

Engineering Mechanics of Composite Materials

11
*

2007

Isaac M. Daniel

Departments of Civil and Mechanical Engineering,
Northwestern University, Evanston, IL, U.S.A.

Ori Ishai

Faculty of Mechanical Engineering,
Technion-Israel Institute of Technology, Haifa, Israel

New York *Oxford*
OXFORD UNIVERSITY PRESS
1994

Oxford University Press

Oxford New York Toronto
Delhi Bombay Calcutta Madras Karachi
Kuala Lumpur Singapore Hong Kong Tokyo
Nairobi Dar es Salaam Cape Town
Melbourne Auckland Madrid

and associated companies in
Berlin Ibadan

Copyright © 1994 by Oxford University Press, Inc.

Published by Oxford University Press, Inc.,
200 Madison Avenue, New York, New York 10016

Oxford is a registered trademark of Oxford University Press

All rights reserved. No part of this publication may be reproduced,
stored in a retrieval system, or transmitted, in any form or by any means,
electronic, mechanical, photocopying, recording, or otherwise,
without the prior permission of Oxford University Press.

Library of Congress Cataloging-in-Publication Data
Daniel, Isaac M.

Engineering mechanics of composite materials/Isaac M. Daniel, Ori Ishai.
p. cm. Includes bibliographical references and index.

ISBN 0-19-507506-4

1. Composite materials—Mechanical properties.
2. Composite materials—Testing.

I. Ishai, Ori, II. Title.

TA418.9.C6D28 1993

620.1'18—dc20 93-11047

9 8 7 6 5 4 3 2 1

Printed in the United States of America
on acid-free paper

Engineering Mechanics of Composite Materials

*To my wife Elaine
my children Belinda, Rebecca and Max
and the memory of my parents Mordochai and Bella Daniel*

ISAAC M. DANIEL

To my wife Yael

ORI ISHAI

Preface

Although the underlying concepts of composite materials go back to antiquity, the technology was essentially developed and most of the progress occurred in the last three decades, and this development was accompanied by a proliferation of literature in the form of reports, conference proceedings, journals, and a few dozen books. Despite this plethora of literature, or because of it, we are constantly faced with a dilemma when asked to recommend a single introductory text for beginning students and engineers. This has convinced us that there is a definite need for a simple and up to date introductory textbook aimed at senior undergraduates, graduate students, and engineers entering the field of composite materials.

This book is designed to meet the above needs as a teaching textbook and as a self-study reference. It only requires knowledge of undergraduate mechanics of materials, although some knowledge of elasticity and especially anisotropic elasticity might be helpful.

The book starts with definitions and an overview of the current status of composites technology. The basic concepts and characteristics, including properties of constituents and typical composite materials of interest and in current use are discussed in Chapter 2. To keep the volume of material covered manageable, we omitted any extensive discussion of micromechanics. We felt that, although relevant, micromechanics is not essential in the analysis and design of composites. In Chapter 3 we deal with the elastic macromechanical response of the unidirectional lamina, including constitutive relations in terms of mathematical stiffnesses and compliances and in terms of engineering properties. We also deal with transformation relations for these mechanical properties. We conclude with a short discussion of micromechanical predictions of elastic properties. In Chapter 4 we begin with a discussion of microscopic failure mechanisms, which leads into the main treatment of failure from the macroscopic point of view. Four basic macroscopic failure theories are discussed in detail. Classical lamination theory, including hygrothermal effects, is developed in detail and then applied to stress and failure analyses of multidirectional laminates in Chapters 5, 6, and 7. We conclude Chapter 7 with a design methodology for structural

composites, including a design example discussed in detail. Experimental methods for characterization and testing of the constituents and the composite material are described in Chapter 8.

Whenever applicable, in every chapter example problems are solved and a list of unsolved problems is given. Computational procedures are emphasized throughout and flow charts for computations are presented.

The material in this book, which can be covered in one semester, is based on lecture notes that we have developed over the last fifteen years in teaching formal courses and condensed short courses at our respective institutions, and we have incorporated much of the feedback received from students. We hope this book is received as a useful and clear guide for introducing students and professionals to the field of composite materials.

We acknowledge with deep gratitude the outstanding, dedicated, and enthusiastic support provided by two people in the preparation of this work. Mrs. Yolande Mallian typed and proofread the entire manuscript, including equations and tables, with painstaking exactitude. Dr. Cho-Liang Tsai diligently and ably performed many computations and prepared all the illustrations.

Evanston, Ill.
Haifa, Israel
May 1993

I.M.D.
O.I.

Contents

1. Introduction	3
1.1 Definition and Characteristics	3
1.2 Historical Development	4
1.3 Overview of Advantages and Limitations of Composite Materials	5
1.3.1 Micromechanics	8
1.3.2 Macromechanics	8
1.3.3 Mechanical Characterization	8
1.3.4 Structural Design and Optimization	8
1.3.5 Fabrication Technology	9
1.3.6 Maintainability, Serviceability, and Durability	9
1.3.7 Cost Effectiveness	9
1.4 Significance and Objectives of Composite Materials Science and Technology	10
1.5 Current Status and Future Prospects	10
2. Basic Concepts and Characteristics	12
2.1 Structural Performance of Conventional Materials	12
2.2 Geometric and Physical Definitions	13
2.2.1 Type of Material	13
2.2.2 Homogeneity	13
2.2.3 Heterogeneity or Inhomogeneity	14
2.2.4 Isotropy	14
2.2.5 Anisotropy/Orthotropy	14
2.3 Material Response	15
2.4 Types and Classification of Composite Materials	19
2.5 Lamina, Laminate; Characteristics and Configurations	21
2.6 Scales of Analysis; Micromechanics, Macromechanics	23
2.7 Basic Lamina Properties	25
2.8 Degrees of Anisotropy	26
2.9 Constituent Materials and Properties	27
2.9.1 Fibers	27
2.9.2 Matrices	30
2.10 Properties of Typical Composite Materials	31

3. Elastic Behavior of Unidirectional Lamina	37
3.1 Stress-Strain Relations	37
3.1.1 General Anisotropic Material	37
3.1.2 Specially Orthotropic Material	41
3.1.3 Transversely Isotropic Material	42
3.1.4 Orthotropic Material under Plane Stress	45
3.1.5 Isotropic Material	47
3.2 Relations between Mathematical and Engineering Constants	48
3.3 Stress-Strain Relations for Thin Lamina	54
3.4 Transformation of Stress and Strain	55
3.5 Transformation of Elastic Parameters	57
3.6 Transformation of Stress-Strain Relations in Terms of Engineering Constants	61
3.7 Transformation Relations for Engineering Constants	64
3.8 Micromechanical Predictions of Elastic Constants	70
3.8.1 Scope and Approaches	70
3.8.2 Longitudinal Properties	72
3.8.3 Transverse Modulus	73
3.8.4 In-Plane Shear Modulus	74
4. Strength of Unidirectional Lamina	85
4.1 Micromechanics of Failure; Failure Mechanisms	85
4.1.1 Longitudinal Tension	85
4.1.2 Longitudinal Compression	90
4.1.3 Transverse Tension	93
4.1.4 Transverse Compression	99
4.1.5 In-Plane Shear	100
4.2 Macromechanical Strength Parameters	102
4.3 Macromechanical Failure Theories	106
4.4 Maximum Stress Theory	108
4.5 Maximum Strain Theory	111
4.6 Deviatoric Strain Energy Theory (Tsai-Hill)	114
4.7 Interactive Tensor Polynomial Theory (Tsai-Wu)	116
4.8 Computational Procedure for Determination of Lamina Strength	120
4.9 Applicability of Various Failure Theories	126
5. Elastic Behavior of Multidirectional Laminates	142
5.1 Basic Assumptions	142
5.2 Strain-Displacement Relations	143
5.3 Stress-Strain Relations of Layer within a Laminate	145
5.4 Force and Moment Resultants	146
5.5 General Load-Deformation Relations: Laminate Stiffnesses	149
5.6 Inversion of Load-Deformation Relations: Laminate Compliances	152
5.7 Symmetric Laminates	153
5.7.1 Symmetric Laminates with Isotropic Layers	155

5.7.2 Symmetric Laminates with Specially Orthotropic Layers (Symmetric Crossply Laminates)	156
5.7.3 Symmetric Angle-Ply Laminates	157
5.8 Balanced Laminates	157
5.8.1 Antisymmetric Laminates	158
5.8.2 Antisymmetric Crossply Laminates	159
5.8.3 Antisymmetric Angle-Ply Laminates	161
5.9 Orthotropic Laminates: Transformation of Laminate Stiffnesses and Compliances	162
5.10 Quasi-Isotropic Laminates	164
5.11 Design Considerations	166
5.12 Laminate Engineering Properties	168
5.13 Computational Procedure for Determination of Engineering Elastic Properties	177
5.14 Comparison of Elastic Parameters of Unidirectional and Angle-Ply Laminates	178
5.15 Carpet Plots for Multidirectional Laminates	181
6. Hygrothermal Effects	189
6.1 Introduction	189
6.1.1 Physical and Chemical Effects	189
6.1.2 Effects on Mechanical Properties	190
6.1.3 Hygrothermoelastic (HTE) Effects	190
6.2 Hygrothermal Effects on Mechanical Behavior	190
6.3 Coefficients of Thermal and Moisture Expansion of Unidirectional Lamina	194
6.4 Hygrothermal Strains in Unidirectional Lamina	198
6.5 Hygrothermoelastic Stress–Strain Relations	200
6.6 Hygrothermoelastic Strain–Stress Relations	203
6.7 Physical Significance of Hygrothermal Forces	204
6.8 Hygrothermal Stress–Strain Relations	206
6.9 Coefficients of Thermal and Moisture Expansion of Multidirectional Laminates	206
6.10 Coefficients of Thermal and Moisture Expansion of Balanced/Symmetric Laminates	207
6.11 Hygrothermoelastic Isotropy and Stability	209
6.12 Coefficients of Thermal Expansion of Unidirectional and Multidirectional Carbon/Epoxy Laminates	212
6.13 Hygrothermoelastic Stress Analysis of Multidirectional Laminates	213
6.14 Residual Stresses	215
6.15 Warpage	221
6.16 Computational Procedure for Hygrothermoelastic Analysis of Multidirectional Laminates	225
7. Stress and Failure Analysis of Multidirectional Laminates	234
7.1 Introduction	234

7.2	Types of Failure	235
7.3	Stress Analysis and Safety Factors for First-Ply Failure of Symmetric Laminates (In-Plane Loading)	235
7.4	Strength Components for First-Ply Failure of Symmetric Laminates	238
7.5	Computational Procedure for Stress and Failure Analysis of General Multidirectional Laminates (First-Ply Failure)	244
7.6	Comparison of Strengths of Unidirectional and Angle-Ply Laminates (First-Ply Failure)	246
7.7	Carpet Plots for Strength of Multidirectional Laminates (First-Ply Failure)	248
7.8	Effect of Hygrothermal History on Strength of Multidirectional Laminates (First-Ply Failure; Tsai–Wu Criterion)	250
7.9	Computational Procedure for Stress and Failure Analysis of Multidirectional Laminates under Combined Mechanical and Hygrothermal Loading (First-Ply Failure; Tsai–Wu Criterion)	252
7.10	Micromechanics of Progressive Failure: Stiffness Reduction	254
7.11	Progressive and Ultimate Laminate Failure	259
7.12	Analysis of Progressive Laminate Failure	261
7.13	Interlaminar Stresses and Strength of Multidirectional Laminates: Edge Effects	265
	7.13.1 Introduction	265
	7.13.2 Angle-Ply Laminates	265
	7.13.3 Crossply Laminates	266
	7.13.4 Effects of Stacking Sequence	268
	7.13.5 Interlaminar Strength	272
7.14	Interlaminar Fracture Toughness	275
7.15	Design Methodology for Structural Composite Materials	278
7.16	Illustration of Design Process: Design of a Pressure Vessel	281
	7.16.1 Aluminum Reference Vessel	282
	7.16.2 Crossply $[0_m/90_n]_s$ Laminates	283
	7.16.3 Angle-Ply $[\pm\theta]_{ns}$ Laminates	283
	7.16.4 $[90/\pm\theta]_{ns}$ Laminates	285
	7.16.5 $[0/\pm\theta]_{ns}$ Laminates	286
	7.16.6 Quasi-Isotropic $[0/\pm 45/90]_{ns}$ Laminates	286
	7.16.7 Summary and Comparison of Results	286
7.17	Ranking of Composite Laminates	288
8.	Experimental Methods for Characterization and Testing of Composite Materials	299
8.1	Introduction	299
8.2	Characterization of Constituent Materials	300
	8.2.1 Fiber Characterization	300
	8.2.2 Matrix Characterization	304
8.3	Physical Characterization of Composite Materials	306
	8.3.1 Density	306

8.3.2 Fiber Volume Ratio	306
8.3.3 Void Volume Ratio (Porosity)	307
8.3.4 Coefficients of Thermal Expansion	309
8.3.5 Coefficients of Moisture Expansion	310
8.4 Determination of Tensile Properties of Unidirectional Lamina	312
8.5 Determination of Compressive Properties of Unidirectional Lamina	316
8.6 Determination of Shear Properties of Unidirectional Lamina	321
8.7 Determination of Interlaminar Strength	331
8.7.1 Interlaminar Shear Strength	331
8.7.2 Interlaminar Tensile Strength	333
8.8 Determination of Interlaminar Fracture Toughness	336
8.8.1 Mode I Testing	336
8.8.2 Mode II Testing	339
8.8.3 Mixed Mode Testing	343
8.8.4 Mode III Testing	345
8.9 Biaxial Testing	347
8.9.1 Introduction	347
8.9.2 Off-Axis Uniaxial Test	347
8.9.3 Crossbeam Sandwich Specimen	350
8.9.4 Flat Plate Specimen	352
8.9.5 Thin-Wall Tubular Specimen	352
8.10 Characterization of Composites with Stress Concentrations	357
8.10.1 Introduction	357
8.10.2 Laminates with Holes	357
8.10.3 Laminates with Cracks	364
8.11 Summary and Discussion	368
<i>Answers to Selected Problems</i>	379
<i>Index</i>	385

Engineering Mechanics of Composite Materials

Chapter 1

Introduction

1.1. Definition and Characteristics

A structural composite is a material system consisting of two or more phases on a macroscopic scale, whose mechanical performance and properties are designed to be superior to those of the constituent materials acting independently. One of the phases is usually discontinuous, stiffer, and stronger and is called *reinforcement*, whereas the less stiff and weaker phase is continuous and is called *matrix* (Fig. 1.1). Sometimes, because of chemical interactions or other processing effects, an additional phase, called *interphase*, exists between the reinforcement and the matrix. The properties of a composite material depend

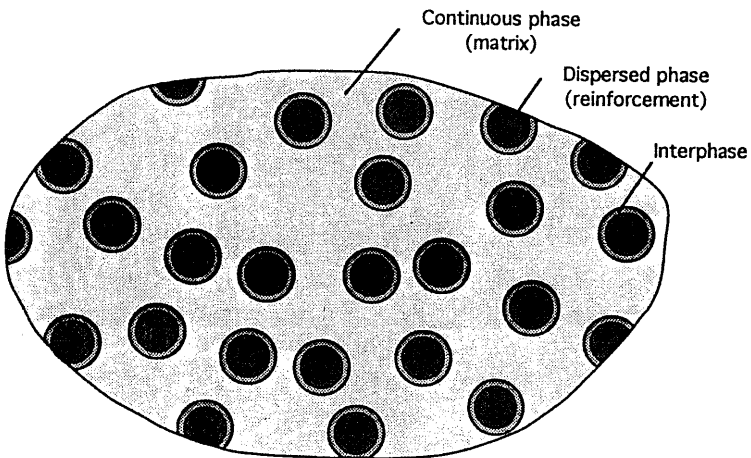


Fig. 1.1 Phases of a composite material.

on the properties of the constituents, geometry, and distribution of the phases. One of the most important parameters is the volume (or weight) fraction of reinforcement, or fiber volume ratio. The distribution of the reinforcement determines the homogeneity or uniformity of the material system. The more nonuniform is the reinforcement distribution, the more heterogeneous is the material and the higher is the probability of failure in the weakest areas. The geometry and orientation of the reinforcement affect the anisotropy of the system.

The phases of the composite system have different roles that depend on the type and application of the composite material. In the case of low to medium performance composite materials, the reinforcement, usually in the form of short fibers or particles, provides some stiffening but only local strengthening of the material. The matrix, on the other hand, is the main load-bearing constituent governing the mechanical properties of the material. In the case of high performance structural composites, the usually continuous-fiber reinforcement is the backbone of the material that determines its stiffness and strength in the direction of the fibers. The matrix phase provides protection and support for the sensitive fibers and local stress transfer from one fiber to another. The interphase, although small in size, can play an important role in controlling the failure mechanisms, fracture toughness, and overall stress-strain behavior of the material.

1.2. Historical Development

Historically, the concept of fibrous reinforcement is very old. There are biblical references to straw-reinforced clay bricks in ancient Egypt. Iron rods were used to reinforce masonry in the nineteenth century, leading to the development of steel-reinforced concrete. Phenolic resin reinforced with asbestos fibers was introduced in the beginning of the twentieth century. The first fiberglass boat was made in 1942; reinforced plastics were also used in aircraft and electrical components at this time. Filament winding was invented in 1946 and incorporated into missile applications in the 1950s. The first boron and high strength carbon fibers were introduced in the early 1960s, with applications of advanced composites to aircraft components by 1968. Metal matrix composites such as boron/aluminum were introduced in 1970. Dupont developed Kevlar (or aramid) fibers in 1973. Starting in the late 1970s applications of composites expanded widely to the aircraft, automotive, sporting goods, and biomedical industries. The 1980s marked a significant increase in high modulus fiber utilization. Now emphasis is being placed on development of newer metal/matrix and ceramic/matrix composites, as well as carbon/carbon composites, for high temperature applications. Applications abound, including underground pipes and containers, boats, ground vehicles, aircraft and aerospace structures, automotive

components, sports equipment, biomedical products, and many other products designed to have high mechanical performance and/or environmental stability coupled with low weight (see Figs. 1.2–1.7).

1.3 Overview of Advantages and Limitations of Composite Materials

Composites have unique advantages over monolithic materials, such as high strength, high stiffness, long fatigue life, low density, and adaptability to the

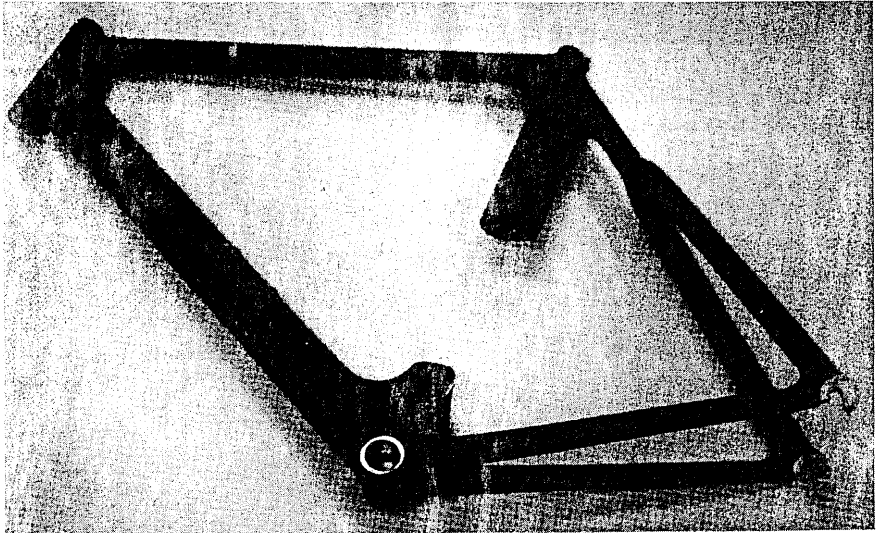


Fig. 1.2 Bicycle frame made of carbon/epoxy composite weighing 13 N (3 lb).

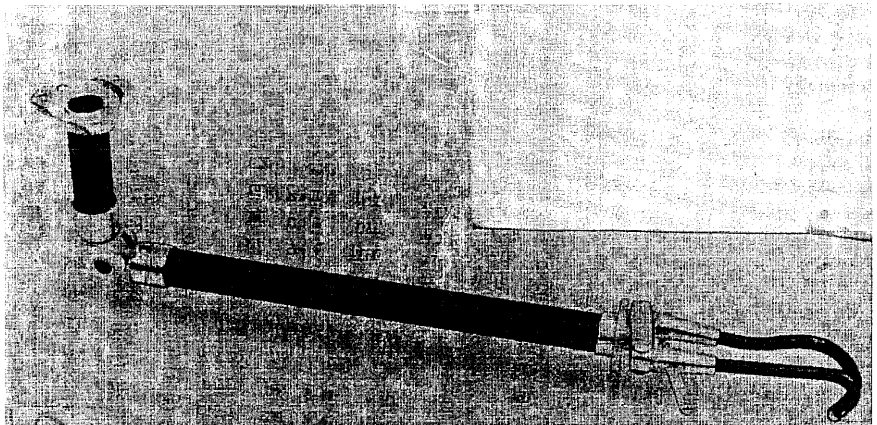


Fig. 1.3 Artificial limb incorporating carbon/epoxy components.

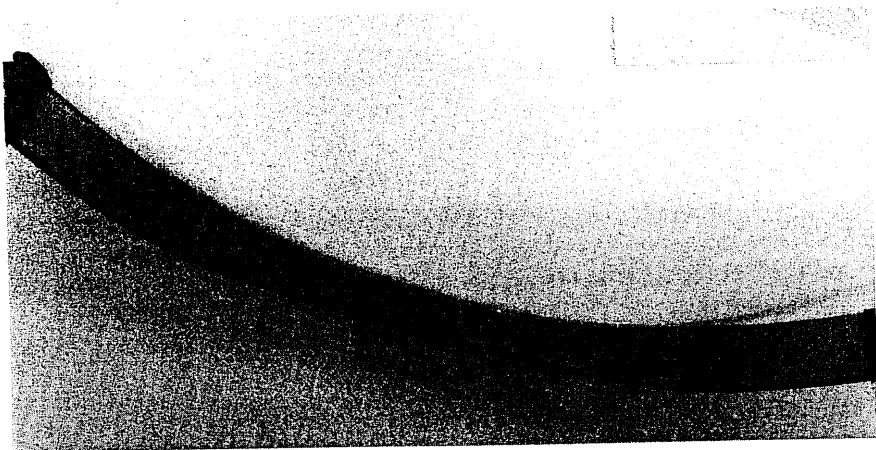


Fig. 1.4 Automobile leaf spring made of glass/polyester composite weighing 36 N (8 lb) compared with original steel spring which weighed 285 N (64 lb).

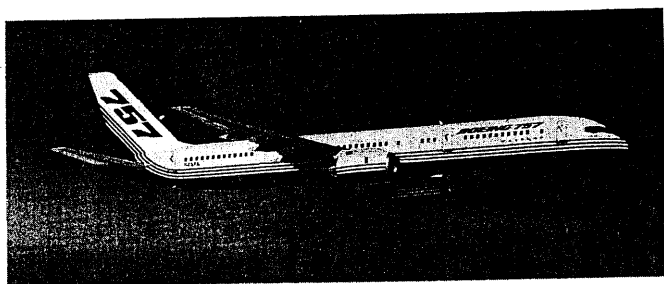


Fig. 1.5 Boeing 757 commercial aircraft with a large number of composite material components. (Courtesy of Boeing Commercial Airplane Group.)

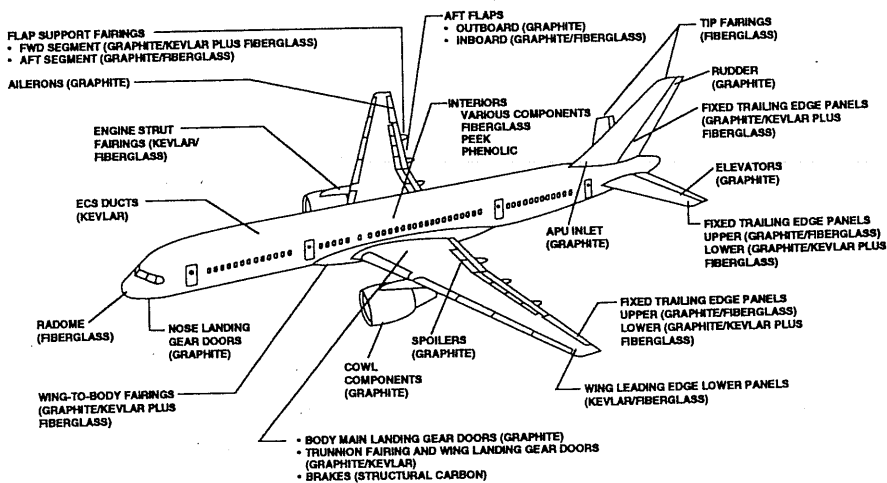


Fig. 1.6 Diagram illustrating the various components of the Boeing 757 aircraft made of composite materials. (Courtesy of Boeing Commercial Airplane Group.)

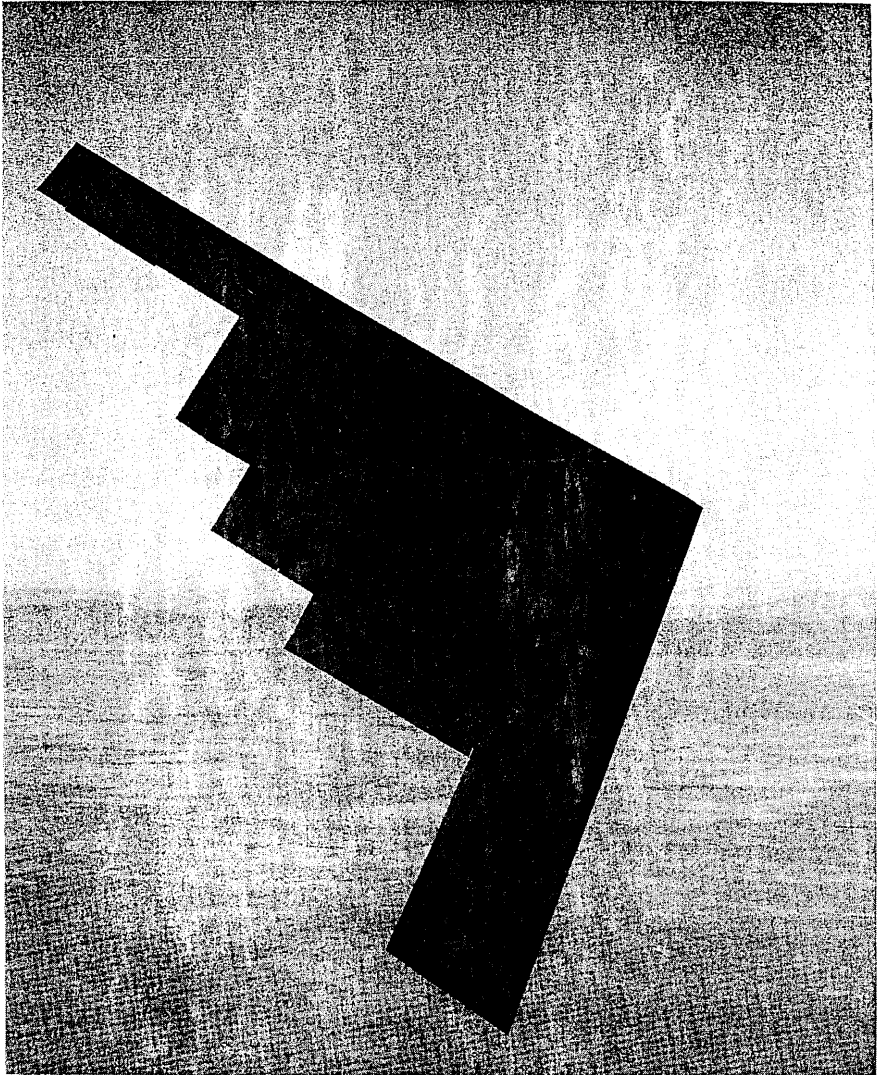


Fig. 1.7 B-2 stealth bomber made almost entirely of composite materials. (Courtesy of Dr. R. Ghezler, Northrop Corporation.)

intended function of the structure. Additional improvements can be realized in corrosion resistance, wear resistance, appearance, temperature-dependent behavior, thermal stability, thermal insulation, thermal conductivity, and acoustic insulation. The basis of the superior structural performance of composite materials lies in the high specific strength (strength to density ratio) and high specific stiffness (modulus to density ratio) and in the anisotropic and heterogeneous character of the material. The latter provides the composite system with many degrees of freedom for optimum configuration of the material.

Composites also have some limitations that conventional monolithic materials do not have. Below is a brief discussion of the advantages and limitations of composites and conventional structural materials (mainly metals) when compared on the basis of micromechanics, macromechanics, material characterization, design and optimization, fabrication technology, maintenance and durability, and cost effectiveness.

1.3.1 Micromechanics

When viewed on the scale of the fiber dimensions, composites have the advantage of high stiffness and high strength fibers. The usually low fracture toughness of the fiber is enhanced by the energy dissipation at the fiber/matrix interface and matrix ductility. The stress transfer capability of the matrix enables the development of multiple-site failure mechanisms. On the other hand, the fibers exhibit a relatively high scatter in strength. Local stress concentrations around the fibers reduce the transverse tensile strength appreciably. Conventional materials are more sensitive to their microstructure and local irregularities, which influence the brittle or ductile behavior of the material.

1.3.2 Macromechanics

In the macromechanical analysis, in which the material is treated as quasihomogeneous, its anisotropy can be used to advantage. The average material behavior can be controlled and predicted from the properties of the constituents. However, the anisotropic analysis is more complex and more dependent on the computational procedures. On the other hand, the analysis for conventional materials is much simpler due to their isotropy and homogeneity.

1.3.3 Mechanical Characterization

The analysis of composite structures requires the input of average material properties. These properties can be predicted on the basis of the properties and arrangement of the constituents. However, experimental verification of analysis or independent characterization requires a comprehensive test program for determination of a large number (more than 10) of basic material parameters. In the case of conventional materials, mechanical characterization is simple, as only two elastic constants and two strength values suffice.

1.3.4. Structural Design and Optimization

Composites afford the unique possibility of designing the material and structure in one unified and concurrent process. The large number of degrees of freedom

available enable material optimization for several given constraints simultaneously, such as minimum weight and maximum dynamic stability. However, the numerous available options make the process more involved and the analysis more complex. In the case of conventional materials, optimization is limited due to the few degrees of freedom available, usually one or two geometric parameters.

1.3.5. Fabrication Technology

The fabrication process is one of the most important steps in the application of composite materials. Structural parts, rather than generic material form, are fabricated with relatively simple tooling. A variety of fabrication methods suitable for several applications are available. They include autoclave molding, filament winding, pultrusion, and resin transfer molding (RTM). Structural components consisting of different materials, such as honeycomb sandwich structures, can be manufactured in one step by the so-called co-curing process. Thus the number of parts to be assembled and the number of required joints can be reduced. On the negative side, composite fabrication is still dependent on skilled hand labor with limited automation and standardization. This requires more stringent and extensive quality control procedures.

In the case of conventional materials, material fabrication and structure fabrication are two separate processes. Structures usually necessitate complex tooling and elaborate assembly with multiple joints.

1.3.6 Maintainability, Serviceability, and Durability

Composites can operate in hostile environments for long periods of time. They have long fatigue lives and are easily maintainable and repaired. However, they suffer from sensitivity to hygrothermal environments. Service-induced damage growth may be internal, requiring sophisticated, nondestructive techniques for its detection and monitoring. Sometimes it is necessary to apply protective coatings against erosion, surface damage, and lightning strike.

Conventional materials, usually metals, are susceptible to corrosion in hostile environments. Discrete flaws and cracks may be induced in service and may grow and propagate to catastrophic failure. Although detection of these defects may be easier, repair of conventional materials is not simple.

1.3.7 Cost Effectiveness

One of the important advantages of composites is reduction in acquisition and/or life cycle costs. This is effected through weight savings, lower tooling costs,

reduced number of parts, and fewer assembly operations. This advantage is somewhat diluted when one considers the high cost of raw materials, fibers and prepreg (resin preimpregnated fibers), and auxiliary materials used in fabrication and assembly with composite materials. In the case of conventional structural materials, the low cost of raw materials is more than offset by the high cost of tooling, machining, and assembly.

1.4 Significance and Objectives of Composite Materials Science and Technology

The study of composites is a philosophy of material design that allows for the optimum material composition along with structural design and optimization in one concurrent and interactive process. It is a science and technology requiring close interaction of various disciplines such as structural design and analysis, materials science, mechanics of materials, and process engineering. The scope of composite materials research and technology consists of the following tasks:

1. Investigation of basic characteristics of the constituent and composite materials.
2. Material optimization for given service conditions.
3. Development of effective and efficient fabrication procedures and understanding of their effect on material properties.
4. Development of analytical procedures for determining material properties and prediction of structural behavior.
5. Development of effective experimental methods for material characterization, stress analysis, and failure analysis.
6. Nondestructive evaluation of material integrity and structural reliability.
7. Assessment of durability, flaw criticality, and life prediction.

1.5 Current Status and Future Prospects

The technology of composite materials has experienced a rapid development in the last two decades. Some of the underlying reasons and motivations for this development are (1) significant progress in materials science and technology in the area of fibers, polymers, and ceramics; (2) requirements for high performance materials in aircraft and aerospace structures; and (3) development of powerful and sophisticated numerical methods for structural analysis using modern computer technology and the availability of powerful desk-top computers for the engineering community.

The initial driving force in the technology development was weight savings. Later, cost competitiveness with more conventional materials became equally

important. To these two requirements today is added the need for quality assurance, reproducibility, and predictability of behavior over the lifetime of the structure.

New developments continue in all areas. For example, new types of carbon fibers are being introduced with higher ultimate strains. Thermoplastic matrices are used under certain conditions because they are tough, have low sensitivity to moisture effects, and are more easily amenable to mass production and repair. The use of woven fabric and short fiber reinforcement is receiving more attention. The design of structures and systems capable of operating at elevated temperatures has spurred intensive research in high temperature composites, such as metal/matrix, ceramic/matrix, and carbon/carbon composites.

The utilization of conventional and new composite materials is intimately related to the development of fabrication methods. The manufacturing process is one of the most important stages in controlling the properties and ensuring the quality of the finished product. Quality control inspection and automation are being introduced in the manufacturing process.

The technology of composite materials, although still developing, has reached a state of maturity. Prospects for the future are bright for a variety of reasons. The cost of the basic constituents is decreasing due to market expansion. The fabrication process is becoming less costly as more experience is accumulated, techniques are improved, and automation is introduced. Newer high volume applications, such as in the automotive industry, will expand the use of composites greatly. The need for energy conservation motivates more uses of lightweight materials and products. Finally, the availability of many good interactive computer programs make structural design and analysis simpler and more manageable for engineers who have a basic undergraduate education.

Chapter 2

Basic Concepts and Characteristics

2.1 Structural Performance of Conventional Materials

Conventional monolithic materials can be divided into three broad categories: metals, ceramics, and polymers. Although there is considerable variability in properties within each category, each group of materials has some characteristic properties that are more distinct for that group. In the case of ceramics one must make a distinction between two forms, bulk and fiber.

Table 2.1 presents a list of properties and a rating of the three groups of materials with regard to each property. The advantage or desirability is ranked as: superior (++), good (+), poor (-), and variable (v). Thus, for example, metals are superior with regard to stiffness and hygroscopic sensitivity, but they have high density and are subject to chemical corrosion (-). Ceramics in bulk form have low tensile strength and toughness (-) but good thermal stability, high hardness, low creep, and high erosion resistance (+). Ceramics in fibrous form behave very differently from those in bulk form and have some unique advantages. They rank highest with regard to tensile strength, stiffness, creep, and thermal stability (++). The biggest advantage that polymers have is their low density (++), but they rank poorly with respect to stiffness, creep, hardness, thermal and dimensional stability, and erosion resistance (-). The observations above show that no single material possesses all the advantages for a given application (property) and that it would be highly desirable to combine materials in ways that utilize the best of each constituent in a synergistic way. A good combination, for example, would be ceramic fibers in a polymeric matrix.

Table 2.1 Structural Performance Ranking of Conventional Materials

Property	Metals	Ceramics		Polymers
		Bulk	Fibers	
Tensile strength	+	-	++	v
Stiffness	++	v	++	-
Fracture toughness	+	-	v	+
Impact strength	+	-	v	+
Fatigue endurance	+	v	+	+
Creep	v	v	++	-
Hardness	+	+	+	-
Density	-	+	+	++
Dimensional stability	+	v	+	-
Thermal stability	v	+	++	-
Hygroscopic sensitivity	++	v	+	v
Weatherability	v	v	v	+
Erosion resistance	+	+	+	-
Corrosion Resistance	-	v	v	+

++, superior; +, good; -, poor; v, variable.

2.2 Geometric and Physical Definitions

2.2.1 Type of Material

Depending on the number of its constituents or phases, a material is called **single phase** (or monolithic), **bi phase** (or two-phase), **three phase**, and **multi-phase**. The different phases of a structural composite have distinct physical and mechanical properties and characteristic dimensions much larger than molecular or grain dimensions.

2.2.2 Homogeneity

A material is called **homogeneous** if its properties are the same at every point or are independent of location. The concept of homogeneity is associated with a scale or characteristic volume and the definition of the properties involved. Depending on the scale or volume observed, the material can be more homogeneous or less homogeneous. If low variability exists from point to point on a macroscopic scale, the material is referred to as **quasi homogeneous**.

2.2.3 Heterogeneity or Inhomogeneity

A material is heterogeneous or inhomogeneous if its properties vary from point to point or depend on location. As in the case above, the concept of heterogeneity is associated with a scale or characteristic volume. As this scale decreases, the same material can be regarded as homogeneous, quasi homogeneous, or heterogeneous.

In Figure 2.1, for example, the material is considered homogeneous and anisotropic on a macroscopic scale, because it has a similar composition at different locations (A and B) but properties varying with orientation. On a microscopic scale, the material is heterogeneous and isotropic, having different but orientation-independent properties within characteristic volumes **a** and **b**.

2.2.4 Isotropy

Many material properties, such as stiffness, strength, thermal expansion, and thermal conductivity, are associated with a direction or axis. A material is **isotropic** when its properties are the same in all directions or are independent of the orientation of reference axes.

2.2.5 Anisotropy/Orthotropy

A material is **anisotropic** when its properties at a point vary with direction or depend on the orientation of reference axes. If the properties of the material

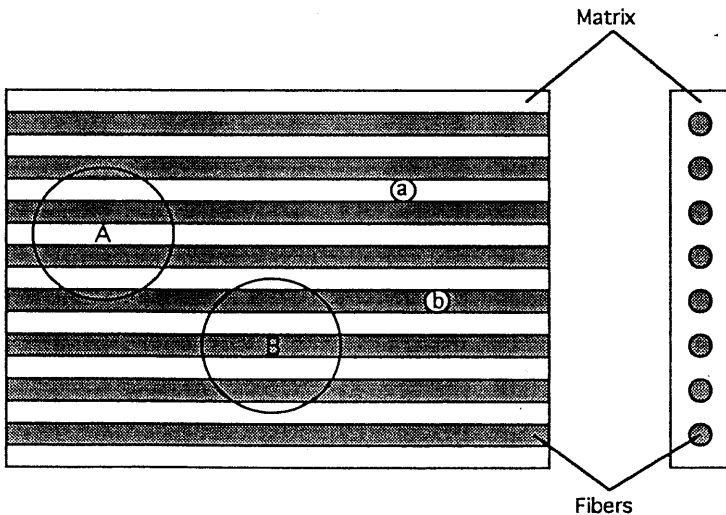


Fig. 2.1 Macroscopic (A,B) and microscopic (a,b) scales of observation for unidirectional layer.

along any direction are the same as those along a symmetric direction with respect to a plane, then that plane is defined as a **plane of material symmetry**. A material may have zero, one, two, three, or an infinite number of planes of material symmetry through a point. A material without any planes of symmetry is called **general anisotropic** (or aeolotropic). At the other extreme, an isotropic material has an infinite number of planes of symmetry.

Of special relevance to composite materials are **orthotropic** materials, i.e., materials having at least three mutually perpendicular planes of symmetry. The intersections of these planes define three mutually perpendicular axes, called **principal axes** of material symmetry or simply **principal material axes**.

2.3 Material Response

Some of the intrinsic characteristics of the materials discussed before are revealed in their response to simple mechanical loading, e.g., uniaxial normal stress and pure shear stress, as illustrated in Figure 2.2. An isotropic material under uniaxial tensile loading undergoes an axial deformation (strain), ϵ_x , in the loading direction, a transverse deformation (strain), ϵ_y , and no shear deformation:

$$\begin{aligned}\epsilon_x &= \frac{\sigma_x}{E} \\ \epsilon_y &= -\frac{\nu \sigma_x}{E} \\ \gamma_{xy} &= 0\end{aligned}\tag{2.1}$$

where

ϵ_x , ϵ_y , γ_{xy} = Axial, transverse, and shear strains, respectively

σ_x = Axial stress

E = Young's modulus

ν = Poisson's ratio

Under pure shear loading τ_{xy} , the material undergoes a pure shear deformation, i.e., a square element deforms into a diamond-shaped one with equal and

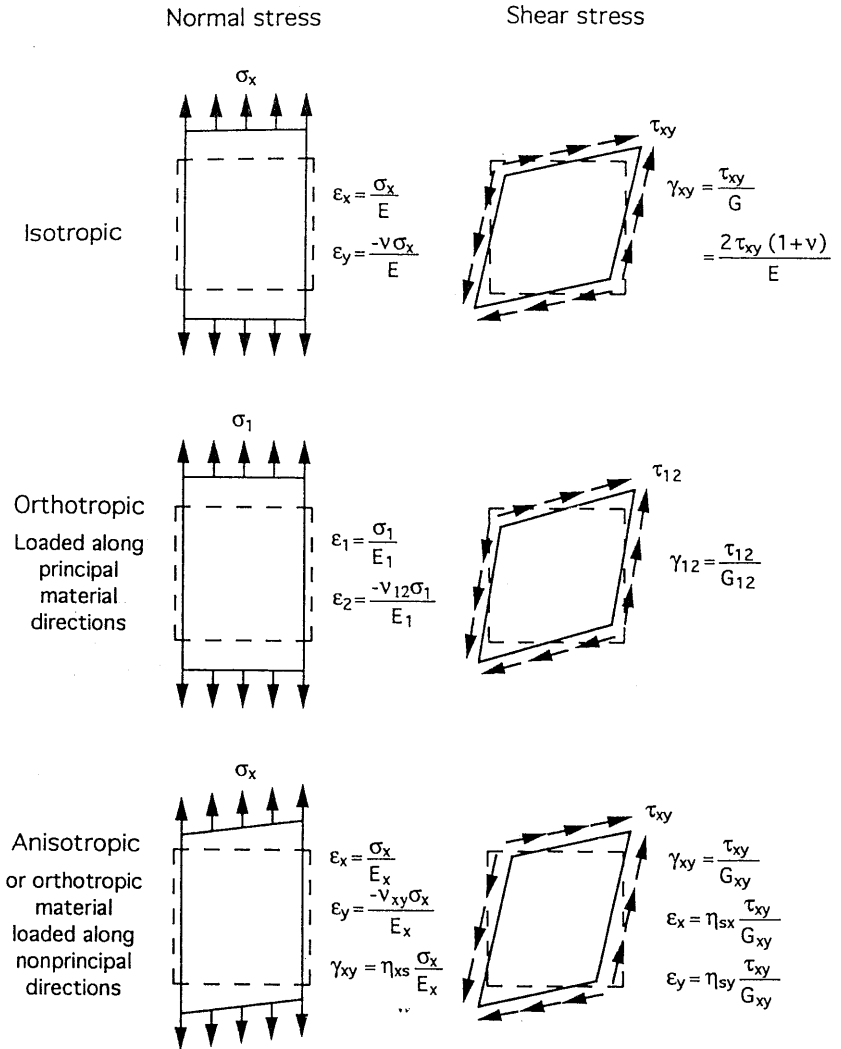


Fig. 2.2 Response of various types of materials under uniaxial normal and pure shear loading.

unchanged side lengths. The shear-strain (change of angle), γ_{xy} , and the normal strains ϵ_x, ϵ_y are

$$\gamma_{xy} = \frac{\tau_{xy}}{G} = \frac{2\tau_{xy} (1 + \nu)}{E}$$

$$\epsilon_x = \epsilon_y = 0$$

(2.2)

where

τ_{xy} = Shear stress

G = Shear modulus

As indicated in Eq. (2.2), the shear modulus is not an independent constant, but is related to Young's modulus and Poisson's ratio.

An orthotropic material loaded in uniaxial tension along one of its principal material axes (1) undergoes deformations similar to those of an isotropic material and given by

$$\begin{aligned}\epsilon_1 &= \frac{\sigma_1}{E_1} \\ \epsilon_2 &= -\frac{\nu_{12} \sigma_1}{E_1} \\ \gamma_{12} &= 0\end{aligned}\tag{2.3}$$

where

$\epsilon_1, \epsilon_2, \gamma_{12}$ = Axial, transverse and shear strains, respectively

σ_1 = Axial normal stress

E_1 = Axial modulus in the 1-direction

ν_{12} = Poisson's ratio associated with loading in the
1-direction and strain in the 2-direction

Under pure shear loading, τ_{12} , along the principal material axes, the material undergoes pure shear deformation, i.e., a square element deforms into a diamond-shaped one with unchanged side lengths. The strains are

$$\begin{aligned}\gamma_{12} &= \frac{\tau_{12}}{G_{12}} \\ \epsilon_1 &= \epsilon_2 = 0\end{aligned}\tag{2.4}$$

Here, the shear modulus, G_{12} , is an independent material constant and is not related to the Young's moduli or Poisson's ratios.

In both cases discussed before, normal loading does not produce shear strain and pure shear loading does not produce normal strains. Thus normal loading and shear deformation (as well as pure shear loading and normal strains) are independent or uncoupled.

A general anisotropic material under uniaxial tension, or an orthotropic material under uniaxial tension along a direction other than a principal material axis, undergoes axial, transverse, and shear deformations given by

$$\begin{aligned}\epsilon_x &= \frac{\sigma_x}{E_x} \\ \epsilon_y &= -\frac{\nu_{xy}\sigma_x}{E_x} \\ \gamma_{xy} &= \eta_{kx} \frac{\sigma_x}{E_x}\end{aligned}\tag{2.5}$$

where

$\epsilon_x, \epsilon_y, \gamma_{xy}$ = Axial, transverse, and shear strains, respectively

σ_x = Axial normal stress

E_x = Axial modulus in x -direction

ν_{xy} = Poisson's ratio associated with loading in the
 x -direction and strain in the y -direction

η_{kx} = Shear coupling coefficient (the first
subscript denotes normal loading in the x -direction;
the second subscript denotes shear strain)

This mode of response characterized by η_{kx} , is called **shear coupling effect** and will be discussed in detail in Chapter 3.

Under pure shear loading, τ_{xy} , along the same axes, the material undergoes both shear and normal deformations, i.e., a square element deforms into a parallelogram with unequal sides. The shear and normal strains are given by

$$\begin{aligned}\gamma_{xy} &= \frac{\tau_{xy}}{G_{xy}} \\ \epsilon_x &= \eta_{sx} \frac{\tau_{xy}}{G_{xy}} \\ \epsilon_y &= \eta_{sy} \frac{\tau_{xy}}{G_{xy}}\end{aligned}\tag{2.6}$$

where

G_{xy} = Shear modulus referred to the x - and y -axes

η_{sx}, η_{sy} = Shear coupling coefficients (to be discussed later)

The above discussion illustrates the increasing complexity of material response with increasing anisotropy and the need to introduce additional material constants to describe this response.

2.4 Types and Classification of Composite Materials

Two-phase composite materials are classified into three broad categories depending on the type, geometry, and orientation of the reinforcement phase, as illustrated in the chart of Figure 2.3.

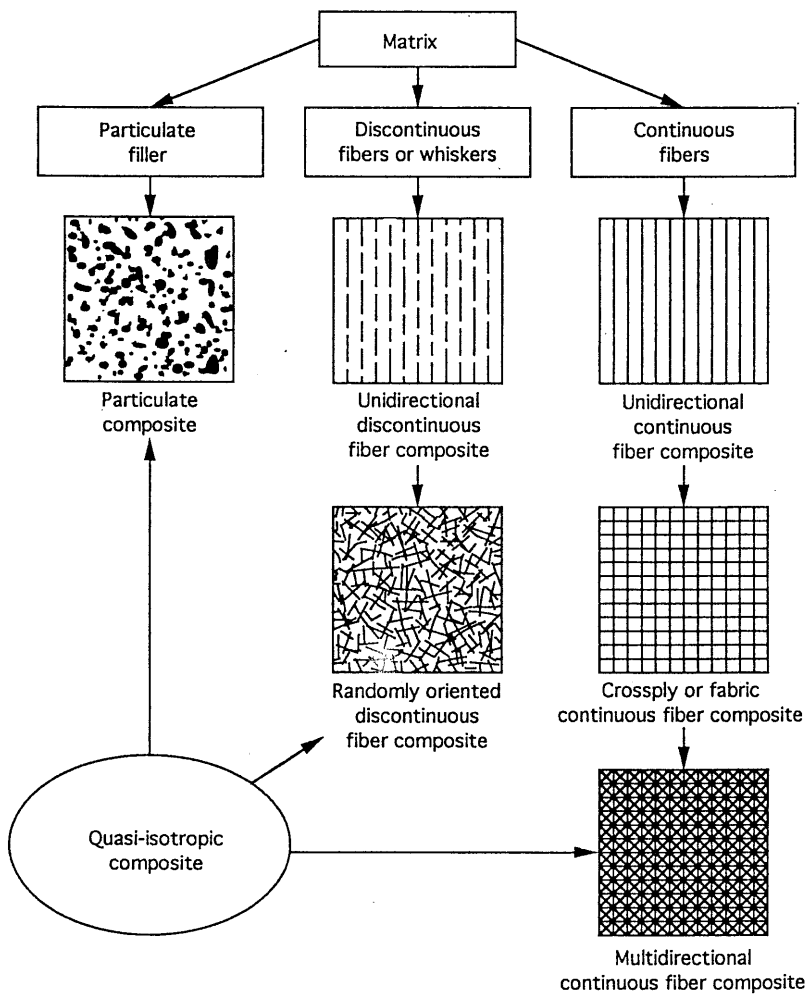


Fig. 2.3 Classification of composite material systems.

Particulate composites consist of particles of various sizes and shapes randomly dispersed within the matrix. Because of the randomness of particle distribution, these composites can be regarded as quasi homogeneous on a scale larger than the particle size and spacing and quasi-isotropic. Particulate composites may consist of nonmetallic particles in a nonmetallic matrix (concrete, glass reinforced with mica flakes, brittle polymers reinforced with rubberlike particles); metallic particles in nonmetallic matrices (aluminium particles in polyurethane rubber used in rocket propellants); metallic particles in metallic matrices (lead particles in copper alloys to improve machinability); and nonmetallic particles in metallic matrices (silicon carbide particles in aluminium, SiC(p)/Al).

Discontinuous or short-fiber composites contain short fibers or whiskers as the reinforcing phase. These short fibers, which can be fairly long compared with the diameter, can be either all oriented along one direction or randomly oriented. In the first instance the composite material tends to be markedly anisotropic or, more specifically, orthotropic, whereas in the second it can be regarded as quasi-isotropic.

Continuous fiber composites are reinforced by long continuous fibers and are the most efficient from the point of view of stiffness and strength. The continuous fibers can be all parallel (unidirectional continuous fiber composite), can be oriented at right angles to each other (crossply or woven fabric continuous fiber composite), or can be oriented along several directions (multidirectional continuous fiber composite). In the latter case, for a certain number of fiber directions and distribution of fibers, the composite can be characterized as a quasi-isotropic material.

Fiber-reinforced composites can be classified into broad categories according to the matrix used: polymer, metal, ceramic, and carbon matrix composites (Table 2.2). **Polymer matrix composites** include thermoset (epoxy, polyimide, polyester) or thermoplastic (poly-ether-ether-ketone, polysulfone) resins reinforced with glass, carbon (graphite), aramid (Kevlar), or boron fibers. They are used primarily in relatively low temperature applications. **Metal matrix composites** consist of metals or alloys (aluminum, magnesium, titanium, copper) reinforced with boron, carbon (graphite), or ceramic fibers. Their maximum use temperature is limited by the softening or melting temperature of the metal matrix. **Ceramic matrix composites** consist of ceramic matrices (silicon carbide, aluminum oxide, glass-ceramic, silicon nitride) reinforced with ceramic fibers. They are best suited for very high temperature applications. **Carbon/carbon composites** consist of carbon or graphite matrix reinforced with graphite yarn or fabric. They have unique properties of relatively high strength at high temperatures coupled with low thermal expansion and low density.

In addition to the types discussed above, there are **laminated composites**. These consist of thin layers of different materials bonded together, such as bi-metals, clad metals, plywood and formica.

Table 2.2 Types of Composite Materials

Matrix type	Fiber	Matrix
Polymer	E-glass	Epoxy
	S-glass	Polyimide
	Carbon (graphite)	Polyester
	Aramid (Kevlar)	Thermoplastics
	Boron	(PEEK, polysulfone, etc.)
Metal	Boron	Aluminum
	Borsic	Magnesium
	Carbon (graphite)	Titanium
	Silicon carbide	Copper
	Alumina	
Ceramic	Silicon carbide	Silicon carbide
	Alumina	Alumina
	Silicon nitride	Glass-ceramic
		Silicon nitride
Carbon	Carbon	Carbon

2.5 Lamina, Laminate; Characteristics and Configurations

A **lamina**, or ply, is a plane (or curved) layer of unidirectional fibers or woven fabric in a matrix. In the case of unidirectional fibers, it is also referred to as **unidirectional lamina (UD)**. The lamina is an orthotropic material with principal material axes in the direction of the fibers (longitudinal), normal to the fibers in the plane of the lamina (in-plane transverse), and normal to the plane of the lamina (Fig. 2.4). These principal axes are designated as 1, 2, and 3, respectively.

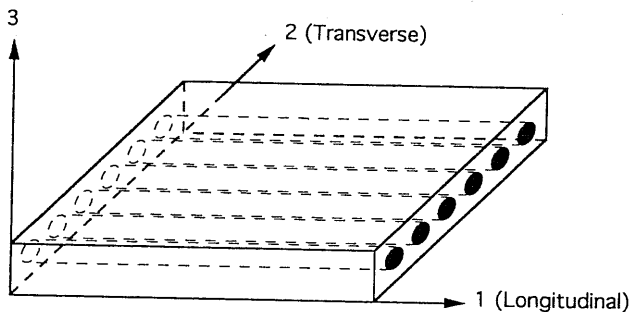


Fig. 2.4 Unidirectional lamina and principal coordinate axes.

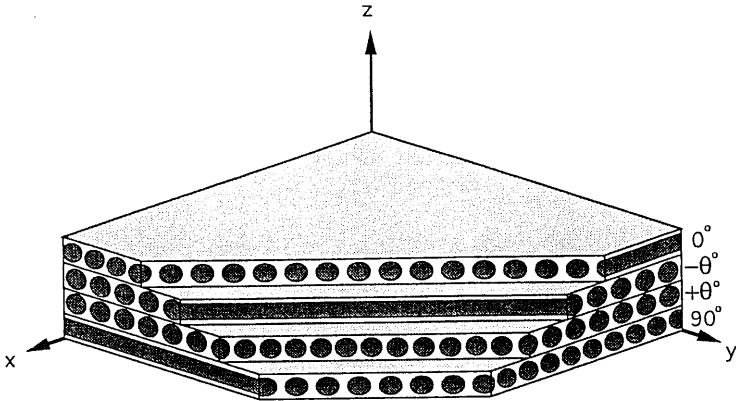


Fig. 2.5 Multidirectional laminate and reference coordinate system.

ively. In the case of a woven fabric composite, the warp and the fill directions are the in-plane principal directions.

A **laminate** is made up of two or more unidirectional laminae or plies stacked together at various orientations (Fig. 2.5). The laminae (or plies, or layers) can be of various thicknesses and consist of different materials. Since the principal material axes differ from ply to ply, it is more convenient to analyze laminates using a common fixed system of coordinates (x,y,z) , as shown. The orientation of a given ply is given by the angle between the reference x -axis and the major principal material axis (fiber orientation) of the ply, measured in a counterclockwise direction on the x - y plane.

Composite laminates containing plies of two or more different types of materials are called **hybrid composites** and, more specifically, **interply hybrid composites**. For example, a composite laminate may be made up of unidirectional glass/epoxy, carbon/epoxy and aramid/epoxy layers stacked together in a specified sequence. In some cases it may be advantageous to intermingle different types of fibers, such as glass and carbon or aramid and carbon, within the same unidirectional ply. Such composites are called **intraply hybrid composites**. Of course, one could combine intraply hybrid layers with other layers to form an **intraply-interply hybrid composite**.

Composite laminates are designated in a manner indicating the number, type, orientation, and stacking sequence of the plies. The configuration of the laminate indicating its ply composition is called **lay-up**. The configuration indicating, in addition to the ply composition, the exact location or sequence of the various plies is called the **stacking sequence**. Following are some examples of laminate designations:

Unidirectional 6-ply:	$[0/0/0/0/0/0] = [0_6]$
Crossply symmetric:	$[0/90/90/0] = [0/90]_s$ $[0/90/0] = [0/\overline{90}]_s$
Angle-ply symmetric:	$[+45/-45/-45/45] = [\pm 45]_s$ $[30/-30/30/-30/-30/30/-30/30] = [\pm 30]_{2s}$
Angle-ply asymmetric:	$[30/-30/30/-30/30/-30/30/-30] = [\pm 30]_4$
Multi directional:	$[0/45/-45/-45/45/0] = [0/\pm 45]_s$ $[0/0/45/-45/0/0/0/0/-45/45/0/0] = [0_2/\pm 45/0_2]_s$ $[0/15/-15/15/-15/0] = [0/\pm 15/\pm 15/0]_T = [0/(\pm 15)_2/0]_T$
Hybrid:	$[0^K/0^K/45^C/-45^C/90^G/-45^C/45^C/0^K/0^K]_T = [0_2^K/\pm 45^C/\overline{90^G}]_s$

where subscripts and symbols signify the following:

- number subscript = Multiple of plies or group of plies
- s = Symmetric sequence
- T = Total (number of plies)
- Overbar denotes that laminate is symmetric about the midplane of the ply

In the case of the hybrid laminate, superscripts K , C , and G denote Kevlar (aramid), carbon (graphite), and glass fibers, respectively.

2.6 Scales of Analysis, Micromechanics, Macromechanics

Composite materials can be viewed and analyzed at different levels and on different scales, depending on the particular characteristics and behavior under consideration. A schematic diagram of the various levels of consideration and the corresponding types of analysis is shown in Figure 2.6.

At the constituent level the scale of observation is on the order of the fiber diameter, particle size, or matrix interstices between reinforcement. **Micromechanics** is the study of the interactions of the constituents on this microscopic level. It deals with the state of deformation and stress in the constituents and local failures, such as matrix failure (tensile, compressive, shear), fiber failure (tensile, buckling, splitting), and interface/interphase failure (debonding). An example of the complex stress distributions on the transverse cross section of a transversely loaded unidirectional composite is illustrated in Figure 2.7.

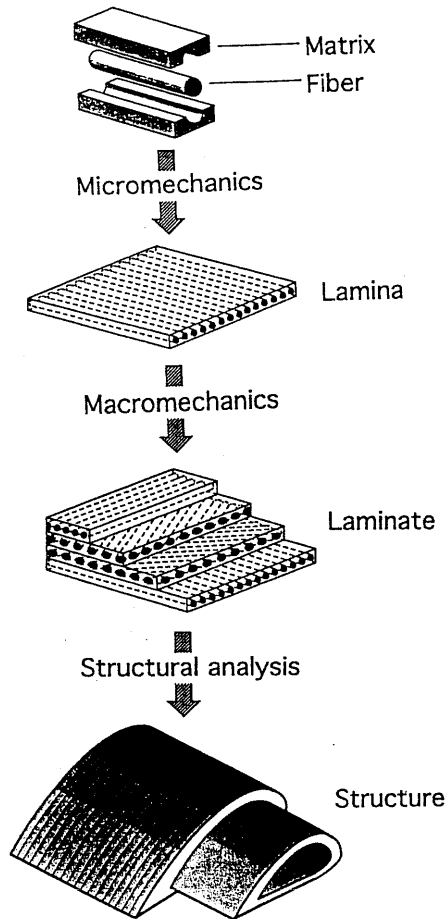


Fig. 2.6 Levels of observation and types of analysis for composite materials.

Micromechanics is particularly important in the study of properties such as strength, fracture toughness, and fatigue life, which are strongly influenced by local characteristics that cannot be integrated or averaged. Micromechanics also allows the prediction of average behavior at the lamina level as a function of constituent properties and local conditions.

At the lamina level it is usually more expeditious to consider the material homogeneous, albeit anisotropic, and use average properties in the analysis. This type of analysis is called **macromechanics** and considers the unidirectional lamina as a quasi homogeneous anisotropic material with its own average stiffness and strength properties. Failure criteria may be expressed in terms of average stresses and overall lamina strengths without reference to any particular local failure mechanisms. This approach is recommended in the study of the

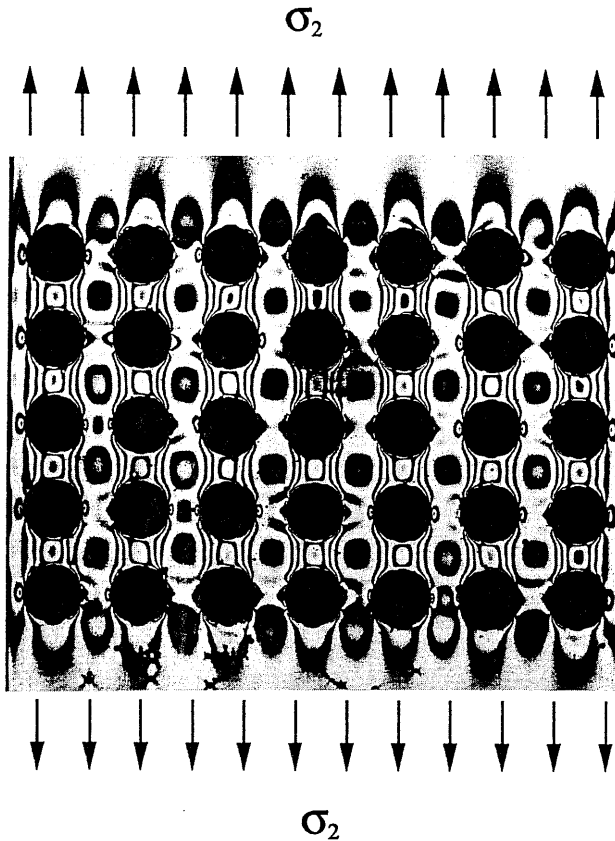


Fig. 2.7 Isochromatic fringe patterns in a model of transversely loaded unidirectional composite.

overall elastic or viscoelastic behavior of composite laminates or structures, which assumes material continuity.

At the laminate level the macromechanical analysis is applied in the form of lamination theory dealing with overall behavior as a function of lamina properties and stacking sequence. Finally, at the component or structure level, methods such as finite element analysis coupled with lamination theory give the overall behavior of the structure as well as the state of stress in each lamina.

2.7 Basic Lamina Properties

The approach followed in this textbook is based on macromechanics. The unidirectional lamina or ply is considered the basic building block of any laminate

or composite structure. The basic material properties necessary for analysis and design are the average ply properties. With reference to Figure 2.4, the unidirectional ply is characterized by the following properties:

- E_1, E_2, E_3 = Young's moduli along the principal ply directions
 G_{12}, G_{23}, G_{13} = Shear moduli in 1-2, 2-3, and 1-3 planes, respectively
 (these are equal to $G_{21}, G_{32},$ and $G_{31},$ respectively)
 $\nu_{12}, \nu_{23}, \nu_{13}$ = Poisson's ratios (the first subscript denotes the loading direction, and the second subscript denotes the strain direction; these Poisson's ratios are different from $\nu_{21}, \nu_{32},$ and $\nu_{31},$ i.e., subscripts are not interchangeable)
 F_{1t}, F_{2t}, F_{3t} = Tensile strengths along the principal ply directions
 F_{1c}, F_{2c}, F_{3c} = Compressive strengths along the principal ply directions
 F_{12}, F_{23}, F_{13} = Shear strengths in 1-2, 2-3, and 1-3 planes, respectively
 (these are equal to $F_{21}, F_{32},$ and $F_{31},$ respectively)
 $\alpha_1, \alpha_2, \alpha_3$ = Coefficients of thermal expansion
 $\beta_1, \beta_2, \beta_3$ = Coefficients of moisture expansion
 $\kappa_1, \kappa_2, \kappa_3$ = Coefficients of thermal conductivity

In addition to the above, the composite lamina is characterized by the following properties:

$$\text{Fiber volume ratio: } V_f = \frac{\text{volume of fibers}}{\text{volume of composite}}$$

$$\text{Fiber weight ratio: } W_f = \frac{\text{weight of fibers}}{\text{weight of composite}}$$

$$\text{Matrix volume ratio: } V_m = \frac{\text{volume of matrix}}{\text{volume of composite}}$$

$$\text{Matrix weight ratio: } W_m = 1 - W_f = \frac{\text{weight of matrix}}{\text{weight of composite}}$$

$$\text{Void volume ratio: } V_v = 1 - V_f - V_m = \frac{\text{volume of voids}}{\text{volume of composite}}$$

2.8 Degrees of Anisotropy

Some material properties, such as density, specific heat, absorptivity, and emittance, have no directionality associated with them and are described by one

scalar quantity for both isotropic and anisotropic materials. On the other hand, properties such as stiffness, Poisson's ratio, strength, thermal expansion, moisture expansion, thermal conductivity, and electrical conductivity are associated with direction and are a function of orientation in anisotropic materials. Fiber composite materials can exhibit various degrees of anisotropy in the various properties. The largest differences occur between properties in the longitudinal (fiber) and transverse (normal to the fiber) directions. Ratios of some properties along these two directions for some typical composite materials are listed in Table 2.3.

2.9 Constituent Materials and Properties

2.9.1 Fibers

A large variety of fibers are available as reinforcement for composites. The desirable characteristics of most reinforcing fibers are high strength, high stiffness, and relatively low density. Each type of fiber has its own advantages and disadvantages, as listed in Table 2.4. Table 2.5 lists specific fibers with their manufacturer, strength, modulus, and density. Extensive discussions of fiber reinforcements for composite materials can be found elsewhere.¹⁻³

Glass fibers are the most commonly used ones in low to medium performance composites because of their high tensile strength and low cost. They are somewhat limited in composite applications because of their relatively low stiffness, low fatigue endurance, and rapid property degradation with exposure to severe hygrothermal conditions. Aramid (or Kevlar) fibers have higher stiffness and lower density, but they are limited by very low compressive strength in the

Table 2.3 Degrees of Anisotropy

	E_1/E_2	E_1/G_{12}	F_1/F_{2t}	α_1/α_2
Silicon carbide/ceramic	1.09	2.35	17.8	0.93
Boron/aluminum	1.71	5.01	11.6	0.30
Silicon carbide/aluminum	1.73	5.02	17	0.52
S-glass/epoxy	2.44	5.06	28	0.23
E-glass/epoxy	4.42	8.76	17.7	0.13
Boron/epoxy	9.27	37.4	24.6	0.20
Carbon/epoxy	13.64	19.1	41.4	-0.07
Kevlar/epoxy	15.3	27.8	260	-0.07
GY-70/epoxy	40	70	90	-0.05

Table 2.4 Advantages and Disadvantages of Reinforcing Fibers

Fiber	Advantages	Disadvantages
E-glass, S-glass	High strength Low cost	Low stiffness Short fatigue life High temperature sensitivity
Aramid (Kevlar)	High tensile strength Low density	Low compressive strength High moisture absorption
Boron	High stiffness High compressive strength	High cost
Carbon (AS4, T300, C6000)	High strength High stiffness	Moderately high cost
Graphite (GY-70, pitch)	Very high stiffness	Low strength High cost
Ceramic (silicon carbide, alumina)	High stiffness High use temperature	Low strength High cost

Table 2.5 Fiber Properties

Type	Manufacturer	Tensile strength MPa (ksi)	Modulus GPa (Msi)	Density (g/cm ³)
E-glass	Corning	3,450 (500)	72.5 (10.5)	2.54
S-glass	Corning	4,480 (650)	85.6 (12.4)	2.49
Carbon				
AS4	Hercules	3,730 (540)	235 (34)	1.81
T300	Union Carbide	2,760–3,450 (400–500)	228 (33)	1.76
HTS	Hercules	2,830 (410)	248 (36)	1.82
IM-6	Hercules	4,480 (650)	290 (42)	1.80
IM-7	Hercules	5,170 (750)	290 (42)	1.80
Graphite				
T-50	Union Carbide	2,070 (300)	393 (57)	1.67
GY-70	Celanese	1,725 (250)	517 (75)	1.86
Pitch, type P	Union Carbide	1,725 (250)	345 (50)	2.02
Boron	AVCO	3,280–3660 (475–530)	365–414 (53–60)	2.1–3.0
Kevlar (aramid)	DuPont	3,800 (550)	131 (19)	1.45
Silicon carbide				
5.6 mil/C (SCS-2)	Textron	4,140 (600)	400 (58)	3.05
Nicalon	Nippon Carbon	2,070 (300)	172 (25)	2.60
Alumina				
FP-2	Dupont	1,725 (250)	380 (55)	3.70
Nextel 610	3M	1,900 (275)	370 (54)	3.75
Saphikon	Saphikon	3,100 (450)	380 (55)	3.80
Silica	—	5,800 (840)	72.5 (10.5)	2.19
Tungsten	—	4,140 (600)	414 (60)	19.3

composite and high moisture absorption. Boron fibers, not widely used at present, are useful in local stiffening applications because of their high stiffness.

Carbon (graphite) fibers come in many types with a range of stiffnesses and strengths, depending on the processing temperatures. High strength and high stiffness carbon fibers (AS4, T300, C6000), are processed at temperatures between 1200° and 1500°C (2200° and 2700°F). Ultrahigh stiffness graphite fibers (GY-70, Pitch) are processed at temperatures between 2000° and 3000°C (3600° and 5400°F). The increase in stiffness is achieved at the expense of strength, as shown in Table 2.5. Ceramic fibers such as silicon carbide and aluminum oxide have high stiffness and moderate strength and are used in metal–matrix and ceramic–matrix composites for high temperature applications.

Most fibers behave linearly to failure, as shown in Figure 2.8. Carbon fibers, such as the AS4 fiber, however, display a nonlinear stiffening effect. One important property of the fiber related to strength and stiffness is the ultimate strain or strain to failure, because it influences greatly the strength of the composite laminate.

As mentioned previously, the basis of the superior performance of composites lies in the high specific strength (strength to density ratio) and high specific stiffness (modulus to density ratio). These two properties are controlled by the fibers. A two-dimensional comparative representation of some typical fibers from the point of view of specific strength and specific modulus is shown in Figure 2.9.

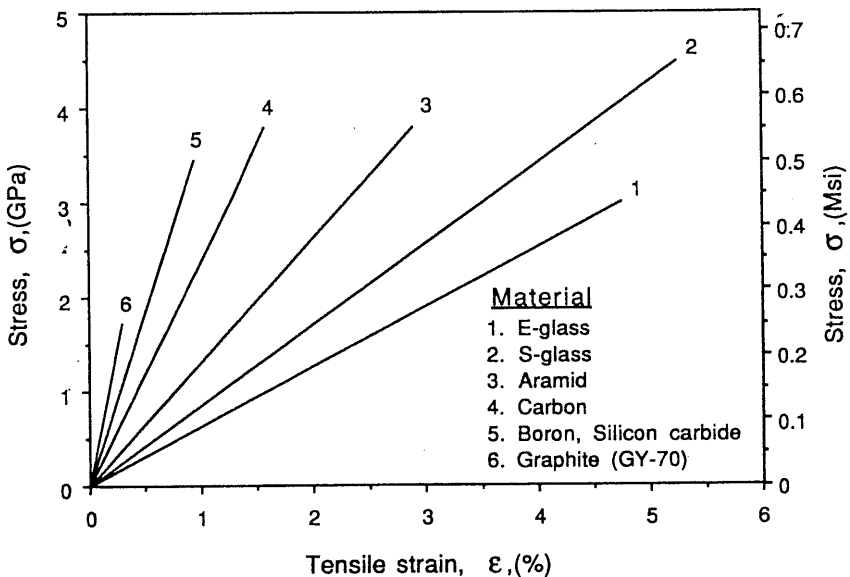


Fig. 2.8 Stress–strain curves of typical reinforcing fibers.

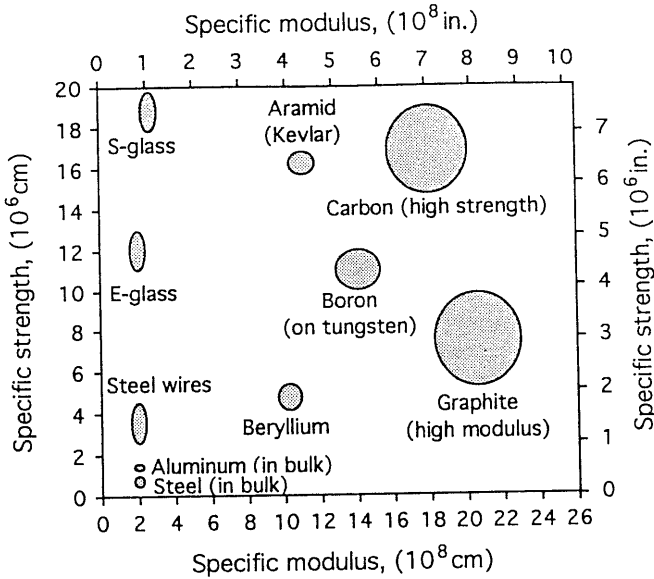


Fig. 2.9 Performance map of fibers used in structural composite materials.

2.9.2 Matrices

As shown in Table 2.2, four types of matrices are used in composites: polymeric, metallic, ceramic, and carbon. The most commonly used matrices are polymeric, which can be thermosets (epoxies, polyimide, polyester) or thermoplastics (polysulfone, poly-ether-ether-ketone). The most highly developed of these are epoxies of DGEBA type (diglycidyl ether of bisphenol A). They can be formulated with a range of stiffnesses as shown in Figure 2.10. There are two types of epoxies, those cured at a low temperature (120°C ; 250°F) and used in components exposed to low or moderate temperature variations (e.g., sporting goods) and those cured at a higher temperature (175°C ; 350°F) and used in high performance components exposed to high temperature and moisture variations (e.g., aircraft structures). Polyimide matrices are used for high temperature applications, up to 370°C (700°F). Polyesters are used in quick-curing systems for commercial products. Thermoplastics are more compatible with hot forming and injection molding fabrication methods and can be applied at temperatures up to 400°C (750°F).

Metal matrices are recommended for high temperature applications up to approximately 800°C (1500°F). Commonly used metal matrices include aluminum, magnesium, and titanium alloys. Their use temperature is limited by the melting point.

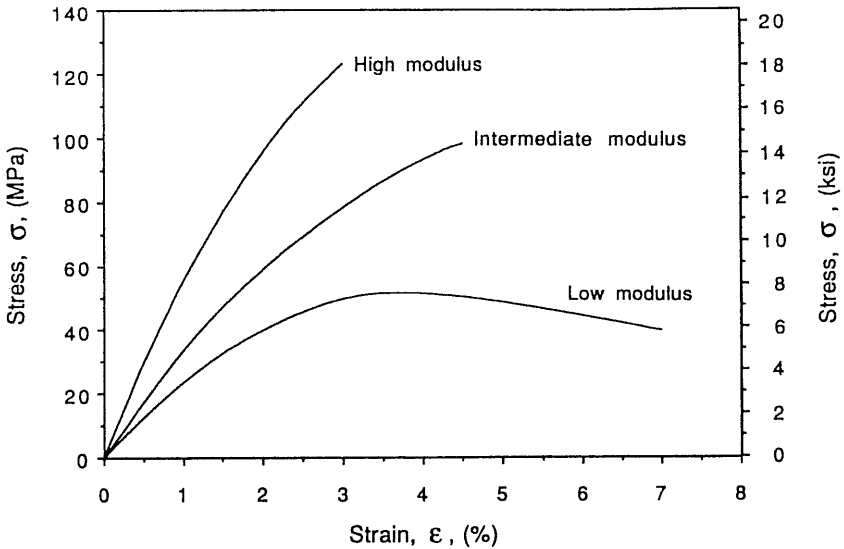


Fig. 2.10 Stress-strain curves of epoxy matrix resins of different moduli.

For higher temperature applications exceeding 1000°C (1800°F), glass, glass ceramic, ceramic, and carbon matrices are used. Glass ceramic matrices, such as lithium aluminosilicate (LAS) and calcium aluminosilicate (CAS), and ceramics such as reaction-bonded silicon nitride, are used with silicon carbide fibers. Carbon matrix is used by vapor depositing pyrolytic graphite onto a graphite fiber preform. The resulting composite can be used at temperatures up to 2600°C (4700°F). Stress-strain curves of three typical matrices, epoxy, aluminum and glass ceramic, are shown in Figure 2.11.

2.10 Properties of Typical Composite Materials

Composite materials incorporating the various constituents discussed before display a wide range of characteristics. As mentioned, the quality of performance of composite materials can be rated on the basis of specific strength and specific modulus. A comparative representation of the performance of typical structural composites from the point of view of these properties is shown in Figure 2.12. The range shown for the composites corresponds to the variation between quasi-isotropic and unidirectional laminates. As can be seen, most composites have higher specific modulus and specific strength than metals. Among the various composites, carbon/epoxy in its unidirectional form seems to combine the highest specific modulus and strength.

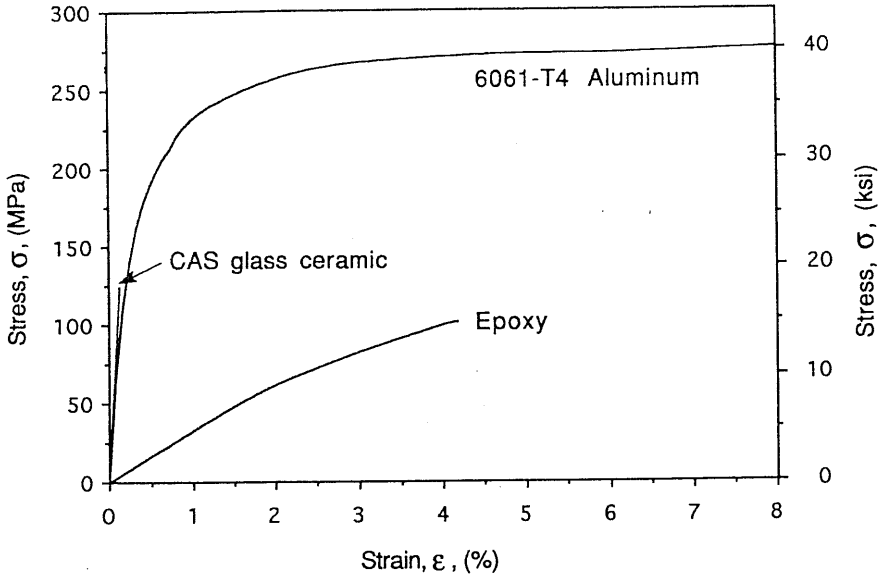


Fig. 2.11 Stress-strain curves of three typical matrices.

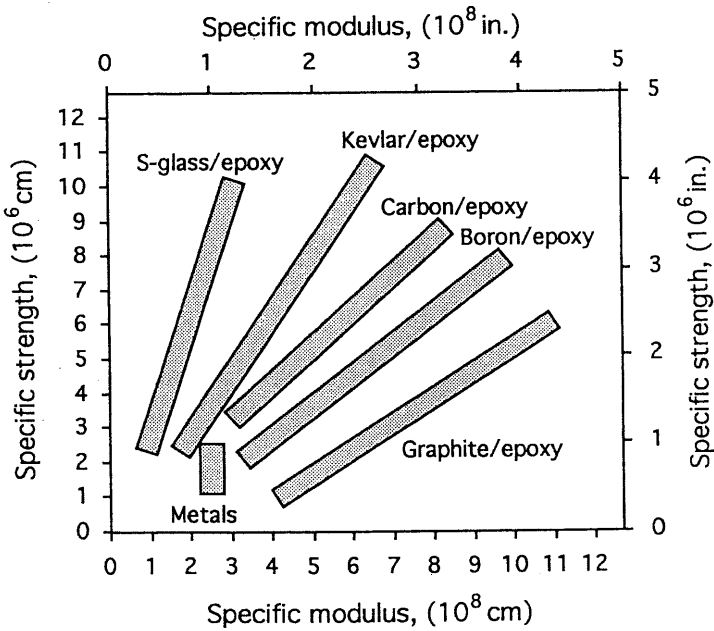


Fig. 2.12 Performance map of structural composites.

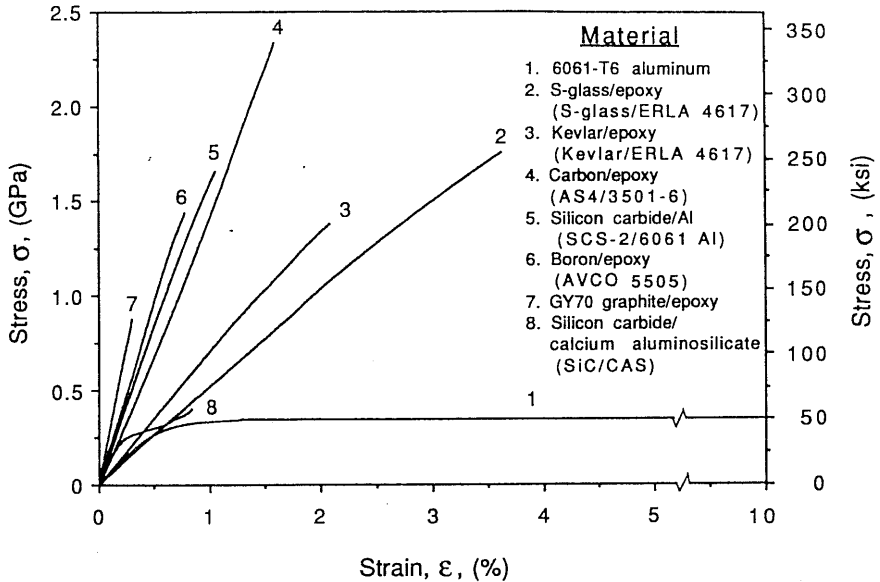


Fig. 2.13 Stress-strain curves of typical unidirectional composites in fiber direction.

The behavior of unidirectional composites in the fiber direction, especially the stiffness, is usually dominated by the fiber properties. Stress-strain curves of typical unidirectional composites in the fiber direction are shown in Figure 2.13 and compared with that of aluminum. Some general trends can be observed. As the stiffness increases, the ultimate strain decreases. For a certain group of materials (identified as materials 4, 5, 6, and 7 in Fig. 2.13) the increase in stiffness is accompanied by a drastic decrease in strength and ultimate strain. The behavior of unidirectional composites in the transverse to the fiber direction, especially the strength, is dominated by the matrix properties. Stress-strain curves of typical unidirectional composites in the transverse to the fiber direction are shown in Figure 2.14. All of these materials exhibit quasilinear behavior with relatively low ultimate strains and strengths. In particular, the four polymer-matrix composites depicted in Figure 2.14 show almost equal transverse strengths.

A more comprehensive list of properties of typical composite materials is given in Table 2.6. This is followed by Table 2.7, showing for comparison similar properties of three structural metals, aluminum, steel, and titanium. The composite properties listed are at ambient temperature (24°C; 75°F) and zero moisture conditions. The values listed are typical for these material systems but can vary from batch to batch of the same material. They can be used for instructional and preliminary design purposes. For a final design of a component, it is recommended that the designer obtain more exact properties for the particular batch of material used.

Table 2.6 Properties of Typical Unidirectional Composite Materials

Property	E-glass/ epoxy	S-glass/ epoxy	Woven- glass/ epoxy (7781/5245C)	Kevlar/epoxy (Aramid 149/ epoxy)	Carbon/epoxy (AS4/3501-6)	Carbon/PEEK (AS4/APC2)
Fiber volume ratio, (V_f)	0.55	0.50	0.45	0.60	0.63	0.58
Density (ρ , g/cm ³ [lb/in ³])	2.10 (0.076)	2.00 (0.072)	2.20 (0.080)	1.38 (0.050)	1.58 (0.057)	1.57 (0.057)
Longitudinal modulus (E_1 , GPa [Msi])	39 (5.7)	43 (6.3)	29.7 (4.31)	87 (12.6)	142 (20.6)	131 (19.1)
Transverse modulus (E_2 , GPa [Msi])	8.6 (1.24)	8.9 (1.29)	29.7 (4.31)	5.5 (0.80)	10.3 (1.50)	8.7 (1.27)
In-plane shear modulus (G_{12} , GPa [Msi])	3.8 (0.54)	4.5 (0.66)	5.3 (0.77)	2.2 (0.31)	7.2 (1.04)	5.0 (0.73)
Major Poisson's ratio (ν_{12})	0.28	0.27	0.17	0.34	0.27	0.28
Minor Poisson's ratio (ν_{21})	0.06	0.06	0.17	0.02	0.02	0.02
Longitudinal tensile strength (F_{1t} , MPa [ksii])	1,080 (157)	1,280 (185)	367 (53)	1,280 (185)	2,280 (330)	2,060 (299)
Transverse tensile strength (F_{2t} , MPa [ksii])	39 (5.7)	49 (7.1)	367 (53)	30 (4.2)	57 (8.3)	78 (11.4)
In-plane shear strength (F_6 , MPa [ksii])	89 (12.9)	69 (10.0)	97.1 (14.1)	49 (7.1)	71 (10.3)	157 (22.8)
Ultimate longitudinal tensile strain (ϵ_{1t}^u)	0.028	0.029	0.025	0.015	0.015	0.016
Ultimate transverse tensile strain (ϵ_{2t}^u)	0.005	0.006	0.025	0.005	0.006	0.009
Longitudinal compressive strength (F_{1c} , MPa [ksii])	620 (90)	690 (100)	549 (80)	335 (49)	1,440 (209)	1,080 (156)
Transverse compressive strength (F_{2c} , MPa [ksii])	128 (18.6)	158 (22.9)	549 (80)	158 (22.9)	228 (33)	196 (28.4)
Longitudinal thermal expansion coefficient, (α_1 , $10^{-6}/^\circ\text{C}$ [$10^{-6}/^\circ\text{F}$])	7.0 (3.9)	5.0 (2.8)	10.0 (5.6)	-2.0 (-1.1)	-0.9 (-0.5)	-0.2 (-0.1)
Transverse thermal expansion coefficient (α_2 , $10^{-6}/^\circ\text{C}$ [$10^{-6}/^\circ\text{F}$])	21 (11.7)	26 (14.4)	10.0 (5.6)	60 (33)	27 (15)	24 (13.3)
Longitudinal moisture expansion coefficient (β_1)	0	0	0.06	0	0.01	0
Transverse moisture expansion coefficient (β_2)	0.2	0.2	0.06	0.3	0.2	0.3

Table 2.6 Continued

Property	Carbon/epoxy (IM6/SC1081)	Carbon/polyimide (Mod I/ WRD9371)	Graphite/ epoxy (GY-70/934)	Boron/ epoxy (B5.6/5505)	Boron/ aluminum (B4/6061 Al)	Silicon carbide/ aluminum (SCS2/ 6061 Al)	Silicon carbide/ ceramic (SiC/CAS)
Fiber volume ratio, (V_f)	0.65	0.45	0.57	0.50	0.50	0.43	0.39
Density (ρ , g/cm ³ [lb/in ³])	1.60 (0.058)	1.54 (0.056)	1.59 (0.058)	2.03 (0.073)	2.65 (0.096)	2.85 (0.103)	2.72 (0.098)
Longitudinal modulus (E_1 , GPa [Msi])	177 (25.7)	216 (31.3)	294 (42.7)	201 (29.2)	235 (34.1)	204 (29.6)	121 (17.6)
Transverse modulus (E_2 , GPa [Msi])	10.8 (1.57)	5.0 (0.72)	6.4 (0.92)	21.7 (3.15)	137 (19.9)	118 (17.1)	112 (16.2)
In-plane shear modulus (G_{12} , GPa [Msi])	7.6 (1.1)	4.5 (0.65)	4.9 (0.71)	5.4 (0.78)	47 (6.8)	41 (5.9)	44 (6.4)
Major Poisson's ratio (ν_{12})	0.27	0.25	0.23	0.17	0.30	0.27	0.20
Minor Poisson's ratio (ν_{21})	0.02	0.01	0.01	0.02	0.17	0.12	0.18
Longitudinal tensile strength (F_{1r} , MPa [ksi])	2,860 (414)	807 (117)	589 (85.3)	1,380 (200)	1,373 (199)	1,462 (212)	393 (57)
Transverse tensile strength (F_{2r} , MPa [ksi])	49 (7.1)	15 (2.2)	29.4 (4.3)	56 (8.1)	118 (17.1)	86 (12.5)	22 (3.2)
In-plane shear strength (F_6 , MPa [ksi])	83 (12.0)	22 (3.2)	49.1 (7.1)	62 (9.1)	128 (18.5)	113 (16.4)	—
Ultimate longitudinal tensile strain (ϵ_{1t}^u)	0.016	0.004	0.002	0.007	0.006	0.009	0.008
Ultimate transverse tensile strain (ϵ_{2t}^u)	0.005	0.003	0.005	0.003	0.001	0.001	0.0002
Longitudinal compressive strength (F_{1c} , MPa [ksi])	1,875 (270)	655 (95)	491 (71.1)	1,600 (232)	1,573 (228)	2,990 (434)	—
Transverse compressive strength (F_{2c} , MPa [ksi])	246 (36)	71 (10.2)	98.1 (14.2)	125 (18)	157 (22.8)	285 (41.4)	—
Longitudinal thermal expansion coefficient, (α_1 , 10 ⁻⁶ /°C [10 ⁻⁶ /°F])	-0.3 (-0.2)	0	-0.1 (-0.06)	6.1 (3.4)	6.0 (3.3)	9.1 (5.0)	4.05 (2.25)
Transverse thermal expansion coefficient (α_2 , 10 ⁻⁶ /°C [10 ⁻⁶ /°F])	30 (16.7)	25.3 (14.1)	26 (14.4)	30 (17)	20.0 (11.1)	17.8 (9.9)	4.15 (2.35)
Longitudinal moisture expansion coefficient (β_1)	0	0	0	0	0	0	0
Transverse moisture expansion coefficient (β_2)	0.2	0.2	0.3	0.2	0	0	0

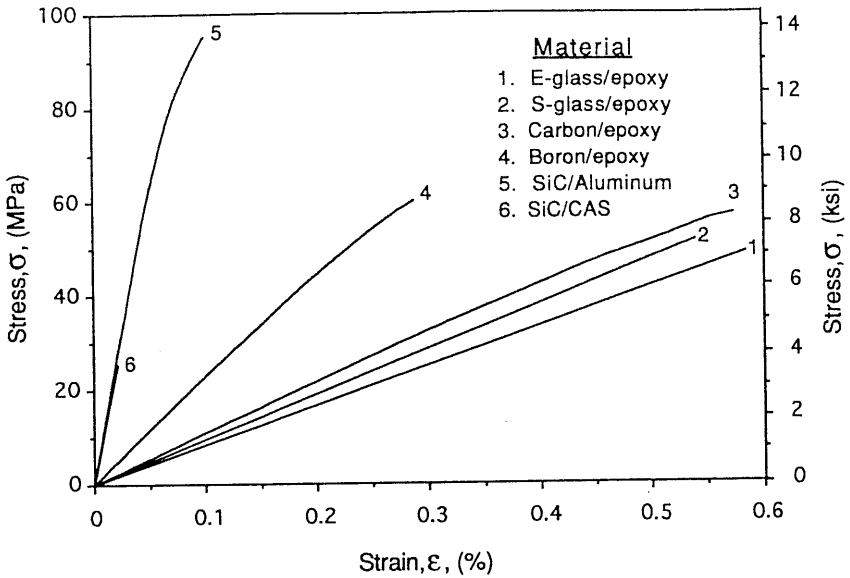


Fig. 2.14 Stress-strain curves of typical unidirectional composites in the transverse direction.

Table 2.7 Properties of Typical Structural Metals

Property	Aluminum (2024 T3)	Steel (AISI 1025)	Titanium (MILT)
Density (ρ , g/cm ³ [lb/in ³])	2.80 (0.101)	7.80 (0.282)	4.40 (0.159)
Young's modulus (E , GPa [Msi])	73 (10.4)	207 (30)	108 (15.7)
Shear modulus (G , GPa [Msi])	26.6 (3.86)	79 (11.4)	42.4 (6.1)
Poisson's ratio (ν)	0.33	0.30	0.30
Tensile strength (F_t , MPa [ksi])	414 (60)	394 (57)	550 (80)
Compressive strength (F_c , MPa [ksi])	217 (31)	394 (57)	475 (69)
Shear strength (F_s , MPa [ksi])	248 (36)	248 (36)	295 (43)
Coefficient of thermal expansion (α , 10 ⁻⁶ /°C [10 ⁻⁶ /°F])	23 (13)	11 (6)	11 (6)

References

1. E. Fitzer, *Carbon Fibres and Their Composites*, Springer-Verlag, Berlin, 1985.
2. A. R. Bunsell (Ed.), *Fiber Reinforcements for Composite Materials*, Elsevier, Amsterdam, 1988.
3. K. K. Chawla, *Ceramic Matrix Composites*, Chapman and Hall, London, 1993.

Chapter 3

Elastic Behavior of Unidirectional Lamina

3.1 Stress–Strain Relations

3.1.1 General Anisotropic Material

The state of stress at a point in a general continuum can be represented by nine stress components σ_{ij} (where $i, j = 1, 2, 3$) acting on the sides of an elemental cube with sides parallel to the axes 1, 2, 3 of a reference coordinate system (Fig. 3.1). Similarly, the state of deformation is represented by nine strain components, ϵ_{ij} . In the most general case the stress and strain components are related by the generalized Hooke's law as follows:

$$\begin{bmatrix} \sigma_{11} \\ \sigma_{22} \\ \sigma_{33} \\ \sigma_{23} \\ \sigma_{31} \\ \sigma_{12} \\ \sigma_{32} \\ \sigma_{13} \\ \sigma_{21} \end{bmatrix} = \begin{bmatrix} C_{1111} & C_{1122} & C_{1133} & C_{1123} & C_{1131} & C_{1112} & C_{1132} & C_{1113} & C_{1121} \\ C_{2211} & C_{2222} & C_{2233} & C_{2223} & C_{2231} & C_{2212} & C_{2232} & C_{2213} & C_{2221} \\ C_{3311} & C_{3322} & C_{3333} & C_{3323} & C_{3331} & C_{3312} & C_{3332} & C_{3313} & C_{3321} \\ C_{2311} & C_{2322} & C_{2333} & C_{2323} & C_{2331} & C_{2312} & C_{2332} & C_{2313} & C_{2321} \\ C_{3111} & C_{3122} & C_{3133} & C_{3123} & C_{3131} & C_{3112} & C_{3132} & C_{3113} & C_{3121} \\ C_{1211} & C_{1222} & C_{1233} & C_{1223} & C_{1231} & C_{1212} & C_{1232} & C_{1213} & C_{1221} \\ C_{3211} & C_{3222} & C_{3233} & C_{3223} & C_{3231} & C_{3212} & C_{3232} & C_{3213} & C_{3221} \\ C_{1311} & C_{1322} & C_{1333} & C_{1323} & C_{1331} & C_{1312} & C_{1332} & C_{1313} & C_{1321} \\ C_{2111} & C_{2122} & C_{2133} & C_{2123} & C_{2131} & C_{2112} & C_{2132} & C_{2113} & C_{2121} \end{bmatrix} \begin{bmatrix} \epsilon_{11} \\ \epsilon_{22} \\ \epsilon_{33} \\ \epsilon_{23} \\ \epsilon_{31} \\ \epsilon_{12} \\ \epsilon_{32} \\ \epsilon_{13} \\ \epsilon_{21} \end{bmatrix} \quad (3.1)$$

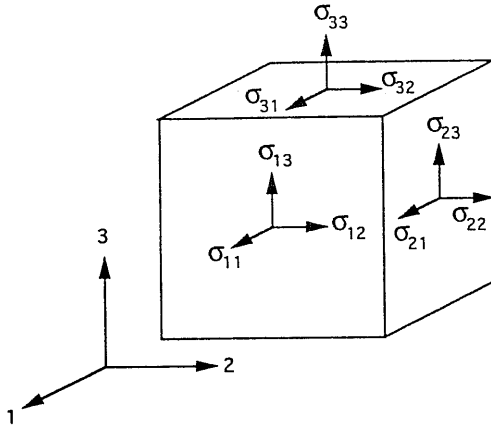


Fig. 3.1 State of stress at a point of a continuum.

and

$$\begin{bmatrix} \epsilon_{11} \\ \epsilon_{22} \\ \epsilon_{33} \\ \epsilon_{23} \\ \epsilon_{31} \\ \epsilon_{12} \\ \epsilon_{32} \\ \epsilon_{13} \\ \epsilon_{21} \end{bmatrix} = \begin{bmatrix} S_{1111} & S_{1122} & S_{1133} & S_{1123} & S_{1131} & S_{1112} & S_{1132} & S_{1113} & S_{1121} \\ S_{2211} & S_{2222} & S_{2233} & S_{2223} & S_{2231} & S_{2212} & S_{2232} & S_{2213} & S_{2221} \\ S_{3311} & S_{3322} & S_{3333} & S_{3323} & S_{3331} & S_{3312} & S_{3332} & S_{3313} & S_{3321} \\ S_{2311} & S_{2322} & S_{2333} & S_{2323} & S_{2331} & S_{2312} & S_{2332} & S_{2313} & S_{2321} \\ S_{3111} & S_{3122} & S_{3133} & S_{3123} & S_{3131} & S_{3112} & S_{3132} & S_{3113} & S_{3121} \\ S_{1211} & S_{1222} & S_{1233} & S_{1223} & S_{1231} & S_{1212} & S_{1232} & S_{1213} & S_{1221} \\ S_{3211} & S_{3222} & S_{3233} & S_{3223} & S_{3231} & S_{3212} & S_{3232} & S_{3213} & S_{3221} \\ S_{1311} & S_{1322} & S_{1333} & S_{1323} & S_{1331} & S_{1312} & S_{1332} & S_{1313} & S_{1321} \\ S_{2111} & S_{2122} & S_{2133} & S_{2123} & S_{2131} & S_{2112} & S_{2132} & S_{2113} & S_{2121} \end{bmatrix} \begin{bmatrix} \sigma_{11} \\ \sigma_{22} \\ \sigma_{33} \\ \sigma_{23} \\ \sigma_{31} \\ \sigma_{12} \\ \sigma_{32} \\ \sigma_{13} \\ \sigma_{21} \end{bmatrix} \quad (3.2)$$

or, in indicial notation

$$\sigma_{ij} = C_{ijkl} \epsilon_{kl} \quad (i, j, k, l = 1, 2, 3) \quad (3.3)$$

$$\epsilon_{ij} = S_{ijkl} \sigma_{kl}$$

where

C_{ijkl} = Stiffness components

S_{ijkl} = Compliance components

Repeated subscripts in the relations above imply summation for all values of that subscript. The compliance matrix $[S_{ijkl}]$ is the inverse of the stiffness matrix $[C_{ijkl}]$.

Thus, in general, it would require 81 elastic constants to characterize a material fully. However, the symmetry of the stress and strain tensors

$$\begin{aligned}\sigma_{ij} &= \sigma_{ji} \\ \epsilon_{ij} &= \epsilon_{ji}\end{aligned}\tag{3.4}$$

reduces the number of independent elastic constants to 36.

It is customary in mechanics of composites to use a contracted notation for the stress, strain, stiffness, and compliance tensors as follows:

$$\begin{aligned}\sigma_{11} &= \sigma_1 \\ \sigma_{22} &= \sigma_2 \\ \sigma_{33} &= \sigma_3 \\ \sigma_{23} &= \tau_{23} = \sigma_4 = \tau_4 \\ \sigma_{31} &= \tau_{31} = \sigma_5 = \tau_5 \\ \sigma_{12} &= \tau_{12} = \sigma_6 = \tau_6 \\ \epsilon_{11} &= \epsilon_1 \\ \epsilon_{22} &= \epsilon_2 \\ \epsilon_{33} &= \epsilon_3 \\ 2\epsilon_{23} &= \gamma_{23} = \epsilon_4 = \gamma_4 \\ 2\epsilon_{31} &= \gamma_{31} = \epsilon_5 = \gamma_5 \\ 2\epsilon_{12} &= \gamma_{12} = \epsilon_6 = \gamma_6\end{aligned}\tag{3.6}$$

$$\begin{aligned}C_{1111} &= C_{11}, C_{1122} = C_{12}, C_{1133} = C_{13}, C_{1123} = 2C_{14}, C_{1131} = 2C_{15}, C_{1112} = 2C_{16} \\ C_{2211} &= C_{21}, C_{2222} = C_{22}, C_{2233} = C_{23}, C_{2223} = 2C_{24}, C_{2231} = 2C_{25}, C_{2212} = 2C_{26} \\ C_{3311} &= C_{31}, C_{3322} = C_{32}, C_{3333} = C_{33}, C_{3323} = 2C_{34}, C_{3331} = 2C_{35}, C_{3312} = 2C_{36} \\ C_{2311} &= C_{41}, C_{2322} = C_{42}, C_{2333} = C_{43}, C_{2323} = 2C_{44}, C_{2331} = 2C_{45}, C_{2312} = 2C_{46} \\ C_{3111} &= C_{51}, C_{3122} = C_{52}, C_{3133} = C_{53}, C_{3123} = 2C_{54}, C_{3131} = 2C_{55}, C_{3112} = 2C_{56} \\ C_{1211} &= C_{61}, C_{1222} = C_{62}, C_{1233} = C_{63}, C_{1223} = 2C_{64}, C_{1231} = 2C_{65}, C_{1212} = 2C_{66}\end{aligned}\tag{3.7}$$

Thus the stress-strain relations for an anisotropic body can be written in the contracted notation as

$$\begin{bmatrix} \sigma_1 \\ \sigma_2 \\ \sigma_3 \\ \tau_4 \\ \tau_5 \\ \tau_6 \end{bmatrix} = \begin{bmatrix} C_{11} & C_{12} & C_{13} & C_{14} & C_{15} & C_{16} \\ C_{21} & C_{22} & C_{23} & C_{24} & C_{25} & C_{26} \\ C_{31} & C_{32} & C_{33} & C_{34} & C_{35} & C_{36} \\ C_{41} & C_{42} & C_{43} & C_{44} & C_{45} & C_{46} \\ C_{51} & C_{52} & C_{53} & C_{54} & C_{55} & C_{56} \\ C_{61} & C_{62} & C_{63} & C_{64} & C_{65} & C_{66} \end{bmatrix} \begin{bmatrix} \epsilon_1 \\ \epsilon_2 \\ \epsilon_3 \\ \gamma_4 \\ \gamma_5 \\ \gamma_6 \end{bmatrix} \quad (3.8)$$

$$\begin{bmatrix} \epsilon_1 \\ \epsilon_2 \\ \epsilon_3 \\ \gamma_4 \\ \gamma_5 \\ \gamma_6 \end{bmatrix} = \begin{bmatrix} S_{11} & S_{12} & S_{13} & S_{14} & S_{15} & S_{16} \\ S_{21} & S_{22} & S_{23} & S_{24} & S_{25} & S_{26} \\ S_{31} & S_{32} & S_{33} & S_{34} & S_{35} & S_{36} \\ S_{41} & S_{42} & S_{43} & S_{44} & S_{45} & S_{46} \\ S_{51} & S_{52} & S_{53} & S_{54} & S_{55} & S_{56} \\ S_{61} & S_{62} & S_{63} & S_{64} & S_{65} & S_{66} \end{bmatrix} \begin{bmatrix} \sigma_1 \\ \sigma_2 \\ \sigma_3 \\ \tau_4 \\ \tau_5 \\ \tau_6 \end{bmatrix} \quad (3.9)$$

or, in indicial notation,

$$\sigma_i = C_{ij} \epsilon_j \quad (i, j = 1, 2, 3, \dots, 6) \quad (3.10)$$

$$\epsilon_i = S_{ij} \sigma_j$$

Energy considerations require additional symmetries. The work per unit volume is expressed as

$$W = \frac{1}{2} C_{ij} \epsilon_i \epsilon_j \quad (3.11)$$

The stress-strain relation, Eq. (3.10), can be obtained by differentiating Eq. (3.11):

$$\sigma_i = \frac{\partial W}{\partial \epsilon_i} = C_{ij} \epsilon_j \quad (3.12)$$

By differentiating again we obtain

$$C_{ij} = \frac{\partial^2 W}{\partial \epsilon_i \partial \epsilon_j} \quad (3.13)$$

In a similar manner, by reversing the order of differentiation, we obtain

$$C_{ji} = \frac{\partial^2 W}{\partial \epsilon_j \partial \epsilon_i} \quad (3.14)$$

Since the order of differentiation of W is immaterial, Eqs. (3.13) and (3.14) yield

$$C_{ij} = C_{ji} \quad (3.15)$$

In a similar manner we can show that

$$S_{ij} = S_{ji} \quad (3.16)$$

i.e., the stiffness and compliance matrices are symmetric. Thus the state of stress (or strain) at a point can be described by six components of stress (or strain), and the stress-strain Eqs. (3.8) and (3.9) are expressed in terms of 21 independent stiffness (or compliance) constants.

3.1.2 Specially Orthotropic Material

In the case of an orthotropic material (which has three mutually perpendicular planes of material symmetry) the stress-strain relations in general have the same form as Eqs. (3.8) and (3.9). However, the number of independent elastic constants is reduced to nine, as various stiffness and compliance terms are interrelated. This is clearly seen when the reference system of coordinates is selected along principal planes of material symmetry, i.e., in the case of a **specially orthotropic** material. Then,

$$\begin{bmatrix} \sigma_1 \\ \sigma_2 \\ \sigma_3 \\ \tau_4 \\ \tau_5 \\ \tau_6 \end{bmatrix} = \begin{bmatrix} C_{11} & C_{12} & C_{13} & 0 & 0 & 0 \\ C_{12} & C_{22} & C_{23} & 0 & 0 & 0 \\ C_{13} & C_{23} & C_{33} & 0 & 0 & 0 \\ 0 & 0 & 0 & C_{44} & 0 & 0 \\ 0 & 0 & 0 & 0 & C_{55} & 0 \\ 0 & 0 & 0 & 0 & 0 & C_{66} \end{bmatrix} \begin{bmatrix} \epsilon_1 \\ \epsilon_2 \\ \epsilon_3 \\ \gamma_4 \\ \gamma_5 \\ \gamma_6 \end{bmatrix} \quad (3.17)$$

and

$$\begin{bmatrix} \epsilon_1 \\ \epsilon_2 \\ \epsilon_3 \\ \gamma_4 \\ \gamma_5 \\ \gamma_6 \end{bmatrix} = \begin{bmatrix} S_{11} & S_{12} & S_{13} & 0 & 0 & 0 \\ S_{12} & S_{22} & S_{23} & 0 & 0 & 0 \\ S_{13} & S_{23} & S_{33} & 0 & 0 & 0 \\ 0 & 0 & 0 & S_{44} & 0 & 0 \\ 0 & 0 & 0 & 0 & S_{55} & 0 \\ 0 & 0 & 0 & 0 & 0 & S_{66} \end{bmatrix} \begin{bmatrix} \sigma_1 \\ \sigma_2 \\ \sigma_3 \\ \tau_4 \\ \tau_5 \\ \tau_6 \end{bmatrix} \quad (3.18)$$

It is clearly shown that an orthotropic material can be characterized by nine independent elastic constants. This number does not change by changing the reference system of coordinates to one in which the stiffness and compliance matrices in Eqs. (3.17) and (3.18) above are fully populated. The terms of either the stiffness or compliance matrix can be obtained by inversion of the other. Thus relationships can be obtained between C_{ij} and S_{ij} .

Three important observations can be made with respect to the stress-strain relations in Eqs. (3.17) and (3.18):

1. No interaction exists between normal stresses $\sigma_1, \sigma_2, \sigma_3$ and shear strains $\gamma_4, \gamma_5, \gamma_6$; i.e., normal stresses acting along principal material directions produce only normal strains.
2. No interaction exists between shear stresses τ_4, τ_5, τ_6 , and normal strains $\epsilon_1, \epsilon_2, \epsilon_3$; i.e., shear stresses acting on principal material planes produce only shear strains.
3. No interaction exists between shear stresses and shear strains on different planes; i.e., a shear stress acting on a principal plane produces a shear strain only on that plane.

3.1.3 Transversely Isotropic Material

An orthotropic material is called **transversely isotropic** when one of its principal planes is a **plane of isotropy**, i.e., at every point there is a plane on which the mechanical properties are the same in all directions. Many unidirectional composites with fibers packed in a hexagonal array, or close to it, can be considered transversely isotropic, with the 2-3 plane (normal to the fibers) as the plane of isotropy (Fig. 3.2). This is the case with unidirectional carbon/epoxy, aramid/epoxy, and glass/epoxy composites with relatively high fiber volume ratios.

The stress-strain relations for a transversely isotropic material are simplified by noting that subscripts 2 and 3 (for a 2-3 plane of isotropy) in the material constants are interchangeable in Eqs. (3.17) and (3.18), i.e.,

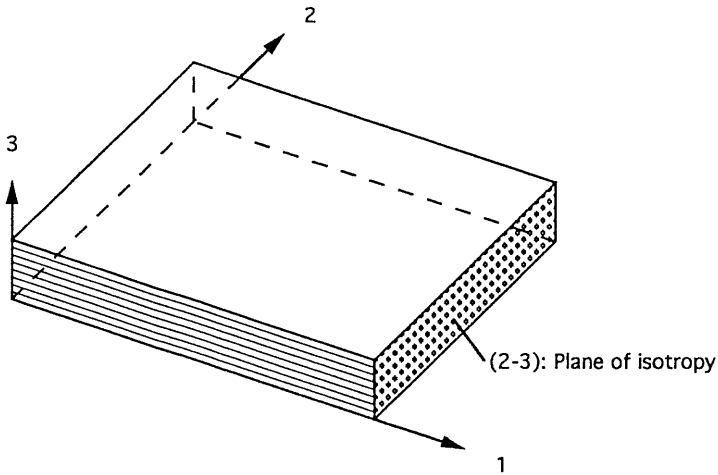


Fig. 3.2 Orthotropic material with transverse isotropy.

$$\begin{aligned}
 C_{12} &= C_{13} \\
 C_{22} &= C_{33}
 \end{aligned}
 \tag{3.19}$$

and

$$\begin{aligned}
 S_{12} &= S_{13} \\
 S_{22} &= S_{33}
 \end{aligned}$$

Also, subscripts 5 and 6 are interchangeable; thus

$$\begin{aligned}
 C_{55} &= C_{66} \\
 S_{55} &= S_{66}
 \end{aligned}
 \tag{3.20}$$

Furthermore, the simple stress transformation illustrated in Figure 3.3 shows that stiffness C_{44} (or compliance S_{44}) is not independent. Considering an element with sides parallel to the 2- and 3-axes (Fig. 3.3a) under pure shear stress $\tau_0 = \tau_{23}$ and resulting shear strain $\gamma_0 = \gamma_{23}$, we have from Eq. (3.17).

$$\tau_4 = \tau_{23} = C_{44} \gamma_{23} = C_{44} \gamma_4 = \tau_0
 \tag{3.21}$$

The state of stress shown in Figure 3.3a is equivalent to that of an element rotated by 45° and subjected to equal tensile and compressive normal stresses (Fig. 3.3b),

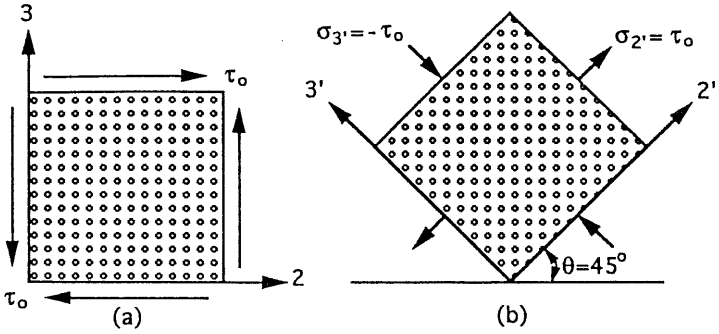


Fig. 3.3 Stress transformations on plane of isotropy of transversely isotropic material.

$$\sigma_{2'} = \tau_0$$

$$\sigma_{3'} = -\tau_0$$

(3.22)

resulting in normal strains such that

$$\epsilon_{2'} = -\epsilon_{3'} = \frac{\gamma_{23}}{2}$$

(3.23)

$$\epsilon_1 = 0$$

Then, from Eq. (3.17),

$$\begin{aligned} \sigma_{2'} &= C_{2'2'} \epsilon_{2'} + C_{2'3'} \epsilon_{3'} \\ &= C_{22} \epsilon_{2'} - C_{23} \epsilon_{2'} \end{aligned}$$

or

$$\sigma_{2'} = \epsilon_{2'} (C_{22} - C_{23}) = \frac{\gamma_{23}}{2} (C_{22} - C_{23})$$

(3.24)

since

$$C_{2'2'} = C_{22}$$

$$C_{2'3'} = C_{23}$$

due to transverse isotropy.

From Eqs. (3.21), (3.22), and (3.24), we obtain

$$C_{44} = \frac{C_{22} - C_{23}}{2} \quad (3.25)$$

Thus, the stress-strain relations for a transversely isotropic material reduce to

$$\begin{bmatrix} \sigma_1 \\ \sigma_2 \\ \sigma_3 \\ \tau_4 \\ \tau_5 \\ \tau_6 \end{bmatrix} = \begin{bmatrix} C_{11} & C_{12} & C_{12} & 0 & 0 & 0 \\ C_{12} & C_{22} & C_{23} & 0 & 0 & 0 \\ C_{12} & C_{23} & C_{22} & 0 & 0 & 0 \\ 0 & 0 & 0 & \frac{C_{22} - C_{23}}{2} & 0 & 0 \\ 0 & 0 & 0 & 0 & C_{55} & 0 \\ 0 & 0 & 0 & 0 & 0 & C_{55} \end{bmatrix} \begin{bmatrix} \epsilon_1 \\ \epsilon_2 \\ \epsilon_3 \\ \gamma_4 \\ \gamma_5 \\ \gamma_6 \end{bmatrix} \quad (3.26)$$

and the inverse relations are reduced to

$$\begin{bmatrix} \epsilon_1 \\ \epsilon_2 \\ \epsilon_3 \\ \gamma_4 \\ \gamma_5 \\ \gamma_6 \end{bmatrix} = \begin{bmatrix} S_{11} & S_{12} & S_{12} & 0 & 0 & 0 \\ S_{12} & S_{22} & S_{23} & 0 & 0 & 0 \\ S_{12} & S_{23} & S_{22} & 0 & 0 & 0 \\ 0 & 0 & 0 & 2(S_{22} - S_{23}) & 0 & 0 \\ 0 & 0 & 0 & 0 & S_{55} & 0 \\ 0 & 0 & 0 & 0 & 0 & S_{55} \end{bmatrix} \begin{bmatrix} \sigma_1 \\ \sigma_2 \\ \sigma_3 \\ \tau_4 \\ \tau_5 \\ \tau_6 \end{bmatrix} \quad (3.27)$$

The relations above show that an orthotropic material with transverse isotropy is characterized by only five independent elastic constants.

3.1.4 Orthotropic Material under Plane Stress

In most structural applications composite materials are used in the form of thin laminates loaded in the plane of the laminate. Thus composite laminae (or laminates) can be considered to be under a condition of plane stress with all stress components in the out-of-plane direction (3-direction) being zero, i.e.,

$$\begin{aligned} \sigma_3 &= 0 \\ \tau_{23} = \tau_4 &= 0 \\ \tau_{13} = \tau_5 &= 0 \end{aligned} \quad (3.28)$$

The orthotropic stress-strain relations (Eq. 3.17) reduce to

$$\begin{bmatrix} \sigma_1 \\ \sigma_2 \\ 0 \\ 0 \\ 0 \\ \tau_6 \end{bmatrix} = \begin{bmatrix} C_{11} & C_{12} & C_{13} & 0 & 0 & 0 \\ C_{12} & C_{22} & C_{23} & 0 & 0 & 0 \\ C_{13} & C_{23} & C_{33} & 0 & 0 & 0 \\ 0 & 0 & 0 & C_{44} & 0 & 0 \\ 0 & 0 & 0 & 0 & C_{55} & 0 \\ 0 & 0 & 0 & 0 & 0 & C_{66} \end{bmatrix} \begin{bmatrix} \epsilon_1 \\ \epsilon_2 \\ \epsilon_3 \\ \gamma_4 \\ \gamma_5 \\ \gamma_6 \end{bmatrix} \quad (3.29)$$

which, in expanded form, are

$$\begin{aligned} \sigma_1 &= C_{11} \epsilon_1 + C_{12} \epsilon_2 + C_{13} \epsilon_3 \\ \sigma_2 &= C_{12} \epsilon_1 + C_{22} \epsilon_2 + C_{23} \epsilon_3 \\ 0 &= C_{13} \epsilon_1 + C_{23} \epsilon_2 + C_{33} \epsilon_3 \\ \gamma_4 &= \gamma_5 = 0 \\ \tau_6 &= C_{66} \gamma_6 \end{aligned} \quad (3.30)$$

Eliminating strain ϵ_3 from Eq. (3.30), we obtain

$$\begin{aligned} \sigma_1 &= \left(C_{11} - \frac{C_{13} C_{13}}{C_{33}} \right) \epsilon_1 + \left(C_{12} - \frac{C_{13} C_{23}}{C_{33}} \right) \epsilon_2 \\ &= Q_{11} \epsilon_1 + Q_{12} \epsilon_2 \\ \sigma_2 &= \left(C_{12} - \frac{C_{23} C_{13}}{C_{33}} \right) \epsilon_1 + \left(C_{22} - \frac{C_{23} C_{23}}{C_{33}} \right) \epsilon_2 \\ &= Q_{12} \epsilon_1 + Q_{22} \epsilon_2 \\ \tau_6 &= C_{66} \gamma_6 = Q_{66} \gamma_6 \end{aligned}$$

or

$$\begin{bmatrix} \sigma_1 \\ \sigma_2 \\ \tau_6 \end{bmatrix} = \begin{bmatrix} Q_{11} & Q_{12} & 0 \\ Q_{12} & Q_{22} & 0 \\ 0 & 0 & Q_{66} \end{bmatrix} \begin{bmatrix} \epsilon_1 \\ \epsilon_2 \\ \gamma_6 \end{bmatrix} \quad (3.31)$$

or, in brief,

$$[\sigma]_{1,2} = [Q]_{1,2} [\epsilon]_{1,2}$$

where the reduced stiffness matrix components are

$$Q_{ij} = C_{ij} - \frac{C_{i3} C_{j3}}{C_{33}} \quad (i, j, = 1, 2, 6) \quad (3.32)$$

The inverse relation is written as

$$\begin{bmatrix} \epsilon_1 \\ \epsilon_2 \\ \gamma_6 \end{bmatrix} = \begin{bmatrix} S_{11} & S_{12} & 0 \\ S_{12} & S_{22} & 0 \\ 0 & 0 & S_{66} \end{bmatrix} \begin{bmatrix} \sigma_1 \\ \sigma_2 \\ \tau_6 \end{bmatrix} \quad (3.33)$$

or, in brief,

$$[\epsilon]_{1,2} = [S]_{1,2} [\sigma]_{1,2}$$

Thus, the in-plane stress-strain relations for an orthotropic layer under plane stress can be expressed in terms of only four independent elastic parameters, i.e., the reduced stiffnesses Q_{11} , Q_{12} , Q_{22} , Q_{66} or the compliances S_{11} , S_{12} , S_{22} , S_{66} . It should be noted that, under plane stress, the nonzero out-of-plane strain ϵ_3 (or ϵ_2) is related to the in-plane stresses σ_1 and σ_2 through the compliances S_{13} and S_{23} . This requires two additional independent elastic parameters over and above the four needed for the in-plane stress-strain relations.

3.1.5 Isotropic Material

An isotropic material is characterized by an infinite number of planes of material symmetry through a point. For such a material, subscripts 1, 2, and 3 in the material constants are interchangeable. Then the stress-strain relations in Eq. (3.17) are reduced to

$$\begin{bmatrix} \sigma_1 \\ \sigma_2 \\ \sigma_3 \\ \tau_4 \\ \tau_5 \\ \tau_6 \end{bmatrix} = \begin{bmatrix} C_{11} & C_{12} & C_{12} & 0 & 0 & 0 \\ C_{12} & C_{11} & C_{12} & 0 & 0 & 0 \\ C_{12} & C_{12} & C_{11} & 0 & 0 & 0 \\ 0 & 0 & 0 & \frac{C_{11}-C_{12}}{2} & 0 & 0 \\ 0 & 0 & 0 & 0 & \frac{C_{11}-C_{12}}{2} & 0 \\ 0 & 0 & 0 & 0 & 0 & \frac{C_{11}-C_{12}}{2} \end{bmatrix} \begin{bmatrix} \epsilon_1 \\ \epsilon_2 \\ \epsilon_3 \\ \gamma_4 \\ \gamma_5 \\ \gamma_6 \end{bmatrix} \quad (3.34)$$

Thus, an isotropic material is fully characterized by only two independent constants, e.g., the stiffnesses C_{11} and C_{12} .

The conclusions discussed before regarding the required number of independent elastic constants for the various types of materials are summarized in Table 3.1.

3.2 Relations between Mathematical and Engineering Constants

The stress-strain relations discussed before acquire more physical meaning when expressed in terms of the familiar engineering constants, i.e., moduli and Poisson's ratios. Relations between mathematical and engineering constants are obtained by conducting imaginary elementary experiments as illustrated in Figures 3.4 and 3.5.

If an orthotropic material element is subjected to uniaxial tensile loading in the longitudinal direction, σ_1 , then, from Eq. (3.18) we have

$$\begin{aligned}\epsilon_1 &= S_{11} \sigma_1 \\ \epsilon_2 &= S_{12} \sigma_1 \\ \epsilon_3 &= S_{13} \sigma_1 \\ \gamma_4 &= \gamma_5 = \gamma_6 = 0\end{aligned}\tag{3.35}$$

From engineering considerations we have

Table 3.1 Independent Elastic Constants for Various Types of Materials

Material	No. of independent elastic constants
1. General anisotropic material	81
2. Anisotropic material considering symmetry of stress and strain tensors ($\sigma_{ij} = \sigma_{ji}$; $\epsilon_{ij} = \epsilon_{ji}$)	36
3. Anisotropic material with elastic energy considerations	21
4. General orthotropic material	9
5. Orthotropic material with transverse isotropy	5
6. Isotropic material	2

$$\epsilon_1 = \frac{\sigma_1}{E_1}$$

$$\epsilon_2 = -\frac{\nu_{12}}{E_1} \sigma_1$$

$$\epsilon_3 = -\frac{\nu_{13}}{E_1} \sigma_1 \quad (3.36)$$

$$\gamma_4 = \gamma_5 = \gamma_6 = 0$$

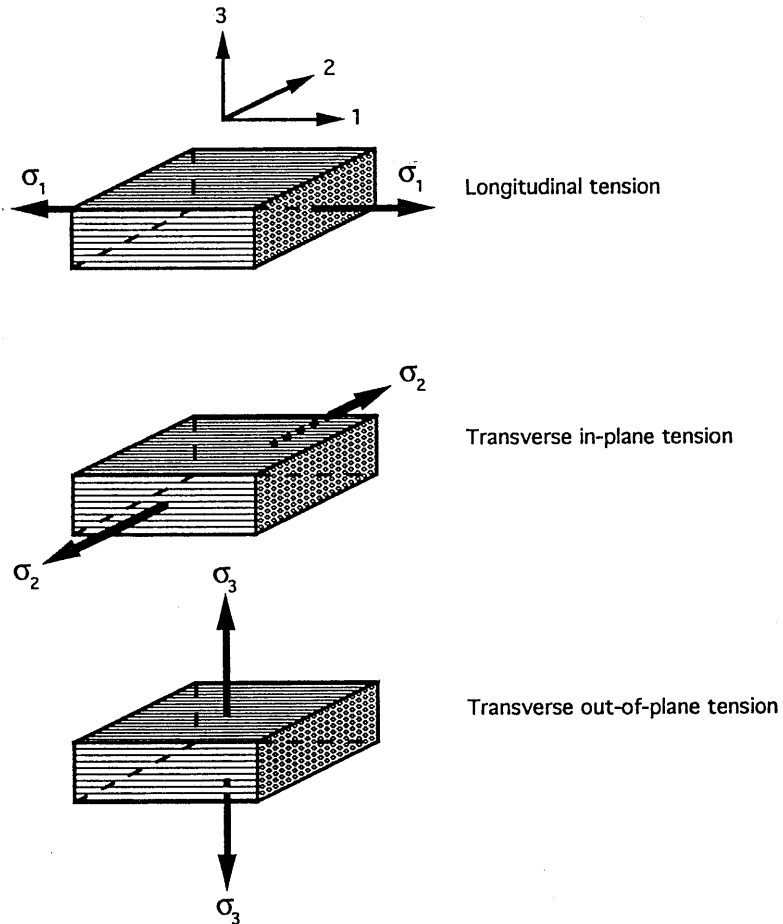


Fig. 3.4 Elementary experiments for obtaining relations between mathematical and engineering constants (normal stress loading).

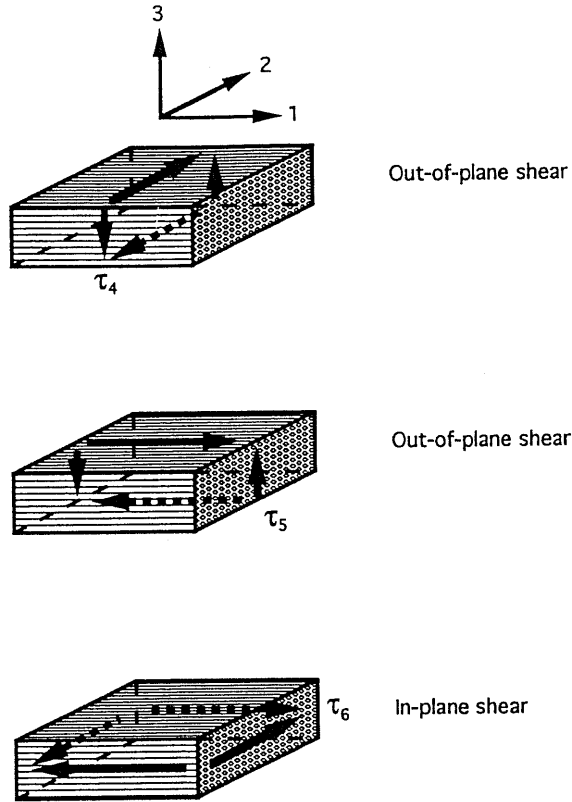


Fig. 3.5 Elementary experiments for obtaining relations between mathematical and engineering constants (shear loading).

Recall that the first and second subscripts in Poisson's ratio denote stress and strain directions, respectively.

From Eqs. (3.35) and (3.36) we obtain the relations

$$S_{11} = \frac{1}{E_1}, S_{12} = -\frac{\nu_{12}}{E_1}, S_{13} = -\frac{\nu_{13}}{E_1} \quad (3.37)$$

If a material element is subjected to uniaxial tensile loading in the in-plane transverse direction, σ_2 , we have in a similar fashion

$$\epsilon_1 = S_{12} \sigma_2 = -\frac{\nu_{21}}{E_2} \sigma_2$$

$$\epsilon_2 = S_{22} \sigma_2 = \frac{\sigma_2}{E_2}$$

$$\epsilon_3 = S_{23} \sigma_2 = -\frac{\nu_{23}}{E_2} \sigma_2 \quad (3.38)$$

$$\gamma_4 = \gamma_5 = \gamma_6 = 0$$

from which we obtain the relations

$$S_{12} = -\frac{\nu_{21}}{E_2}, S_{22} = \frac{1}{E_2}, S_{23} = -\frac{\nu_{23}}{E_2} \quad (3.39)$$

Uniaxial normal loading in the out-of-plane transverse direction, σ_3 , yields the following

$$\epsilon_1 = S_{13} \sigma_3 = -\frac{\nu_{31}}{E_3} \sigma_3$$

$$\epsilon_2 = S_{23} \sigma_3 = -\frac{\nu_{32}}{E_3} \sigma_3 \quad (3.40)$$

$$\epsilon_3 = S_{33} \sigma_3 = \frac{\sigma_3}{E_3}$$

from which we obtain the relations

$$S_{13} = -\frac{\nu_{31}}{E_3}, S_{23} = -\frac{\nu_{32}}{E_3}, S_{33} = \frac{1}{E_3} \quad (3.41)$$

In-plane pure shear loading, τ_6 , yields

$$\epsilon_1 = \epsilon_2 = \epsilon_3 = \gamma_4 = \gamma_5 = 0$$

$$\gamma_6 = S_{66} \tau_6 = \frac{\tau_6}{G_{12}} \quad (3.42)$$

from which we obtain

$$S_{66} = \frac{1}{G_{12}} \quad (3.43)$$

Out-of-plane pure shear loading in the 2–3 plane, τ_4 , yields

$$\epsilon_1 = \epsilon_2 = \epsilon_3 = \gamma_5 = \gamma_6 = 0 \quad (3.44)$$

$$\gamma_4 = S_{44} \tau_4 = \frac{\tau_4}{G_{23}}$$

from which we obtain

$$S_{44} = \frac{1}{G_{23}} \quad (3.45)$$

Finally, out-of-plane pure shear loading in the 1–3 plane, τ_5 , yields

$$\begin{aligned} \epsilon_1 = \epsilon_2 = \epsilon_3 = \gamma_4 = \gamma_6 = 0 \\ \gamma_5 = S_{55} \tau_5 = \frac{\tau_5}{G_{13}} \end{aligned} \quad (3.46)$$

from which we obtain

$$S_{55} = \frac{1}{G_{13}} \quad (3.47)$$

The stress–strain relations in Eq. (3.18) can then be expressed in terms of engineering constants as follows:

$$\begin{bmatrix} \epsilon_1 \\ \epsilon_2 \\ \epsilon_3 \\ \gamma_4 \\ \gamma_5 \\ \gamma_6 \end{bmatrix} = \begin{bmatrix} \frac{1}{E_1} & -\frac{\nu_{21}}{E_2} & -\frac{\nu_{31}}{E_3} & 0 & 0 & 0 \\ -\frac{\nu_{12}}{E_1} & \frac{1}{E_2} & -\frac{\nu_{32}}{E_3} & 0 & 0 & 0 \\ -\frac{\nu_{13}}{E_1} & -\frac{\nu_{23}}{E_2} & \frac{1}{E_3} & 0 & 0 & 0 \\ 0 & 0 & 0 & \frac{1}{G_{23}} & 0 & 0 \\ 0 & 0 & 0 & 0 & \frac{1}{G_{13}} & 0 \\ 0 & 0 & 0 & 0 & 0 & \frac{1}{G_{12}} \end{bmatrix} \begin{bmatrix} \sigma_1 \\ \sigma_2 \\ \sigma_3 \\ \tau_4 \\ \tau_5 \\ \tau_6 \end{bmatrix} \quad (3.48)$$

From the symmetry of the compliance matrix $[S_{ij}]$ and the above we conclude that

$$\begin{aligned} \frac{\nu_{12}}{E_1} &= \frac{\nu_{21}}{E_2} \\ \frac{\nu_{13}}{E_1} &= \frac{\nu_{31}}{E_3} \\ \frac{\nu_{23}}{E_2} &= \frac{\nu_{32}}{E_3} \end{aligned} \quad (3.49)$$

and in general

$$\frac{\nu_{ij}}{E_i} = \frac{\nu_{ji}}{E_j} \quad \text{or} \quad \frac{\nu_{ij}}{\nu_{ji}} = \frac{E_i}{E_j} \quad (i, j = 1, 2, 3)$$

(Note: The above can also be deduced from Betti's reciprocal law according to which transverse deformation due to a stress applied in the longitudinal direction is equal to the longitudinal deformation due to an equal stress applied in the transverse direction.¹)

As seen above, the relations between compliances S_{ij} and engineering constants are fairly simple. This, however, is not the case for the relations between stiffnesses C_{ij} and engineering constants. To obtain such relationships, we need first to invert the compliance matrix $[S_{ij}]$ and express the stiffnesses C_{ij} as a function of the compliances S_{ij} as follows:

$$\begin{aligned} C_{11} &= \frac{S_{22} S_{33} - S_{23}^2}{S} \\ C_{22} &= \frac{S_{33} S_{11} - S_{13}^2}{S} \\ C_{33} &= \frac{S_{11} S_{22} - S_{12}^2}{S} \\ C_{12} &= \frac{S_{13} S_{23} - S_{12} S_{33}}{S} \\ C_{23} &= \frac{S_{12} S_{13} - S_{23} S_{11}}{S} \\ C_{13} &= \frac{S_{12} S_{23} - S_{13} S_{22}}{S} \\ C_{44} &= \frac{1}{S_{44}}, \quad C_{55} = \frac{1}{S_{55}}, \quad C_{66} = \frac{1}{S_{66}} \end{aligned} \quad (3.50)$$

where

$$S = \begin{vmatrix} S_{11} & S_{12} & S_{13} \\ S_{12} & S_{22} & S_{23} \\ S_{13} & S_{23} & S_{33} \end{vmatrix} \quad (3.51)$$

Substituting the relations between S_{ij} and engineering constants in the above, we obtain²

$$\begin{aligned}
 C_{11} &= \frac{1 - \nu_{23} \nu_{32}}{E_2 E_3 \Delta} \\
 C_{22} &= \frac{1 - \nu_{13} \nu_{31}}{E_1 E_3 \Delta} \\
 C_{33} &= \frac{1 - \nu_{12} \nu_{21}}{E_1 E_2 \Delta} \\
 C_{12} &= \frac{\nu_{21} + \nu_{31} \nu_{23}}{E_2 E_3 \Delta} = \frac{\nu_{12} + \nu_{13} \nu_{32}}{E_1 E_3 \Delta} \\
 C_{23} &= \frac{\nu_{32} + \nu_{12} \nu_{31}}{E_1 E_3 \Delta} = \frac{\nu_{23} + \nu_{21} \nu_{13}}{E_1 E_2 \Delta} \\
 C_{13} &= \frac{\nu_{13} + \nu_{12} \nu_{23}}{E_1 E_2 \Delta} = \frac{\nu_{31} + \nu_{21} \nu_{32}}{E_2 E_3 \Delta} \\
 C_{44} &= G_{23}, \quad C_{55} = G_{13}, \quad C_{66} = G_{12}
 \end{aligned} \tag{3.52}$$

where

$$\Delta = \frac{1}{E_1 E_2 E_3} \begin{vmatrix} 1 & -\nu_{21} & -\nu_{31} \\ -\nu_{12} & 1 & -\nu_{32} \\ -\nu_{13} & -\nu_{23} & 1 \end{vmatrix} \tag{3.53}$$

It should be noted that in the case of a transversely isotropic material with the 2–3 plane as the plane of isotropy

$$\begin{aligned}
 E_2 &= E_3 \\
 G_{12} &= G_{13} \\
 \nu_{12} &= \nu_{13}
 \end{aligned} \tag{3.54}$$

3.3 Stress–Strain Relations for Thin Lamina

A thin, unidirectional lamina is assumed to be under a state of plane stress; therefore, the stress–strain relations in Eqs. (3.31) and (3.33) are applicable. They relate the in-plane stress components with the in-plane strain components along the principal material axes:

$$\begin{bmatrix} \sigma_1 \\ \sigma_2 \\ \tau_6 \end{bmatrix} = \begin{bmatrix} Q_{11} & Q_{12} & 0 \\ Q_{12} & Q_{22} & 0 \\ 0 & 0 & Q_{66} \end{bmatrix} \begin{bmatrix} \epsilon_1 \\ \epsilon_2 \\ \gamma_6 \end{bmatrix} \tag{3.31 bis}$$

and

$$\begin{bmatrix} \epsilon_1 \\ \epsilon_2 \\ \gamma_6 \end{bmatrix} = \begin{bmatrix} S_{11} & S_{12} & 0 \\ S_{12} & S_{22} & 0 \\ 0 & 0 & S_{66} \end{bmatrix} \begin{bmatrix} \sigma_1 \\ \sigma_2 \\ \tau_6 \end{bmatrix} \quad (3.33 \text{ bis})$$

The relations above can be expressed in terms of engineering constants by noting that

$$\begin{aligned} S_{11} &= \frac{1}{E_1} \\ S_{22} &= \frac{1}{E_2} \\ S_{12} &= -\frac{\nu_{12}}{E_1} = -\frac{\nu_{21}}{E_2} \\ S_{66} &= \frac{1}{G_{12}} \end{aligned} \quad (3.55)$$

and

$$\begin{aligned} Q_{11} &= \frac{E_1}{1 - \nu_{12} \nu_{21}} \\ Q_{22} &= \frac{E_2}{1 - \nu_{12} \nu_{21}} \\ Q_{12} &= \frac{\nu_{21} E_1}{1 - \nu_{12} \nu_{21}} = \frac{\nu_{12} E_2}{1 - \nu_{12} \nu_{21}} \\ Q_{66} &= G_{12} \end{aligned} \quad (3.56)$$

Thus, as far as the in-plane stress-strain relations are concerned, the unidirectional lamina can be fully characterized by four independent constants—the four reduced stiffnesses Q_{11} , Q_{22} , Q_{12} and Q_{66} ; or the four compliances S_{11} , S_{22} , S_{12} , and S_{66} ; or four engineering constants E_1 , E_2 , G_{12} , and ν_{12} . Poisson's ratio ν_{21} is not independent, as it is related to ν_{12} , E_1 and E_2 by Eq. (3.49).

3.4 Transformation of Stress and Strain

Normally, the lamina principal axes (1, 2) do not coincide with the loading or reference axes (x, y) (Fig. 3.6). Then, the stress and strain components referred

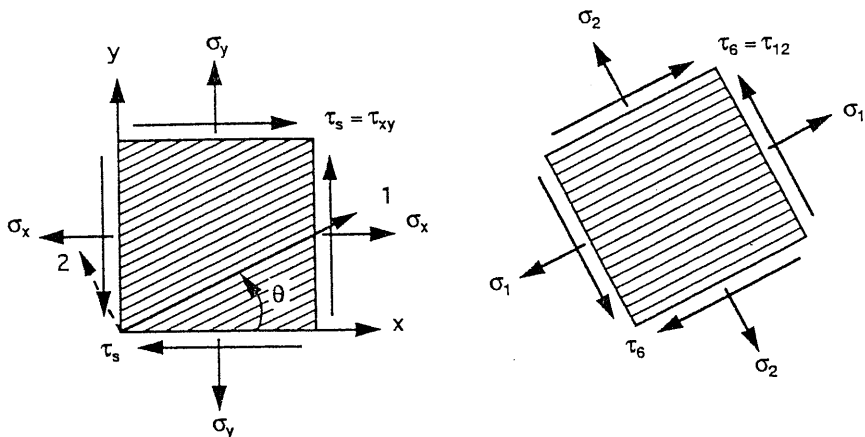


Fig. 3.6 Stress components in unidirectional lamina referred to loading and material axes.

to the principal material axes (1, 2) can be expressed in terms of those referred to the loading axes (x, y) by the following transformation relations:

$$\begin{bmatrix} \sigma_1 \\ \sigma_2 \\ \tau_6 \end{bmatrix} = [T] \begin{bmatrix} \sigma_x \\ \sigma_y \\ \tau_s \end{bmatrix} \quad (3.57)$$

or, in brief,

$$[\sigma]_{1,2} = [T] [\sigma]_{x,y}$$

and

$$\begin{bmatrix} \epsilon_1 \\ \epsilon_2 \\ \frac{1}{2}\gamma_6 \end{bmatrix} = [T] \begin{bmatrix} \epsilon_x \\ \epsilon_y \\ \frac{1}{2}\gamma_s \end{bmatrix} \quad (3.58)$$

or, in brief,

$$[\epsilon]_{1,2} = [T] [\epsilon]_{x,y}$$

where the transformation matrix $[T]$ is given by

$$[T] = \begin{bmatrix} m^2 & n^2 & 2mn \\ n^2 & m^2 & -2mn \\ -mn & mn & m^2 - n^2 \end{bmatrix} \quad (3.59)$$

and

$$m = \cos\theta, \quad n = \sin\theta$$

The angle θ is measured positive counterclockwise from the x -axis to the 1-axis.

By inversion of the relations above we obtain

$$\begin{bmatrix} \sigma_x \\ \sigma_y \\ \tau_s \end{bmatrix} = [T^{-1}] \begin{bmatrix} \sigma_1 \\ \sigma_2 \\ \tau_6 \end{bmatrix} \quad (3.60)$$

and

$$\begin{bmatrix} \epsilon_x \\ \epsilon_y \\ \frac{1}{2}\gamma_s \end{bmatrix} = [T^{-1}] \begin{bmatrix} \epsilon_1 \\ \epsilon_2 \\ \frac{1}{2}\gamma_6 \end{bmatrix} \quad (3.61)$$

where

$$[T^{-1}] = [T(-\theta)] = \begin{bmatrix} m^2 & n^2 & -2mn \\ n^2 & m^2 & 2mn \\ mn & -mn & m^2 - n^2 \end{bmatrix} \quad (3.62)$$

In the contracted notation used here, the subscript s in the above equations corresponds to shear stress or strain components referred to the x - y system of coordinates, i.e., $\tau_s = \tau_{xy}$ and $\gamma_s = \gamma_{xy}$. The subscript 6, as mentioned before, is a contraction of the subscripts 12.

The laws of stress and strain transformation are independent of material properties, i.e., they are the same for isotropic or anisotropic materials.

3.5 Transformation of Elastic Parameters

The stress-strain relations in Eqs. (3.31) and (3.33) show that, when the lamina is loaded only in tension or compression along the principal material axes, there

is no shear strain. Similarly, when the lamina is loaded under pure shear, τ_6 , along the principal axes (1, 2) only a shear strain, γ_6 , is produced along these axes. Thus there is no coupling between normal stresses and shear deformation and between shear stress and normal strains. This is not the case when the lamina is loaded along arbitrary axes x and y . Then, the stress-strain relations are expressed in the form

$$\begin{bmatrix} \sigma_x \\ \sigma_y \\ \tau_s \end{bmatrix} = \begin{bmatrix} Q_{xx} & Q_{xy} & Q_{xs} \\ Q_{yx} & Q_{yy} & Q_{ys} \\ Q_{sx} & Q_{sy} & Q_{ss} \end{bmatrix} \begin{bmatrix} \epsilon_x \\ \epsilon_y \\ \gamma_s \end{bmatrix} \quad (3.63)$$

or, in brief,

$$[\sigma]_{x,y} = [Q]_{x,y} [\epsilon]_{x,y}$$

with the reduced stiffness matrix fully populated. However, the number of independent constants is still four, as in the case of Eq. (3.31). What is needed, then, is the relationship between the transformed stiffnesses $[Q]_{x,y}$ and principal stiffnesses $[Q]_{1,2}$.

Equation (3.63) can be rewritten in the form

$$\begin{bmatrix} \sigma_x \\ \sigma_y \\ \tau_s \end{bmatrix} = \begin{bmatrix} Q_{xx} & Q_{xy} & 2Q_{xs} \\ Q_{yx} & Q_{yy} & 2Q_{ys} \\ Q_{sx} & Q_{sy} & 2Q_{ss} \end{bmatrix} \begin{bmatrix} \epsilon_x \\ \epsilon_y \\ \frac{1}{2}\gamma_s \end{bmatrix} \quad (3.64)$$

Introducing the stress-strain relation Eq. (3.31) into the transformation relation Eq. (3.60) we have

$$\begin{aligned} \begin{bmatrix} \sigma_x \\ \sigma_y \\ \tau_s \end{bmatrix} &= [T^{-1}] \begin{bmatrix} \sigma_1 \\ \sigma_2 \\ \tau_6 \end{bmatrix} = [T^{-1}] \begin{bmatrix} Q_{11} & Q_{12} & 0 \\ Q_{12} & Q_{22} & 0 \\ 0 & 0 & Q_{66} \end{bmatrix} \begin{bmatrix} \epsilon_1 \\ \epsilon_2 \\ \gamma_6 \end{bmatrix} \\ &= [T^{-1}] \begin{bmatrix} Q_{11} & Q_{12} & 0 \\ Q_{12} & Q_{22} & 0 \\ 0 & 0 & 2Q_{66} \end{bmatrix} \begin{bmatrix} \epsilon_1 \\ \epsilon_2 \\ \frac{1}{2}\gamma_6 \end{bmatrix} = [T^{-1}] \begin{bmatrix} Q_{11} & Q_{12} & 0 \\ Q_{12} & Q_{22} & 0 \\ 0 & 0 & 2Q_{66} \end{bmatrix} [T] \begin{bmatrix} \epsilon_x \\ \epsilon_y \\ \frac{1}{2}\gamma_s \end{bmatrix} \end{aligned} \quad (3.65)$$

Comparison of Eqs. (3.64) and (3.65) leads to the following transformation relation for the stiffness matrix:

$$\begin{bmatrix} Q_{xx} & Q_{xy} & 2Q_{xs} \\ Q_{yx} & Q_{yy} & 2Q_{ys} \\ Q_{sx} & Q_{sy} & 2Q_{ss} \end{bmatrix} = [T^{-1}] \begin{bmatrix} Q_{11} & Q_{12} & 0 \\ Q_{12} & Q_{22} & 0 \\ 0 & 0 & 2Q_{66} \end{bmatrix} [T] \quad (3.66)$$

From the relation above we obtain the transformed reduced stiffnesses as a function of the principal lamina stiffnesses:

$$\begin{aligned} Q_{xx} &= m^4 Q_{11} + n^4 Q_{22} + 2m^2 n^2 Q_{12} + 4m^2 n^2 Q_{66} \\ Q_{yy} &= n^4 Q_{11} + m^4 Q_{22} + 2m^2 n^2 Q_{12} + 4m^2 n^2 Q_{66} \\ Q_{xy} &= m^2 n^2 Q_{11} + m^2 n^2 Q_{22} + (m^4 + n^4) Q_{12} - 4m^2 n^2 Q_{66} \\ Q_{xs} &= m^3 n Q_{11} - mn^3 Q_{22} + (mn^3 - m^3 n) Q_{12} + 2(mn^3 - m^3 n) Q_{66} \\ Q_{ys} &= mn^3 Q_{11} - m^3 n Q_{22} + (m^3 n - mn^3) Q_{12} + 2(m^3 n - mn^3) Q_{66} \\ Q_{ss} &= m^2 n^2 Q_{11} + m^2 n^2 Q_{22} - 2m^2 n^2 Q_{12} + (m^2 - n^2)^2 Q_{66} \end{aligned} \quad (3.67)$$

The transformed strain–stress relations can be obtained either by direct inversion of the stress–strain relations in Eq. (3.63) or by transformation of the strain–stress relations in Eq. (3.33) referred to the principal material axes. The transformed strain–stress relations are

$$\begin{bmatrix} \epsilon_x \\ \epsilon_y \\ \gamma_s \end{bmatrix} = \begin{bmatrix} S_{xx} & S_{xy} & S_{xs} \\ S_{yx} & S_{yy} & S_{ys} \\ S_{sx} & S_{sy} & S_{ss} \end{bmatrix} \begin{bmatrix} \sigma_x \\ \sigma_y \\ \tau_s \end{bmatrix} \quad (3.68)$$

or, in brief,

$$[\epsilon]_{x,y} = [S]_{x,y} [\sigma]_{x,y}$$

which can be rewritten in the form

$$\begin{bmatrix} \epsilon_x \\ \epsilon_y \\ \frac{1}{2}\gamma_s \end{bmatrix} = \begin{bmatrix} S_{xx} & S_{xy} & S_{xs} \\ S_{yx} & S_{yy} & S_{ys} \\ \frac{1}{2}S_{sx} & \frac{1}{2}S_{sy} & \frac{1}{2}S_{ss} \end{bmatrix} \begin{bmatrix} \sigma_x \\ \sigma_y \\ \tau_s \end{bmatrix} \quad (3.69)$$

A series of transformations similar to those of Eq. (3.65) gives

$$\begin{aligned}
 \begin{bmatrix} \epsilon_x \\ \epsilon_y \\ \frac{1}{2}\gamma_s \end{bmatrix} &= [T^{-1}] \begin{bmatrix} \epsilon_1 \\ \epsilon_2 \\ \frac{1}{2}\gamma_6 \end{bmatrix} = [T^{-1}] \begin{bmatrix} S_{11} & S_{12} & 0 \\ S_{12} & S_{22} & 0 \\ 0 & 0 & \frac{1}{2}S_{66} \end{bmatrix} \begin{bmatrix} \sigma_1 \\ \sigma_2 \\ \tau_6 \end{bmatrix} \\
 &= [T^{-1}] \begin{bmatrix} S_{11} & S_{12} & 0 \\ S_{12} & S_{22} & 0 \\ 0 & 0 & \frac{1}{2}S_{66} \end{bmatrix} [T] \begin{bmatrix} \sigma_x \\ \sigma_y \\ \tau_s \end{bmatrix} \quad (3.70)
 \end{aligned}$$

Comparison of Eqs. (3.69) and (3.70) leads to the following transformation relation for the compliance matrix:

$$\begin{bmatrix} S_{xx} & S_{xy} & S_{xs} \\ S_{yx} & S_{yy} & S_{ys} \\ \frac{1}{2}S_{sx} & \frac{1}{2}S_{sy} & \frac{1}{2}S_{ss} \end{bmatrix} = [T^{-1}] \begin{bmatrix} S_{11} & S_{12} & 0 \\ S_{12} & S_{22} & 0 \\ 0 & 0 & \frac{1}{2}S_{66} \end{bmatrix} [T] \quad (3.71)$$

This relation leads to the following ones for the transformed compliances as a function of the principal lamina compliances:

$$\begin{aligned}
 S_{xx} &= m^4 S_{11} + n^4 S_{22} + 2m^2 n^2 S_{12} + m^2 n^2 S_{66} \\
 S_{yy} &= n^4 S_{11} + m^4 S_{22} + 2m^2 n^2 S_{12} + m^2 n^2 S_{66} \\
 S_{xy} &= m^2 n^2 S_{11} + m^2 n^2 S_{22} + (m^4 + n^4) S_{12} - m^2 n^2 S_{66} \\
 S_{xs} &= 2m^3 n S_{11} - 2mn^3 S_{22} + 2(mn^3 - m^3 n) S_{12} + (mn^3 - m^3 n) S_{66} \\
 S_{ys} &= 2mn^3 S_{11} - 2m^3 n S_{22} + 2(m^3 n - mn^3) S_{12} + (m^3 n - mn^3) S_{66} \\
 S_{ss} &= 4m^2 n^2 S_{11} + 4m^2 n^2 S_{22} - 8m^2 n^2 S_{12} + (m^2 - n^2)^2 S_{66}
 \end{aligned} \quad (3.72)$$

Table 3.2 Relations for Stiffness and Compliance Transformation

	$S_{11}(Q_{11})$	$S_{22}(Q_{22})$	$S_{12}(Q_{12})$	$S_{66}(4Q_{66})$
$S_{xx}(Q_{xx})$	m^4	n^4	$2m^2 n^2$	$m^2 n^2$
$S_{yy}(Q_{yy})$	n^4	m^4	$2m^2 n^2$	$m^2 n^2$
$S_{xy}(Q_{xy})$	$m^2 n^2$	$m^2 n^2$	$(m^4 + n^4)$	$-m^2 n^2$
$S_{ss}(4Q_{ss})$	$4m^2 n^2$	$4n^2 m^2$	$-8m^2 n^2$	$(m^2 - n^2)^2$
$S_{xs}(2Q_{xs})$	$2m^3 n$	$-2mn^3$	$2(mn^3 - m^3 n)$	$(mn^3 - m^3 n)$
$S_{ys}(2Q_{ys})$	$2mn^3$	$-2nm^3$	$2(m^3 n - mn^3)$	$(m^3 n - mn^3)$

$$m = \cos\theta, n = \sin\theta.$$

The transformation relations are presented in tabular form for easy reference in Table 3.2.

3.6 Transformation of Stress–Strain Relations in Terms of Engineering Constants

The strain–stress relations referred to the principal material axes as given by Eqs. (3.33) and (3.55) are

$$\begin{bmatrix} \epsilon_1 \\ \epsilon_2 \\ \gamma_6 \end{bmatrix} = \begin{bmatrix} S_{11} & S_{12} & 0 \\ S_{12} & S_{22} & 0 \\ 0 & 0 & S_{66} \end{bmatrix} \begin{bmatrix} \sigma_1 \\ \sigma_2 \\ \tau_6 \end{bmatrix} = \begin{bmatrix} \frac{1}{E_1} & -\frac{\nu_{21}}{E_2} & 0 \\ -\frac{\nu_{12}}{E_1} & \frac{1}{E_2} & 0 \\ 0 & 0 & \frac{1}{G_{12}} \end{bmatrix} \begin{bmatrix} \sigma_1 \\ \sigma_2 \\ \tau_6 \end{bmatrix} \quad (3.73)$$

These relations, when transformed to the x - y coordinate system, are expressed by Eq. (3.68) in terms of mathematical compliance constants, S_{xx} , S_{yy} , S_{xy} , etc. To obtain the relationships between these constants and engineering parameters, we conduct simple imaginary experiments on an element with sides parallel to the x - and y -axes. For example, the elements of the first column of the compliance matrix in Eq. (3.68) are the strain components, ϵ_x , ϵ_y , and γ_s produced by a unit normal stress $\sigma_x = 1$.

A uniaxial stress σ_x produces the following strains:

$$\begin{aligned} \epsilon_x &= \frac{\sigma_x}{E_x} \\ \epsilon_y &= -\frac{\nu_{xy}}{E_x} \sigma_x \\ \gamma_s &= \frac{\eta_{xs}}{E_x} \sigma_x \end{aligned} \quad (3.74)$$

In the above, Poisson's ratio ν_{xy} corresponding to stress in the x -direction and strain in the y -direction is the negative ratio of the transverse strain ϵ_y to the axial strain ϵ_x . The shear coupling coefficient η_{xs} , corresponding to normal stress in the x -direction and shear strain in the x - y plane, is the ratio of the shear strain γ_s (γ_{xy}) to the axial strain ϵ_x .

In a similar manner, a uniaxial stress σ_y produces the following strains

$$\begin{aligned}
 \epsilon_x &= -\frac{\nu_{yx}}{E_y} \sigma_y \\
 \epsilon_y &= \frac{\sigma_y}{E_y} \\
 \gamma_s &= \frac{\eta_{ys}}{E_y} \sigma_y
 \end{aligned} \tag{3.75}$$

with Poisson's ratio ν_{yx} and shear coupling coefficient η_{ys} defined as before.

A pure shear stress τ_s (τ_{xy}) produces the following strains

$$\begin{aligned}
 \epsilon_x &= \frac{\eta_{sx}}{G_{xy}} \tau_s \\
 \epsilon_y &= \frac{\eta_{sy}}{G_{xy}} \tau_s \\
 \gamma_s &= \frac{\tau_s}{G_{xy}}
 \end{aligned} \tag{3.76}$$

where the shear coupling coefficients η_{sx} and η_{sy} are the ratios of the normal strains ϵ_x and ϵ_y to the shear strain γ_s , respectively, for the pure shear loading applied. Here, the first subscript s denotes shear stress in the x - y plane and the second subscripts x and y denote normal strains in the x - and y -directions, respectively.

By superposition of the three loadings discussed above we obtain the following strain-stress relations in terms of engineering constants:

$$\begin{bmatrix} \epsilon_x \\ \epsilon_y \\ \gamma_s \end{bmatrix} = \begin{bmatrix} \frac{1}{E_x} & -\frac{\nu_{yx}}{E_y} & \frac{\eta_{sx}}{G_{xy}} \\ -\frac{\nu_{xy}}{E_x} & \frac{1}{E_y} & \frac{\eta_{sy}}{G_{xy}} \\ \frac{\eta_{xs}}{E_x} & \frac{\eta_{ys}}{E_y} & \frac{1}{G_{xy}} \end{bmatrix} \begin{bmatrix} \sigma_x \\ \sigma_y \\ \tau_s \end{bmatrix} \tag{3.77}$$

From symmetry considerations of the compliance matrix we obtain

$$\begin{aligned}
 \frac{\nu_{xy}}{E_x} &= \frac{\nu_{yx}}{E_y} & \frac{\nu_{xy}}{\nu_{yx}} &= \frac{E_x}{E_y} \\
 \frac{\eta_{xs}}{E_x} &= \frac{\eta_{sx}}{G_{xy}} & \text{or} & \quad \frac{\eta_{xs}}{\eta_{sx}} &= \frac{E_x}{G_{xy}} \\
 \frac{\eta_{ys}}{E_y} &= \frac{\eta_{sy}}{G_{xy}} & & \quad \frac{\eta_{ys}}{\eta_{sy}} &= \frac{E_y}{G_{xy}}
 \end{aligned} \tag{3.78}$$

Comparison of equivalent strain–stress relations in Eqs. (3.68) and (3.77) yields the following relationships:

$$\begin{aligned}
 S_{xx} &= \frac{1}{E_x} \\
 S_{yy} &= \frac{1}{E_y} \\
 S_{ss} &= \frac{1}{G_{xy}} \\
 S_{xy} = S_{yx} &= -\frac{\nu_{xy}}{E_x} = -\frac{\nu_{yx}}{E_y} \\
 S_{xs} = S_{sx} &= \frac{\eta_{xs}}{E_x} = \frac{\eta_{sx}}{G_{xy}} \\
 S_{ys} = S_{sy} &= \frac{\eta_{ys}}{E_y} = \frac{\eta_{sy}}{G_{xy}}
 \end{aligned} \tag{3.79}$$

or

$$\begin{aligned}
 E_x &= \frac{1}{S_{xx}} \\
 E_y &= \frac{1}{S_{yy}} \\
 G_{xy} &= \frac{1}{S_{ss}} \\
 \nu_{xy} &= -\frac{S_{yx}}{S_{xx}}; \quad \nu_{yx} = -\frac{S_{xy}}{S_{yy}} \\
 \eta_{xs} &= \frac{S_{sx}}{S_{xx}}; \quad \eta_{sx} = \frac{S_{xs}}{S_{ss}} \\
 \eta_{ys} &= \frac{S_{sy}}{S_{yy}}; \quad \eta_{sy} = \frac{S_{ys}}{S_{ss}}
 \end{aligned} \tag{3.80}$$

The relations in Eq. (3.77) can be inverted to yield stress–strain relations in terms of engineering constants. These relations would be more complex than the strain–stress relations in Eq. (3.77).

3.7 Transformation Relations for Engineering Constants

Using the relations between engineering constants and compliances, Eqs. (3.79) and (3.80), in the compliance transformation relations, Eq. (3.72), we obtain the following transformation relations for the engineering constants:

$$\begin{aligned}
 \frac{1}{E_x} &= \frac{m^2}{E_1} (m^2 - n^2 \nu_{12}) + \frac{n^2}{E_2} (n^2 - m^2 \nu_{21}) + \frac{m^2 n^2}{G_{12}} \\
 \frac{1}{E_y} &= \frac{n^2}{E_1} (n^2 - m^2 \nu_{12}) + \frac{m^2}{E_2} (m^2 - n^2 \nu_{21}) + \frac{m^2 n^2}{G_{12}} \\
 \frac{1}{G_{xy}} &= \frac{4m^2 n^2}{E_1} (1 + \nu_{12}) + \frac{4m^2 n^2}{E_2} (1 + \nu_{21}) + \frac{(m^2 - n^2)^2}{G_{12}} \\
 \frac{\nu_{xy}}{E_x} &= \frac{\nu_{yx}}{E_y} = \frac{m^2}{E_1} (m^2 \nu_{12} - n^2) + \frac{n^2}{E_2} (n^2 \nu_{21} - m^2) + \frac{m^2 n^2}{G_{12}} \\
 \frac{\eta_{xs}}{E_x} &= \frac{\eta_{sx}}{G_{xy}} = \frac{2mn}{E_1} (m^2 - n^2 \nu_{12}) - \frac{2mn}{E_2} (n^2 - m^2 \nu_{21}) + \frac{mn^3 - m^3 n}{G_{12}} \\
 \frac{\eta_{ys}}{E_y} &= \frac{\eta_{sy}}{G_{xy}} = \frac{2mn}{E_1} (n^2 - m^2 \nu_{12}) - \frac{2mn}{E_2} (m^2 - n^2 \nu_{21}) + \frac{m^3 n - mn^3}{G_{12}}
 \end{aligned} \tag{3.81}$$

A computational procedure for calculation of transformed elastic constants is illustrated by the flow chart in Figure 3.7. It is assumed that the input consists of the basic engineering constants E_1 , E_2 , G_{12} , and ν_{12} referred to the principal material axes of the lamina and obtained from characterization tests. Then, relations in Eqs. (3.55) and (3.56) are used to obtain the reduced principal compliances and stiffnesses S_{ij} and Q_{ij} . The transformation relations in Eqs. (3.67) and (3.72) are used to obtain the transformed lamina stiffnesses $[Q]_{x,y}$ and compliances $[S]_{x,y}$. Finally, relations in Eq. (3.80) are used to obtain the transformed engineering constants (E_x , E_y , G_{xy} , ν_{xy} , ν_{yx} , η_{xs} , η_{ys} , η_{sx} , η_{sy}) referred to the x - y system of coordinates. Alternatively, relations in Eq. (3.81) can be used to obtain the transformed engineering constants directly from the given engineering constants referred to the principal material axes.

The variation of the transformed engineering constants with fiber orientation is illustrated in Figures 3.8 and 3.9 for a typical carbon/epoxy (AS4/3501-6) unidirectional material. Young's modulus decreases monotonically from its maximum value E_1 at $\theta = 0^\circ$ to its minimum E_2 at $\theta = 90^\circ$. The shear modulus G_{xy} peaks at $\theta = 45^\circ$ and reaches its minimum values at $\theta = 0^\circ$ and $\theta = 90^\circ$. Poisson's ratio ν_{xy} varies monotonically from its maximum value ν_{12} at $\theta = 0^\circ$ to

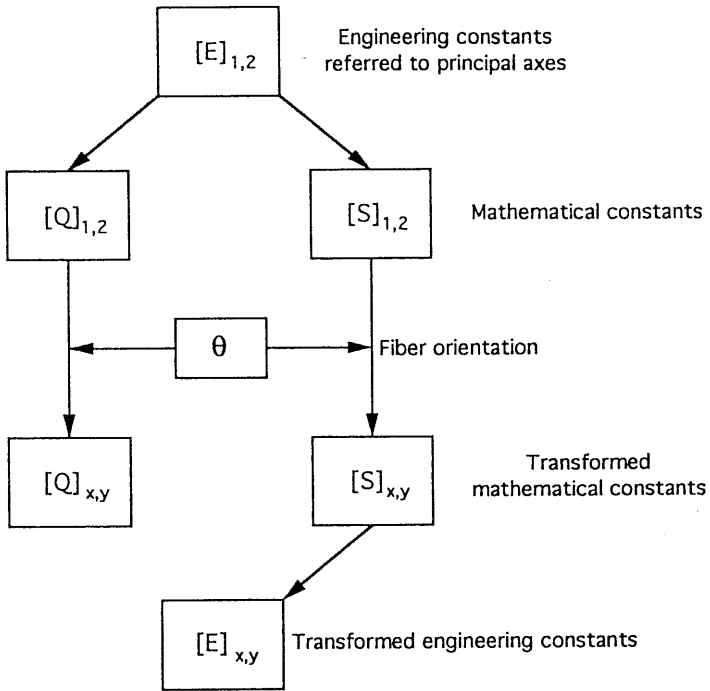


Fig. 3.7 Flow chart for determination of transformed elastic constants of unidirectional lamina.

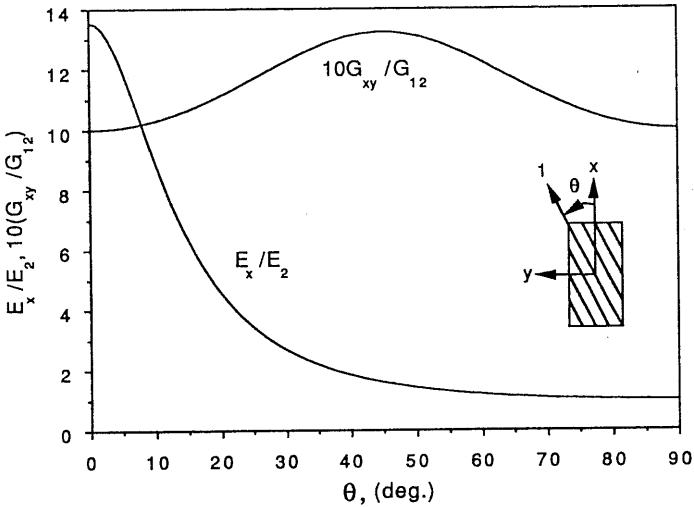


Fig. 3.8 Young's modulus and shear modulus of unidirectional composite as a function of fiber orientation (AS4/3501-6 carbon/epoxy).

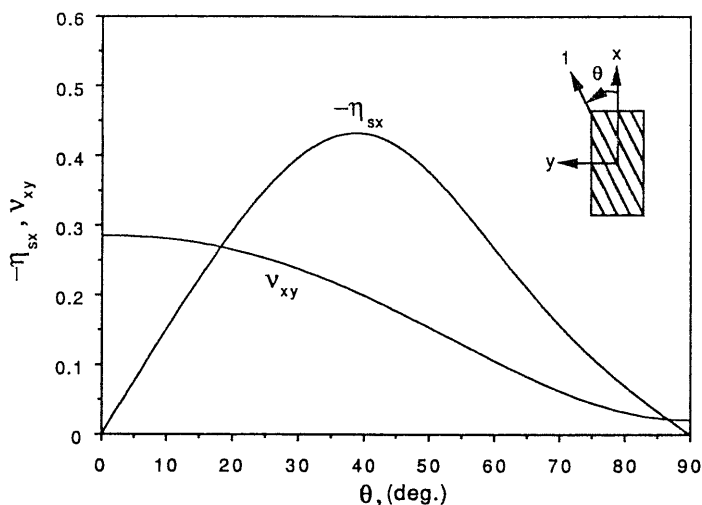


Fig. 3.9 Poisson's ratio and shear coupling coefficient of unidirectional composite as a function of fiber orientation (AS4/3501-6 carbon/epoxy).

its minimum value ν_{21} at $\theta = 90^\circ$. The shear coupling coefficient η_{sx} is negative throughout and peaks at around $\theta = 38^\circ$. The curves in Figures 3.8 and 3.9 are typical of high stiffness, highly anisotropic composites. The form of the variation of elastic constants depends on the relative magnitudes of the basic constants referred to the principal material axes. An example of a mildly anisotropic woven-glass/epoxy laminate (E-glass style 142/FR-4 epoxy) is illustrated in Figures 3.10 and 3.11. Here, Young's modulus decreases from a maximum value

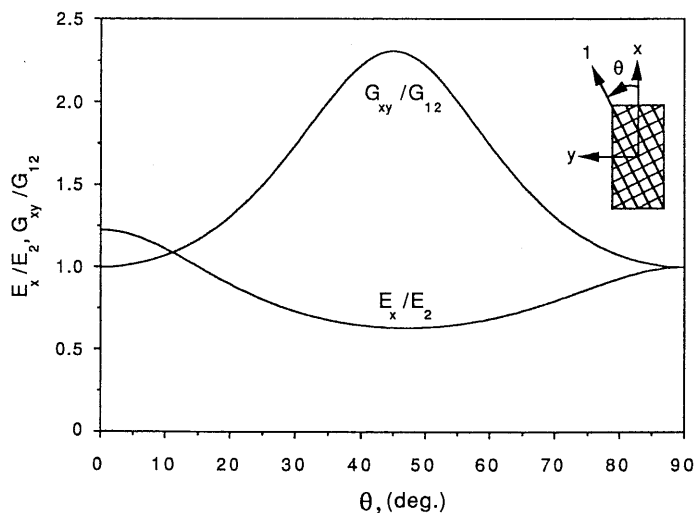


Fig. 3.10 Young's modulus and shear modulus of woven-glass/epoxy as a function of warp fiber orientation (IBM style 142/FR-4 epoxy).

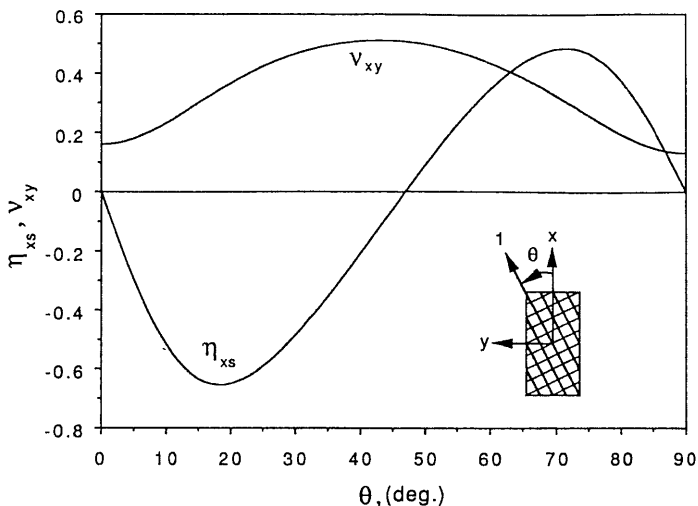


Fig. 3.11 Poisson's ratio and shear coupling coefficient of woven-glass/epoxy as a function of warp fiber orientation (IBM style 142/FR-4 epoxy).

at $\theta = 0^\circ$ to an absolute minimum at $\theta = 45^\circ$, and then it increases to a local maximum at $\theta = 90^\circ$. The shear modulus behaves similarly as in the case of carbon/epoxy, but it attains a maximum value at $\theta = 45^\circ$ that is much higher than the Young's modulus. Poisson's ratio has minimum values at $\theta = 0^\circ$ and $\theta = 90^\circ$, and it peaks at $\theta \cong 45^\circ$. The shear coupling coefficient changes signs as shown.

Sample Problem 3.1

Transformation of Young's Modulus

Given the basic lamina properties E_1 , E_2 , G_{12} and ν_{12} , it is required to determine Young's modulus E_x at an angle $\theta = 45^\circ$ with the fiber direction (Fig. 3.12). From Eq. (3.81) we obtain the following exact relation:

$$\left(\frac{1}{E_x}\right)_{\theta=45^\circ} = \frac{1 - \nu_{12}}{4E_1} + \frac{1 - \nu_{21}}{4E_2} + \frac{1}{4G_{12}} \quad (3.82)$$

The above relation can be simplified for the case of a high stiffness composite for which

$$E_1 \gg E_2 \text{ and } \nu_{21} \ll 1$$

In that case we obtain the following approximate expression:

$$(E_x)_{\theta = 45^\circ} \cong \frac{4G_{12} E_2}{G_{12} + E_2} \quad (3.83)$$

This means that Young's modulus at 45° with the fiber direction is a matrix-dominated property, since it depends primarily on E_2 and G_{12} , which are matrix-dominated properties.

Sample Problem 3.2

Transformation of Shear Modulus

Given the basic lamina properties E_1 , E_2 , G_{12} , and ν_{12} , it is required to determine the shear modulus G_{xy} at 45° with the fiber direction (see Fig. 3.12). From Eq. (3.81) we obtain the following exact relation:

$$\left(\frac{1}{G_{xy}}\right)_{\theta = 45^\circ} = \frac{1 + \nu_{12}}{E_1} + \frac{1 + \nu_{21}}{E_2} \quad (3.84)$$

For a high stiffness composite, for which $E_1 \gg E_2$ and $\nu_{21} \ll 1$, we obtain

$$(G_{xy})_{\theta = 45^\circ} \cong E_2 \quad (3.85)$$

which means that in this case the above shear modulus is a matrix-dominated property.

Sample Problem 3.3

Transformation of Poisson's Ratio

Given the basic lamina properties E_1 , E_2 , G_{12} , and ν_{12} , it is required to determine Poisson's ratio ν_{xy} at 45° with the fiber direction (Fig. 3.12). From Eq. (3.81) we obtain the following exact relation:

$$\left(\frac{\nu_{xy}}{E_x}\right)_{\theta = 45^\circ} = \frac{1}{4E_1} (\nu_{12} - 1) + \frac{1}{4E_2} (\nu_{21} - 1) + \frac{1}{4G_{12}} \quad (3.86)$$

For a high stiffness composite, for which $E_1 \gg E_2$ and $\nu_{21} \ll 1$, and taking into consideration the approximate relation in Eq. (3.83), we obtain

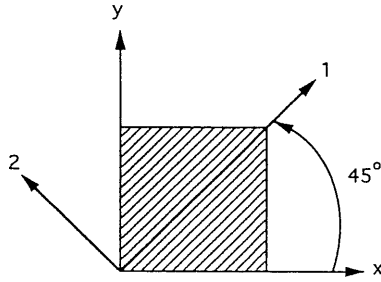


Fig. 3.12 Unidirectional lamina with fiber orientation at 45° with reference axis.

$$(\nu_{xy})_{\theta=45^\circ} \cong \frac{E_2 - G_{12}}{E_2 + G_{12}} \quad (3.87)$$

which means that in this case Poisson's ratio is a matrix-dominated property.

Sample Problem 3.4

Transformation of Shear Coupling Coefficient

Given the basic lamina properties E_1 , E_2 , G_{12} , and ν_{12} , it is required to determine the shear coupling coefficient η_{sx} at $\theta = 45^\circ$ with the fiber direction (Fig. 3.12). From Eq. (3.81) we obtain the following exact relation:

$$\left(\frac{\eta_{sx}}{G_{xy}}\right)_{\theta=45^\circ} = \frac{1}{2E_1}(1 - \nu_{12}) - \frac{1}{2E_2}(1 - \nu_{21}) = \frac{1}{2}\left(\frac{1}{E_1} - \frac{1}{E_2}\right) \quad (3.88)$$

This relation can be simplified as follows for the case of a high stiffness composite:

$$\left(\frac{\eta_{sx}}{G_{xy}}\right)_{\theta=45^\circ} \cong -\frac{1}{2E_2} \quad (3.89)$$

Recalling from Eq. (3.85) that in this case $(G_{xy})_{\theta=45^\circ} \cong E_2$, we obtain

$$(\eta_{sx})_{\theta=45^\circ} \cong -\frac{1}{2} \quad (3.90)$$

3.8 Micromechanical Predictions of Elastic Constants

3.8.1 Scope and Approaches

It was shown in the foregoing that the in-plane elastic behavior of a unidirectional lamina may be fully described in terms of four basic lamina properties, such as E_1 , E_2 , G_{12} , and ν_{12} . In the macromechanical approach these constants are assumed to be known from direct experimental characterization of the unidirectional material. These properties can vary a great deal even for the same material, as constituent properties and geometric parameters vary from batch to batch. It may not always be practical to characterize each batch of material experimentally. It is desirable to have reliable predictions of lamina properties as a function of constituent properties and geometric characteristics, such as fiber volume ratio and geometric packing parameters. Typical transverse cross sections of unidirectional composites are shown in Figure 3.13. It is shown that composites with low fiber volume ratio tend to have a random fiber distribution, whereas fibers in composites with high fiber volume ratio tend to nest in near hexagonal packing. One objective of micromechanics is to obtain functional relationships for the elastic constants of the composite in the form

$$C_{ij} = f(E_f, E_m, \nu_f, \nu_m, V_f, V_m, V_v, S, A) \quad (3.91)$$

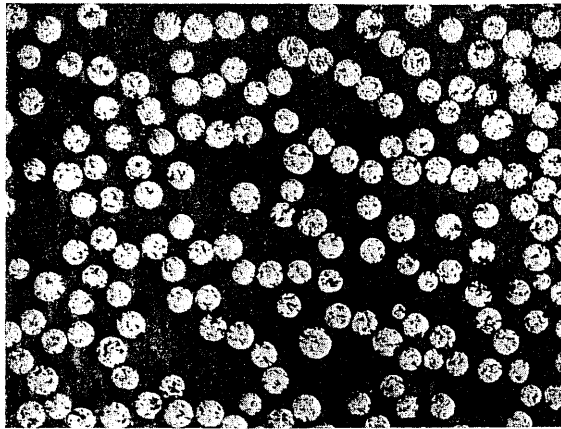
where S and A denote geometrical parameters describing the shape and array of the reinforcement.

A variety of methods have been used to predict properties of composite materials.³ The approaches used fall into the following general categories:

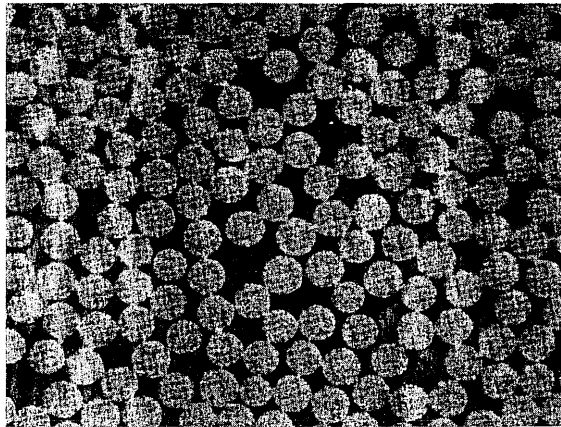
1. Mechanics of materials
2. Numerical
3. Self-consistent field
4. Bounding (variational approach)
5. Semi-empirical
6. Experimental

The mechanics of materials approach is based on simplifying assumptions of either uniform strain or uniform stress in the constituents. The mechanics of materials predictions are adequate for longitudinal properties such as Young's modulus E_1 and major Poisson's ratio ν_{12} . These properties are not sensitive to fiber shape and distribution. On the other hand, the mechanics of materials approach underestimates the transverse and shear properties, i.e., transverse modulus E_2 and shear modulus G_{12} .

Numerical approaches using finite differences, finite element, or boundary element methods yield the best predictions; however, they are time consuming



(a)



(b)

Fig. 3.13 Photomicrographs of typical transverse sections of unidirectional composites. (a) Silicon carbide/glass ceramic (SiC/CAS); average fiber diameter 15 μm ; fiber volume ratio, $V_f = 0.40$. (b) Carbon/epoxy (AS4/3501-6); fiber diameter 8 μm ; fiber volume ratio, $V_f = 0.70$.

and they do not yield closed form expressions. Results are usually presented in the form of families of curves.^{4,5}

In the self-consistent field approach a simplified composite model is considered consisting of a typical fiber surrounded by a cylindrical matrix phase. This composite element is considered embedded in a larger (infinite), homogeneous medium whose properties are identical to the average properties of the composite material. Classical elasticity theory has been used to obtain closed form solutions for the various elastic constants of the composite.^{6,7} This approach, because of the gross geometric simplifications involved, neglects

interaction effects between fibers and as a result tends to underestimate composite properties for higher fiber volume ratios.

Variational methods based on energy principles have been developed to establish bounds on effective properties.^{8,9} The bounds are close to each other in the case of longitudinal properties (E_1, ν_{12}), but they can be far apart in the case of transverse and shear properties (E_2, G_{12}).

Semi-empirical relationships have been developed to circumvent the difficulties with the theoretical approaches above and to facilitate computation.¹⁰ The so-called Halpin–Tsai relationships have a consistent form for all properties and represent an attempt at judicious interpolation between the series and parallel models used in the mechanics of materials approach or between the upper and lower bounds of the variational approach. This is expressed in terms of a parameter ξ , which is a measure of the reinforcing efficiency (or load transfer) and is determined with the aid of experiment.

The micromechanics of load transfer and the correlation between constituent properties and average composite properties must be ultimately verified experimentally. Photoelastic models have proven useful in illustrating stress transfer and determining local stress distributions and stress concentrations for composites of various constituents and various geometric parameters.¹¹

Micromechanics of composites in general and the various methods discussed above have been discussed extensively in the literature. Here, only simplified approaches and final expressions are given for determination of the basic elastic properties of the lamina.

3.8.2 Longitudinal Properties

Properties related to loading in the fiber direction, E_1 and ν_{12} , are dominated by the fibers that are usually stronger, stiffer, and have a lower ultimate strain. All predictions in this case and experimental results are very close to the rule of mixtures prediction. The longitudinal modulus is given by

$$E_1 = V_f E_{1f} + V_m E_m \quad (3.92)$$

where E_{1f} and E_m are longitudinal fiber and matrix moduli, respectively and V_f and V_m are the fiber and matrix volume ratios, respectively. In the relation above it is assumed that the fiber can be anisotropic with different properties in the axial and transverse (radial) directions and that the matrix is isotropic. The rule of mixtures prediction for the major (longitudinal) Poisson's ratio is also very close to all other predictions and experimental results and is given by a similar relation

$$\nu_{12} = V_f \nu_{12f} + V_m \nu_m \quad (3.93)$$

where ν_{12f} is the longitudinal Poisson's ratio of the fiber and ν_m is Poisson's ratio of the matrix.

3.8.3 Transverse Modulus

In the case of transverse normal loading, the state of stress in the matrix surrounding the fibers is complex and more affected by interaction from neighboring fibers. The transverse modulus is a matrix-dominated property and sensitive to the local state of stress. Approaches that are based on assumptions of simplified stress distributions do not yield accurate results.

In the mechanics of materials approach the fibers and matrix are assumed to be under uniform stress. The composite is represented by a series model of matrix and fiber elements yielding the following relation for transverse modulus:

$$\frac{1}{E_2} = \frac{V_f}{E_{2f}} + \frac{V_m}{E_m} \quad (3.94)$$

or

$$E_2 = \frac{E_{2f} E_m}{V_f E_m + V_m E_{2f}} \quad (3.95)$$

where E_{2f} is the transverse modulus of the fiber. The matrix modulus E_m in Eqs. (3.94) and (3.95) is usually replaced by

$$E'_m = \frac{E_m}{1 - \nu_m^2} \quad (3.96)$$

where ν_m is Poisson's ratio of the matrix. This accounts for the constraint imposed on the matrix by the fibers in the fiber direction. Thus Eq. (3.95) is modified as follows:

$$E_2 = \frac{E_{2f} E'_m}{V_f E'_m + V_m E_{2f}} \quad (3.97)$$

The mechanics of materials prediction above tends to underestimate the transverse modulus.

The self-consistent field model and the variational bounding method yield complex expressions for transverse modulus in terms of other properties, such as bulk modulus and transverse shear modulus.^{3,9}

The Halpin-Tsai semi-empirical relationship is a practical one, once the right choice is made for the parameter ξ .¹⁰

$$E_2 = E_m \frac{1 + \xi_1 \eta_1 V_f}{1 - \eta_1 V_f} \tag{3.98}$$

where

$$\eta_1 = \frac{E_{2f} - E_m}{E_{2f} + \xi_1 E_m}$$

and ξ_1 is the reinforcing efficiency factor for transverse loading. The prediction above tends to agree with experimental results for values of ξ_1 between 1 and 2. If a reliable experimental value of E_2 is available for a composite, then the value of ξ_1 can be obtained by using Eq. (3.98) and can be used to predict E_2 for a wide range of fiber volume ratios of the same composite. The variation of transverse modulus as a function of fiber volume ratio for several composite materials obtained by the relation above is shown in Figure 3.14. Similar results have been obtained by Adams and Doner⁴ using numerical methods.

3.8.4 In-Plane Shear Modulus

The behavior of unidirectional composites under in-plane (longitudinal) shear loading is also dominated by the matrix properties and the local stress distri-

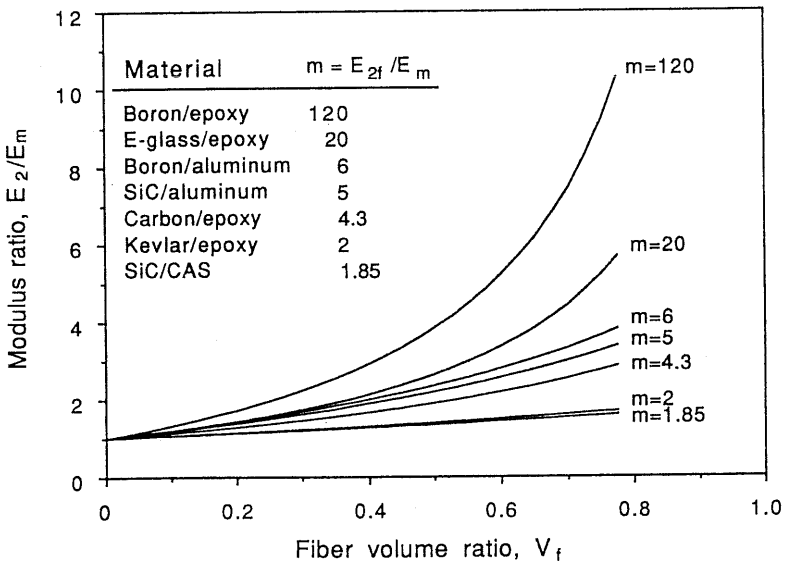


Fig. 3.14 Transverse modulus of unidirectional composites as a function of fiber volume ratio (Halpin-Tsai equations¹⁰).

butions. The mechanics of materials approach uses a series model under uniform stress and yields the following relation:

$$\frac{1}{G_{12}} = \frac{V_f}{G_{12f}} + \frac{V_m}{G_m} \tag{3.99}$$

or

$$G_{12} = \frac{G_{12f} G_m}{V_f G_m + V_m G_{12f}} \tag{3.100}$$

where G_{12f} and G_m are the shear moduli of the fiber and matrix, respectively. As in the case of transverse modulus, this approach tends to underestimate the in-plane shear modulus.

The Halpin–Tsai semi-empirical relation in this case is

$$G_{12} = G_m \frac{1 + \xi_2 \eta_2 V_f}{1 - \eta_2 V_f} \tag{3.101}$$

where

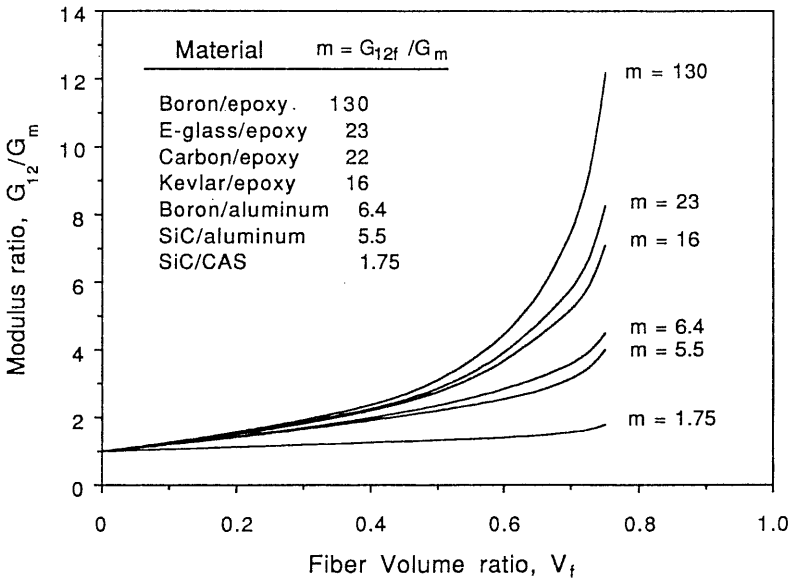


Fig. 3.15 In-plane shear modulus of unidirectional composites as a function of fiber volume ratio. (From Adams and Doner⁵).

$$\eta_2 = \frac{G_{12f} - G_m}{G_{12f} + \xi_2 G_m}$$

and ξ_2 = reinforcing efficiency factor for in-plane shear.

Best agreement with experimental results has been found for $\xi_2 = 1$. For $\xi_2 = 1$, the relation in Eq. (3.101) becomes

$$G_{12} = G_m \frac{(G_{12f} + G_m) + V_f (G_{12f} - G_m)}{(G_{12f} + G_m) - V_f (G_{12f} - G_m)} \quad (3.102)$$

This expression is identical to that derived by the self-consistent field model and to the lower bound of the variational approach. The variation of in-plane shear modulus as a function of fiber volume ratio for several composite materials obtained from numerical results by Adams and Doner⁵ is shown in Figure 3.15.

References

1. E. Betti, *Il Nuovo Cimento*, Ser. 2, Vols. 7 and 8, 1872.
2. R. M. Jones, *Mechanics of Composite Materials*, Hemisphere Publishing Co., New York, 1975.
3. Z. Hashin, "Analysis of Composite Materials—A Survey," *J. Appl. Mech.*, Vol. 50, 1983, pp. 481–505.
4. D. F. Adams and D. R. Doner, "Transverse Normal Loading of a Unidirectional Composite," *J. Composite Materials*, Vol. 1, 1967, pp. 152–164.
5. D. F. Adams and D. R. Doner, "Longitudinal Shear Loading of a Unidirectional Composite," *J. Composite Materials*, Vol. 1, 1967, pp. 4–17.
6. R. Hill, "Theory of Mechanical Properties of Fibre-Strengthened Materials: III, Self-Consistent Model," *J. Mech. Phys. Solids*, Vol. 13, 1965, p. 189.
7. J. M. Whitney and M. B. Riley, "Elastic Properties of Fiber Reinforced Composite Materials," *AIAA J.*, Vol. 4, 1966, p. 1537.
8. B. Paul, "Prediction of Elastic Constants of Multiphase Materials," *Trans. Metal., Soc. AIME*, Vol. 218, 1960, pp. 36–41.
9. Z. Hashin and B. W. Rosen, "The Elastic Moduli of Fiber-Reinforced Materials," *J. Appl. Mech.*, Vol. 21, 1964, pp. 233–242.
10. J. C. Halpin and S. W. Tsai, *Effects of Environmental Factors on Composite Materials*, Air Force Technical Report AFML-TR-67-423, Wright Aeronautical Labs, Dayton, OH, 1967.
11. I. M. Daniel, "Photoelastic Investigation of Composites," in *Composite Materials*, Vol. 2, "Mechanics of Composite Materials" (Vol. Ed., G. P. Sendeckyj; Series Eds., L. J. Broutman and R. H. Krock), Academic Press, New York, 1974.

PROBLEMS

- 3.1 Derive relations in Eqs. (3.52) and (3.53) from Eqs. (3.18), (3.48), (3.50), and (3.51).
- 3.2 Assuming that the stiffness and compliance matrices are positive definite, i.e., they have positive principal values (C_{11} , C_{22} , $C_{33} > 0$), and using Eqs. (3.48) to (3.53), prove that Poisson's ratios of an orthotropic material must satisfy the condition

$$|\nu_{ij}| < \left(\frac{E_i}{E_j}\right)^{1/2} \quad (i, j = 1, 2, 3)$$

- 3.3 Derive transformation relations for Q_{xx} , Q_{xy} , Q_{xs} , and Q_{ss} (Eq. 3.67).
- 3.4 Derive transformation relation for E_x (Eq. 3.81).
- 3.5 Derive transformation relation for G_{xy} (Eq. 3.81).
- 3.6 Derive transformation relation for ν_{xy} (Eq. 3.81).
- 3.7 Derive transformation relation for η_{xs} (Eq. 3.81).
- 3.8 Show that the transformed stiffness Q_{xx} can be expressed in the form

$$Q_{xx} = U_1 + U_2 \cos 2\theta + U_3 \cos 4\theta$$

Determine U_1 , U_2 , and U_3 , and show that they are invariants, i.e., independent of orientation of coordinate axes.

- 3.9 Using the equations of stiffness transformation, prove that the quantity $Q_{11} + Q_{22} + 2Q_{12}$ is an invariant, i.e., it is independent of axes orientation, by showing that

$$Q_{xx} + Q_{yy} + 2Q_{xy} = Q_{11} + Q_{22} + 2Q_{12}$$

for any angle θ between the fiber direction and the reference axes.

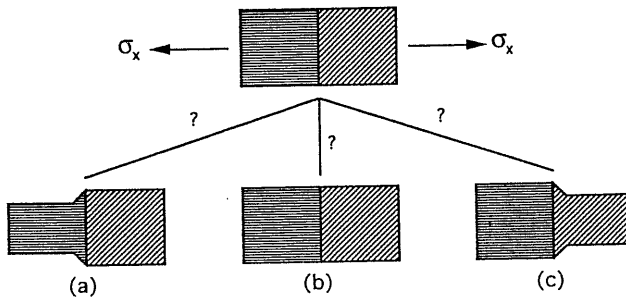
- 3.10** Write stress-strain relations for a unidirectional lamina in terms of engineering constants referred to an arbitrary coordinate system (x, y) .
- 3.11** A specimen is made by joining along one edge two unidirectional laminae at 0° and 45° to the loading axis, as shown below. How is the specimen going to deform in the transverse direction (a , b , or c) for a material of the following properties? Prove your answer by numerical computation.

$$E_1 = 145 \text{ GPa (21 Msi)}$$

$$E_2 = 10.4 \text{ GPa (1.5 Msi)}$$

$$G_{12} = 7.6 \text{ GPa (1.1 Msi)}$$

$$\nu_{12} = 0.28$$



- 3.12** Knowing E_1 , E_2 , ν_{12} and $(E_x)_{\theta=45^\circ}$ (modulus at 45° to the fiber direction), determine G_{12} , first exactly and then using approximation for high stiffness composites.
- 3.13** Knowing E_1 , E_2 , G_{12} , and ν_{12} for a unidirectional lamina, determine $(\nu_{xy})_{\theta=45^\circ}$, first exactly and then using approximation for high stiffness composites. Compare numerical values for a carbon-epoxy material having the following properties:

$$E_1 = 145 \text{ GPa (21 Msi)}, E_2 = 10.45 \text{ GPa (1.5 Msi)},$$

$$G_{12} = 6.9 \text{ GPa (1.0 Msi)}, \nu_{12} = 0.28$$

- 3.14** Compare exact and approximate values of Young's modulus at 45° with the fiber direction for the material of problem 3.13.
- 3.15** Compare exact and approximate values of the shear modulus $(G_{xy})_{\theta=45^\circ}$ for the material of problem 3.13.

- 3.16** Compare exact and approximate values of $(\eta_{sx})_{\theta=45^\circ}$ for the material of problem 3.13.
- 3.17** Find a general expression for the coupling coefficient η_{sx} for a unidirectional composite with fiber orientation $\theta = 45^\circ$ in terms of lamina properties. Then, obtain an approximate expression for a high stiffness composite. Is η_{sx} a fiber-dominated or matrix-dominated property?
- 3.18** Determine Poisson's ratio ν_{xy} at angle $\theta = 30^\circ$ with the fiber direction for a material with the following properties:

$$E_1/E_2 = 3, G_{12}/E_2 = 0.5 \text{ and } \nu_{12} = 0.25$$

- 3.19** A unidirectional lamina is characterized by determining E_1 and E_2 . Subsequently, it is loaded at an angle $\theta = 30^\circ$ with the fibers and the modulus $(E_x)_{\theta=30^\circ}$ is determined. Obtain a relationship for the modulus $(E_x)_{\theta=45^\circ}$ in terms of E_1 , E_2 and $(E_x)_{\theta=30^\circ}$.
- 3.20** A unidirectional lamina is loaded at angles $\theta = 30^\circ$ and 60° with the fiber direction and the corresponding moduli $(E_x)_{\theta=30^\circ}$ and $(E_x)_{\theta=60^\circ}$ are obtained. Determine a relationship between these two moduli and E_1 and E_2 . Find an approximate expression for E_2 in terms of $(E_x)_{\theta=30^\circ}$ and $(E_x)_{\theta=60^\circ}$ for a high stiffness composite ($E_1 \gg E_2$).
- 3.21** A woven carbon/epoxy composite has identical moduli and Poisson's ratios in the warp and fill directions, $E_1 = E_2$ and $\nu_{12} = \nu_{21} = 0.02$. Determine the maximum values of Poisson's ratio, $(\nu_{xy})_{\max}$, shear coupling coefficient, $(\eta_{sx})_{\max}$, and the corresponding angles θ with the principal directions.
- 3.22** Determine the extreme values of the shear coupling coefficient η_{sx} and corresponding angles with the principal directions for a woven-glass/epoxy composite with the following properties:

$$E_1 = 15.8 \text{ GPa (2.3 Msi)}$$

$$E_2 = 12.9 \text{ GPa (1.9 Msi)}$$

$$G_{12} = 2.7 \text{ GPa (0.4 Msi)}$$

$$\nu_{12} = 0.16$$

- 3.23** Using the transformation relation for E_x in Eq. (3.81), determine its maximum and minimum values (by using derivatives of E_x with respect

to θ). Prove that E_x can have a maximum value for some value of θ ($0 < \theta < 90^\circ$) when

$$G_{12} > \frac{E_1}{2(1 + \nu_{12})}$$

(This means that for some orthotropic materials, the off-axis modulus E_x can be higher than E_1 .)

- 3.24** Using the same procedure as in the preceding problem, prove that E_x can have a minimum value for some value of θ ($0^\circ < \theta < 90^\circ$) when

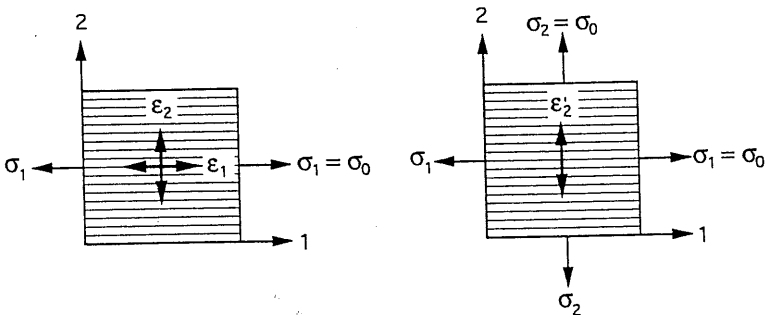
$$G_{12} < \frac{E_1}{2[(E_1/E_2) + \nu_{12}]}$$

(This means that for some orthotropic materials, the off-axis modulus E_x can be lower than E_2 .)

- 3.25** Using the same procedure as in Problem 3.23, prove that E_x attains its maximum value E_1 at $\theta = 0^\circ$ and its minimum value E_2 at $\theta = 90^\circ$ when

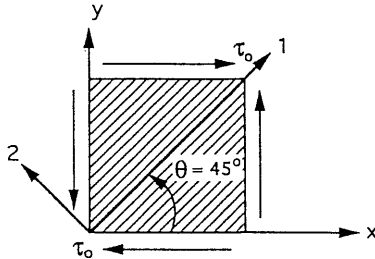
$$\frac{E_1}{2[(E_1/E_2) + \nu_{12}]} < G_{12} < \frac{E_1}{2(1 + \nu_{12})}$$

- 3.26** A unidirectional lamina is loaded under a uniaxial stress $\sigma_1 = \sigma_0$, and principal strains ϵ_1 and ϵ_2 are measured. Compute transverse strain ϵ'_2 of the same lamina loaded under equal biaxial normal stresses $\sigma_1 = \sigma_2 = \sigma_0$ as a function of ϵ_1 and ϵ_2 obtained before and the modulus ratio $k_E = E_1/E_2$.



- 3.27** For a unidirectional lamina loaded in pure shear τ_0 at 45° with the fiber direction, obtain expressions for the three strain components ϵ_x , ϵ_y , and

γ_s as a function of the basic engineering properties $E_1, E_2, G_{12}, \nu_{12}$ (and/or ν_{21}), and the shear stress τ_0 . Obtain first the exact relations and then the approximate ones for a high stiffness composite.



3.28 An off-axis unidirectional lamina is loaded as shown and the strain ϵ_x in the x -direction is measured with a strain gage.

- a. Find an expression for the shear coupling coefficient η_{sx} in terms of $E_x, G_{xy}, \sigma_x, \tau_s$, and the measured strain ϵ_x .
- b. Determine the shear strain γ_s for the following values:

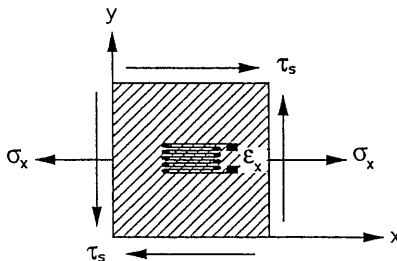
$$\epsilon_x = 2 \times 10^{-3} \text{ m/m}$$

$$E_x = 58.7 \text{ GPa (8.5 Msi)}$$

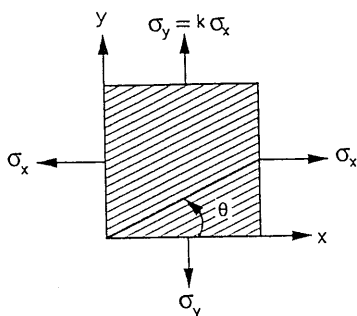
$$G_{xy} = 9.7 \text{ GPa (1.4 Msi)}$$

$$\sigma_x = 193 \text{ MPa (28 ksi)}$$

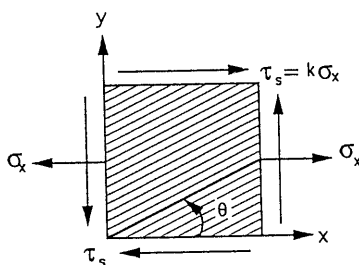
$$\tau_s = 48.3 \text{ MPa (7 ksi)}$$



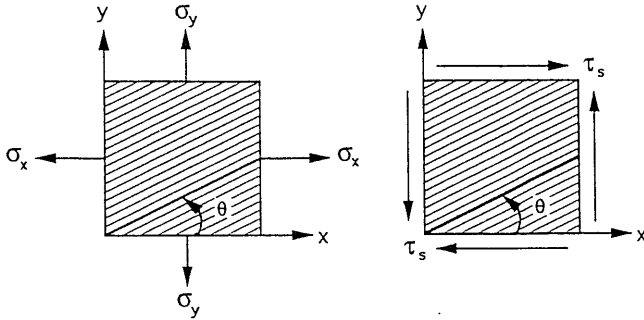
3.29 An off-axis unidirectional lamina is loaded under biaxial normal loading along the x - and y -axes. Find an expression for the ratio of the two normal stresses, $k = \sigma_y/\sigma_x$, such that there is no shear deformation in the lamina. Obtain first an exact expression and then an approximate one for a high stiffness composite, with $E_2 = 2G_{12}$.



- 3.30** An off-axis unidirectional lamina is loaded as shown under uniaxial tension and in-plane shear at an angle to the fiber direction. Express the normal strains ϵ_x and ϵ_y in terms of the engineering properties (E_x , E_y , G_{xy} , ν_{xy} , ν_{yx} , η_{xs} , η_{ys} , η_{sx} , η_{sy}). What relation must the engineering properties satisfy, so that for a certain ratio of σ_x/τ_s , the material behaves as an infinitely rigid one, i.e., $\epsilon_x = \epsilon_y = 0$? What is the stress ratio σ_x/τ_s in that case?

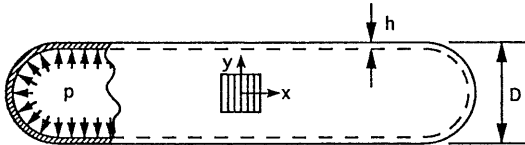


- 3.31** For the same lamina and loading of Problem 3.30
- Determine the ratio $k = \tau_s/\sigma_x$ in terms of the off-axis engineering constants (E_x , E_y , G_{xy} , ν_{xy} , ν_{yx} , η_{xs} , η_{ys} , η_{sx} , η_{sy}) for which the shear strain $\gamma_s = 0$.
 - What relationship must the engineering constants satisfy in order that $\epsilon_y = 0$ for the above loading ratio?
 - For the same loading ratio, under what condition is $\epsilon_x = 0$?
- 3.32** A unidirectional lamina is loaded as shown, first under biaxial normal loading σ_x and σ_y and then under pure shear τ_s , both at the same angle θ with the fiber direction. The strains produced by the first (biaxial) loading are ϵ_x^A , ϵ_y^A and γ_s^A ; the strains produced by the second (shear) loading are ϵ_x^S , ϵ_y^S and γ_s^S . Develop expressions for ϵ_x^A and γ_s^A in terms of σ_x , σ_y , ϵ_x^A , τ_s , ϵ_x^S , ϵ_y^S , E_x and E_y .



- 3.33 Two cylindrical pressure vessels made of the same unidirectional lamina but with different fiber orientations were loaded as shown and gave the following strain readings:

Cylinder A



Diameter: $D = 100 \text{ mm}$

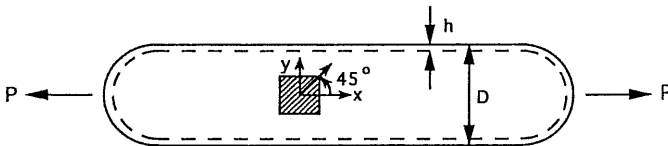
Thickness: $h = 5 \text{ mm}$

Hoop wound (i.e., fibers in circumferential direction)

Internal pressure: $p = 20 \text{ MPa}$

Measured strains: $\epsilon_x = 8 \times 10^{-3}$, $\epsilon_y = \epsilon_\theta = 2.75 \times 10^{-3}$

Cylinder B



Diameter: $D = 100 \text{ mm}$

Thickness: $h = 5 \text{ mm}$

Helically wound at $\theta = 45^\circ$

Axial load: $P = 147 \text{ kN}$

Measured strain: $\epsilon_x = 7 \times 10^{-3}$

Assuming $\nu_{12} = 0.3$, determine lamina moduli E_1 , E_2 , G_{12} .

- 3.34 Determine the transverse modulus E_2 of a carbon/epoxy composite with the following properties:

$$E_{2f} = 14.8 \text{ GPa (2.15 Msi)}$$

$$E_m = 3.45 \text{ GPa (0.5 Msi)}$$

$$\nu_m = 0.36$$

$$V_f = 0.65$$

using the mechanics of materials approach and the Halpin–Tsai relationship with $\xi_1 = 1$.

- 3.35** Determine the transverse modulus E_2 of silicon carbide/aluminum (SiC/Al) composite with the properties

$$E_{2f} = 366 \text{ GPa (53 Msi)}$$

$$E_m = 69 \text{ GPa (10 Msi)}$$

$$\nu_m = 0.33$$

$$V_f = 0.40$$

using the mechanics of materials approach and the Halpin–Tsai relationship with $\xi_1 = 2$.

- 3.36** Determine the in-plane shear modulus G_{12} of a glass/epoxy composite with the properties

$$G_f = 28.3 \text{ GPa (4.10 Msi)}$$

$$G_m = 1270 \text{ MPa (184 ksi)}$$

$$V_f = 0.55$$

using the mechanics of materials approach and the Halpin–Tsai relationship with $\xi_2 = 1$.

Chapter 4

Strength of Unidirectional Lamina

4.1 Micromechanics of Failure; Failure Mechanisms

In the preceding chapter, the elastic behavior of the lamina was discussed primarily from a macroscopic point of view with only a brief review of the micromechanical relationships between lamina and constituent properties. In the case of failure phenomena and strength of a lamina, it is important to understand first the underlying failure mechanisms and processes within the constituents of the composite and their effect on the ultimate macroscopic behavior (see Sect. 2.6). For this reason, the micromechanics of failure is dealt with here in more detail and with more emphasis than was the micromechanics of elastic behavior in Chapter 3 and precedes the macromechanical discussion.

The failure mechanisms and processes on a micromechanical scale vary with type of loading and are intimately related to the properties of the constituents, i.e., fiber, matrix, and interface–interphase. These processes and predictions of macroscopic strength are discussed below for various types of loading.

4.1.1 Longitudinal Tension

Under longitudinal tension, the phase with the lower ultimate strain will fail first. For perfectly bonded fibers, the average longitudinal stress in the composite, σ_1 , is given by the rule of mixtures as

$$\sigma_1 = \sigma_f V_f + \sigma_m V_m \quad (4.1)$$

where

σ_f, σ_m = Average longitudinal stresses in the fiber and matrix, respectively

V_f, V_m = fiber and matrix volume ratios, respectively

Under the simple deterministic assumption of uniform strengths, two cases are distinguished depending on the relative magnitudes of the ultimate tensile strains of the constituents.

In the case in which the ultimate tensile strain of the fiber is lower than that of the matrix, i.e., when

$$\epsilon_{ft}^u < \epsilon_{mt}^u \quad (4.2)$$

the composite will fail when its longitudinal strain reaches the ultimate tensile strain in the fiber (Fig. 4.1). Then, the longitudinal tensile strength of the composite can be approximated by the relation

$$F_{1t} \cong F_{ft} V_f + \sigma'_m V_m \quad (4.3)$$

where

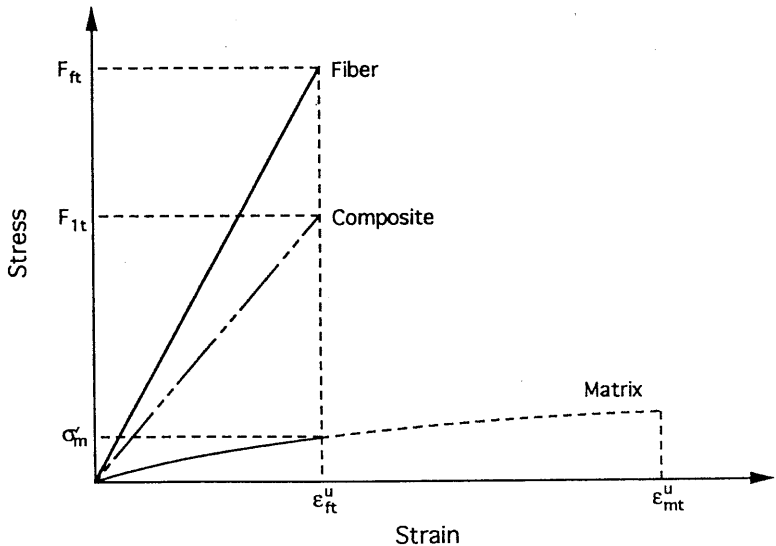


Fig. 4.1 Longitudinal stress-strain curves for composite and constituents for case of fiber-dominated strength ($\epsilon_{ft}^u < \epsilon_{mt}^u$).

F_{1t} = Longitudinal composite tensile strength

F_{ft} = Longitudinal fiber tensile strength

σ'_m = Average longitudinal matrix stress

when ultimate fiber strain is reached.

Assuming linear elastic behavior for the constituents, Eq. (4.3) is written as

$$\begin{aligned} F_{1t} &\cong F_{ft} V_f + E_m \epsilon_{ft}^u V_m \\ &= F_{ft} \left(V_f + V_m \frac{E_m}{E_f} \right) \end{aligned} \quad (4.4)$$

For composites with very stiff fibers, i.e., when $E_f \gg E_m$, and reasonable values of V_f , the above relation can be further simplified as

$$F_{1t} \cong F_{ft} V_f \quad (4.5)$$

When the ultimate tensile strain of the matrix is lower than that of the fiber, i.e., when

$$\epsilon_{mt}^u < \epsilon_{ft}^u \quad (4.6)$$

the composite fails when its longitudinal strain reaches the ultimate tensile strain of the matrix (Fig. 4.2). Then the longitudinal tensile strength of the composite can be approximated by the relation

$$F_{1t} \cong \sigma'_f V_f + F_{mt} V_m \quad (4.7)$$

which can be further approximated as

$$F_{1t} \cong F_{mt} \left(V_f \frac{E_f}{E_m} + V_m \right) \quad (4.8)$$

where

F_{mt} = Matrix tensile strength

σ'_f = Longitudinal fiber stress when ultimate matrix strain is reached

The results above do not take into consideration the statistical distribution of fiber and matrix strengths. In the case of fiber-dominated strength, for exam-

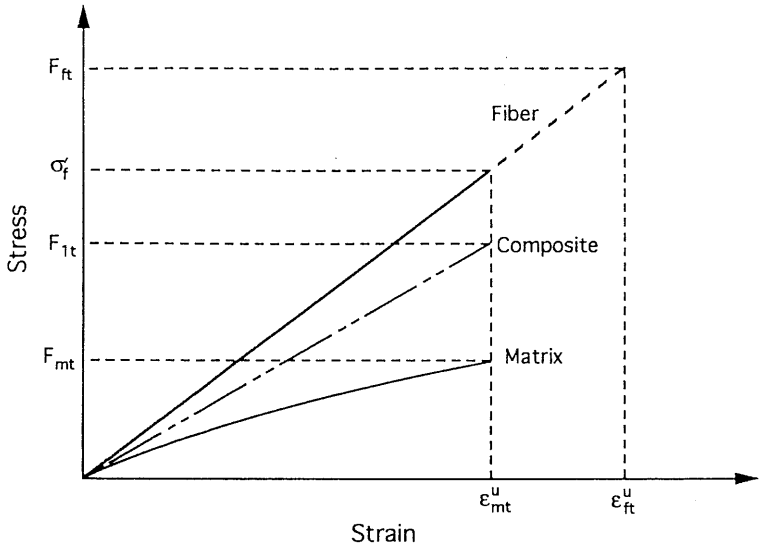


Fig. 4.2 Longitudinal stress-strain curves for composite and constituents for case of matrix-dominated strength ($\epsilon_{mt}^u < \epsilon_{ft}^u$).

ple, fiber strength varies from point to point and from fiber to fiber. Not all fibers fail simultaneously, but isolated single fiber breaks (singlets) occur at weak points. A nonuniform state of stress is developed around the fiber break (Fig. 4.3).¹ An interfacial shear stress results with a high peak near the fiber break and helps transfer the stress to the broken fiber. The stress transmitted by the fiber is zero at the break but increases gradually to the far-field value at some characteristic distance, δ , from the break. This is the same distance at which the interfacial shear stress drops to zero. The effect of the fiber break on adjacent fibers is a local increase in both fiber stress and interfacial shear stress. The net effect of a single fiber break is to reduce the load-carrying fiber length by the ineffective length 2δ .

Depending on the properties of the constituents, these initial fiber breaks produce different types of failure in their vicinity (Fig. 4.4).² These failure mechanisms take the following forms: (1) transverse matrix cracking in composites with a brittle matrix and a relatively strong interface, (2) fiber matrix debonding in the case of a relatively weak interface and/or relatively high ultimate fiber strain, and (3) conical shear fractures in matrix in the case of a relatively ductile matrix and a strong interface. In most cases the damage is localized and arrested by the adjacent fibers. The net effect of this localized damage is to increase the ineffective length of the fiber.

As the load increases the single fiber breaks increase in density and interact to produce adjacent fiber breaks (e.g., doublets, triplets) (Fig. 4.5). These

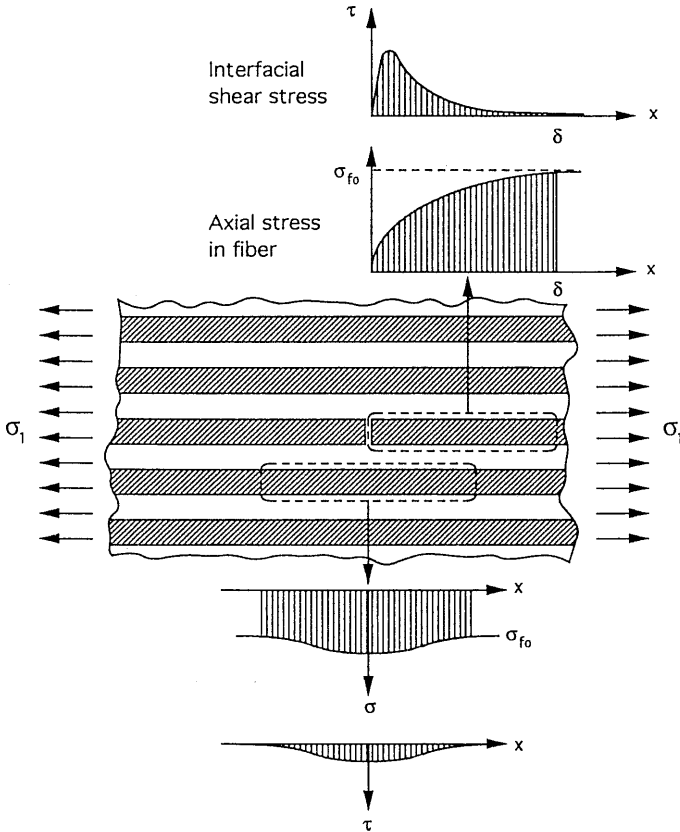


Fig. 4.3 Local stress distributions around a fiber break in a unidirectional composite under longitudinal tension.

localized failures interact and eventually coalesce to produce catastrophic failure. The exact sequence of events and the final failure pattern vary with constituent properties and the fiber volume ratio. Typical failure patterns under longitudinal tension are shown in Figure 4.6 for two composite materials, boron/epoxy and S-glass/epoxy. The boron/epoxy shows more brittle failure and limited fiber/matrix debonding, whereas the glass/epoxy shows extensive interfacial debonding associated with the relatively high ultimate strain of the glass fiber. These results can be incorporated into a statistical analysis to yield the overall composite strength in terms of the fiber volume ratio and the parameters of the statistical distribution of fiber strengths.¹

In the case of brittle-matrix composites, such as ceramic/matrix composites, the failure strain of the matrix is usually lower than that of the fibers and damage initiates with the development of multiple matrix cracks analogous to the fiber

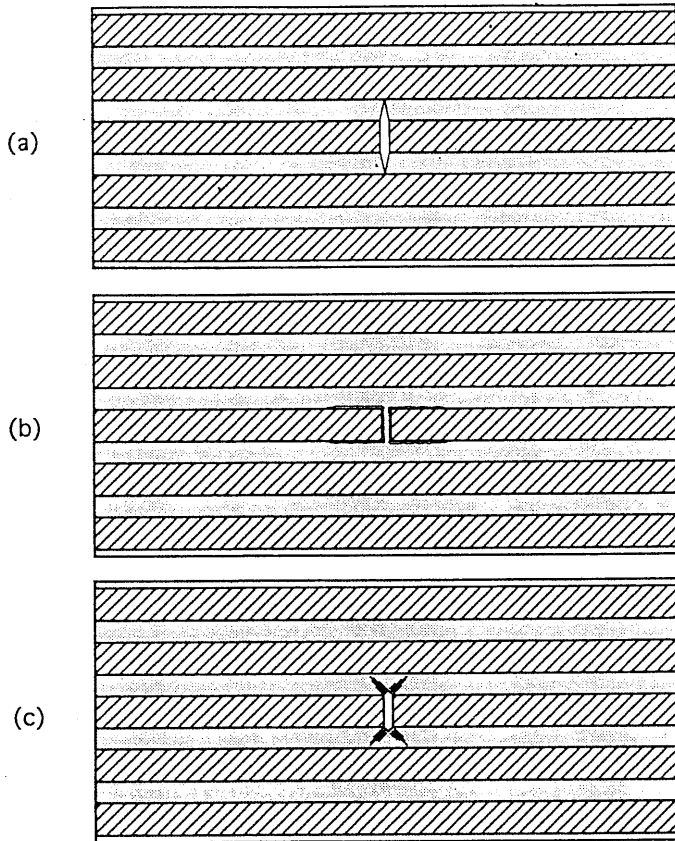


Fig. 4.4 Failure mechanisms around single fiber break in unidirectional composite under longitudinal tension. (a) Transverse matrix cracking for brittle matrix and relatively strong interface. (b) Fiber-matrix debonding for relatively weak interface and/or relatively high fiber ultimate strain. (c) Conical shear fractures in relatively ductile matrix.

breaks discussed before (Fig. 4.7). These cracks produce local stress distributions with high interfacial shear stresses and increased tensile stress in adjacent fibers. These cracks are accompanied or followed by fiber/matrix debonding and fiber breaks. A typical fractograph of such a failure in a silicon carbide/glass ceramic composite is shown in Figure 4.8. It shows clearly the transverse matrix crack, fiber breaks, and fiber pullout. Analysis of stresses and failure mechanisms of such composites provides predictions of longitudinal tensile strength as a function of material and geometric parameters.³

4.1.2 Longitudinal Compression

Under longitudinal compression, failure is assumed to be associated with microbuckling or kinking of the fibers within the matrix (Figs. 4.9, 4.10). At

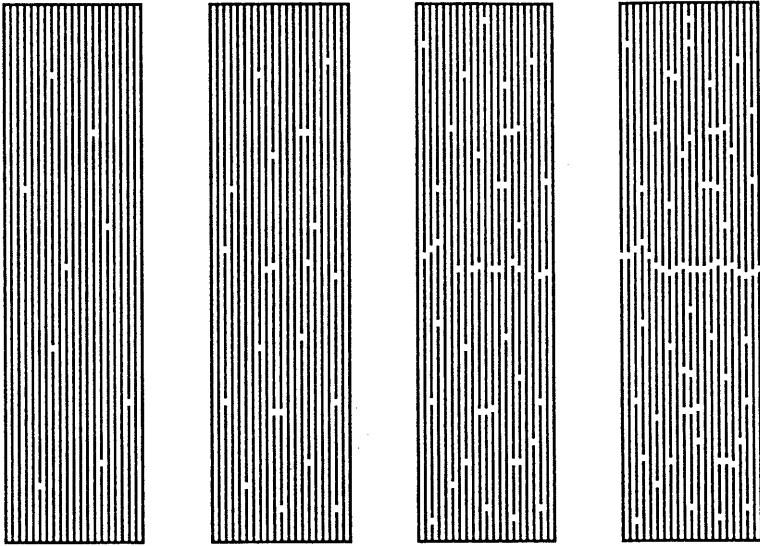


Fig. 4.5 Failure sequence in unidirectional composite with fiber-dominated strength under longitudinal tensile loading.

low values of fiber volume ratio, the extensional or out-of-phase mode of microbuckling is predicted with a compressive strength:⁴

$$F_{1c} \cong 2V_f \left[\frac{E_m E_f V_f}{3(1-V_f)} \right]^{1/2} \quad (4.9)$$

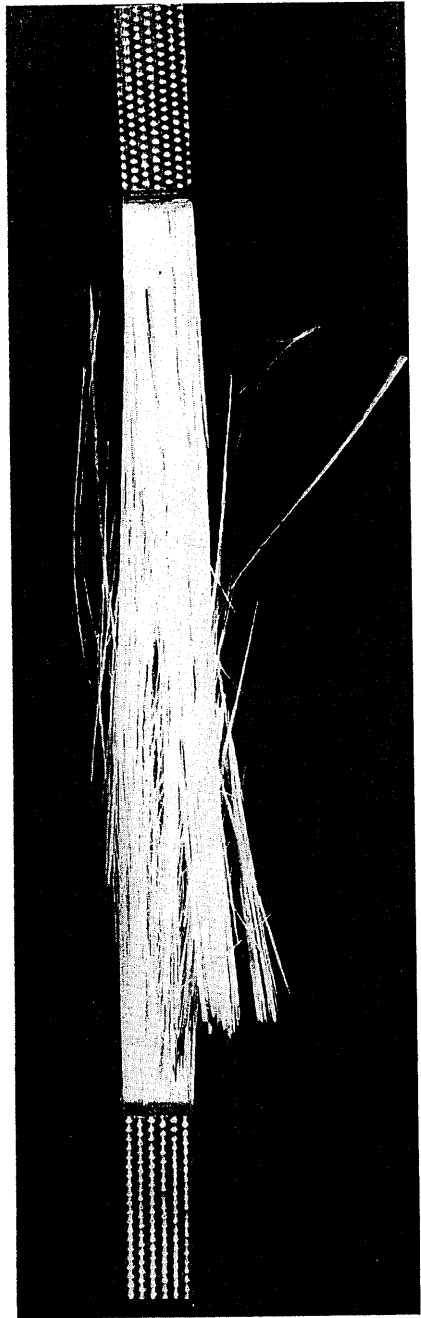
At higher values of V_f the shear or in-phase mode is predicted with a compressive strength:⁴

$$F_{1c} \cong \frac{G_m}{1 - V_f} \quad (4.10)$$

Tensile and compressive stresses in a fiber due to in-phase buckling lead to the formation of kink zones, which can cause pronounced deformation in ductile fibers such as aramid or fracture planes in brittle fibers such as carbon (Fig. 4.10). Figures 4.11 and 4.12 show typical fractographs of unidirectional carbon/epoxy loaded in longitudinal compression. Figure 4.12a shows the stepped nature of the macroscopic failure surface resulting from microbuckling, kinking, and fiber fractures.⁵ Figure 4.12b shows an enlarged view of the same fracture surface showing cracking of the fibers in the direction normal to the axis of microbuckling. As the fiber volume ratio increases, debonding precedes in-phase microbuckling and failure results from the three-dimensional state of



Boron/epoxy



S-glass/epoxy

Fig. 4.6 Typical failure patterns of unidirectional composites under longitudinal tension.

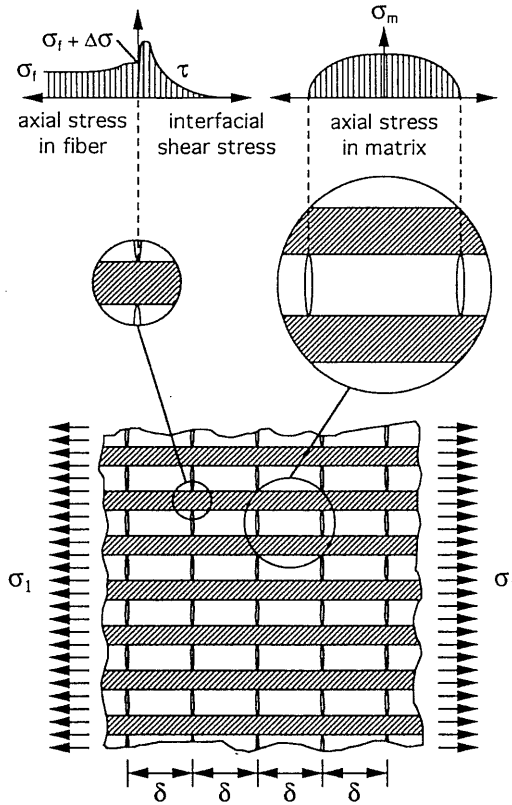


Fig. 4.7 Matrix cracking and local stress distributions in unidirectional brittle matrix composite under longitudinal tension.

stress. At the highest values of V_f for well-aligned fibers one may encounter pure compressive failure, which can be related to shear failure of the fibers.

Another failure mode more likely for the case of high fiber volume ratios is the shear mode governed by the shear strength of the fiber (Fig. 4.13). The predicted strength based on this mode is

$$F_{1c} = 2F_{6f} \left[V_f + (1 - V_f) \frac{E_m}{E_f} \right] \tag{4.11}$$

where F_{6f} is the shear strength of the fiber.

4.1.3 Transverse Tension

The most critical loading of a unidirectional composite is transverse tensile loading. This type of loading results in high stress and strain concentrations in the



Fig. 4.8 Scanning electron microscope (SEM) fractograph of longitudinal tensile failure in silicon carbide/glass ceramic (SiC/CAS) composite.

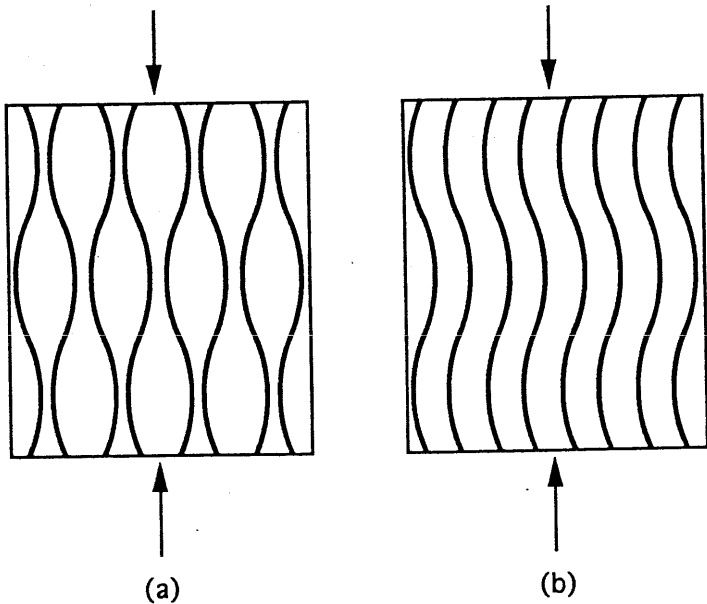


Fig. 4.9 Microbuckling modes in a unidirectional composite under longitudinal compression. (a) Out-of-phase or extensional mode. (b) In-phase or shear mode.

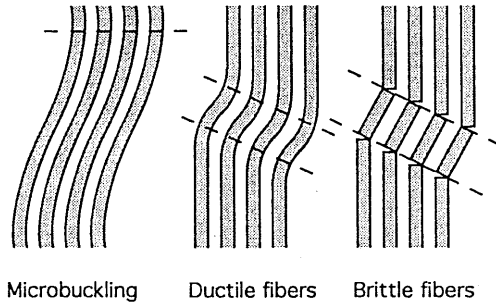


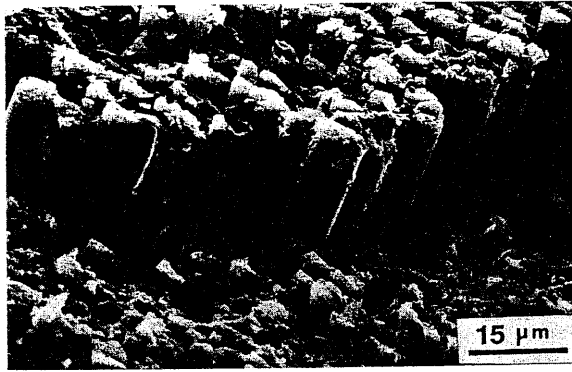
Fig. 4.10 Microbuckling leading to formation of kink zones with excessive deformation or fracture planes for ductile or brittle fibers, respectively.



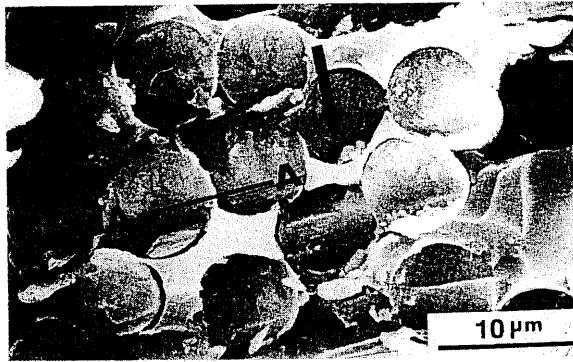
Fig. 4.11 Kink band in unidirectional IM6/3501-6 carbon/epoxy under longitudinal compressive loading.

matrix and interface/interphase. Stress distributions around the fiber can be obtained analytically by finite element, finite difference, complex variable, or boundary element methods and experimentally by means of two- and three-dimensional photoelastic models. The critical stresses and strains usually occur at the fiber/matrix interface.

The peak stress in the matrix for a square array is the axial stress at the interface along the loading direction (Fig. 4.14) The stress concentration factor,



(a)



(b)

Fig. 4.12 Fractograph of carbon/epoxy composite under longitudinal compression.⁵
 (a) Stepped macroscopic fracture surface resulting from microbuckling and kinking.
 (b) Arrow indicates direction of crack propagation normal to microbuckling axis A-A.

defined as the ratio of this peak stress to the applied average stress, is shown in Figure 4.15 as a function of fiber volume ratio for three typical composites. Results shown were obtained by finite difference⁶ and photoelastic⁷ methods. The boron/epoxy material with a fiber to matrix modulus ratio of 120 represents one of the most severe cases. In most other cases the values of stress concentration are lower.

A more characteristic quantity for a transversely loaded composite is the strain concentration factor that is related to the stress concentration factor as follows:⁷

$$k_\epsilon = \frac{\epsilon_{\max}}{\epsilon_2} \cong k_\sigma \left(\frac{E_2}{E_m} \right) \frac{(1 + \nu_m)(1 - 2\nu_m)}{1 - \nu_m} \quad (4.12)$$

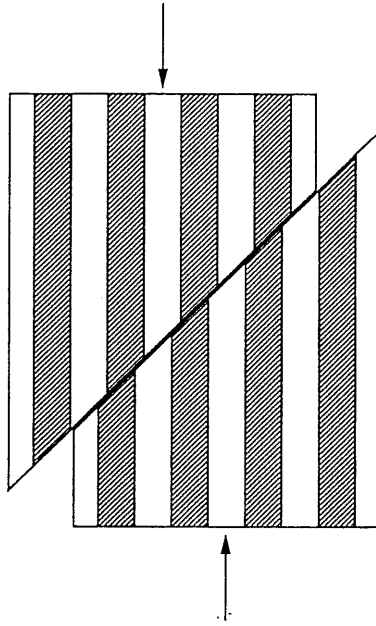


Fig. 4.13 Shear failure mode of unidirectional composite under longitudinal compression.

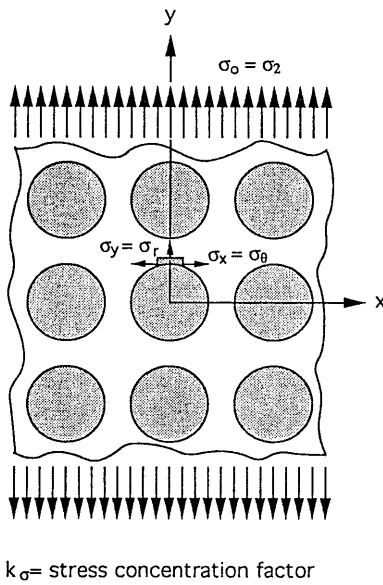


Fig. 4.14 Local stresses in transversely loaded unidirectional composite.

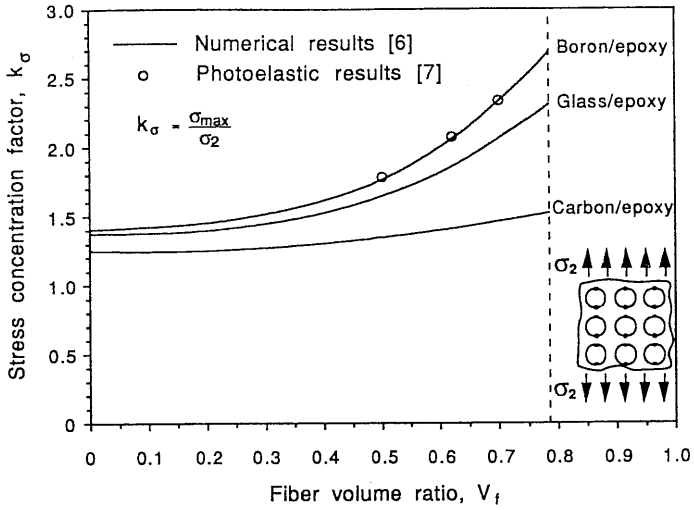


Fig. 4.15 Stress concentration in matrix of unidirectional composites with square fiber array under transverse tension.

where ϵ_{max} and ϵ_2 are the maximum and average strains, respectively and ν_m the matrix Poisson's ratio. In the expression above it was assumed that the fibers are much stiffer than and perfectly bonded to the matrix. The variation of the strain concentration factor with fiber volume ratio for a boron/epoxy composite is shown in Figure 4.16. It is shown how it increases sharply for fiber volume ratios over 0.5.

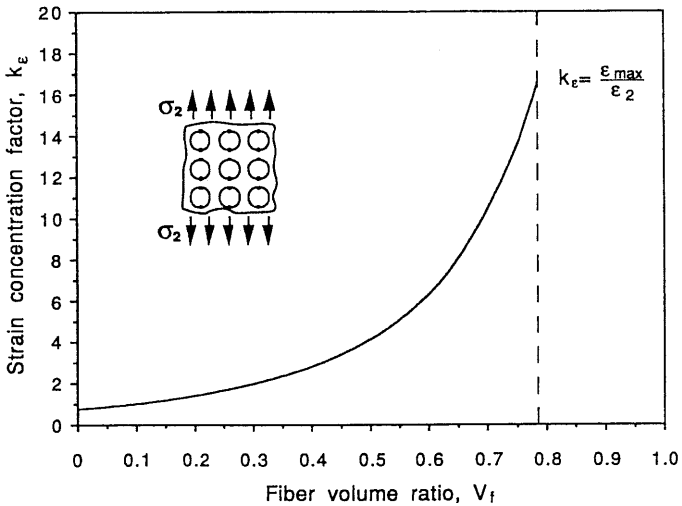


Fig. 4.16 Strain concentration factor in matrix of unidirectional boron/epoxy composite under transverse tension.

In predicting failure of a transversely loaded composite, the residual stresses and strains due to curing of the matrix, or thermal stresses and strains due to thermal expansion mismatch, must be taken into account. Assuming a maximum tensile stress or strain failure criterion and linear elastic behavior to failure for the matrix, one can predict the following transverse tensile strength for a unidirectional composite

$$F_{2t} = \frac{1}{k_{\sigma}} (F_{mt} - \sigma_{rm}) \quad (4.13)$$

for the maximum tensile stress criterion, and

$$F_{2t} = \frac{1 - \nu_m}{k_{\sigma} (1 + \nu_m) (1 - 2\nu_m)} (F_{mt} - \epsilon_{rm} E_m) \quad (4.14)$$

for the maximum tensile strain criterion with very stiff perfectly bonded fibers, where σ_{rm} and ϵ_{rm} are the radial (maximum) residual stress and residual strain, respectively.

This prediction is based on a local deterministic failure criterion at a point. In reality, as in the case of longitudinal tensile loading, failure takes the form of isolated interfacial microcracks increasing in number with loading and finally coalescing into a catastrophic macrocrack (Fig. 4.17). Typical failure patterns under transverse tension are shown in Figure 4.18 for two composite materials, carbon/high modulus epoxy and carbon/polyimide. Typical fractographs of transverse tensile failure are shown in Figures 4.19, 4.20, and 4.21.

4.1.4 Transverse Compression

Under transverse compression a unidirectional composite may fail under a number of failure mechanisms. The high compressive stress concentration at the interface may cause compressive failure in the matrix and/or fiber crushing. The predicted composite strength for this failure mechanism is

$$F_{2c} = \frac{F_{mc} + \sigma_{rm}}{k_{\sigma}} \quad (4.15)$$

where F_{mc} is the compressive strength of the matrix and σ_{rm} is the maximum residual radial stress at the interface. High interfacial shear stresses may cause matrix shear failure and/or debonding leading to an overall shear failure mode, as illustrated schematically in Figure 4.22.

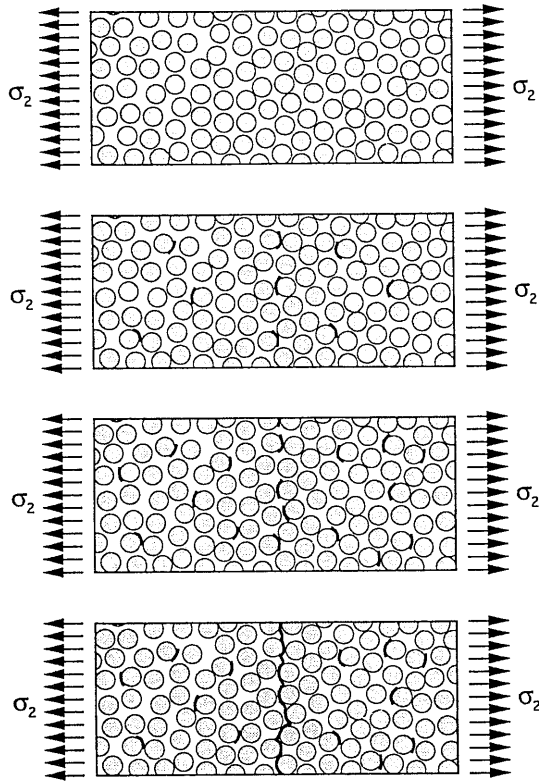


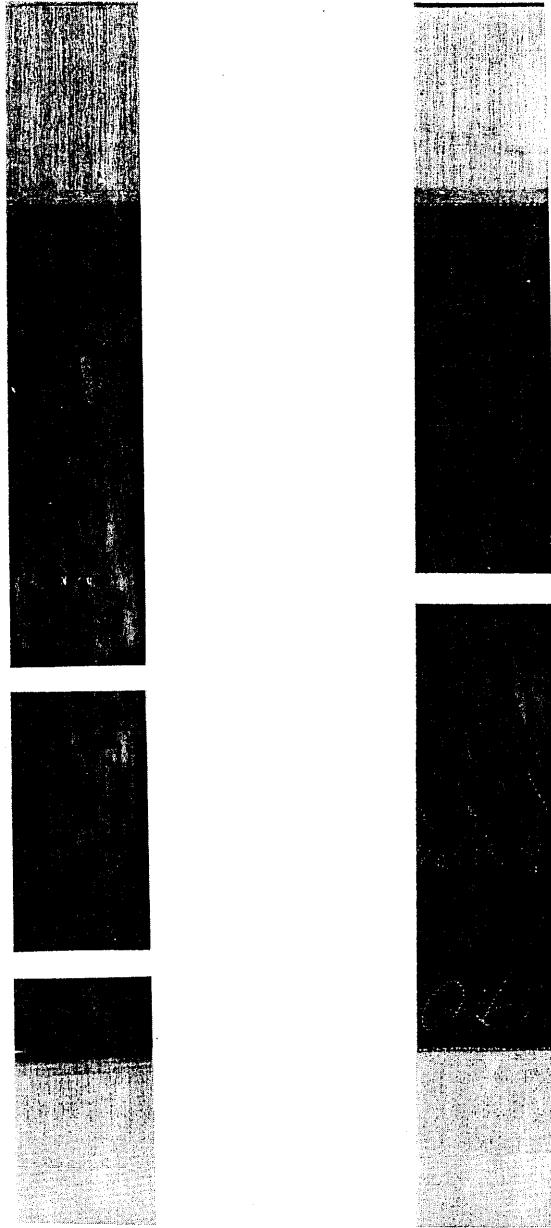
Fig. 4.17 Progressive microcracking leading to ultimate failure in unidirectional composite under transverse tension.

4.1.5 In-Plane Shear

Under in-plane shear, as illustrated in Figure 4.23, a high shear stress concentration develops at the fiber–matrix interface. The variation of the shear stress concentration factor with material and fiber volume ratio has been obtained by a finite difference procedure.⁹ The high shear stress at the interface can cause shear failure in the matrix and/or fiber–matrix debonding (Fig. 4.23). Figure 4.24 shows the failure pattern of a carbon/epoxy composite under in-plane shear. The in-plane shear strength of the composite based on matrix shear failure can be predicted as

$$F_6 = \frac{F_{ms}}{k_\tau} \quad (4.16)$$

where F_{ms} is the matrix shear strength and k_τ the shear stress concentration factor.



Carbon/high modulus epoxy

Carbon/polyimide

Fig. 4.18 Typical failure patterns of unidirectional composites under transverse tension.

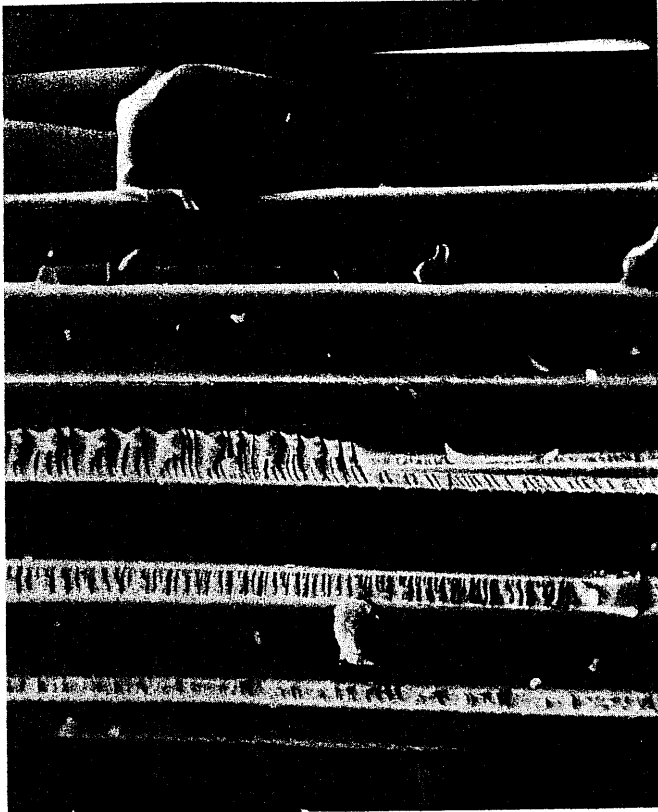


Fig. 4.19 Scanning electron microscope (SEM) fractograph of transverse tensile failure in E-glass/epoxy composite (brittle matrix).⁸

4.2 Macromechanical Strength Parameters

As discussed before, the failure mechanisms vary greatly with material properties and type of loading. Strength predictions are based on micromechanical analyses and point failure criteria. Even when the predictions are accurate with regard to failure initiation at critical points, they are only approximate as far as global failure of the lamina is concerned. Furthermore, the possible interaction of failure mechanisms makes it difficult to obtain reliable strength predictions under a general type of loading. For these reasons, a macromechanical or phenomenological approach to failure analysis may be preferable.

From the macromechanical point of view, the strength of a lamina is an anisotropic property, i.e., it varies with orientation. It is desirable, for example, to correlate the strength along an arbitrary direction to some basic strength parameters. A lamina may be characterized by a number of basic strength parameters

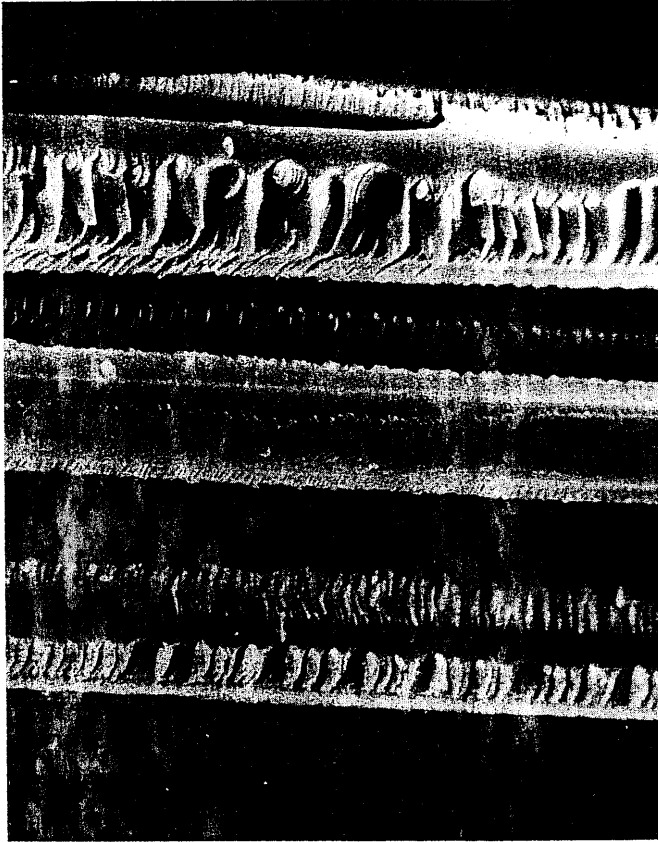


Fig. 4.20 Scanning electron microscope (SEM) fractograph of transverse tensile failure in E-glass/epoxy composite (ductile matrix).⁸

referred to its principal material directions in a manner analogous to the stiffness parameters defined before. For in-plane loading, a lamina may be characterized by five strength parameters, as listed in Figure 4.25. All strength parameters are used in their absolute numerical values.

This characterization recognizes the fact that most composite materials have different strengths in tension and compression. No distinction is necessary between positive and negative shear strength as long as it is referred to the principal material directions. This is illustrated in Figure 4.26 where a unidirectional lamina is subjected to positive and negative shear stress according to the sign convention used in mechanics of materials. As can be observed, both cases are equivalent to equal tensile and compressive normal loading at 45° with the fiber direction. Thus the sign of the shear stress is immaterial. The shear strength

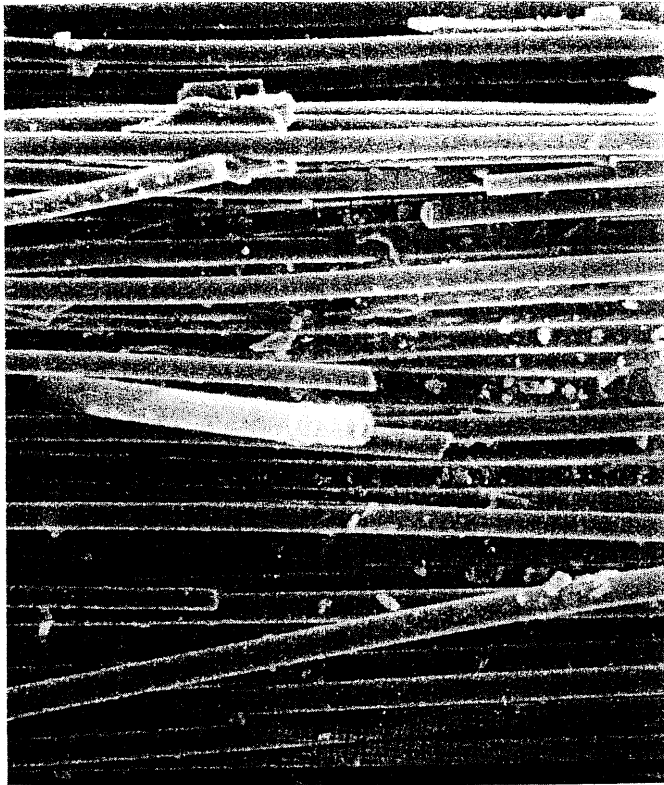


Fig. 4.21 Scanning electron microscope (SEM) fractograph of transverse tensile failure in silicon carbide/glass ceramic (SiC/CAS) composite.

referred to the principal material directions does not depend on the difference between tensile and compressive strengths of the material.

However, this is not the case when the shear stress is applied at an angle with the principal material directions. Figure 4.27 shows an example of a lamina loaded in shear at 45° with the fiber direction. As can be observed, positive shear stress corresponds to a tensile stress in the fiber direction and an equal compressive stress in the transverse to the fiber direction, whereas negative shear stress corresponds to a compressive stress in the fiber direction and an equal tensile stress in the transverse direction. Since most composites have different tensile and compressive strengths and they are weakest in transverse tension, it follows that in this case the lamina would be stronger under positive shear.

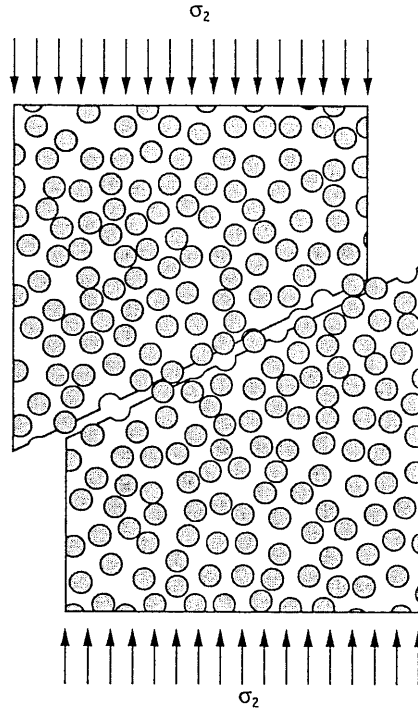


Fig. 4.22 Shear failure mode in unidirectional composite under transverse compression.

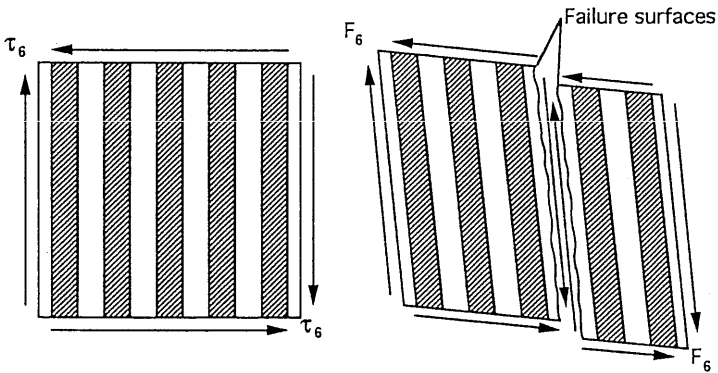


Fig. 4.23 Failure mode of unidirectional composite under in-plane shear.

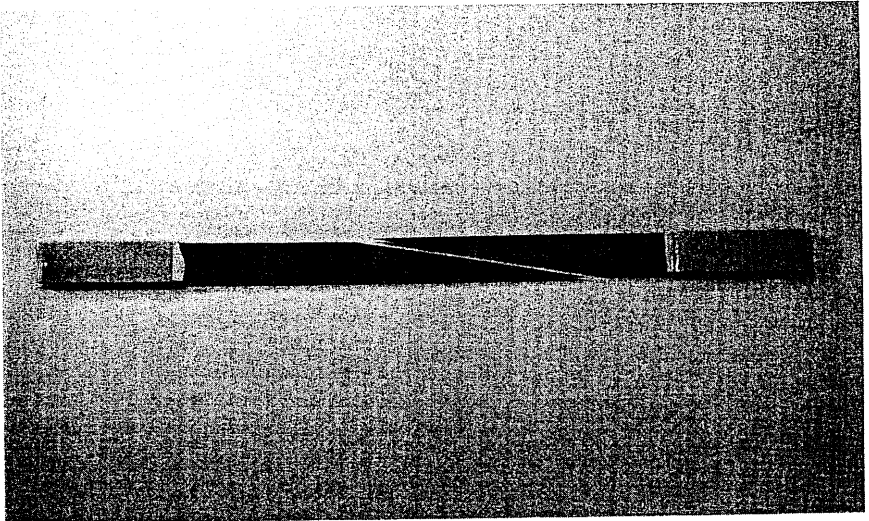


Fig. 4.24 Failure pattern of unidirectional carbon/epoxy composite under in-plane shear (10° off-axis specimen loaded in axial tension).

Four additional lamina strength parameters, which are relevant in three-dimensional analysis, are the out-of-plane or interlaminar tensile, compressive, and shear strengths, F_{3t} , F_{3c} , F_{23} , and F_{13} . For transversely isotropic composites, with the 2–3 as the plane of isotropy, $F_{3t} \cong F_{2t}$, $F_{3c} \cong F_{2c}$, and $F_{13} \cong F_{12} = F_6$.

Given a state of stress, the principal stresses and their directions are obtained by stress transformation that is independent of material properties. The principal strains and their directions are obtained by using the appropriate anisotropic stress–strain relations and strain transformation. In general, the principal stress, principal strain, and material symmetry directions do not coincide. Since strength varies with orientation, maximum stress alone is not the critical factor in failure. Anisotropic failure theories are needed that take into account both the stress and strength variation with orientation.

4.3 Macromechanical Failure Theories

Failure criteria for homogeneous isotropic materials, such as maximum normal stress (Rankine), maximum shear stress (Tresca), maximum distortional energy (von Mises), and so forth, are well established. Macromechanical failure theories for composites have been proposed by extending and adapting isotropic failure theories to account for the anisotropy in stiffness and strength of the composite. Surveys of anisotropic failure theories have been given by Sandhu¹⁰ and Owen and Rice.¹¹ More than forty such theories have been proposed in recent years.

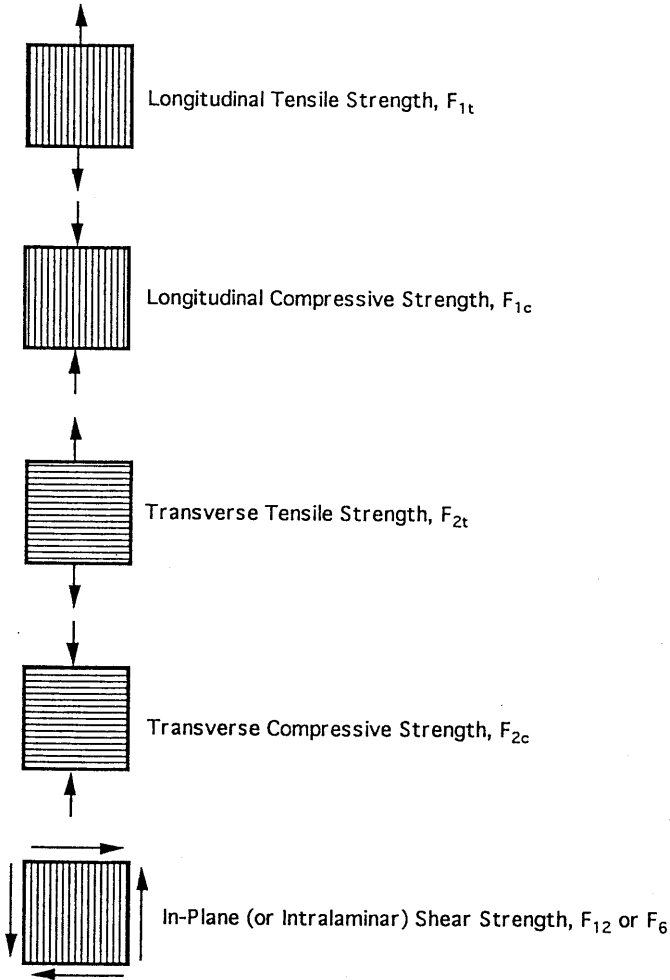


Fig. 4.25 Basic strength parameters of unidirectional lamina.

Almost all of them are based on assumptions of homogeneity and linear stress-strain behavior to failure. All theories can be expressed in terms of the basic strength parameters referred to the principal material axes (Fig. 4.25). Some theories do not account for interaction of stress components while others do so to varying degrees. Some interaction theories require additional strength properties obtained by biaxial testing.

Of all failure theories available, the following four are considered representative and are more widely used:

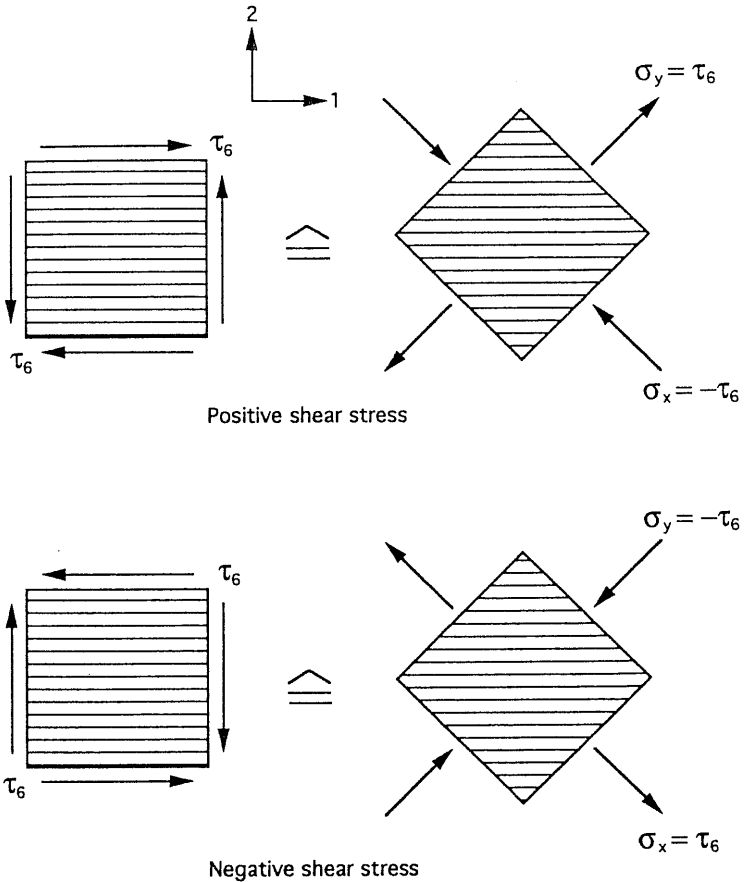


Fig. 4.26 Positive and negative shear stress acting along principal material directions.

1. Maximum stress theory.
2. Maximum strain theory.
3. Deviatoric strain energy theory for anisotropic materials (Tsai-Hill).
4. Interactive tensor polynomial theory (Tsai-Wu).

4.4 Maximum Stress Theory

According to the maximum stress theory, failure occurs when at least one stress component along one of the principal material axes exceeds the corresponding strength in that direction. The stresses acting on a lamina are resolved along

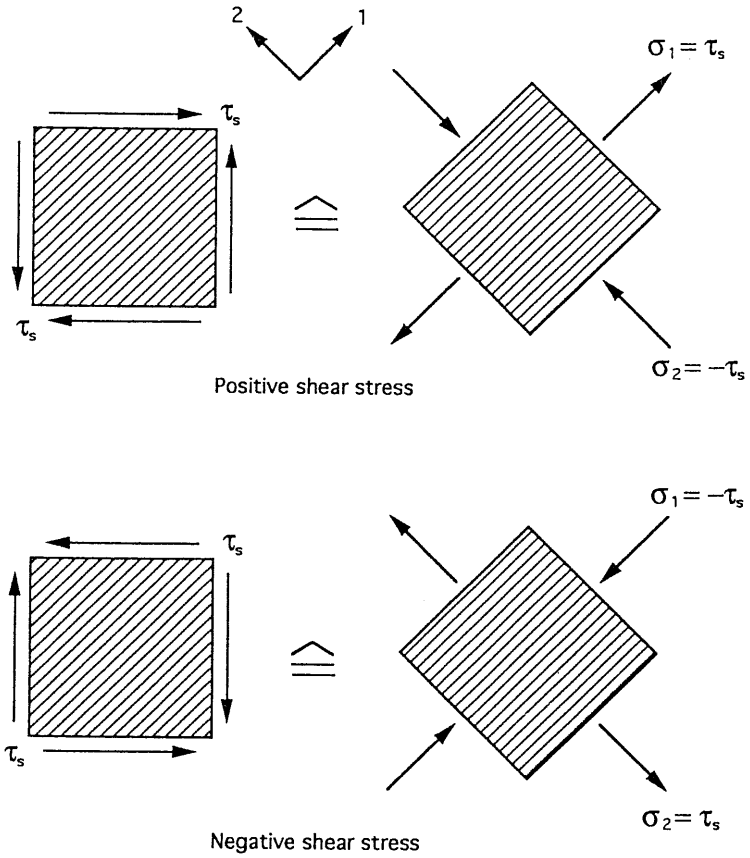


Fig. 4.27 Positive and negative shear stress acting at 45° with principal material directions.

the principal material axes ($\sigma_1, \sigma_2, \tau_6$), and the failure condition is expressed in the form of three subcriteria:

$$\sigma_1 = \begin{cases} F_{1t} & \text{when } \sigma_1 > 0 \\ -F_{1c} & \text{when } \sigma_1 < 0 \end{cases} \quad (4.17a)$$

$$\sigma_2 = \begin{cases} F_{2t} & \text{when } \sigma_2 > 0 \\ -F_{2c} & \text{when } \sigma_2 < 0 \end{cases} \quad (4.17b)$$

$$|\tau_6| = F_6 \quad (4.17c)$$

For a two-dimensional state of stress with $\tau_6 = 0$, the failure envelope takes the form of a rectangle as shown in Figure 4.28.

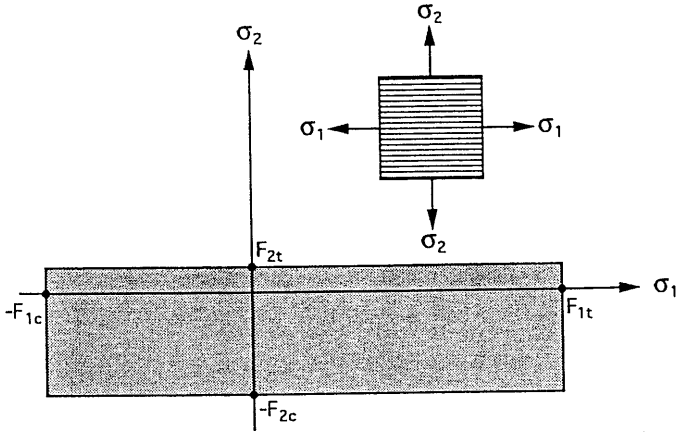


Fig. 4.28 Failure envelope for unidirectional lamina under biaxial normal loading (maximum stress theory).

In the more general case, the stresses are transformed along the principal material axes, and each stress component is related to the corresponding strength parameter. Consider, for example, the case of uniaxial loading of an off-axis lamina (Fig. 4.29). The stress components along the principal material axes are

$$\begin{aligned}
 \sigma_1 &= \sigma_x \cos^2\theta \\
 \sigma_2 &= \sigma_x \sin^2\theta \\
 \tau_6 &= -\sigma_x \sin\theta \cos\theta
 \end{aligned}
 \tag{4.18}$$

By equating the stress components in Eq. (4.18) with the corresponding strengths, we obtain the following ultimate values of σ_x , i.e., the off-axis strength F_x :
 when $\sigma_x > 0$

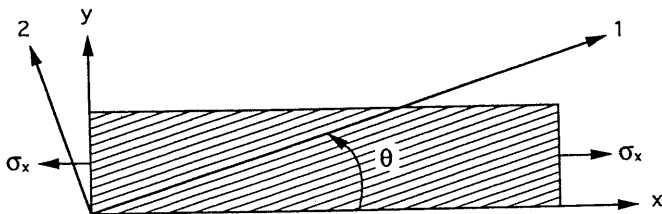


Fig. 4.29 Uniaxial loading of off-axis unidirectional lamina.

$$F_{xt} = \frac{F_{1t}}{\cos^2\theta} \quad (4.19a)$$

$$F_{xt} = \frac{F_{2t}}{\sin^2\theta} \quad (4.19b)$$

$$F_{xt} = \frac{F_6}{\sin\theta \cos\theta} \quad (4.19c)$$

and when $\sigma_x < 0$

$$F_{xc} = \frac{F_{1c}}{\cos^2\theta} \quad (4.20a)$$

$$F_{xc} = \frac{F_{2c}}{\sin^2\theta} \quad (4.20b)$$

$$F_{xc} = \frac{F_6}{\sin\theta \cos\theta} \quad (4.20c)$$

It should be noted that in the case of shear stress and strength referred to the principal material axes, the sign of the shear stress is immaterial and only absolute values need be used.

Using the strength properties of a material such as E-glass/epoxy from Table 2.6, one can obtain the variation of lamina strength as a function of fiber orientation (Fig. 4.30). By taking the lowest values of the predicted strength, we obtain a failure envelope for F_x as a function of θ . This envelope is characterized by cusps at the intersections of the curves for the various subcriteria. Three regions can be identified, corresponding to three different modes of failure, fiber failure (tensile and compressive), in-plane shear failure, and transverse normal stress failure (tensile and compressive).

The maximum stress theory is more applicable for the brittle modes of failure of the material, closer to transverse and longitudinal tension, and does not take into account any stress interaction under a general biaxial state of stress.

4.5 Maximum Strain Theory

According to the maximum strain theory, failure occurs when at least one of the strain components along the principal material axes exceeds the corresponding ultimate strain in that direction. This theory allows for some interaction of stress

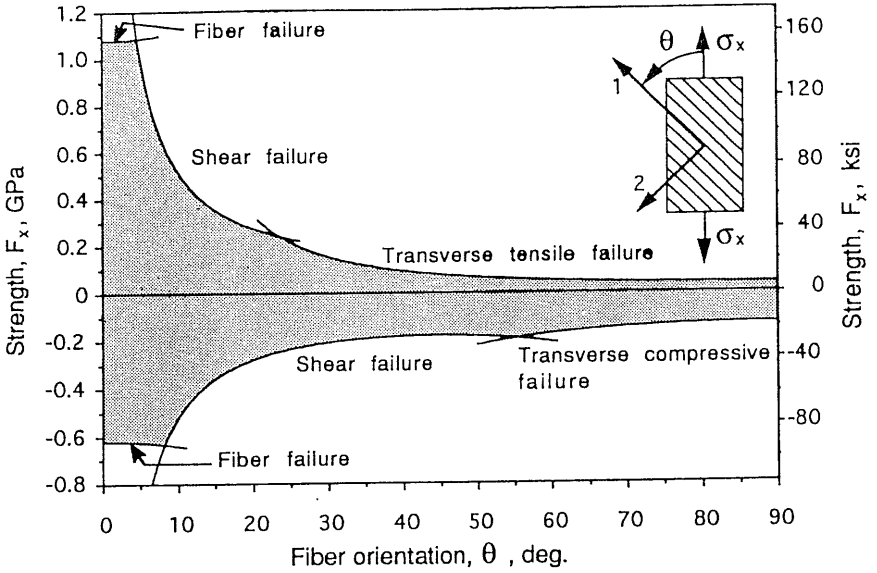


Fig. 4.30 Uniaxial strength of off-axis E-glass/epoxy unidirectional lamina as a function of fiber orientation.

components due to Poisson's effect. It is expressed in the form of the following three subcriteria:

$$\epsilon_1 = \begin{cases} \epsilon_{1t}'' & \text{when } \epsilon_1 > 0 \\ \epsilon_{1c}'' & \text{when } \epsilon_1 < 0 \end{cases} \quad (4.21a)$$

$$\epsilon_2 = \begin{cases} \epsilon_{2t}'' & \text{when } \epsilon_2 > 0 \\ \epsilon_{2c}'' & \text{when } \epsilon_2 < 0 \end{cases} \quad (4.21b)$$

$$|\gamma_6| = 2|\epsilon_{12}| = \gamma_6'' \quad (4.21c)$$

where ϵ_1 , ϵ_2 , γ_6 are the strain components referred to the principal material axes and

ϵ_{1t}'' = Ultimate longitudinal tensile strain

ϵ_{1c}'' = Ultimate longitudinal compressive strain

ϵ_{2t}'' = Ultimate transverse tensile strain

ϵ_{2c}'' = Ultimate transverse compressive strain

γ_6'' = Ultimate in-plane shear strain

To apply the theory for a given general biaxial state of stress, the stress components along the principal material axes σ_1 , σ_2 , and τ_6 are first obtained by stress transformation, and then the corresponding strain components ϵ_1 , ϵ_2 , and γ_6 are obtained by means of the lamina stress-strain relations in Eq. (3.73).

$$\begin{aligned}\epsilon_1 &= \frac{\sigma_1}{E_1} - \nu_{21} \frac{\sigma_2}{E_2} = \frac{1}{E_1} (\sigma_1 - \nu_{12} \sigma_2) \\ \epsilon_2 &= \frac{\sigma_2}{E_2} - \nu_{12} \frac{\sigma_1}{E_1} = \frac{1}{E_2} (\sigma_2 - \nu_{21} \sigma_1) \\ \gamma_6 &= \frac{\tau_6}{G_{12}}\end{aligned}\quad (3.73 \text{ bis})$$

The ultimate strains for the lamina obtained by uniaxial or pure shear testing are related to the basic strength parameters of the lamina as follows:

$$\begin{aligned}\epsilon_{1t}^u &= \frac{F_{1t}}{E_1} \\ \epsilon_{1c}^u &= -\frac{F_{1c}}{E_1} \\ \epsilon_{2t}^u &= \frac{F_{2t}}{E_2} \\ \epsilon_{2c}^u &= -\frac{F_{2c}}{E_2} \\ \gamma_6^u &= \frac{F_6}{G_{12}}\end{aligned}\quad (4.22)$$

In view of the relations in Eqs. (3.73) and (4.22), the failure subcriteria in Eq. (4.21) can be expressed in terms of stresses as follows:

$$\sigma_1 - \nu_{12} \sigma_2 = \begin{cases} F_{1t} & \text{when } \epsilon_1 > 0 \\ -F_{1c} & \text{when } \epsilon_1 < 0 \end{cases}\quad (4.23a)$$

$$\sigma_2 - \nu_{21} \sigma_1 = \begin{cases} F_{2t} & \text{when } \epsilon_2 > 0 \\ -F_{2c} & \text{when } \epsilon_2 < 0 \end{cases}\quad (4.23b)$$

$$|\tau_6| = F_6\quad (4.23c)$$

For a two-dimensional state of stress with $\tau_6 = 0$, the failure envelope takes the form of a parallelogram with its center off the origin of the σ_1 , σ_2 coordinate system (Fig. 4.31).

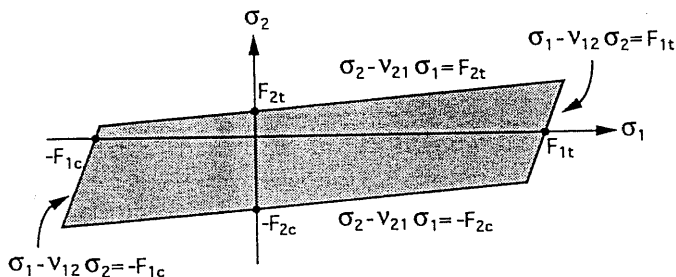


Fig. 4.31 Failure envelope for unidirectional lamina under biaxial normal loading (maximum strain theory).

4.6 Deviatoric Strain Energy Theory (Tsai-Hill)

The deviatoric or distortional energy has been proposed by many investigators (e.g., von Mises, Hencky, Nadai, Novozhilov) in various forms as a failure criterion for isotropic ductile metals. For a two-dimensional state of stress referred to the principal stress directions, the von Mises yield criterion has the form

$$\sigma_1^2 + \sigma_2^2 - \sigma_1 \sigma_2 = \sigma_{yp}^2 \quad (4.24)$$

where σ_{yp} is the yield stress.

Hill¹² modified this criterion for the case of ductile metals with anisotropy and proposed the following form:

$$A \sigma_1^2 + B \sigma_2^2 + C \sigma_1 \sigma_2 + D \tau_6^2 = 1 \quad (4.25)$$

where A , B , C , and D are material parameters characteristic of the current state of anisotropy. The above form cannot be technically referred to as distortional energy criterion, since distortion cannot be separated from dilatation in anisotropic materials.

Azzi and Tsai¹³ adapted this criterion to orthotropic composite materials, i.e., a unidirectional lamina with transverse isotropy. The parameters of Eq. (4.25) can be related to the basic strength parameters of the lamina by conducting imaginary elementary experiments as discussed previously in Section 3.6 (Figs. 3.4 and 3.5).

For uniaxial longitudinal loading to failure, $\sigma_1^u = F_1$, $\sigma_2 = \tau_6 = 0$, Eq. (4.25) yields

$$A = \frac{1}{F_1^2} \quad (4.26)$$

For uniaxial transverse loading to failure, $\sigma_2^u = F_2$, $\sigma_1 = \tau_6 = 0$, Eq. (4.25) yields

$$B = \frac{1}{F_2^2} \quad (4.27)$$

For in-plane shear loading to failure $\sigma_1 = \sigma_2 = 0$, $\tau_6^u = F_6$, Eq. (4.25) yields

$$D = \frac{1}{F_6^2} \quad (4.28)$$

The superscript u in the above denotes ultimate value of stress at failure.

The remaining parameter C , accounting for interaction between normal stresses σ_1 and σ_2 , must be determined by means of a biaxial test. Under equal biaxial normal loading, $\sigma_1 = \sigma_2 \neq 0$, $\tau_6 = 0$, it can be assumed that the material follows the maximum stress criterion, i.e., failure will occur when the transverse stress σ_2 reaches the transverse strength value, F_2 , which is much lower than the longitudinal strength F_1 . Equation (4.25) then yields

$$C = -\frac{1}{F_1^2} \quad (4.29)$$

Substituting the values of the parameters A , B , C , and D into Eq. (4.25), we obtain the Tsai–Hill criterion

$$\frac{\sigma_1^2}{F_1^2} + \frac{\sigma_2^2}{F_2^2} + \frac{\tau_6^2}{F_6^2} - \frac{\sigma_1 \sigma_2}{F_1^2} = 1 \quad (4.30)$$

In the above no distinction is made between tensile and compressive strengths. However, the appropriate strength values can be used in Eq. (4.30) according to the signs of the normal stresses σ_1 and σ_2 . Thus

$$F_1 = \begin{cases} F_{1t} & \text{when } \sigma_1 > 0 \\ F_{1c} & \text{when } \sigma_1 < 0 \end{cases} \quad (4.31a)$$

$$F_2 = \begin{cases} F_{2t} & \text{when } \sigma_2 > 0 \\ F_{2c} & \text{when } \sigma_2 < 0 \end{cases} \quad (4.31b)$$

The failure envelope described by the Tsai–Hill criterion in Eq. (4.30) is a closed surface in the σ_1 , σ_2 , τ_6 space. Failure envelopes for constant values of $k = \tau_6/F_6$ have the form

$$\frac{\sigma_1^2}{F_1^2} + \frac{\sigma_2^2}{F_2^2} - \frac{\sigma_1 \sigma_2}{F_1^2} = 1 - k^2 \quad (4.32)$$

The above form represents four different elliptical arcs joined at the σ_1, σ_2 axes.

Consider, for example, the case of uniaxial off-axis loading shown in Figure 4.29. By transforming the applied stress σ_x along the principal material axes (Eq. 4.18) and substituting into Eq. (4.30), we obtain the following equation for the axial strength F_x ($\sigma_x^u = F_x$):

$$\frac{1}{F_x^2} = \frac{m^4}{F_1^2} + \frac{n^4}{F_2^2} + \left[\frac{1}{F_6^2} - \frac{1}{F_1^2} \right] m^2 n^2 \quad (4.33)$$

where $m = \cos\theta$ and $n = \sin\theta$.

In the case of advanced high strength composites the longitudinal strength is much higher than the shear strength, i.e., $F_1 \gg F_6$. Then, Eq. (4.33) can be approximated by the following

$$\frac{1}{F_x^2} \cong \frac{m^4}{F_1^2} + \frac{n^4}{F_2^2} + \frac{m^2 n^2}{F_6^2} \quad (4.34)$$

The Tsai–Hill failure theory is expressed in terms of a single criterion instead of the three subcriteria required in the maximum stress and maximum strain theories. The Tsai–Hill theory allows for considerable interaction among the stress components σ_1, σ_2 , and τ_6 . One disadvantage, however, is that it does not distinguish directly between tensile and compressive strengths. The strength parameters in Eq. (4.30) must be specified according to the given state of stress.

4.7 Interactive Tensor Polynomial Theory (Tsai–Wu)

The first attempt to develop a general failure theory for anisotropic materials without the limitations of previous theories was discussed by Gol'denblat and Kopnov.¹⁴ This theory is capable of predicting strength under general states of stress for which no experimental data are available. It uses the concept of strength tensors, which allows for transformation from one coordinate system to another. It has the form of an invariant formed from stress and strain tensor components, and, most important, it has the capability to account for the difference between tensile and compressive strengths. The proposed original form of the criterion (in contracted notation) is

$$(f_i \sigma_i)^\alpha + (f_{ij} \sigma_i \sigma_j)^\beta + (f_{ijk} \sigma_i \sigma_j \sigma_k)^\gamma + \dots = 1 \quad (4.35)$$

where repeated subscripts in a term imply summation, with $i, j, k = 1, 2, \dots, 6$. The coefficients $f_i, f_{ij}, f_{ijk}, \dots$, are strength tensors of second, fourth, sixth, and higher orders and can be related to the basic strength constants of the material. To make the criterion homogeneous, the exponents are taken as $\alpha = 1, \beta = 1/2$, and $\gamma = 1/3$. In its simplest form the criterion takes the form

$$f_i \sigma_i + [f_{ij} \sigma_i \sigma_j]^{1/2} = 1 \quad (4.36)$$

Tsai and Wu¹⁵ proposed a modified tensor polynomial theory by assuming the existence of a failure surface in the stress space. In contracted notation it takes the form

$$f_i \sigma_i + f_{ij} \sigma_i \sigma_j = 1 \quad (4.37)$$

where f_i, f_{ij} are second and fourth order strength tensors, and $i, j = 1, 2, \dots, 6$. In expanded form and for a plane state of stress, the Tsai–Wu criterion in Eq. (4.37) is expressed as

$$\begin{aligned} f_1 \sigma_1 + f_2 \sigma_2 + f_6 \tau_6 + f_{11} \sigma_1^2 + f_{22} \sigma_2^2 + f_{66} \tau_6^2 + \\ + 2f_{12} \sigma_1 \sigma_2 + 2f_{16} \sigma_1 \tau_6 + 2f_{26} \sigma_2 \tau_6 = 1 \end{aligned} \quad (4.38)$$

The linear terms in this expression allow for the distinction between tensile and compressive strengths. The term f_{12} accounts for the interaction between normal stresses σ_1 and σ_2 .

Since the strength of a lamina loaded under pure shear τ_6 along its principal material axes (Fig. 4.26) is independent of the sign of the shear stress, all linear terms in τ_6 must vanish. Thus

$$f_6 = f_{16} = f_{26} = 0 \quad (4.39)$$

The remaining coefficients of the quadratic Tsai–Wu criterion are obtained by applying elementary loading conditions to the lamina. Thus, for longitudinal tensile loading to failure $\sigma_1^u = F_{1t}$, $\sigma_2 = \tau_6 = 0$,

$$f_1 F_{1t} + f_{11} F_{1t}^2 = 1 \quad (4.40)$$

and for longitudinal compressive loading $\sigma_1^u = -F_{1c}$, $\sigma_2 = \tau_6 = 0$,

$$-f_1 F_{1c} + f_{11} F_{1c}^2 = 1 \quad (4.41)$$

Equations (4.40) and (4.41) yield the values of coefficients f_1 and f_{11} as

$$f_1 = \frac{1}{F_{1t}} - \frac{1}{F_{1c}} \quad (4.42)$$

$$f_{11} = \frac{1}{F_{1t} F_{1c}} \quad (4.43)$$

Similarly, for transverse uniaxial tensile and compressive loadings we obtain

$$f_2 = \frac{1}{F_{2t}} - \frac{1}{F_{2c}} \quad (4.44)$$

$$f_{22} = \frac{1}{F_{2t} F_{2c}} \quad (4.45)$$

For pure shear loading to failure, $\tau_6^u = F_6$, $\sigma_1 = \sigma_2 = 0$, we obtain

$$f_{66} = \frac{1}{F_6^2} \quad (4.46)$$

The remaining coefficient f_{12} must be obtained by some type of biaxial testing. Under equal biaxial normal loading, $\sigma_1^u = \sigma_2^u = F_{(12)}$, $\tau_6 = 0$, we obtain

$$(f_1 + f_2)F_{(12)} + (f_{11} + f_{22} + 2f_{12})F_{(12)}^2 = 1 \quad (4.47)$$

where $F_{(12)}$ is the experimentally determined strength under equal biaxial tensile loading ($\sigma_1 = \sigma_2$). Equation (4.47) is then solved for f_{12} and, using the relations in Eqs. (4.42) to (4.45) between f_1 , f_2 , f_{11} , and f_{22} and the strength parameters, we obtain

$$f_{12} = \frac{1}{2F_{(12)}^2} \left[1 - F_{(12)} \left(\frac{1}{F_{1t}} - \frac{1}{F_{1c}} + \frac{1}{F_{2t}} - \frac{1}{F_{2c}} \right) - F_{(12)}^2 \left(\frac{1}{F_{1t} F_{1c}} + \frac{1}{F_{2t} F_{2c}} \right) \right] \quad (4.48)$$

Thus, f_{12} is a function of the basic strength parameters plus the equal biaxial strength $F_{(12)}$.

Direct biaxial testing is not easy or practical to perform. An easier test producing a biaxial state of stress is the off-axis tensile test, i.e., uniaxial loading σ_x at an angle θ with the fiber direction. For $\theta = 45^\circ$, Eq. (4.18) yields

$$\sigma_1 = \sigma_2 = |\tau_6| = \frac{1}{2} F_{45t} \quad (4.49)$$

where F_{45t} is the off-axis tensile strength of the lamina at 45° with the fiber direction. Substituting the above in Eq. (4.38) we obtain

$$2F_{45t}(f_1 + f_2) + F_{45t}^2(f_{11} + f_{22} + f_{66} + 2f_{12}) = 4 \quad (4.50)$$

Solving for f_{12} we obtain

$$f_{12} = \frac{2}{F_{45t}^2} \left[1 - \frac{F_{45t}}{2} \left(\frac{1}{F_{1t}} - \frac{1}{F_{1c}} + \frac{1}{F_{2t}} - \frac{1}{F_{2c}} \right) - \frac{F_{45t}^2}{4} \left(\frac{1}{F_{1t} F_{1c}} + \frac{1}{F_{2t} F_{2c}} + \frac{1}{F_6^2} \right) \right] \quad (4.51)$$

In many cases the interaction coefficient f_{12} is not critical, and an approximation suffices. A good approximation is

$$f_{12} \cong -\frac{1}{2}(f_{11} f_{22})^{1/2} \quad (4.52)$$

This relation is compatible with the von Mises yield criterion in Eq. (4.24) for isotropic materials where

$$f_{11} = f_{22} = \frac{1}{\sigma_{yp}^2}$$

The Tsai–Wu failure criterion is operationally simple and readily amenable to computational procedures. The theory satisfies the invariant requirements of coordinate transformation, following normal tensor transformation laws. The strength tensors display similar symmetry properties as the stiffnesses and compliances. The interaction terms can be treated as separate components if the appropriate experimental data are available. The theory, through its linear terms, accounts for the difference in tensile and compressive strengths.

The off-axis strength of unidirectional E-glass/epoxy (Table 2.6) was computed by means of the Tsai–Wu criterion and plotted as a function of fiber orientation in Figure 4.32, using the approximate relation in Eq. (4.52) for f_{12} . Superimposed in the figure is the prediction of the Tsai–Hill theory. It is seen that the predictions of the two theories are almost indistinguishable for the tensile strength, but they deviate somewhat for the compressive strength. The off-axis strength is not very sensitive to the interaction coefficient f_{12} . Considering

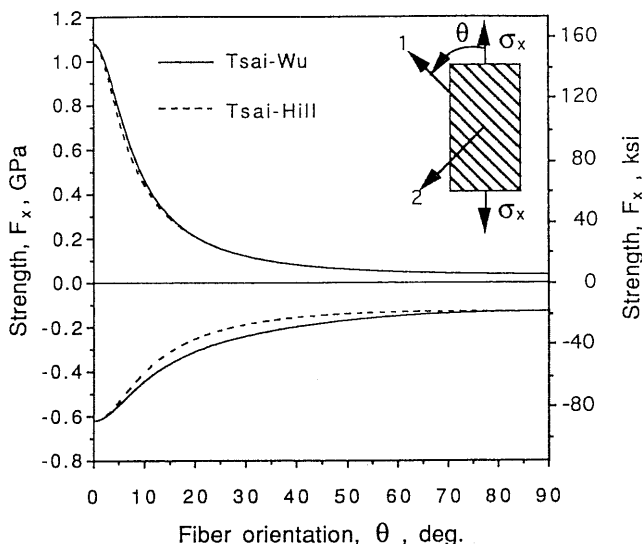


Fig. 4.32 Uniaxial strength of off-axis E-glass/epoxy unidirectional lamina as a function of fiber orientation (comparison of Tsai–Wu and Tsai–Hill failure criteria).

the usual scatter in measured strengths, the differences between the two theories are not significant.

The reduced form of the Tsai–Wu criterion is

$$f_1 \sigma_1 + f_2 \sigma_2 + f_{11} \sigma_1^2 + f_{22} \sigma_2^2 + f_{66} \tau_6^2 + 2f_{12} \sigma_1 \sigma_2 = 1 \quad (4.53)$$

with the coefficients f_i, f_{ij} defined as before. The failure envelope described by Eq. (4.53) is a closed surface in the $\sigma_1, \sigma_2, \tau_6$ space. Failure envelopes for constant values of shear stress $\tau_6 = kF_6$ have the form

$$f_1 \sigma_1 + f_2 \sigma_2 + f_{11} \sigma_1^2 + f_{22} \sigma_2^2 + 2f_{12} \sigma_1 \sigma_2 = 1 - k^2 \quad (4.54)$$

and are illustrated in Figure 4.33 for the same E-glass/epoxy material (Table 2.6).

4.8 Computational Procedure for Determination of Lamina Strength

As mentioned before, the Tsai–Wu criterion is operationally simple; therefore, it is the preferred one for computation. The goal of this computation is twofold:

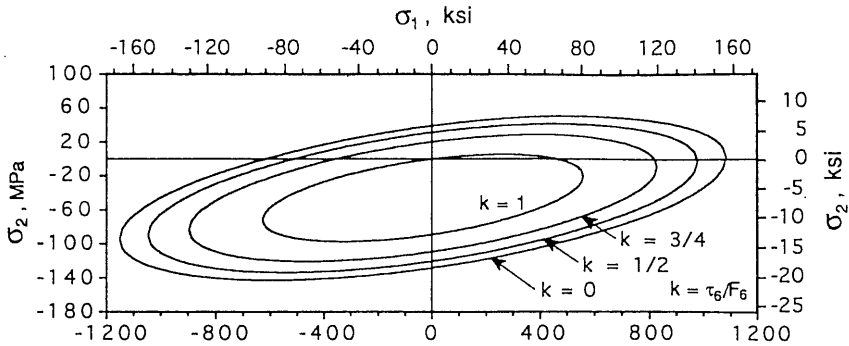


Fig. 4.33 Failure envelopes for unidirectional E-glass/epoxy lamina under biaxial loading with different levels of shear stress (Tsai–Wu criterion).

to determine the safety factor for a given loading and the strength components of the lamina referred to any system of coordinates.

The safety factor S_f for a given state of stress σ_i ($\sigma_1, \sigma_2, \tau_6$) is a multiplier that is applied to all stress components to produce a critical or failure state as defined by the selected failure criterion, say, the Tsai–Wu criterion. Thus, for a given state of stress ($\sigma_1, \sigma_2, \tau_6$), the state of stress at failure is ($S_f \sigma_1, S_f \sigma_2, S_f \tau_6$). Substitution of the critical stresses in the Tsai–Wu criterion in Eq. (4.53) yields

$$f_1 S_f \sigma_1 + f_2 S_f \sigma_2 + f_{11} S_f^2 \sigma_1^2 + f_{22} S_f^2 \sigma_2^2 + f_{66} S_f^2 \tau_6^2 + 2f_{12} S_f^2 \sigma_1 \sigma_2 = 1 \tag{4.55}$$

or

$$aS_f^2 + bS_f - 1 = 0 \tag{4.56}$$

where

$$a = f_{11} \sigma_1^2 + f_{22} \sigma_2^2 + f_{66} \tau_6^2 + 2f_{12} \sigma_1 \sigma_2$$

$$b = f_1 \sigma_1 + f_2 \sigma_2 \tag{4.57}$$

Thus the problem of determining the safety factor reduces to that of solving the quadratic Eq. (4.56).

A flow chart for computation of the safety factor as well as the strength components of a unidirectional lamina based on the Tsai–Wu criterion is shown

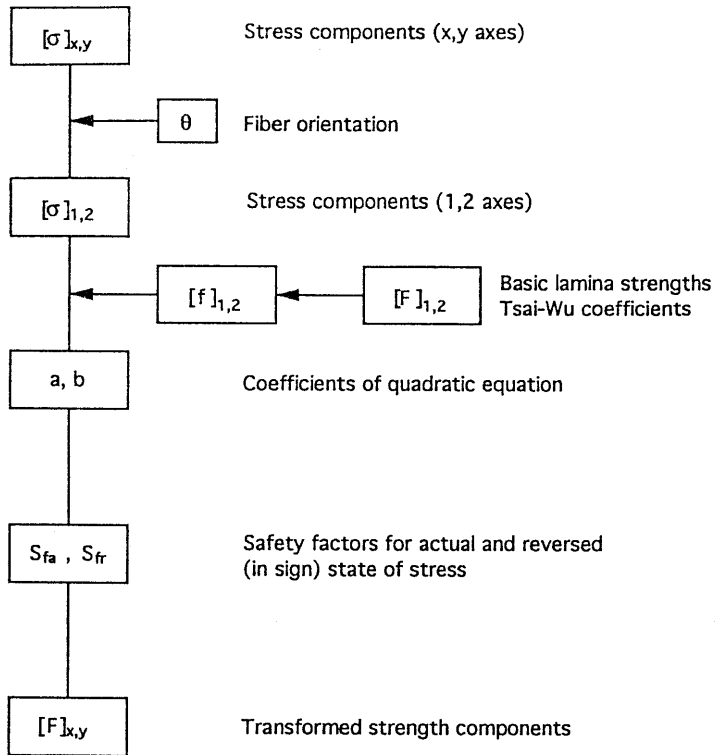


Fig. 4.34 Flow chart for computation of safety factors and lamina strengths based on Tsai-Wu failure criterion.

in Figure 4.34. The procedure for determination of safety factors consists of the following steps:

- Step 1** Enter given stress components σ_x , σ_y , τ_s referred to the (x,y) coordinate system.
- Step 2** Enter fiber orientation θ , i.e., angle between x -axis and fiber direction (1-direction) measured positive counterclockwise.
- Step 3** Calculate stress components σ_1 , σ_2 , τ_6 referred to the principal material directions using the stress transformation relations in Eq. (3.57).
- Step 4** Enter basic lamina strengths F_{1b} , F_{1c} , F_{2b} , F_{2c} , F_6 for the material.
- Step 5** Compute Tsai-Wu coefficients f_1 , f_2 , f_{11} , f_{22} , f_{66} , and f_{12} using Eqs. (4.42), (4.43), (4.44), (4.45), (4.46), and (4.52).
- Step 6** Compute coefficients a and b of the quadratic Eq. (4.56) using Eq. (4.57).

Step 7 Obtain roots of the quadratic equation S_{fa} and S_{fr} for the actual and reversed (in sign) state of stress, respectively.

The procedure above is modified slightly for computation of the transformed lamina strengths, by introducing separately a unit applied normal stress in the x - and y -directions and a unit applied shear stress.

To obtain the strength components F_{xt} and F_{xc} along the x -axis the following state of stress is entered

$$\begin{aligned}\sigma_x &= 1 \\ \sigma_y &= 0 \\ \tau_s &= 0\end{aligned}\tag{4.58}$$

Then the roots of the quadratic equation will give the strength components along the x -axis as

$$\begin{aligned}F_{xt} &= S_{fa} && \text{(tensile strength)} \\ F_{xc} &= S_{fr} && \text{(compressive strength)}\end{aligned}$$

To obtain the strength components along the y -axis the following stresses are entered

$$\begin{aligned}\sigma_x &= 0 \\ \sigma_y &= 1 \\ \tau_s &= 0\end{aligned}\tag{4.59}$$

Then the strength components are

$$\begin{aligned}F_{yt} &= S_{fa} && \text{(tensile strength)} \\ F_{yc} &= S_{fr} && \text{(compressive strength)}\end{aligned}$$

To obtain the shear strength F_s referred to the x,y -axes the following stresses are entered:

$$\begin{aligned}\sigma_x &= 0 \\ \sigma_y &= 0 \\ \tau_s &= 1\end{aligned}\tag{4.60}$$

which yield the following shear strengths:

$$F_s^{(+)} = S_{fa} \quad (\text{positive shear strength})$$

$$F_s^{(-)} = S_{fr} \quad (\text{negative shear strength})$$

Sample Problem 4.1

Transformation of Shear Strength

Given the basic lamina strengths F_1 , F_2 , and F_6 it is required to determine the shear strength F_s at 45° with the fiber direction according to the Tsai–Hill criterion (Fig. 4.35). The transformed stresses along the principal material directions are

$$\sigma_1 = 2mn \tau_s = \tau_s$$

$$\sigma_2 = -2mn \tau_s = -\tau_s$$

(4.61)

$$\tau_6 = (m^2 - n^2) \tau_s = 0$$

Substitution into the Tsai–Hill criterion in Eq. (4.30) yields

$$\frac{\tau_s^2}{F_1^2} + \frac{\tau_s^2}{F_2^2} + \frac{\tau_s^2}{F_1^2} = 1$$

and at failure, $\tau_s = F_s$,

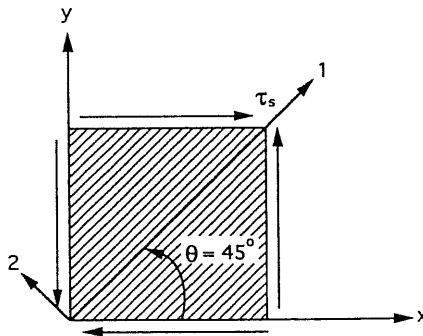


Fig. 4.35 Unidirectional lamina under pure shear loading at 45° with fiber direction.

$$\frac{1}{F_s^2} = \frac{2}{F_1^2} + \frac{1}{F_2^2} \tag{4.62}$$

For a high (fiber) strength composite with $F_1 \gg F_2$,

$$F_s \cong F_2 \tag{4.63}$$

or

$$\begin{aligned} F_s^{(+)} &= F_{2c} \\ F_s^{(-)} &= F_{2t} \end{aligned} \tag{4.64}$$

As discussed in Section 4.2, this result shows that the positive shear strength at 45° with the fiber direction is controlled by the transverse compressive strength F_{2c} of the lamina, whereas the negative shear strength is controlled by the transverse tensile strength F_{2t} . The same result is obtained by using the Tsai–Wu criterion, or the maximum stress theory.

Sample Problem 4.2

Biaxial Strength

Consider a unidirectional lamina loaded under equal biaxial normal stress $\sigma_x = \sigma_y = \sigma_o$ at an angle θ with the fiber direction (Fig. 4.36). It is required to determine the biaxial strength $F_{(xy)}$ according to the Tsai–Wu criterion.

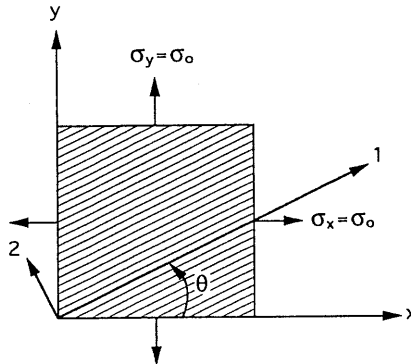


Fig. 4.36 Unidirectional lamina under equal biaxial normal loading.

The transformed stresses along the principal material directions are

$$\begin{aligned}\sigma_1 &= \sigma_x m^2 + \sigma_y n^2 = \sigma_o \\ \sigma_2 &= \sigma_x n^2 + \sigma_y m^2 = \sigma_o \\ \tau_6 &= (\sigma_x - \sigma_y) mn = 0\end{aligned}\quad (4.65)$$

and at failure,

$$\sigma_1 = \sigma_2 = \sigma_o = F_{(12)} \quad (4.66)$$

Substitution into the Tsai–Wu criterion (Eq. 4.53) yields:

$$F_{(12)}(f_1 + f_2) + F_{(12)}^2(f_{11} + f_{22} + 2f_{12}) = 1 \quad (4.67)$$

which can be solved for $F_{(12)}$.

For a high strength composite with $F_1 \gg F_2$ it follows that

$$f_1 \ll f_2; \quad f_{11} \ll f_{22}; \quad \text{and } f_{12} \ll f_{22} \quad (4.68)$$

and Eq. (4.67) yields

$$F_{(12)} \cong \frac{-f_2 \pm \sqrt{f_2^2 + 4f_{22}}}{2f_{22}} \quad (4.69)$$

and, after substitution of f_2 and f_{22} from relations in Eqs. (4.44) and (4.45), the two roots of Eq. (4.69) yield the tensile and compressive biaxial strengths

$$\begin{aligned}F_{(12)t} &\cong F_{2t} \\ F_{(12)c} &\cong F_{2c}\end{aligned}\quad (4.70)$$

It can be concluded that for a high (fiber) strength composite, the strength under equal biaxial normal loading is an isotropic property, i.e., it is independent of fiber orientation.

4.9 Applicability of Various Failure Theories

The four failure theories discussed before are representative and the most widely used. The validity and applicability of a specific theory depend on the convenience of application and agreement with experimental results. Since failure

modes depend greatly on material properties and type of loading, it would seem that the applicability of the various theories is also related to the type of material and failure modes. A comparison of the four failure theories is summarized in Table 4.1 from the points of view of physical basis, operational convenience, and required experimental input.

For example, the maximum stress and strain theories are more applicable when brittle behavior is predominant, typically in the first quadrant of the failure envelope, i.e., $\sigma_1 > 0$, $\sigma_2 > 0$. Of these two theories, only the maximum strain theory allows for a small degree of stress interaction through Poisson's ratio effect. These theories, although conceptually simple, are inconvenient for computational operations because they consist of three conditional subcriteria. The necessary experimental parameters can be obtained by standard characterization testing of the unidirectional material.

The interactive theories, such as the Tsai–Hill and Tsai–Wu theories, are more applicable when ductile behavior under shear or compression loading is predominant. The Tsai–Hill theory is based on Hill's theory for ductile anisotropic materials and adapted to the more brittle heterogeneous composites by a

Table 4.1 Comparison of Failure Theories

Theory	Physical basis	Operational convenience	Required experimental characterization
Maximum stress	Tensile behavior of brittle material No stress interaction	Inconvenient	Few parameters by simple testing
Maximum strain	Tensile behavior of brittle material Some stress interaction	Inconvenient	Few parameters by simple testing
Deviatoric strain energy (Tsai–Hill)	Ductile behavior of anisotropic materials “Curve fitting” for heterogeneous brittle composites	Can be programmed Different functions required for tensile and compressive strengths	Biaxial testing is needed in addition to uniaxial testing
Interactive tensor polynomial (Tsai–Wu)	Mathematically consistent Reliable “curve fitting”	General and comprehensive; operationally simple	Numerous parameters Comprehensive experimental program needed

form of “curve fitting.” Although suitable for computational operations, each quadrant of the failure envelope in the σ_1 - σ_2 space requires a different input because of the inability of the theory to account automatically for tensile and compressive strengths. Although the coefficient accounting for the σ_1 - σ_2 interaction can be approximated, a more precise determination requires some form of biaxial testing.

The Tsai–Wu theory is mathematically consistent and operationally simple. The additional coefficients in the criterion allow for distinction between tensile and compressive strengths. It represents a more reliable form of “curve fitting.” Although the interaction coefficient f_{12} can be approximated, a more precise determination requires biaxial testing. A comprehensive material characterization program is desirable to determine accurately the numerous required material parameters.

Composite materials that exhibit pronounced transitions between brittle and ductile behavior with type of loading would be best described by hybrid or combined failure criteria. Figure 4.37 shows such a hybrid failure envelope combining the maximum strain theory in the first quadrant ($\sigma_1 > 0, \sigma_2 > 0$) and an interactive theory in the remaining quadrants.

Most of the experimental data available for comparison with theoretical predictions are in the first quadrant. These type of data are easily obtained by off-axis tensile testing. Given the usual scatter in strength data, all four theories seem to give satisfactory predictions. More significant differences among the theories appear in the other quadrants where compressive stresses are present. Unfortunately there is a dearth of experimental data under such biaxial stress conditions. In the few cases in which such data are available, it appears that the Tsai–Wu theory fits them best. When material behavior and mode of failure are not known and when a conservative approach is required, it is recommended to use all four theories and determine the most conservative envelope in each quadrant (Fig. 4.38).

All four theories were expressed in two-dimensional form. They can all be extended or formulated for a general three-dimensional state of stress. Determi-

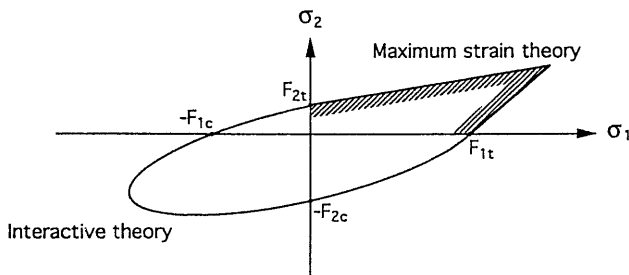


Fig. 4.37 Hybrid failure envelope incorporating two failure criteria.

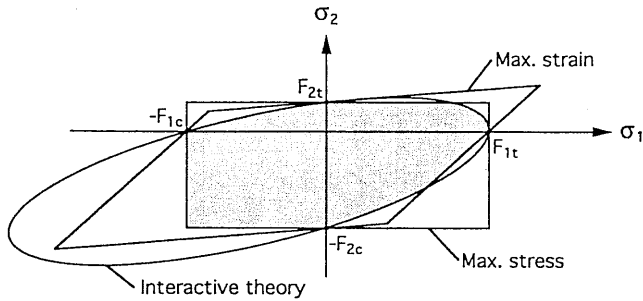


Fig. 4.38 Illustration of “conservative approach” in design by using different failure theories.

nation of all the relevant experimental parameters in this case would be more complicated and verification of theoretical predictions with experiment more difficult. The three-dimensional analysis and its experimental investigation are beyond the scope of this book and not necessary in the treatment of thin composite structures, which are assumed to be under a state of plane stress.

References

1. B. W. Rosen, “Tensile Failure of Fibrous Composites,” *AIAA J*, Vol. 2, 1964, pp. 1985–1991.
2. J. Mullin, J. M. Berry, and A. Gatti, “Some Fundamental Fracture Mechanisms Applicable to Advanced Filament Reinforced Composites,” *J. Composite Materials*, Vol. 2, No. 1, 1968, pp. 82–103.
3. J.-W. Lee and I. M. Daniel, “Deformation and Failure of Longitudinally Loaded Brittle-Matrix Composites,” in *Composite Materials: Testing and Design, (Tenth Volume)* ASTM STP 1120, Glen C. Grimes, Ed., American Society for Testing and Materials, Philadelphia, 1992, pp. 204–221.
4. B. W. Rosen, “Mechanics of Composite Strengthening,” Ch. 3, in *Fiber Composite Materials*, ASM, Metals Park, OH, 1965.
5. L. Shikhmanter, I. Eldror, and B. Cina, “Fractography of Unidirectional CFRP Composites,” *J Materials Sci*, Vol. 24, 1989, pp. 167–172.
6. D. F. Adams and D. R. Doner, “Transverse Normal Loading of a Unidirectional Composite,” *J. Composite Materials*, Vol. 1, 1967, pp. 152–164.
7. I. M. Daniel, “Photoelastic Investigation of Composites,” in *Composite Materials*, Vol. 2, “Mechanics of Composite Materials” (Vol. Ed. G. P. Sendeckyj, Series Eds. L. J. Broutman and R. H. Krock), Academic Press, 1974, pp. 433–489.
8. O. Ishai, “Failure of Unidirectional Composites in Tension,” *J. Eng. Mech. Div.*, Proc. of the ASCE, Vol. 97, No. EM2, 1971, pp. 205–221.
9. D. F. Adams and D. R. Doner, “Longitudinal Shear Loading of a Unidirectional Composite,” *J Composite Materials*, Vol. 1, No. 1, 1967, pp. 4–17.
10. R. S. Sandhu, “A Survey of Failure Theories of Isotropic and Anisotropic

- Materials," Air Force Flight Dynamics Laboratory, Technical Report AFFDL-TR-72-71, Wright Aeronautical Labs, Dayton, OH, 1972.
11. M. J. Owen and D. J. Rice, "Biaxial Strength Behavior of Glass Reinforced Polyester Resins," *Composite Materials: Testing and Design (Sixth Conference)*, ASTM STP 787, I. M. Daniel, Ed., American Society for Testing and Materials, Philadelphia, 1982, pp. 124-144.
 12. R. Hill, "A Theory of the Yielding and Plastic Flow of Anisotropic Metals," *Proceedings of the Royal Society, Series A*, Vol. 193, 1948.
 13. V. D. Azzi and S. W. Tsai, "Anisotropic Strength of Composites," *Exp. Mech.*, Vol. 5, No. 9, 1965, pp. 283-288.
 14. I. I. Gol'denblat and V. A. Kopnov, "Strength of Glass-Reinforced Plastics in Complex Stress State," *Mekhanika Polimerov*, Vol. 1, 1965, pp. 70-78 (in Russian); English translation: *Polymer Mechanics*, Vol. 1, Faraday Press, 1966, p. 54.
 15. S. W. Tsai and E. M. Wu, "A General Theory of Strength for Anisotropic Materials," *J. Composite Materials*, Vol. 5, 1971, pp. 58-80.

Problems

- 4.1 Determine the longitudinal modulus E_1 and the longitudinal tensile strength F_{1t} for a unidirectional E-glass/epoxy composite with the following constituent properties:

Fiber volume ratio: $V_f = 0.65$

Fiber modulus: $E_f = 69 \text{ GPa (10 Msi)}$

Matrix modulus: $E_m = 3.45 \text{ GPa (0.5 Msi)}$

Fiber tensile strength: $F_{ft} = 3,450 \text{ MPa (500 ksi)}$

Matrix tensile strength: $F_{mt} = 104 \text{ MPa (15 ksi)}$

Assume linear elastic behavior to failure for both fiber and matrix. Everything else being equal, how does the strength F_{1t} vary with E_f ?

- 4.2 Determine the longitudinal modulus E_1 and the longitudinal tensile strength F_{1t} for a unidirectional carbon/epoxy composite with the following properties:

$$V_f = 0.65$$

$$E_{1f} = 235 \text{ GPa (34 Msi)}$$

$$E_m = 4.14 \text{ GPa (0.6 Msi)}$$

$$F_{ft} = 3,450 \text{ MPa (500 ksi)}$$

$$F_{mt} = 104 \text{ MPa (15 ksi)}$$

- 4.3 Determine the longitudinal modulus E_1 and longitudinal tensile strength F_{1t} of a unidirectional silicon carbide/ceramic composite with the following properties:

$$V_f = 0.40$$

$$E_f = 172 \text{ GPa (25 Msi)}$$

$$E_m = 97 \text{ GPa (14 Msi)}$$

$$F_{ft} = 1,930 \text{ MPa (280 ksi)}$$

$$F_{mt} = 138 \text{ MPa (20 ksi)}$$

(Note: Strength is defined here as the composite stress at failure initiation of one of the phases.)

- 4.4 A unidirectional E-glass/epoxy composite is loaded in transverse tension. Obtain the stress concentration factor from Figure 4.15 and calculate the transverse tensile strength based on the maximum stress and maximum strain criteria, for the following constituent and composite properties:

$$V_f = 0.65$$

$$E_f = 69 \text{ GPa (10 Msi)}$$

$$E_m = 3.45 \text{ GPa (0.5 Msi)}$$

$$\nu_m = 0.36$$

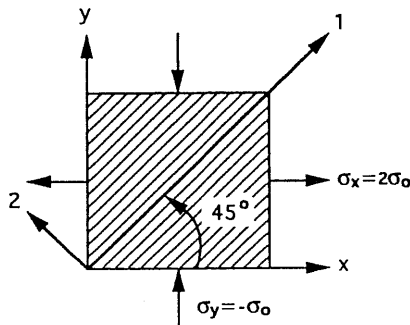
$$F_{mt} = 104 \text{ MPa (15 ksi)}$$

(Neglect residual stresses.)

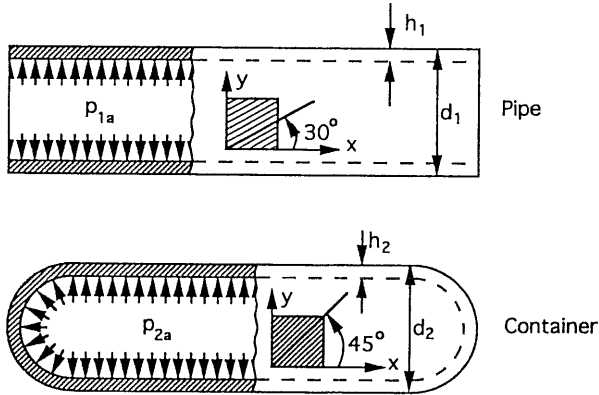
- 4.5 A unidirectional lamina is loaded under biaxial normal loading $\sigma_x = -2\sigma_y = 2\sigma_0$ at 45° with the fiber direction as shown. The basic strength properties of the material are

$$F_{1t} = F_{1c} = 3F_{2c} = 5F_6 = 12F_{2t} = 600 \text{ MPa (87 ksi)}$$

Determine the stress level σ_0^u at failure of the lamina according to the maximum stress theory. What is the failure mode?



- 4.6 A thin-wall pipe is made of a unidirectional glass/epoxy with the fiber direction at 30° with its axis and has an allowable pressure p_{1a} . A container (closed ends) made of the same material with the fiber direction at 45° with its axis has the same outer diameter but twice the wall thickness of the pipe ($d_2 = d_1$, $h_2 = 2h_1$). Relate the allowable pressure p_{2a} of the container to that of the pipe p_{1a} assuming the same safety factor based on the maximum stress theory with the following relations: $F_{1t} \gg F_6 > F_{2t}$.



- 4.7 A unidirectional S-glass/epoxy lamina is loaded in tension at an angle to the fiber direction. Using the maximum strain criterion, determine the off-axis strength, F_{xt} , and the fiber orientation θ at which the predictions of in-plane shear and transverse tensile failure coincide.

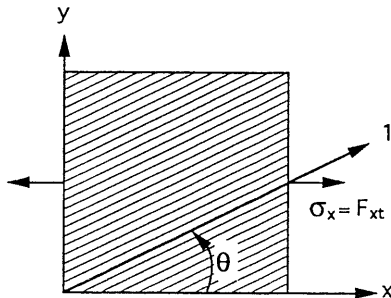
$$F_{1t} = 1,280 \text{ MPa (185 ksi)}$$

$$F_{2t} = 49 \text{ MPa (7.1 ksi)}$$

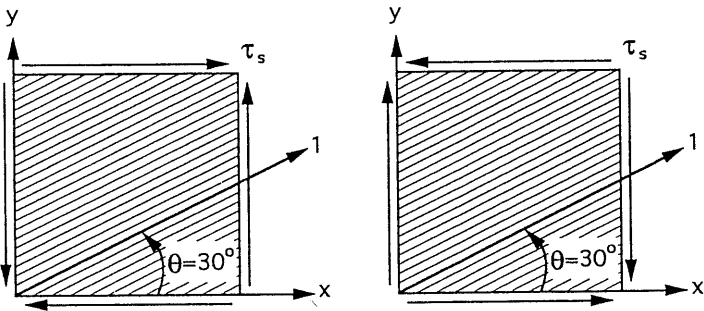
$$F_6 = 69 \text{ MPa (10 ksi)}$$

$$\nu_{12} = 0.27$$

$$\nu_{21} = 0.06$$



- 4.8 For the off-axis lamina under positive and negative shear stress as shown, and using the maximum strain failure theory, express the positive and negative shear strengths, $F_s^{(+)}$ and $F_s^{(-)}$, in terms of the basic lamina strengths (F_{1t} , F_{1c} , \dots , etc.) and material Poisson's ratios. Assume $F_{1t} > F_{1c} \gg F_{2c} > F_{2t}$ and $F_6 = F_{2t}$.



- 4.9 A unidirectional lamina is loaded under equal biaxial compression at 30° and -60° with the fiber direction as shown. Calculate the ultimate value σ_o'' using the maximum strain theory for the following properties:

$$F_6 = F_{2t} = 55 \text{ MPa (8 ksi)}$$

$$E_1 = 145 \text{ GPa (21 Msi)}$$

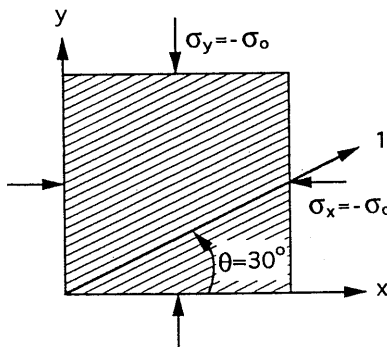
$$E_2 = 10.4 \text{ GPa (1.5 Msi)}$$

$$G_{12} = 6.9 \text{ GPa (1 Msi)}$$

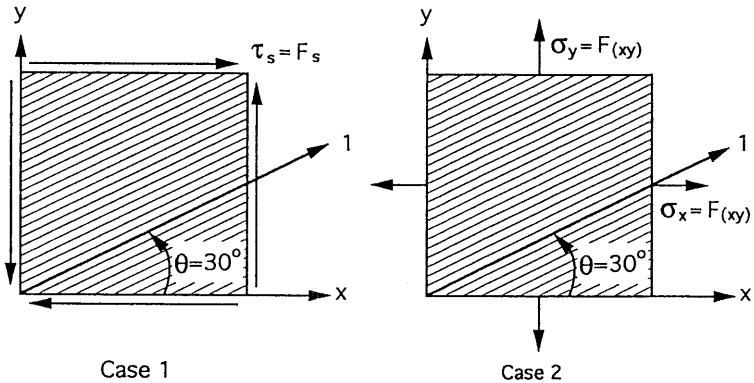
$$\nu_{12} = 0.27$$

$$F_{1c} = 1,725 \text{ MPa (250 ksi)}$$

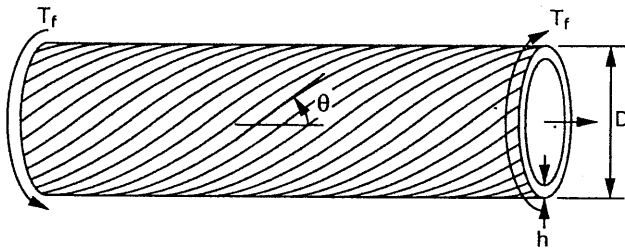
$$F_{2c} = 207 \text{ MPa (30 ksi)}$$



4.10 A unidirectional carbon/epoxy lamina with fiber direction at 30° with the reference x -axis is loaded under pure shear (case 1) and equal biaxial normal tensile stress (case 2) as shown. It was found for case 1 that the positive shear strength was four times the negative shear strength, $F_s^{(+)} = 4F_s^{(-)}$. Based on this finding, calculate the biaxial strength $F_{(xy)}$ for case 2. Use the maximum strain theory with the following material properties: $F_{1t} = F_{1c} = 10 F_{2c} = 16 F_6 = 1,600 \text{ MPa}$ (230 ksi) $\gg F_{2t}$; $E_1 \gg E_2$; $\nu_{12} = 0.25$.

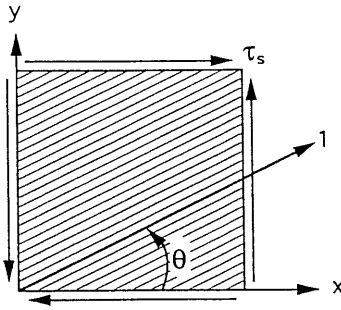


4.11 A thin-wall tube made of a unidirectional lamina with a fiber direction θ with its axis is loaded in torsion as shown. Using the maximum strain theory, plot torsional strength, T_f , versus θ (for $0^\circ \leq \theta \leq 90^\circ$) for the following material properties: $E_1 = 10E_2$, $\nu_{12} = 0.25$, $F_{1t} = F_{1c} = 2F_{2c} = 4F_6 = 10F_{2t} = 1,000 \text{ MPa}$ (145 ksi).

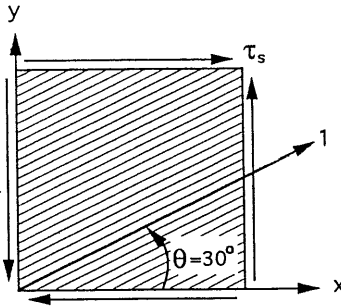


4.12 For the data in problem 4.11, calculate the transition fiber direction angles θ_1 and θ_2 at which the failure mode shifts from shear to transverse compression and from transverse compression to shear, respectively.

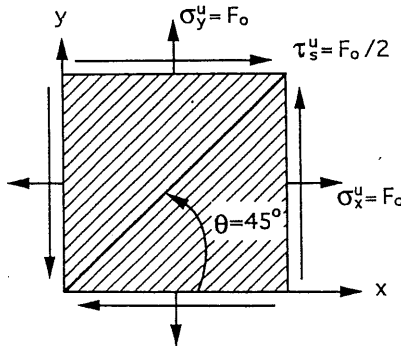
4.13 Express the Tsai–Hill failure criterion for pure shear loading of a lamina at an angle θ with the principal material axes and find an expression for the shear stress at failure $\tau_s^u = F_s$ in terms of F_1 , F_2 , F_6 .



- 4.14 A unidirectional lamina is loaded in pure shear τ_s at an angle $\theta = 30^\circ$ with the fiber direction. Determine the shear stress at failure $\tau_s^u = F_s$ using the Tsai–Hill failure criterion and the following data: $F_{1t} = 2,070$ MPa (300 ksi), $F_{2c} = 228$ MPa (33 ksi), $F_6 = 69$ MPa (10 ksi).



- 4.15 Using the Tsai–Hill failure criterion, determine the strength of a lamina under equal biaxial tension and shear at 45° with the fiber direction as shown, i.e., determine $\sigma_x^u = \sigma_y^u = 2\tau_s^u = F_0$ at failure in terms of F_1 and F_2 .



- 4.16 An off-axis lamina is loaded as shown. Determine $\sigma_x = -\sigma_y = F_o$ at failure using the Tsai–Hill and maximum stress failure criteria for a material of the following properties:

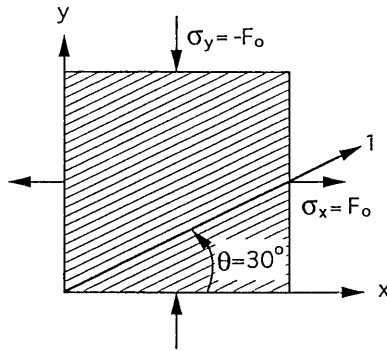
$$F_{1t} = 2,280 \text{ MPa (330 ksi)}$$

$$F_{2t} = 59 \text{ MPa (8.5 ksi)}$$

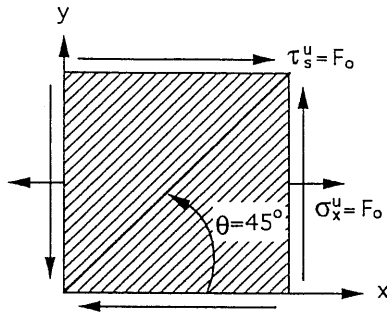
$$F_6 = 69 \text{ MPa (10 ksi)}$$

$$F_{1c} = 1,450 \text{ MPa (210 ksi)}$$

$$F_{2c} = 228 \text{ MPa (33 ksi)}$$

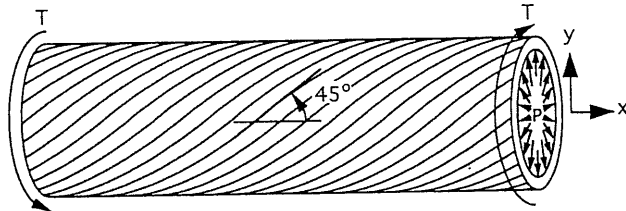


- 4.17 Using the Tsai–Hill failure criterion, determine the strength of a lamina under uniaxial tension and shear of equal magnitude at 45° with the fiber direction, i.e., determine $\sigma_x^u = \tau_s^u = F_o$ at failure in terms of F_1 , F_2 , and F_6 .

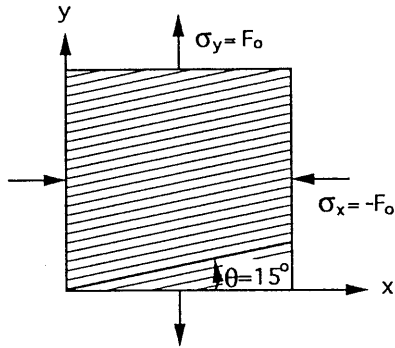


- 4.18 A thin-wall tube is made of a unidirectional carbon/epoxy with fiber direction at 45° to its axis. The tube is loaded under combined internal pressure and torsion producing a normal hoop stress $\sigma_y = \sigma_o$ and a shear stress $\tau_s = 2\sigma_o$. Calculate the ultimate value of σ_o^u at failure of the tube

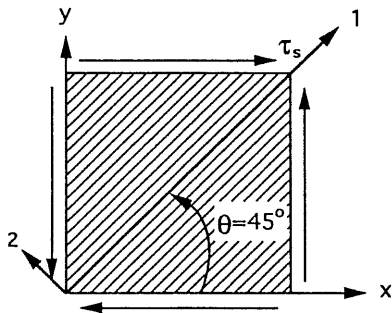
according to the Tsai–Hill failure criterion for the following material properties: $F_{1t} = F_{1c} = 10F_{2c} = 20F_6 = 30F_{2t} = 1,800$ MPa (260 ksi).



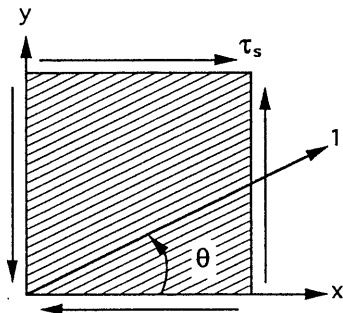
- 4.19** The off-axis strength of a unidirectional lamina can be higher than F_1 at some angle between 0° and 90° . Using the Tsai–Hill failure criterion (Eq. 4.33) find a relationship among F_1 , F_2 , and F_6 such that $F_x > F_1$ for some angle $0^\circ < \theta < 90^\circ$.
- 4.20** For the same conditions above find a relationship among F_1 , F_2 , and F_6 such that $F_x < F_2$ for same angle $0^\circ < \theta < 90^\circ$.
- 4.21** Prove relations in Eq. (4.39).
- 4.22** Calculate and compare the values of the coefficient f_{12} of the Tsai–Wu criterion for the E-glass/epoxy material of Table 2.6 from relations in Eqs. (4.48), (4.51), and (4.52). Assume $F_{(12)} = F_{2t}$ in Eq. (4.48) and $F_{45t} = 2F_{2t}$ in Eq. (4.51).
- 4.23** Calculate and compare values of the coefficient f_{12} of the Tsai–Wu criterion for the carbon/epoxy (AS4/3501-6) material of Table 2.6 from relations in Eqs. (4.48), (4.51), and (4.52) under the same assumptions as in Problem 4.22.
- 4.24** Using the Tsai–Wu failure criterion, determine the strength of a lamina under the loading shown. Obtain first the exact solution for the ultimate value of F_o in terms of the Tsai–Wu coefficients f_1 , f_2 , f_{11} , etc. Then, obtain an approximate solution in terms of lamina strengths (F_{1t} , F_{1c} , F_{2t} , etc.) for high strength composites, i.e., when $f_1 \ll f_2$, $f_{11} \ll f_{22}$, $f_{12} \ll f_{22}$.



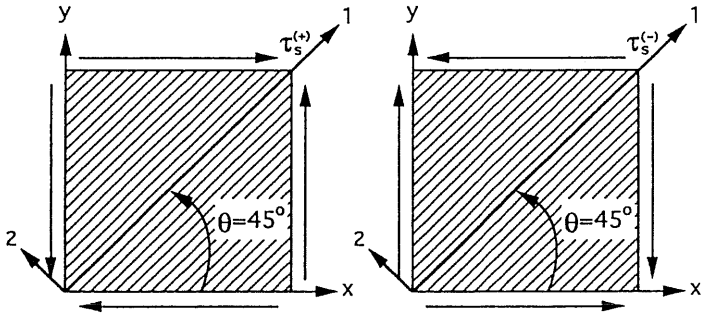
- 4.25 Using the Tsai–Wu failure criterion for pure shear loading of a lamina at an angle of 45° with the fiber direction, express the shear stress at failure $\tau_s^u = F_s$ in terms of the Tsai–Wu coefficients. Obtain approximate expression when $F_{1t} > F_{1c} \gg F_{2c} > F_{2t}$.



- 4.26 Using the Tsai–Wu failure criterion for pure shear loading of a lamina at an angle θ with the fiber direction, express the shear stress at failure $\tau_s^u = F_s$ in terms of the Tsai–Wu coefficients. Find approximation for composites with much higher longitudinal than transverse strengths.

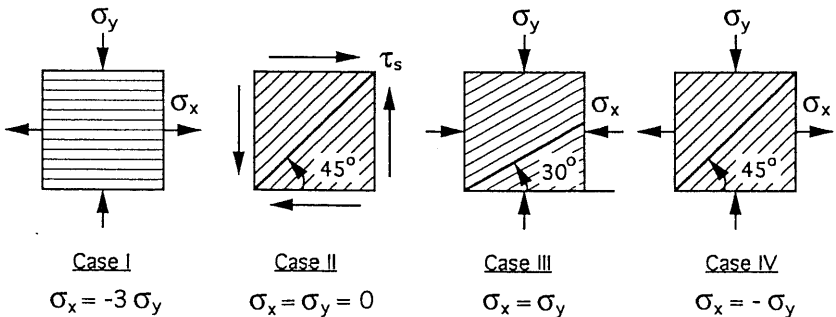


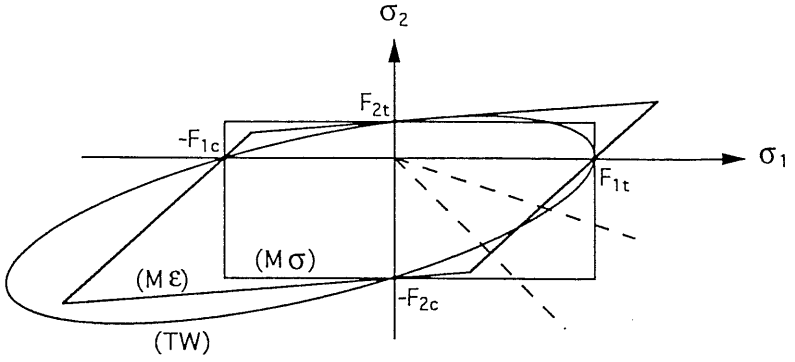
- 4.27 For the off-axis lamina under positive and negative shear stress as shown, express the positive and negative shear strengths, $F_s^{(+)}$ and $F_s^{(-)}$, using the Tsai–Wu failure theory in terms of the polynomial coefficients ($f_1, f_2, f_{11}, f_{22}, f_{12}$). Then, obtain approximate values for $F_s^{(+)}$ and $F_s^{(-)}$ in terms of the basic lamina strengths (F_{1t}, F_{1c}, \dots , etc.) by assuming $f_1 \ll f_2, f_{11} \ll f_{22}, f_{12} \ll f_{22}$.



- 4.28 For the off-axis lamina of problem 4.27, obtain expressions for the coefficient f_{12} of the Tsai–Wu criterion in terms of the basic strength parameters and the positive or negative shear strength, $F_s^{(+)}$ or $F_s^{(-)}$. Compare the values of f_{12} based on $F_s^{(+)}$ and $F_s^{(-)}$ by assuming $f_1 \ll f_2, f_{11} \ll f_{22}$.
- 4.29 Three failure envelopes are illustrated for a given unidirectional material based on three failure theories: maximum stress ($M\sigma$), maximum strain ($M\epsilon$), and Tsai–Wu (TW). Rank the three theories from the most conservative to the least conservative for each of the following loading cases:

Hint: Plot σ_1 versus σ_2 (loading path) for each loading case and relate to failure envelopes.





Chapter 5

Elastic Behavior of Multidirectional Laminates

5.1 Basic Assumptions

It is apparent that the overall behavior of a multidirectional laminate is a function of the properties and stacking sequence of the individual layers. The so-called classical lamination theory predicts the behavior of the laminate within the framework of the following assumptions:¹⁻³

1. Each layer (lamina) of the laminate is quasihomogeneous and orthotropic.
2. The laminate is thin with its lateral dimensions much larger than its thickness and is loaded in its plane only, i.e., the laminate and its layers (except for their edges) are in a state of plane stress ($\sigma_z = \tau_{xz} = \tau_{yz} = 0$).
3. All displacements are small compared with the thickness of the laminate ($|u|, |v|, |w| \ll h$).
4. Displacements are continuous throughout the laminate.
5. In-plane displacements vary linearly through the thickness of the laminate, i.e., u and v displacements in the x - and y -directions are linear functions of z .
6. Transverse shear strains γ_{xz} and γ_{yz} are negligible. This assumption and the preceding one imply that straight lines normal to the middle surface remain straight and normal to that surface after deformation.
7. Strain-displacement and stress-strain relations are linear.
8. Normal distances from the middle surface remain constant, i.e., the transverse normal strain ϵ_z is negligible (compared with the in-plane strains ϵ_x and ϵ_y).

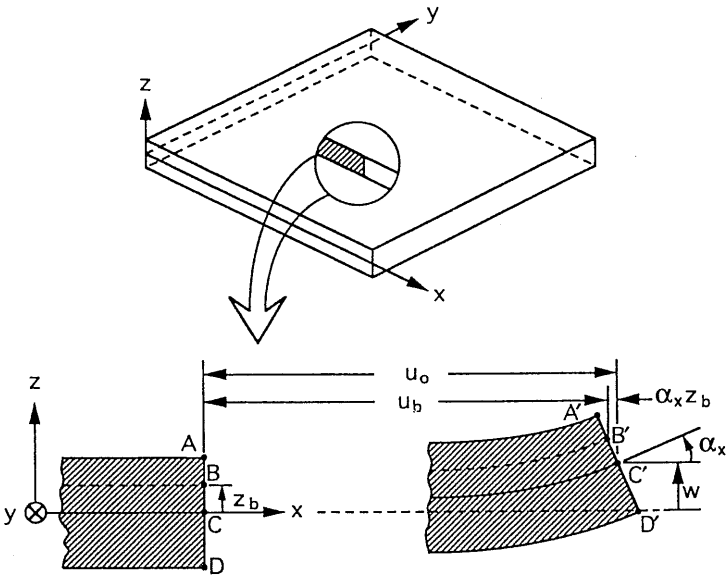


Fig. 5.1 Laminate section before (ABCD) and after (A'B'C'D') deformation.

5.2 Strain-Displacement Relations

Figure 5.1 shows a section of the laminate normal to the y -axis before and after deformation. The xy plane is equidistant from the top and bottom surfaces of the laminate and is called the *reference plane*.

The reference plane displacements u_o and v_o in the x - and y -directions and the out-of-plane displacement w in the z -direction are functions of x and y only:

$$\begin{aligned}
 u_o &= u_o(x,y) \\
 v_o &= v_o(x,y) \\
 w &= f(x,y)
 \end{aligned}
 \tag{5.1}$$

The rotations of the x - and y -axes are

$$\begin{aligned}
 \alpha_x &= \frac{\partial w}{\partial x} \\
 \alpha_y &= \frac{\partial w}{\partial y}
 \end{aligned}
 \tag{5.2}$$

The in-plane displacement components of a point B of coordinate z_b are (Fig. 5.1)

$$\begin{aligned} u_b &= u_o - \alpha_x z_b \\ v_b &= v_o - \alpha_y z_b \end{aligned} \quad (5.3)$$

and in general,

$$\begin{aligned} u &= u_o - z \frac{\partial w}{\partial x} \\ v &= v_o - z \frac{\partial w}{\partial y} \end{aligned} \quad (5.4)$$

where z is the coordinate variable of a general point of the cross section.

For small displacements, the classical strain-displacement relations of elasticity yield

$$\begin{aligned} \epsilon_x &= \frac{\partial u}{\partial x} = \frac{\partial u_o}{\partial x} - z \frac{\partial^2 w}{\partial x^2} \\ \epsilon_y &= \frac{\partial v}{\partial y} = \frac{\partial v_o}{\partial y} - z \frac{\partial^2 w}{\partial y^2} \\ \gamma_{xy} &= \gamma_s = \frac{\partial u}{\partial y} + \frac{\partial v}{\partial x} = \frac{\partial u_o}{\partial y} + \frac{\partial v_o}{\partial x} - 2z \frac{\partial^2 w}{\partial x \partial y} \\ \epsilon_z &= \gamma_{xz} = \gamma_{yz} = 0 \end{aligned} \quad (5.5)$$

Noting that the strain components on the reference plane are expressed as

$$\begin{aligned} \epsilon_x^o &= \frac{\partial u_o}{\partial x} \\ \epsilon_y^o &= \frac{\partial v_o}{\partial y} \\ \gamma_{xy}^o &= \gamma_s^o = \frac{\partial u_o}{\partial y} + \frac{\partial v_o}{\partial x} \end{aligned} \quad (5.6)$$

and the curvatures of the laminate as

$$\begin{aligned}\kappa_x &= -\frac{\partial^2 w}{\partial x^2} \\ \kappa_y &= -\frac{\partial^2 w}{\partial y^2} \\ \kappa_{xy} = \kappa_s &= -\frac{2\partial^2 w}{\partial x \partial y}\end{aligned}\quad (5.7)$$

we can relate the strains at any point in the laminate to the reference plane strains and the laminate curvatures as follows:

$$\begin{bmatrix} \epsilon_x \\ \epsilon_y \\ \gamma_s \end{bmatrix} = \begin{bmatrix} \epsilon_x^o \\ \epsilon_y^o \\ \gamma_s^o \end{bmatrix} + z \begin{bmatrix} \kappa_x \\ \kappa_y \\ \kappa_s \end{bmatrix}\quad (5.8)$$

5.3 Stress-Strain Relations of Layer within a Laminate

Consider an individual layer k in a multidirectional laminate whose midplane is at a distance z_k from the laminate reference plane (Fig. 5.2). The stress-strain relations for this layer referred to its material axes are

$$\begin{bmatrix} \sigma_1 \\ \sigma_2 \\ \tau_6 \end{bmatrix}_k = \begin{bmatrix} Q_{11} & Q_{12} & 0 \\ Q_{21} & Q_{22} & 0 \\ 0 & 0 & Q_{66} \end{bmatrix}_k \begin{bmatrix} \epsilon_1 \\ \epsilon_2 \\ \gamma_6 \end{bmatrix}_k\quad (5.9)$$

and after transformation to the laminate coordinate system

$$\begin{bmatrix} \sigma_x \\ \sigma_y \\ \tau_s \end{bmatrix}_k = \begin{bmatrix} Q_{xx} & Q_{xy} & Q_{xs} \\ Q_{yx} & Q_{yy} & Q_{ys} \\ Q_{sx} & Q_{sy} & Q_{ss} \end{bmatrix}_k \begin{bmatrix} \epsilon_x \\ \epsilon_y \\ \gamma_s \end{bmatrix}_k\quad (5.10)$$

Substituting the expressions for the strains from Eq. (5.8), we obtain

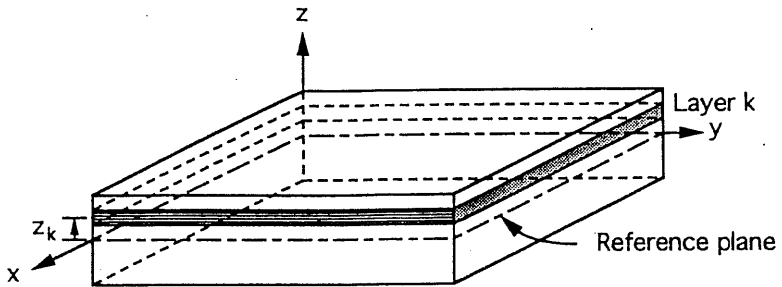


Fig. 5.2 Layer k within laminate.

$$\begin{bmatrix} \sigma_x \\ \sigma_y \\ \tau_{s,k} \end{bmatrix} = \begin{bmatrix} Q_{xx} & Q_{xy} & Q_{xs} \\ Q_{yx} & Q_{yy} & Q_{ys} \\ Q_{sx} & Q_{sy} & Q_{ss,k} \end{bmatrix} \begin{bmatrix} \epsilon_x^o \\ \epsilon_y^o \\ \gamma_s^o \end{bmatrix} + z \begin{bmatrix} Q_{xx} & Q_{xy} & Q_{xs} \\ Q_{yx} & Q_{yy} & Q_{ys} \\ Q_{sx} & Q_{sy} & Q_{ss,k} \end{bmatrix} \begin{bmatrix} \kappa_x \\ \kappa_y \\ \kappa_s \end{bmatrix} \quad (5.11)$$

or, in brief,

$$[\sigma]_{x,y}^k = [Q]_{x,y}^k [\epsilon^o]_{x,y} + z [Q]_{x,y}^k [\kappa]_{x,y}$$

From Eqs. (5.8) and (5.11) it is seen that whereas the strains vary linearly through the thickness, the stresses do not. Because of the discontinuous variation of the transformed stiffness matrix $[Q]_{x,y}$ from layer to layer, the stresses may also vary discontinuously from layer to layer. This is illustrated by the hypothetical four-layer laminate in Figure 5.3 under uniaxial stress in the x -direction. For a certain linear strain variation through the thickness, which can result from axial and flexural loading, the variation of the modulus E_x from layer to layer can cause the discontinuous stress variation illustrated. In many applications the stress gradient through the layer thickness is disregarded. The average stresses in each layer are determined by knowing the reference plane strains $[\epsilon^o]_{x,y}$, the curvatures $[\kappa]_{x,y}$ of the laminate, the location of the layer midplane z_k , and its transformed stiffness matrix $[Q]_{x,y}$.

5.4 Force and Moment Resultants

Because of the discontinuous variation of stresses from layer to layer, it is more convenient to deal with the integrated effect of these stresses on the laminate. Thus we seek expressions relating forces and moments to laminate deformation. The stresses acting on a layer k of a laminate (Fig. 5.2) given by Eq. (5.11)

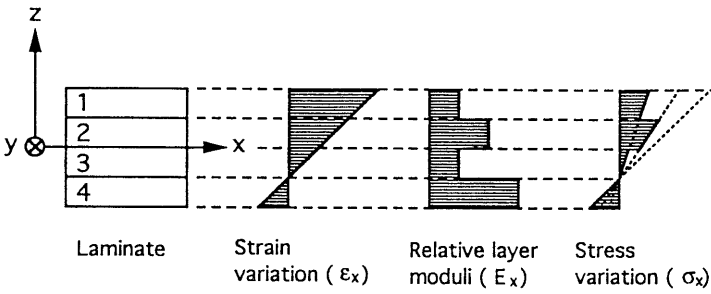


Fig. 5.3 Illustration of linear strain variation and discontinuous stress variation in multi-directional laminate.

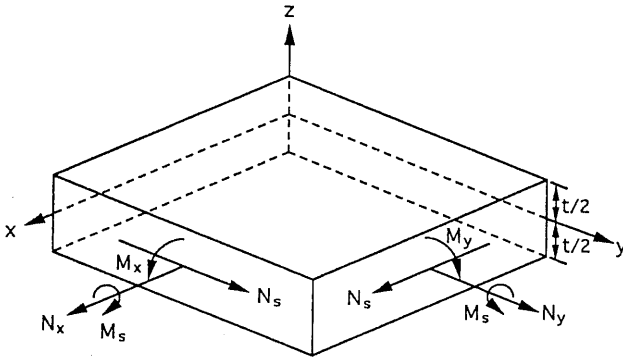


Fig. 5.4 Element of single layer with force and moment resultants.

can be replaced by resultant forces and moments as shown in Figure 5.4 and given below:

$$\begin{aligned}
 N_x^k &= \int_{-t/2}^{t/2} \sigma_x dz \\
 N_y^k &= \int_{-t/2}^{t/2} \sigma_y dz \\
 N_{xy}^k &= N_s^k = \int_{-t/2}^{t/2} \tau_s dz
 \end{aligned}
 \tag{5.12}$$

and

$$\begin{aligned}
 M_x^k &= \int_{-t/2}^{t/2} \sigma_x z dz \\
 M_y^k &= \int_{-t/2}^{t/2} \sigma_y z dz \\
 M_{xy}^k &= M_s^k = \int_{-t/2}^{t/2} \tau_s z dz
 \end{aligned} \tag{5.13}$$

where

z = The coordinate variable of a point in the cross section

t = Layer thickness

N_x^k, N_y^k = Normal forces per unit length

N_s^k = Shear force per unit length

M_x^k, M_y^k = Bending moments per unit length

M_s^k = Twisting moment per unit length

In the case of a multilayer laminate the total force and moment resultants are obtained by summing the effects for all layers. Thus, for the n -ply laminate in Figure 5.5, the force and moment resultants are obtained as

$$\begin{bmatrix} N_x \\ N_y \\ N_s \end{bmatrix} = \sum_{k=1}^n \int_{h_{k-1}}^{h_k} \begin{bmatrix} \sigma_x \\ \sigma_y \\ \tau_s \end{bmatrix}_k dz \tag{5.14}$$

and

$$\begin{bmatrix} M_x \\ M_y \\ M_s \end{bmatrix} = \sum_{k=1}^n \int_{h_{k-1}}^{h_k} \begin{bmatrix} \sigma_x \\ \sigma_y \\ \tau_s \end{bmatrix}_k z dz \tag{5.15}$$

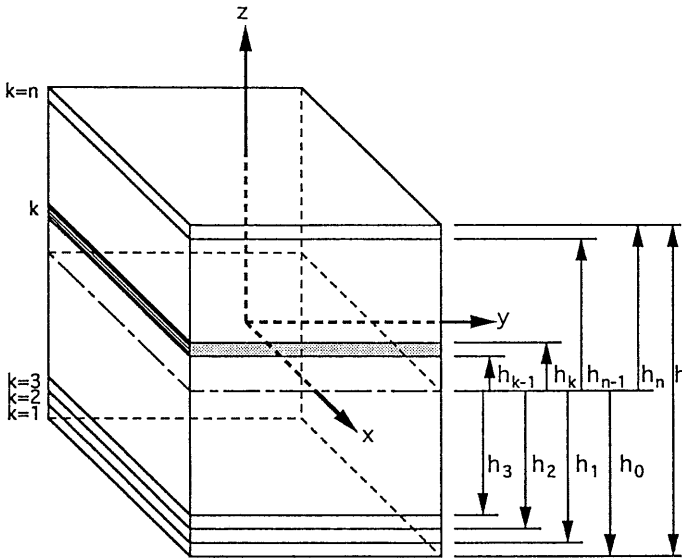


Fig. 5.5 Multidirectional laminate with coordinate notation of individual plies.

where h_k and h_{k-1} are the z -coordinates of the upper and lower surfaces of layer k .

5.5 General Load-Deformation Relations: Laminate Stiffnesses

Substituting Eq. (5.11) for the layer stresses in Eqs. (5.14) and (5.15) above, we obtain

$$\begin{aligned}
 \begin{bmatrix} N_x \\ N_y \\ N_s \end{bmatrix} &= \sum_{k=1}^n \left\{ \begin{bmatrix} Q_{xx} & Q_{xy} & Q_{xs} \\ Q_{yx} & Q_{yy} & Q_{ys} \\ Q_{sx} & Q_{sy} & Q_{ss} \end{bmatrix}_{kl} \begin{bmatrix} \epsilon_x^o \\ \epsilon_y^o \\ \gamma_s^o \end{bmatrix} \int_{h_{k-1}}^{h_k} dz \right. \\
 &+ \left. \begin{bmatrix} Q_{xx} & Q_{xy} & Q_{xs} \\ Q_{yx} & Q_{yy} & Q_{ys} \\ Q_{sx} & Q_{sy} & Q_{ss} \end{bmatrix}_{kl} \begin{bmatrix} \kappa_x \\ \kappa_y \\ \kappa_s \end{bmatrix} \int_{h_{k-1}}^{h_k} z dz \right\} \quad (5.16)
 \end{aligned}$$

and

$$\begin{aligned}
 \begin{bmatrix} M_x \\ M_y \\ M_s \end{bmatrix} &= \sum_{k=1}^n \left\{ \begin{bmatrix} Q_{xx} & Q_{xy} & Q_{xs} \\ Q_{yx} & Q_{yy} & Q_{ys} \\ Q_{sx} & Q_{sy} & Q_{ss} \end{bmatrix}_k \begin{bmatrix} \epsilon_x^o \\ \epsilon_y^o \\ \gamma_s^o \end{bmatrix} \int_{h_{k-1}}^{h_k} z dz \right. \\
 &\quad \left. + \begin{bmatrix} Q_{xx} & Q_{xy} & Q_{xs} \\ Q_{yx} & Q_{yy} & Q_{ys} \\ Q_{sx} & Q_{sy} & Q_{ss} \end{bmatrix}_k \begin{bmatrix} \kappa_x \\ \kappa_y \\ \kappa_s \end{bmatrix} \int_{h_{k-1}}^{h_k} z^2 dz \right\} \quad (5.17)
 \end{aligned}$$

In the expressions above, the stiffnesses $[Q]_{x,y}^k$, reference plane strains $[\epsilon^o]_{x,y}$, and curvatures $[\kappa]_{x,y}$ are taken outside the integration operation since they are not functions of z . Of these quantities only the stiffnesses are unique for each layer k , whereas the reference plane strains and curvatures refer to the entire laminate and are the same for all plies. Thus $[\epsilon^o]_{x,y}$ and $[\kappa]_{x,y}$ can be factored outside the summation sign as follows:

$$\begin{aligned}
 [N]_{x,y} &= \left[\sum_{k=1}^n [Q]_{x,y}^k \int_{h_{k-1}}^{h_k} dz \right] [\epsilon^o]_{x,y} \\
 &\quad + \left[\sum_{k=1}^n [Q]_{x,y}^k \int_{h_{k-1}}^{h_k} z dz \right] [\kappa]_{x,y} \quad (5.18) \\
 &= \left[\sum_{k=1}^n [Q]_{x,y}^k (h_k - h_{k-1}) \right] [\epsilon^o]_{x,y} \\
 &\quad + \left[\frac{1}{2} \sum_{k=1}^n [Q]_{x,y}^k (h_k^2 - h_{k-1}^2) \right] [\kappa]_{x,y} \\
 &= [A]_{x,y} [\epsilon^o]_{x,y} + [B]_{x,y} [\kappa]_{x,y}
 \end{aligned}$$

and

$$\begin{aligned}
 [M]_{x,y} &= \left[\frac{1}{2} \sum_{k=1}^n [Q]_{x,y}^k (h_k^2 - h_{k-1}^2) \right] [\epsilon^o]_{x,y} \\
 &\quad + \left[\frac{1}{3} \sum_{k=1}^n [Q]_{x,y}^k (h_k^3 - h_{k-1}^3) \right] [\kappa]_{x,y} \quad (5.19) \\
 &= [B]_{x,y} [\epsilon^o]_{x,y} + [D]_{x,y} [\kappa]_{x,y}
 \end{aligned}$$

where

$$\begin{aligned}
 A_{ij} &= \sum_{k=1}^n Q_{ij}^k (h_k - h_{k-1}) \\
 B_{ij} &= \frac{1}{2} \sum_{k=1}^n Q_{ij}^k (h_k^2 - h_{k-1}^2) \\
 D_{ij} &= \frac{1}{3} \sum_{k=1}^n Q_{ij}^k (h_k^3 - h_{k-1}^3)
 \end{aligned} \tag{5.20}$$

with $i, j = x, y, s$.

Thus, in full form the force-deformation relations are

$$\begin{bmatrix} N_x \\ N_y \\ N_s \end{bmatrix} = \begin{bmatrix} A_{xx} & A_{xy} & A_{xs} \\ A_{yx} & A_{yy} & A_{ys} \\ A_{sx} & A_{sy} & A_{ss} \end{bmatrix} \begin{bmatrix} \epsilon_x^o \\ \epsilon_y^o \\ \gamma_s^o \end{bmatrix} + \begin{bmatrix} B_{xx} & B_{xy} & B_{xs} \\ B_{yx} & B_{yy} & B_{ys} \\ B_{sx} & B_{sy} & B_{ss} \end{bmatrix} \begin{bmatrix} \kappa_x \\ \kappa_y \\ \kappa_s \end{bmatrix} \tag{5.21}$$

and the moment-deformation relations are

$$\begin{bmatrix} M_x \\ M_y \\ M_s \end{bmatrix} = \begin{bmatrix} B_{xx} & B_{xy} & B_{xs} \\ B_{yx} & B_{yy} & B_{ys} \\ B_{sx} & B_{sy} & B_{ss} \end{bmatrix} \begin{bmatrix} \epsilon_x^o \\ \epsilon_y^o \\ \gamma_s^o \end{bmatrix} + \begin{bmatrix} D_{xx} & D_{xy} & D_{xs} \\ D_{yx} & D_{yy} & D_{ys} \\ D_{sx} & D_{sy} & D_{ss} \end{bmatrix} \begin{bmatrix} \kappa_x \\ \kappa_y \\ \kappa_s \end{bmatrix} \tag{5.22}$$

The expressions above can be combined into one general expression relating in-plane forces and moments to reference plane strains and curvatures.

$$\begin{bmatrix} N_x \\ N_y \\ N_s \\ M_x \\ M_y \\ M_s \end{bmatrix} = \begin{bmatrix} A_{xx} & A_{xy} & A_{xs} & B_{xx} & B_{xy} & B_{xs} \\ A_{yx} & A_{yy} & A_{ys} & B_{yx} & B_{yy} & B_{ys} \\ A_{sx} & A_{sy} & A_{ss} & B_{sx} & B_{sy} & B_{ss} \\ B_{xx} & B_{xy} & B_{xs} & D_{xx} & D_{xy} & D_{xs} \\ B_{yx} & B_{yy} & B_{ys} & D_{yx} & D_{yy} & D_{ys} \\ B_{sx} & B_{sy} & B_{ss} & D_{sx} & D_{sy} & D_{ss} \end{bmatrix} \begin{bmatrix} \epsilon_x^o \\ \epsilon_y^o \\ \gamma_s^o \\ \kappa_x \\ \kappa_y \\ \kappa_s \end{bmatrix} \tag{5.23}$$

or, in brief,

$$\begin{bmatrix} N \\ M \end{bmatrix} = \begin{bmatrix} A & B \\ B & D \end{bmatrix} \begin{bmatrix} \epsilon^o \\ \kappa \end{bmatrix} \tag{5.24}$$

It should be noted that all of the above matrices are symmetric, i.e.,

$$A_{ij} = A_{ji}$$

$$B_{ij} = B_{ji}$$

$$D_{ij} = D_{ji}$$

with $i, j = x, y, s$.

The relations above are expressed in terms of three laminate stiffness matrices, $[A]$, $[B]$, and $[D]$, which are functions of the geometry, material properties and stacking sequence of the individual plies, as defined in Eq. (5.20). They are the average elastic parameters of the multidirectional laminate with the following significance:

A_{ij} are extensional stiffnesses, or in-plane laminate moduli, relating in-plane loads to in-plane strains.

B_{ij} are coupling stiffnesses, or in-plane/flexure coupling laminate moduli, relating in-plane loads to curvatures and moments to in-plane strains. Thus, if $B_{ij} \neq 0$, in-plane forces produce flexural and twisting deformations; moments produce extension of the middle surface in addition to flexure and twisting.

D_{ij} are bending or flexural laminate stiffnesses relating moments to curvatures.

5.6 Inversion of Load-Deformation Relations: Laminate Compliances

Since multidirectional laminates are characterized by stress discontinuities from ply to ply, it is preferable to work with strains, which are continuous through the thickness. For this reason it is necessary to invert the load-deformation relations (Eq. 5.23) and express strains and curvatures as a function of applied loads and moments.

Equation (5.23) can be rewritten as follows by performing matrix inversions:

$$\begin{bmatrix} \epsilon_x^o \\ \epsilon_y^o \\ \gamma_s^o \\ \kappa_x \\ \kappa_y \\ \kappa_s \end{bmatrix} = \begin{bmatrix} a_{xx} & a_{xy} & a_{xs} & b_{xx} & b_{xy} & b_{xs} \\ a_{yx} & a_{yy} & a_{ys} & b_{yx} & b_{yy} & b_{ys} \\ a_{sx} & a_{sy} & a_{ss} & b_{sx} & b_{sy} & b_{ss} \\ c_{xx} & c_{xy} & c_{xs} & d_{xx} & d_{xy} & d_{xs} \\ c_{yx} & c_{yy} & c_{ys} & d_{yx} & d_{yy} & d_{ys} \\ c_{sx} & c_{sy} & c_{ss} & d_{sx} & d_{sy} & d_{ss} \end{bmatrix} \begin{bmatrix} N_x \\ N_y \\ N_s \\ M_x \\ M_y \\ M_s \end{bmatrix} \quad (5.25)$$

or, in brief,

$$\begin{bmatrix} \epsilon^o \\ \kappa \end{bmatrix} = \begin{bmatrix} a & b \\ c & d \end{bmatrix} \begin{bmatrix} N \\ M \end{bmatrix} \quad (5.26)$$

Here, matrices $[a]$, $[b]$, $[c]$, and $[d]$ are the laminate compliance matrices obtained from the stiffness matrices as follows:³

$$\begin{aligned} [a] &= [A^{-1}] - \{[B^*][D^{*-1}]\}[C^*] \\ [b] &= [B^*][D^{*-1}] \\ [c] &= -[D^{*-1}][C^*] \\ [d] &= [D^{*-1}] \end{aligned} \quad (5.27)$$

where

$$\begin{aligned} [A^{-1}] &= \text{inverse of matrix } [A] \\ [B^*] &= -[A^{-1}][B] \\ [C^*] &= [B][A^{-1}] \\ [D^*] &= [D] - \{[B][A^{-1}]\}[B] \end{aligned}$$

It should be noted that, while the individual compliance matrices are symmetric, the combined 6×6 matrix of Eq. (5.25) is not, since in general $[b] \neq [c]$. Actually, $[c]$ is the transpose of matrix $[b]$, i.e., it is obtained from matrix $[b]$ by interchanging columns and rows. Thus the compliances that relate reference plane strains to applied moments are not identical to those that relate curvatures to in-plane loads.

5.7 Symmetric Laminates

A laminate is called **symmetric** when for each layer on one side of a reference plane (middle surface) there is a corresponding layer at an equal distance from the reference plane on the other side with identical thickness, orientation, and properties. The laminate is symmetric in both geometry and material properties.

Consider the n -layer laminate in Figure 5.6, where identical layers k and k' are symmetrically situated about the reference plane. Then

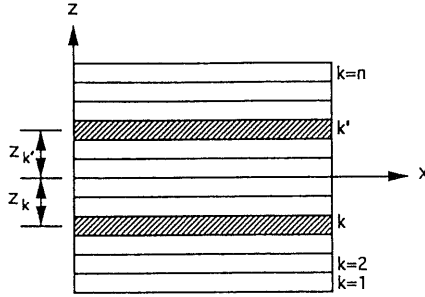


Fig. 5.6 Symmetric laminate with identical layers k and k' .

$$\begin{aligned}
 t_k &= t_{k'} \\
 Q_{ij}^k &= Q_{ij}^{k'} \quad (i, j = x, y, s) \\
 z_k &= -z_{k'}
 \end{aligned} \tag{5.28}$$

and, according to the definition in Eq. (5.20), the coupling stiffnesses are

$$\begin{aligned}
 B_{ij} &= \frac{1}{2} \sum_{k=1}^n Q_{ij}^k (h_k^2 - h_{k-1}^2) \\
 &= \frac{1}{2} \sum_{k=1}^n Q_{ij}^k (h_k + h_{k-1})(h_k - h_{k-1}) \\
 &= \sum_{k=1}^n Q_{ij}^k z_k t_k
 \end{aligned}$$

Since

$$z_k = \frac{1}{2} (h_k + h_{k-1})$$

and

$$t_k = h_k - h_{k-1}$$

For the conditions of symmetry stated before, the sum above will consist of pairs of terms of equal absolute value and opposite signs. Thus, for a symmetric laminate,

$$B_{ij} = 0 \quad (i, j = x, y, s) \quad (5.29)$$

and no coupling exists between in-plane loading and out-of-plane deformation (curvatures) and between bending and twisting moments and in-plane deformation.

The load-deformation relations in this case reduce to

$$\begin{bmatrix} N_x \\ N_y \\ N_s \end{bmatrix} = \begin{bmatrix} A_{xx} & A_{xy} & A_{xs} \\ A_{yx} & A_{yy} & A_{ys} \\ A_{sx} & A_{sy} & A_{ss} \end{bmatrix} \begin{bmatrix} \epsilon_x^o \\ \epsilon_y^o \\ \gamma_s^o \end{bmatrix} \quad (5.30)$$

and

$$\begin{bmatrix} M_x \\ M_y \\ M_s \end{bmatrix} = \begin{bmatrix} D_{xx} & D_{xy} & D_{xs} \\ D_{yx} & D_{yy} & D_{ys} \\ D_{sx} & D_{sy} & D_{ss} \end{bmatrix} \begin{bmatrix} \kappa_x \\ \kappa_y \\ \kappa_s \end{bmatrix} \quad (5.31)$$

Some special types of symmetric laminates are discussed below.

5.7.1 Symmetric Laminates with Isotropic Layers

If the layers are isotropic although not all of the same material, the layer stiffnesses of each pair of symmetrically situated layers k and k' are

$$\begin{aligned} Q_{xx}^k &= Q_{yy}^k = Q_{xx}^{k'} = Q_{yy}^{k'} = \frac{E_k}{1 - \nu_k^2} \\ Q_{xs}^k &= Q_{ys}^k = Q_{xs}^{k'} = Q_{ys}^{k'} = 0 \\ Q_{xy}^k &= Q_{xy}^{k'} = \frac{\nu_k E_k}{1 - \nu_k^2} \\ Q_{ss}^k &= Q_{ss}^{k'} = \frac{E_k}{2(1 + \nu_k)} \end{aligned} \quad (5.32)$$

The above relations lead to

$$\begin{aligned} A_{xx} &= A_{yy} \\ A_{xs} &= A_{ys} = 0 \\ D_{xx} &= D_{yy} \\ D_{xs} &= D_{ys} = 0 \end{aligned} \quad (5.33)$$

and the load-deformation relations take the form

$$\begin{bmatrix} N_x \\ N_y \\ N_s \end{bmatrix} = \begin{bmatrix} A_{xx} & A_{xy} & 0 \\ A_{xy} & A_{xx} & 0 \\ 0 & 0 & A_{ss} \end{bmatrix} \begin{bmatrix} \epsilon_x^o \\ \epsilon_y^o \\ \gamma_s^o \end{bmatrix} \quad (5.34)$$

and

$$\begin{bmatrix} M_x \\ M_y \\ M_s \end{bmatrix} = \begin{bmatrix} D_{xx} & D_{xy} & 0 \\ D_{xy} & D_{xx} & 0 \\ 0 & 0 & D_{ss} \end{bmatrix} \begin{bmatrix} \kappa_x \\ \kappa_y \\ \kappa_s \end{bmatrix} \quad (5.35)$$

5.7.2 Symmetric Laminates with Specially Orthotropic Layers (Symmetric Crossply Laminates)

The layers of a symmetric laminate with specially orthotropic layers have principal material axes coinciding with the laminate axes, e.g., $[0/90/0]$, $[0/90]_{ns}$. Because of symmetry, the coupling stiffnesses $B_{ij} = 0$, i.e., there is no coupling between in-plane loading and out-of-plane deformation.

Assuming that the k th layer is oriented with its principal 1-direction along the x -axis, we have

$$\begin{aligned} Q_{xx}^k &= Q_{11}^k = \frac{E_1^k}{1 - \nu_{12}^k \nu_{21}^k} \\ Q_{xy}^k &= Q_{12}^k = \frac{\nu_{21}^k E_1^k}{1 - \nu_{12}^k \nu_{21}^k} \\ Q_{yy}^k &= Q_{22}^k = \frac{E_2^k}{1 - \nu_{12}^k \nu_{21}^k} \\ Q_{xs}^k &= Q_{16}^k = 0 \\ Q_{ys}^k &= Q_{26}^k = 0 \\ Q_{ss}^k &= Q_{66}^k = G_{12}^k \end{aligned} \quad (5.36)$$

From the above it follows that

$$A_{xs} = A_{ys} = 0 \quad (5.37)$$

and

$$D_{xs} = D_{ys} = 0 \quad (5.37)$$

The load-deformation relations then are reduced to

$$\begin{bmatrix} N_x \\ N_y \\ N_s \end{bmatrix} = \begin{bmatrix} A_{xx} & A_{xy} & 0 \\ A_{yx} & A_{yy} & 0 \\ 0 & 0 & A_{ss} \end{bmatrix} \begin{bmatrix} \epsilon_x^o \\ \epsilon_y^o \\ \gamma_s^o \end{bmatrix} \quad (5.38)$$

and

$$\begin{bmatrix} M_x \\ M_y \\ M_s \end{bmatrix} = \begin{bmatrix} D_{xx} & D_{xy} & 0 \\ D_{yx} & D_{yy} & 0 \\ 0 & 0 & D_{ss} \end{bmatrix} \begin{bmatrix} \kappa_x \\ \kappa_y \\ \kappa_s \end{bmatrix} \quad (5.39)$$

5.7.3 Symmetric Angle-Ply Laminates

Laminates containing plies oriented at $+\theta$ and $-\theta$ directions are called *angle-ply laminates*. They can be symmetric or asymmetric. If such a laminate consists of an odd number of alternating $+\theta$ and $-\theta$ plies of equal thickness, then it is symmetric, e.g., $[\theta/-\theta/\theta/-\theta/\theta]_s$. The shear coupling terms A_{xs} , A_{ys} , D_{xs} , and D_{ys} are nonzero, but their magnitude decreases with increasing number of layers for the same overall laminate thickness.

5.8 Balanced Laminates

A laminate is balanced when it consists of pairs of layers with identical thickness and elastic properties but have $+\theta$ and $-\theta$ orientations of their principal material axes with respect to the laminate reference axes. For such a laminate, the in-plane shear coupling terms are

$$A_{is} = \sum_{k=1}^n Q_{is}^k (h_k - h_{k-1}) = \sum_{k=1}^n Q_{is}^k t_k \quad (5.40)$$

where $i = x, y$.

The transformed coupling stiffness of a layer of orientation θ is given in terms of the principal stiffnesses by Eq. (3.67). For example,

$$Q_{xs}(\theta) = m^3 n(Q_{11} - Q_{12} - 2Q_{66}) + mn^3(Q_{12} - Q_{22} + 2Q_{66}) \quad (5.41)$$

where $m = \cos \theta$ and $n = \sin \theta$.

The same coupling stiffness for the ply of $-\theta$ orientation would have the same magnitude but opposite sign because the terms $m^3 n$ and nm^3 above are odd in $n = \sin \theta$. Thus

$$Q_{is}(\theta) = -Q_{is}(-\theta) \quad (5.42)$$

For each balanced pair of layers k and k'

$$t_k = t_{k'}$$

$$\theta_k = -\theta_{k'}$$

Then, from Eqs. (5.40) and (5.42), we conclude that

$$A_{is} = 0 \quad (i = x, y)$$

The fact that the in-plane shear coupling stiffnesses A_{is} are zero is a defining characteristic of a balanced laminate.

A balanced laminate can be symmetric, antisymmetric, or asymmetric. For example, a laminate consisting of pairs of θ_1 and $-\theta_1$ and θ_2 and $-\theta_2$ plies can be arranged in the following lay-ups:

Symmetric:	$[\pm\theta_1/\pm\theta_2]_s$
Antisymmetric:	$[\theta_1/\theta_2/-\theta_2/-\theta_1]$
Asymmetric:	$[\theta_1/\theta_2/-\theta_1/-\theta_2]$

In general, the bending/twisting coupling stiffnesses D_{is} are not zero unless the laminate is antisymmetric, as we can see below.

5.8.1 Antisymmetric Laminates

An antisymmetric laminate is a special case of a balanced laminate, having its balanced $+\theta$ and $-\theta$ pairs symmetrically situated about the middle surface.

In this case the bending/twisting coupling stiffnesses are

$$D_{is} = \frac{1}{3} \sum_{k=1}^n Q_{is}^k (h_k^3 - h_{k-1}^3) = 0 \quad (5.43)$$

since

$$(h_k^3 - h_{k-1}^3) = (h_k^3 - h_{k'-1}^3)$$

and

$$Q_{is}^k = -Q_{is}^{k'}$$

for the symmetrically situated balanced pair of k and k' (or θ and $-\theta$) layers.

The coupling stiffnesses B_{ij} for antisymmetric laminates are in general non-zero, and they vary according to the specific lay-up. The overall load-deformation relations for this class of laminates are

$$\begin{bmatrix} N_x \\ N_y \\ N_s \\ M_x \\ M_y \\ M_s \end{bmatrix} = \begin{bmatrix} A_{xx} & A_{xy} & 0 & B_{xx} & B_{xy} & B_{xs} \\ A_{yx} & A_{yy} & 0 & B_{yx} & B_{yy} & B_{ys} \\ 0 & 0 & A_{ss} & B_{sx} & B_{sy} & B_{ss} \\ B_{xx} & B_{xy} & B_{xs} & D_{xx} & D_{xy} & 0 \\ B_{yx} & B_{yy} & B_{ys} & D_{yx} & D_{yy} & 0 \\ B_{sx} & B_{sy} & B_{ss} & 0 & 0 & D_{ss} \end{bmatrix} \begin{bmatrix} \epsilon_x^o \\ \epsilon_y^o \\ \gamma_s^o \\ \kappa_x \\ \kappa_y \\ \kappa_s \end{bmatrix} \quad (5.44)$$

5.8.2 Antisymmetric Crossply Laminates

Antisymmetric crossply laminates consist of 0° and 90° plies arranged in such a way that for every 0° ply at a distance z from the midplane there is a 90° ply of the same material and thickness at a distance $-z$ from the midplane. By definition then, this laminate has an even number of plies.

For every pair k and k' of 0° and 90° plies we have

$$\begin{aligned} z_k &= -z_{k'} \\ t_k &= t_{k'} \\ Q_{xx}^k &= Q_{yy}^{k'} \\ Q_{yy}^k &= Q_{xx}^{k'} \\ Q_{xy}^k &= Q_{xy}^{k'} \\ Q_{xs}^k &= Q_{ys}^k = Q_{xs}^{k'} = Q_{ys}^{k'} = 0 \end{aligned} \quad (5.45)$$

Then, it follows from the definitions of laminate stiffnesses that

$$\begin{aligned}
 A_{xx} &= A_{yy} \\
 A_{xs} &= A_{ys} = 0 \\
 B_{xx} &= -B_{yy} \\
 B_{xy} &= B_{xs} = B_{ys} = B_{ss} = 0 \\
 D_{xx} &= D_{yy} \\
 D_{xs} &= D_{ys} = 0
 \end{aligned} \tag{5.46}$$

The overall load-deformation relations are

$$\begin{bmatrix} N_x \\ N_y \\ N_s \\ M_x \\ M_y \\ M_s \end{bmatrix} = \begin{bmatrix} A_{xx} & A_{xy} & 0 & B_{xx} & 0 & 0 \\ A_{yx} & A_{xx} & 0 & 0 & -B_{xx} & 0 \\ 0 & 0 & A_{ss} & 0 & 0 & 0 \\ \hline B_{xx} & 0 & 0 & D_{xx} & D_{xy} & 0 \\ 0 & -B_{xx} & 0 & D_{yx} & D_{xx} & 0 \\ 0 & 0 & 0 & 0 & 0 & D_{ss} \end{bmatrix} \begin{bmatrix} \epsilon_x^o \\ \epsilon_y^o \\ \gamma_s^o \\ \kappa_x \\ \kappa_y \\ \kappa_s \end{bmatrix} \tag{5.47}$$

For crossply laminates with alternating 0° and 90° plies, the coupling stiffness B_{xx} approaches zero as the number of plies increases for a constant laminate thickness.

Sample Problem 5.1

Stiffnesses of Antisymmetric Crossply Laminate

It is required to derive approximate expressions for stiffnesses A_{xx} , A_{xy} , A_{ss} , B_{xx} , D_{xx} , D_{xy} , and D_{ss} of a $[0/90]$ antisymmetric crossply laminate in terms of the basic lamina properties (E_1 , E_2 , G_{12} and ν_{12}) and the lamina thickness t . It is assumed that the composite material contains high stiffness fibers such that $E_1 \gg E_2$ and $\nu_{21} \ll 1$.

From the definitions of laminate stiffnesses we obtain

$$\begin{aligned}
 A_{xx} &= \sum_{k=1}^n Q_{xx}^k (h_k - h_{k-1}) = (Q_{11} + Q_{22}) t \\
 &= \frac{t}{1 - \nu_{12} \nu_{21}} (E_1 + E_2) \cong (E_1 + E_2) t
 \end{aligned} \tag{5.48}$$

$$\begin{aligned}
 A_{xy} &= \sum_{k=1}^n Q_{xy}^k (h_k - h_{k-1}) = 2 Q_{12} t \\
 &= \frac{2 \nu_{12} E_2 t}{1 - \nu_{12} \nu_{21}} \cong 2 \nu_{12} E_2 t
 \end{aligned} \tag{5.49}$$

$$A_{ss} = \sum_{k=1}^n Q_{ss}^k (h_k - h_{k-1}) = 2 G_{12} t \quad (5.50)$$

$$B_{xx} = \frac{1}{2} \sum_{k=1}^n Q_{xx}^k (h_k^2 - h_{k-1}^2) \cong \frac{t^2}{2} (E_1 - E_2) \quad (5.51)$$

$$D_{xx} = \frac{1}{3} \sum_{k=1}^n Q_{xx}^k (h_k^3 - h_{k-1}^3) \cong \frac{t^3}{3} (E_1 + E_2) \quad (5.52)$$

$$D_{xy} = \frac{1}{3} \sum_{k=1}^n Q_{xy}^k (h_k^3 - h_{k-1}^3) \cong \frac{2}{3} t^3 \nu_{12} E_2 \quad (5.53)$$

$$D_{ss} = \frac{1}{3} \sum_{k=1}^n Q_{ss}^k (h_k^3 - h_{k-1}^3) = \frac{2}{3} t^3 G_{12} \quad (5.54)$$

5.8.3 Antisymmetric Angle-Ply Laminates

Antisymmetric angle-ply laminates consist of pairs of plies of $+\theta_i$ and $-\theta_i$ orientations ($0 < \theta_i < 90$), symmetrically situated about the middle plane and having the same thickness and elastic properties. Because of antisymmetry

$$A_{is} = D_{is} = 0 \quad \text{with } i = x, y$$

For every balanced pair of k and k' plies with orientations θ and $-\theta$ we have

$$\begin{aligned} z_k &= -z_{k'} \\ t_k &= t_{k'} \\ Q_{xx}^k &= Q_{xx}^{k'} \\ Q_{yy}^k &= Q_{yy}^{k'} \\ Q_{xy}^k &= Q_{xy}^{k'} \\ Q_{xs}^k &= -Q_{xs}^{k'} \\ Q_{ys}^k &= -Q_{ys}^{k'} \\ Q_{ss}^k &= Q_{ss}^{k'} \end{aligned} \quad (5.55)$$

Then, from the definition of B_{ij} it follows that

$$B_{xx} = B_{yy} = B_{xy} = B_{ss} = 0$$

and the overall load-deformation relations take the form

$$\begin{bmatrix} N_x \\ N_y \\ N_s \\ M_x \\ M_y \\ M_s \end{bmatrix} = \begin{bmatrix} A_{xx} & A_{xy} & 0 & 0 & 0 & B_{xs} \\ A_{yx} & A_{yy} & 0 & 0 & 0 & B_{ys} \\ 0 & 0 & A_{ss} & B_{sx} & B_{sy} & 0 \\ 0 & 0 & B_{xs} & D_{xx} & D_{xy} & 0 \\ 0 & 0 & B_{ys} & D_{yx} & D_{yy} & 0 \\ B_{sx} & B_{sy} & 0 & 0 & 0 & D_{ss} \end{bmatrix} \begin{bmatrix} \epsilon_x^o \\ \epsilon_y^o \\ \gamma_s^o \\ \kappa_x \\ \kappa_y \\ \kappa_s \end{bmatrix} \quad (5.56)$$

A more special case of this class of laminates is the antisymmetric regular angle-ply laminate, consisting of an even number of plies alternating between θ and $-\theta$ in orientation, i.e., $[\theta/-\theta/\theta/.../\theta/-\theta]_n$.

The nonzero coupling stiffnesses B_{xs} and B_{ys} decrease and approach zero as the number of plies increases for the same overall laminate thickness.

5.9 Orthotropic Laminates: Transformation of Laminate Stiffnesses and Compliances

A balanced symmetric laminate has its ply orientations parallel to or balanced about two perpendicular axes \bar{x} and \bar{y} , referred to as *principal laminate axes* (Fig. 5.7). On a macroscopic scale, this laminate can be treated as a homogeneous orthotropic material with the \bar{x} and \bar{y} axes as the principal axes of the equivalent material. This type of laminate is called an *orthotropic laminate*.

By definition, the in-plane/flexure coupling stiffnesses and the in-plane shear coupling stiffnesses are zero, i.e.,

$$B_{ij} = 0 \quad (i, j = \bar{x}, \bar{y}, \bar{s})$$

and

$$A_{i\bar{s}} = 0 \quad (i = \bar{x}, \bar{y})$$

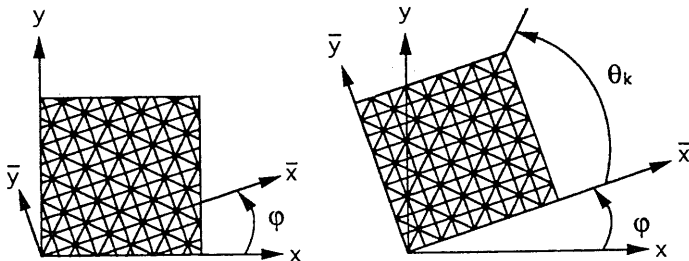


Fig. 5.7 Notation for coordinate transformation in orthotropic laminate.

Thus, the force-deformation relations referred to the $\bar{x}\bar{y}$ system of coordinates are

$$\begin{bmatrix} N_{\bar{x}} \\ N_{\bar{y}} \\ N_{\bar{s}} \end{bmatrix} = \begin{bmatrix} A_{\bar{x}\bar{x}} & A_{\bar{x}\bar{y}} & 0 \\ A_{\bar{y}\bar{x}} & A_{\bar{y}\bar{y}} & 0 \\ 0 & 0 & A_{\bar{s}\bar{s}} \end{bmatrix} \begin{bmatrix} \epsilon_{\bar{x}}^o \\ \epsilon_{\bar{y}}^o \\ \gamma_{\bar{s}}^o \end{bmatrix} \quad (5.57)$$

These relations, when referred to the xy system (Fig. 5.7), take the form

$$\begin{bmatrix} N_x \\ N_y \\ N_s \end{bmatrix} = \begin{bmatrix} A_{xx} & A_{xy} & A_{xs} \\ A_{yx} & A_{yy} & A_{ys} \\ A_{sx} & A_{sy} & A_{ss} \end{bmatrix} \begin{bmatrix} \epsilon_x^o \\ \epsilon_y^o \\ \gamma_s^o \end{bmatrix} \quad (5.58)$$

or, in brief,

$$[N]_{x,y} = [A]_{x,y}[\epsilon^o]_{x,y}$$

Equations (5.57) and (5.58) are entirely analogous to Eqs. (3.31) and (3.63), where the following correspondences are noted:

$$\begin{bmatrix} \bar{x} \\ \bar{y} \\ \bar{s} \end{bmatrix} \rightarrow \begin{bmatrix} 1 \\ 2 \\ 6 \end{bmatrix}, \quad \varphi \rightarrow \theta$$

$$\begin{bmatrix} N_{\bar{x}} \\ N_{\bar{y}} \\ N_{\bar{s}} \end{bmatrix} \rightarrow \begin{bmatrix} \sigma_1 \\ \sigma_2 \\ \tau_6 \end{bmatrix}, \quad \begin{bmatrix} N_x \\ N_y \\ N_s \end{bmatrix} \rightarrow \begin{bmatrix} \sigma_x \\ \sigma_y \\ \tau_s \end{bmatrix}$$

$$\begin{bmatrix} \epsilon_{\bar{x}}^o \\ \epsilon_{\bar{y}}^o \\ \gamma_{\bar{s}}^o \end{bmatrix} \rightarrow \begin{bmatrix} \epsilon_1 \\ \epsilon_2 \\ \gamma_6 \end{bmatrix}, \quad \begin{bmatrix} \epsilon_x^o \\ \epsilon_y^o \\ \gamma_s^o \end{bmatrix} \rightarrow \begin{bmatrix} \epsilon_x \\ \epsilon_y \\ \gamma_s \end{bmatrix}$$

$$\begin{bmatrix} A_{\bar{x}\bar{x}} & A_{\bar{x}\bar{y}} & 0 \\ A_{\bar{y}\bar{x}} & A_{\bar{y}\bar{y}} & 0 \\ 0 & 0 & A_{\bar{s}\bar{s}} \end{bmatrix} \rightarrow \begin{bmatrix} Q_{11} & Q_{12} & 0 \\ Q_{21} & Q_{22} & 0 \\ 0 & 0 & Q_{66} \end{bmatrix}$$

$$\begin{bmatrix} A_{xx} & A_{xy} & A_{xs} \\ A_{yx} & A_{yy} & A_{ys} \\ A_{sx} & A_{sy} & A_{ss} \end{bmatrix} \rightarrow \begin{bmatrix} Q_{xx} & Q_{xy} & Q_{xs} \\ Q_{yx} & Q_{yy} & Q_{ys} \\ Q_{sx} & Q_{sy} & Q_{ss} \end{bmatrix}$$

Table 5.1 Relations for Stiffness and Compliance Transformation of Orthotropic Laminates

	$a_{\bar{x}\bar{x}}(A_{\bar{x}\bar{x}})$	$a_{\bar{y}\bar{y}}(A_{\bar{y}\bar{y}})$	$a_{\bar{x}\bar{y}}(A_{\bar{x}\bar{y}})$	$a_{\bar{s}\bar{s}}(4A_{\bar{s}\bar{s}})$
$a_{xx}(A_{xx})$	m^4	n^4	$2m^2n^2$	m^2n^2
$a_{yy}(A_{yy})$	n^4	m^4	$2m^2n^2$	m^2n^2
$a_{xy}(A_{xy})$	m^2n^2	m^2n^2	$(m^4 + n^4)$	$-m^2n^2$
$a_{ss}(4A_{ss})$	$4m^2n^2$	$4m^2n^2$	$-8m^2n^2$	$(m^2 - n^2)^2$
$a_{xs}(2A_{xs})$	$2m^3n$	$-2mn^3$	$2(mn^3 - m^3n)$	$(mn^3 - m^3n)$
$a_{ys}(2A_{ys})$	$2mn^3$	$-2nm^3$	$2(m^3n - mn^3)$	$(m^3n - mn^3)$

$m = \cos\phi, n = \sin\phi.$

Then, the relations described in Table 5.1, analogous to those in Table 3.2, hold true for the laminate stiffnesses and compliances.

5.10 Quasi-Isotropic Laminates

There is a special class of orthotropic laminates for which the elastic properties are independent of orientation, i.e., the in-plane stiffnesses and compliances and all engineering elastic constants are identical in all directions. Referring to Figure 5.8, this condition is expressed as

$$\begin{aligned}
 [A]_{\bar{x}, \bar{y}} &= [A]_{x,y} = \text{constant} \\
 [a]_{\bar{x}, \bar{y}} &= [a]_{x,y} = \text{constant}
 \end{aligned}
 \tag{5.59}$$

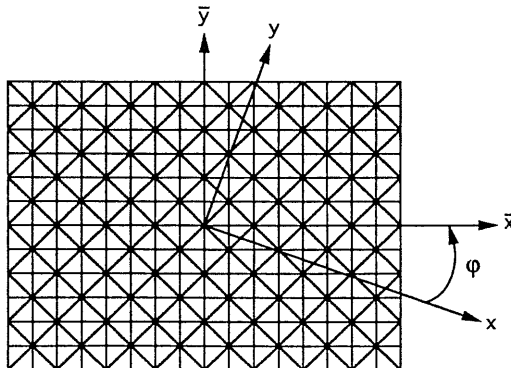


Fig. 5.8 Quasi-isotropic laminate.

or, in terms of engineering constants,

$$\begin{aligned}\bar{E}_{\bar{x}} &= \bar{E}_x = \text{constant} \\ \bar{G}_{\bar{x}\bar{y}} &= \bar{G}_{xy} = \text{constant} \\ \bar{\nu}_{\bar{x}\bar{y}} &= \bar{\nu}_{xy} = \text{constant} \\ \bar{\eta}_{\bar{x}\bar{s}} &= \bar{\eta}_{\bar{y}\bar{s}} = \bar{\eta}_{xs} = \bar{\eta}_{ys} = 0\end{aligned}\tag{5.60}$$

where symbols with overbar denote effective laminate properties. All of the above properties are invariant with respect to orientation φ .

All shear coupling coefficients are zero because all quasi-isotropic laminates are balanced; therefore, $A_{xs} = A_{ys} = 0$. The simplest type of quasi-isotropic laminate is one of $[0/60/-60]_s$ lay-up. Another type is the so-called $\pi/4$ quasi-isotropic laminate, or $[0/\pm 45/90]_s$. In general any laminate of

$$\left[0/\frac{\pi}{n}/\frac{2\pi}{n}/\dots/\frac{n-1}{n}\pi \right]_s$$

or

$$\left[\frac{\pi}{n}/\frac{2\pi}{n}/\dots/\pi \right]_s$$

lay-up is quasi-isotropic for any integer n greater than 2.

Sample Problem 5.2

Quasi-Isotropic $[0/\pm 45/90]_s$ Laminate

It is required to prove that the $[0/\pm 45/90]_s$ laminate is quasi-isotropic. Referring to Figure 5.8 and the specific laminate lay-up, we observe that

$$\begin{aligned}A_{\bar{x}\bar{x}} &= A_{\bar{y}\bar{y}} = (A_{xx})_{\varphi=45^\circ} \\ A_{\bar{s}\bar{s}} &= (A_{ss})_{\varphi=45^\circ}\end{aligned}\tag{5.61}$$

From the stiffness transformation relations (Table 5.1) and Eq. (5.61) we obtain for $\varphi = 45^\circ$

$$(A_{ss})_{\varphi=45^\circ} = A_{\bar{s}\bar{s}} = \frac{1}{2}(A_{\bar{x}\bar{x}} - A_{\bar{y}\bar{y}})\tag{5.62}$$

The stiffness A_{xx} along any arbitrary direction φ is

$$A_{xx} = (m^4 + n^4) A_{\bar{x}\bar{x}} + 2 m^2 n^2 A_{\bar{x}\bar{y}} + 4 m^2 n^2 A_{\bar{y}\bar{y}}$$

and, in view of Eq. (5.62),

$$\begin{aligned} A_{xx} &= (m^4 + n^4) A_{\bar{x}\bar{x}} + 2 m^2 n^2 (A_{\bar{x}\bar{y}} + A_{\bar{x}\bar{x}} - A_{\bar{x}\bar{y}}) \\ &= (m^4 + n^4 + 2 m^2 n^2) A_{\bar{x}\bar{x}} = (m^2 + n^2)^2 A_{\bar{x}\bar{x}} = A_{\bar{x}\bar{x}} \end{aligned} \quad (5.63)$$

Similarly we can prove that

$$A_{xy} = A_{\bar{x}\bar{y}} \quad (5.64)$$

$$A_{ss} = A_{\bar{s}\bar{s}} \quad (5.65)$$

$$A_{xs} = A_{ys} = 0 \quad (5.66)$$

5.11 Design Considerations

The coupling stiffnesses B_{ij} , A_{is} , and D_{is} complicate the analysis and design of multilayer and multidirectional laminates.

The bending coupling stiffnesses $B_{ij}(i,j = x,y,s)$, coupling in-plane loading with out-of-plane deformation, are responsible for laminate warpage due to cool-down after curing and to hygrothermal environment variations. It is therefore desirable in general to eliminate this type of coupling by selecting a symmetric layup. It is conceivable that in some special designs such a coupling might be used to advantage, such as laminate shells subjected to aerodynamic loading. In other cases of nonsymmetric laminates, it is possible to minimize bending coupling by selecting an appropriate stacking sequence.

Shear coupling stiffnesses A_{xs} and A_{ys} cause in-plane shear deformations under in-plane normal loading and normal in-plane deformation under in-plane shear loading. These stiffnesses become zero for a balanced or a crossply lay-up. For unbalanced laminates it is advisable to select the stacking sequence that minimizes the shear coupling stiffnesses.

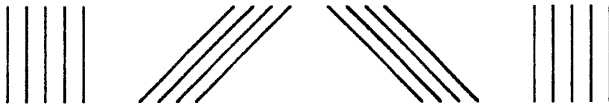
Torsion coupling stiffnesses D_{xs} and D_{ys} are responsible for twisting deformation under cylindrical flexure and may produce interlaminar stresses under bending. These stiffnesses are zero only for antisymmetric (special case of balanced) or crossply lay-ups. In other cases it is possible to minimize the torsion coupling stiffnesses by a proper choice of stacking sequence.

The only lay-up for which all three types of coupling stiffnesses B_{ij} , A_{is} , and D_{is} are zero is the crossply symmetric lay-up, e.g., $[0/90_2]_s$. One can design

symmetric and balanced laminates where $B_{ij} = 0$ and $A_{is} = 0$, but in general $D_{is} \neq 0$. However, by proper selection of the stacking sequence, e.g., by increasing the number of layers for the same overall laminate thickness, D_{is} can be minimized.

Consider, for example, a laminate consisting of ten 0° plies, four 45° plies, and four -45° plies arranged in the following three stacking sequences:

Balanced/asymmetric: $[0_5/45_4/-45_4/0_5]$



This stacking sequence is definitely not recommended because of its asymmetry and coarse ply distribution. The shear coupling stiffnesses A_{is} and torsion coupling stiffnesses D_{is} are zero, but the extension/bending coupling stiffnesses (B_{ij}) are nonzero. The coarseness of the ply distribution would make any interlaminar edge stresses present more serious. It has been shown analytically that interlaminar edge stresses are a function of the stacking sequence and decrease as the thickness of the various layers decreases.⁴

Balanced/symmetric: $[0_5/45_2/-45_2]_s$



This stacking sequence is balanced and symmetric; therefore, $B_{ij} = 0$ and $A_{is} = 0$. However, the torsion coupling stiffnesses D_{is} are nonzero and are relatively high due to the coarseness of the ply distribution. It represents an adequate but not the best design.

Balanced/symmetric: $[0_2/45_2/0_2/-45_2/0]_s$



The bending coupling stiffnesses B_{ij} and shear coupling stiffnesses A_{is} are zero again. The nonzero torsion coupling stiffnesses D_{is} are relatively low, near their minimum, because of the fine ply distribution. This design is rec-

ommended. The absolute minimum for D_{is} is obtained by selecting an even finer ply distribution, e.g., $[0/45/0/-45/0/45/0/-45/0]_s$. Although this design represents an optimum mechanically, it may make the fabrication process more complicated.

Whenever possible it is recommended to select a symmetric and balanced lay-up with fine ply interdispersion in order to eliminate bending coupling and shear coupling and to minimize torsion coupling. Thus warpage and unexpected distortions will be avoided, interlaminar stresses will be reduced, and the analysis will become considerably simpler.

5.12 Laminate Engineering Properties

Simple relations can be derived for engineering properties as a function of laminate stiffnesses for the special case of a symmetric balanced laminate. Consider an element of such a laminate under uniaxial loading N_x as shown in Figure 5.9. Then, by definition, the Young's modulus \bar{E}_x and Poisson's ratio $\bar{\nu}_{xy}$ of the laminate are given by

$$\begin{aligned}\bar{E}_x &= \frac{N_x}{h\epsilon_x^o} \\ \bar{\nu}_{xy} &= -\frac{\epsilon_y^o}{\epsilon_x^o}\end{aligned}\quad (5.67)$$

where ϵ_x^o , ϵ_y^o are the normal strains in the x - and y -directions, respectively, and h is the laminate thickness. Symbols with an overbar denote effective laminate

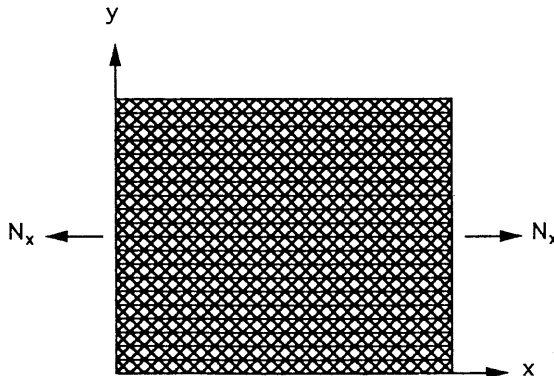


Fig. 5.9 Symmetric balanced laminate under uniaxial loading.

properties, and the x and y axes here are the principal laminate axes (denoted before as \bar{x} and \bar{y}).

The force-deformation relations are

$$\begin{bmatrix} N_x \\ 0 \\ 0 \end{bmatrix} = \begin{bmatrix} A_{xx} & A_{xy} & 0 \\ A_{yx} & A_{yy} & 0 \\ 0 & 0 & A_{ss} \end{bmatrix} \begin{bmatrix} \epsilon_x^o \\ \epsilon_y^o \\ 0 \end{bmatrix} \quad (5.68)$$

There is no shear strain γ_s^o under the applied loading because the laminate is balanced.

Equations (5.68) in expanded form are ($A_{xy} = A_{yx}$)

$$\begin{aligned} N_x &= A_{xx} \epsilon_x^o + A_{xy} \epsilon_y^o \\ 0 &= A_{xy} \epsilon_x^o + A_{yy} \epsilon_y^o \end{aligned} \quad (5.69)$$

From Eqs. (5.69) and (5.67) we obtain

$$\begin{aligned} \bar{E}_x &= \frac{1}{h} \left[A_{xx} - \frac{A_{xy}^2}{A_{yy}} \right] \\ \bar{\nu}_{xy} &= \frac{A_{xy}}{A_{yy}} \end{aligned} \quad (5.70)$$

Similarly, by considering a uniaxial loading N_y in the y -direction we obtain

$$\begin{aligned} \bar{E}_y &= \frac{1}{h} \left[A_{yy} - \frac{A_{xy}^2}{A_{xx}} \right] \\ \bar{\nu}_{yx} &= \frac{A_{xy}}{A_{xx}} \end{aligned} \quad (5.71)$$

For pure shear loading N_s we obtain

$$\bar{G}_{xy} = \frac{A_{ss}}{h} \quad (5.72)$$

The shear coupling coefficients for this balanced laminate are zero:

$$\bar{\eta}_{xs} = \bar{\eta}_{ys} = \bar{\eta}_{sx} = \bar{\eta}_{sy} = 0 \quad (5.73)$$

Expressions for engineering properties in terms of laminate stiffnesses are more complicated for more general types of laminates, such as symmetric but not balanced laminates. In that case it is preferable to develop relations in terms of laminate compliances. For symmetric laminates the bending coupling stiffnesses B_{ij} and compliances b_{ij} and c_{ij} , with $i, j = x, y, s$, are zero. Thus the reference plane strains are related only to in-plane forces as follows:

$$\begin{bmatrix} \epsilon_x^o \\ \epsilon_y^o \\ \gamma_s^o \end{bmatrix} = \begin{bmatrix} a_{xx} & a_{xy} & a_{xs} \\ a_{yx} & a_{yy} & a_{ys} \\ a_{sx} & a_{sy} & a_{ss} \end{bmatrix} \begin{bmatrix} N_x \\ N_y \\ N_s \end{bmatrix} \quad (5.74)$$

where $[a]$ is the extensional laminate compliance matrix, which is the inverse of the corresponding stiffness matrix

$$[a] = [A]^{-1} \quad (5.75)$$

A symmetric laminate may be treated on a macroscopic scale as a homogeneous orthotropic material. Its elastic behavior is analogous to that of a unidirectional lamina, and thus similar expressions can be used between average stresses and strains and effective laminate constants. Thus, Eq. (5.74) can be written in terms of engineering constants by replacing the lamina constants in Eq. (3.77) with corresponding laminate moduli and noting that the average laminate stresses are

$$\begin{bmatrix} \bar{\sigma}_x \\ \bar{\sigma}_y \\ \bar{\tau}_s \end{bmatrix} = \begin{bmatrix} N_x \\ N_y \\ N_s \end{bmatrix} \frac{1}{h} \quad (5.76)$$

Thus the strain-force relations for the laminate are written in terms of engineering constants as follows:

$$\begin{bmatrix} \epsilon_x^o \\ \epsilon_y^o \\ \gamma_s^o \end{bmatrix} = \begin{bmatrix} \frac{1}{\bar{E}_x} & -\frac{\bar{\nu}_{yx}}{\bar{E}_y} & \frac{\bar{\eta}_{sx}}{\bar{G}_{xy}} \\ -\frac{\bar{\nu}_{xy}}{\bar{E}_x} & \frac{1}{\bar{E}_y} & \frac{\bar{\eta}_{sy}}{\bar{G}_{xy}} \\ \frac{\bar{\eta}_{xs}}{\bar{E}_x} & \frac{\bar{\eta}_{ys}}{\bar{E}_y} & \frac{1}{\bar{G}_{xy}} \end{bmatrix} \begin{bmatrix} N_x \\ N_y \\ N_s \end{bmatrix} \frac{1}{h} \quad (5.77)$$

where

\bar{E}_x, \bar{E}_y = Laminate effective Young's moduli in the
x- and y-directions, respectively

$\bar{\nu}_{xy}, \bar{\nu}_{yx}$ = Laminate effective Poisson's ratios

$\bar{\eta}_{xs}, \bar{\eta}_{ys}, \bar{\eta}_{sx}, \bar{\eta}_{sy}$ = Laminate effective shear coupling
coefficients

By equating corresponding terms in the compliance matrices of Eqs. (5.74) and (5.77), we obtain the following relations, analogous to Eqs (3.80):

$$\begin{aligned} \bar{E}_x &= \frac{1}{h a_{xx}}, & \bar{E}_y &= \frac{1}{h a_{yy}}, & \bar{G}_{xy} &= \frac{1}{h a_{ss}} \\ \bar{\nu}_{xy} &= -\frac{a_{yx}}{a_{xx}}, & \bar{\nu}_{yx} &= -\frac{a_{xy}}{a_{yy}}, & \bar{\eta}_{sx} &= \frac{a_{xs}}{a_{ss}} \\ \bar{\eta}_{xs} &= \frac{a_{sx}}{a_{xx}}, & \bar{\eta}_{ys} &= \frac{a_{sy}}{a_{yy}}, & \bar{\eta}_{sy} &= \frac{a_{ys}}{a_{ss}} \end{aligned} \quad (5.78)$$

The symmetry of the compliance matrix implies the following relations among the laminate engineering constants, as in the case of the single unidirectional lamina (Eq. 3.78):

$$\begin{aligned} \frac{\bar{\nu}_{xy}}{\bar{E}_x} &= \frac{\bar{\nu}_{yx}}{\bar{E}_y} \\ \frac{\bar{\eta}_{xs}}{\bar{E}_x} &= \frac{\bar{\eta}_{sx}}{\bar{G}_{xy}} \\ \frac{\bar{\eta}_{ys}}{\bar{E}_y} &= \frac{\bar{\eta}_{sy}}{\bar{G}_{xy}} \end{aligned} \quad (5.79)$$

Thus, in order to calculate the engineering properties of a symmetric laminate using Eq. (5.78) one needs to calculate the extensional stiffness matrix $[A]$ and then invert it to obtain the compliance matrix $[a]$.

Expressions for engineering constants of general asymmetric laminates can be obtained from the general strain-load relations (Eq. 5.25) that reduce to Eq. (5.74) for in-plane loading. Thus, using the normal definitions of engineering properties in terms of average in-plane stresses and strains, one obtains that relations in Eq. (5.78) are equally valid for general laminates. For example, comparison of engineering constants of a $[0/90]$ asymmetric and a $[0/90]_s$ symmetric laminate leads to the correct conclusion that the Young's moduli are different for the two laminates. This is because in Eq. (5.78) the compliance matrices $[a_{ij}]$ are different for the two laminates due to coupling effects.

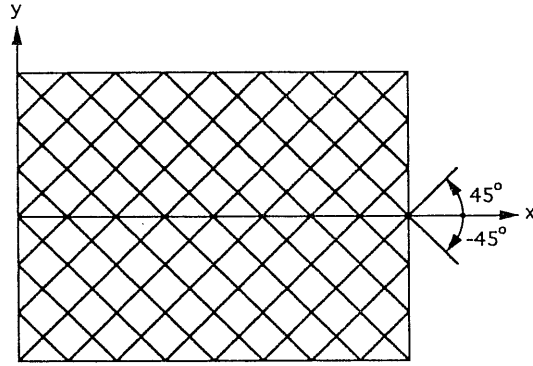


Fig. 5.10 $[\pm 45]_{ns}$ angle-ply laminate.

Sample Problem 5.3

Axial Modulus of Angle-Ply Laminate

It is required to determine Young's modulus \bar{E}_x of a $[\pm 45]_{ns}$ laminate in terms of the basic lamina properties (Fig. 5.10). For this balanced symmetric laminate we can apply Eq. (5.70)

$$\bar{E}_x = \frac{1}{h} \left[A_{xx} - \frac{A_{xy}^2}{A_{yy}} \right] \quad (5.70 \text{ bis})$$

where

$$\begin{aligned} A_{xx} &= \sum_{k=1}^{4n} (Q_{xx})^k t_k = h Q_{xx} \\ A_{xy} &= \sum_{k=1}^{4n} (Q_{xy})^k t_k = h Q_{xy} \\ A_{yy} &= \sum_{k=1}^{4n} (Q_{yy})^k t_k = h Q_{yy} \end{aligned} \quad (5.80)$$

where t_k is the ply thickness, h the laminate thickness and Q_{xx} , Q_{yy} , Q_{xy} the transformed 45° lamina stiffnesses.

From the stiffness transformation relations in Eq. (3.67) we obtain

$$(Q_{xx})_{\theta=\pm 45^\circ} = (Q_{yy})_{\theta=\pm 45^\circ} = \frac{1}{4}(Q_{11} + Q_{22} + 2Q_{12} + 4Q_{66}) \quad (5.81)$$

$$(Q_{xy})_{\theta=\pm 45^\circ} = \frac{1}{4}(Q_{11} + Q_{22} + 2Q_{12} - 4Q_{66}) \quad (5.82)$$

Then,

$$A_{xx} = A_{yy} = \frac{h}{4}(Q_{11} + Q_{22} + 2Q_{12} + 4Q_{66}) \quad (5.83)$$

$$A_{xy} = \frac{h}{4}(Q_{11} + Q_{22} + 2Q_{12} - 4Q_{66}) \quad (5.84)$$

From Eqs. (5.70) and (5.80) it follows that

$$\begin{aligned} \bar{E}_x &= \left(Q_{xx} - \frac{Q_{xy}^2}{Q_{yy}} \right)_{\theta=\pm 45^\circ} = \left(Q_{xx} - \frac{Q_{xy}^2}{Q_{xx}} \right)_{\theta=\pm 45^\circ} \\ &= \frac{1}{Q_{xx}}(Q_{xx} + Q_{xy})(Q_{xx} - Q_{xy}) \quad (\text{for } \theta = \pm 45^\circ) \end{aligned} \quad (5.85)$$

and from Eqs. (5.81) and (5.82)

$$\bar{E}_x = \frac{4(Q_{11} + Q_{22} + 2Q_{12}) Q_{66}}{Q_{11} + Q_{22} + 2Q_{12} + 4Q_{66}} \quad (5.86)$$

For composites with high stiffness fibers

$$Q_{11} \gg Q_{22}$$

$$Q_{11} \gg Q_{12} \quad (5.87)$$

$$Q_{11} \gg Q_{66}$$

and then Eq. (5.86) reduces to

$$\bar{E}_x \cong \frac{4Q_{11} Q_{66}}{Q_{11}} = 4Q_{66} = 4G_{12} \quad (5.88)$$

This result shows that the axial Young's modulus of a $[\pm 45]_{ns}$ laminate is a matrix-dominated property since it depends primarily on the in-plane shear modulus G_{12} of the lamina. This was also true for the case of the $[45]$ off-axis lamina (see Eq. 3.83).

Sample Problem 5.4

Shear Modulus of Angle-Ply Laminate

It is required to determine the shear modulus \bar{G}_{xy} of a $[\pm 45]_{ns}$ laminate as a function of the basic lamina properties (Fig. 5.10). This is obtained from Eq. (5.72)

$$\bar{G}_{xy} = \frac{A_{ss}}{h} \quad (5.72 \text{ bis})$$

where

$$A_{ss} = \sum_{k=1}^{4n} (Q_{ss})^k t_k = h (Q_{ss})_{\theta=\pm 45^\circ} \quad (5.89)$$

From the stiffness transformation relations in Eq. (3.67) we obtain

$$(Q_{ss})_{\theta=\pm 45^\circ} = \frac{1}{4} (Q_{11} + Q_{22} - 2Q_{12}) \quad (5.90)$$

and then, using Eqs. (5.72) and (5.89),

$$\bar{G}_{xy} = (Q_{ss})_{\theta=\pm 45^\circ} = \frac{1}{4} (Q_{11} + Q_{22} - 2Q_{12}) \quad (5.91)$$

For composites with high stiffness fibers

$$\bar{G}_{xy} \cong \frac{Q_{11}}{4} \cong \frac{E_1}{4} \quad (5.92)$$

Thus the shear modulus of a $[\pm 45]_{ns}$ laminate is a fiber dominated property since it depends primarily on the longitudinal lamina modulus E_1 .

Sample Problem 5.5

Poisson's Ratio of Angle-Ply Laminate

It is required to determine Poisson's ratio $\bar{\nu}_{xy}$ of a $[\pm 45]_{ns}$ laminate as a function of the basic lamina properties (Fig. 5.10). This is obtained from Eq. (5.70).

$$\bar{v}_{xy} = \frac{A_{xy}}{A_{yy}} \quad (5.70 \text{ bis})$$

Substituting Eqs. (5.83) and (5.84) into Eq. (5.70) yields

$$\bar{v}_{xy} = \frac{Q_{11} + Q_{22} + 2Q_{12} - 4Q_{66}}{Q_{11} + Q_{22} + 2Q_{12} + 4Q_{66}} \quad (5.93)$$

For composites with high stiffness fibers

$$\bar{v}_{xy} \cong \frac{Q_{11} - 4Q_{66}}{Q_{11} + 4Q_{66}} \cong \frac{E_1 - 4G_{12}}{E_1 + 4G_{12}} \quad (5.94)$$

Sample Problem 5.6

Engineering Constants of $[0/\pm 45/90]_s$ Quasi-Isotropic Laminate

For the $[0/\pm 45/90]_s$ laminate discussed before

$$A_{ij} = \sum_{k=1}^n Q_{ij}^k t_k = t \sum_{k=1}^n Q_{ij}^k = \frac{h}{n} \sum_{k=1}^n Q_{ij}^k \quad (5.95)$$

where

$$i, j = x, y, s$$

$$t = \text{Lamina thickness}$$

$$h = \text{Laminate thickness}$$

The transformed lamina stiffnesses Q_{xx} of the four different ply orientations are

$$Q_{xx(\theta=0^\circ)} = Q_{11}$$

$$Q_{xx(\theta=90^\circ)} = Q_{22}$$

$$Q_{xx(\theta=45^\circ)} = Q_{xx(\theta=-45^\circ)} = \frac{1}{4}(Q_{11} + Q_{22} + 2Q_{12} + 4Q_{66})$$

Thus from Eq. (5.95) we obtain

$$A_{xx} = A_{yy} = \frac{h}{8}(3Q_{11} + 3Q_{22} + 2Q_{12} + 4Q_{66}) \quad (5.96)$$

Similarly, from the relations

$$Q_{xy(\theta=0^\circ)} = Q_{xy(\theta=90^\circ)} = Q_{12}$$

$$Q_{xy(\theta=45^\circ)} = Q_{xy(\theta=-45^\circ)} = \frac{1}{4}(Q_{11} + Q_{22} + 2Q_{12} - 4Q_{66})$$

we obtain

$$A_{xy} = \frac{h}{8}(Q_{11} + Q_{22} + 6Q_{12} - 4Q_{66}) \quad (5.97)$$

and from the relations

$$Q_{ss(\theta=0^\circ)} = Q_{ss(\theta=90^\circ)} = Q_{66}$$

$$Q_{ss(\theta=45^\circ)} = Q_{ss(\theta=-45^\circ)} = \frac{1}{4}(Q_{11} + Q_{22} - 2Q_{12})$$

we obtain

$$A_{ss} = \frac{h}{8}(Q_{11} + Q_{22} - 2Q_{12} + 4Q_{66}) \quad (5.98)$$

Introducing Eqs. (5.96) and (5.97) into (5.70), we obtain

$$\begin{aligned} \bar{E}_x &= \frac{1}{hA_{xx}}(A_{xx} + A_{xy})(A_{xx} - A_{xy}) \\ &= \frac{(Q_{11} + Q_{22} + 2Q_{12})(Q_{11} + Q_{22} - 2Q_{12} + 4Q_{66})}{(3Q_{11} + 3Q_{22} + 2Q_{12} + 4Q_{66})} \end{aligned} \quad (5.99)$$

For a high stiffness composite

$$E_1 \gg E_2, \nu_{21} \ll 1, Q_{11} \gg Q_{22}, Q_{11} \gg Q_{12}, Q_{11} \cong E_1$$

and Eq. (5.99) becomes

$$\bar{E}_x = \bar{E}_y \cong \frac{E_1(E_1 + 4G_{12})}{3E_1 + 4G_{12}} \quad (5.100)$$

Similarly, from the same Eqs. (5.96), (5.97) and (5.70) we obtain

$$\bar{\nu}_{xy} = \frac{A_{xy}}{A_{yy}} = \frac{Q_{11} + Q_{22} + 6Q_{12} - 4Q_{66}}{3Q_{11} + 3Q_{22} + 2Q_{12} + 4Q_{66}} \quad (5.101)$$

which, for a high stiffness composite, becomes

$$\bar{\nu}_{xy} \cong \frac{E_1 - 4G_{12}}{3E_1 + 4G_{12}} \quad (5.102)$$

Finally, from Eqs. (5.72) and (5.98) we obtain

$$\bar{G}_{xy} = \frac{A_{ss}}{h} = \frac{1}{8}(Q_{11} + Q_{22} - 2Q_{12} + 4Q_{66}) \quad (5.103)$$

which, for a high stiffness composite, becomes

$$\bar{G}_{xy} \cong \frac{1}{8}(E_1 + 4G_{12}) \quad (5.104)$$

5.13 Computational Procedure for Determination of Engineering Elastic Properties

A flow chart for the determination of engineering properties of multidirectional laminates is given in Figure 5.11. It consists of the following steps:

- Step 1** Enter engineering properties of unidirectional layer, E_1 , E_2 , ν_{12} , and G_{12} .
- Step 2** Calculate layer stiffnesses Q_{11} , Q_{22} , Q_{12} , and Q_{66} referred to its principal material axes using Eq. (3.56).
- Step 3** Enter fiber orientation or principal material axis orientation, θ_k , of layer k .
- Step 4** Calculate transformed stiffnesses $[Q]_{x,y}$ of layer k referred to the laminate coordinate system (x,y) , using Eq. (3.67).
- Step 5** Enter through the thickness coordinates of layer k surfaces h_k and h_{k-1} .
- Step 6** Calculate laminate stiffness matrices $[A]$, $[B]$, and $[D]$ using Eq. (5.20).
- Step 7** Calculate laminate compliance matrix $[a]$, using relations in Eq. (5.27), or by inversion of 6×6 stiffness matrix of Eq. (5.23).
- Step 8** Enter total laminate thickness, h .
- Step 9** Calculate laminate engineering properties referred to the x - and y -axes using Eq. (5.78).

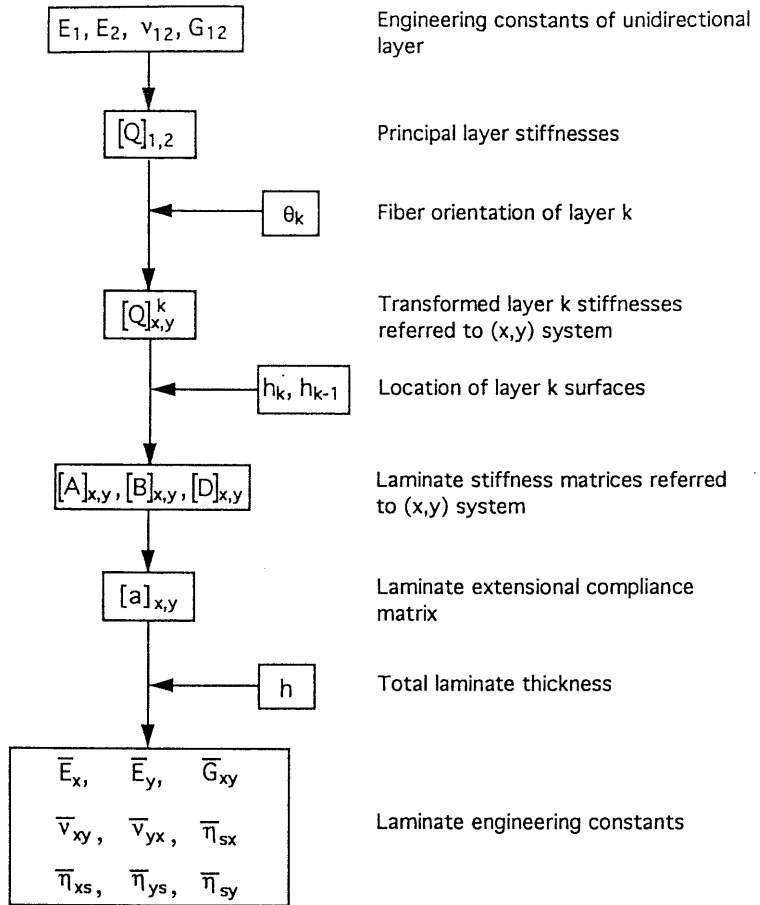


Fig. 5.11 Flow chart for computation of engineering elastic properties of multidirectional laminates.

5.14 Comparison of Elastic Parameters of Unidirectional and Angle-Ply Laminates

Exact and approximate expressions for the elastic properties of a $[\pm 45]_{ns}$ angle-ply laminate were obtained before, [see Eqs. (5.86), (5.88), and (5.91) through (5.94)]. In addition to these results it should be mentioned that the laminate shear coupling coefficients $\bar{\eta}_{xs}$, $\bar{\eta}_{sx}$, $\bar{\eta}_{ys}$, and $\bar{\eta}_{sy}$ are zero since the laminate is balanced. It is of interest to compare the properties of the angle-ply laminate with those of the 45° off-axis lamina obtained before, [see Eqs. (3.82) through (3.90)].

Numerical results for all properties above, exact and approximate, were obtained for a typical carbon/epoxy material (AS4/3501-6; Table 2.6) and compared in Table 5.2. It is seen that values obtained by the approximation formulas

Table 5.2 Comparison of Engineering Constants of [45] Unidirectional and [± 45]_s Angle-Ply Carbon/Epoxy Laminates (AS4/3501-6)

Property	[45]			[± 45] _s		
	Approximation formula	Approximate value	Exact value	Approximation formula	Approximate value	Exact value
\bar{E}_{xx} GPa (Msi)	$\frac{4 G_{12} E_2}{G_{12} + E_2}$	17.0 (2.46)	16.7 (2.43)	$4 G_{12}$	28.7 (4.16)	24.4 (3.54)
\bar{G}_{xy} GPa (Msi)	E_2	10.4 (1.50)	9.3 (1.34)	$E_1/4$	35.5 (5.15)	36.9 (5.35)
$\bar{\nu}_{xy}$	$\frac{E_2 - G_{12}}{E_2 + G_{12}}$	0.18	0.16	$\frac{E_1 - 4 G_{12}}{E_1 + 4 G_{12}}$	0.66	0.69
$\bar{\eta}_{lx}$	$-\frac{2 G_{12}}{E_2 + G_{12}}$	-0.82	-0.75	0	0	0
$\bar{\eta}_{ly}$	-0.50	-0.50	-0.42	0	0	0

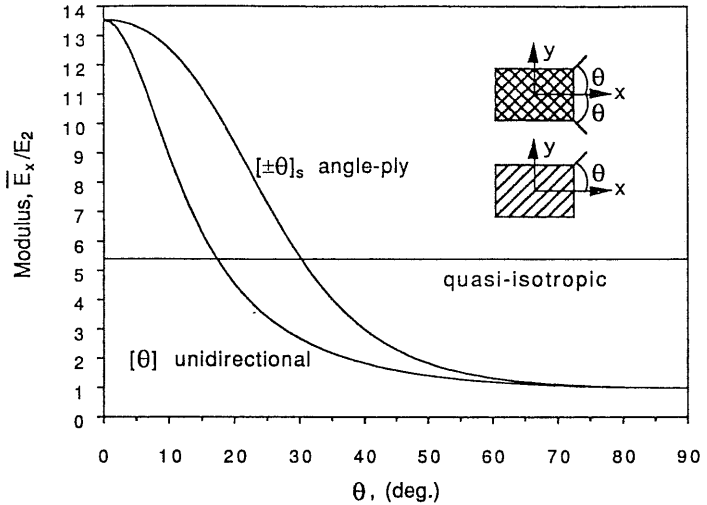


Fig. 5.12 Young's modulus of unidirectional and angle-ply laminates as a function of fiber orientation compared with that of a quasi-isotropic laminate (AS4/3501-6 carbon/epoxy).

are close to the exact values. The differences between the unidirectional lamina and angle-ply laminate are illustrated in Figures 5.12 to 5.15. The Young's modulus, shear modulus, Poisson's ratio, and shear coupling coefficient are plotted as a function of fiber orientation for the AS4/3501-6 carbon/epoxy material. Results for a quasi-isotropic laminate are also plotted for reference.

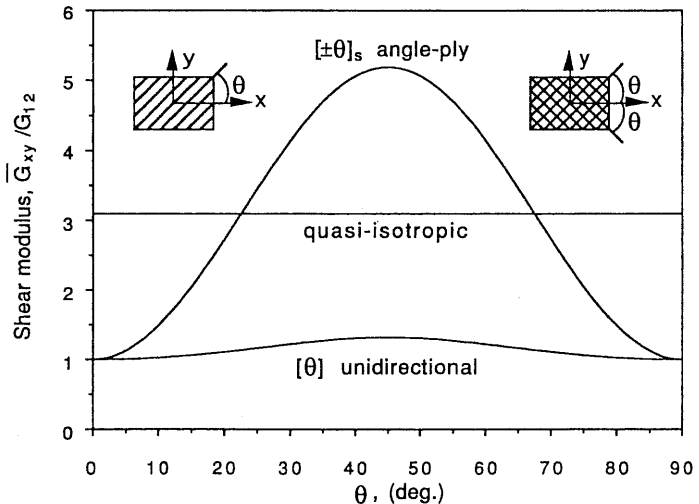


Fig. 5.13 Shear modulus of unidirectional and angle-ply laminates as a function of fiber orientation compared with that of a quasi-isotropic laminate (AS4/3501-6 carbon/epoxy).

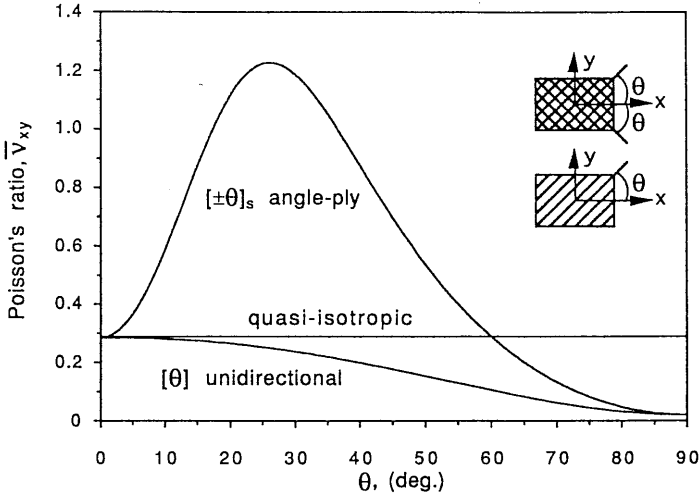


Fig. 5.14 Poisson's ratio of unidirectional and angle-ply laminates as a function of fiber orientation compared with that of a quasi-isotropic laminate (AS4/3501-6 carbon/epoxy).

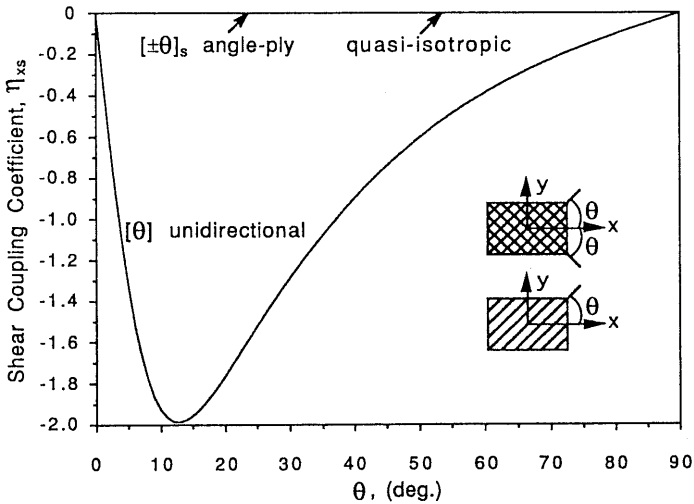


Fig. 5.15 Shear coupling coefficient of unidirectional and angle-ply laminates as a function of fiber orientation compared with that of a quasi-isotropic laminate (AS4/3501-6 carbon/epoxy).

5.15 Carpet Plots for Multidirectional Laminates

Many design applications involve lay-ups consisting of various numbers of 0° , 90° , and $\pm 45^\circ$ plies. These lay-ups are balanced since the $+45^\circ$ plies are balanced by an equal number of -45° plies. A designation for such a general lay-

up is $[0_m/90_n/(\pm 45)_p]_s$ where m , n , and p denote the number of 0° , 90° , and $(\pm 45^\circ)$ plies, respectively. The in-plane engineering constants for a symmetric laminate depend only on the proportion of the various plies in the entire laminate and not on the exact stacking sequence. Thus in-plane engineering constants are a function of the fractional values α , β , and γ , where

$$\alpha = \frac{2m}{N}$$

$$\beta = \frac{2n}{N} \tag{5.105}$$

$$\gamma = \frac{4p}{N}$$

$$N = 2(m + n + 2p) = \text{total number of plies}$$

For a given material with known basic lamina properties, in-plane properties for the general $[0_m/90_n/(\pm 45)_p]_s$ laminate can be obtained as a function of α , β , and γ . Although such computations can be performed readily using available computer programs, it is sometimes useful and practical for the designer to have

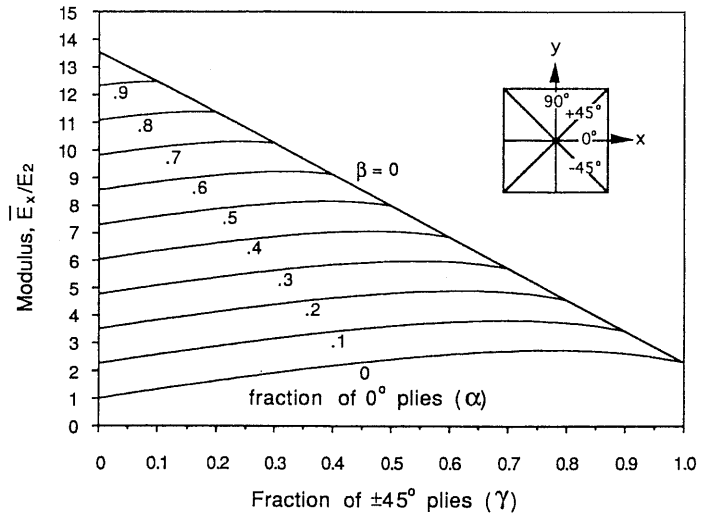


Fig. 5.16 Carpet plot for Young's modulus of $[0_m/90_n/(\pm 45)_p]_s$ carbon/epoxy laminates (AS4/3501-6) (α , β , and γ are fractions of 0° , 90° , and $\pm 45^\circ$ plies, respectively).

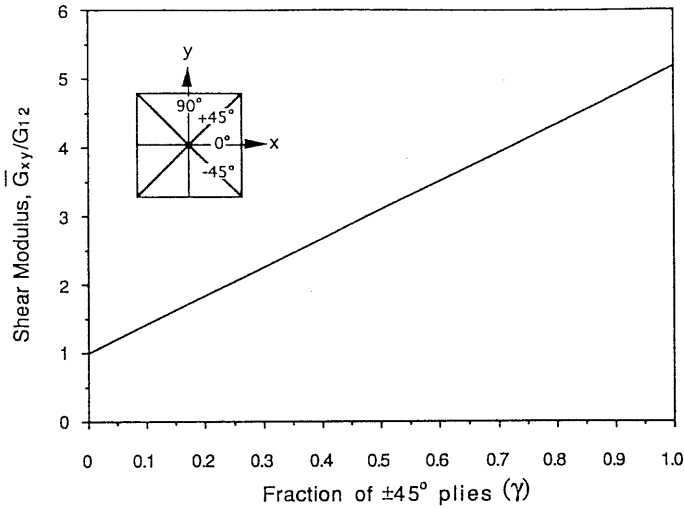


Fig. 5.17 Carpet plot for shear modulus of $[0_m/90_n/(\pm 45)_p]_s$ carbon/epoxy laminates (AS4/3501-6 (α , β , and γ are fractions of 0° , 90° , and $\pm 45^\circ$ plies, respectively).

so-called “carpet plots.” A carpet plot is a parametric family of curves with one of α , β , or γ as a variable and the other two as parameters, keeping in mind that $\alpha + \beta + \gamma = 1$. Such plots for Young’s modulus, shear modulus, and Poisson’s ratio are shown in Figures 5.16 to 5.18 for the AS4/3501-6 carbon/epoxy material (see Table 2.6).

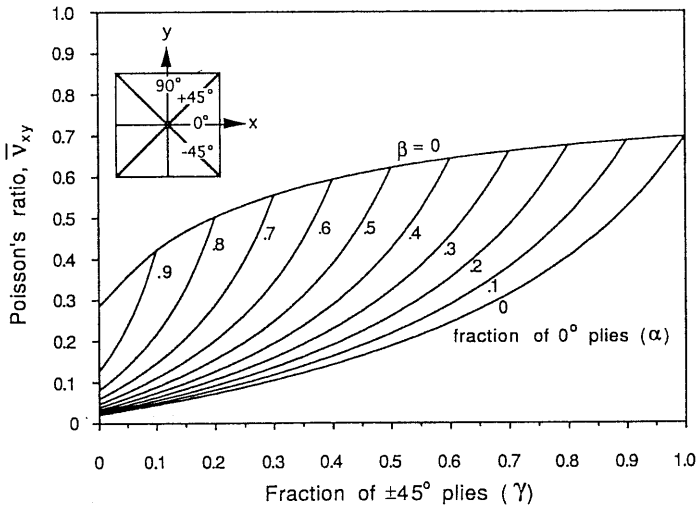


Fig. 5.18 Carpet plot for Poisson’s ratio of $[0_n/90_n/(\pm 45)_p]_s$ carbon/epoxy laminates (AS4/3501-6 (α , β , and γ are fractions of 0° , 90° , and $\pm 45^\circ$ plies, respectively).

References

1. K. S. Pister and S. B. Dong, "Elastic Bending of Layered Plates," *J. Eng. Mech. Division*, ASCE, 1959, pp. 1-10.
2. E. Reissner and Y. Stavsky, "Bending and Stretching of Certain Types of Heterogeneous Anisotropic Elastic Plates," *J. Appl. Mech.*, 1961, pp. 402-408.
3. R. M. Jones, *Mechanics of Composite Materials*, Hemisphere Publ. Co., New York, 1975.
4. N. J. Pagano and R. B. Pipes, "The Influence of Stacking Sequence on Laminate Strength," *J. Comp. Materials*, Vol. 5, 1971, pp. 50-57.

PROBLEMS

5.1 Identify each of the following laminates by name (i.e., symmetric, balanced, and so forth) and indicate which terms of the $[A]$, $[B]$, and $[D]$ matrices are zero for each laminate.

- a. $[\pm\theta]$
- b. $[0/\pm 45]$
- c. $[0/90_2]_s$
- d. $[0/45/90/-45]$
- e. $[0/\pm 30/\mp 30/0]$
- f. $[0/90/0/90]$
- g. $[30/-45/-30/45]$
- h. $[-45/30/-30/45]$
- i. $[\pm 45/\mp 45]$

5.2 Name two types of laminates, with specific examples, for which

$$B_{ij} = 0$$

$$A_{xs} = A_{ys} = D_{xs} = D_{ys} = 0$$

5.3 Which terms of the $[A]$, $[B]$, and $[D]$ matrices are zero for the following laminates?

$$[\alpha/-\alpha/\alpha/-\alpha/\alpha]$$

$$[\alpha/-\alpha/-\alpha/\alpha]$$

$$[\alpha/-\alpha/\alpha/-\alpha]$$

5.4 For an $[\alpha/-\alpha]_n$ laminate, determine B_{xs} in terms of the total laminate thickness, h , the number of plies, the basic lamina stiffnesses Q_{11} , Q_{12} , Q_{22} , and Q_{66} (referred to the lamina material axes), and the ply orientation α .

5.5 Compute all terms of the A , B , and D matrices for a $[0/90]$ laminate with the following lamina properties:

$$E_1 = 145 \text{ GPa (21 Msi)} \qquad E_2 = 10.5 \text{ GPa (1.5 Msi)}$$

$$G_{12} = 7.5 \text{ GPa (1.1 Msi)} \qquad \nu_{12} = 0.28$$

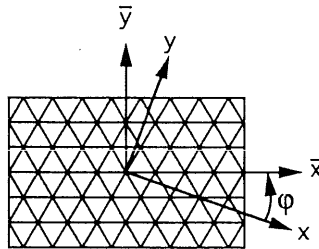
lamina thickness: $t = 0.25 \text{ mm (0.01 inch)}$

- 5.6 Compute all terms of the $[A]$ and $[B]$ matrices for a $[+45/-45]$ laminate with the lamina properties of problem 5.5.
- 5.7 Evaluate the $[B]$ matrix for a $[+45/-45]$ laminate in terms of the lamina engineering properties $E_1, E_2, \nu_{12}, G_{12}$, and the lamina thickness t .
- 5.8 Compute all terms of the A matrix for a $[0/\pm 45]$ laminate with the lamina properties of problem 5.5.
- 5.9 Determine and compare the terms of the $[B]$ matrix for laminates $[0_2/90_2]$ and $[0/90]_2$ in terms of lamina properties Q_{ij} and thickness t .
- 5.10 An antisymmetric $[\pm 45]$ laminate consists of two carbon/epoxy layers of thickness t . The elastic properties of the lamina are as follows:

$$E_1 = 15 E_o, \quad E_2 = E_o, \quad G_{12} = 0.6 E_o, \quad \nu_{12} = 0.3$$

Determine the laminate stiffnesses $[A], [B],$ and $[D]$ in terms of E_o and t . Obtain approximate solutions by assuming $E_1 \gg E_2 > G_{12}$.

- 5.11 Show that the $[0/\pm 60]_s$ laminate is quasi-isotropic, i.e., $A_{xx} = A_{\bar{x}\bar{x}}$ for any angle ϕ .



- 5.12 Prove Eqs. (5.64) through (5.66) in sample problem 5.2.
- 5.13 Prove that a laminate of

$$\left[\frac{\pi}{n} \frac{2}{n} \frac{-\pi}{\pi} / \dots \frac{k\pi}{n} / \dots \frac{n-1}{n} \frac{-\pi}{\pi} \right]_s$$

layup is quasi-isotropic, i.e., that all extensional stiffnesses A_{ij} are independent of orientation of reference axes.

- 5.14** Prove that for a $[\pm 45]_s$ angle-ply laminate, the in-plane lamina shear modulus G_{12} is related to the laminate modulus and Poisson's ratio as follows:

$$G_{12} = \frac{\bar{E}_x}{2(1 + \bar{\nu}_{xy})}$$

(Hint: see sample problems 5.3 and 5.5.)

- 5.15** Determine \bar{E}_x , \bar{G}_{xy} , and $\bar{\nu}_{xy}$ for a $[\pm 45]_s$ angle-ply laminate with the lamina properties of problem 5.5.
- 5.16** Determine Poisson's ratio $\bar{\nu}_{xy}$ for a $[\pm 30]_s$ angle-ply laminate with the lamina properties of problem 5.5.
- 5.17** Determine Poisson's ratio $\bar{\nu}_{xy}$ for a $[0/\pm 45]_s$ laminate with the lamina properties of problem 5.5.
- 5.18** Show that for a quasi-isotropic laminate the following relation holds among axial modulus, shear modulus and Poisson's ratio:

$$\bar{G}_{xy} = \frac{\bar{E}_x}{2(1 + \bar{\nu}_{xy})}$$

- 5.19** A laminate of $[0/\pm 45/90]_s$ layup is loaded under in-plane biaxial loading

$$N_x = N_o$$

$$N_y = 2N_o$$

$$N_s = 0$$

and the resulting strains are

$$\varepsilon_x = 1.3 \times 10^{-3}$$

$$\varepsilon_y = 5.1 \times 10^{-3}$$

Determine Poisson's ratio $\bar{\nu}_{xy}$.

- 5.20 An asymmetric $[0/90]$ laminate is subjected to biaxial loading $N_x = N_y = N_o$ and the following strains and curvatures are obtained: $\varepsilon_x^o = \varepsilon_y^o = \varepsilon_o$; $\kappa_x = -\kappa_y = \kappa_o$. Assuming $\bar{\nu}_{xy} \ll 1$, obtain an expression for the laminate modulus \bar{E}_x as a function of its relevant stiffness parameters A_{ij} , B_{ij} , and D_{ij} .
- 5.21 For the laminate of problem 5.20 above made of AS4/3501-6 carbon/epoxy (see Table 2.6) determine the load N_o corresponding to a curvature $\kappa_x = 2 \times 10^{-3} \text{ mm}^{-1} (0.051 \text{ in}^{-1})$. The layer thickness is $t = 0.1 \text{ mm} (0.004 \text{ in.})$.
- 5.22 A symmetric and unbalanced laminate for which $\bar{E}_x = \bar{E}_y$ and $\bar{\eta}_{xs} = \bar{\eta}_{ys}$ is loaded in pure shear $N_x = N_o$ and the normal strain ε_x is measured.
- Determine the shear strain γ_o produced under biaxial compressive loading $N_x = N_y = -N_o$ of the same laminate as a function of ε_x .
 - Determine Poisson's ratio $\bar{\nu}_{xy}$ of this laminate if the normal strain ε_x under biaxial loading is zero.
- 5.23 A symmetric crossply laminate is designed such that $\bar{E}_x = 5 \bar{E}_y$. The relative lamina moduli are $E_1 = 14 E_2$. Determine the approximate ratio r between the number of 0° plies to that of the 90° plies assuming $E_1 \gg E_2$.
- 5.24 Two samples were cut from a $[0/90]_s$ laminate, one along the 0° direction and the other at 45° . The measured moduli from these samples were $(\bar{E}_x)_{\theta=0^\circ} = 80 \text{ GPa} (11.6 \text{ Msi})$ and $(\bar{E}_x)_{\theta=45^\circ} = 24 \text{ GPa} (3.5 \text{ Msi})$. Determine the lamina moduli E_1 and G_{12} assuming $E_1 \gg E_2$.
- 5.25 Based on the results of problem 5.24 above, compute the approximate properties \bar{E}_x , \bar{G}_{xy} and $\bar{\nu}_{xy}$ of a quasi-isotropic laminate of the same material. Verify the relationship of problem 5.18.

Chapter 6

Hygrothermal Effects

6.1 Introduction

The fabrication process of composite materials may introduce reversible and irreversible effects due to the processing thermal cycle and chemical changes and due to the mismatch in thermal properties of the constituents. The most common manifestation of these effects are residual stresses and warpage.

After fabrication, composite structures operate in a variety of thermal and moisture environments that may have a pronounced impact on their performance. These hygrothermal effects are a result of the temperature and moisture content variations and are related to the difference in thermal and hygric properties of the constituents.

Processing and environmental effects are similar in nature. They can be viewed and analyzed from the microscopic point of view, on the scale of the fiber diameter, or from the macroscopic point of view, by considering the overall effects on the lamina, which is treated as a homogeneous material.

Analysis of the processing and hygrothermal effects is an important component of the overall structural design and analysis. The performance of a composite structure is a function of its environmental history, temperature and moisture distributions, processing and hygrothermal stresses, and property variations with temperature and moisture. Hygrothermal effects can be categorized as follows:

6.1.1 Physical and Chemical Effects

Moisture absorption and desorption processes in polymer/matrix composites depend on the current hygrothermal state and on the environment.¹ The glass transition temperature of the polymeric matrix varies with the moisture content. Polymerization processes are a function of the hygrothermal properties of the

constituent materials and the composite and the current hygrothermal state. Material degradation and corrosion can be related to hygrothermal factors.

6.1.2 Effects on Mechanical Properties

Elastic and viscoelastic (time-dependent) properties may vary with temperature and moisture concentration. Failure and strength characteristics, especially interfacial and matrix-dominated ones, may vary with temperature and moisture content.

6.1.3 Hygrothermoelastic (HTE) Effects

The composite material undergoes reversible deformations related to thermal expansion (α) and moisture expansion (β) coefficients. Intralaminar and interlaminar stresses are developed as a result of the thermoelastic and hygroelastic inhomogeneity and anisotropy of the material.

6.2 Hygrothermal Effects on Mechanical Behavior

The hygrothermal state affects the stress-strain behavior of composite materials in two different ways; the properties of the constituents may vary with temperature and moisture concentration, and fabrication residual stresses are altered by the hygrothermal state. Since the fibers are usually the least sensitive to environment, hygrothermal effects are most noticeable in matrix dominated properties, e.g., transverse tensile, transverse compressive, and in-plane shear properties.

Effects of temperature on stress-strain behavior of typical composites are illustrated in Figures 6.1 to 6.4. Figure 6.1 shows the transverse stress-strain behavior of a carbon/epoxy (AS4/3501-6) composite at various temperatures.² It is seen that the transverse modulus decreases steadily with increasing temperature, although the strength and ultimate strain are not affected much. Figure 6.2 shows similar stress-strain curves for in-plane shear loading. The in-plane shear modulus and strength decrease with increasing temperature, but the ultimate shear strain remains nearly constant. Figure 6.3 shows the effect of temperature on the transverse stress-strain behavior of a silicon carbide/aluminum (SiC/Al; SCS-2/6061 Al) unidirectional composite. The initial modulus is not affected, but the yield stress decreases and the ultimate strain increases with increasing temperature. A similar behavior is displayed by the same material under in-plane shear loading (Fig. 6.4).

The influence of moisture concentration is similar to that of temperature on polymer matrix composites, and it is more pronounced at elevated temperatures. Figure 6.5 shows that a 1% moisture concentration produces a very small differ-

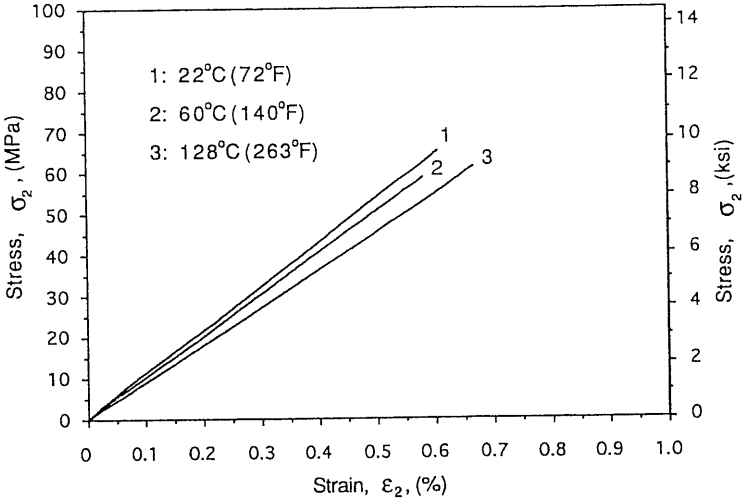


Fig. 6.1 Transverse tensile stress-strain curves for dry AS4/3501-6 carbon/epoxy composite at various temperatures.²

ence in the shear stress versus shear strain behavior of a carbon/epoxy composite at room temperature; however, it has a noticeable effect at the elevated temperature of 90°C (195°F). The most deleterious effects on stiffness and strength are produced by a combination of elevated temperature and high moisture concentration.^{3,4} This is further illustrated in Figure 6.6, where it is shown that the

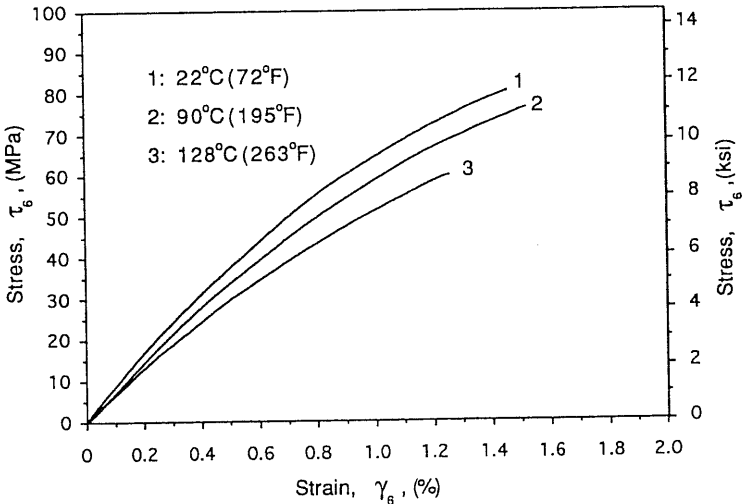


Fig. 6.2 In-plane shear stress-strain curves for unidirectional AS4/3501-6 carbon/epoxy composite at various temperatures.²

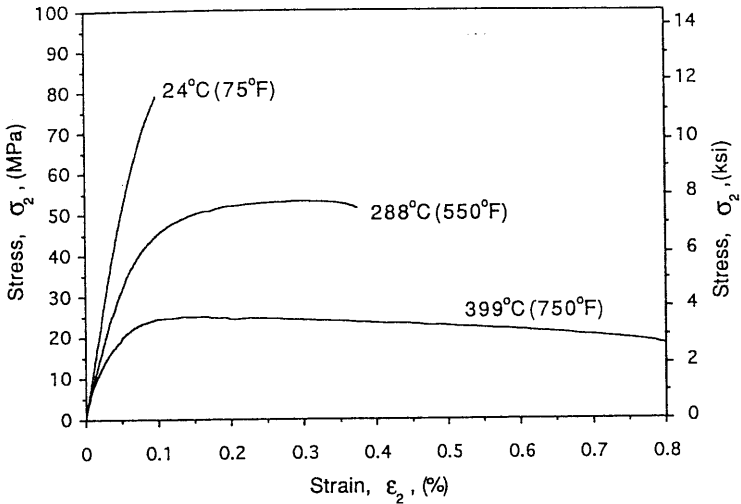


Fig. 6.3 Transverse tensile stress–strain curves for unidirectional silicon carbide/aluminum (SCS-2/6061Al) composite at various temperatures.

torsional stiffness under cyclic loading degrades most at high temperature and moisture concentration.

Table 6.1 illustrates in a quantitative way the degradation in stiffnesses and strengths with temperature of a unidirectional intermediate strength carbon/epoxy.⁵ It is seen that the longitudinal modulus and tensile strength decrease by approximately 5% and 10% at 121°C (250°F) and 177°C (350°F) respect-

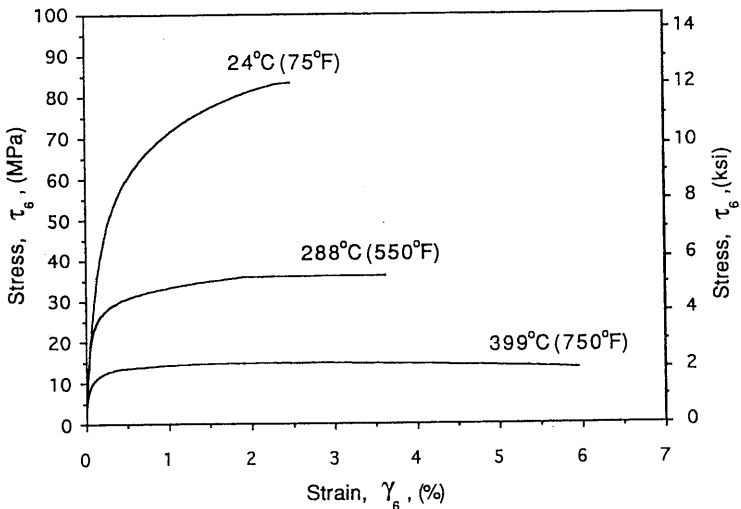


Fig. 6.4 In-plane shear stress–strain curves for unidirectional silicon carbide/aluminum (SCS-2/6061Al) composite at various temperatures.

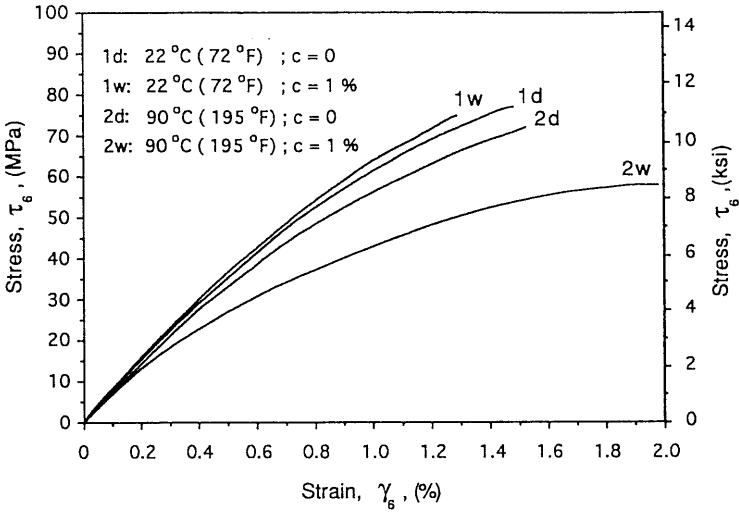


Fig. 6.5 In-plane shear stress–strain curves for unidirectional AS4/3501-6 carbon/epoxy composite illustrating effects of temperature and moisture concentration.

ively. Matrix-dominated properties, such as transverse and in-plane shear moduli and their corresponding strengths, degrade by 50% or more at 177°C (350°F), with the strengths degrading somewhat more than the moduli. Longitudinal and transverse compressive strengths decrease to 40% and 60% of their room temperature values, respectively, at 177°C (350°F).

The effect of long term hygrothermal exposure on matrix-dominated proper-

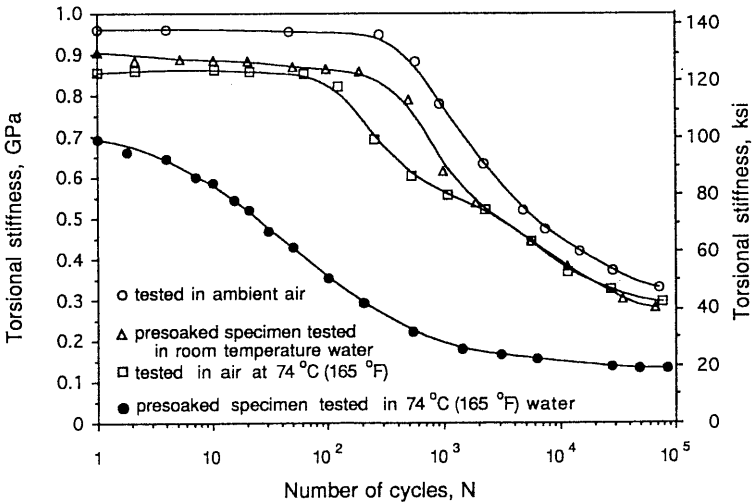


Fig. 6.6 Torsional stiffness degradation of carbon/epoxy composite under cyclic loading under various hygrothermal conditions.

Table 6.1 Temperature Effects on Elastic and Strength Properties of a Typical Intermediate Strength Carbon/Epoxy Composite.⁵

Normalized property	Temperature, T, °C (°F)		
	24 (75)	121 (250)	177 (350)
Longitudinal modulus			
$E_1(T)/E_1(T_0)$	1	0.95	0.93
Transverse modulus			
$E_2(T)/E_2(T_0)$	1	0.87	0.50
In-plane shear modulus			
$G_{12}(T)/G_{12}(T_0)$	1	0.87	0.50
Longitudinal tensile strength			
$F_{1t}(T)/F_{1t}(T_0)$	1	0.96	0.90
Transverse tensile strength			
$F_{2t}(T)/F_{2t}(T_0)$	1	0.82	0.45
Longitudinal compressive strength			
$F_{1c}(T)/F_{1c}(T_0)$	1	0.78	0.40
Transverse compressive strength			
$F_{2c}(T)/F_{2c}(T_0)$	1	0.87	0.60
In-plane shear strength			
$F_6(T)/F_6(T_0)$	1	0.70	0.40

T_0 = reference room temperature; T = current temperature.

ties depends on the composition and type of matrix resin. Glass/fiber composites with rubber-modified epoxy matrix exhibited high strength degradation when exposed to hot and humid ambient conditions compared with composites having a standard (unmodified) "brittle" epoxy matrix, which showed a slight improvement in strength.^{4,6}

6.3 Coefficients of Thermal and Moisture Expansion of Unidirectional Lamina

The hygrothermal behavior of a unidirectional lamina is fully characterized in terms of two principal coefficients of thermal expansion (CTE), α_1 and α_2 , and two principal coefficients of moisture expansion (CME), β_1 and β_2 (Fig. 6.7). These coefficients can be related to the geometric and material properties of the constituents.

Approximate micromechanical relations for the coefficients of thermal expansion were given by Schapery⁷ for isotropic constituents. The longitudinal coefficient for a continuous fiber composite is given by the relation

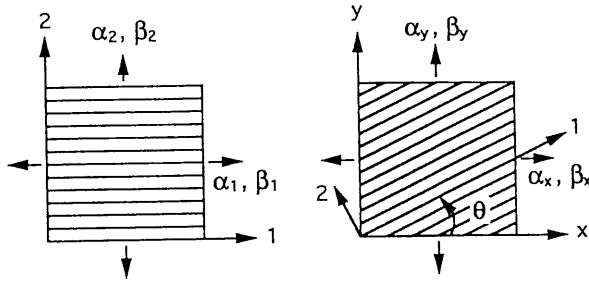


Fig. 6.7 Coefficients of thermal and moisture expansion of a unidirectional lamina.

$$\alpha_1 = \frac{E_f \alpha_f V_f + E_m \alpha_m V_m}{E_f V_f + E_m V_m} = \frac{(E\alpha)_1}{E_1} \tag{6.1}$$

where

E_f, E_m = Fiber and matrix moduli, respectively

α_f, α_m = Fiber and matrix coefficients of thermal expansion, respectively

V_f, V_m = Fiber and matrix volume ratios, respectively

$$(E\alpha)_1 = E_f \alpha_f V_f + E_m \alpha_m V_m$$

E_1 = Longitudinal composite modulus (by rule of mixtures)

This relation is similar to the rule of mixtures for longitudinal modulus and gives fairly accurate results. It is identical to that obtained by the self-consistent scheme discussed before.

The relation for the transverse coefficient of thermal expansion based on energy principles⁷ is

$$\alpha_2 = \alpha_f V_f(1 + \nu_f) + \alpha_m V_m(1 + \nu_m) - \nu_{12} \alpha_1 \tag{6.2}$$

where

ν_f, ν_m = Poisson's ratios of fiber and matrix, respectively

$\nu_{12} = \nu_f V_f + \nu_m V_m$ = Major Poisson's ratio of composite lamina as obtained by the rule of mixtures Eq. (3.93)

α_1 = Longitudinal CTE of lamina as obtained by Eq. (6.1)

In many cases, such as carbon and aramid composites, the fibers are orthotropic, i.e., they have different properties in the axial and transverse directions. Properties for composites with orthotropic constituents were obtained by Hashin.⁸ The relation for the transverse CTE is

$$\alpha_2 = \alpha_{2f} V_f \left(1 + \nu_{12f} \frac{\alpha_{1f}}{\alpha_{2f}} \right) + \alpha_{2m} V_m \left(1 + \nu_{12m} \frac{\alpha_{1m}}{\alpha_{2m}} \right) - (\nu_{12f} V_f + \nu_{12m} V_m) \frac{(E\alpha)_1}{E_1} \quad (6.3)$$

where

α_{1f}, α_{2f} = Axial and transverse CTE's of fiber, respectively

α_{1m}, α_{2m} = Axial and transverse CTE's of matrix, respectively

ν_{12f}, ν_{12m} = Axial Poisson's ratios of fiber and matrix, respectively

$$(E\alpha)_1 = E_{1f} \alpha_{1f} V_f + E_{1m} \alpha_{1m} V_m \quad (6.4)$$

$$E_1 = E_{1f} V_f + E_{1m} V_m \quad (6.5)$$

In most cases the matrix can be considered isotropic, and the orientation designation of the matrix properties in Eqs. (6.3) through (6.5) can be dropped.

The coefficients of thermal expansion are obtained by measuring strains as a function of temperature and determining the slopes of the thermal strain versus temperature curves. Thermal strains versus temperature curves are shown in Figure 6.8 for three material systems, S-glass/epoxy, carbon/epoxy and Kevlar/epoxy.⁹ It is seen that the CTEs in general are not constant but they vary with temperature. The S-glass/epoxy system is the least anisotropic material thermally with both principal coefficients positive. The carbon/epoxy and Kevlar/epoxy display negative longitudinal coefficients of thermal expansion, with the Kevlar/epoxy being the most thermally anisotropic material. Coefficients of thermal expansion of some typical composite materials are listed in Table 6.2.

Once the principal coefficients α_1 and α_2 are known, the coefficients referred to any system of coordinates x, y can be obtained by the following transformation relations, which are the same as those for strain transformation (Fig. 6.7):

$$\begin{aligned} \alpha_x &= \alpha_1 m^2 + \alpha_2 n^2 \\ \alpha_y &= \alpha_1 n^2 + \alpha_2 m^2 \\ \alpha_{xy} &= \alpha_s = 2(\alpha_1 - \alpha_2)mn \end{aligned} \quad (6.6)$$

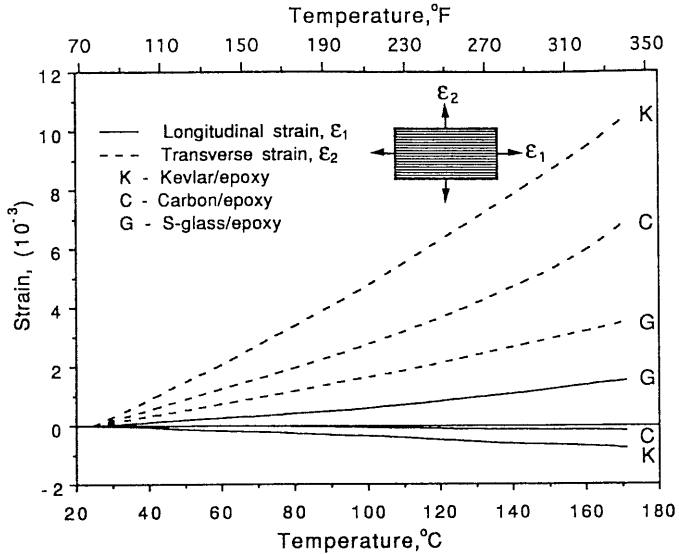


Fig. 6.8 Thermal strains as a function of temperature for three representative unidirectional composites.⁹

Table 6.2 Coefficients of Thermal Expansion of Unidirectional Composite Materials⁹

Material	Longitudinal coefficient of thermal expansion, α_1 $10^{-6}/^{\circ}\text{C}$ ($10^{-6}/^{\circ}\text{F}$)				Transverse coefficient of thermal expansion, α_2 $10^{-6}/^{\circ}\text{C}$ ($10^{-6}/^{\circ}\text{F}$)			
	24°C	(75°F)	177°C	(350°F)	24°C	(75°F)	177°C	(350°F)
Boron/epoxy (boron/AVCO 5505)	6.1	(3.4)	6.1	(3.4)	30.3	(16.9)	37.8	(21.0)
Boron/polyimide (boron/WRD 9371)	4.9	(2.7)	4.9	(2.7)	28.4	(15.8)	28.4	(15.8)
Carbon/epoxy (AS4/3501-6)	-0.9	(-0.5)	-0.9	(-0.5)	27.0	(15.0)	34.2	(19.0)
Carbon/polyimide (modmor I/WRD 9371)	-0.4	(-0.2)	-0.4	(-0.2)	25.3	(14.1)	25.3	(14.1)
S-glass/epoxy (Scotchply 1009-26-5901)	3.8	(2.1)	3.8	(2.1)	16.7	(9.3)	54.9	(30.5)
S-glass/epoxy (S-glass/ERLA 4617)	6.6	(3.7)	14.1	(7.9)	19.7	(10.9)	26.5	(14.7)
Kevlar/epoxy (Kevlar 49/ERLA 4617)	-4.0	(-2.2)	-5.7	(-3.2)	57.6	(32.0)	82.8	(46.0)

where $m = \cos\theta$, $n = \sin\theta$.

Micromechanical relations for the coefficients of moisture expansion are entirely analogous. However, some simplification results by taking into consideration the fact that usually the fiber (carbon, boron, glass) does not absorb moisture, i.e., $\beta_f = \beta_{1f} = \beta_{2f} = 0$. Then the relations for the longitudinal and transverse coefficients of moisture expansion for isotropic constituents take the form

$$\beta_1 = \beta_m \frac{E_m V_m}{E_f V_f + E_m V_m} = \beta_m \frac{E_m V_m}{E_1} \quad (6.7)$$

and

$$\beta_2 = \beta_m \frac{V_m}{E_1} [(1 + \nu_m)E_f V_f + (V_m - \nu_f V_f)E_m] \quad (6.8)$$

For orthotropic constituents, the equations above take the form

$$\beta_1 = \beta_{1m} \frac{E_{1m} V_m}{E_1} \quad (6.9)$$

and

$$\beta_2 = \beta_{2m} \frac{V_m}{E_1} \left[\left(1 + \nu_{12m} \frac{\beta_{1m}}{\beta_{2m}} \right) E_1 - (\nu_{12f} V_f + \nu_{12m} V_m) E_{1m} \frac{\beta_{1m}}{\beta_{2m}} \right] \quad (6.10)$$

For a composite with isotropic matrix but orthotropic fibers, β_1 is given by Eq. (6.7) and β_2 takes the form

$$\beta_2 = \beta_m \frac{V_m}{E_1} [(1 + \nu_m)E_{1f} V_f + (V_m - \nu_{12f} V_f)E_m] \quad (6.11)$$

The transformation relations for β_1 and β_2 are entirely analogous to Eq. (6.6) for the CTEs.

6.4 Hygrothermal Strains in Unidirectional Lamina

A lamina undergoes hygrothermal deformation when subjected to a uniform change in temperature $\Delta T = T - T_o$ and change in moisture concentration $\Delta c = c - c_o$, where (T_o, c_o) is a reference hygrothermal state. Assuming the thermal and moisture deformations to be uncoupled and the thermal and moisture expansion coefficients to be constant (which is a good approximation for most

composites under normal service conditions), the hygrothermal strains referred to the principal material axes of the lamina are

$$\begin{aligned}
 e_1 &= \alpha_1 \Delta T + \beta_1 \Delta c \\
 e_2 &= \alpha_2 \Delta T + \beta_2 \Delta c \\
 e_6 &= 0
 \end{aligned}
 \tag{6.12}$$

The transformed hygrothermal strains referred to the x, y coordinate system of Figure 6.7 are

$$\begin{aligned}
 e_x &= e_1 m^2 + e_2 n^2 \\
 e_y &= e_1 n^2 + e_2 m^2 \\
 e_{xy} &= e_s = 2(e_1 - e_2)mn
 \end{aligned}
 \tag{6.13}$$

where $m = \cos\theta$ and $n = \sin\theta$. The variation of the normal and shear hygrothermal strains e_x and e_s with fiber orientation θ is shown in Figure 6.9.

Substituting e_1 and e_2 from Eq. (6.12) into Eq. (6.13) and in view of relations in Eq. (6.6), we obtain

$$\begin{aligned}
 e_x &= \alpha_x \Delta T + \beta_x \Delta c \\
 e_y &= \alpha_y \Delta T + \beta_y \Delta c \\
 e_s &= \alpha_s \Delta T + \beta_s \Delta c
 \end{aligned}
 \tag{6.14}$$

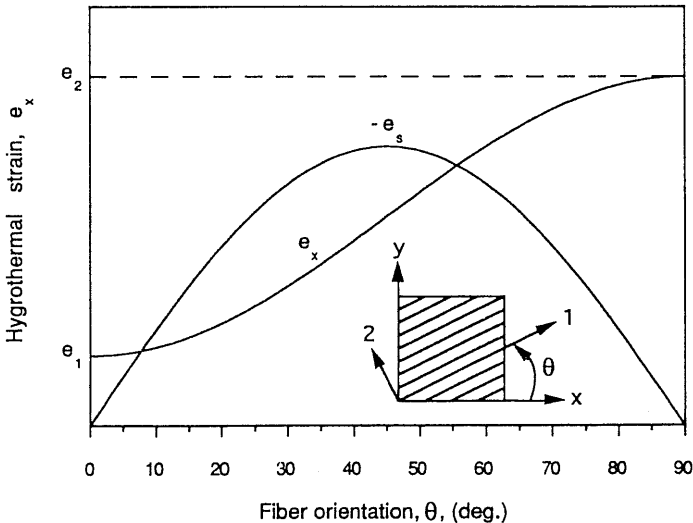


Fig. 6.9 Variation of hygrothermal strains with fiber orientation in unidirectional lamina.

where $\alpha_x, \alpha_y, \alpha_s$ and $\beta_x, \beta_y, \beta_s$ are the transformed lamina coefficients of thermal and moisture expansion.

6.5 Hygrothermoelastic Stress–Strain Relations

When a multidirectional laminate is subjected to mechanical ($[N]$, $[M]$) and hygrothermal (ΔT , Δc) loading, a lamina k within the laminate is under a state of stress $[\sigma]_{x,y}^k$ and deformation $[\epsilon]_{x,y}^k$. The hygrothermoelastic superposition principle states that the strains $[\epsilon]_{x,y}^k$ in lamina k within the laminate are equal to the sum of the strains produced by the existing stresses in the lamina, $[\sigma]_{x,y}^k$, and the free (unrestrained) hygrothermal strains of the lamina, i.e.,

$$\begin{bmatrix} \epsilon_x \\ \epsilon_y \\ \gamma_s \end{bmatrix}_k = \begin{bmatrix} S_{xx} & S_{xy} & S_{xs} \\ S_{yx} & S_{yy} & S_{ys} \\ S_{sx} & S_{sy} & S_{ss} \end{bmatrix}_k \begin{bmatrix} \sigma_x \\ \sigma_y \\ \tau_s \end{bmatrix}_k + \begin{bmatrix} e_x \\ e_y \\ e_s \end{bmatrix}_k \quad (6.15)$$

or, in brief,

$$[\epsilon]_{x,y}^k = [S]_{x,y}^k [\sigma]_{x,y}^k + [e]_{x,y}^k$$

Equations (6.15) can be inverted to give the stresses in lamina k as follows:

$$\begin{bmatrix} \sigma_x \\ \sigma_y \\ \tau_s \end{bmatrix}_k = \begin{bmatrix} Q_{xx} & Q_{xy} & Q_{xs} \\ Q_{yx} & Q_{yy} & Q_{ys} \\ Q_{sx} & Q_{sy} & Q_{ss} \end{bmatrix}_k \begin{bmatrix} \epsilon_x - e_x \\ \epsilon_y - e_y \\ \gamma_s - e_s \end{bmatrix}_k \quad (6.16)$$

or, in view of the relations in Eq. (5.8)

$$\begin{bmatrix} \sigma_x \\ \sigma_y \\ \tau_s \end{bmatrix}_k = \begin{bmatrix} Q_{xx} & Q_{xy} & Q_{xs} \\ Q_{yx} & Q_{yy} & Q_{ys} \\ Q_{sx} & Q_{sy} & Q_{ss} \end{bmatrix}_k \begin{bmatrix} \epsilon_x^o + z\kappa_x - e_x \\ \epsilon_y^o + z\kappa_y - e_y \\ \gamma_s^o + z\kappa_s - e_s \end{bmatrix}_k \quad (6.17)$$

or, in brief,

$$[\sigma]_{x,y}^k = [Q]_{x,y}^k [\epsilon^o]_{x,y} + [Q]_{x,y}^k [\kappa]_{x,y} z - [Q]_{x,y}^k [e]_{x,y}^k \quad (6.18)$$

As mentioned in Chapter 5, stresses in the laminate may vary discontinuously from lamina to lamina. Therefore a more convenient form of expressing the stress–strain relations in Eq. (6.17) is in terms of force and moment resultants for the entire laminate.

Integration of the stresses from Eq. (6.17) across the thickness of each lamina k and summation for all laminae in the laminate gives the force resultants.

$$\begin{aligned}
 [N]_{x,y} &= \sum_{k=1}^n \int_{h_{k-1}}^{h_k} [\sigma]_{x,y}^k dz \\
 &= \sum_{k=1}^n \int_{h_{k-1}}^{h_k} [Q]_{x,y}^k \{ [\epsilon^o]_{x,y} + z[\kappa]_{x,y} - [e]_{x,y}^k \} dz
 \end{aligned}$$

or

$$\begin{bmatrix} N_x \\ N_y \\ N_s \end{bmatrix} = \sum_{k=1}^n \int_{h_{k-1}}^{h_k} \begin{bmatrix} Q_{xx} & Q_{xy} & Q_{xs} \\ Q_{yx} & Q_{yy} & Q_{ys} \\ Q_{sx} & Q_{sy} & Q_{ss} \end{bmatrix}_k \left\{ \begin{bmatrix} \epsilon_x^o \\ \epsilon_y^o \\ \gamma_s^o \end{bmatrix} + z \begin{bmatrix} \kappa_x \\ \kappa_y \\ \kappa_s \end{bmatrix} - \begin{bmatrix} e_x \\ e_y \\ e_s \end{bmatrix}_k \right\} dz$$

or, in view of Eqs. (5.18) through (5.22),

$$\begin{bmatrix} N_x \\ N_y \\ N_s \end{bmatrix} = \begin{bmatrix} A_{xx} & A_{xy} & A_{xs} \\ A_{yx} & A_{yy} & A_{ys} \\ A_{sx} & A_{sy} & A_{ss} \end{bmatrix} \begin{bmatrix} \epsilon_x^o \\ \epsilon_y^o \\ \gamma_s^o \end{bmatrix} + \begin{bmatrix} B_{xx} & B_{xy} & B_{xs} \\ B_{yx} & B_{yy} & B_{ys} \\ B_{sx} & B_{sy} & B_{ss} \end{bmatrix} \begin{bmatrix} \kappa_x \\ \kappa_y \\ \kappa_s \end{bmatrix} - \begin{bmatrix} N_x^{HT} \\ N_y^{HT} \\ N_s^{HT} \end{bmatrix} \tag{6.19}$$

where the laminate stiffness matrices $[A]$ and $[B]$ are defined as in Eq. (5.20), $[N^{HT}]_{x,y}$ are the hygrothermal force resultants defined as

$$\begin{bmatrix} N_x^{HT} \\ N_y^{HT} \\ N_s^{HT} \end{bmatrix} = \sum_{k=1}^n \begin{bmatrix} Q_{xx} & Q_{xy} & Q_{xs} \\ Q_{yx} & Q_{yy} & Q_{ys} \\ Q_{sx} & Q_{sy} & Q_{ss} \end{bmatrix}_k \begin{bmatrix} e_x \\ e_y \\ e_s \end{bmatrix}_k t_k \tag{6.20}$$

and $t_k = h_k - h_{k-1}$ is the thickness of lamina k .

In a similar fashion, integration of the stresses from Eq. (6.17) multiplied by the z -coordinate across the thickness of the lamina k and summation for all laminae in the laminate gives the moment resultants

$$\begin{aligned}
 [M]_{x,y} &= \sum_{k=1}^n \int_{h_{k-1}}^{h_k} [\sigma]_{x,y}^k z dz \\
 &= \sum_{k=1}^n \int_{h_{k-1}}^{h_k} [Q]_{x,y}^k \{ [\epsilon^o]_{x,y} + z[\kappa]_{x,y} - [e]_{x,y}^k \} z dz
 \end{aligned}$$

or, in view of Eqs. (5.18) through (5.22),

$$\begin{bmatrix} M_x \\ M_y \\ M_s \end{bmatrix} = \begin{bmatrix} B_{xx} & B_{xy} & B_{xs} \\ B_{yx} & B_{yy} & B_{ys} \\ B_{sx} & B_{sy} & B_{ss} \end{bmatrix} \begin{bmatrix} \epsilon_x^o \\ \epsilon_y^o \\ \gamma_s^o \end{bmatrix} + \begin{bmatrix} D_{xx} & D_{xy} & D_{xs} \\ D_{yx} & D_{yy} & D_{ys} \\ D_{sx} & D_{sy} & D_{ss} \end{bmatrix} \begin{bmatrix} \kappa_x \\ \kappa_y \\ \kappa_s \end{bmatrix} - \begin{bmatrix} M_x^{HT} \\ M_y^{HT} \\ M_s^{HT} \end{bmatrix} \quad (6.21)$$

where the laminate stiffness matrices $[B]$ and $[D]$ are defined as before in Eq. (5.20), $[M^{HT}]_{x,y}$ are the hygrothermal moment resultants defined as

$$\begin{bmatrix} M_x^{HT} \\ M_y^{HT} \\ M_s^{HT} \end{bmatrix} = \sum_{k=1}^n \begin{bmatrix} Q_{xx} & Q_{xy} & Q_{xs} \\ Q_{yx} & Q_{yy} & Q_{ys} \\ Q_{sx} & Q_{sy} & Q_{ss} \end{bmatrix}_k \begin{bmatrix} e_x \\ e_y \\ e_s \end{bmatrix}_k z_k t_k \quad (6.22)$$

t_k is the lamina k thickness, and $z_k = (h_k + h_{k-1})/2$ is the z -coordinate to the midplane of lamina k . Equations (6.19) and (6.21) can be rewritten in the form

$$\begin{bmatrix} N_x \\ N_y \\ N_s \end{bmatrix} + \begin{bmatrix} N_x^{HT} \\ N_y^{HT} \\ N_s^{HT} \end{bmatrix} = \begin{bmatrix} \bar{N}_x \\ \bar{N}_y \\ \bar{N}_s \end{bmatrix} = \begin{bmatrix} A_{xx} & A_{xy} & A_{xs} \\ A_{yx} & A_{yy} & A_{ys} \\ A_{sx} & A_{sy} & A_{ss} \end{bmatrix} \begin{bmatrix} \epsilon_x^o \\ \epsilon_y^o \\ \gamma_s^o \end{bmatrix} + \begin{bmatrix} B_{xx} & B_{xy} & B_{xs} \\ B_{yx} & B_{yy} & B_{ys} \\ B_{sx} & B_{sy} & B_{ss} \end{bmatrix} \begin{bmatrix} \kappa_x \\ \kappa_y \\ \kappa_s \end{bmatrix} \quad (6.23)$$

$$\begin{bmatrix} M_x \\ M_y \\ M_s \end{bmatrix} + \begin{bmatrix} M_x^{HT} \\ M_y^{HT} \\ M_s^{HT} \end{bmatrix} = \begin{bmatrix} \bar{M}_x \\ \bar{M}_y \\ \bar{M}_s \end{bmatrix} = \begin{bmatrix} B_{xx} & B_{xy} & B_{xs} \\ B_{yx} & B_{yy} & B_{ys} \\ B_{sx} & B_{sy} & B_{ss} \end{bmatrix} \begin{bmatrix} \epsilon_x^o \\ \epsilon_y^o \\ \gamma_s^o \end{bmatrix} + \begin{bmatrix} D_{xx} & D_{xy} & D_{xs} \\ D_{yx} & D_{yy} & D_{ys} \\ D_{sx} & D_{sy} & D_{ss} \end{bmatrix} \begin{bmatrix} \kappa_x \\ \kappa_y \\ \kappa_s \end{bmatrix} \quad (6.24)$$

or, in brief,

$$[\bar{N}]_{x,y} = [N]_{x,y} + [N^{HT}]_{x,y} = [A][\epsilon^o]_{x,y} + [B][\kappa]_{x,y} \quad (6.25)$$

$$[\bar{M}]_{x,y} = [M]_{x,y} + [M^{HT}]_{x,y} = [B][\epsilon^o]_{x,y} + [D][\kappa]_{x,y} \quad (6.26)$$

where $[\bar{N}]$ and $[\bar{M}]$ are total force and moment resultants equal to the respective sums of their mechanical and hygrothermal components.

The above relations can also be presented in a combined abbreviated form as

$$\begin{bmatrix} \overline{N} \\ \overline{M} \end{bmatrix} = \begin{bmatrix} A & B \\ B & D \end{bmatrix} \begin{bmatrix} \epsilon^o \\ \kappa \end{bmatrix} \quad (6.27)$$

Thus the force-deformation and moment deformation relations are identical to those derived before for mechanical loading only (Eqs. 5.21 to 5.24), except for the fact that here the hygrothermal forces and moments are added to the mechanically applied forces and moments.

6.6 Hygrothermoelastic Strain-Stress Relations

As mentioned in Chapter 5, it is preferable to work with strains because they are continuous through the laminate thickness and because the applied loads are independent variables. Inversion of the load-deformation and moment-deformation relations in Eqs. (6.23) and (6.24) yields the following relations, which are identical to Eq. (5.25) except for the substitution of total forces and moments for the mechanical forces and moments.

$$\begin{bmatrix} \epsilon_x^o \\ \epsilon_y^o \\ \gamma_s^o \\ \kappa_x \\ \kappa_y \\ \kappa_s \end{bmatrix} = \begin{bmatrix} a_{xx} & a_{xy} & a_{xs} & b_{xx} & b_{xy} & b_{xs} \\ a_{yx} & a_{yy} & a_{ys} & b_{yx} & b_{yy} & b_{ys} \\ a_{sx} & a_{sy} & a_{ss} & b_{sx} & b_{sy} & b_{ss} \\ c_{xx} & c_{xy} & c_{xs} & d_{xx} & d_{xy} & d_{xs} \\ c_{yx} & c_{yy} & c_{ys} & d_{yx} & d_{yy} & d_{ys} \\ c_{sx} & c_{sy} & c_{ss} & d_{sx} & d_{sy} & d_{ss} \end{bmatrix} \begin{bmatrix} \overline{N}_x \\ \overline{N}_y \\ \overline{N}_s \\ \overline{M}_x \\ \overline{M}_y \\ \overline{M}_s \end{bmatrix} \quad (6.28)$$

or, in brief,

$$\begin{bmatrix} \epsilon^o \\ \kappa \end{bmatrix} = \begin{bmatrix} a & b \\ c & d \end{bmatrix} \begin{bmatrix} \overline{N} \\ \overline{M} \end{bmatrix} \quad (6.29)$$

where $[a]$, $[b]$, $[c]$, and $[d]$ are the laminate compliance matrices related to the stiffness matrices $[A]$, $[B]$, and $[D]$ by Eq. (5.27) or obtained by direct inversion of the 6×6 stiffness matrix in Eq. (5.23).

6.7 Physical Significance of Hygrothermal Forces

The concept of hygrothermal forces, as defined in Eq. (6.20), is not a mathematical abstraction but can be understood in physical terms. For example, consider the hygrothermal force N_x^{HT} given by

$$N_x^{HT} = \sum_{k=1}^n [Q_{xx} e_x + Q_{xy} e_y + Q_{xs} e_s]_k t_k \quad (6.30)$$

The quantity in brackets represents the stress σ_x required to produce a deformation equal to the free (unrestrained) hygrothermal deformation (e_x, e_y, e_s) in lamina k . This quantity multiplied by the thickness t_k of the lamina gives the force necessary to deform lamina k in the same manner as it is deformed by the free hygrothermal deformation. Finally, the sum of all these lamina forces adds up to the total hygrothermal force N_x^{HT} .

Consider, for example, the case of a composite beam made of several layers and subjected to a temperature change $\Delta T = \Delta T_o$ (Fig. 6.10). This temperature change will result in a net axial strain $\epsilon = \epsilon_o$ without any external forces, i.e., $N = 0$. Thus, for case (a) in Figure 6.10 we have

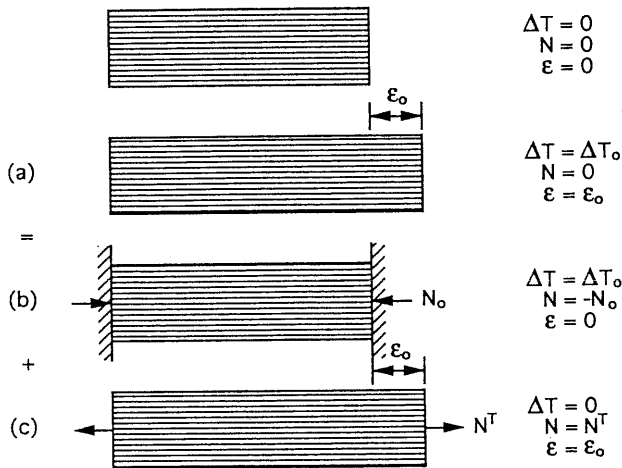


Fig. 6.10 Illustration of physical significance of thermal force.

$$\Delta T = \Delta T_o$$

$$N = 0$$

$$\epsilon = \epsilon_o$$

This case can be viewed as the superposition of cases (b) and (c) shown in Figure 6.10 for which we have, respectively,

$$\Delta T = \Delta T_o$$

$$N = -N_o$$

$$\epsilon = 0$$

and

$$\Delta T = 0$$

$$N = N^T$$

$$\epsilon = \epsilon_o$$

For case (b) using the relation in Eq. (6.19) and the definition in Eq. (6.20) with conditions $[\epsilon^o] = 0$ and $[\kappa] = 0$, we obtain

$$N = -N_o = - \sum_{k=1}^n Q^k e^k t_k \quad (6.31)$$

For the combination of cases (b) and (c) we have

$$\Sigma N = 0 = N^T - N_o$$

Thus

$$N^T = N_o = \sum_{k=1}^n Q^k e^k t_k \quad (6.32)$$

which means that the thermal force N^T is equal to the reaction N_o of the fixed-end beam under thermal loading, or the mechanical force necessary to produce a strain equal to the purely thermal strain of the laminate.

6.8 Hygrothermal Stress–Strain Relations

In the absence of externally applied mechanical forces and moments, i.e., when $[N] = 0$ and $[M] = 0$, the hygrothermoelastic relations in Eqs. (6.23) and (6.24) reduce to

$$\begin{bmatrix} N_x^{HT} \\ N_y^{HT} \\ N_s^{HT} \end{bmatrix} = \begin{bmatrix} A_{xx} & A_{xy} & A_{xs} \\ A_{yx} & A_{yy} & A_{ys} \\ A_{sx} & A_{sy} & A_{ss} \end{bmatrix} \begin{bmatrix} \epsilon_x^o \\ \epsilon_y^o \\ \gamma_s^o \end{bmatrix} + \begin{bmatrix} B_{xx} & B_{xy} & B_{xs} \\ B_{yx} & B_{yy} & B_{ys} \\ B_{sx} & B_{sy} & B_{ss} \end{bmatrix} \begin{bmatrix} \kappa_x \\ \kappa_y \\ \kappa_s \end{bmatrix} \quad (6.33)$$

$$\begin{bmatrix} M_x^{HT} \\ M_y^{HT} \\ M_s^{HT} \end{bmatrix} = \begin{bmatrix} B_{xx} & B_{xy} & B_{xs} \\ B_{yx} & B_{yy} & B_{ys} \\ B_{sx} & B_{sy} & B_{ss} \end{bmatrix} \begin{bmatrix} \epsilon_x^o \\ \epsilon_y^o \\ \gamma_s^o \end{bmatrix} + \begin{bmatrix} D_{xx} & D_{xy} & D_{xs} \\ D_{yx} & D_{yy} & D_{ys} \\ D_{sx} & D_{sy} & D_{ss} \end{bmatrix} \begin{bmatrix} \kappa_x \\ \kappa_y \\ \kappa_s \end{bmatrix} \quad (6.34)$$

The hygrothermal forces $[N^{HT}]$ and moments $[M^{HT}]$ are defined as in Eqs. (6.20) and (6.22).

Inversion of the relations above yields the reference plane strains $[\epsilon^o]$ and curvatures $[\kappa]$ produced by purely hygrothermal changes:

$$\begin{bmatrix} \epsilon_x^o \\ \epsilon_y^o \\ \gamma_s^o \end{bmatrix} = \begin{bmatrix} a_{xx} & a_{xy} & a_{xs} \\ a_{yx} & a_{yy} & a_{ys} \\ a_{sx} & a_{sy} & a_{ss} \end{bmatrix} \begin{bmatrix} N_x^{HT} \\ N_y^{HT} \\ N_s^{HT} \end{bmatrix} + \begin{bmatrix} b_{xx} & b_{xy} & b_{xs} \\ b_{yx} & b_{yy} & b_{ys} \\ b_{sx} & b_{sy} & b_{ss} \end{bmatrix} \begin{bmatrix} M_x^{HT} \\ M_y^{HT} \\ M_s^{HT} \end{bmatrix} \quad (6.35)$$

$$\begin{bmatrix} \kappa_x \\ \kappa_y \\ \kappa_s \end{bmatrix} = \begin{bmatrix} c_{xx} & c_{xy} & c_{xs} \\ c_{yx} & c_{yy} & c_{ys} \\ c_{sx} & c_{sy} & c_{ss} \end{bmatrix} \begin{bmatrix} N_x^{HT} \\ N_y^{HT} \\ N_s^{HT} \end{bmatrix} + \begin{bmatrix} d_{xx} & d_{xy} & d_{xs} \\ d_{yx} & d_{yy} & d_{ys} \\ d_{sx} & d_{sy} & d_{ss} \end{bmatrix} \begin{bmatrix} M_x^{HT} \\ M_y^{HT} \\ M_s^{HT} \end{bmatrix} \quad (6.36)$$

6.9 Coefficients of Thermal and Moisture Expansion of Multidirectional Laminates

For purely hygrothermal loading, i.e., $[N] = 0$ and $[M] = 0$, the reference plane strains can also be related to the effective, or laminate, coefficients of thermal and moisture expansion as

$$\begin{bmatrix} \epsilon_x^o \\ \epsilon_y^o \\ \gamma_s^o \end{bmatrix} = \begin{bmatrix} \bar{\alpha}_x \\ \bar{\alpha}_y \\ \bar{\alpha}_s \end{bmatrix} \Delta T + \begin{bmatrix} \bar{\beta}_x \\ \bar{\beta}_y \\ \bar{\beta}_s \end{bmatrix} \Delta c \quad (6.37)$$

where $[\bar{\alpha}]_{x,y}$ and $[\bar{\beta}]_{x,y}$ are the coefficients of thermal expansion and moisture expansion of the laminate, respectively. These can be determined by comparing Eqs. (6.35) and (6.37) and equating the right-hand sides of those equations.

The coefficients of thermal expansion are obtained by setting $\Delta T = 1$ and $\Delta c = 0$ in the above relations. Thus

$$\begin{bmatrix} \bar{\alpha}_x \\ \bar{\alpha}_y \\ \bar{\alpha}_s \end{bmatrix} = \begin{bmatrix} a_{xx} & a_{xy} & a_{xs} \\ a_{yx} & a_{yy} & a_{ys} \\ a_{sx} & a_{sy} & a_{ss} \end{bmatrix} \begin{bmatrix} N_x^T \\ N_y^T \\ N_s^T \end{bmatrix} + \begin{bmatrix} b_{xx} & b_{xy} & b_{xs} \\ b_{yx} & b_{yy} & b_{ys} \\ b_{sx} & b_{sy} & b_{ss} \end{bmatrix} \begin{bmatrix} M_x^T \\ M_y^T \\ M_s^T \end{bmatrix} \quad (6.38)$$

where $[N^T]_{x,y}$ and $[M^T]_{x,y}$ are the resultant thermal forces and moments as defined in Eqs. (6.20) and (6.22) in the absence of moisture concentration change ($\Delta c = 0$).

The coefficients of moisture expansion are obtained by setting in Eq. (6.37) $\Delta T = 0$ and $\Delta c = 1$. Then

$$\begin{bmatrix} \bar{\beta}_x \\ \bar{\beta}_y \\ \bar{\beta}_s \end{bmatrix} = \begin{bmatrix} a_{xx} & a_{xy} & a_{xs} \\ a_{yx} & a_{yy} & a_{ys} \\ a_{sx} & a_{sy} & a_{ss} \end{bmatrix} \begin{bmatrix} N_x^H \\ N_y^H \\ N_s^H \end{bmatrix} + \begin{bmatrix} b_{xx} & b_{xy} & b_{xs} \\ b_{yx} & b_{yy} & b_{ys} \\ b_{sx} & b_{sy} & b_{ss} \end{bmatrix} \begin{bmatrix} M_x^H \\ M_y^H \\ M_s^H \end{bmatrix} \quad (6.39)$$

where $[N^H]_{x,y}$ and $[M^H]_{x,y}$ are the resultant hygric forces and moments as defined in Eqs. (6.20) and (6.22) in the absence of temperature change ($\Delta T = 0$).

In the case of symmetric laminates Eqs. (6.38) and (6.39) are simplified by noting that the coupling compliance matrices $[b]$ and $[c]$ are zero.

6.10 Coefficients of Thermal and Moisture Expansion of Balanced/Symmetric Laminates

In the case of symmetric and balanced laminates a more direct determination can be made of the coefficients of thermal and moisture expansion in terms of the laminate stiffnesses. The hygrothermal stress-strain relations in Eq. (6.33) referred to the principal laminate axes \bar{x} and \bar{y} reduce to

$$\begin{bmatrix} N_{\bar{x}}^{HT} \\ N_{\bar{y}}^{HT} \\ N_{\bar{s}}^{HT} \end{bmatrix} = \begin{bmatrix} A_{\bar{x}\bar{x}} & A_{\bar{x}\bar{y}} & 0 \\ A_{\bar{y}\bar{x}} & A_{\bar{y}\bar{y}} & 0 \\ 0 & 0 & A_{\bar{s}\bar{s}} \end{bmatrix} \begin{bmatrix} \epsilon_{\bar{x}}^0 \\ \epsilon_{\bar{y}}^0 \\ \gamma_{\bar{s}}^0 \end{bmatrix} = \begin{bmatrix} A_{\bar{x}\bar{x}} & A_{\bar{x}\bar{y}} & 0 \\ A_{\bar{y}\bar{x}} & A_{\bar{y}\bar{y}} & 0 \\ 0 & 0 & A_{\bar{s}\bar{s}} \end{bmatrix} \begin{bmatrix} \bar{\alpha}_{\bar{x}} \Delta T + \bar{\beta}_{\bar{x}} \Delta c \\ \bar{\alpha}_{\bar{y}} \Delta T + \bar{\beta}_{\bar{y}} \Delta c \\ \bar{\alpha}_{\bar{s}} \Delta T + \bar{\beta}_{\bar{s}} \Delta c \end{bmatrix} \quad (6.40)$$

By setting $\Delta T = 1$ and $\Delta c = 0$, the relations above can be written as follows in an expanded form ($A_{\bar{x}\bar{y}} = A_{\bar{y}\bar{x}}$)

$$\begin{aligned} A_{\bar{x}\bar{x}} \bar{\alpha}_{\bar{x}} + A_{\bar{x}\bar{y}} \bar{\alpha}_{\bar{y}} &= N_{\bar{x}}^T \\ A_{\bar{x}\bar{y}} \bar{\alpha}_{\bar{x}} + A_{\bar{y}\bar{y}} \bar{\alpha}_{\bar{y}} &= N_{\bar{y}}^T \\ A_{\bar{s}\bar{s}} \bar{\alpha}_{\bar{s}} &= N_{\bar{s}}^T \end{aligned} \quad (6.41)$$

From the definition of thermal force resultants in Eq. (6.20), by setting $\Delta T = 1$ and $\Delta c = 0$, we obtain for the balanced laminate

$$N_{\bar{s}}^T = \sum_{k=1}^n [Q_{\bar{s}\bar{x}} \alpha_{\bar{x}} + Q_{\bar{s}\bar{y}} \alpha_{\bar{y}} + Q_{\bar{s}\bar{s}} \alpha_{\bar{s}}]_k t_k = 0$$

since

$$\begin{aligned} Q_{\bar{s}\bar{x}}(\theta) &= -Q_{\bar{s}\bar{x}}(-\theta) \quad \text{and} \quad \alpha_{\bar{x}}(\theta) = \alpha_{\bar{x}}(-\theta) \\ Q_{\bar{s}\bar{y}}(\theta) &= -Q_{\bar{s}\bar{y}}(-\theta) \quad \text{and} \quad \alpha_{\bar{y}}(\theta) = \alpha_{\bar{y}}(-\theta) \\ Q_{\bar{s}\bar{s}}(\theta) &= Q_{\bar{s}\bar{s}}(-\theta) \quad \text{and} \quad \alpha_{\bar{s}}(\theta) = -\alpha_{\bar{s}}(-\theta) \end{aligned}$$

The coefficients of thermal expansion along the principal laminate axes are obtained from the system of Eq. (6.41) as follows:

$$\begin{aligned} \bar{\alpha}_{\bar{x}} &= \frac{A_{\bar{y}\bar{y}} N_{\bar{x}}^T - A_{\bar{x}\bar{y}} N_{\bar{y}}^T}{A_{\bar{x}\bar{x}} A_{\bar{y}\bar{y}} - A_{\bar{x}\bar{y}}^2} \\ \bar{\alpha}_{\bar{y}} &= \frac{A_{\bar{x}\bar{x}} N_{\bar{y}}^T - A_{\bar{x}\bar{y}} N_{\bar{x}}^T}{A_{\bar{x}\bar{x}} A_{\bar{y}\bar{y}} - A_{\bar{x}\bar{y}}^2} \\ \bar{\alpha}_{\bar{s}} &= 0 \end{aligned} \quad (6.42)$$

These coefficients can be transformed to an arbitrary system of coordinates (x, y) making an angle φ with the principal laminate axes \bar{x}, \bar{y} (Fig. 5.7) as follows:

$$\begin{aligned}
 \bar{\alpha}_x &= m^2 \bar{\alpha}_{\bar{x}} + n^2 \bar{\alpha}_{\bar{y}} \\
 \bar{\alpha}_y &= n^2 \bar{\alpha}_{\bar{x}} + m^2 \bar{\alpha}_{\bar{y}} \\
 \bar{\alpha}_s &= 2mn (\bar{\alpha}_{\bar{x}} - \bar{\alpha}_{\bar{y}})
 \end{aligned} \tag{6.43}$$

where $m = \cos\varphi$ and $n = \sin\varphi$.

The principal coefficients of moisture expansion for the laminate are obtained in an entirely analogous manner by setting $\Delta T = 0$ and $\Delta c = 1$:

$$\begin{aligned}
 \bar{\beta}_{\bar{x}} &= \frac{A_{\bar{y}\bar{y}} N_{\bar{x}}^H - A_{\bar{x}\bar{y}} N_{\bar{y}}^H}{A_{\bar{x}\bar{x}} A_{\bar{y}\bar{y}} - A_{\bar{x}\bar{y}}^2} \\
 \bar{\beta}_{\bar{y}} &= \frac{A_{\bar{x}\bar{x}} N_{\bar{y}}^H - A_{\bar{x}\bar{y}} N_{\bar{x}}^H}{A_{\bar{x}\bar{x}} A_{\bar{y}\bar{y}} - A_{\bar{x}\bar{y}}^2} \\
 \bar{\beta}_s &= 0
 \end{aligned} \tag{6.44}$$

The transformed coefficients of moisture expansion are

$$\begin{aligned}
 \bar{\beta}_x &= m^2 \bar{\beta}_{\bar{x}} + n^2 \bar{\beta}_{\bar{y}} \\
 \bar{\beta}_y &= n^2 \bar{\beta}_{\bar{x}} + m^2 \bar{\beta}_{\bar{y}} \\
 \bar{\beta}_s &= 2mn (\bar{\beta}_{\bar{x}} - \bar{\beta}_{\bar{y}})
 \end{aligned} \tag{6.45}$$

6.11 Hygrothermoelastic Isotropy and Stability

A symmetric orthotropic laminate with identical elastic and thermoelastic (or hygroelastic) properties along at least **two perpendicular** axes (\bar{x}, \bar{y}) has identical thermoelastic (or hygroelastic) properties in **all directions** and is called **thermoelastic** (or **hygroelastic**) **isotropic**.

Consider, for example, the symmetric orthotropic laminate in Figure 5.7 with \bar{x} and \bar{y} as the principal laminate axes. The condition stated above is expressed as

$$\begin{aligned}
 \bar{\alpha}_{\bar{x}} &= \bar{\alpha}_{\bar{y}} = \bar{\alpha} \\
 \bar{E}_{\bar{x}} &= \bar{E}_{\bar{y}} \\
 \nu_{\bar{x}\bar{y}} &= \nu_{\bar{y}\bar{x}}
 \end{aligned} \tag{6.46}$$

Then, by the transformation relations in Eq. (6.43), we obtain for any arbitrary direction x at an angle φ with the \bar{x} -axis (Fig. 5.7),

$$\bar{\alpha}_x = m^2 \bar{\alpha}_x + n^2 \bar{\alpha}_y = \bar{\alpha}(m^2 + n^2) = \bar{\alpha} \quad (6.47)$$

where $m = \cos\phi$, $n = \sin\phi$, and $\bar{\alpha}$ = invariant coefficient of thermal expansion. Examples of such laminates are those of $[\pm 45]_{ns}$ and $[0/90]_{ns}$ lay-up.

Composite materials such as carbon/epoxy and Kevlar/epoxy with $E_1 \gg E_2$ and $|\alpha_1| \ll \alpha_2$ have the additional characteristic that

$$\bar{\alpha}_x = \bar{\alpha}_y = \bar{\alpha} \ll \alpha_2$$

Such materials are defined as **thermoelastic stable and isotropic**. Similarly, for hygroelastic characteristics such materials have the property

$$\bar{\beta}_x = \bar{\beta}_y = \bar{\beta} \ll \beta_2$$

Such materials are defined as **hygroelastic stable and isotropic**.

Sample Problem 6.1

Coefficient of Thermal Expansion of $[\pm 45]_s$ Laminate

It is required to calculate the coefficient of thermal expansion $\bar{\alpha}_x$ of a carbon/epoxy $[\pm 45]_s$ laminate. For this material the following observations can be made:

$$\begin{aligned} Q_{11} &\cong E_1, & Q_{22} &\cong E_2 \ll E_1 \\ Q_{12} &\cong \nu_{12}E_2 = \nu_{21}E_1 < E_2 \ll E_1 \\ Q_{66} &= G_{12} < E_2 \ll E_1 \\ \alpha_1 &\cong 0, & \alpha_2 &= \alpha \end{aligned} \quad (6.48)$$

The transformed coefficients of thermal expansion of the 45° layer are

$$\begin{bmatrix} \alpha_x \\ \alpha_y \\ \frac{1}{2}\alpha_s \end{bmatrix} = \begin{bmatrix} m^2 & n^2 & -2mn \\ n^2 & m^2 & 2mn \\ mn & -mn & (m^2 - n^2) \end{bmatrix} \begin{bmatrix} \alpha_1 \\ \alpha_2 \\ \frac{1}{2}\alpha_6 \end{bmatrix} = \begin{bmatrix} \frac{1}{2} & \frac{1}{2} & -1 \\ \frac{1}{2} & \frac{1}{2} & 1 \\ \frac{1}{2} & -\frac{1}{2} & 0 \end{bmatrix} \begin{bmatrix} 0 \\ \alpha \\ 0 \end{bmatrix} \quad (6.49)$$

Thus

$$(\alpha_x)_{45^\circ} = (\alpha_y)_{45^\circ} = (\alpha_x)_{-45^\circ} = \frac{1}{2} \alpha \quad (6.50)$$

$$(\alpha_s)_{45^\circ} = -(\alpha_s)_{-45^\circ} = -\alpha$$

The transformed lamina stiffnesses are

$$\begin{aligned}
 (Q_{xx})_{45^\circ} &= (Q_{yy})_{45^\circ} = (Q_{xx})_{-45^\circ} = (Q_{yy})_{-45^\circ} \\
 &= \frac{1}{4}(Q_{11} + Q_{22} + 2Q_{12} + 4Q_{66}) \\
 (Q_{xy})_{45^\circ} &= (Q_{xy})_{-45^\circ} = \frac{1}{4}(Q_{11} + Q_{22} + 2Q_{12} - 4Q_{66}) \\
 (Q_{ss})_{45^\circ} &= (Q_{ss})_{-45^\circ} = \frac{1}{4}(Q_{11} + Q_{22} - 2Q_{12}) \\
 (Q_{xs})_{45^\circ} &= (Q_{ys})_{45^\circ} = -(Q_{xs})_{-45^\circ} = -(Q_{ys})_{-45^\circ} \\
 &= \frac{1}{4}(Q_{11} - Q_{22})
 \end{aligned} \tag{6.51}$$

From the definition of thermal forces we have

$$\begin{aligned}
 \begin{bmatrix} N_x^T \\ N_y^T \\ N_s^T \end{bmatrix} &= \begin{bmatrix} Q_{xx} & Q_{xy} & Q_{xs} \\ Q_{yx} & Q_{yy} & Q_{ys} \\ Q_{sx} & Q_{sy} & Q_{ss} \end{bmatrix}_{45^\circ} \begin{bmatrix} \alpha_x \\ \alpha_y \\ \alpha_s \end{bmatrix}_{45^\circ} 2t\Delta T \\
 &+ \begin{bmatrix} Q_{xx} & Q_{xy} & Q_{xs} \\ Q_{yx} & Q_{yy} & Q_{ys} \\ Q_{sx} & Q_{sy} & Q_{ss} \end{bmatrix}_{-45^\circ} \begin{bmatrix} \alpha_x \\ \alpha_y \\ \alpha_s \end{bmatrix}_{-45^\circ} 2t\Delta T
 \end{aligned} \tag{6.52}$$

where t is the ply thickness.

Substituting the relations in Eqs. (6.50) and (6.51) in the above we obtain

$$\begin{aligned}
 N_x^T &= N_y^T = (Q_{xx} \alpha_x + Q_{xy} \alpha_y + Q_{xs} \alpha_s)_{45^\circ} h\Delta T \\
 N_s^T &= 0
 \end{aligned} \tag{6.53}$$

where $h = 4t$ is the laminate thickness.

From Eq. (6.42) (in which $\Delta T = 1$), we obtain

$$\begin{aligned}
 \bar{\alpha}_x &= \bar{\alpha}_y = \frac{N_x^T}{A_{xx} + A_{xy}} \\
 \bar{\alpha}_s &= 0
 \end{aligned} \tag{6.54}$$

Noting that in this case

$$(A_{xx} + A_{xy}) = h (Q_{xx} + Q_{xy})_{45^\circ}$$

and substituting Eq. (6.53) into Eq. (6.54) with $\Delta T = 1$, we obtain

$$\bar{\alpha}_x = \bar{\alpha}_y = \left[\frac{Q_{xx} \alpha_x + Q_{xy} \alpha_y + Q_{xs} \alpha_s}{Q_{xx} + Q_{xy}} \right]_{45^\circ} \quad (6.55)$$

Taking Eqs. (6.50), and (6.51) into consideration, we obtain

$$\begin{aligned} \bar{\alpha}_x = \bar{\alpha}_y &= \frac{\alpha}{2} \frac{(Q_{xx} + Q_{xy} - 2Q_{xs})}{Q_{xx} + Q_{xy}} \\ &= \frac{\alpha}{2} \frac{(Q_{11} + Q_{22} + 2Q_{12} - Q_{11} + Q_{22})}{Q_{11} + Q_{22} + 2Q_{12}} \\ &= \alpha \frac{(Q_{22} + Q_{12})}{Q_{11} + Q_{22} + 2Q_{12}} \end{aligned} \quad (6.56)$$

from which it follows, for high fiber stiffness composites, that

$$\bar{\alpha}_x = \bar{\alpha}_y \cong \frac{E_2(1 + \nu_{12}) \alpha_2}{E_2(1 + \nu_{12}) + E_1(1 + \nu_{21})} \cong \frac{E_2(1 + \nu_{12})\alpha_2}{E_1} \quad (6.57)$$

and

$$\bar{\alpha}_x = \bar{\alpha}_y \ll \alpha_2$$

Thus the $[\pm 45]_s$ laminate is thermoelastic isotropic, and, in the case of carbon/epoxy, its coefficient of thermal expansion in any direction is much lower than the transverse CTE α_2 . For carbon/epoxy (AS4/3501-6) in particular $\bar{\alpha}_x \cong 0.093 \alpha_2 \cong \alpha_2/11$, i.e., the CTE of a $[\pm 45]_s$ carbon/epoxy laminate is fiber dominated.

6.12 Coefficients of Thermal Expansion of Unidirectional and Multidirectional Carbon/Epoxy Laminates

A typical carbon/epoxy composite, the AS4/3501-6, has the following principal coefficients of thermal expansion:

$$\alpha_1 = -0.9 \times 10^{-6}/^\circ\text{C} \quad (-0.5 \times 10^{-6}/^\circ\text{F})$$

$$\alpha_2 = 27 \times 10^{-6}/^\circ\text{C} \quad (15 \times 10^{-6}/^\circ\text{F})$$

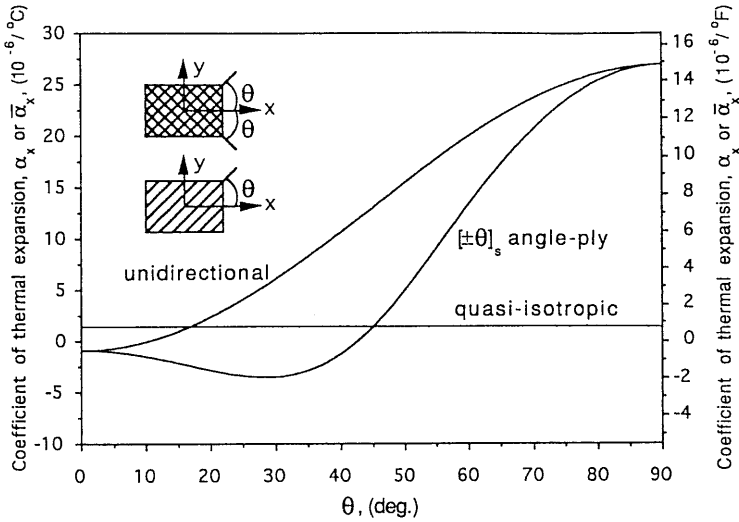


Fig. 6.11 Coefficients of thermal expansion of unidirectional and angle-ply laminates as a function of fiber orientation compared with that of a thermally isotropic laminate (e.g., $[0/90]_s$) (AS4/3501-6 carbon/epoxy).

The variation of the transformed CTE, α_x , for a unidirectional lamina with fiber orientation θ is illustrated in Figure 6.11, where it is compared with the $\bar{\alpha}_x$ of the angle-ply laminate $[\pm\theta]_s$ and the quasi-isotropic laminate. It is interesting to note that the variation of $\bar{\alpha}_x$ with angle θ for the angle-ply laminate is not monotonic and has a local minimum at $\theta \cong 28^\circ$.

A carpet plot of the CTE for the general class of $[0_m/90_n/(\pm 45)_p]_s$ laminates is shown in Figure 6.12 as a function of the percentages of the 0° , $(\pm 45^\circ)$, and 90° plies. It can be seen that there are many laminates with exactly zero CTE, a fact of great importance in the design of dimensionally stable structures, such as space antennae, mirrors, and other aerospace components and structures.

6.13 Hygrothermoelastic Stress Analysis of Multidirectional Laminate

Given a hygrothermomechanical loading $[\bar{N}]$ and $[\bar{M}]$, as defined in Eqs. (6.23) and (6.24), the reference plane strains and curvatures of the laminate are obtained from Eq. (6.29) repeated here:

$$\begin{bmatrix} \epsilon^o \\ \kappa \end{bmatrix} = \begin{bmatrix} a & b \\ c & d \end{bmatrix} \begin{bmatrix} \bar{N} \\ \bar{M} \end{bmatrix} \tag{6.29 bis}$$

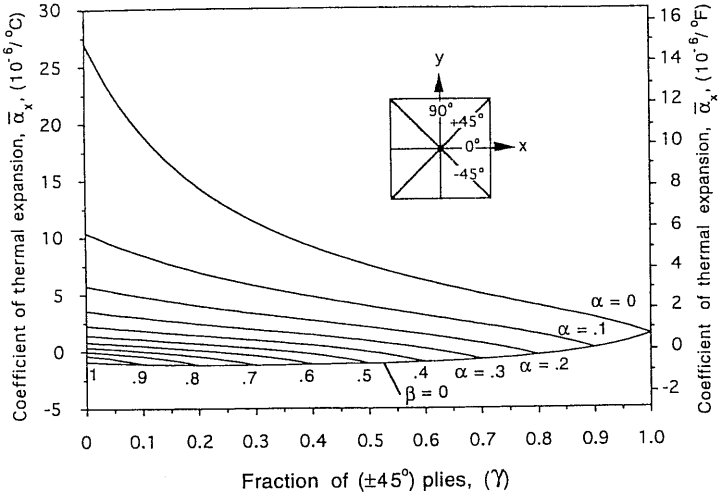


Fig. 6.12 Carpet plot for principal coefficient of thermal expansion of $[0_m/90_n/(\pm 45)_p]_s$ carbon/epoxy laminates (AS4/3501-6) (α , β , and γ are fractions of 0° , 90° , and $\pm 45^\circ$ plies, respectively).

The total (net) strains in layer k at a distance z from the reference plane are

$$\begin{bmatrix} \epsilon_x \\ \epsilon_y \\ \gamma_{s,k} \end{bmatrix} = \begin{bmatrix} \epsilon_x^o \\ \epsilon_y^o \\ \gamma_s^o \end{bmatrix} + z \begin{bmatrix} K_x \\ K_y \\ K_s \end{bmatrix} \tag{5.8 bis}$$

Based on the hygrothermoelastic principle stated in Eq. (6.15), the hygrothermal strains of layer k are obtained as

$$\begin{bmatrix} \epsilon_{xe} \\ \epsilon_{ye} \\ \gamma_{se,k} \end{bmatrix} = \begin{bmatrix} \epsilon_x \\ \epsilon_y \\ \gamma_{s,k} \end{bmatrix} - \begin{bmatrix} e_x \\ e_y \\ e_s \end{bmatrix}_k \tag{6.58}$$

The stresses in layer k referred to the laminate coordinate axes (x,y) can be obtained by

$$\begin{bmatrix} \sigma_{xe} \\ \sigma_{ye} \\ \tau_{se,k} \end{bmatrix} = \begin{bmatrix} Q_{xx} & Q_{xy} & Q_{xs} \\ Q_{yx} & Q_{yy} & Q_{ys} \\ Q_{sx} & Q_{sy} & Q_{ss,k} \end{bmatrix} \begin{bmatrix} \epsilon_{xe} \\ \epsilon_{ye} \\ \gamma_{se,k} \end{bmatrix} \tag{6.59}$$

These stresses can be transformed to the lamina axes (1,2) by the transformation relation

$$\begin{bmatrix} \sigma_{1e} \\ \sigma_{2e} \\ \tau_{6e} \end{bmatrix} = [T] \begin{bmatrix} \sigma_{xe} \\ \sigma_{ye} \\ \tau_{se} \end{bmatrix}$$

where

$$[T] = \begin{bmatrix} m^2 & n^2 & 2mn \\ n^2 & m^2 & -2mn \\ -mn & mn & m^2 - n^2 \end{bmatrix}$$

and $m = \cos\theta$, $n = \sin\theta$.

These stresses can also be obtained by first transforming the hygrothermal strains from Eq. (6.58) to the lamina principal axes and then using the stress-strain relations for the lamina referred to its principal axes as follows:

$$\begin{bmatrix} \epsilon_{1e} \\ \epsilon_{2e} \\ \frac{1}{2}\gamma_{6e} \end{bmatrix} = [T] \begin{bmatrix} \epsilon_{xe} \\ \epsilon_{ye} \\ \frac{1}{2}\gamma_{se} \end{bmatrix} = \begin{bmatrix} \epsilon_1 - e_1 \\ \epsilon_2 - e_2 \\ \frac{1}{2}\gamma_6 \end{bmatrix} \quad (6.60)$$

and

$$\begin{bmatrix} \sigma_{1e} \\ \sigma_{2e} \\ \tau_{6e} \end{bmatrix}_k = \begin{bmatrix} Q_{11} & Q_{12} & 0 \\ Q_{21} & Q_{22} & 0 \\ 0 & 0 & Q_{66} \end{bmatrix}_k \begin{bmatrix} \epsilon_{1e} \\ \epsilon_{2e} \\ \gamma_{6e} \end{bmatrix}_k \quad (6.61)$$

In the absence of mechanical loading, the total loading $[\bar{N}]$ and $[\bar{M}]$ in Eq. (6.29) is replaced by the hygrothermal forces and moments $[N^{HT}]$ and $[M^{HT}]$. Then, Eqs. (6.59) and (6.61) above give the purely hygrothermal stresses in each layer.

6.14 Residual Stresses

Residual stresses are introduced in multidirectional laminates during fabrication. On a micromechanical scale, residual stresses are introduced in unidirectional layers in and around individual fibers due to the mismatch in thermal properties

of the constituents. These stresses are accounted for in the analysis and design of laminates by using lamina properties determined macroscopically by standard testing. In addition, there exist residual stresses on a macroscopic level, the so-called lamination residual stresses, due to the thermal anisotropy of the layers. These stresses are similar in nature to the hygrothermal stresses discussed before.

During processing at elevated temperatures there is a certain temperature level at which the composite material is assumed to be stress free. This temperature level may be taken as the glass transition temperature of the polymer matrix, or the melting temperature of the metal matrix, or the sintering temperature of the ceramic matrix. Residual stresses develop in the initially stress-free laminate if the thermally anisotropic plies are oriented in different directions. Residual stresses are a function of many parameters, such as ply orientation and stacking sequence, curing process, fiber volume ratio, and other material and processing variables.

Lamination residual stresses can be analyzed by using lamination theory and lamina material properties.¹⁰⁻¹² Experimentally, they can be determined using embedded strain gage techniques.^{9,13-15} It has been shown by viscoelastic analysis that residual stresses are also a function of the cooldown path in the curing cycle.^{16,17} For a given temperature drop over a specified length of time, there is an optimum cooldown path that minimizes curing residual stresses. A more precise analysis of residual stresses should take into consideration the viscoelastic properties and the irreversible polymerization (or chemical) shrinkage of the matrix.¹⁶⁻¹⁹

The procedure for elastic analysis of residual stresses is as follows: The difference ΔT between ambient and stress-free temperature is introduced in Eqs. (6.14) to obtain the free thermal strains in each layer; then, the thermal forces and moments are determined using the definitions in Eqs. (6.20) and (6.22). The hygrothermal stress-strain relations in Eqs. (6.33) and (6.34) or (6.35) and (6.36) are solved for the reference plane strains $[\epsilon^0]$ and curvatures $[\kappa]$. Then, following the procedure discussed in section 6.13, the residual (hygrothermal) stresses are obtained for each individual layer of the laminate.

As an example, residual stresses in a ply of a $[\pm\theta]_s$ angle-ply carbon/epoxy laminate were calculated as a function of the fiber orientation θ and plotted in Figure 6.13. The properties of carbon/epoxy (AS4/3501-6) in Table 2.6 with a temperature difference of $\Delta T = 110^\circ\text{C}$ (200°F) were used. The normal lamina stresses σ_{1e} and σ_{2e} are equal and opposite in sign and reach maximum absolute values for $\theta = 45^\circ$. In the case of a $[\pm 45]_s$ laminate, which is the same as a $[0/90]_s$ laminate rotated by 45° , the maximum transverse residual stress σ_{2e} is approximately equal to half the transverse lamina strength, F_{2t} .

A clear manifestation of lamination residual stresses is shown for hybrid laminates in Figure 6.14.⁹ Before failure the laminate was flat under the self-

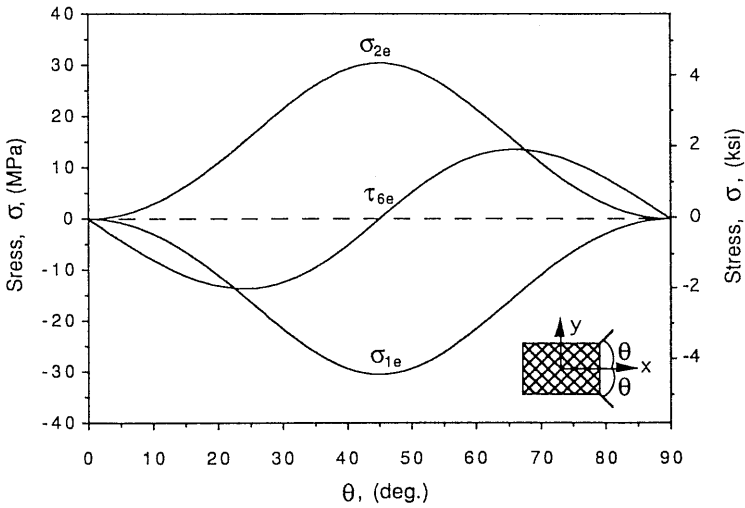


Fig. 6.13 Residual stresses at room temperature in layer of $[\pm\theta]_s$ carbon/epoxy laminate (AS4/3501-6; a temperature difference $\Delta T = 110^\circ\text{C}$ (200°F) was assumed).

equilibrated residual stresses. In the $[\pm 45^{\text{C}}/0^{\text{G}}/0^{\text{C}}]_s$ laminate (where superscripts C and G denote carbon and glass, respectively) failure of the 0° carbon plies caused delamination of the outer three-ply ($\pm 45^{\text{C}}/0^{\text{G}}$) sublaminates. The compressive residual stresses in the $\pm 45^\circ$ carbon plies and tensile residual stress in the 0° glass ply of this sublaminates caused the warpage shown in the asymmetric sublaminates. In the $[0^{\text{G}}/\pm 45^{\text{C}}/0^{\text{G}}]_s$ laminates, the outer three-ply ($0^{\text{G}}/\pm 45^{\text{C}}$) sublaminates delaminated and warped as shown due to the tensile residual stress in the 0° glass ply and compressive residual stress in the $\pm 45^\circ$ carbon plies of the sublaminates.

Sample Problem 6.2

Residual Stresses in Crossply Symmetric Laminate

It is required to calculate the residual stresses in a $[0/90]_s$ crossply symmetric laminate in terms of the temperature difference ΔT and the lamina mechanical and thermal properties (Fig. 6.15).¹²

The general procedure is to determine the thermal forces $[N^T]$, the reference plane strains from Eq. (6.29), and the thermal strains and stresses using Eqs. (6.58) and (6.59) or (6.60) and (6.61). In the present case a more direct approach may be taken by making some observations.

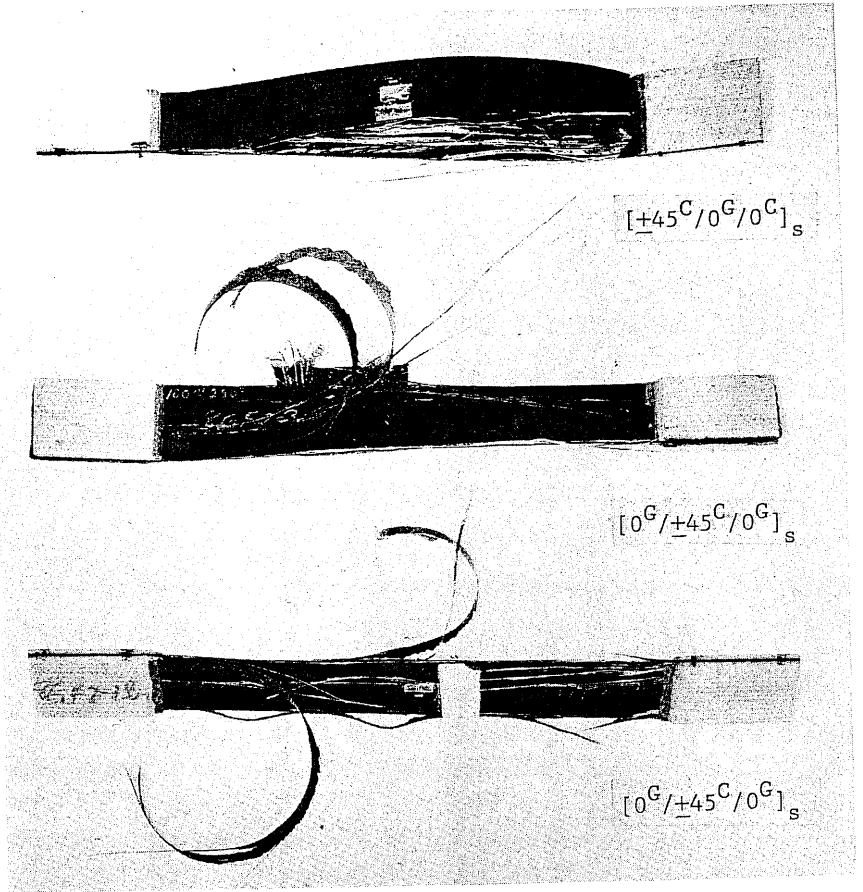


Fig. 6.14 Characteristic failure patterns in three carbon/S-glass/epoxy specimens under uniaxial tensile loading, illustrating presence of residual stresses.⁹

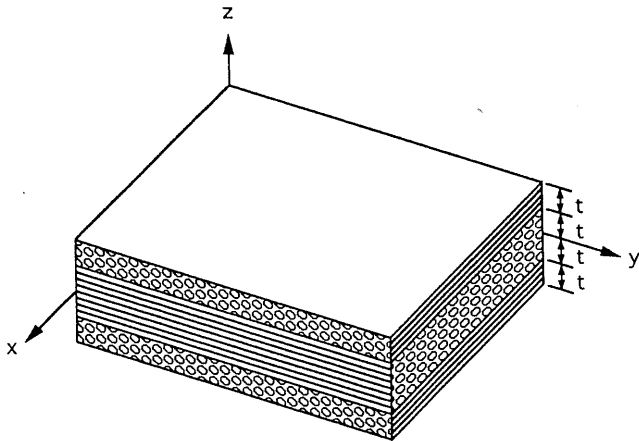


Fig. 6.15 Crossply symmetric laminate.

The laminate lay-up implies that

$$\begin{aligned}\epsilon_x^o &= \epsilon_y^o, \quad \gamma_s^o = 0 \\ \kappa_x &= \kappa_y = \kappa_s = 0\end{aligned}\quad (6.62)$$

Also, from the laminate symmetry and lay-up, it follows that

$$\begin{aligned}A_{xx} &= A_{yy}, \quad A_{xs} = A_{ys} = 0 \\ [B] &= 0 \\ N_x^T &= N_y^T, \quad N_s^T = 0 \\ M_x^T &= M_y^T = M_s^T = 0\end{aligned}\quad (6.63)$$

The hygrothermal stress-strain relations in Eq. (6.33) reduce to

$$\begin{bmatrix} N_x^T \\ N_y^T \\ 0 \end{bmatrix} = \begin{bmatrix} A_{xx} & A_{xy} & 0 \\ A_{yx} & A_{yy} & 0 \\ 0 & 0 & A_{ss} \end{bmatrix} \begin{bmatrix} \epsilon_x^o \\ \epsilon_y^o \\ 0 \end{bmatrix}\quad (6.64)$$

which, in view of Eqs. (6.62) and (6.63) reduce to

$$N_x^T = N_y^T = (A_{xx} + A_{xy})\epsilon_x^o$$

or

$$\epsilon_x^o = \epsilon_y^o = \frac{N_x^T}{A_{xx} + A_{xy}}\quad (6.65)$$

The hygrothermal force N_x^T is obtained from its defining relation (Eq. 6.20) as

$$N_x^T = 2t(Q_{11} \alpha_1 + Q_{12} \alpha_2 + Q_{22} \alpha_2 + Q_{12} \alpha_1)\Delta T\quad (6.66)$$

where t is the lamina thickness.

Substituting the above into Eq. (6.65) and evaluating A_{xx} and A_{xy} for the laminate, we obtain

$$\epsilon_x^o = \epsilon_y^o = \frac{(Q_{11} + Q_{12})\alpha_1 + (Q_{22} + Q_{12})\alpha_2}{Q_{11} + Q_{22} + 2Q_{12}} \Delta T\quad (6.67)$$

The residual (thermal) strains in the 0° ply, for example, are then

$$\begin{aligned}\epsilon_{1e} &= \epsilon_x^o - e_1 = \epsilon_x^o - \alpha_1 \Delta T \\ \epsilon_{2e} &= \epsilon_y^o - e_2 = \epsilon_y^o - \alpha_2 \Delta T\end{aligned}\quad (6.68)$$

and, substituting from Eq. (6.67),

$$\begin{aligned}\epsilon_{1e} &= \Delta T(\alpha_2 - \alpha_1) \frac{Q_{22} + Q_{12}}{Q_{11} + Q_{22} + 2Q_{12}} \\ \epsilon_{2e} &= \Delta T(\alpha_1 - \alpha_2) \frac{Q_{11} + Q_{12}}{Q_{11} + Q_{22} + 2Q_{12}}\end{aligned}\quad (6.69)$$

Finally, the residual stresses in the 0° ply are obtained as follows:

$$\begin{aligned}\sigma_{1e} &= Q_{11} \epsilon_{1e} + Q_{12} \epsilon_{2e} = \Delta T(\alpha_2 - \alpha_1) \frac{Q_{11} Q_{22} - Q_{12}^2}{Q_{11} + Q_{22} + 2Q_{12}} \\ \sigma_{2e} &= Q_{12} \epsilon_{1e} + Q_{22} \epsilon_{2e} = \Delta T(\alpha_1 - \alpha_2) \frac{Q_{11} Q_{22} - Q_{12}^2}{Q_{11} + Q_{22} + 2Q_{12}}\end{aligned}\quad (6.70)$$

For a high fiber stiffness composite the stresses above can be approximated as

$$\begin{aligned}\sigma_{1e} &= \Delta T(\alpha_2 - \alpha_1) \frac{Q_{11} Q_{22} (1 - \nu_{12}\nu_{21})}{Q_{11}(1 + \nu_{21}) + Q_{22}(1 + \nu_{12})} \\ &\cong \Delta T(\alpha_2 - \alpha_1) \frac{E_2}{1 + \frac{E_2}{E_1}(1 + \nu_{12})} \cong \Delta T(\alpha_2 - \alpha_1) E_2 \\ \sigma_{2e} &\cong \Delta T(\alpha_1 - \alpha_2) \frac{E_2}{1 + \frac{E_2}{E_1}(1 + \nu_{12})} \cong \Delta T(\alpha_1 - \alpha_2) E_2\end{aligned}\quad (6.71)$$

For carbon fiber composites where $|\alpha_1| \ll \alpha_2$,

$$\sigma_{1e} = -\sigma_{2e} \cong \Delta T \alpha_2 E_2$$

It is seen that the residual stresses in the fiber and transverse to the fiber directions are of equal magnitude and opposite sign, which satisfies equilibrium conditions. For a temperature drop during cooldown, this means that there is a

transverse tensile stress and longitudinal compressive stress since $\Delta T < 0$ and $\alpha_2 > \alpha_1$. The stresses in the 90° ply referred to its principal axes are identical to those of the 0° ply. The results above obtained for a $[0/90]_s$ lay-up are identical to those for a $[\pm 45]_s$ laminate.

6.15 Warpage

Warpage, or out-of-plane deformation, occurs in asymmetric laminates under uniform hygrothermal loading. It is a result of the induced hygrothermal stresses and the laminate asymmetry (Fig. 6.16). Bending asymmetries result from an asymmetric lay-up, designed for a specific purpose, or from inadvertently introduced process or material nonuniformities as well as thermal and moisture gradients through the thickness. Warpage can be calculated by classical lamination theory using lamina material properties.^{12,19–22}

Integration of the curvature-deflection relations

$$\begin{aligned}\kappa_x &= -\frac{\partial^2 w}{\partial x^2} \\ \kappa_y &= -\frac{\partial^2 w}{\partial y^2} \\ \kappa_s &= -\frac{2\partial^2 w}{\partial x\partial y}\end{aligned}\tag{5.7 bis}$$

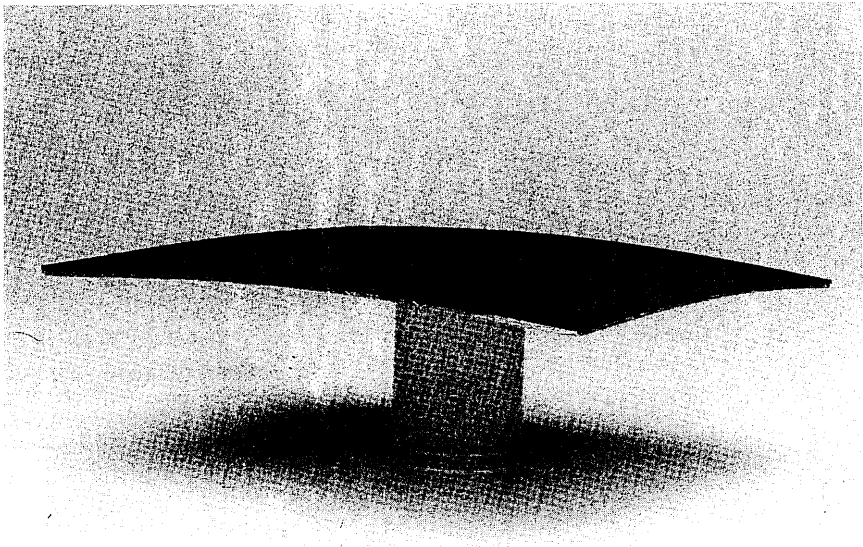


Fig. 6.16 Warpage in hybrid laminate made of a $[\pm 45]_s$ carbon/epoxy (AS4/3502) laminate bonded to an aluminum (2024) plate.

yields the out-of-plane deflection w

$$w = -\frac{1}{2}(\kappa_x x^2 + \kappa_y y^2 + \kappa_{xy} xy) + (\text{rigid body motion}) \quad (6.72)$$

Warpage is described by the quadratic part of this expression.

The curvatures are also related to the hygrothermal forces and moments as shown in Eqs. (6.29):

$$[\kappa]_{x,y} = [c][N^{HT}]_{x,y} + [d][M^{HT}]_{x,y} \quad (6.73)$$

which, substituted into Eq. (6.72), yields the specific equation for w describing the warpage.

Sample Problem 6.3

Warpage of Crossply Antisymmetric Laminate

It is required to calculate the warpage of a $[0/90]$ crossply antisymmetric laminate in terms of the uniform temperature change ΔT and the lamina mechanical and thermal properties (Fig. 6.17.)^{12,22}

The thermal force and moment resultants are

$$\begin{bmatrix} N_x^T \\ N_y^T \\ 0 \end{bmatrix} = \frac{h\Delta T}{2} \begin{bmatrix} Q_{11} & Q_{12} & 0 \\ Q_{21} & Q_{22} & 0 \\ 0 & 0 & Q_{66} \end{bmatrix} \begin{bmatrix} \alpha_1 \\ \alpha_2 \\ 0 \end{bmatrix} + \frac{h\Delta T}{2} \begin{bmatrix} Q_{22} & Q_{21} & 0 \\ Q_{12} & Q_{11} & 0 \\ 0 & 0 & Q_{66} \end{bmatrix} \begin{bmatrix} \alpha_2 \\ \alpha_1 \\ 0 \end{bmatrix} \quad (6.74)$$

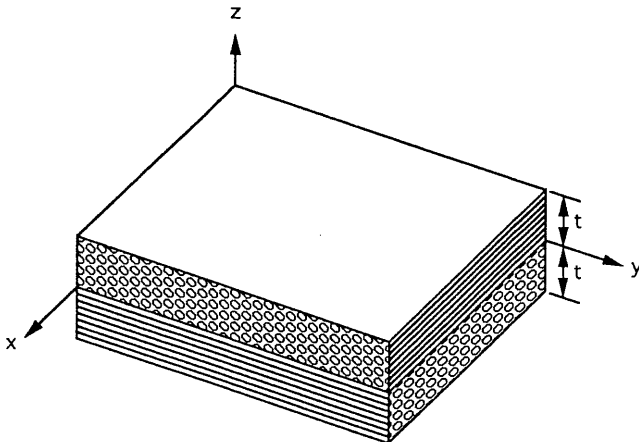


Fig. 6.17 $[0/90]$ antisymmetric crossply laminate.

and

$$\begin{bmatrix} M_x^T \\ M_y^T \\ 0 \end{bmatrix} = \frac{h^2 \Delta T}{8} \begin{bmatrix} Q_{11} & Q_{12} & 0 \\ Q_{21} & Q_{22} & 0 \\ 0 & 0 & Q_{66} \end{bmatrix} \begin{bmatrix} \alpha_1 \\ \alpha_2 \\ 0 \end{bmatrix} - \frac{h^2 \Delta T}{8} \begin{bmatrix} Q_{22} & Q_{21} & 0 \\ Q_{12} & Q_{11} & 0 \\ 0 & 0 & Q_{66} \end{bmatrix} \begin{bmatrix} \alpha_2 \\ \alpha_1 \\ 0 \end{bmatrix} \quad (6.75)$$

The following observations can be made for the specific lay-up considered:

$$\begin{aligned} \epsilon_x^o &= \epsilon_y^o, & \gamma_s^o &= 0 \\ \kappa_x &= -\kappa_y, & \kappa_s &= 0 \\ N_x^T &= N_y^T, & N_s^T &= 0 \\ M_x^T &= -M_y^T, & M_s^T &= 0 \end{aligned} \quad (6.76)$$

Furthermore,

$$\begin{aligned} B_{xx} &= -B_{yy} \\ B_{xy} &= B_{xs} = B_{ss} = 0 \end{aligned} \quad (6.77)$$

The thermal force deformation relations in Eqs. (6.33) and (6.34) reduce to

$$\begin{aligned} N_x^T &= (A_{xx} + A_{xy}) \epsilon_x^o + B_{xx} \kappa_x \\ M_x^T &= B_{xx} \epsilon_x^o + (D_{xx} - D_{xy}) \kappa_x \end{aligned} \quad (6.78)$$

The system of Eqs. (6.78) can be solved for the two unknowns ϵ_x^o and κ_x .

$$\epsilon_x^o = \epsilon_y^o = \frac{(D_{xx} - D_{xy})N_x^T - B_{xx} M_x^T}{(A_{xx} + A_{xy})(D_{xx} - D_{xy}) - B_{xx}^2} \quad (6.79)$$

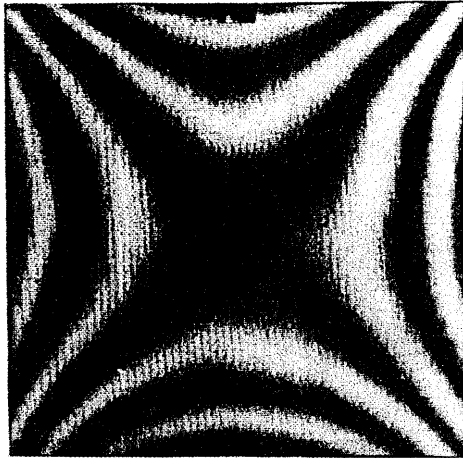
and

$$\kappa_x = -\kappa_y = \frac{(A_{xx} + A_{xy})M_x^T - B_{xx} N_x^T}{(A_{xx} + A_{xy})(D_{xx} - D_{xy}) - B_{xx}^2} \quad (6.80)$$

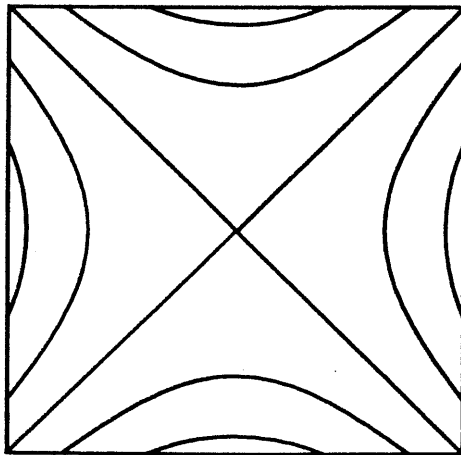
Substitution of Eq. (6.80) into Eq. (6.72) yields the equation of the warped surface as:

$$w = -\frac{1}{2} \frac{(A_{xx} + A_{xy})M_x^T - B_{xx} N_x^T}{(A_{xx} + A_{xy})(D_{xx} - D_{xy}) - B_{xx}^2} (x^2 - y^2) \quad (6.81)$$

which represents a hyperbolic paraboloid or saddle-shaped surface. Predicted contours of this surface for a woven-glass/epoxy antisymmetric laminate are shown in Figure 6.18. They are in good agreement with the moiré fringe pattern, which depicts the same contours.²²



(a)



(b)

Fig. 6.18 Contours of warped surface obtained by shadow moiré method and predicted by analysis for $[0_6/90_6]$ woven-glass/epoxy laminate; (a) experimental, (b) predicted. (Experimental and predicted fringes are loci of points of 0.60 mm [0.023 in.] constant out-of-plane displacement with respect to points on neighboring fringe).²²

6.16 Computational Procedure for Hygrothermoelastic Analysis of Multidirectional Laminates

A flow chart for hygrothermoelastic analysis of multidirectional laminates is shown in Figure 6.19. It consists of two main branches. The left-hand branch is similar to the flow chart in Figure 5.11 used for computation of laminate stiffnesses and compliances and has been discussed before. The right-hand branch consists of the following steps:

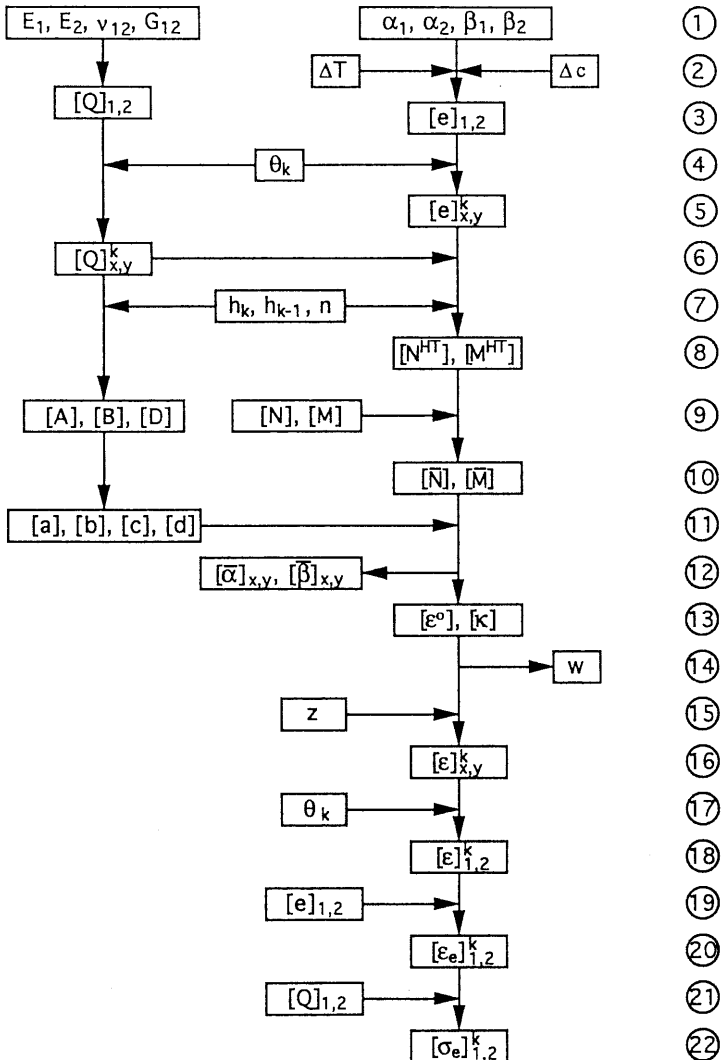


Fig. 6.19 Flow chart for hygrothermoelastic analysis of multidirectional laminates.

- Step 1** Enter lamina coefficients of thermal and moisture expansion α_1 , α_2 , β_1 and β_2 .
- Step 2** Enter temperature and moisture concentration differences, ΔT and Δc .
- Step 3** Calculate free lamina hygrothermal strains e_1 and e_2 referred to its principal material axes (1,2) using Eq. (6.12).
- Step 4** Enter ply (or principal axis) orientation, θ_k , of lamina k .
- Step 5** Calculate transformed free lamina hygrothermal strains $(e_x, e_y, e_s)_k$, referred to laminate reference axes (x,y) using Eq. (6.13).
- Step 6** Enter transformed lamina stiffnesses $[Q]_{x,y}^k$ of lamina k from left-hand branch.
- Step 7** Enter through-the-thickness coordinates h_k and h_{k-1} of lamina k surfaces and total number of plies n .
- Step 8** Calculate hygrothermal forces and moments, N^{HT} and M^{HT} , using Eqs. (6.20) and (6.22).
- Step 9** Enter mechanical loading $[N]$ and $[M]$.
- Step 10** Combine hygrothermal and mechanical loading, $[\bar{N}]$ and $[\bar{M}]$.
- Step 11** Enter laminate compliances $[a]$, $[b]$, $[c]$, and $[d]$ from left-hand branch.
- Step 12** Calculate laminate coefficients of thermal and moisture expansion, $\bar{\alpha}_x$, $\bar{\alpha}_y$, $\bar{\beta}_x$, and $\bar{\beta}_y$, using Eqs. (6.38) and (6.39).
- Step 13** Calculate reference plane strains $[\epsilon^o]$ and curvatures $[\kappa]$ using Eq. (6.28).
- Step 14** Calculate warpage w , using Eq. (6.72).
- Step 15** Enter through-the-thickness coordinate, z , of point of interest in lamina k . For a laminate consisting of many thin (compared with the laminate thickness) layers or for any symmetric laminate under in-plane loading, the coordinate of the lamina midplane, $z = z_k$, is used. Then, the computed strains and stresses are the average through-the-thickness strains and stresses in the layer. However, when the laminate consists of few and thick (relative to the laminate thickness) layers and is asymmetric or subjected to bending and twisting, $z = h_k$ and $z = h_{k-1}$ are entered in order to determine the extreme values of the strains and stresses at the top and bottom surfaces of the layer.
- Step 16** Calculate total (net) strains $(\epsilon_x, \epsilon_y, \gamma_s)_k$ in lamina k using Eq. (5.8).
- Step 17** Enter orientation θ_k of lamina k .
- Step 18** Transform total lamina strains $[\epsilon]_{x,y}^k$ to lamina coordinate axes (1,2).
- Step 19** Enter free lamina hygrothermal strains e_1 , e_2 referred to lamina axes (1,2) from step 3.
- Step 20** Calculate hygrothermal strains $[\epsilon_e]_{1,2}^k$ referred to lamina axes (1,2) using Eq. (6.60).
- Step 21** Enter lamina stiffnesses referred to lamina axes (1,2).
- Step 22** Calculate hygrothermal stresses $[\sigma_e]_{1,2}^k$ of lamina k referred to lamina axes (1,2) using Eq. (6.61).

The procedure above reduces to purely hygrothermal stress analysis when the mechanical loading $[N]$ and $[M]$ is zero and to purely mechanical stress analysis when the hygrothermal loading ΔT and Δc is zero.

References

1. G. S. Springer, Ed., *Environmental Effects on Composite Materials*, Technomic, Lancaster, PA, Vol. 1, 1981, Vol. 2, 1984.
2. I. M. Daniel, G. Yaniv, and G. Peimanidis, "Hygrothermal and Strain Rate Effects on Properties of Graphite/Epoxy Composites," *J. Eng. Materials Technol.*, Vol. 110, 1988, pp. 169–173.
3. O. Ishai and A. Mazor, "The Effect of Environmental Loading History on Longitudinal Strength of Glass-Fiber Reinforced Plastics," *Rheol. Acta*, Vol. 13, 1974, pp. 381–394.
4. O. Ishai and U. Arnon, "The Effect of Hygrothermal History on Residual Strength of Glass-Fiber Reinforced Plastic Laminates," *J. Testing Evaluation*, Vol. 5, No. 4, American Society for Testing and Materials, Philadelphia, 1977, pp. 320–326.
5. T. T. Matoi, J. A. Rohlen, and C. H. Hamilton, "Material Properties," Ch. 1.2 in *Advanced Composites Design Guide*, third edition, Vol. 1, Design, (prepared by the Los Angeles Division of the Rockwell International Corp.), Air Force Materials Laboratory, Wright-Patterson Air Force Base, OH, 1973.
6. O. Ishai and U. Arnon, "Instantaneous Effect of Internal Moisture Conditions on Strength of Glass-Fiber Reinforced Plastics," *Advanced Composite Materials—Environmental Effects*, ASTM STP 658, J. R. Vinson, Ed., American Society for Testing and Materials, Philadelphia, 1978, pp. 267–276.
7. R. A. Schapery, "Thermal Expansion Coefficients of Composite Materials Based on Energy Principles," *J. Composite Materials*, Vol. 2, 1968, pp. 380–404.
8. Z. Hashin, "Analysis of Properties of Fiber Composites with Anisotropic Constituents," *J. Appl. Mechanics*, Vol. 46, 1979, pp. 543–550.
9. I. M. Daniel, "Thermal Deformations and Stresses in Composite Materials," *Thermal Stresses in Severe Environments*, D. P. H. Hasselman and R. A. Heller, Eds., Plenum Press, New York, 1980, pp. 607–628.
10. C. C. Chamis, "Lamination Residual Stresses in Crossplied Fiber Composites," in *Proc. of 26th Annual Conf. of SPI, Reinforced Plastics/Composites Div.*, The Society of the Plastics Industry, New York, 1971, Sect. 17-D.
11. H. T. Hahn, "Residual Stresses in Polymer Matrix Composite Laminates," *J. Composite Materials*, Vol. 10, 1976, pp. 266–278.
12. I. G. Zewi, I. M. Daniel, and J. T. Gotro, "Residual Stresses and Warpage in Woven-Glass/Epoxy Laminates," *Exp. Mech.*, Vol. 27, 1987, pp. 44–50.
13. I. M. Daniel and T. Liber, "Lamination Residual Stresses in Fiber Composites," NASA CR-134826, NASA-Lewis Research Center, 1975.
14. I. M. Daniel and T. Liber, "Effect of Laminate Construction on Residual Stresses in Graphite/Polyimide Composites," *Exp. Mech.*, Vol. 17, 1977, pp. 21–25.
15. I. M. Daniel and T. Liber, "Lamination Residual Strains and Stresses in Hybrid Laminates," in: *Composite Materials: Testing and Design* (Fourth Conf.), ASTM STP 617, American Society for Testing and Materials, Philadelphia, 1977, pp. 331–343.

16. Y. Weitsman, "Residual Thermal Stresses Due to Cool-Down of Epoxy-Resin Composites," *J. Appl. Mech.*, Vol. 46, 1979, pp. 563-567.
17. Y. Weitsman and B. D. Harper, "Optimal Cooling of Crossply Composite Laminates and Adhesive Joints," *J. Appl. Mech.*, Vol. 49, 1982, pp. 735-739.
18. I. M. Daniel, T. M. Wang, D. Karalekas, and J. T. Gotro, "Determination of Chemical Cure Shrinkage in Composite Laminates," *J. Composite Technol. Res.*, Vol. 12, 1990, pp. 172-176.
19. T. M. Wang and I. M. Daniel, "Thermoviscoelastic Analysis of Residual Stresses and Warpage in Composite Laminates," *J. Composite Materials*, Vol. 26, 1992, pp. 883-899.
20. C. C. Chamis, "A Theory for Predicting Composite Laminate Warpage Resulting from Fabrication," in *Proc. 30th Tech. Conf., Reinforced Plastics/Composites Inst.*, Society of Plastics Industry, New York, 1975, Sect. 18-C.
21. M. W. Hyer, "Calculations of the Room-Temperature Shapes of Unsymmetric Laminates," *J. Composite Materials*, Vol. 15, 1981, pp. 296-309.
22. I. M. Daniel, T. M. Wang, and J. T. Gotro, "Thermomechanical Behavior of Multi-layer Structures in Microelectronics," *J. Electronic Packaging, Trans. ASME*, Vol. 112, 1990, pp. 11-15.

PROBLEMS

- 6.1 Determine the coefficients of thermal expansion α_1 and α_2 of a unidirectional glass/epoxy lamina of the following properties

$$E_f = 69 \text{ GPa (10 Msi)}$$

$$E_m = 3.80 \text{ GPa (0.55 Msi)}$$

$$\nu_f = 0.22$$

$$\nu_m = 0.36$$

$$\alpha_f = 4.5 \times 10^{-6}/^\circ\text{C} \quad (2.5 \times 10^{-6}/^\circ\text{F})$$

$$\alpha_m = 90 \times 10^{-6}/^\circ\text{C} \quad (50 \times 10^{-6}/^\circ\text{F})$$

$$V_f = 0.55$$

- 6.2 Determine the coefficients of thermal expansion α_1 and α_2 of a unidirectional silicon carbide/aluminum (SCS 2/6061 Al) lamina of the following properties

$$E_f = 410 \text{ GPa (60 Msi)}$$

$$E_m = 69 \text{ GPa (10 Msi)}$$

$$\nu_f = 0.20$$

$$\nu_m = 0.33$$

$$\alpha_f = 1.5 \times 10^{-6}/^\circ\text{C} \quad (0.83 \times 10^{-6}/^\circ\text{F})$$

$$\alpha_m = 23.4 \times 10^{-6}/^\circ\text{C} \quad (13 \times 10^{-6}/^\circ\text{F})$$

$$V_f = 0.44$$

- 6.3 Determine the coefficients of thermal expansion α_1 and α_2 of a unidirectional silicon carbide/glass ceramic composite (SiC/CAS) of the following properties

$$E_f = 170 \text{ GPa (25 Msi)}$$

$$E_m = 98 \text{ GPa (14.2 Msi)}$$

$$\nu_f = 0.20$$

$$\nu_m = 0.20$$

$$\alpha_m = 5.0 \times 10^{-6}/^\circ\text{C} \quad (2.8 \times 10^{-6}/^\circ\text{F})$$

$$\alpha_f = 3.2 \times 10^{-6}/^\circ\text{C} \quad (1.8 \times 10^{-6}/^\circ\text{F})$$

$$V_f = 0.39$$

- 6.4 The measured coefficients of thermal expansion of a unidirectional carbon/epoxy composite of fiber volume ratio $V_f = 0.65$ are

$$\alpha_1 = -0.9 \times 10^{-6}/^\circ\text{C} \quad (-0.5 \times 10^{-6}/^\circ\text{F})$$

$$\alpha_2 = 27 \times 10^{-6}/^\circ\text{C} \quad (15 \times 10^{-6}/^\circ\text{F})$$

Determine the coefficients α_{1f} and α_{2f} of the fiber from the above and the following constituent properties

$$E_{1f} = 235 \text{ GPa (34} \times 10^6 \text{ psi)}$$

$$E_m = 4.1 \text{ GPa (0.6} \times 10^6 \text{ psi)}$$

$$\nu_f = 0.20$$

$$\nu_m = 0.34$$

$$\alpha_m = 41 \times 10^{-6}/^\circ\text{C} \quad (23 \times 10^{-6}/^\circ\text{F})$$

- 6.5 Determine the thermal forces N_x^T , N_y^T , and N_s^T for a $[\pm 45]_s$ carbon/epoxy laminate (AS4/3501-6, Table 2.6) for a temperature difference $\Delta T = 56^\circ\text{C}$ (100°F) in terms of the lamina thickness t .
- 6.6 Determine the thermal forces N_x^T , N_y^T , and N_s^T for a $[\pm 30]_s$ carbon/epoxy laminate (AS4/3501-6, Table 2.6) for a temperature difference of $\Delta T = 56^\circ\text{C}$ (100°F) and lamina thickness $t = 0.127 \text{ mm}$ (0.005 in.).
- 6.7 Following a procedure similar to that described under Sample Problem 6.1, show that the coefficient of thermal expansion $\bar{\alpha}_x$ of a $[0/90]_s$ carbon/epoxy laminate is equal to $[E_2(1 + \nu_{12})\alpha_2]/E_1$, i.e., it is equal to that of the $[\pm 45]_s$ laminate.

- 6.8** Determine the coefficient of thermal expansion $\bar{\alpha}_x$ of a $[\pm 30]_s$ carbon/epoxy laminate (AS4/3501-6, Table 2.6).
- 6.9** Determine the coefficients of thermal expansion of a $[0/90]_s$ laminate as a function of the lamina engineering constants E_1 , E_2 , G_{12} , and ν_{12} and the lamina coefficients of thermal expansion α_1 and α_2 . Find a relationship among the lamina properties such that the CTE of the laminate is zero in all directions.
- 6.10** For a $[0_m/90_n]_s$ crossply laminate obtain a general relation between $r = m/n$ and the lamina properties such that the coefficient of thermal expansion $\bar{\alpha}_x$ along the 0° direction is zero. Determine a specific value of r for a carbon/epoxy material (AS4/3501-6, Table 2.6).
- 6.11** Calculate the coefficients of thermal expansion $\bar{\alpha}_x$ and $\bar{\alpha}_y$ of a $[0/\pm 45]_s$ S-glass/epoxy laminate with properties listed in Table 2.6.
- 6.12** Calculate the coefficients of thermal expansion $\bar{\alpha}_x$ and $\bar{\alpha}_y$ of a $[0/\pm 45]_s$ carbon/epoxy (AS4/3601-6, Table 2.6).
- 6.13** Independently of Sample Problem 6.2, show that the lamina stresses in a $[\pm 45]_s$ carbon/epoxy laminate subjected to a temperature change ΔT are

$$\sigma_{1e} \cong \alpha_2 E_2 \Delta T$$

$$\sigma_{2e} \cong -\alpha_2 E_2 \Delta T$$

assuming that $\alpha_1 \cong 0$ and $E_1 \gg E_2$.

- 6.14** A $[\pm 30]_s$ carbon/epoxy laminate was cured at 180°C (356°F) and cooled down to 23°C (73°F) and dry condition. Then, it was allowed to absorb moisture. Determine the moisture concentration Δc at which the net hygrothermal stresses will be zero for the following lamina properties: $\alpha_1 = \beta_1 \cong 0$; $\alpha_2 = 30 \times 10^{-6}/^\circ\text{C}$ ($16.7 \times 10^{-6}/^\circ\text{F}$), $\beta_2 = 0.55$.
- 6.15** A $[0/90]$ crossply antisymmetric carbon/epoxy laminate is cooled down during curing from 180°C (356°F) to 30°C (86°F) (Fig. 6.17). Compute the curvatures κ_x and κ_y for the following lamina properties:

$$E_1 = 140 \text{ GPa (20.3 Msi)}$$

$$E_2 = 10 \text{ GPa (1.45 Msi)}$$

$$G_{12} = 6 \text{ GPa (0.87 Msi)}$$

$$\nu_{12} = 0.34$$

$$\alpha_1 = \beta_1 \cong 0$$

$$\alpha_2 = 30 \times 10^{-6}/^\circ\text{C} \quad (16.7 \times 10^{-6}/^\circ\text{F})$$

$$\beta_2 = 0.55$$

$$t = 1 \text{ mm (0.040 in.) (layer thickness)}$$

6.16 Determine the maximum lamina stresses σ_{1e} and σ_{2e} for the laminate and conditions of Problem 6.15.

6.17 After cooldown, the dry laminate of Problem 6.15 was exposed to moisture absorption. Determine the moisture concentration at which the laminate will become flat ($\kappa_x = -\kappa_y = 0$).

6.18 A $[\pm 45]$ antisymmetric carbon/epoxy laminate was cooled down during curing from 150°C (302°F) to 50°C (122°F) and the following deformations were measured:

$$\varepsilon_x^o = \varepsilon_y^o = -7.54 \times 10^{-4}, \quad \gamma_s^o = 0$$

$$\kappa_x = \kappa_y = 0, \quad \kappa_s = 2.47 \text{ m}^{-1}$$

Compute the maximum lamina residual stresses σ_{1e} , σ_{2e} , and τ_{6e} for the following properties:

$$E_1 = 150 \text{ GPa (21.7 Msi)}$$

$$E_2 = 10 \text{ GPa (1.45 Msi)}$$

$$G_{12} = 6 \text{ GPa (0.87 Msi)}$$

$$\nu_{12} = 0.30$$

$$\alpha_1 = \beta_1 \cong 0$$

$$\alpha_2 = 30 \times 10^{-6}/^\circ\text{C} \quad (16.7 \times 10^{-6}/^\circ\text{F})$$

$$\beta_2 = 0.5$$

$$t = 1 \text{ mm (0.040 in.) (layer thickness)}$$

6.19 A $[\pm 30]_s$ laminate of the same material as in Problem 6.18 was cured at 180°C (356°F) and cooled down to 30°C (86°F) where it absorbed

0.5% moisture. Determine the hygrothermal lamina stresses σ_{1e} , σ_{2e} , and τ_{6e} for the following measured hygrothermal properties of the laminate:

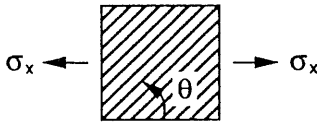
$$\bar{\alpha}_x = -3.45 \times 10^{-6}/^{\circ}\text{C} \quad (-1.92 \times 10^{-6}/^{\circ}\text{F})$$

$$\bar{\alpha}_y = 16.6 \times 10^{-6}/^{\circ}\text{C} \quad (9.22 \times 10^{-6}/^{\circ}\text{F})$$

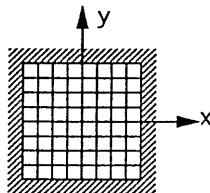
$$\bar{\beta}_x = -0.058$$

$$\bar{\beta}_y = 0.277$$

- 6.20** An off-axis lamina undergoes a temperature rise of ΔT . Determine the uniaxial normal stress σ_x (tensile or compressive) that must be applied in order to prevent shear distortion in the specimen. Find a general expression for σ_x in terms of material properties, ΔT and angle θ .



- 6.21** In Problem 6.20, determine the numerical value of σ_x for a carbon/epoxy lamina (AS4/3501-6, Table 2.6) with $\theta = 45^{\circ}$ and $\Delta T = 56^{\circ}\text{C}$ (100°F).
- 6.22** In Problem 6.20, determine the numerical value of σ_x for silicon carbide/aluminum composite (Table 2.6) with $\theta = 45^{\circ}$ and $\Delta T = 278^{\circ}\text{C}$ (500°F).
- 6.23** A $[0/90]_s$ laminate is clamped on all sides to a rigid frame and undergoes a temperature change ΔT . Determine the force N_x developed for a carbon/epoxy material (AS4/3501-6, Table 2.6) with lamina thickness $t = 0.127 \text{ mm}$ (0.005 in.) and $\Delta T = -56^{\circ}\text{C}$ (-100°F).



- 6.24** In Problem 6.23, determine the force N_x for a silicon carbide/aluminum composite (Table 2.6) with $t = 0.178 \text{ mm}$ (0.007 in.) and $\Delta T = -278^{\circ}\text{C}$ (-500°F).

Chapter 7

Stress and Failure Analysis of Multidirectional Laminates

7.1 Introduction

In the classical lamination theory discussed in Chapter 5, stress-strain or load-deformation relations were developed for multidirectional laminates. It was shown how the laminate deformation can be fully described in terms of the reference plane strains and the curvatures, from which the strains can be obtained at any through-the-thickness location of the laminate. It was pointed out that, whereas strains are continuous (linear) through the thickness, stresses can be discontinuous from layer to layer, depending on the material properties and orientation of the layers (laminae).

Failure analysis of a laminate is much more complex than that of a single lamina. The stresses in the individual laminae are fundamental and control failure initiation and progression in the laminate. Failure of a lamina does not necessarily imply total failure of the laminate, but is only the beginning of an interactive and progressive failure process. Laminate strength theories, like lamina strength theories, are macroscopic and are expressed in terms of the basic lamina strength parameters discussed in Chapter 4. The strength of each individual lamina is assessed separately by referring its stresses to its principal axes (1,2), which vary from lamina to lamina, and by applying a selected failure criterion.

The strength of a multidirectional laminate is a function of many factors, in addition to the fundamental lamina strengths. The varying lamina orientations, stiffnesses, strengths, and coefficients of thermal and moisture expansion affect the directional characteristics of laminate strength. The exact stacking sequence

affects the bending and coupling stiffnesses (D and B) and hence the stresses and strength of the laminate. Finally, the fabrication process affects the residual stresses, which influence the overall strength. Failure or strength analysis takes two forms: (1) analysis of an existing laminate and determination of ultimate loads or safety factors and (2) design of a laminate for a given loading condition.

7.2 Types of Failure

In the failure analysis of a laminate three different types (or definitions) of failure are discussed: (1) initial or first-ply failure (FPF), (2) ultimate laminate failure (ULF), and (3) interlaminar failure. In the first case, the laminate is considered failed when the first layer fails. In the second case the laminate is considered failed when the maximum load level is reached or exceeded, following multilayer failure. In the third case failure is a result of separation between contiguous layers even when the layers themselves remain intact.

The first two definitions above represent two levels in the failure process, the initial and the ultimate, which are analogous to the yield and ultimate stress criteria in elastoplastic materials. The FPF approach is conservative, but it can be used with low safety factors. The ULF approach is more advanced and requires more precise knowledge of loading conditions and stress distributions, and thus it is used with higher safety factors. A general practice in design of primary structures is to keep working loads below levels producing first-ply failure. For example, a general practice in the aircraft industry is to limit maximum strains in carbon/epoxy below 0.4%.

7.3 Stress Analysis and Safety Factors for First-Ply Failure of Symmetric Laminates (In-Plane Loading)

Given a symmetric laminate under general in-plane loading, the average laminate stresses are (Fig. 7.1)

$$\begin{bmatrix} \bar{\sigma}_x \\ \bar{\sigma}_y \\ \bar{\tau}_s \end{bmatrix} = \frac{1}{h} \begin{bmatrix} N_x \\ N_y \\ N_s \end{bmatrix} \quad (5.76 \text{ bis})$$

where h is the laminate thickness.

The laminate strains, which are uniform through the thickness, are equal to the reference plane strains and to the strains of any layer k and are related to the applied forces by the force-deformation relations in Eq. (5.74):

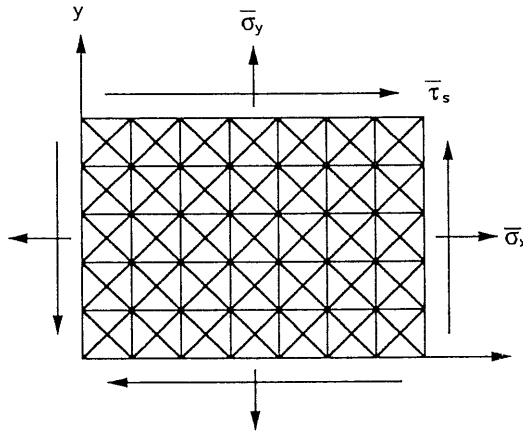


Fig. 7.1 Multidirectional laminate under general in-plane loading.

$$\begin{bmatrix} \bar{\epsilon}_x \\ \bar{\epsilon}_y \\ \bar{\gamma}_s \end{bmatrix} = \begin{bmatrix} \epsilon_x^o \\ \epsilon_y^o \\ \gamma_s^o \end{bmatrix} = \begin{bmatrix} \epsilon_x \\ \epsilon_y \\ \gamma_s \end{bmatrix}_k = \begin{bmatrix} a_{xx} & a_{xy} & a_{xs} \\ a_{yx} & a_{yy} & a_{ys} \\ a_{sx} & a_{sy} & a_{ss} \end{bmatrix} \begin{bmatrix} N_x \\ N_y \\ N_s \end{bmatrix} \quad (7.1)$$

The strains in layer k referred to its principal material axes are obtained by transformation as

$$\begin{bmatrix} \epsilon_1 \\ \epsilon_2 \\ \frac{1}{2}\gamma_6 \end{bmatrix}_k = \begin{bmatrix} m^2 & n^2 & 2mn \\ n^2 & m^2 & -2mn \\ -mn & mn & (m^2 - n^2) \end{bmatrix}_k \begin{bmatrix} \epsilon_x^o \\ \epsilon_y^o \\ \frac{1}{2}\gamma_s^o \end{bmatrix} \quad (7.2)$$

and the corresponding stresses are

$$\begin{bmatrix} \sigma_1 \\ \sigma_2 \\ \tau_6 \end{bmatrix}_k = \begin{bmatrix} Q_{11} & Q_{12} & 0 \\ Q_{21} & Q_{22} & 0 \\ 0 & 0 & Q_{66} \end{bmatrix} \begin{bmatrix} \epsilon_1 \\ \epsilon_2 \\ \gamma_6 \end{bmatrix}_k \quad (7.3)$$

For the FPF approach the selected failure criterion is applied to the state of stress in each layer separately. Thus, for a state of stress $(\sigma_1, \sigma_2, \tau_6)_k$ in layer k , the state of stress at failure of the same layer is $S_{fk}(\sigma_1, \sigma_2, \tau_6)_k$, where S_{fk} is the safety factor for layer k . Substitution of the critical (failure) state of stress in the Tsai-Wu failure criterion in Eq. (4.53) yields

$$f_1 S_{fk} \sigma_{1k} + f_2 S_{fk} \sigma_{2k} + f_{11} S_{fk}^2 \sigma_{1k}^2 + f_{22} S_{fk}^2 \sigma_{2k}^2 + f_{66} S_{fk}^2 \tau_{6k}^2 + 2f_{12} S_{fk}^2 \sigma_{1k} \sigma_{2k} = 1 \quad (7.4)$$

or

$$a S_{fk}^2 + b S_{fk} - 1 = 0 \quad (7.5)$$

where

$$a = f_{11} \sigma_{1k}^2 + f_{22} \sigma_{2k}^2 + f_{66} \tau_{6k}^2 + 2f_{12} \sigma_{1k} \sigma_{2k} \quad (7.6)$$

$$b = f_1 \sigma_{1k} + f_2 \sigma_{2k}$$

The solutions of the quadratic Eq. (7.4) or (7.5) are

$$S_{fk} = \frac{-b \pm \sqrt{b^2 + 4a}}{2a}$$

or

$$S_{fka} = \frac{-b + \sqrt{b^2 + 4a}}{2a} \quad (7.7)$$

and

$$S_{fkr} = \left| \frac{-b - \sqrt{b^2 + 4a}}{2a} \right| \quad (7.8)$$

where S_{fka} is the safety factor of layer k for the actual state of stress (σ_1 , σ_2 , τ_6) $_k$ and S_{fkr} is the safety factor of the same layer k for a state of stress with reversed sign, i.e., ($-\sigma_1$, $-\sigma_2$, $-\tau_6$) $_k$.

The procedure above is carried out repeatedly for all layers of the laminate to find the minimum values of S_{fka} and S_{fkr} . These minimum values are the safety factors of the laminate based on the FPF approach, for the actual and reversed loadings. Thus,

$$\bar{S}_{fa} = (S_{fka})_{\min} \quad (7.9)$$

$$\bar{S}_{fr} = (S_{fkr})_{\min}$$

For a given laminate, the layer that fails first depends on its state of stress. As the laminate loading state varies continuously, the strains (and stresses) in each layer also vary continuously, but FPF can jump from one layer to another in a discontinuous manner. Whereas the failure envelope for any given layer is a continuous surface, the failure envelope for the laminate based on FPF is discontinuous, consisting of portions of envelopes of individual layers.

7.4 Strength Components for First-Ply Failure of Symmetric Laminates

Given a multidirectional laminate, it is required, for example, to determine its axial strength along the x -axis based on FPF. The laminate in Figure 7.1 is assumed to be loaded under unit average stress in the x -direction, i.e.,

$$\bar{\sigma}_x = 1$$

$$\bar{\sigma}_y = 0$$

$$\bar{\tau}_s = 0$$

Then, the reference plane strains and layer k strains are obtained by Eqs. (5.74) and (7.1) as

$$\begin{bmatrix} \epsilon_x^o \\ \epsilon_y^o \\ \gamma_s^o \end{bmatrix} = \begin{bmatrix} \epsilon_x \\ \epsilon_y \\ \gamma_s \end{bmatrix}_k = \begin{bmatrix} a_{xx} & a_{xy} & a_{xs} \\ a_{yx} & a_{yy} & a_{ys} \\ a_{sx} & a_{sy} & a_{ss} \end{bmatrix} \begin{bmatrix} h \\ 0 \\ 0 \end{bmatrix}$$

or

$$\begin{bmatrix} \epsilon_x^o \\ \epsilon_y^o \\ \gamma_s^o \end{bmatrix} = \begin{bmatrix} \epsilon_x \\ \epsilon_y \\ \gamma_s \end{bmatrix}_k = \begin{bmatrix} a_{xx} \\ a_{yx} \\ a_{sx} \end{bmatrix} h \quad (7.10)$$

The strains in layer k along its principal material axes are obtained by transformation as in Eq. (7.2) and the corresponding stresses are obtained as in Eq. (7.3). The critical (failure) state of stress for layer k is $(S_{fk}, 0, 0)$ which substituted in the Tsai–Wu failure criterion Eq. (7.4) gives two safety factors S_{fka} corresponding to $\bar{\sigma}_x = 1$, and S_{fkr} corresponding to $\bar{\sigma}_x = -1$.

The axial tensile and compressive strengths of the laminate are obtained as

$$\begin{aligned}\bar{F}_{xt} &= (S_{fka})_{\min} \\ \bar{F}_{xc} &= (S_{fkr})_{\min}\end{aligned}\tag{7.11}$$

The axial strengths along the y -axis are obtained in a similar manner by assuming the following state of stress in the laminate:

$$\begin{aligned}\bar{\sigma}_x &= 0 \\ \bar{\sigma}_y &= 1 \\ \bar{\tau}_s &= 0\end{aligned}$$

The in-plane shear strength is obtained by assuming the following state of stress:

$$\begin{aligned}\bar{\sigma}_x &= 0 \\ \bar{\sigma}_y &= 0 \\ \bar{\tau}_s &= 1\end{aligned}$$

In the case of quasi-isotropic laminates discussed before (Sect. 5.10), the elastic properties are, by definition, independent of orientation. Thus a uniaxial loading $\bar{\sigma}_x$ produces the same strains ϵ_x and ϵ_y in each layer regardless of the load direction x . Depending on the orientation of the principal layer directions with respect to the loading direction, a different state of stress exists in each layer. Thus failure in each layer and the occurrence of first failure in any layer (FPF) depend on load orientation. This means that quasi-isotropic laminates are not isotropic as far as FPF is concerned. For example, the $[0/\pm 60]_s$ quasi-isotropic laminate would be strongest along a fiber direction (0° , 60° , or -60°) and weakest along a bisector between fiber directions of different plies (30° , -30° , or 90°).

Sample Problem 7.1

Uniaxial Strength of Angle-Ply Laminate

It is required to determine the axial tensile strength \bar{F}_{xt} of a $[\pm 45]_{ns}$ laminate using the Tsai–Hill criterion for FPF. Consider the laminate in Figure 7.2 subjected to a uniaxial stress

$$\bar{\sigma}_x = \frac{N_x}{h}, \quad \bar{\sigma}_y = \bar{\tau}_s = 0.$$

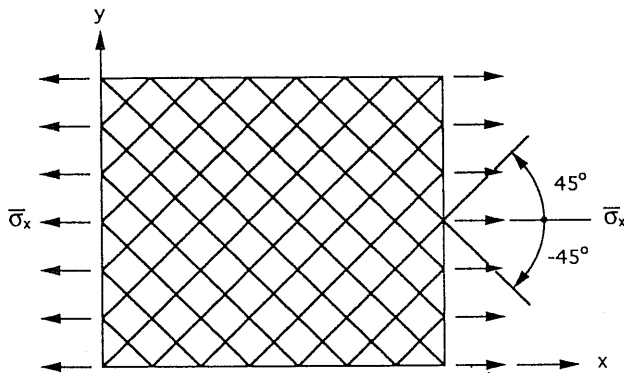


Fig. 7.2 $[\pm 45]_s$ angle-ply laminate under uniaxial loading.

The strains, which are uniform through the thickness, can be related to the applied stress and the laminate engineering properties as

$$\begin{aligned}\epsilon_x^o &= \frac{\bar{\sigma}_x}{\bar{E}_x} \\ \epsilon_y^o &= -\bar{\nu}_{xy} \frac{\bar{\sigma}_x}{\bar{E}_x} \\ \gamma_s^o &= 0\end{aligned}\quad (7.12)$$

The strains in the -45° lamina referred to its principal material axes are obtained from the strain transformation relations in Eq. (3.58) as

$$\begin{aligned}\epsilon_1 &= \epsilon_2 = \frac{1}{2} (\epsilon_x^o + \epsilon_y^o) \\ \gamma_6 &= \epsilon_x^o - \epsilon_y^o\end{aligned}$$

and in view of Eq (7.12)

$$\begin{aligned}\epsilon_1 &= \epsilon_2 = \frac{\bar{\sigma}_x}{2\bar{E}_x} (1 - \bar{\nu}_{xy}) \\ \gamma_6 &= \frac{\bar{\sigma}_x}{\bar{E}_x} (1 + \bar{\nu}_{xy})\end{aligned}\quad (7.13)$$

Referring to relations in Eqs. (5.86) and (5.93) derived for Sample Problems 5.3 and 5.5, we obtain further

$$\epsilon_1 = \epsilon_2 = \frac{\bar{\sigma}_x}{Q_{11} + Q_{22} + 2Q_{12}} \quad (7.14)$$

$$\gamma_6 = \frac{\bar{\sigma}_x}{2Q_{66}}$$

The lamina stresses, obtained from Eq. (3.31), are

$$\begin{aligned} \sigma_1 &= \epsilon_1 (Q_{11} + Q_{12}) = \bar{\sigma}_x \frac{Q_{11} + Q_{12}}{Q_{11} + Q_{22} + 2Q_{12}} \\ \sigma_2 &= \epsilon_1 (Q_{12} + Q_{22}) = \bar{\sigma}_x \frac{Q_{12} + Q_{22}}{Q_{11} + Q_{22} + 2Q_{12}} \\ \tau_6 &= \gamma_6 Q_{66} = \frac{\bar{\sigma}_x}{2} \end{aligned} \quad (7.15)$$

The above stress components can be introduced into the Tsai–Hill criterion to yield an exact value for $\bar{\sigma}_x$ at failure, i.e., \bar{F}_x . An approximate value for the strength can be obtained more easily for the case of a high stiffness composite, i.e., when $E_1 \gg E_2$. Then the lamina stress components in Eq. (7.15) can be approximated as

$$\begin{aligned} \sigma_1 &\cong \bar{\sigma}_x \\ \sigma_2 &\cong (1 + \nu_{12}) \frac{E_2}{E_1} \bar{\sigma}_x \\ \tau_6 &= \frac{\bar{\sigma}_x}{2} \end{aligned} \quad (7.16)$$

Hence $\sigma_2 \ll \sigma_1$ and $\sigma_2 < \tau_6$.

Substituting the above into the Tsai–Hill criterion,

$$\left(\frac{\sigma_1^u}{F_1}\right)^2 + \left(\frac{\sigma_2^u}{F_2}\right)^2 + \left(\frac{\tau_6^u}{F_6}\right)^2 - \frac{\sigma_1^u \sigma_2^u}{F_1^2} = 1$$

we obtain for $\bar{\sigma}_x^u = \bar{F}_{xt}$

$$\bar{F}_{xt}^2 \left[\frac{1}{F_1^2} + \frac{(1 + \nu_{12})^2}{F_2^2} \left(\frac{E_2}{E_1}\right)^2 + \frac{1}{4F_6^2} - \frac{(1 + \nu_{12})}{F_1^2} \left(\frac{E_2}{E_1}\right) \right] \cong 1 \quad (7.17)$$

For a high strength composite with $F_1 \gg F_2$ and $F_1 \gg F_6$, the relation above is further approximated as

$$\bar{F}_{xt}^2 \left[\frac{(1 + \nu_{12})^2}{F_2^2} \left(\frac{E_2}{E_1} \right)^2 + \frac{1}{4 F_6^2} \right] \cong 1 \quad (7.18)$$

or, because $E_2 \ll E_1$,

$$\bar{F}_{xt} \cong 2F_6 \quad (7.19)$$

Thus the uniaxial strength of a $[\pm 45]_{ns}$ angle-ply laminate, for a high stiffness-high strength composite, is controlled primarily by the in-plane shear strength of the unidirectional lamina; hence it is a *matrix-dominated* property. A similar approximation and conclusion holds true for the axial compressive strength \bar{F}_{xc} . Similar results are obtained by using other failure theories.

Sample Problem 7.2

In-Plane Shear Strength of Angle-Ply Laminate

It is required to determine the in-plane shear strength \bar{F}_s of a $[\pm 45]_{ns}$ laminate using the Tsai-Hill criterion for FPF. Consider the laminate in Figure 7.2 under in-plane shear loading

$$\bar{\tau}_s = \frac{N_s}{h}, \quad \bar{\sigma}_x = \bar{\sigma}_y = 0$$

The strains, which are uniform through the thickness, are

$$\epsilon_x^o = \epsilon_y^o = 0 \quad (7.20)$$

$$\gamma_s^o = \frac{\bar{\tau}_s}{G_{xy}}$$

The strains in the $+45^\circ$ ply, obtained by transformation, are

$$\begin{aligned} \epsilon_1 &= mn \gamma_s^o = \frac{\bar{\tau}_s}{2 G_{xy}} \\ \epsilon_2 &= -mn \gamma_s^o = -\frac{\bar{\tau}_s}{2 G_{xy}} \\ \gamma_6 &= 0 \end{aligned} \quad (7.21)$$

and the corresponding stresses are

$$\begin{aligned}\sigma_1 &= \epsilon_1 Q_{11} + \epsilon_2 Q_{12} = (Q_{11} - Q_{12}) \frac{\bar{\tau}_s}{2 G_{xy}} \\ \sigma_2 &= \epsilon_1 Q_{12} + \epsilon_2 Q_{22} = (Q_{12} - Q_{22}) \frac{\bar{\tau}_s}{2 G_{xy}} \\ \tau_6 &= 0\end{aligned}\quad (7.22)$$

or, using the relation in Eq. (5.91) in Sample Problem 5.4, we obtain

$$\begin{aligned}\sigma_1 &= \frac{2(Q_{11} - Q_{12}) \bar{\tau}_s}{Q_{11} + Q_{22} - 2Q_{12}} \\ \sigma_2 &= \frac{2(Q_{12} - Q_{22}) \bar{\tau}_s}{Q_{11} + Q_{22} - 2Q_{12}} \\ \tau_6 &= 0\end{aligned}\quad (7.23)$$

For a high stiffness composite, with $E_1 \gg E_2$, the above stresses can be approximated as

$$\begin{aligned}\sigma_1 &\cong 2\bar{\tau}_s \\ \sigma_2 &\cong -2(1 - \nu_{12}) \frac{E_2}{E_1} \bar{\tau}_s \\ \tau_6 &= 0\end{aligned}\quad (7.24)$$

Thus the $+45^\circ$ ply is under longitudinal tension and transverse compression. The stresses in the -45° ply are of the same magnitude but opposite sign as those of Eq. (7.24). This means that the -45° ply is under longitudinal compression and transverse tension for the same positive shear loading. Since transverse tension is the most severe loading for a typical unidirectional lamina, FPF will occur in the -45° ply.

Substituting the -45° ply stresses in the Tsai–Hill criterion with appropriate consideration for tensile and compressive strengths, we obtain for the ultimate value $\bar{\tau}_s^u = \bar{F}_s$

$$\left(\frac{\sigma_1^u}{F_{1c}^u}\right)^2 + \left(\frac{\sigma_2^u}{F_{2t}^u}\right)^2 - \frac{\sigma_1^u \sigma_2^u}{F_{1c}^u{}^2} = 1$$

or

$$\frac{4\bar{F}_s^2}{F_{1c}^u{}^2} \left[1 + (1 - \nu_{12})^2 \left(\frac{E_2}{E_1}\right)^2 \left(\frac{F_{1c}^u}{F_{2t}^u}\right)^2 + (1 - \nu_{12}) \left(\frac{E_2}{E_1}\right) \right] \cong 1$$

or, because $E_1 \gg E_2$ and assuming $F_{1c} \gg F_{2r}$,

$$\frac{4 \bar{F}_s^2}{F_{1c}^2} \left[1 + (1 - \nu_{12})^2 \left(\frac{E_2}{E_1} \right)^2 \left(\frac{F_{1c}}{F_{2t}} \right)^2 \right] \cong 1$$

from which we obtain

$$\bar{F}_s \cong \frac{F_{1c}}{2} \left[1 + (1 - \nu_{12})^2 \left(\frac{E_2}{E_1} \right)^2 \left(\frac{F_{1c}}{F_{2t}} \right)^2 \right]^{-1/2} \quad (7.25)$$

For a typical carbon/epoxy composite the quantity inside the brackets above is of the order of 3, which means that the shear strength \bar{F}_s is roughly $F_{1c}/2\sqrt{3}$, or approximately 30% of the longitudinal compressive strength of the lamina. It may be concluded that, under shear loading, this angle-ply laminate is utilized more efficiently since at FPF, which is a transverse failure, the longitudinal stress in the ply reaches approximately 60% of its ultimate value ($\sigma_1 \cong 2 \bar{F}_s$). Thus shear strength of a $[\pm 45]_s$ laminate for a high stiffness-high strength composite is primarily a fiber dominated property.

7.5 Computational Procedure for Stress and Failure Analysis of General Multidirectional Laminates (First-Ply Failure)

A flow chart for computation of safety factors and strength components of a general multidirectional laminate is shown in Figure 7.3. It is based on the Tsai-Wu failure criterion and on the FPF approach. The procedure for determination of safety factors consists of the following steps:

- Step 1** Enter basic lamina properties ($E_1, E_2, G_{12}, \nu_{12}$).
- Step 2** Compute ply stiffnesses $[Q]_{1,2}$ referred to its principal material axes, using relations in Eq. (3.56).
- Step 3** Enter orientation of principal material axis, θ_k , of layer k .
- Step 4** Calculate transformed layer stiffnesses $[Q]_{x,y}^k$ of layer k referred to the laminate coordinate system (x,y) , using Eq. (3.67).
- Step 5** Enter through-the-thickness coordinates h_k and h_{k-1} of layer k surfaces.
- Step 6** Calculate laminate stiffness matrices $[A]$, $[B]$, and $[D]$ using Eq. (5.20).
- Step 7** Calculate laminate compliance matrices $[a]$, $[b]$, $[c]$, and $[d]$ using Eq. (5.27).

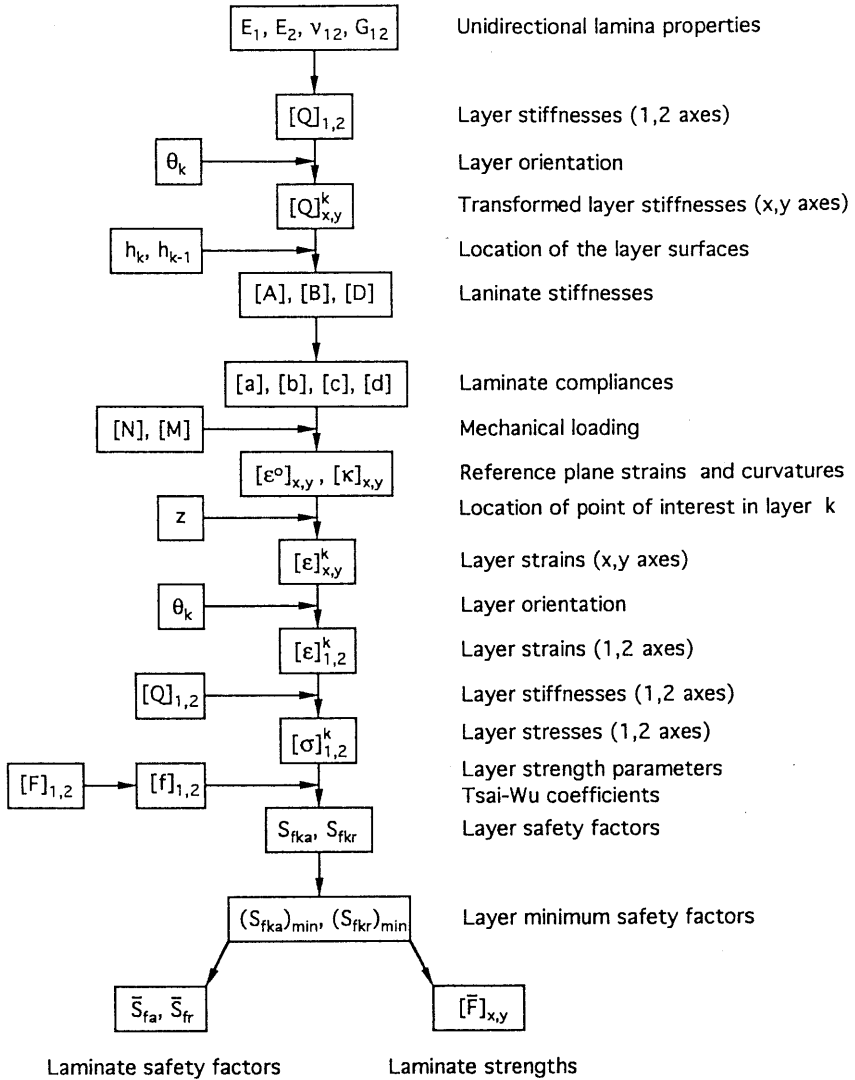


Fig. 7.3 Flow chart for stress and failure analysis of multidirectional laminates (FPF; Tsai-Wu criterion).

- Step 8** Enter mechanical loading, i.e., forces $[N]_{x,y}$ and moments $[M]_{x,y}$.
- Step 9** Calculate reference plane strains, $[\epsilon^o]_{x,y}$ and curvatures $[\kappa]_{x,y}$, using Eq. (5.25).
- Step 10** Enter through-the-thickness coordinate, z , of point of interest in layer k . For a laminate consisting of many thin (compared with the laminate thickness) layers or for any symmetric laminate under in-plane load-

ing, the coordinate of the lamina midplane, $z = z_k$, is used. Then the computed strains and stresses are the average through-the-thickness strains and stresses in the layer. However, when the laminate consists of few and thick (relative to the laminate thickness) layers and is asymmetric or subjected to bending and twisting, $z = h_k$ and $z = h_{k-1}$ are entered in order to determine the extreme values of the strains and stresses at the top and bottom surfaces of the layer.

- Step 11** Calculate layer strains $[\epsilon]_{x,y}^k$ referred to laminate reference axes (x,y) , using Eq. (5.8).
- Step 12** Calculate layer strains $[\epsilon]_{1,2}^k$ referred to layer principal axes $(1,2)$, using Eq. (3.58).
- Step 13** Calculate layer stresses $[\sigma]_{1,2}^k$, referred to the layer principal axes $(1,2)$, using Eq. (3.31).
- Step 14** Enter lamina strengths $[F]_{1,2}$ and calculate Tsai–Wu coefficients f_i, f_{ij} , using Eqs. (4.42) through (4.46) and (4.52).
- Step 15** Calculate layer safety factors, S_{fka}, S_{fkr} , using Eqs. (7.6) through (7.8).
- Step 16a** Determine laminate safety factors, $\bar{S}_{fa}, \bar{S}_{fr}$, using Eq. (7.9).
- Step 16b** Determine laminate strength components, $[\bar{F}]_{x,y}$, by applying unit stress in the respective direction of each component and Eq. (7.11).

7.6 Comparison of Strengths of Unidirectional and Angle-Ply Laminates (First-Ply Failure)

The effect of fiber orientation on the strength of unidirectional and angle-ply laminates is illustrated in Figures 7.4 to 7.6 for a typical carbon/epoxy composite (AS4/3501-6). Figure 7.4 shows that the uniaxial tensile strength of the angle-ply laminate is much higher than that of the off-axis unidirectional material for fiber orientations between 5° and 20° . The maximum ratio between the two strengths occurs for a fiber orientation between 10° and 15° . Figure 7.5 shows the variation of uniaxial compressive strength. The differences between the unidirectional and angle-ply laminates are less pronounced than in the case of tensile strength.

Figure 7.6 shows the variation of in-plane shear strength for unidirectional and angle-ply laminates. In the case of the unidirectional lamina there is a large difference between positive and negative shear strength for reasons discussed before (see Section 4.2). The shear strength of the angle-ply laminate is the same for both positive and negative shear loading and is much higher than either positive or negative shear strength of the unidirectional lamina.

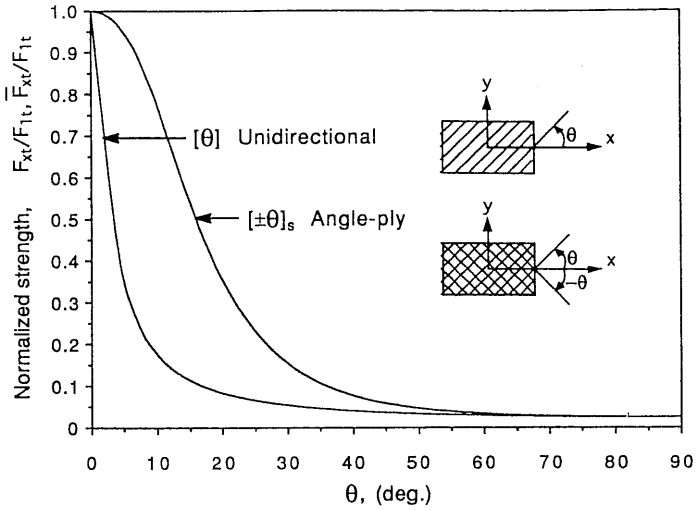


Fig. 7.4 Uniaxial tensile strength of unidirectional and angle-ply laminates as a function of fiber orientation (AS4/3501-6 carbon/epoxy; Tsai-Wu criterion).

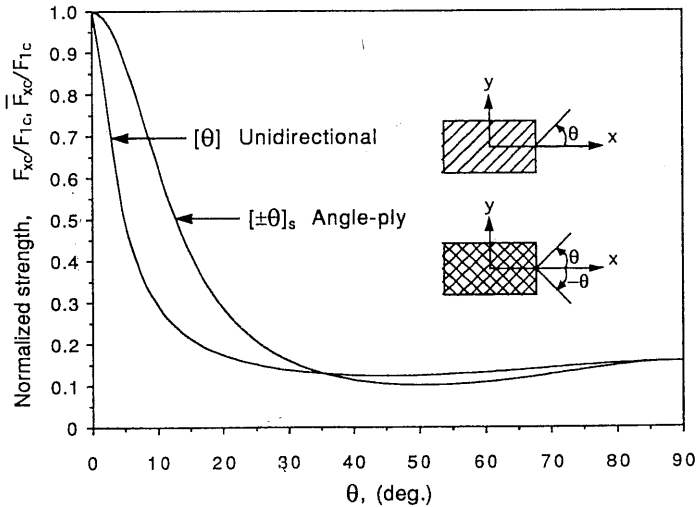


Fig. 7.5 Uniaxial compressive strength of unidirectional and angle-ply laminates as a function of fiber orientation (AS4/3501-6 carbon/epoxy; Tsai-Wu criterion).

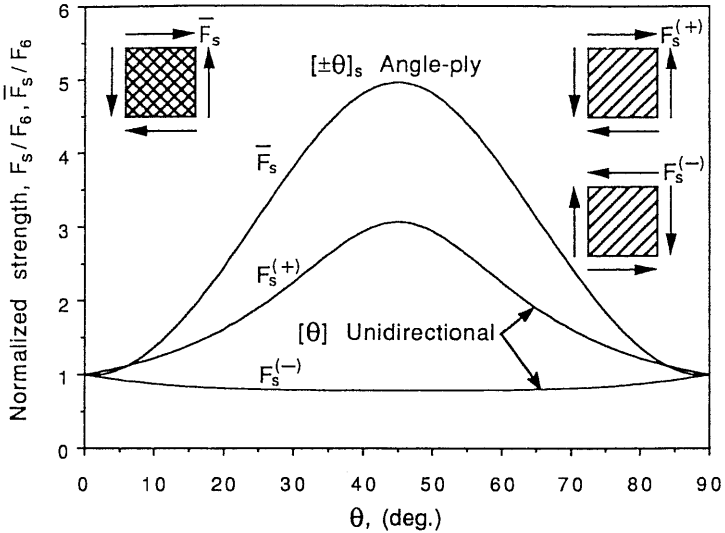


Fig. 7.6 In-plane shear strength of unidirectional and angle-ply laminates as a function of fiber orientation (AS4/3501-6 carbon/epoxy; Tsai-Wu criterion).

7.7 Carpet Plots for Strength of Multidirectional Laminates (First-Ply Failure)

As in the case of elastic properties (Section 5.15) carpet plots can be prepared for strength properties of general multidirectional laminates. A general laminate of $[0_m/90_n/(\pm 45)_p]_s$ lay-up can be described in terms of the fractions α , β , and γ of the 0° , 90° and $(\pm 45^\circ)$ plies, defined as before

$$\alpha = \frac{2m}{N}$$

$$\beta = \frac{2n}{N} \tag{5.105 bis}$$

$$\gamma = \frac{4p}{N}$$

$$N = 2(m+n+2p) = \text{total number of plies}$$

Carpet plots for the uniaxial strength and in-plane shear strength are shown in Figures 7.7 and 7.8 for carbon/epoxy (AS4/3501-6). The gaps and discontinuities in the plot of Figure 7.7 are due to the nature of the FPF approach which causes finite jumps in the calculated strength near the $\beta = 0$ and $\gamma = 0$ values for infinitesimally small increments in β or γ .

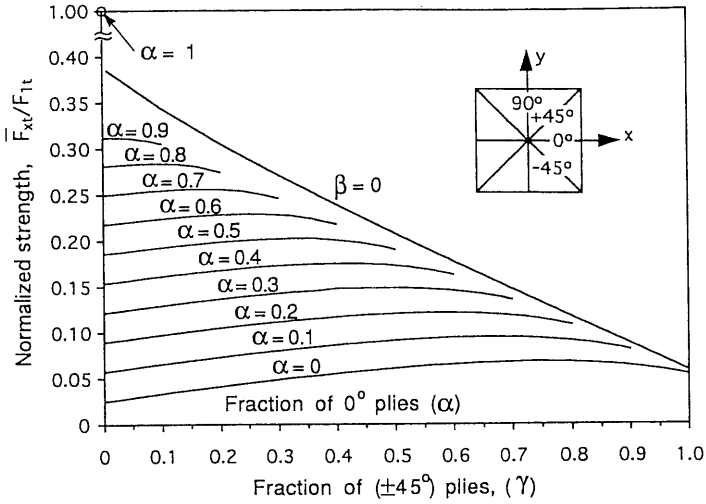


Fig. 7.7 Carpet plot for uniaxial tensile strength of $[0_m/90_n/(\pm 45)_p]_s$ laminates (AS4/3501-6, carbon/epoxy) (α , β , and γ are fractions of 0° , 90° , and $\pm 45^\circ$ plies, respectively).

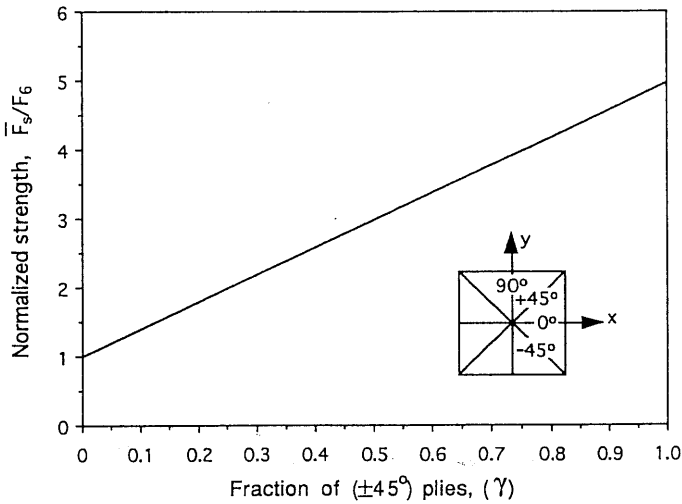


Fig. 7.8 Carpet plot for in-plane shear strength of $[0_m/90_n/(\pm 45)_p]_s$ laminates (AS4/3501-6, carbon/epoxy) (α , β , and γ are fractions of 0° , 90° , and $\pm 45^\circ$ plies, respectively).

7.8 Effect of Hygrothermal History on Strength of Multidirectional Laminates (First-Ply Failure; Tsai–Wu Criterion)

For a given laminate lay-up, under mechanical loading, $[N]$ and $[M]$, and hygrothermal loading ΔT and Δc , application of the failure criterion can yield the following results: (1) safety factor under given loading, (2) laminate strength components, and (3) allowable laminate thickness (of the same basic lay-up) for a given allowable safety factor. The critical stresses at failure of layer k , $(\sigma_{if})_k$, are obtained by multiplying the stresses induced by mechanical loading (σ_i) by the safety factor S_{fk} and combining them with the hygrothermal stresses (σ_{ie}) , where $i = 1, 2, 6$, i.e.,

$$(\sigma_{if})_k = S_{fk} (\sigma_i)_k + (\sigma_{ie})_k \quad (i = 1, 2, 6)$$

Substitution of this state of stress in the Tsai–Wu failure criterion (Eq. 4.53) yields

$$\begin{aligned} & f_1 (S_f \sigma_1 + \sigma_{1e})_k + f_2 (S_f \sigma_2 + \sigma_{2e})_k \\ & + f_{11} (S_f \sigma_1 + \sigma_{1e})_k^2 + f_{22} (S_f \sigma_2 + \sigma_{2e})_k^2 \\ & + f_{66} (S_f \tau_6 + \tau_{6e})_k^2 \\ & + 2f_{12} (S_f \sigma_1 + \sigma_{1e})_k (S_f \sigma_2 + \sigma_{2e})_k - 1 = 0 \end{aligned}$$

or

$$a S_{fk}^2 + b S_{fk} + c = 0 \quad (7.26)$$

where

$$\begin{aligned} a &= f_{11} (\sigma_1^2)_k + f_{22} (\sigma_2^2)_k + f_{66} (\tau_6^2)_k + 2f_{12} (\sigma_1 \sigma_2)_k \\ b &= f_1 (\sigma_1)_k + f_2 (\sigma_2)_k + 2f_{11} (\sigma_1 \sigma_{1e})_k + 2f_{22} (\sigma_2 \sigma_{2e})_k \\ & + 2f_{66} (\tau_6 \tau_{6e})_k + 2f_{12} (\sigma_1 \sigma_{2e} + \sigma_2 \sigma_{1e})_k \\ c &= f_1 (\sigma_{1e})_k + f_2 (\sigma_{2e})_k + f_{11} (\sigma_{1e}^2)_k + f_{22} (\sigma_{2e}^2)_k \\ & + f_{66} (\tau_{6e}^2)_k + 2f_{12} (\sigma_{1e} \sigma_{2e})_k - 1 \end{aligned}$$

The solutions of the quadratic Eq. (7.26) yield the safety factors for the actual and reversed mechanical loading, S_{fka} and S_{fkr} , as

$$S_{fka} = \frac{-b + \sqrt{b^2 - 4ac}}{2a} \quad (7.27)$$

$$S_{fkr} = \left| \frac{-b - \sqrt{b^2 - 4ac}}{2a} \right| \quad (7.28)$$

The minimum values of these factors are the laminate safety factors as given in Eq. (7.9).

The procedure for determining the strength components of the laminate in the presence of hygrothermal stresses is the same as that discussed in Section 7.4. The laminate is assumed loaded by a unit average mechanical stress in the direction of the desired strength component. The laminate safety factors obtained for this unit stress loading combined with the hygrothermal loading yield the desired strength components as given in Eq. (7.11).

In design applications the objective is to determine a specific laminate configuration, number, and orientation of plies for the given mechanical and hygrothermal loading and a given allowable safety factor. The complete design optimization involves many degrees of freedom, both number and orientation of plies. However, if a basic laminate lay-up is selected, the design objective is reduced to finding the allowable thickness of the laminate, consisting of a multiple of the basic lay-up. The approach in that case is to assume a unit laminate thickness $h = 1$. Then the average mechanical stresses applied to the laminate are

$$\begin{bmatrix} \bar{\sigma}_x \\ \bar{\sigma}_y \\ \bar{\tau}_s \end{bmatrix} = \begin{bmatrix} N_x \\ N_y \\ N_s \end{bmatrix} \quad (7.29)$$

The above mechanical loading combined with the given hygrothermal loading gives the state of stress in each lamina k , $(\sigma_i + \sigma_{ie})_k$ for $h = 1$. Failure of the lamina occurs when the mechanical loads or stresses are multiplied by the safety factor, S_{fk} . Following the identical procedure described before, we determine the minimum safety factor, which is the laminate safety factor, \bar{S}_f (\bar{S}_{fa} or \bar{S}_{fr}). Then, the allowable laminate thickness is obtained as

$$h_a = \frac{S_{all}}{\bar{S}_f} \quad (7.30)$$

where

Table 7.1 Failure Analysis of Multidirectional Laminates under Combined Mechanical and Hygrothermal Loading (First-Ply Failure)

Input	Output	Remarks
Average laminate stresses: $\bar{\sigma}_x, \bar{\sigma}_y, \bar{\tau}_s$	Laminate safety factor: $\bar{S}_f = (S_{fk})_{\min}$	Inputs: $N_i, M_i, \Delta T, \Delta c$
Unit laminate stress in given direction: $\bar{\sigma}_i = 1$	Laminate strength components: $\bar{F}_{it} = (S_{fkt})_{\min}$ $\bar{F}_{ic} = (S_{fkc})_{\min}$	Inputs: $N_i = h$ $M_i = 0$ $\Delta T, \Delta c$
Average laminate stresses for unit thickness: $\bar{\sigma}_i = N_i$	Allowable laminate thickness:	Inputs: $N_i, \Delta T, \Delta c$
Allowable safety factor: S_{all}	$h_a = \frac{S_{all}}{(S_{fk})_{\min}}$	Limited to symmetric laminates under in-plane loading: ($M = 0, B_{ij} = 0$)

(i = x, y, s).

 h_a = Allowable laminate thickness S_{all} = Allowable safety factor

This approach is limited to symmetric laminates ($[B] = 0$) under in-plane loading only ($[M] = 0$).

The results of the analysis discussed here, i.e., safety factors, laminate strengths, and laminate sizing are summarized in Table 7.1.

7.9 Computational Procedure for Stress and Failure Analysis of Multidirectional Laminates under Combined Mechanical and Hygrothermal Loading (First-Ply Failure; Tsai–Wu Criterion)

A flow chart for stress and failure analysis under general combined mechanical and hygrothermal loading is shown in Figure 7.9. For the most part the procedure is the same as that described in Section 7.5 for mechanical loading only. The first seven steps in the flow chart of Figure 7.3 are omitted here, and the result, laminate compliances, is used as an input. The procedure illustrated in Figure 7.9 consists of the following steps:

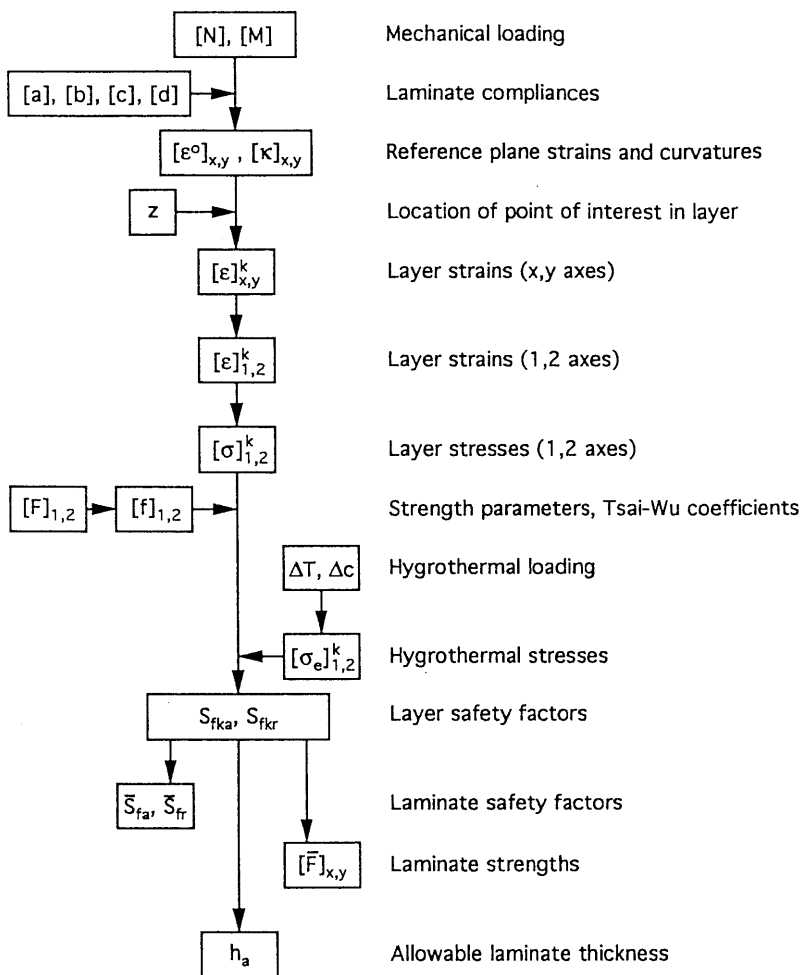


Fig. 7.9 Flow chart for stress and failure analysis of general multidirectional laminates under combined mechanical and hygrothermal loading (FPF; Tsai–Wu criterion).

- Step 1** Enter mechanical loading, i.e., forces $[N]_{x,y}$ and moments $[M]_{x,y}$.
- Step 2** Enter laminate compliances $[a]$, $[b]$, $[c]$, and $[d]$ (from step 7 of Fig. 7.3).
- Step 3** Calculate reference plane strains, $[\epsilon^0]_{x,y}$, and curvatures, $[\kappa]_{x,y}$, using Eq. (5.25).
- Step 4** Enter through-the-thickness coordinate, z , of point of interest in layer k . For a laminate consisting of many thin (compared with the laminate thickness) layers or for any symmetric laminate under in-plane loading, the coordinate of the lamina midplane, $z = z_k$, is used. Then, the

computed strains and stresses are the average through-the-thickness strains and stresses in the layer. However, when the laminate consists of few and thick (relative to the laminate thickness) layers and is asymmetric or subjected to bending and twisting, $z = h_k$ and $z = h_{k-1}$ are entered in order to determine the extreme values of the strains and stresses at the top and bottom surfaces of the layer.

- Step 5** Calculate layer strains referred to laminate axes (x,y) , using Eq. (5.8).
- Step 6** Transform layer strains to layer principal axes, $[\epsilon]_{1,2}^k$ using Eq. (3.58).
- Step 7** Calculate layer stresses $[\sigma]_{1,2}^k$, referred to layer principal axes (1,2), using Eq. (3.31).
- Step 8** Enter lamina strengths $[F]_{1,2}$ and calculate Tsai–Wu coefficients f_i , f_{ij} , using relations in Eqs. (4.42) through (4.46) and (4.52).
- Step 9** Enter hygrothermal loading, ΔT , Δc .
- Step 10** Calculate hygrothermal stresses following the procedure outlined in the flow chart in Figure 6.19.
- Step 11** Introduce combined mechanical and hygrothermal stresses in Tsai–Wu failure criterion and determine layer safety factors, using Eqs. (7.26) through (7.28).
- Step 12a** Determine laminate safety factors, \bar{S}_{fu} , \bar{S}_{fv} , using Eq. (7.9).
- Step 12b** Determine laminate strength components, $[\bar{F}]_{x,y}$, using unit in-plane loading in the respective direction of each component and Eq. (7.11).
- Step 12c** Determine allowable laminate thickness for selected basic layup using Eq. (7.30) for symmetric laminates under in-plane loading ($[B] = 0$, $[M] = 0$).

7.10 Micromechanics of Progressive Failure: Stiffness Reduction

In most cases failure in a multidirectional laminate is initiated in the layer (or layers) with the highest stress normal to the fibers. Failure initiation takes the form of distributed microcracks, which coalesce into macrocracks as illustrated in the case of a unidirectional lamina under transverse tension (see Fig. 4.17). This macrocracking extending across the thickness of the layer constitutes FPF as discussed before.

The failure process is best illustrated for the case of a crossply laminate under uniaxial tension (Fig. 7.10). The axial stress in the 90° layer is uniform initially and, when it reaches a critical value, it produces random microcracks as shown. The microcracks coalesce into roughly evenly spaced macrocracks, resulting in a redistribution of the average axial stress in the 90° ply with zero value at the crack faces and maximum value at the center between cracks. As the applied stress $\bar{\sigma}_x$ is increased, the maximum axial stress in the 90° ply

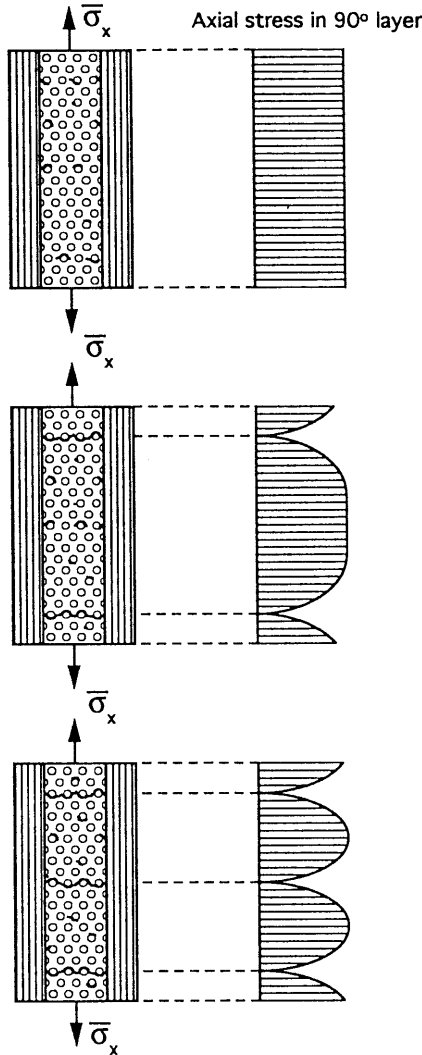


Fig. 7.10 Progressive failure and stress distributions in transverse ply of crossply laminate under uniaxial tension.

increases up to a value equal to the transverse tensile strength of the lamina, F_{2t} , and further macrocracking takes place, resulting in further stress redistribution. This process continues up to a minimum crack spacing, at which point any further increase in applied stress cannot increase the axial stress in the 90° layer to the failure level F_{2t} . This state is called the characteristic damage state (CDS) of the laminate.¹ In most cases the minimum crack spacing is of the order of the layer thickness. The progression of cracking in the 90° layer of a

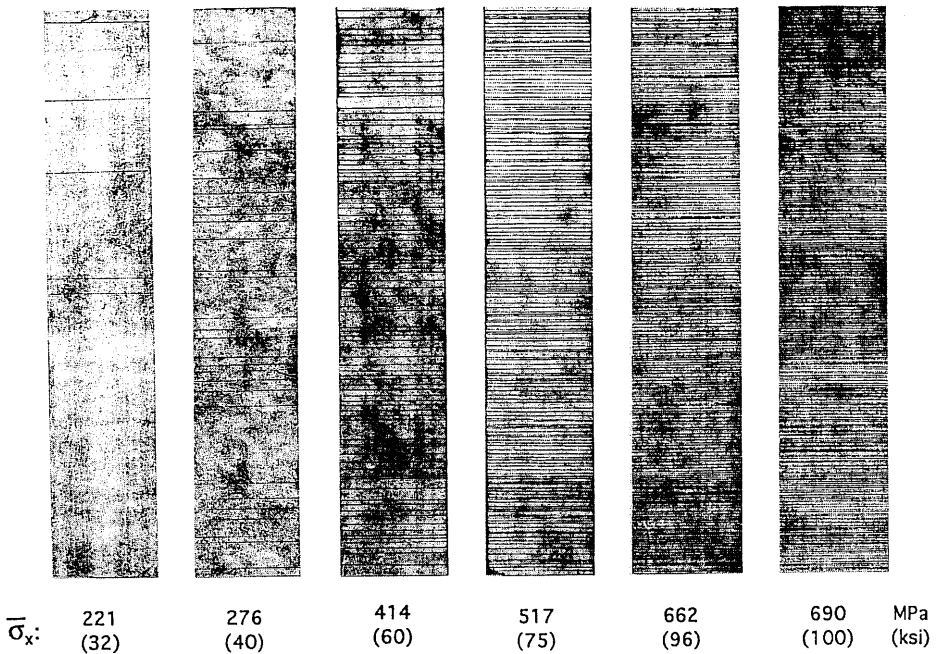


Fig. 7.11 X-radiographs of a $[0/90_2]_s$ carbon/epoxy laminate under uniaxial tensile loading at various applied stress levels.

$[0/90_2]_s$ carbon/epoxy laminate is illustrated by the X-radiographs in Figure 7.11.

As the damage grows, the stiffness of the damaged ply as well as that of the entire laminate is reduced. Analytical models have been developed for predicting the stiffness degradation as a function of damage.²⁻⁸ A shear lag analysis has been used to obtain closed form solutions for stress distributions, transverse matrix crack density and reduced stiffnesses of the damaged plies and the entire laminate as a function of applied stress, properties of the constituent plies, and residual stresses.⁸

The reduced axial modulus of a $[0_m/90_n]_s$ crossply laminate is expressed in the form of a modulus reduction ratio as

$$\rho_E = \frac{\bar{E}'_x}{\bar{E}_x} = \left[1 + \frac{2 E_2 h_2}{\alpha l E_1 h_1} \tanh \frac{\alpha l}{2} + \frac{\sigma_{r1}}{\bar{\sigma}_x} \frac{\bar{E}_x}{E_1} \left(1 - \frac{2}{\alpha l} \tanh \frac{\alpha l}{2} \right) \right]^{-1} \quad (7.31)$$

where

\bar{E}_x, \bar{E}'_x = Initial and reduced modulus of the laminate, respectively

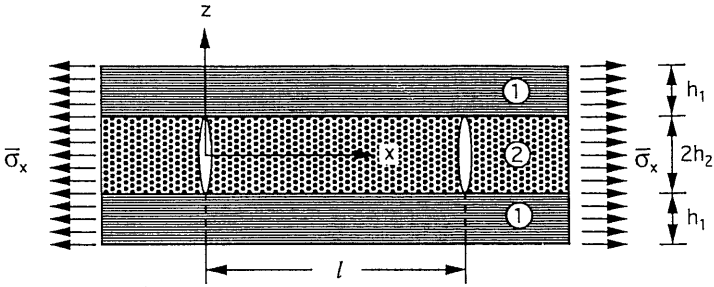


Fig. 7.12 Element of crossply laminate with transverse cracks in 90° layer.

E_1, E_2 = Longitudinal and transverse moduli of lamina

l = Crack spacing

h_1, h_2 = Longitudinal and transverse layer thicknesses, respectively in $[0_m/90_n]_s$ laminate (see Fig. 7.12).

$$\alpha^2 = \frac{3 (h_1 + h_2) \bar{E}_x}{h_1 h_2 E_1 E_2} \cdot \frac{G_{12} G_{23}}{h_1 G_{23} + h_2 G_{12}} \tag{7.32}$$

where

G_{12}, G_{23} = In-plane and out-of-plane shear moduli of lamina

σ_{r1} = Axial residual stress in 0° layer

The reduced effective (in situ) modulus of the cracked transverse layer, E'_2 , is related to the modulus reduction ratio of the laminate as follows:

$$r_2 = \frac{E'_2}{E_2} = \rho_E - \frac{E_1 h_1}{E_2 h_2} (1 - \rho_E) \tag{7.33}$$

The normalized reduced modulus of a $[0/90_2]_s$ carbon/epoxy laminate computed by Eq. (7.31) is plotted versus normalized transverse crack density in Figure 7.13 and compared with experimental results. The normalized in situ modulus of the cracked 90° layer obtained from Eq. (7.33) is plotted versus normalized crack density in Figure 7.14. It is seen that, at the limiting crack density, the laminate modulus is reduced to approximately 90% of its original value, and the in situ modulus of the 90° layer is reduced to approximately 25% of its original value.

Progressive failure under a general in-plane biaxial loading has also been analyzed.^{9,10} Besides Young's modulus, the reduction of the in-plane shear

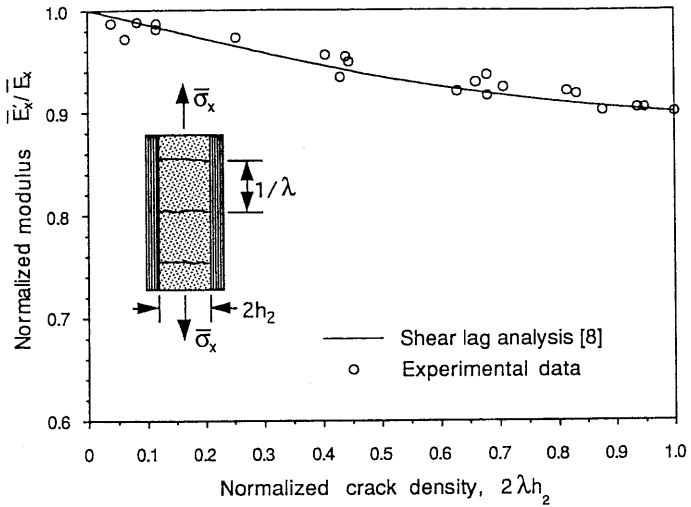


Fig. 7.13 Normalized axial modulus of $[0/90_2]_s$ carbon/epoxy (AS4/3501-6) laminate as a function of normalized transverse crack density.⁸

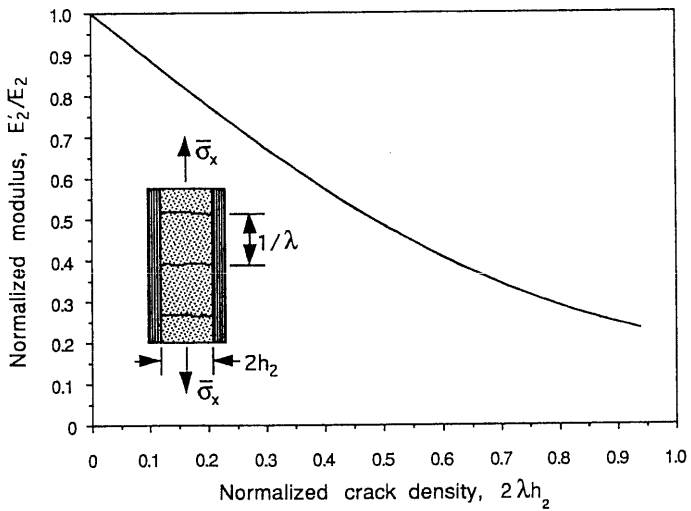


Fig. 7.14 Effective in situ normalized transverse modulus of cracked 90° layer in $[0/90_2]_s$ carbon/epoxy (AS4/3501-6) laminate as a function of normalized transverse crack density.

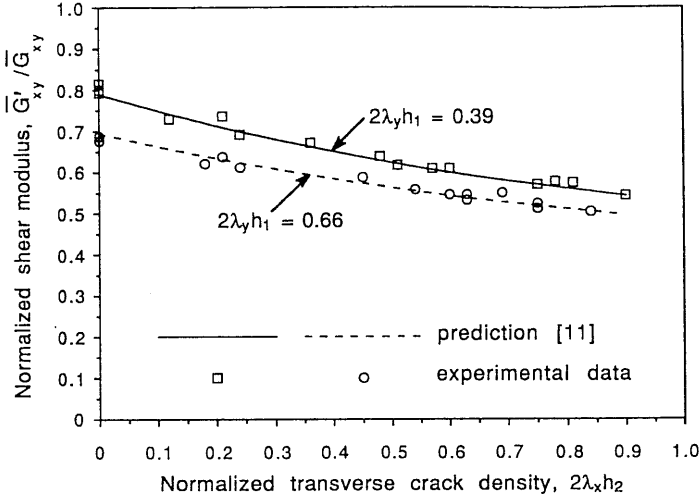


Fig. 7.15 Shear modulus reduction as a function of normalized crack densities of $[0_3/90_3]_s$ crossply carbon/epoxy laminate.¹¹

modulus has been calculated and correlated with the state of damage (cracking) in the laminate.¹¹ The variation of shear modulus for a $[0_3/90_3]_s$ carbon/epoxy laminate as a function of crack spacings is shown in Figure 7.15.

7.11 Progressive and Ultimate Laminate Failure

As discussed before, progressive failure of a lamina within the laminate consists of cracking of the lamina up to a characteristic limiting crack density. Following this FPF, the failure process continues up to ULF. The latter can occur at a much higher load than FPF.

Figure 7.16 illustrates the progression of damage in a $[0/\pm 45/90]_s$ glass/epoxy laminate under uniaxial loading. The first failure mechanism consists of transverse cracking in the 90° layer. These cracks increase in density up to a limiting value or the characteristic damage state. Thereafter, as the load increases, cracking starts in the ± 45 plies precipitating ultimate failure.

Consider for example the stress-strain response of a multidirectional laminate under uniaxial tensile loading (Fig. 7.17). Initially, the laminate behaves linearly, with a stress-strain slope equal to the original laminate modulus \bar{E}_x up to a point (1) where the first ply fails. After this ply reaches its maximum crack density (characteristic damage state), its effective transverse modulus drops to E'_2 and the laminate modulus drops to a value $\bar{E}_x^{(1)}$. If the material behaves in a brittle manner, the modulus drop will be sudden. It will be manifested by a

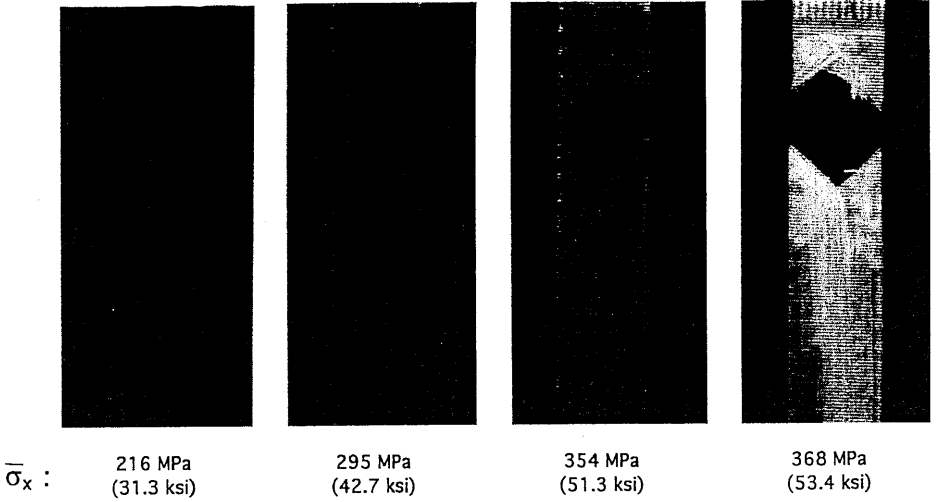


Fig. 7.16 Damage progression in a $[0/\pm 45/90]_s$ glass/epoxy laminate under increasing uniaxial tensile loading.

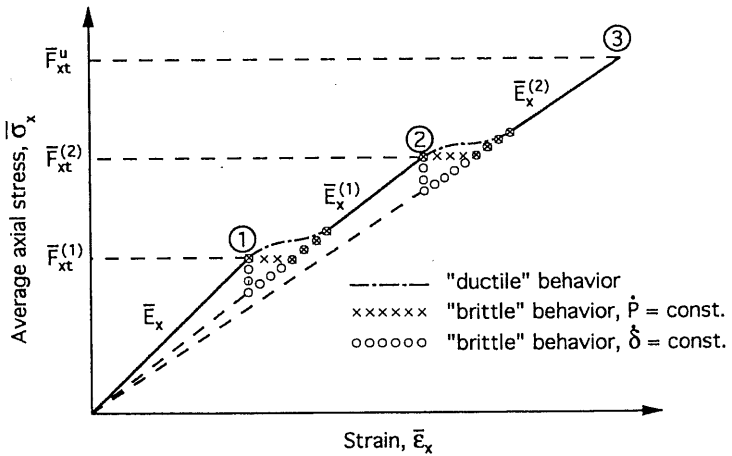


Fig. 7.17 Stress-strain curve of multidirectional laminate under uniaxial tension showing progressive failure ($\dot{P} = \text{constant}$, load rate control; $\dot{\delta} = \text{constant}$, strain rate control).

horizontal or vertical shift in the stress-strain curve, depending on whether the test is conducted under load or strain control, respectively.

Under increasing load the specimen will respond linearly with a stress-strain slope equal to the reduced modulus $\bar{E}_x^{(1)}$ up to point (2), where the next ply or plies fail. Again, if the ply or plies fail instantly in a brittle manner, there will

be a further sudden drop in the modulus to a value $\bar{E}_x^{(2)}$. This value corresponds to the laminate with all the failed plies to date discounted or reduced in stiffness. The drop in modulus will be manifested as a sudden horizontal or vertical shift in the stress-strain curve, depending on the test control mode as discussed before. This progressive failure continues up to a point (say, point 3) where ultimate failure takes place. If the plies fail gradually due to ductile behavior or statistical variation in local strengths and failures, the stress-strain curve will appear smoother with gradual transitions in slope at the points of partial ply failures (Fig. 7.17).

At each stage of failure there is a corresponding strength. Thus, one can define the initial stage (or FPF) and last stage (ULF) tensile strengths, $\bar{F}_{xt}^{(1)}$ and $\bar{F}_{xt}^{(u)}$, respectively. The ratio of these two strengths, φ_L , is a measure of laminate efficiency and indicates the level of fiber strength utilization at FPF:

$$\varphi_L = \frac{\bar{F}_{xt}^{(1)}}{\bar{F}_{xt}^{(u)}} = \frac{\bar{F}_{\text{FPF}}}{\bar{F}_{\text{ULF}}} \quad (7.34)$$

This ratio depends on both the material system and the laminate layup.

A comparison of FPF and ULF of different multidirectional laminates under uniaxial tensile loading is shown in Tables 7.2 and 7.3 as has been done previously for a similar set of materials.¹² The laminate efficiency ratio for $[0/90]_s$ crossply laminates is fairly low for all material systems, ranging from 0.20 for glass/epoxy to 0.42 for boron/epoxy. In the case of $[0_2/\pm 45]_s$ laminates the laminate efficiency ratios are much higher, ranging from 0.33 to 0.88.

7.12 Analysis of Progressive Laminate Failure

The determination of the ultimate strength of a laminate requires an iterative procedure taking into account the damage progression in the various plies. The approach used consists of the following steps:

1. The load required to produce FPF is determined from the lamina stresses using a selected failure criterion (see Fig. 7.9). The lamina stresses are obtained as a function of the loading and are referred first to the laminate coordinates (x,y) and then transformed to the lamina coordinates (1,2).
2. The failed lamina or laminae are replaced with laminae of reduced stiffnesses. These usually are the matrix-dominated stiffnesses, such as E_2 and G_{12} . The stiffness reduction factors can be selected based on analysis as discussed before (see Eq. 7.33), or the affected stiffnesses can be discounted completely (ply discount method). New laminate stiffnesses $[A]$, $[B]$, and $[D]$ are then calculated.

Table 7.2 Comparison of Initial and Ultimate Failures of [0/90]_s Laminates

Material system	First ply failure (FPF)			Ultimate laminate failure (ULF)			Laminate efficiency factor ($\phi_L = \bar{F}_{FPF}/\bar{F}_{ULF}$)
	Strength \bar{F}_{FPF} , MPa (ksi)	Strain (%)	Modulus GPa (Msi)	Strength \bar{F}_{ULF} , MPa (ksi)	Strain (%)	Modulus GPa (Msi)	
Glass/epoxy	111 (16.1)	0.46	24.1 (3.5)	552 (80)	2.75	20.0 (2.9)	0.20
Kevlar/epoxy	241 (34.9)	0.52	46.2 (6.7)	655 (95)	1.50	44.9 (6.5)	0.37
Carbon/epoxy	420 (60.9)	0.50	78.2 (11.3)	1,152 (167)	1.50	82.8 (12.0)	0.36
Boron/epoxy	288 (41.7)	0.35	111.8 (16.2)	690 (100)	0.60	103.5 (15.0)	0.42
Boron/aluminum	163 (23.6)	0.09	187.0 (27.1)	683 (99)	0.58	113.9 (16.5)	0.24

Table 7.3 Comparison of Initial and Ultimate Failures of [0₂/±45]_s Laminates

Material system	First ply failure (FPF)			Ultimate laminate failure (ULF)			Laminate efficiency factor ($\phi_L = \bar{F}_{FPF}/\bar{F}_{ULF}$)
	Strength \bar{F}_{FPF} , MPa (ksi)	Strain (%)	Modulus GPa (Msi)	Strength \bar{F}_{ULF} , MPa (ksi)	Strain (%)	Modulus GPa (Msi)	
Glass/epoxy	265 (38.4)	1.04	25.5 (3.7)	607 (88)	2.75	22.1 (3.2)	0.44
Kevlar/epoxy	607 (88.0)	1.26	48.0 (7.0)	683 (99)	1.50	45.5 (6.6)	0.88
Carbon/epoxy	460 (66.6)	0.53	86.2 (12.5)	1,208 (175)	1.50	80.5 (11.7)	0.38
Boron/epoxy	601 (87.1)	0.53	114.5 (16.6)	745 (108)	0.70	106.4 (15.4)	0.81
Boron/aluminum	259 (37.5)	0.14	185.6 (26.9)	780 (113)	0.60	130.0 (18.8)	0.33

3. Lamina stresses are recalculated and checked against the selected failure criterion to verify that the undamaged laminae do not fail immediately under their increased share of stress following the FPF above.
4. The load is increased until the next ply failure occurs and steps 1, 2, and 3 above are repeated.
5. When the remaining undamaged laminae, at any stage of the progressive ply failures, cannot sustain the stresses, ultimate failure of the laminate occurs.

The computational procedure for the multiple ply failure approach for the case of a symmetric laminate under in-plane loading is illustrated by the flow chart of Figure 7.18 and consists of the following steps:

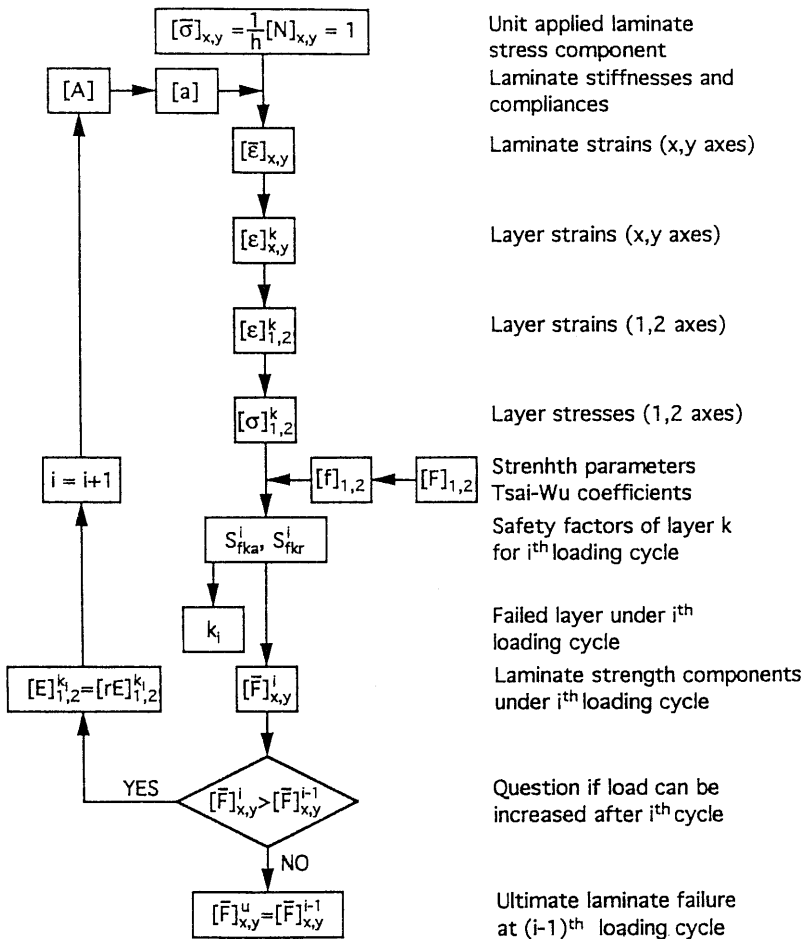


Fig. 7.18 Flow chart for determination of load-deformation curve and failure levels of symmetric laminates under in-plane loading.

Step 1 Enter unit average laminate stress (or load) in desired direction, i.e.,

$$\bar{\sigma}_x = 1 \text{ or } \bar{\sigma}_y = 1 \text{ or } \bar{\tau}_s = 1.$$

- Step 2** Enter laminate extensional stiffnesses $[A]$ and compliances $[a]$ obtained from basic lamina properties and laminate lay-up (steps 1–7 in the flow chart of Figure 7.3).
- Step 3** Calculate average laminate strains $\bar{\epsilon}_x, \bar{\epsilon}_y, \bar{\gamma}_s$ referred to (x,y) axes using Eq. (5.74).
- Step 4** Calculate layer strains $(\epsilon_x, \epsilon_y, \gamma_s)_k$, which are equal to the laminate strains.
- Step 5** Calculate layer strains $(\epsilon_1, \epsilon_2, \gamma_6)_k$ referred to layer principal axes (1,2), using Eq. (3.58).
- Step 6** Calculate layer stresses, $(\sigma_1, \sigma_2, \tau_6)_k$, referred to layer principal axes (1,2), using Eq. (3.31).
- Step 7** Enter lamina strengths, $[F]_{1,2}$, and calculate Tsai–Wu coefficients f_i, f_{ij} , using relations in Eqs. (4.42) through (4.46) and Eq. (4.52).
- Step 8** Calculate layer safety factors, S_{fka} and S_{fkr} , using Eqs. (7.6) through (7.8).
- Step 9a** Identify failed layer, k_i , under i th loading cycle from $S_{fki} = (S_{fk})_{\min}$.
- Step 9b** Determine laminate strength components $[\bar{F}]_{k,y}^i$ for i th loading cycle.
- Step 10** Question whether the computed strength component of the i th loading cycle, \bar{F}^i , is higher than the strength at the previous loading \bar{F}^{i-1} .
- Step 11a** If answer is “yes,” i.e., if loading can be increased, the damaged lamina k_i is replaced with one having the following properties:

$$E_1^{k_i} = r_1 E_1$$

$$E_2^{k_i} = r_2 E_2$$

$$G_{12}^{k_i} = r_{12} G_{12} \quad (7.35)$$

$$\nu_{12}^{k_i} = r_1 \nu_{12}$$

where r_1, r_2, r_{12} are stiffness reduction factors, obtained from analysis or prior experiments. Typical values of these factors are

$$r_1 \cong 1, r_2 \cong r_{12} \cong 0.25$$

The conservative approach is complete ply discount, i.e., $r_1 \cong 1, r_2 \cong r_{12} \cong 0$.

- Step 11b** Go to $i + 1$ loading cycle and recalculate modified laminate stiffnesses $[A]$ and compliances $[a]$. Repeat steps 2 through 10 above. In step 7, the lamina strengths of the failed layer k_i should be made

fictitiously very high to avoid repeated failure indication in the same layer.

Step 12 If answer to question of step 10 is “no,” then ultimate failure occurs at the $(i - 1)$ th loading cycle, i.e. $\bar{F}^u = \bar{F}^{i-1}$.

Hygrothermal loading can be included in the above procedure as in the case of the flow chart for FPF (Fig. 7.9). However, in subsequent loading cycles, the coefficients of thermal and hygric expansion of the failed plies must be modified. The presence of hygrothermal (or residual) stresses also affects the local stresses in the cracked laminate, the extent of layer cracking, and the modulus reduction ratios (Eqs. 7.31 and 7.33). The effect of hygrothermal stresses on the laminate strength decreases with failure level, i.e., it is much less pronounced on ultimate failure than on first ply failure. A similar procedure can be followed for the general case of an asymmetric laminate under general in-plane and moment loading by combining the flow charts of Figures 7.9 and 7.18.

7.13 Interlaminar Stresses and Strength of Multidirectional Laminates: Edge Effects

7.13.1 Introduction

One of the assumptions of the classical lamination theory discussed in Section 5.1 is that the laminate and all its layers are in a state of plane stress, i.e., all out-of-plane stress components are zero, $\sigma_z = \tau_{xz} = \tau_{yz} = 0$. This assumption is justified away from geometric discontinuities, such as free edges. Mechanical and hygrothermal loadings can produce interlaminar stresses, both shear and normal, especially near free edges. Normal tensile interlaminar stresses, or peel stresses, tend to separate the laminae from each other. Interlaminar shear stresses tend to slide one lamina over adjacent ones. In both cases interlaminar stresses can cause interlaminar separation or **delamination**. Interlaminar stresses are a function of the laminate stacking sequence, thus they can be controlled by proper design of the stacking sequence. For example, in some cases a tensile interlaminar normal stress, σ_z , can be transformed into a compressive one by simply rearranging the layer sequence.

There are three types of interlaminar stress problems associated with three types of laminates, $[\pm\theta]$ angle-ply laminates, $[0/90]$ crossply laminates, and laminates combining both angle-ply and crossply configurations.

7.13.2 Angle-Ply Laminates

Consider for example a $[\pm\theta]_s$ angle-ply laminate under average axial tensile stress $\bar{\sigma}_x$ (Fig. 7.19). Each layer is subjected to the same axial stress, $\sigma_x = \bar{\sigma}_x$.

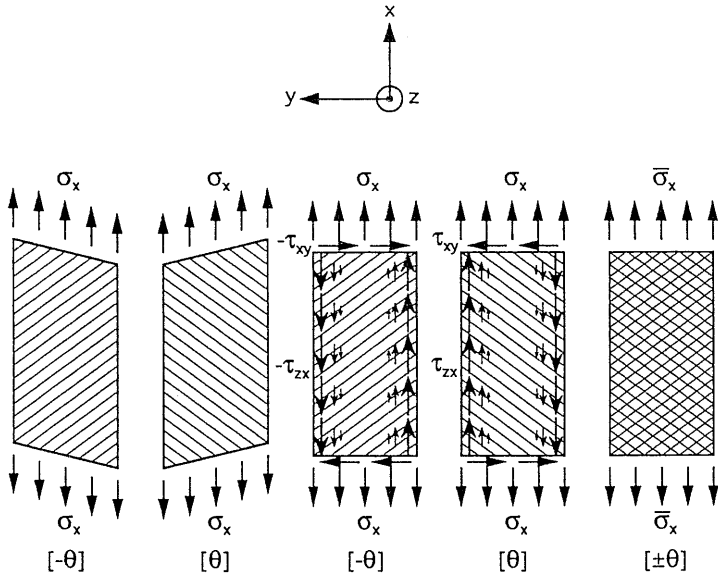


Fig. 7.19 Illustration of generation of interlaminar and intralaminar shear stresses in angle-ply laminate under axial tension.

Because of the off-axis orientation (shear coupling), layers θ and $-\theta$ when considered independently will undergo shear deformations of opposite signs as shown in Figure 7.19. When bonded together in the laminate the layers must have zero shear strain. This is achieved through interlaminar shear stresses τ_{zx} transmitted from one layer to the other. These stresses vary across the width of the specimen, being zero over most of the central region and peaking near the edges (Fig. 7.20). The moment produced by these stresses is equilibrated by intralaminar shear stresses τ_{xy} acting on the transverse cross section of the layer. These stresses are constant over most of the central region and drop to zero at the (stress-free) edges (Fig. 7.20). The interlaminar shear stress (τ_{zx}) is a function of fiber orientation in the $[\pm\theta]_s$ laminate as illustrated in Figure 7.21 for a carbon/epoxy $[\pm\theta]_s$ laminate.¹³ The τ_{zx} stress (as close to the interface and near the edge as can be determined numerically) is zero at $\theta = 60^\circ$ as well as $\theta = 0^\circ$ and $\theta = 90^\circ$. It reaches a peak value (for this carbon/epoxy) at $\theta \cong 35^\circ$. The physical existence of interlaminar stresses was demonstrated by determining axial displacements across the width of a $[\pm 25]_s$ carbon/epoxy specimen by means of the moiré method.¹⁴

7.13.3 Crossply Laminates

A different state of interlaminar stresses arises in the case of crossply laminates. Consider, for example, a $[0/90]_s$ crossply laminate under average axial tensile

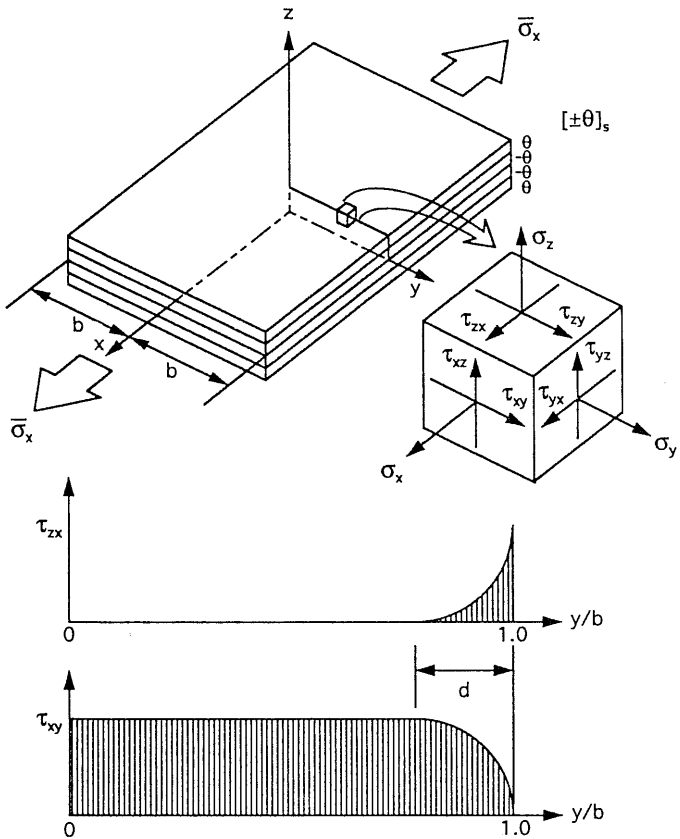


Fig. 7.20 Distribution of interlaminar (τ_{zx}) and intralaminar (τ_{xy}) shear stresses in θ -layer of $[\pm\theta]_s$ angle-ply laminate under axial tension.

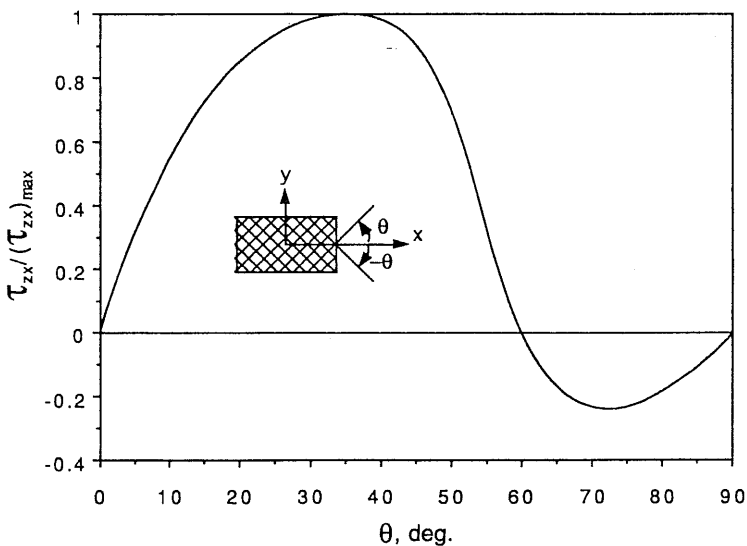


Fig. 7.21 Interlaminar shear stress as a function of fiber orientation.¹³

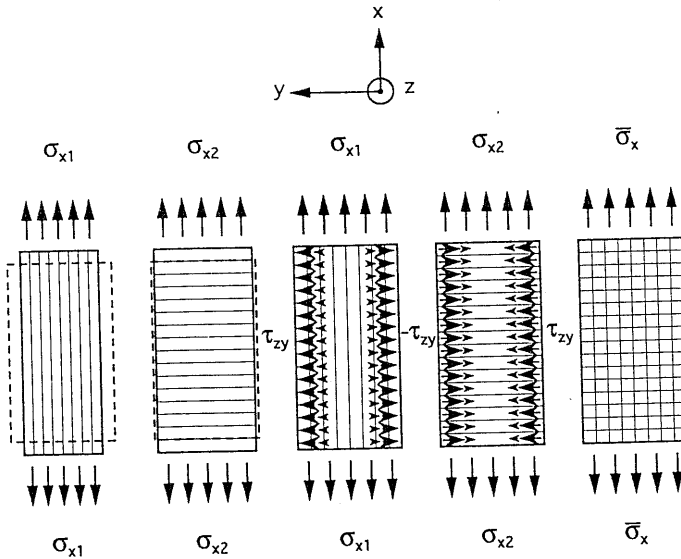


Fig. 7.22 Illustration of generation of interlaminar stresses in crossply laminate under axial tension.

stress $\bar{\sigma}_x$ (Fig. 7.22). The load sharing is such that each layer undergoes the same axial deformation. Because of the different Poisson's ratios, the 0° and 90° layers will undergo different transverse deformations when acting independently. When bonded together in the laminate the 0° and 90° layers must have the same transverse strain. This is achieved through interlaminar shear stresses τ_{zy} , which tend to expand the 0° layer and compress the 90° layer in the y -direction. These stresses vary across the width of the specimen, being zero over the central region and peaking near the free edges.

The development of interlaminar stresses in a crossply laminate is further illustrated in Figure 7.23. Considering a free body diagram of an element of the 0° ply near the edge, one can see that the interlaminar stresses τ_{zy} must be equilibrated by normal stresses σ_y acting on the layer. Moment equilibrium in the yz plane requires interlaminar normal stresses σ_z with a distribution producing a zero force resultant in the z -direction and a moment equal and opposite to that produced by the τ_{zy} and σ_y stresses. For the case under discussion this means high tensile interlaminar normal stresses near the edge, i.e., a tendency for delamination. Of course the sign of all interlaminar stresses is reversed when the applied stress $\bar{\sigma}_x$ is compressive.

7.13.4 Effects of Stacking Sequence

In the case of a general multidirectional laminate all three types of interlaminar stresses are generated near free edges, i.e., σ_z , τ_{xz} , and τ_{zy} . In all cases the

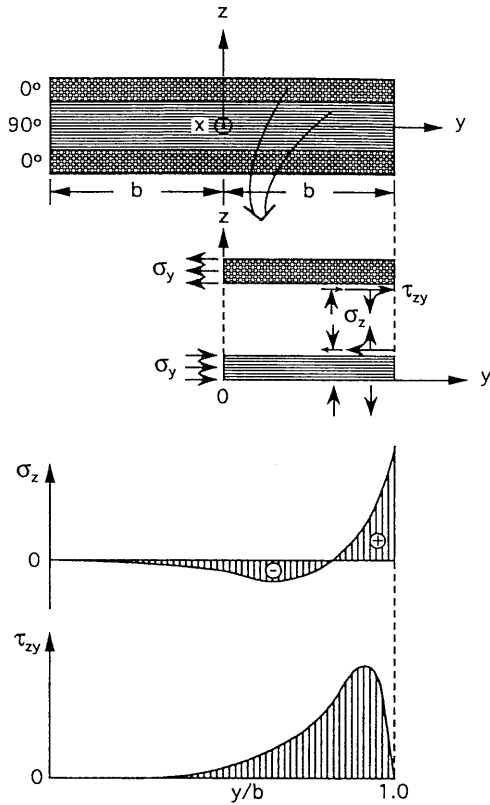


Fig. 7.23 Distribution of interlaminar normal stress σ_z and interlaminar shear stress τ_{zy} in $[0/90]_s$ laminate under axial tension.

magnitude and distribution of interlaminar stresses depend greatly on the stacking sequence of the laminate. The effect of stacking sequence on the interlaminar normal stress σ_z is illustrated in Figure 7.24 for a laminate consisting of $\pm 15^\circ$ and $\pm 45^\circ$ layers under axial tension.¹⁵ The distribution of stress σ_z through the thickness is given for three stacking sequences, $[\pm 15/\pm 45]_s$, $[15/\pm 45/-15]_s$, and $[\pm 45/\pm 15]_s$. It is seen that both the magnitude and sign of the stress can change drastically with stacking sequence. It is obvious that, for design considerations, stacking sequences resulting in low tensile or compressive σ_z stresses should be selected.

The effect of stacking sequence on interlaminar edge stresses, e.g., σ_z , and thereby on strength is dramatically illustrated in the case of laminates with circular holes. In this case edge effects are accentuated by the stress concentration on the edge of the hole. Two boron/epoxy panels of $[0_2/\pm 45/\bar{0}]_s$ and $[\pm 45/0_2/\bar{0}]_s$ stacking sequences with circular holes were loaded in axial tension to failure.¹⁶ These two stacking sequences result, respectively, in tensile and compressive interlaminar normal stresses near the edge of the hole at the point

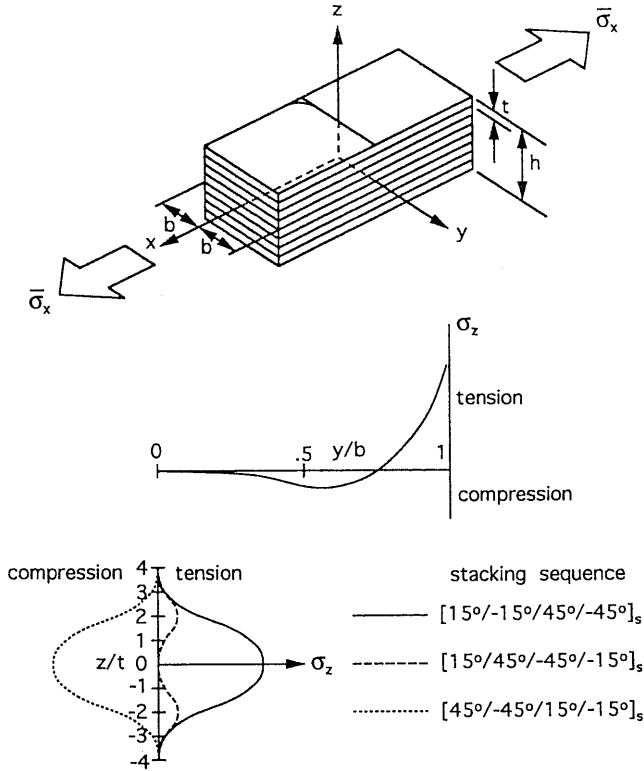
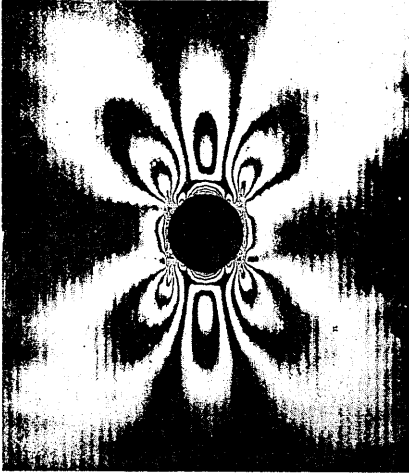


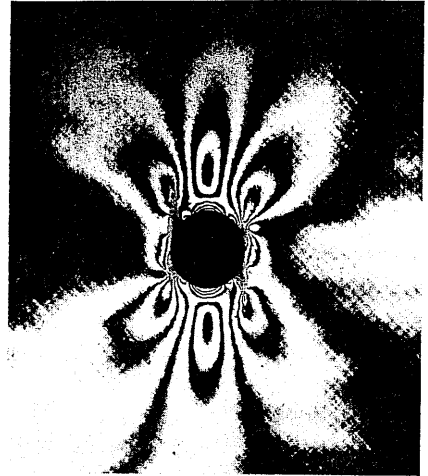
Fig. 7.24 Effect of stacking sequence on through the thickness distribution of interlaminar normal stress σ_z near free edge.¹⁵

of maximum stress concentration. Figure 7.25 shows fringe patterns in a photoelastic coating around the hole near failure. The pattern for the $[0_2/\pm 45/\bar{0}]_s$ specimen is fairly symmetric with lower stress concentration; the pattern for the $[\pm 45/0_2/\bar{0}]_s$ specimen is skewed with higher stress concentration. The failure modes of the two specimens were dramatically different (Fig. 7.26). The $[\pm 45/0_2/\bar{0}]_s$ specimen failed horizontally in a catastrophic manner at an average applied axial stress of 426 MPa (61.7 ksi). The $[0_2/\pm 45/\bar{0}]_s$ specimen failed by vertical cracking in a noncatastrophic manner at an applied axial stress of 527 MPa (76.4 ksi). The specimen then split into two strips that carried a much higher ultimate stress of 725 MPa (105 ksi). Thus stacking sequence can influence, through interlaminar edge effects, the strength and mode of failure. In summary, there are three types of interlaminar stress problems associated with three types of laminates:

1. $[\pm\theta]$ angle-ply laminates exhibit effects of shear coupling mismatch and thus, only τ_{zx} interlaminar shear stresses are generated.



$[0_2/\pm 45/\bar{0}]_s$

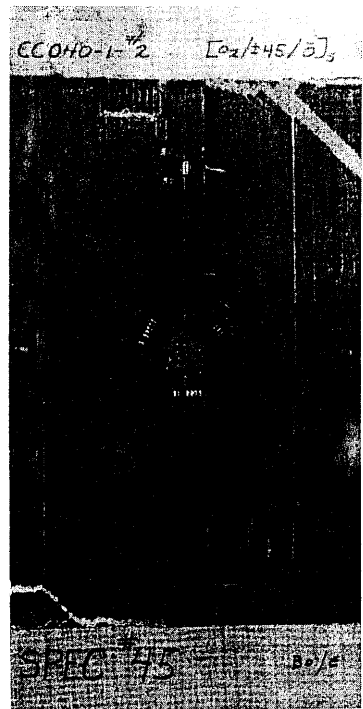


$[\pm 45/0_2/\bar{0}]_s$

Fig. 7.25 Isochromatic fringe patterns in photoelastic coating around hole in boron/epoxy specimens of two different stacking sequences ($\bar{\sigma}_x = 392$ MPa [56.8 ksi]).¹⁶



$[\pm 45/0_2/\bar{0}]_s$



$[0_2/\pm 45/\bar{0}]_s$

Fig. 7.26 Failure patterns of boron/epoxy tensile panels with holes of two different stacking sequences.¹⁶

2. $[0/90]_s$ crossply laminates exhibit effects of Poisson's ratio mismatch and thus only interlaminar shear stresses, τ_{zy} , and interlaminar normal stresses, σ_z , are generated.
3. General multidirectional laminates, combining angle-ply and crossply sublaminates, exhibit effects of both shear coupling and Poisson's ratio mismatch. Thus all three types of interlaminar stresses, σ_z , τ_{zx} , and τ_{zy} , can be generated.

7.13.5 Interlaminar Strength

The analysis and exact determination of interlaminar stresses, which is essential for interlaminar strength evaluation, is highly complex and requires numerical methods that are beyond the scope of this book. Computer programs were developed recently that aim at providing an engineering solution to this problem.¹⁷ In practice the effect of interlaminar stresses can be controlled, since they are confined to a narrow zone near free edges or free hole boundaries. This is usually done by means of edge fastening that constrains the effect of interlaminar tensile (peel) stresses and prevents delamination propagation. As long as the laminate is free of severe delaminations (which can be revealed by non-destructive evaluation), the basic assumptions of Section 5.1 including that of plane stress are valid.

Failure of a laminate under the action of interlaminar stresses cannot be analyzed easily. The lamina failure criteria discussed in Chapter 4 are not applicable. In addition to the basic lamina strengths, interlaminar shear and interlaminar tensile strengths must be determined. These strengths may not be constant material properties but may also depend on the layer (fiber) orientation and the laminate stacking sequence.

Interlaminar strength is a matrix-dominated property, and thus it depends on factors such as moisture and temperature, which affect matrix and interfacial performance. Several test methods are available for determination of interlaminar strength, as will be discussed in Chapter 8. Results from such tests cannot be treated as design allowables, but may be used for comparative parametric investigations or for qualitative evaluation of interlaminar performance. Simplified tests exist that provide a good measure of interlaminar quality and serve as a means of quality control of the fabrication process.

Sample Problem 7.3

Interlaminar Shear Stresses under Flexure

Consider a cantilever beam made of a multidirectional laminate and loaded by a concentrated force P at the free end (Fig. 7.27). The beam is subjected only

to a bending moment M_x and a transverse shear force V_z such that

$$\begin{aligned} M_x &= Px \\ V_z &= P \end{aligned} \tag{7.36}$$

All other forces and moments are zero.

The axial strains at any point of section $a-a$ at a distance z from the reference plane are

$$\begin{bmatrix} \epsilon_x \\ \epsilon_y \\ \gamma_s \end{bmatrix}_a = z \begin{bmatrix} \kappa_x \\ \kappa_y \\ \kappa_s \end{bmatrix}_a \tag{7.37}$$

since the reference plane strains are zero. Referring to Eq. (5.25) and noting that $N_x = N_y = N_s = 0$ and $M_y = M_s = 0$, we can rewrite Eq. (7.37) as

$$\begin{bmatrix} \epsilon_x \\ \epsilon_y \\ \gamma_s \end{bmatrix}_a = z \begin{bmatrix} d_{xx} \\ d_{yx} \\ d_{sx} \end{bmatrix} M_{xa} \tag{7.38}$$

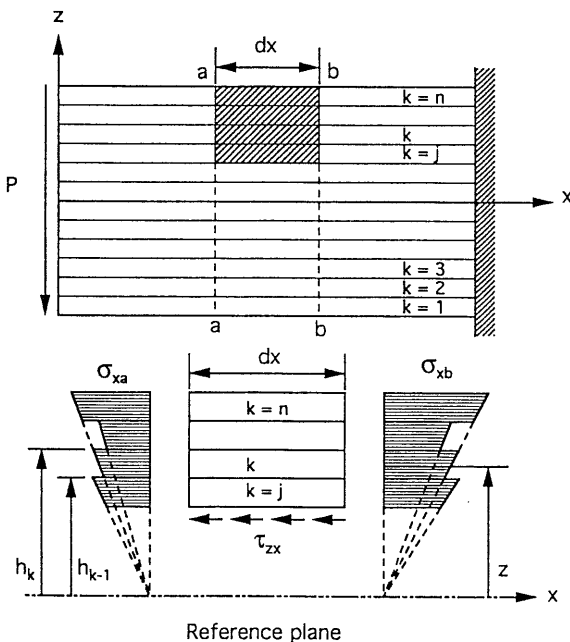


Fig. 7.27 Stresses acting on element of composite cantilever beam.

where d_{ij} are the laminate compliances and M_{xa} the moment at section $a-a$.

Using the constitutive relations for layer k referred to the x - y -coordinate system, we obtain the layer axial stress at section $a-a$ and at location z as

$$\begin{aligned}\sigma_{xa} &= Q_{xx}^k \epsilon_{xa} + Q_{xy}^k \epsilon_{ya} + Q_{xs}^k \gamma_{sa} \\ &= z M_{xa} \left[Q_{xx}^k d_{xx} + Q_{xy}^k d_{yx} + Q_{xs}^k d_{sx} \right] \\ &= z M_{xa} [Q d]_k\end{aligned}\quad (7.39)$$

Similarly, we obtain the axial stress in layer k at section $b-b$ and at location z as

$$\sigma_{xb} = z M_{xb} [Q d]_k \quad (7.40)$$

The crosshatched element of the beam in Figure 7.27 is in equilibrium under the action of the axial normal stresses σ_{xa} and σ_{xb} and the interlaminar shear stress τ_{zx} , acting between layers $j-1$ and j . Equilibrium of forces in the x -direction

$$N_x = 0$$

yields

$$\tau_{zx} dx = dM \sum_{k=j}^n [Q d]_k \int_{h_{k-1}}^{h_k} z dz \quad (7.41)$$

from which we obtain

$$\tau_{zx} = \frac{1}{2} \frac{dM}{dx} \sum_{k=j}^n [Q d]_k \left(h_k^2 - h_{k-1}^2 \right) \quad (7.42)$$

or

$$\tau_{zx} = V_z \sum_{k=j}^n [Q d]_k z_k t_k \quad (7.43)$$

where

$$V_z = \frac{dM}{dx} \quad (\text{shear force})$$

z_k = Coordinate to center of layer k

t_k = Thickness of layer k

7.14 Interlaminar Fracture Toughness

Interlaminar cracking or delamination can occur under three basic modes, opening or peel mode (Mode I), forward sliding shear mode (Mode II), or tearing mode (Mode III), or under combinations thereof (Fig. 7.28). The resistance to delamination growth is expressed in terms of the interlaminar fracture toughness, which has three forms corresponding to the three basic delamination modes. The interlaminar fracture toughness is measured by the strain energy release rate (G_I , G_{II} , or G_{III}), which is the energy dissipated per unit area of delamination growth.

Consider a composite beam delaminated along its midplane over a length, a , and loaded at the ends by loads P as shown in Figure 7.29. The total energy balance is expressed as¹⁸

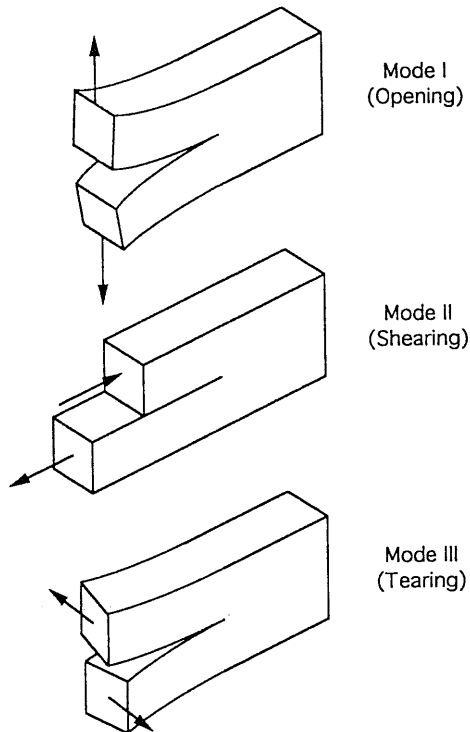


Fig. 7.28 Basic delamination modes in composite material.

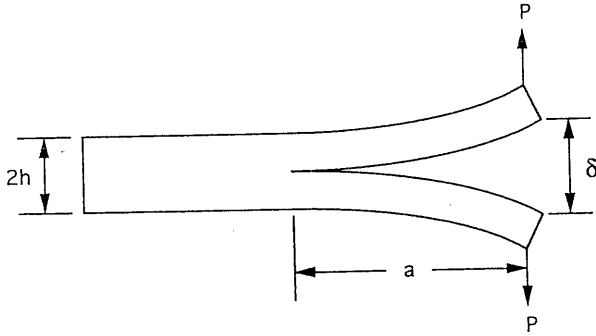


Fig. 7.29 Double cantilever beam (DCB) for measurement of mode I delamination fracture toughness.

$$W = U + T + D \quad (7.44)$$

where

W = External work

U = Elastic strain energy

T = Kinetic energy

D = Dissipative energy associated with fracture

The energy released per unit area of crack extension is expressed as

$$G_I = \frac{1}{b} \frac{dD}{da} = \frac{1}{b} \left[\frac{dW}{da} - \frac{dU}{da} - \frac{dT}{da} \right] \quad (7.45)$$

where b = width of beam. Noting that

$$\frac{dW}{da} = P \frac{d\delta}{da} \quad (7.46)$$

and that, for linear elastic behavior,

$$U = \frac{1}{2} P\delta \quad (7.47)$$

we can rewrite Eq. (7.45) as

$$G_I = \frac{1}{b} \frac{dD}{da} = \frac{1}{2b} \left[P \frac{d\delta}{da} - \delta \frac{dP}{da} - 2 \frac{dT}{da} \right] \quad (7.48)$$

Methods of analysis and applications of the double cantilever beam (DCB) specimen for determination of interlaminar fracture toughness have been discussed in the literature.¹⁹⁻²¹ In the compliance method the strain energy release rate is expressed in terms of the compliance

$$C = \frac{\delta}{P} \quad (7.49)$$

Substituting $\delta = PC$ in Eq. (7.48) and neglecting kinetic energy, we obtain

$$G_I = \frac{P^2}{2b} \frac{dC}{da} \quad (7.50)$$

The compliance C is calculated by considering the DCB specimen as two cantilever beams of length a joined at the crack tip. Thus, for a unidirectional composite DCB specimen with the fiber direction along the longitudinal axis,

$$C = \frac{\delta}{P} = \frac{24}{E_1 b} \left[\frac{1}{3} \left(\frac{a}{h} \right)^3 + \frac{1}{10} \left(\frac{E_1}{G_{31}} \right) \left(\frac{a}{h} \right) \right] \quad (7.51)$$

and

$$G_I = \frac{12 P^2}{E_1 b^2 h} \left[\left(\frac{a}{h} \right)^2 + \frac{1}{10} \left(\frac{E_1}{G_{31}} \right) \right] \quad (7.52)$$

Another commonly used method of analysis is the so-called area method. In this approach the specimen is not modeled as a beam. The energy released per unit area of crack extension is simply calculated as

$$G_I = \frac{1}{2b\Delta a} (P_1 \delta_2 - P_2 \delta_1) \quad (7.53)$$

where load P_1 corresponding to opening deflection δ_1 drops to load P_2 corresponding to deflection δ_2 after a finite increment Δa in crack length (Fig. 7.30). The quantity $\frac{1}{2}(P_1 \delta_2 - P_2 \delta_1)$ in Eq. (7.53) is equal to the shaded area ΔA in Figure 7.30. It should be noted that the relation above is valid only for linear load-deformation response. Variations of the DCB specimen above and other experimental and analytical procedures for determination of strain energy release rates G_I , G_{II} , G_{III} and combinations thereof are discussed in Chapter 8.

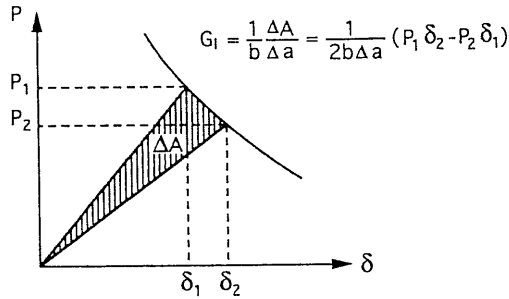


Fig. 7.30 Area method for calculation of strain energy release rate using a double cantilever beam specimen.

7.15 Design Methodology for Structural Composite Materials

The design of composite structures is an integrated process involving material selection, process specification, optimization of laminate configuration, and design of the structural components. Design objectives vary according to the structural application. Specific application requirements define one or a combination of two or more of the following basic design objectives:

1. Design for stiffness.
2. Design for strength (static and fatigue).
3. Design for dynamic stability.
4. Design for environmental stability.
5. Design for damage tolerance.

The design process is guided by certain considerations and optimization criteria. A major consideration in aerospace applications is weight savings. In commercial applications, such as in the automotive and sports industries, an additional consideration is cost competitiveness with more conventional materials and processes. For critical applications of all types, in addition to the above requirements, the need is added for assurance of quality, durability, and reliability over the lifetime of the structure. The various design objectives, structural and material requirements, and typical materials and applications are summarized in Table 7.4.

Applications such as aircraft control surfaces, underground and underwater vessels, thin skins in compression, and sport products such as bicycles and tennis rackets require small deflections under working loads, high buckling loads, and low weight. The design objective in these cases is high stiffness and low weight,

Table 7.4 Design Methodology for Structural Composite Materials

Design objective	Structural requirements	Material requirements	Typical materials	Typical applications
Design for stiffness	Small deflections High buckling loads Low weight	High stiffness fibers in sandwich or hybrid laminates for high flexural rigidity	Carbon, graphite, boron, and Kevlar fiber composites	Aircraft control surfaces Underground, underwater vessels Thin skins in compression Sporting goods
Design for strength	High load capacity (static, dynamic) Low weight	High lamina strength with high degree of fiber utilization High stiffness-strength ratio High interlaminar strength	Carbon, Kevlar (in tension), and S-glass fiber composites	Pressure vessels Trusses (tension members) Thin skins in sandwich panels, ribs, joints
Design for dynamic control and stability	Long fatigue life High resonance frequency Vibration control Low centrifugal forces	High strength fibers Fibers with high specific stiffness (E/ρ) Ductile matrices or hybridization with high damping layers	Carbon, graphite fibers Thermoplastic matrices Interleaving with thermoplastic layers	Engine components Aircraft components Helicopter rotor blades Flywheels
Design for environmental stability	High dimensional stability under extreme environmental fluctuations	Low coefficients of thermal and moisture expansion Laminate design for hygrothermoelastic isotropy High stiffness anisotropic fibers	Carbon, graphite, and Kevlar fiber composites	Radar and space antennae Space mirrors Solar reflectors
Design for damage tolerance	High impact resistance High compressive strength after impact damage Resistance to damage growth	High fracture toughness (intra- and interlaminar) Energy absorbent interlayers Woven laminates	Tough epoxy matrices, thermoplastic matrices Interleaving	Ballistic armour Bullet-proof vests Impact resistant structures

i.e., high specific stiffness. This requires selection of high stiffness fibers in general, such as boron, carbon, graphite, and aramid. For high flexural stiffness, a sandwich construction with composite skins and low density aluminum honeycomb or foam cores, or a hybrid laminate with high stiffness outer layers and low stiffness (and low cost) inner layers, are recommended.

Pressure vessels, truss members in tension, thin composite skins in sandwich panels, ribs, and joints require high load carrying capacity (static and dynamic) combined with low weight. A design for strength is indicated. This requires the selection of high strength fibers, such as carbon, aramid (in tension only), and S-glass. The optimum laminate is one with a high efficiency ratio, ρ_L , and a high degree of fiber strength utilization.²² The first one, as defined in Eq. (7.34), is the ratio of the FPF to the ultimate laminate failure strength and depends primarily on the material system. The second one is measured by the ratio of the longitudinal stress reached in the lamina at FPF to its longitudinal strength and depends primarily on the laminate layup for a given loading. Both of these are related to the principal modulus and principal strength ratios of the lamina²²

$$\rho_E = \frac{E_1}{E_2} \quad (7.54)$$

$$\rho_F = \frac{F_1}{F_2} \quad (7.55)$$

and their ratio, lamina stiffness-strength ratio,

$$\rho_{EF} = \frac{\rho_E}{\rho_F} = \frac{E_1/E_2}{F_1/F_2} \quad (7.56)$$

The ideal laminate, optimized for strength and minimum weight, would be one with high fiber strength utilization and with all its layers failing simultaneously in their fiber direction.

In addition to in-plane stresses, interlaminar stresses must be taken into account. Thus, in addition to meeting the requirements for in-plane loading, selected laminates must maintain high interlaminar normal and shear strengths and high interlaminar fracture toughness. These properties are primarily dominated by the matrix characteristics.

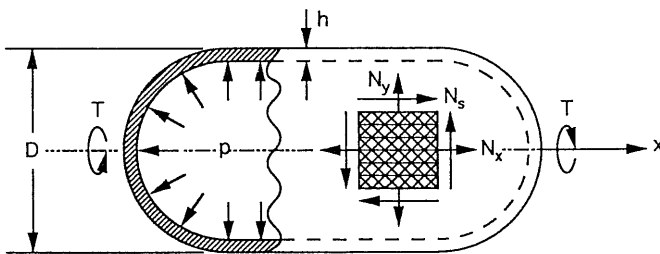
Rotating structural components such as turbine blades, rotor blades, and flywheels, as well as components subjected to vibration and flutter, must have long fatigue life, low mass, high stiffness, high damping, and high resonance frequency and allow for better vibration control. A design for dynamic control and stability is required. This is achieved by using high strength fibers (carbon), fibers with high specific modulus (E/ρ), tough matrices, and hybridization with soft and high damping interlayers.

Space structures (radar and space antennae, mirrors, and solar reflectors) require high dimensional stability under extreme environmental fluctuations. A design for environmental stability is indicated, requiring high modulus thermally anisotropic fibers, such as carbon, graphite (GY-70), and aramid in laminates designed for thermoelastic and hygroelastic isotropic behavior (see Sect. 6.11).

Impact-resistant structures such as ballistic armour and bullet-proof vests require materials and laminates with high impact resistance and high compressive strength after impact. A design for damage tolerance is recommended. Aramid (Kevlar) fibers and tough matrices such as thermoplastics and laminates with selective interleaving can provide the necessary impact and damage propagation resistance.

7.16 Illustration of Design Process: Design of a Pressure Vessel

A thin-wall cylindrical pressure vessel is loaded by internal pressure, p , and an external torque, T , as shown in Figure 7.31. It is also given that the vessel operates at room temperature and dry conditions and that curing residual stresses can be neglected. It is required to find the optimum composite material system and lay-up to achieve minimum weight and to compare it with an aluminum reference vessel. The allowable safety factor is $S_{all} = 2.0$. The design of the aluminum vessel is based on the von Mises criterion with a material yield strength $\sigma_{yp} = 242 \text{ MPa}$ (35 ksi). The density of aluminum is given as $\rho = 2.8 \text{ g/cm}^3$ (0.101 lb/in.^3). The design of the composite laminate is based on the Tsai–Wu failure criterion for FPF. Balanced symmetric laminates are to be



$$\begin{aligned}
 p &= 2.07 \text{ MPa (300 psi)} \\
 T &= 283 \text{ kN}\cdot\text{m (2.5}\times 10^6 \text{ lb}\cdot\text{in.)} \\
 D &= 89 \text{ cm (35 in.)}
 \end{aligned}$$

Fig. 7.31 Thin wall cylindrical pressure vessel under internal pressure and torque loading.

investigated of three candidate composite materials, S-glass/epoxy, Kevlar/epoxy, and carbon/epoxy.

The unit loads acting on an element of the cylindrical shell along the axial and hoop directions (x and y) are obtained as follows:

$$\begin{aligned} N_x &= \bar{\sigma}_x h = \frac{pD}{4} \\ N_y &= \bar{\sigma}_y h = \frac{pD}{2} \\ N_s &= \bar{\tau}_s h \cong \frac{2T}{\pi D^2} \end{aligned} \quad (7.57)$$

Substituting the data given, we obtain

$$\begin{aligned} N_x &= 460 \text{ kN/m} \\ N_y &= 920 \text{ kN/m} \\ N_s &= 228 \text{ kN/m} \end{aligned} \quad (7.58)$$

The principal stresses for the above state of stress are

$$\begin{aligned} \bar{\sigma}_1 &= \frac{1,014}{h} \quad (\text{in kPa}) \\ \bar{\sigma}_2 &= \frac{366}{h} \quad (\text{in kPa}) \\ \bar{\sigma}_3 &= 0 \end{aligned} \quad (7.59)$$

7.16.1 Aluminum Reference Vessel

According to the von Mises yield criterion,

$$[(\bar{\sigma}_1 - \bar{\sigma}_2)^2 + (\bar{\sigma}_2 - \bar{\sigma}_3)^2 + (\bar{\sigma}_3 - \bar{\sigma}_1)^2]^{1/2} = \frac{\sqrt{2} \sigma_{yp}}{S_{all}} \quad (7.60)$$

Substituting the numerical results of Eq. (7.59) and the given data in Eq. (7.60), we obtain

$$\frac{1,257}{h_a} = 170,766 \text{ kPa}$$

which yields

$$h_a = 7.36 \text{ mm (0.290 in.)}$$

7.16.2 Crossply $[0_m/90_n]_s$ Laminates

Since the ratio of hoop stress to axial stress is 2:1, a similar ratio between the number of 90° and 0° layers, or $n:m$, is selected initially. The process of optimization for a given type of lay-up is best carried out by using one of several available computer programs.²³⁻²⁵

Initially the safety factor S_f is obtained for a $[0/90_2]_s$ lay-up of the material investigated, the thickness of which is $h_o = 6t$, i.e., six ply thicknesses. The multiples m_i and n_i for the initial trial are obtained as

$$m_i = \frac{n_i}{2} \cong \frac{S_{all}}{S_f} = \frac{2}{S_f} \quad (7.61)$$

and the allowable laminate thickness is $h_a = 6mt = mh_o$. The optimum choice from the point of view of weight is reached by trying different values of m and n around the initial guess until the sum ($m + n$) is minimized. Results for the three materials investigated are tabulated in Table 7.5.

Table 7.5 Optimum $[0_m/90_n]_s$ Lay-up for Three Composite Materials

	S-glass/epoxy	Kevlar/epoxy	Carbon/epoxy
Ply thickness, (t , mm)	0.165	0.127	0.127
m	10	12	10
n	28	29	22
Safety factor, S_f	2.017	2.029	2.043
Optimum lay-up*	$[0_{10}/90_{28}]_s$	$[0_{12}/90_{29}]_s$	$[0_{10}/90_{22}]_s$
Laminate thickness (h , mm)	12.54	10.41	8.13

*To reduce interlaminar stresses, it is recommended to interdisperse the plies and minimize layer thicknesses as discussed before in Section 5.11.

7.16.3 Angle-Ply $[\pm\theta]_{ns}$ Laminates

Optimization of this type of laminate involves only one variable, θ . This is accomplished by selecting the angle θ for the basic laminate unit $[\pm\theta]_s$ that maximizes the safety factor S_f . The basic laminate unit has a thickness $h_o = 4t$, i.e., four ply thicknesses. Then the allowable laminate thickness is

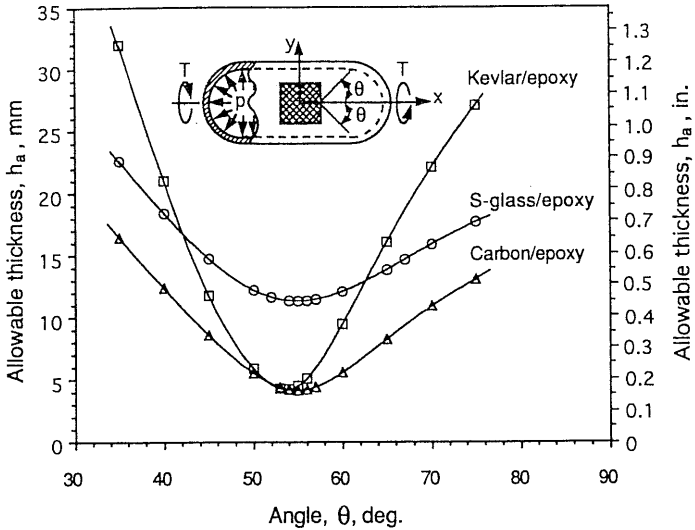


Fig. 7.32 Effect of lamination angle on allowable thickness of $[\pm\theta]_{ns}$ angle-ply laminate in pressure vessel.

$$h_a = \frac{S_{all}}{S_f} h_o = \frac{8t}{S_f} \quad (7.62)$$

To find the optimum θ , the allowable (required) thickness h_a was computed and plotted versus θ for the three materials considered in Figure 7.32. It is interesting to note that the optimum angle θ corresponding to the minimum allowable thickness is almost the same for all three materials, 55° for S-glass/epoxy and carbon/epoxy and 54° for Kevlar/epoxy. Although the three materials considered have comparable strength properties, the variation of the required minimum laminate thickness with angle θ is very different for each material (Fig. 7.32). The curve for Kevlar/epoxy shows the sharpest variation with angle, but it has roughly the same minimum ($h_a = 4.24$ mm) as that of carbon/epoxy ($h_a = 4.14$ mm). Although the strength properties of S-glass/epoxy are higher than those of Kevlar/epoxy, the required minimum thickness for S-glass/epoxy is much higher ($h_a = 11.37$ mm). The results above are tabulated in Table 7.6.

The results obtained illustrate the important fact that the structural efficiency of a laminate is not only a function of the lamina strength properties but also of its lamina stiffnesses and their ratios (degree of anisotropy) as discussed before in Eqs. (7.54) to (7.56).²²

Table 7.6 Optimum $[\pm\theta]_{ns}$ Lay-up for Three Composite Materials

	S-glass/epoxy	Kevlar/epoxy	Carbon/epoxy
Ply thickness (t , mm)	0.165	0.127	0.127
Optimum θ (degrees)	55	54	55
Safety factor (S_f , $n = 1$)	0.116	0.240	0.246
Minimum allowable thickness (h_a , mm)	11.37	4.24	4.14
Optimum lay-up	$[\pm 55]_{18s}$	$[\pm 54]_{9s}$	$[\pm 55]_{9s}$
Safety factor (S_f , optimum lay-up)	2.091	2.125	2.209
Laminate thickness (h , mm, optimum lay-up)	11.89	4.57	4.57

7.16.4 $[90/\pm\theta]_{ns}$ Laminates

Optimization of the $[90/\pm\theta]_{ns}$ laminate again involves only one variable, θ . Safety factors are computed for the basic laminate unit $[90/\pm\theta]_s$ for the three materials investigated for various values of θ . The minimum allowable thickness for each laminate is obtained as

$$h_a = \frac{S_{all}}{S_f} \cdot h_o = \frac{12t}{S_f} \quad (7.63)$$

Results are tabulated in Table 7.7. The optimum angle θ was found to be 48° , 45° , and 45° for the S-glass/epoxy, Kevlar/epoxy, and carbon/epoxy materials, respectively. Again, as in the previous case of the $[\pm\theta]_{ns}$ laminates, the

Table 7.7 Optimum $[90/\pm\theta]_{ns}$ Lay-up for Three Composite Materials

	S-glass/epoxy	Kevlar/epoxy	Carbon/epoxy
Ply thickness (t , mm)	0.165	0.127	0.127
Optimum θ (degrees)	48	45	45
Safety factor (S_f , $n = 1$)	0.155	0.240	0.335
Minimum allowable thickness (h_a , mm)	12.76	6.35	4.55
Optimum lay-up	$[90/\pm 48]_{13s}$	$[90/\pm 45]_{9s}$	$[90/\pm 45]_{6s}$
Safety factor (S_f , optimum lay-up)	2.018	2.159	2.012
Laminate thickness (h , mm, optimum lay-up)	12.87	6.86	4.57

Table 7.8 Optimum $[0/\pm\theta]_{ns}$ Lay-up for Three Composite Materials

	S-glass/epoxy	Kevlar/epoxy	Carbon/epoxy
Ply thickness (t , mm)	0.165	0.127	0.127
Optimum θ (degrees)	75	67	67
Safety factor (S_f , $n = 1$)	0.157	0.254	0.293
Minimum allowable thickness (h_a , mm)	12.61	6.01	5.21
Optimum lay-up	$[0/\pm 75]_{13s}$	$[0/\pm 67]_{8s}$	$[0/\pm 67]_{7s}$
Safety factor, (S_f , optimum lay-up)	2.041	2.029	2.047
Laminate thickness (h , mm, optimum lay-up)	12.87	6.10	5.33

Kevlar/epoxy material appears much better than the S-glass/epoxy because of its higher laminate efficiency and fiber utilization factors.

7.16.5 $[0/\pm\theta]_{ns}$ Laminates

Optimization of the $[0/\pm\theta]_{ns}$ laminate is similar to the previous one. Safety factors and minimum allowable laminate thicknesses are calculated as before in Eq. (7.63). Results are tabulated in Table 7.8. The optimum angle θ was found to be 75° , 67° , and 67° for the S-glass/epoxy, Kevlar/epoxy, and carbon/epoxy materials, respectively. As in the previous case the required laminate thickness for the S-glass/epoxy material was approximately double that for the other two materials.

7.16.6 Quasi-Isotropic $[0/\pm 45/90]_{ns}$ Laminates

Quasi-isotropic $[0/\pm 45/90]_{ns}$ laminates are investigated for reference purposes. Safety factors are calculated for the basic unit ($n = 1$) and allowable thicknesses computed as before

$$h_a = \frac{S_{all}}{S_f} h_o = \frac{16t}{S_f} \quad (7.64)$$

Results are tabulated in Table 7.9. As can be seen, this is the least efficient lay-up for all three materials.

7.16.7 Summary and Comparison of Results

Results of the optimum lay-ups for the three composite materials considered and the relative weight savings compared with an aluminum pressure vessel are

Table 7.9 Optimum $[0/\pm 45/90]_{ns}$ Lay-up for Three Composite Materials

	S-glass/epoxy	Kevlar/epoxy	Carbon/epoxy
Safety factor ($S_f, n = 1$)	0.181	0.257	0.361
Minimum allowable thickness (h_a, mm)	14.59	7.91	5.63
Minimum n	12	8	6
Optimum lay-up	$[0/\pm 45/90]_{12s}$	$[0/\pm 45/90]_{8s}$	$[0/\pm 45/90]_{6s}$
Safety factor ($S_f, \text{optimum lay-up}$)	2.173	2.055	2.169
Laminate thickness ($h, \text{mm, optimum lay-up}$)	15.84	8.13	6.10

summarized in Table 7.10. The optimum lay-up for all three materials is the angle-ply $[\pm\theta]_{ns}$ lay-up. Given the fixed ply thicknesses for the materials, total laminate thicknesses were obtained that resulted in safety factors slightly higher than the allowable one ($S_{all} = 2.0$). Both, the Kevlar/epoxy and carbon/epoxy materials resulted in the same laminate thickness, which is less than half of the required one for the S-glass/epoxy material. The relative weight savings compared with the aluminum reference pressure vessel were calculated as follows:

$$\text{Weight savings} = \frac{\Delta W}{W} = \frac{W_{al} - W_{comp}}{W_{al}}$$

or

$$\frac{\Delta W}{W} = 1 - \frac{\rho_{comp} h_{comp}}{\rho_{al} h_{al}} \tag{7.65}$$

Table 7.10 Summary of Optimum Lay-Ups for Three Composite Materials

	S-glass/epoxy	Kevlar/epoxy	Carbon/epoxy
Density ($\rho, \text{g/cm}^3$)	2.0	1.4	1.6
Ply thickness (t, mm)	0.165	0.127	0.127
Optimum lay-up	$[\pm 55]_{18s}$	$[\pm 54]_{9s}$	$[\pm 55]_{9s}$
Safety factor ($S_f, \text{optimum lay-up}$)	2.091	2.125	2.209
Laminate thickness ($h, \text{mm, optimum lay-up}$)	11.89	4.57	4.57
Weight savings compared to aluminum ($\Delta W/W, \%$)	-15.4	69.0	64.5

As shown in Table 7.10, there are weight savings of 69% and 64.5% in the Kevlar/epoxy and carbon/epoxy designs, but a weight increase of 15.4% in the S-glass/epoxy design.

7.17 Ranking of Composite Laminates

The results above are summarized in bar-graph form in Figure 7.33. Here the different composite laminate options are ranked according to their weight per unit wall area. A clear trend is observed that is common for the three material systems considered, i.e., minimum weight for $[\pm\theta]_{ns}$ angle-ply configurations with $\theta \cong 55^\circ$ and significantly higher weights for crossply $[0_m/90_n]_s$ and quasi-isotropic $[0/\pm 45/90]_{ns}$ lay-ups.

The design procedure illustrated before can be very time consuming if all potential lay-ups are examined for each material system considered. Based on this illustration and prior experience, a shortened ranking procedure is recommended:

1. Select a material system and determine the best lay-up for this system to achieve minimum weight.
2. Compare different material systems for this lay-up.
3. Select the material system giving the lowest weight in step (2) and repeat step (1) for this material system.

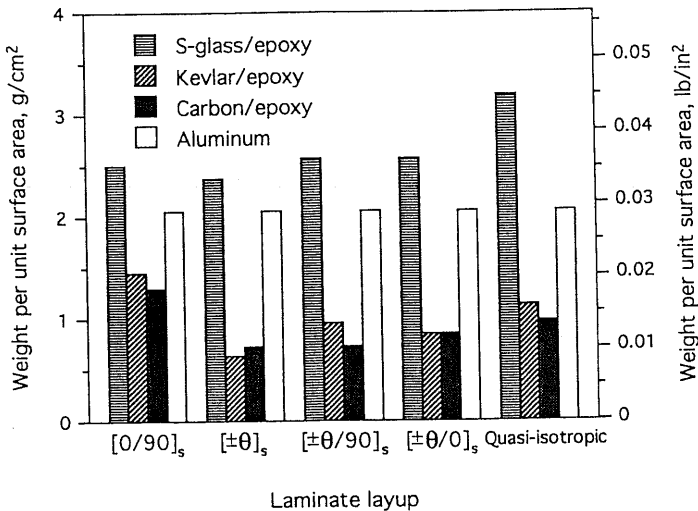


Fig. 7.33 Ranking of different material systems and laminate lay-ups according to weight for pressure vessel design example.

It should be pointed out that the above sizing and ranking procedure is based on FPF, which is considered a conservative approach for many applications. A less conservative approach may be based on ULF, using higher allowable safety factors. In this approach, the carbon/epoxy system with its high ultimate strength would rank much more favorably than the other candidate material systems. This is related to the lower structural efficiency ratio, ϕ_L , of this carbon/epoxy, which means that its fiber strength is not utilized efficiently at FPF (see Tables 7.2 and 7.3). At ULF, which in many cases is related to fiber failure, the carbon/epoxy laminate is significantly stronger.

References

1. K. L. Reifsnider and J. E. Masters, "An Investigation of Cumulative Damage Development in Quasi-Isotropic Graphite/Epoxy Laminates," in *Damage in Composite Materials*, ASTM STP 775, K. L. Reifsnider, Ed., American Society for Testing and Materials, Philadelphia, 1982, pp. 40–62.
2. A. L. Highsmith and K. L. Reifsnider, "Stiffness Reduction Mechanisms in Composite Laminates," in *Damage in Composite Materials*, ASTM SPT 775, K. L. Reifsnider, Ed., American Society for Testing and Materials, Philadelphia, 1982, pp. 103–117.
3. R. Talreja, "Transverse Cracking and Stiffness Reduction in Composite Laminates," *J. Composite Materials*, Vol. 19, 1985, pp. 355–375.
4. Z. Hashin, "Analysis of Cracked Laminates: A Variational Approach," *Mech. Materials*, Vol. 4, 1985, pp. 121–136.
5. S. L. Ogin, P. A. Smith, and P. W. R. Beaumont, "Matrix Cracking and Stiffness Reduction During the Fatigue of [0/90] GFRP Laminates," *Composite Sci. Technol.*, Vol. 22, 1985, pp. 23–31.
6. N. Laws and G. J. Dvorak, "Progressive Transverse Cracking in Composite Laminates," *J. Composite Materials*, Vol. 22, 1988, pp. 900–916.
7. S. G. Lim and C. S. Hong, "Prediction of Transverse Cracking and Stiffness Reduction in Cross-Ply Laminated Composites," *J. Composite Materials*, Vol. 23, 1989, pp. 695–713.
8. J.-W. Lee and I. M. Daniel, "Progressive Transverse Cracking of Crossply Composite Laminates," *J. Composite Materials*, Vol. 24, 1990, pp. 1225–1243.
9. C.-L. Tsai, I. M. Daniel, and J.-W. Lee, "Progressive Matrix Cracking of Crossply Composite Laminates Under Biaxial Loading," in *Microcracking-Induced Damage in Composites*, G. J. Dvorak and D. C. Lagoudas, Eds., Proc. of ASME 1990 Winter Annual Meeting, AMD-Vol. 111, MD-Vol. 22, American Soc. of Mechanical Engineers, New York, 1990, pp. 9–18.
10. I. M. Daniel and C.-L. Tsai, "Analytical/Experimental Study of Cracking in Composite Laminates Under Biaxial Loading," *Composites Engineering*, Vol. 1, 1991, pp. 355–362.
11. C.-L. Tsai and I. M. Daniel, "The Behavior of Cracked Crossply Laminates Under Shear Loading," *Int. J. Solids Structures*, Vol. 29, 1992, pp. 3251–3267.
12. J. C. Halpin, "Structure-Property Relations and Reliability Concepts," *J. Composite Materials*, Vol. 6, 1972, pp. 208–231.

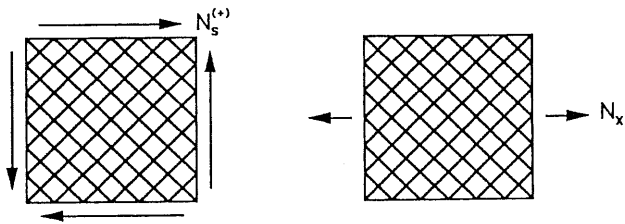
13. R. B. Pipes and N. J. Pagano, "Interlaminar Stresses in Composite Laminates Under Uniform Axial Extension," *J. Composite Materials*, Vol. 4, 1970, pp. 538-548.
14. R. B. Pipes and I. M. Daniel, "Moiré Analysis of the Interlaminar Shear Edge Effect in Laminated Composites," *J. Composite Materials*, Vol. 5, 1971, pp. 255-259.
15. N. J. Pagano and R. B. Pipes, "The Influence of Stacking Sequence on Laminate Strength," *J. Composite Materials*, Vol. 5, 1971, pp. 50-57.
16. I. M. Daniel, R. E. Rowlands, and J. B. Whiteside, "Effects of Material and Stacking Sequence on Behavior of Composite Plates With Holes," *Exp. Mech.*, Vol. 14, 1974, pp. 1-9.
17. N. J. Pagano, "Automated System for Composite Analysis (ASCA)," Software Package, Ad Tech Systems, Inc., Dayton, OH, 1991.
18. K. Hellan, *Introduction to Fracture Mechanics*, McGraw-Hill Book Co., New York, 1984.
19. J. M. Whitney, C. E. Browning, and W. Hoogsteden, "A Double Cantilever Beam Test for Characterizing Mode I Delamination of Composite Materials," *J. Reinforced Plastics Composites* Vol. 1, 1982, pp. 297-313.
20. A. A. Aliyu and I. M. Daniel, "Effects of Strain Rate on Delamination Fracture Toughness of Graphite/Epoxy," in *Delamination and Debonding of Materials*, ASTM STP 876, W. S. Johnson, Ed., American Society for Testing and Materials, Philadelphia, 1985, pp. 336-348.
21. N. Sela and O. Ishai, "Interlaminar Fracture Toughness and Toughening of Laminated Composite Materials: A Review," *Composites*, Vol. 20, 1989, pp. 423-435.
22. O. Ishai, S. Krishnamachari, and L. J. Broutman, "Structural Design Optimization of Composite Laminates," *J. Reinforced Plastics Composites*, Vol. 7, 1988, pp. 459-474.
23. O. Ishai, *Microcomputer Program for Analysis of Mechanical Behavior of Multi-material Composite Laminates*, LIN 925 PC Version, Technion, Israel Institute of Technology, Haifa, 1990.
24. S. C. Wooh and I. M. Daniel, *ICAN—Interactive Composite Analysis*, Version 1.02, Northwestern University, Evanston, IL, 1992.
25. S. W. Tsai, *Composites Design*, 4th Ed., Think Composites, Dayton, OH, 1988.

PROBLEMS

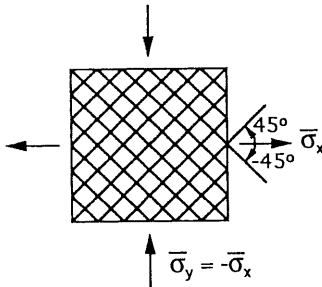
- 7.1 A $[0/90]_s$ laminate is subjected to uniaxial loading N_x . Which of the following four answers is a correct approximation of the ratio of stresses σ_2 to σ_1 in the 90° and 0° layers, respectively, before FPF?
- $\frac{\sigma_2}{\sigma_1} \cong 2 E_2/E_1$
 - $\frac{\sigma_2}{\sigma_1} \cong E_2/E_1$
 - $\frac{\sigma_2}{\sigma_1} \cong \nu_{12} E_2/E_1$
 - $\frac{\sigma_2}{\sigma_1} \cong E_2/\nu_{12} E_1$
- 7.2 Determine the FPF strength of a $[0/90]_s$ laminate under uniaxial tension or compression based on (a) the maximum stress criterion and (b) the Tsai–Wu criterion (material: AS4/3501-6 carbon/epoxy, Table 2.6).
- 7.3 Determine the axial tensile strength \bar{F}_{xt} at FPF of a $[\pm 45]_s$ laminate using the Tsai–Wu criterion. Obtain an exact expression and then an approximate one for a high stiffness–high strength composite.
- 7.4 Determine exact and approximate values for the axial tensile strength \bar{F}_{xt} at FPF of a $[\pm 45]_s$ laminate using the Tsai–Hill criterion for the following materials listed in Table 2.6:
- E-glass/epoxy
 - Kevlar/epoxy
 - Carbon/epoxy (AS4/3501-6)
- 7.5 Determine exact and approximate values for the axial compressive strength \bar{F}_{xc} at FPF of a $[\pm 45]_s$ laminate using the Tsai–Hill criterion for the following materials listed in Table 2.6:
- E-glass/epoxy
 - Kevlar/epoxy
 - Carbon/epoxy (AS4/3501-6)
- 7.6 Determine exact and approximate values for the shear strength \bar{F}_s at FPF of a $[\pm 45]_s$ laminate using the Tsai–Hill criterion for the following materials listed in Table 2.6:
- E-glass/epoxy
 - Kevlar/epoxy
 - Carbon/epoxy (AS4/3501-6)

7.7 A $[\pm 45]_{ns}$ laminate is loaded in pure shear and uniaxial tension as shown. Which one of the four following statements is wrong?

- The tensile strength \bar{F}_{xt} is primarily controlled by the lamina in-plane shear strength F_6 .
- The positive laminate shear strength $\bar{F}_s^{(+)}$ is equal to the negative shear strength $\bar{F}_s^{(-)}$.
- The tensile strength \bar{F}_{xt} is primarily controlled by the lamina transverse tensile strength F_{2t} .
- The laminate shear strength $\bar{F}_s^{(-)}$ is primarily controlled by the fiber strength.



7.8 A $[\pm 45]_{ns}$ laminate is loaded biaxially as shown. Determine the magnitude of the biaxial stress $\bar{F}_o = \bar{\sigma}_x^u$ at FPF using both the maximum stress and Tsai–Wu criteria (material: AS4/3501-6 carbon/epoxy, Table 2.6). Hint: Transform the $[\pm 45]_s$ into a $[0/90]_s$ lay-up.

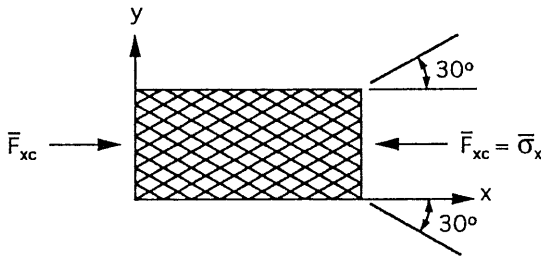


7.9 For the laminate and loading of Problem 7.8 the biaxial stress at FPF based on the maximum stress criterion is one of the following. Select correct answer.

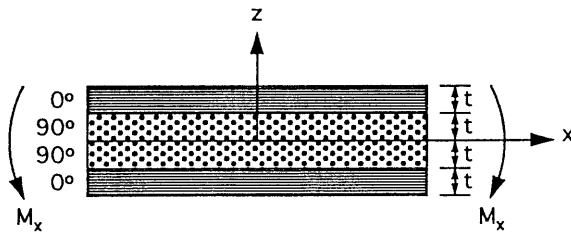
- $\bar{F}_o = F_6$
- $\bar{F}_o = F_{2c}$
- $\bar{F}_o = F_{2t}$
- $\bar{F}_o = F_{1c}$

7.10 A $[\pm 30]_s$ laminate is loaded in uniaxial compression as shown. Determine the compressive strength \bar{F}_{xc} at FPF according to the maximum strain theory for the following given properties:

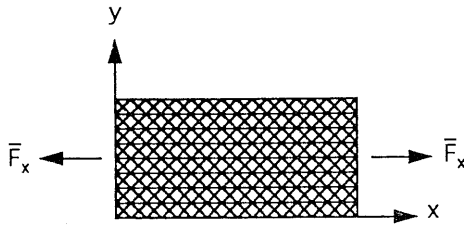
$$\begin{aligned} \epsilon_{1t}'' &= 0.015 & \epsilon_{2t}'' &= 0.006 \\ \epsilon_{1c}'' &= -0.015 & \epsilon_{2c}'' &= -0.024 \\ \gamma_6'' &= 0.015 \\ \bar{E}_x &= 61.4 \text{ GPa (8.9 Msi)} & \bar{\nu}_{xy} &= 1.2 \end{aligned}$$



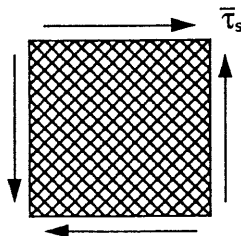
7.11 A beam of a symmetric crossply laminate $[0/90]_s$ is loaded under pure bending M_x in the 0° direction as shown. Determine the maximum σ_1 and σ_2 stresses in the top ply in terms of the lamina stiffnesses Q_{ij} , thickness t , laminate bending stiffnesses D_{ij} , and the applied moment M_x . (Note: $\epsilon_x = z\kappa_x$, $\epsilon_y = z\kappa_y$.)



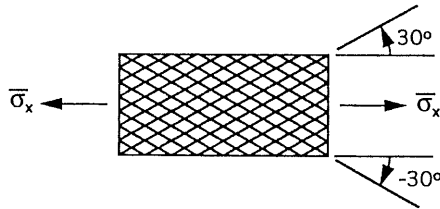
7.12 Determine the axial tensile strength \bar{F}_{xt} at FPF of a $[0/\pm 45]_s$ laminate by the Tsai–Hill criterion. Obtain exact and approximate expressions for a high strength–high stiffness composite in terms of the lamina properties, the laminate modulus \bar{E}_x and Poisson’s ratio $\bar{\nu}_{xy}$.



- 7.13 Determine exact and approximate values for the strength \bar{F}_{xt} of the above Problem 7.12 for the carbon/epoxy material AS4/3501-6 listed in Table 2.6 using the maximum stress theory. What is the prevailing failure mode? The laminate modulus is $\bar{E}_x = 64.1$ GPa (9.30 Msi) and Poisson's ratio is $\bar{\nu}_{xy} = 0.65$.
- 7.14 Determine the uniaxial tensile and compressive strengths at FPF for the $[0/90]_s$ laminate of Problem 7.2, taking into account the residual stresses due to cooldown $\Delta T = -150^\circ\text{C}$ (-270°F) during curing. Use both maximum stress and Tsai-Wu criteria. What are the failure modes in tension and compression? Thermal stresses are given as $\sigma_{2e} = -\sigma_{1e} = 39$ MPa (5.65 ksi) for both layers.
- 7.15 A $[0/90]_s$ laminate is cured at an elevated temperature and cooled down to room temperature. What is the effect of increasing the moisture concentration Δc on the FPF uniaxial laminate strength \bar{F}_x ? Neglect the effect of moisture on unidirectional lamina properties. Select the correct answer:
- Reduction in compressive strength and increase in tensile strength.
 - Increase in compressive strength and reduction in tensile strength.
 - No effect on compressive strength and increase in tensile strength.
 - Increase in both tensile and compressive strengths.
- 7.16 A $[\pm 45]_{ns}$ carbon/epoxy (AS4/3501-6) laminate is loaded under pure shear as shown. Determine the shear strength \bar{F}_s at FPF taking into account the residual stresses due to the hygrothermal loading $\Delta T = -150^\circ\text{C}$ (-270°F) and $\Delta c = 0.5\%$. Compare results based on the maximum stress and Tsai-Wu criteria and identify the failure mode.

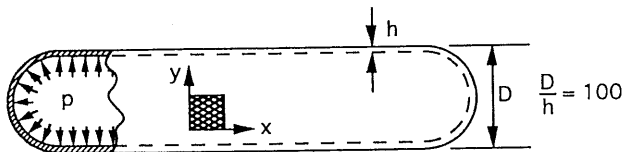


- 7.17 Determine the biaxial stress \bar{F}_o of Problem 7.8 taking into account the residual stresses due to the hygrothermal loading $\Delta T = -150^\circ\text{C}$ (-270°F) and $\Delta c = 0.5\%$.
- 7.18 A $[\pm 30]_{ns}$ angle-ply laminate is loaded under a uniaxial stress $\bar{\sigma}_x$ and a hygrothermal loading $\Delta T = -150^\circ\text{C}$ (-270°F) and $\Delta c = 0.5\%$. Determine (a) the residual stresses due to hygrothermal loading alone, (b) the mechanical stresses due to applied stress $\bar{\sigma}_x$ as a function of this stress, and (c) the axial tensile strength \bar{F}_{xt} at FPF under the combined mechanical and hygrothermal loading. Use both the maximum stress and Tsai-Wu criteria and identify the prevailing failure mode (material: AS4/3501-6 carbon/epoxy, Table 2.6).



- 7.19 Determine the axial compressive strength of the laminate of Problem 7.18 above for the same hygrothermal conditions. What is the failure mechanism in this case?
- 7.20 Determine the ultimate laminate failure tensile strength and the laminate efficiency ratio φ_L for the $[0/90]_s$ laminate of Problem 7.2, using the maximum stress criterion and total ply discount method.
- 7.21 The laminate efficiency ratio $\varphi_L = \bar{F}_{\text{FPF}}/\bar{F}_{\text{ULF}}$ (ratio of FPF to ultimate laminate failure strength) for a $[0/90]_s$ laminate is approximately equal to one of the following ratios. Select the correct one.
- $\varphi_L \cong F_{2t}/F_{1t}$
 - $\varphi_L \cong E_2 F_{2t}/E_1 F_{1t}$
 - $\varphi_L \cong \begin{pmatrix} \nu_{12} \\ \nu_{21} \end{pmatrix} \begin{pmatrix} F_{2t} \\ F_{1t} \end{pmatrix}$
 - $\varphi_L \cong \begin{pmatrix} E_2 \\ E_1 \end{pmatrix} \begin{pmatrix} F_{1t} \\ F_{2t} \end{pmatrix}$
- 7.22 Determine the FPF and ULF uniaxial tensile strengths of a $[0/90_2]_s$ carbon/epoxy laminate using the maximum stress criterion and total ply

- discount method. Plot the stress-strain curve to failure (material: AS4/3501-6 carbon/epoxy, Table 2.6).
- 7.23 For a $[0_m/90_n]_s$ carbon/epoxy (AS4/3501-6) laminate under axial tension compute the laminate efficiency factor as a function of m and n . Use the maximum stress criterion for FPF.
- 7.24 What is the effect of temperature reduction on the uniaxial tensile strength \bar{F}_{xt} of a $[\pm 45]_s$ laminate? Select correct answer based on the maximum stress criterion.
- Increase in FPF strength but no effect on ULF strength.
 - Reduction in FPF strength but no effect on ULF strength.
 - Increase in both FPF and ULF strengths.
 - No effect on either FPF or ULF strength.
- 7.25 A cantilever beam of a carbon/epoxy $[0/\pm 45/90]_s$ laminate is subjected to a concentrated force P at the free end (see Fig. 7.27). Determine the force P at initiation of delamination for the properties of AS4/3501-6 carbon/epoxy listed in Table 2.6 and interlaminar shear strength $F_{zx} = 90$ MPa (13 ksi).
- 7.26 A thin-walled cylindrical pressure vessel made of a $[\pm 30]_{ns}$ carbon/epoxy laminate was cured at 180°C (356°F) and cooled down to 30°C (86°F). Subsequently, it absorbed 0.5% moisture by volume and was loaded by an internal pressure $p = 1$ MPa (145 psi). Calculate (a) the stresses in each layer due to the pressure loading only, (b) the stresses due to the hygrothermal loading only, and (c) the total stresses due to the combined mechanical and hygrothermal loading (material: AS4/3501-6 carbon/epoxy, Table 2.6).



The $[\pm 30]_s$ laminate properties are

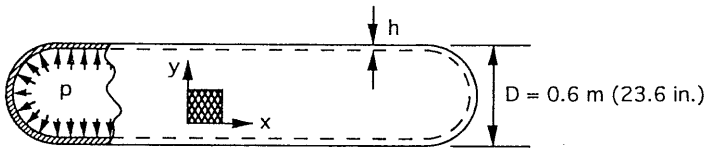
$$\bar{E}_x = 57.8 \text{ GPa (8.38 Msi)} \quad \bar{\alpha}_x = -3.47 \times 10^{-6}/^\circ\text{C} \quad (-1.93 \times 10^{-6}/^\circ\text{F})$$

$$\bar{E}_y = 14.0 \text{ GPa (2.03 Msi)} \quad \bar{\alpha}_y = 13.28 \times 10^{-6}/^\circ\text{C} \quad (7.38 \times 10^{-6}/^\circ\text{F})$$

$$\bar{G}_{xy} = 29.5 \text{ GPa (4.27 Msi)} \quad \bar{\beta}_x = -7.50 \times 10^{-3}$$

$$\bar{\nu}_{xy} = 1.18 \quad \bar{\beta}_y = 0.107$$

- 7.27 For the pressure vessel of Problem 7.26 calculate the allowable pressure for FPF based on the maximum stress criterion and an allowable safety factor $S_{all} = 2.0$. What is the expected failure mode?
- 7.28 A thin-wall cylindrical pressure vessel made of a $[\pm 60]_{ns}$ S-glass/epoxy laminate was cured at 100°C (212°F), cooled down to 20°C (68°F), and stored in a dry environment. For a design internal pressure of $p = 1.2 \text{ MPa}$ (174 psi), calculate the required wall thickness (h_a) for an allowable safety factor $S_{all} = 2.0$. Use both the maximum stress and Tsai–Wu failure criteria for first ply failure and compare results (material: S-glass/epoxy, Table 2.6).



Measured laminate thermal strains due to cooldown:

$$\bar{\epsilon}_x^T = -1.45 \times 10^{-3}, \quad \bar{\epsilon}_y^T = -3.47 \times 10^{-4}, \quad \bar{\gamma}_s^T = 0$$

Mechanical (pressure) strains given for $h = 1.0 \text{ mm}$ (0.039 in.):

$$\bar{\epsilon}_x^M = 8.25 \times 10^{-3}, \quad \bar{\epsilon}_y^M = 1 \times 10^{-2}, \quad \bar{\gamma}_s^M = 0$$

- 7.29 A thin-wall cylindrical pressure vessel of the same overall dimensions as that of Problem 7.28 is made of a $[\pm 60]_{ns}$ carbon/epoxy laminate (AS4/3501-6, Table 2.6). It is subjected to a hygrothermal loading $\Delta T = -150^\circ\text{C}$ (-270°F) and $\Delta c = 0.005$. For a design pressure $p = 1.2 \text{ MPa}$ (174 psi) and allowable safety factor $S_{all} = 2.0$.
- Determine the required wall thickness and compare it with the corresponding thickness obtained for the S-glass/epoxy vessel of Problem 7.28. Use both the maximum stress and Tsai–Wu failure criteria.
 - Determine the required thickness for a pressure vessel of the same overall dimensions made of aluminum with a yield stress of $\sigma_{yp} = 200 \text{ MPa}$ (29 ksi) using the von Mises failure theory.
 - Compare the required thicknesses for the aluminum and carbon/epoxy vessels and calculate the weight savings of the carbon/epoxy vessel with respect to the aluminum one.

The laminate strains produced by cooldown and moisture absorption were measured as

$$\bar{\epsilon}_x^{HT} = -1.46 \times 10^{-3}$$

$$\bar{\epsilon}_y^{HT} = 4.83 \times 10^{-3}$$

$$\bar{\gamma}_s^{HT} = 0$$

Strains due to pressure loading only for a 1 mm (0.039 in.) thick vessel are given as

$$\bar{\epsilon}_x^M = 5.47 \times 10^{-3}$$

$$\bar{\epsilon}_y^M = 2.54 \times 10^{-3}$$

$$\bar{\gamma}_s^M = 0$$

The densities of aluminum and carbon/epoxy are 2.8 g/cm^3 and 1.60 g/cm^3 , respectively.

Chapter 8

Experimental Methods for Characterization and Testing of Composite Materials

8.1 Introduction

The analysis and design of composite structures requires the input of reliable experimental data. As in the case of analysis, experimental characterization can be done on several scales; micromechanical, macromechanical, and structural. Testing of composite materials has three major objectives: determination of basic properties of the unidirectional lamina for use as an input in structural design and analysis; investigation and verification of analytical predictions of mechanical behavior; and independent experimental study of material and structural behavior for specific geometries and loading conditions. Under these general objectives, specific types and applications of testing include the following:

1. Characterization of constituent materials, i.e., fiber, matrix and interphase, for use in micromechanics analyses. Knowing these properties, one can predict, in principle, the behavior of the lamina and hence of laminates and structures.
2. Characterization of basic unidirectional lamina which forms the basic building block of all laminated structures.
3. Determination of interlaminar properties.
4. Material behavior under special conditions of loading, e.g., multiaxial, fatigue, creep, impact, and high rate loading.
5. Experimental stress and failure analysis of composite laminates and structures, especially those involving geometric discontinuities such as free edges, cutouts, joints, and ply dropoffs.
6. Assessment of structural integrity by means of nondestructive testing.

A variety of experimental methods are used for the various applications above. Most of these deal with measurement of deformation or strains. Experimental methods for composite materials are much more complex than for isotropic materials and require significant modifications. Test methods and extensive related references have been reviewed in the literature.¹⁻⁵

8.2 Characterization of Constituent Materials

Constituent properties are important for understanding and predicting the macroscopic behavior of composite materials by means of micromechanics. These include physical and mechanical properties of fibers and matrices.

8.2.1 Fiber Characterization

The most commonly measured properties of fibers are the longitudinal modulus, tensile strength, and ultimate tensile strain.⁵⁻⁸ A mechanical test method is described in ASTM specification D3379-75.⁵ The method is recommended for fibers with an elastic modulus greater than 21 GPa (3 Msi). The filament is mounted along the centerline of a slotted paper tab and axial alignment is accomplished without damaging the fiber (Fig. 8.1). After the specimen is mounted in the test machine the paper tab is cut to allow for filament elongation. Specimens of various gage lengths are tested to failure at a constant crosshead rate, and the load-displacement curve is obtained.

To determine the elastic modulus of the fiber, the measured load displacement curves must be corrected for the system compliance. The measured or "apparent" compliance is assumed to be the sum of the fiber and system compliances.

$$C_a = \frac{u}{P} = \frac{u_f}{P} + \frac{u_s}{P} = \frac{1}{AE_{1f}} + \frac{u_s}{P} \quad (8.1)$$

where

C_a = Apparent compliance

u = Crosshead displacement

u_f = Actual fiber elongation

u_s = Displacement due to system compliance

P = Load

l = Fiber gage length

E_{1f} = Longitudinal fiber modulus

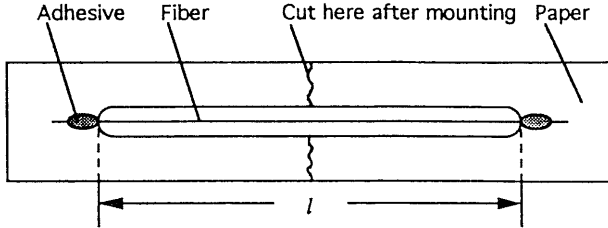


Fig. 8.1 Fiber specimen mounted on slotted paper tab (ASTM D3379-75).⁵

The system compliance, $C_s = u_s/P$, is obtained as the zero gage length intercept by plotting the apparent compliance obtained from the various specimens versus fiber length. A typical compliance versus gage length curve is shown in Figure 8.2 for a silicon carbide fiber. The fiber modulus is determined from Eq. (8.1). The cross sectional area A is determined by measurements of representative fiber cross sections under the microscope.

The fiber strength is simply obtained from the maximum load as

$$F_{ft} = \frac{P_{\max}}{A} \tag{8.2}$$

The ultimate strain is obtained from the maximum fiber elongation

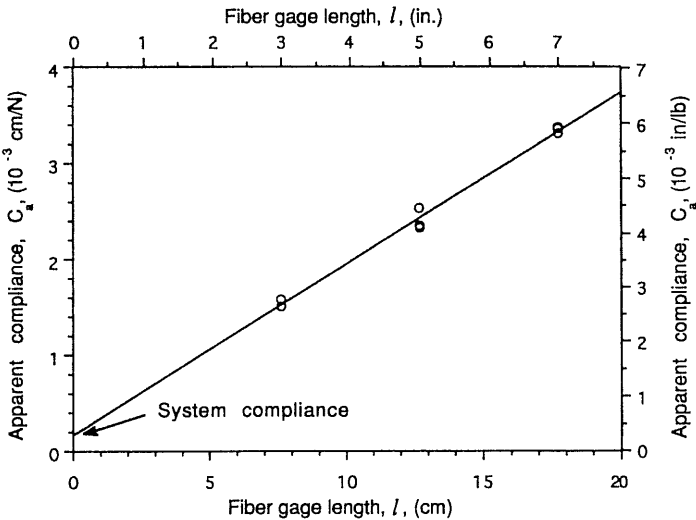


Fig. 8.2 Apparent compliance versus fiber gage length for silicon carbide fiber (SCS-2, Textron Specialty Materials).

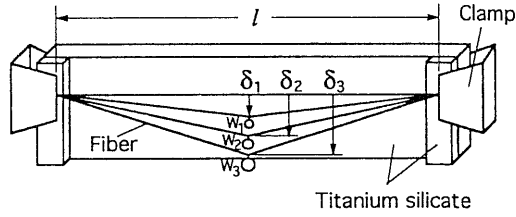


Fig. 8.3 Fixture for stiffness measurement of fiber.⁸

$$\epsilon_{ft}^{\mu} = \frac{(u_f)_{\max}}{l} \quad (8.3)$$

A new mechanical test method suitable for measuring fiber stiffness at various temperatures has been described recently.⁸ A length of fiber is fixed at the ends on a plate of very low thermal expansion material (Fig. 8.3). Titanium silicate, having a coefficient of thermal expansion of $0.3 \times 10^{-7}/^{\circ}\text{C}$ ($1.7 \times 10^{-8}/^{\circ}\text{F}$), can be used as the support plate. The fiber is fixed to the titanium silicate plate over a span length l with the plate held vertically inside a furnace. Small incremental weights, W_1 , W_2 , W_3 , etc., are suspended at the center of the fiber and the corresponding deflections, δ_1 , δ_2 , δ_3 , etc., are recorded photographically. The equilibrium condition yields the following relation

$$\frac{W_i}{2} = \frac{\sigma A \delta_i}{\sqrt{(l/2)^2 + \delta_i^2}} \quad (8.4)$$

where

σ = Stress in fiber

A = Cross sectional area of fiber

From geometric considerations we obtain the following relation for the strain in the fiber

$$\epsilon = \epsilon_0 + \epsilon_w = \epsilon_0 + \frac{2\sqrt{(l/2)^2 + \delta_i^2} - l}{l} \quad (8.5)$$

where

ϵ_0 = Initial strain

ϵ_w = Strain produced by deflection under weight

The stress obtained from Eq. 8.4 is plotted versus the weight-induced strain obtained from Eq. (8.5), i.e.,

$$\sigma = \frac{W_i}{2A} \sqrt{(l/2\delta_i)^2 + 1} \tag{8.6}$$

versus

$$\epsilon_w = \sqrt{1 + (2\delta_i/l)^2} - 1 \tag{8.7}$$

A typical stress-strain curve for an intermediate modulus carbon fiber (IM6, Hercules, Inc.) is shown in Figure 8.4.

In addition to mechanical properties, thermal properties of fibers are very important. Relatively few results are available for coefficients of thermal expansion of fibers.^{8,9} In a recently described method for measurement of the coefficient of thermal expansion, a length of fiber is fixed loosely at the ends of a titanium silicate plate (Fig. 8.5).⁸ A constant weight W is suspended at the center

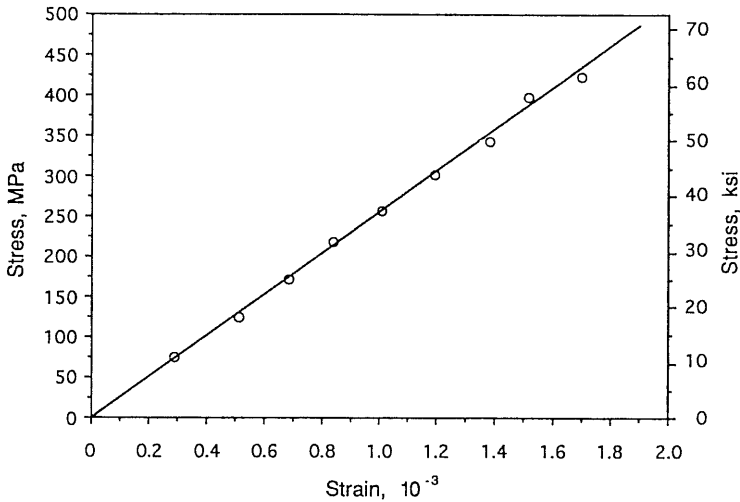


Fig. 8.4 Stress-strain curve of carbon fiber (IM6, Hercules, Inc.).⁸

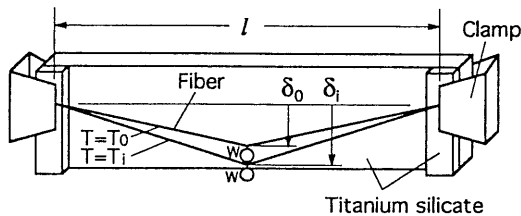


Fig. 8.5 Deflection of fiber with fixed ends under suspended load at various temperatures.⁸

and the deflection δ_0 at room temperature T_0 is measured optically. The stretched length of the fiber under these conditions (T_0 and W) is

$$L_0 = 2\sqrt{(l/2)^2 + \delta_0^2} \quad (8.8)$$

The temperature is then raised to the next step T_i and the corresponding deflection δ_i is measured. The new fiber length is then

$$L_i = 2\sqrt{(l/2)^2 (1 + \alpha_r \Delta T)^2 + \delta_i^2} \quad (8.9)$$

where

α_r = Coefficient of thermal expansion of mounting plate material (titanium silicate)

$\Delta T = T_i - T_0$ = temperature difference

The difference in fiber length $L_i - L_0$ is due primarily to the thermal expansion and in a smaller part to any possible changes in the fiber stiffness with temperature. For small loads and fibers of high modulus not varying much with temperature, the mechanical changes are negligible. Then, the thermal strain is given by

$$\epsilon^T \cong \frac{L_i - L_0}{L_0} \cong \sqrt{\frac{(1 + \alpha_r \Delta T)^2 + (2\delta_i/l)^2}{1 + (2\delta_0/l)^2}} - 1 \quad (8.10)$$

The thermal strain obtained from Eq. 8.10 is plotted versus temperature, and the coefficient of thermal expansion at any temperature is the slope of the curve at that temperature. A typical thermal strain versus temperature curve for a silicon carbide fiber (Nicalon, Nippon Carbon Co.) is shown in Figure 8.6. The technique described here was modified for stiff large diameter fibers, such as boron and silicon carbide (SCS type) filaments.⁸

In addition to the longitudinal properties above, there is need to measure other properties of fibers, especially anisotropic fibers such as carbon and aramid (Kevlar) fibers. Properties of interest are the longitudinal shear modulus, G_{12f} , longitudinal Poisson's ratio, ν_{12f} , transverse modulus, E_{2f} , and transverse coefficient of thermal expansion α_{2f} . Methods for direct measurement of these properties are not available in general or are currently under development.

8.2.2 Matrix Characterization

Polymeric matrices are characterized by casting the material in sheet form and cutting and testing coupons from these sheets. The specimens are usually pris-

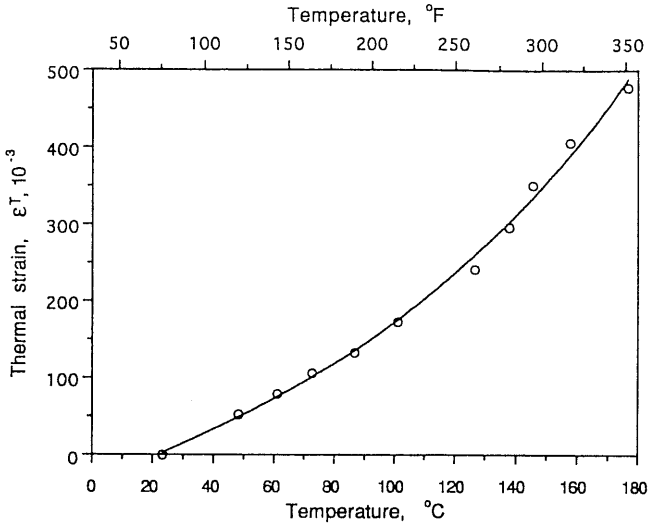


Fig. 8.6 Thermal strain versus temperature for silicon carbide fiber (Nicalon NLM-202, Nippon Carbon Co.).⁸

matic or dogbone in shape. The suggested geometry and dimensions depend on the sheet thickness and are described in ASTM specifications D638-89, D638-89M, and D882-83.^{5,10} Strains are measured by means of strain gages or an extensometer. When the specimen thickness is small and/or the material stiffness is low, optical techniques are recommended. Uniaxial tensile tests to failure yield the following properties: Young's modulus, E_m , Poisson's ratio, ν_m , tensile strength F_{mT} , and ultimate tensile strain, ϵ_{mT}^u . In the above, it is assumed that the matrix is isotropic and that its bulk properties are the same as the in situ properties in the composite.

Metallic matrices are characterized in a similar way by testing coupons of the matrix metal. However, the bulk properties of the metal or metallic alloy may be appreciably different from the in situ properties of the matrix within the composite due to the heat treatment during the fabrication process and interactions with the fibers. In such cases, it is important to identify the condition of the matrix within the composite and to characterize a bulk material of similar properties. For example, in the fabrication of silicon carbide/aluminum composites (such as SCS-2/6061-Al), the matrix within the composite after processing is considered equivalent to bulk aluminum of T4 temper.

Ceramic matrices can also be tested in bulk form to obtain elastic properties. However, strength and failure characteristics are not the same as those of the ceramic matrix within the composite. These properties can be obtained indirectly by testing the composite material.

8.3 Physical Characterization of Composite Materials

Physical characterization of composites includes the determination of density, fiber volume ratio, void volume ratio, coefficients of thermal expansion, coefficients of moisture expansion, and heat conduction coefficients.

8.3.1 Density

The procedure for measuring the density of a composite material is the same as that used for any other solid and is based on ASTM specification D792-86.⁵ The procedure consists of the following steps:

1. Weigh specimen in air to the nearest 0.1 mg.
2. Attach specimen to analytical balance with a thin wire and weigh while the specimen and portion of the wire are immersed in distilled water.
3. Weigh wire alone, partially immersed up to the same point as in the previous step.

The density of the material at 23°C (73.4°F) is determined as follows:

$$\rho = \frac{a}{a + w - b} (0.9975) \quad (8.11)$$

where,

ρ = Density (in g/cm³)

a = Weight of specimen in air

b = Apparent weight of fully immersed specimen and partially immersed wire

w = Apparent weight of partially immersed wire

0.9975 = density of distilled water at 23°C (in g/cm³)

8.3.2 Fiber Volume Ratio

A variety of methods exist for determination of fiber volume ratio, an important property of a composite. When it can be confirmed that the composite material has zero or negligible (less than 1%) porosity, the fiber volume ratio can be obtained from the densities of the composite and the constituents by the following gravimetric relation:

$$V_f = \frac{\rho_c - \rho_m}{\rho_f - \rho_m} \quad (8.12)$$

where

ρ_c, ρ_m, ρ_f = Densities of composite, matrix, and fiber, respectively.

The ignition or burnout method, based on ASTM specification D2584-68 (1985), can be applied to composites having inorganic fibers in an organic matrix, such as glass/epoxy and boron/epoxy composites.⁵ A sample of the composite material is oven dried, weighed, and then heated in a crucible until the matrix is completely burnt. The residue is washed of the ashes, dried, and weighed. The fiber volume ratio is obtained as

$$V_f = \frac{W_f/\rho_f}{W_c/\rho_c} \quad (8.13)$$

where

W_c, W_f = Weight of composite and fibers, respectively.

The acid digestion method, described in ASTM specifications D3171-76 (1982) and D3553-76 (1989), is used with composites having a matrix that is soluble in some acid that does not attack the fiber.⁵ A sample of the composite material is dried and weighed. Then it is immersed in an acid solution to dissolve the matrix. The type of acid used is one that dissolves the matrix without attacking the fibers. The residue is filtered, washed, dried, and weighed, and the fiber volume ratio is determined by Eq. (8.13).

The fiber volume ratio can also be determined reliably by optical techniques based on image analysis of photomicrographs of transverse (to the fibers) cross sections of the composite. An elementary approach consists of counting the number of fiber cross sections and fractions thereof within the frame of the photomicrograph, calculating the total area of the fiber cross sections and dividing it by the total area photographed. More sophisticated image analysis techniques are also used and can determine both fiber volume ratio and void volume ratio in one operation, as will be discussed below.

8.3.3 Void Volume Ratio (Porosity)

The void volume ratio (or porosity ratio) is obtained as described in ASTM specification D2734-70 (1985).⁵ It is expressed in terms of the quantities measured in the acid digestion or ignition methods as follows:

$$V_v = 1 - \frac{W_f/\rho_f + (W_c - W_f)/\rho_m}{W_c/\rho_c} \quad (8.14)$$

In the above relation the void volume ratio, which is usually a small number, is expressed as the difference between two much larger numbers; therefore the result is very sensitive to the measurement accuracy involved.

A preferred method for determination of porosity in a composite is the image analysis method mentioned before. A photomicrograph of a cross section of a carbon/epoxy composite, for example, shows the fibers, matrix and voids as light grey, dark grey, and black, respectively (Fig. 8.7). In the image analysis procedure, the specimen cross section is viewed by a video camera, which transmits the image in digital form to the "image grabber" of a PC computer. The image is converted into a rectangular array of integers, corresponding to the digitized grey level of each picture element (pixel). The image processing board in the PC processes this digital image information and represents it in the form of a grey level histogram, such as the one shown in Figure 8.8. This histogram summarizes the grey level content of the image. It shows for each grey level the number of pixels in the image that have that grey level. The three peaks of

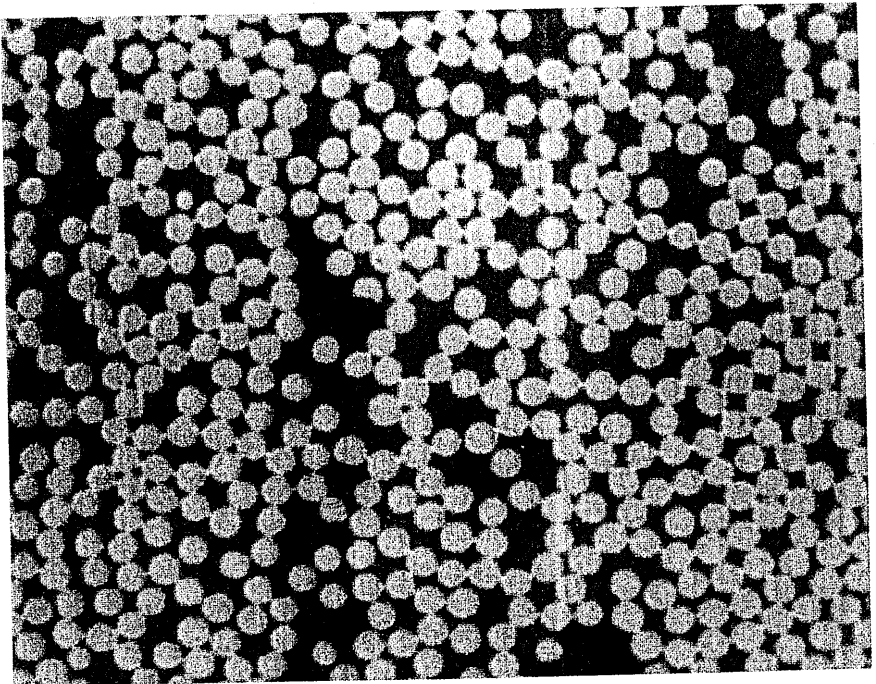


Fig. 8.7 Digitized image of carbon/epoxy cross section used for determination of fiber volume and void volume ratios.

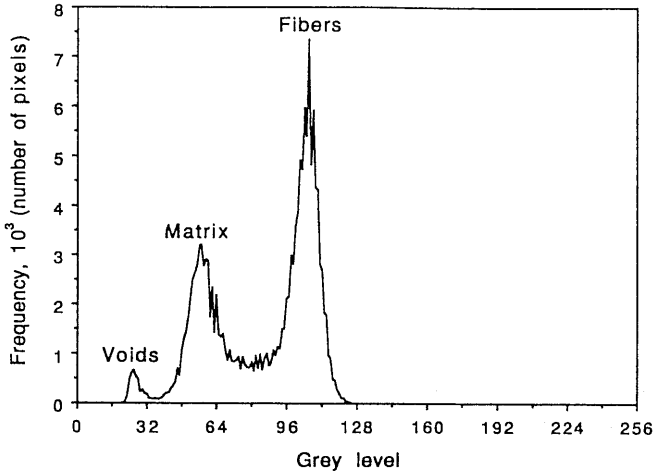


Fig. 8.8 Trimodal grey level histogram of the image of Figure 8.7.

the histogram of Figure 8.8 correspond to the porosity, matrix, and fibers. The pixels closest to the three peaks above are separated by a thresholding process into three groups corresponding to porosity, matrix, and fibers. The void volume, matrix volume, and fiber volume ratios are obtained as follows:

$$\begin{aligned}
 V_v &= \frac{n_1}{N} \\
 V_m &= \frac{n_2}{N} \\
 V_f &= \frac{n_3}{N}
 \end{aligned}
 \tag{8.15}$$

where

$$\begin{aligned}
 n_1, n_2, n_3 &= \text{Number of pixels corresponding to grey levels associated with} \\
 &\quad \text{porosity, matrix, and fibers, respectively} \\
 N &= \text{Total number of pixels}
 \end{aligned}$$

8.3.4 Coefficients of Thermal Expansion

As mentioned before in Chapter 6, the thermal behavior of a unidirectional lamina can be fully characterized in terms of the two principal coefficients of thermal expansion, α_1 and α_2 . Determination of these coefficients consists of measuring the corresponding thermal strains in a unidirectional composite speci-

men as a function of temperature. These measurements can be made by means of interferometric, dilatometric, optical noninterferometric or strain gage methods.¹¹⁻¹⁹ The interferometric method is the most sensitive one and can give results for the coefficients α_1 and α_2 with a resolution of $10^{-8}/^\circ\text{C}$. The dilatometer also gives results with high precision, but it requires one specimen for each coefficient.

Strain gages have been shown to be a practical and adequate means of measuring thermal strains in composites.¹¹⁻¹⁴ However, they must be properly compensated for the purely thermal output. One method of temperature compensation employs an identical gage bonded to a reference material of known thermal expansion exposed to the same temperature as the composite specimen.¹¹ The true thermal strain in the composite is given by

$$\epsilon_{tc} = \epsilon_{ac} - \epsilon_{ar} + \epsilon_{tr} \quad (8.16)$$

where

ϵ_{tc} = True thermal strain in composite specimen

ϵ_{ac} = Apparent strain in composite specimen

ϵ_{tr} = True thermal strain in reference specimen

ϵ_{ar} = Apparent strain in reference specimen

Reference materials used are usually ceramics of low and stable coefficient of thermal expansion, such as fused quartz ($\alpha_r = 0.7 \times 10^{-6}/^\circ\text{C}$) and titanium silicate ($\alpha_r = 0.03 \times 10^{-6}/^\circ\text{C}$). For a temperature change of ΔT , the true thermal strain in the reference material is $\alpha_r \Delta T$.

A unidirectional composite specimen is usually instrumented with two-gage rosettes to record thermal strains along the fiber (1) and transverse to the fiber (2) directions (Fig. 8.9). For better results it is preferable to use gages on both surfaces of the specimen, or even embedded gages, to correct for any possible bending of the specimen due to asymmetries or small thermal gradients through the thickness. Measured thermal strains are plotted versus temperature as shown in Figure 8.9. The slopes of these curves at any point give the coefficients of thermal expansion. Thermal strain curves for typical composites were shown in Figure 6.8 and typical results in Table 6.2.

8.3.5 Coefficients of Moisture Expansion

The hygric (moisture) behavior of a unidirectional lamina, like the thermal behavior, can be fully characterized in terms of two principal coefficients of

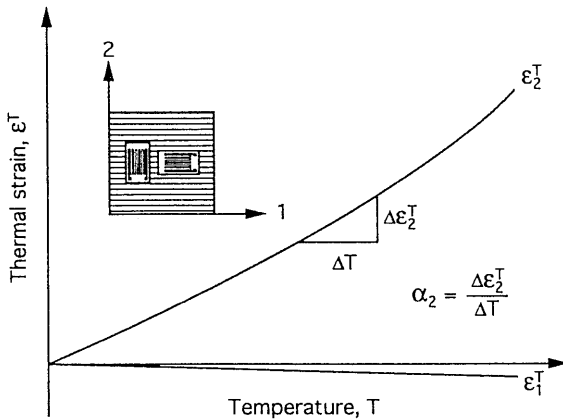


Fig. 8.9 Measurement of coefficients of thermal expansion by means of strain gages.

moisture expansion, β_1 and β_2 . Determination of these coefficients consists of measuring the principal direction strains in a unidirectional composite as a function of moisture concentration. Specimens are preconditioned by drying them in an oven at a moderately high temperature (65°C ; 150°F) for approximately two hours. Subsequently they are exposed to the moisture conditioning environment. Moisture absorption can be accomplished by immersing the specimens in a water bath inside an oven at a moderately high temperature, e.g., 50°C (120°F).

Moisture expansion or swelling has been measured by means of a micrometer or a caliper gage.^{20,21} The application of strain gages has been difficult because conventional strain gage adhesives are attacked by moisture.¹ Furthermore, the presence of the gage on the surface of the specimen may inhibit locally the process of moisture diffusion. A newer method utilizing embedded strain gages has been shown to be more reliable and consistent than previously used techniques.²² The method consists of embedding encapsulated strain gages in the midplane of the specimen. The technique results in good adhesion without the need for additional adhesive and does not cause any local disturbance in moisture diffusion, since the gage is located at a plane of symmetry.

Unidirectional specimens with and without embedded strain gages are dried (preconditioned) and then immersed in a 50°C (120°F) water bath inside an oven. The embedded gages in the immersed specimen are connected to a data logger and monitored continuously throughout the duration of conditioning. Specimens without gages exposed to the same environment are removed periodically from the water bath and weighed on an analytical balance to determine the relative weight gain, M . The average moisture concentration c representing the relative volume occupied by water is related to the weight gain as follows:

$$c = \frac{V_w}{V_c} = \frac{W_w/\rho_w}{W_c/\rho_c} = \frac{\rho_c}{\rho_w} \frac{W_w}{W_c} = \frac{\rho_c}{\rho_w} M \quad (8.17)$$

where

V_w, V_c = Volumes of water and composite, respectively

W_w, W_c = Weights of water and composite, respectively

ρ_w, ρ_c = Densities of water and composite, respectively

The measured hygric strains are plotted versus average moisture concentration c as illustrated in Figure 8.10 for a carbon/epoxy composite. The slopes of these curves yield the coefficients of moisture expansion β_1 and β_2 .

8.4 Determination of Tensile Properties of Unidirectional Lamina

Uniaxial tensile tests are conducted on unidirectional laminae to determine the following properties:

E_1, E_2 : Longitudinal and transverse Young's moduli, respectively

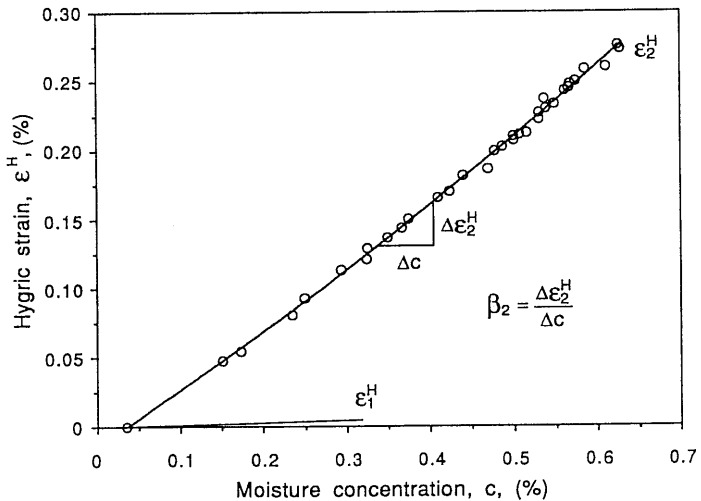


Fig. 8.10 Hygric strains in unidirectional AS4/3501-6 carbon/epoxy composite as a function of moisture concentration.

- ν_{12}, ν_{21} : Major and minor Poisson's ratios, respectively
- F_{1t}, F_{2t} : Longitudinal and transverse tensile strengths, respectively
- $\epsilon_{1t}^u, \epsilon_{2t}^u$: Longitudinal and transverse ultimate tensile strains, respectively

Tensile specimens are straight-sided coupons of constant cross section with adhesively bonded beveled glass/epoxy tabs (Fig. 8.11). More details are given in ASTM specification D3039-76 (1989).⁵ The longitudinal (0°) coupon is usually 1.27 cm (0.50 in.) wide, while the transverse (90°) coupon is 2.54 cm (1.0 in.) wide. Recommended thicknesses are 0.5 to 2.5 mm (0.020 to 0.100 in.),

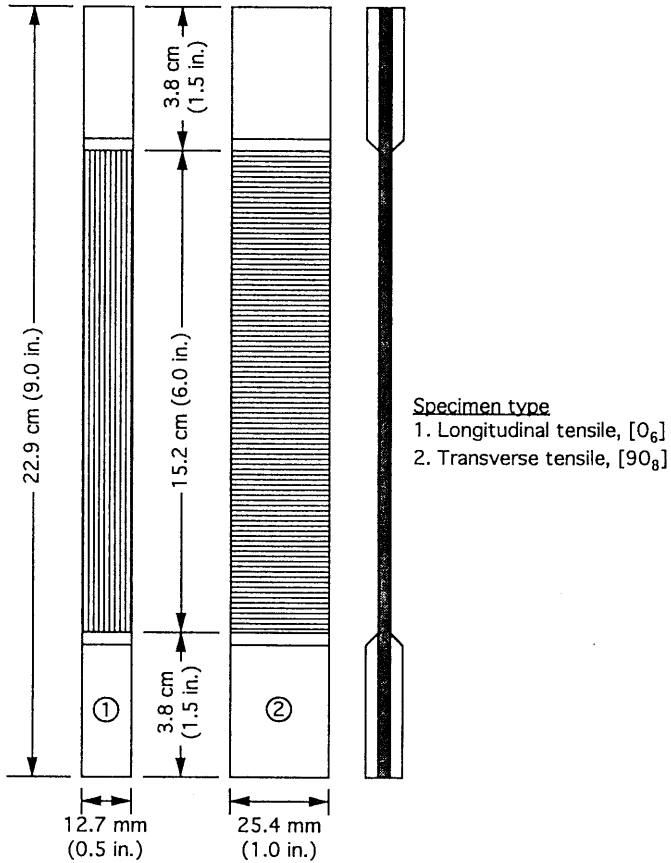


Fig. 8.11 Specimen geometries for determination of tensile properties of unidirectional lamina.

usually six plies for the longitudinal specimen and at least eight plies for the transverse one. Both specimens have an overall length of 22.9 cm (9.0 in.) and a gage length of 15.2 cm (6.0 in.). The specimens are loaded to failure under uniaxial tensile loading. A continuous record of load and deformation is obtained by an appropriate digital data acquisition system. Axial and transverse strains are obtained by means of a pair of two-gage rosettes mounted on both sides of the specimen. In some cases when the transverse strain is not needed for determination of Poisson's ratio, the axial deformation alone is recorded with an extensometer mounted on the specimen. Typical stress-strain curves for 0° and 90° carbon/epoxy specimens are shown in Figures 8.12 and 8.13. Results obtained from these curves are shown in the figures as well as in Table 2.6. Typical fractures of unidirectional tensile coupons were shown in Figures 4.6 and 4.18. Failure of the 0° specimens consists of fiber fractures, matrix splitting, and fiber pullout. The latter mechanism is much more pronounced in the "brooming" failure pattern of glass/epoxy. Transverse (90°) specimens fail in a brittle manner by matrix tensile failure between fibers.

Sometimes the unidirectional material to be characterized is prepared in thin-wall tubular form, following the same fabrication procedure used for tubular structures. Rings approximately 2.54 cm (1.0 in.) wide are machined from a thin-wall composite cylinder. They are instrumented on the outer surface with strain gages along the axial and hoop directions. They are mounted in a specially designed fixture and loaded to failure under internal pressure (Fig. 8.14). The rings are thus subjected to uniaxial hoop stress equivalent to the axial stress in a flat coupon. The hoop stress σ_θ is obtained from the internal pressure p as

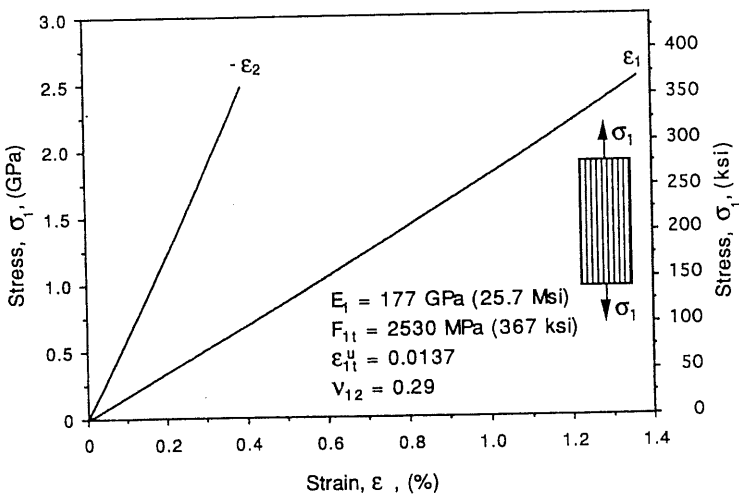


Fig. 8.12 Stress-strain curves for $[0_6]$ carbon/epoxy specimen under uniaxial tensile loading (IM6G/3501-6).

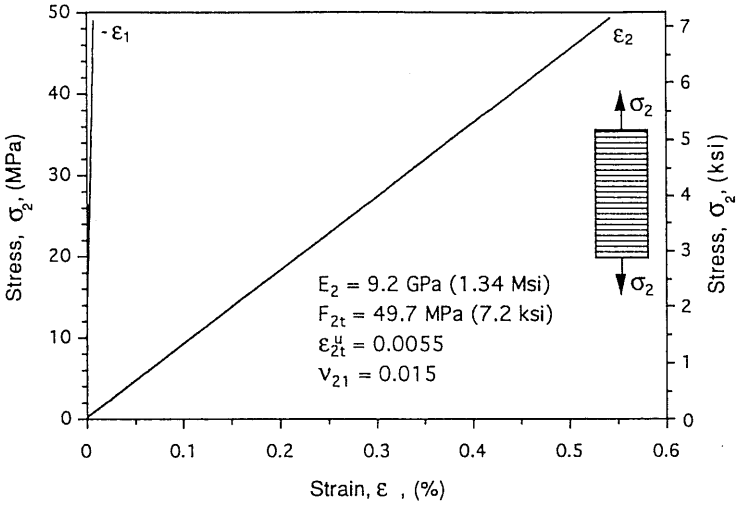


Fig. 8.13 Stress-strain curves for $[90_8]$ carbon/epoxy specimen under uniaxial tensile loading (IM6G/3501-6).

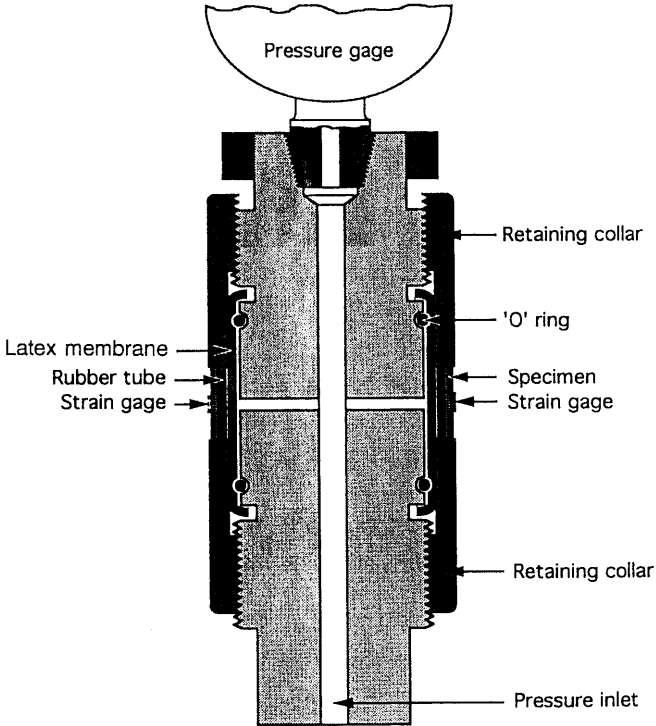


Fig. 8.14 Sketch of fixture for subjecting composite ring specimen to uniform tensile hoop stress.

$$\sigma_{\theta} = \frac{p\bar{r}}{h} \quad (8.18)$$

where \bar{r} is the mean radius and h the wall thickness. A record is obtained of the pressure and strain gage signals up to failure and stress-strain curves similar to those of Figures 8.12 and 8.13 are obtained.

8.5 Determination of Compressive Properties of Unidirectional Lamina

Compression testing of composites is one of the most difficult types of testing because of the tendency for premature failure due to crushing or buckling. Over the years, many test methods have been developed and used, incorporating a variety of specimen designs and loading fixtures. These methods have been reviewed elsewhere.¹

Compression test methods can be classified into three broad categories. In the first one (type I) specimens with a very short but unsupported gage length are used. One of these, the so-called Celanese test, makes use of coupon specimens, 14.1 cm (5.5 in.) long, 15 to 20 plies thick, and 0.64 cm (0.25 in.) wide as described in ASTM D-3410-87.⁵ The coupons are tabbed with long tapered glass/epoxy tabs, leaving a gage section 1.27 cm (0.5 in.) long. Load is introduced through friction by means of split conical collet grips, which fit into matching sleeves that in turn fit into a snugly fitting cylindrical shell. One major disadvantage of this fixture is that it requires a perfect cone-to-cone contact. This contact is not normally achieved due to small variations in tab thickness. Instead, contact can be limited to two lines on opposite sides of the specimen. This unstable condition causes a lateral shift in the grips, which then produces high frictional forces in the enveloping cylinder. This situation can result in erroneously high values for the stiffness and compressive strength.

The IITRI test method represents a modification of the method above.²³ The conical grips are replaced with trapezoidal wedges. This eliminates the problem of line contact, since surface-to-surface contact can be attained at all positions of the wedges. Furthermore, it permits precompression of the specimen tabs to prevent slippage in the early stages of loading. The lateral alignment of the fixture top and bottom halves is assured by a guidance system consisting of two parallel roller bushings. The specimen, grips, and fixture assembly are illustrated in Figure 8.15. Strains are measured by means of strain gages mounted on both sides of the specimen to verify that it fails in compression and not by buckling. This is the case when strain readings from both faces of the specimen are nearly the same up to failure. Typical results obtained with this fixture for a carbon/epoxy material are plotted in Figures 8.16 and 8.17.

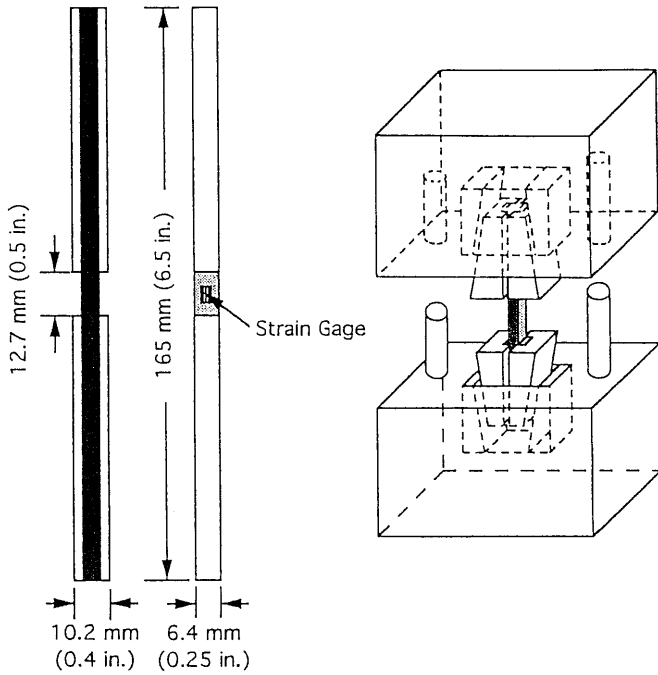


Fig. 8.15 IITRI compression test specimen and fixture.

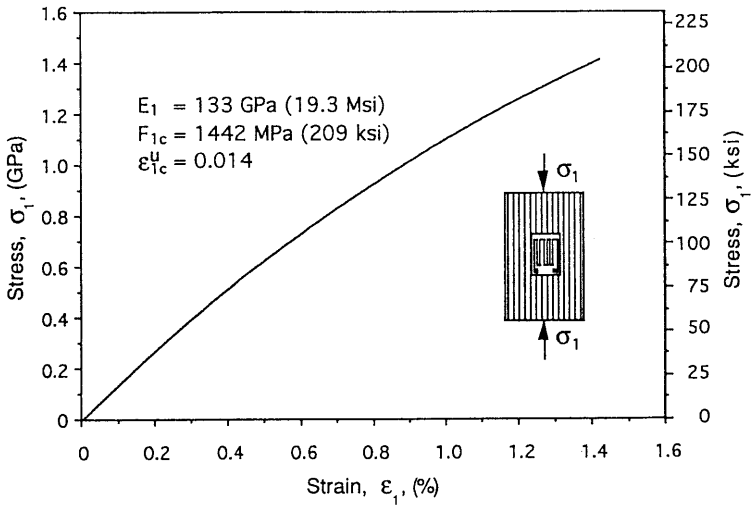


Fig. 8.16 Stress–strain curve for $[0_{16}]$ carbon/epoxy specimen under uniaxial compressive loading (AS4/3501-6).

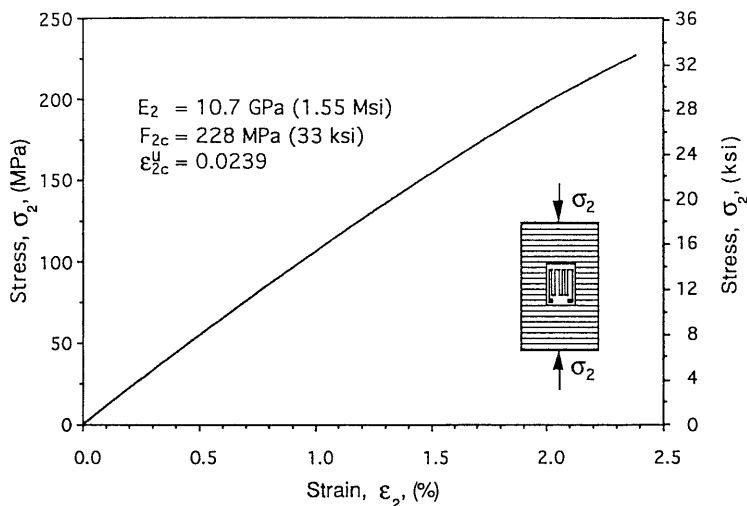


Fig. 8.17 Stress–strain curve for $[90_{16}]$ carbon/epoxy specimen under uniaxial compressive loading (AS4/3501-6).

In the second category of test methods (type II), a relatively long, fully supported specimen is used. The test specimen is similar to the tensile coupon discussed before but slightly shorter and with longer tabs. The fixture provides contact support over the entire gage length of the specimen. The type II tests yield data similar to those obtained by the type I tests, except in the case of 0° specimens, for which they give consistently low values. This may be due to some premature buckling despite the lateral support.

In the third category of compression test methods (type III) the composite laminate is bonded to a honeycomb core that provides the required lateral support. Sandwich specimens can be tested in direct edgewise compression or in pure bending.

In the first case two composite coupons are bonded to a honeycomb block as described in ASTM standard C364-61 (1988).⁵ The specimen has a rectangular cross section with a width of the order of 50 mm (2 in.) (Fig. 8.18). The unsupported length should be limited to prevent buckling and should not exceed twelve times the total specimen thickness (ASTM C364-61).⁵ The loaded ends are reinforced with a potting compound, such as epoxy syntactic foam, which fills the honeycomb cells at the ends. The ends are fitted inside grooved cylindrical rods that are loaded between two metal plates. It is very important to machine the loaded surfaces parallel to each other and to ensure that the loading surfaces of the testing machine are parallel. Results are very critically dependent on the parallelism of the loaded surfaces, and for this reason this type of test is not widely used.

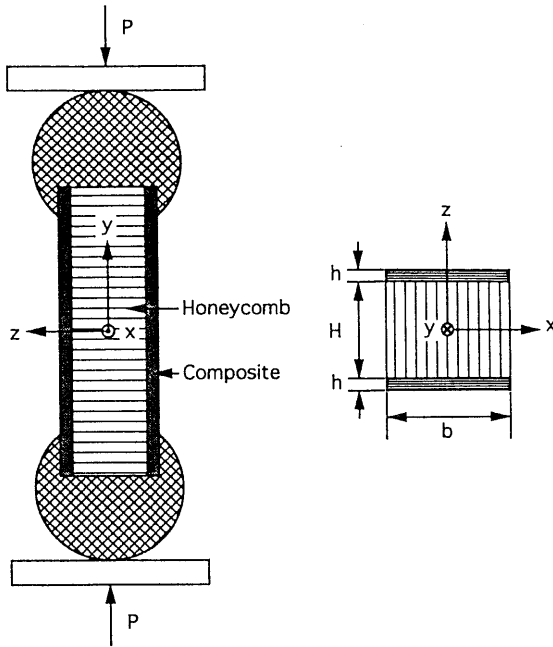


Fig. 8.18 Sandwich column specimen for direct compression testing of composites.

The sandwich flexure specimen consists of a honeycomb core with a composite skin or facing sheet bonded on the top (compressive) side and a metal sheet bonded on the bottom (tensile) side (Fig. 8.19). The beam is loaded in four point bending at two quarter-span points, which subjects the top composite skin to nearly uniform compression as described in ASTM standard C393-62 (1988).⁵ The overall beam is 56 cm (22 in.) long and 2.54 cm (1 in.) wide; the honeycomb core is 3.8 cm (1.5 in.) deep, and the thicknesses of the composite

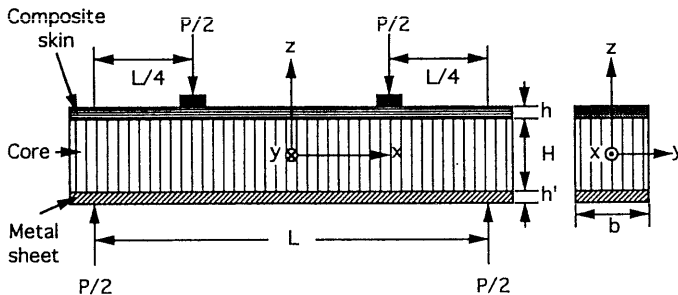


Fig. 8.19 Sandwich beam specimen for compression testing of composites.

and metal faces are adjusted to ensure compressive failure in the top face. This is ensured when

$$L/h \geq 4 F_{xc}/F_{cs} \quad (8.19)$$

where

L = Span length

h = Composite facing thickness

F_{xc} = Compressive strength of composite facing

F_{cs} = Allowable core shear stress

If the beam is not long enough, core shear failure may occur instead of composite compressive failure.

The beam is loaded through hard rubber pads on the top face or loading blocks embedded in the honeycomb core next to the metal sheet to prevent local crushing. Strains are measured by means of strain gages mounted on the composite facing. The center deflection can also be monitored with a deflectometer. The stress in the composite facing is determined by assuming uniform deformation in the face sheets and neglecting the bending stresses in the core, i.e.

$$\bar{\sigma}_x = \frac{N_x}{h} = \frac{PL}{4bh(2H + h + h')} \quad (8.20)$$

The elastic properties are obtained from the strain readings as

$$E_x = \frac{\bar{\sigma}_x}{\epsilon_x} = \frac{PL}{4bh \epsilon_x (2H + h + h')} \quad (8.21)$$

$$\nu_{xy} = - \frac{\epsilon_y}{\epsilon_x} \quad (8.22)$$

Results obtained from sandwich beam tests tend to be higher than those obtained by the other methods discussed, probably because of the restraint produced by the honeycomb and the biaxial state of stress induced in the composite facing.

8.6 Determination of Shear Properties of Unidirectional Lamina

Full characterization of a unidirectional composite requires the determination of lamina properties under in-plane shear parallel to the fibers, i.e., shear modulus, G_{12} , shear strength, F_6 , and ultimate shear strain γ_6^u . There are four generally accepted test methods for determination of these properties: (1) the $[\pm 45]_{ns}$ coupon test, (2) the 10° off-axis test, (3) the rail shear test, and (4) the torsion test.

The first test method utilizes an 8-ply $[\pm 45]_{2s}$ coupon of the same dimensions as the 90° unidirectional tensile coupon discussed before (Fig. 8.20).²⁴ The test procedure is described in ASTM standard D3518-76 (1982).⁵ When

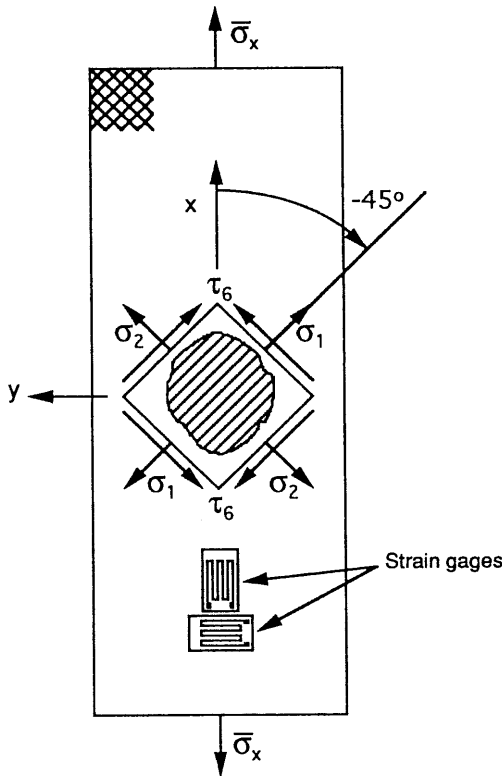


Fig. 8.20 $[\pm 45]_{ns}$ angle-ply specimen under uniaxial tension for the determination of in-plane lamina shear properties.

this coupon is subjected to a uniaxial tensile stress, $\bar{\sigma}_x$, the stresses acting on a lamina element shown are

$$\begin{aligned}\sigma_1 &= \frac{\bar{\sigma}_x}{2} + \tau_{xy} \\ \sigma_2 &= \frac{\bar{\sigma}_x}{2} - \tau_{xy} \\ \tau_6 &= \frac{\bar{\sigma}_x}{2}\end{aligned}\tag{8.23}$$

where τ_{xy} is the in-plane shear stress generated because of the shear coupling mismatch (see Figs. 7.19 and 7.20). The in-plane lamina strains are

$$\epsilon_1 = \epsilon_2 = \frac{\bar{\epsilon}_x + \bar{\epsilon}_y}{2}\tag{8.24}$$

$$\gamma_6 = \bar{\epsilon}_x - \bar{\epsilon}_y\tag{8.25}$$

where $\bar{\epsilon}_x$ and $\bar{\epsilon}_y$ are the axial and transverse strains in the coupon measured with two-gage rosettes. This in-plane (or intralaminar) shear modulus of the unidirectional lamina is obtained from the initial slope of the τ_6 vs. γ_6 curve as

$$G_{12} = \frac{\bar{\sigma}_x}{2(\bar{\epsilon}_x - \bar{\epsilon}_y)}\tag{8.26}$$

This value of the modulus is not affected by the edge effects present in this specimen or by the biaxial state of stress existing in the lamina.

Equation (8.26) can be rewritten in the following form (by dividing numerator and denominator by $\bar{\epsilon}_x$):

$$G_{12} = \frac{\bar{E}_x}{2(1 + \bar{\nu}_{xy})}\tag{8.27}$$

Thus the lamina shear modulus G_{12} can be obtained in terms of the axial modulus \bar{E}_x and Poisson's ratio $\bar{\nu}_{xy}$ of the $[\pm 45]_{ns}$ laminate (see Sample Problems 5.3 and 5.5 and Problem 5.14).

The above method tends to overestimate the in-plane shear strength of the lamina because of the constraint imposed on the lamina by the adjacent plies. In estimating this strength the method does not take into account edge effects or the influence of the other stress components σ_1 and σ_2 on the lamina (see Sample Problem 7.1). A typical shear stress versus shear strain curve obtained from a $[\pm 45]_{2s}$ carbon/epoxy coupon is shown in Figure 8.21.

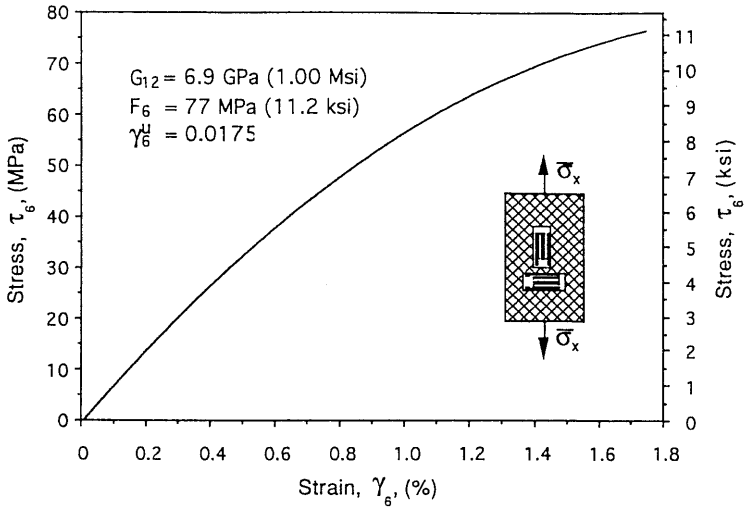


Fig. 8.21 Shear stress versus shear strain in $[\pm 45]_{2s}$ carbon/epoxy specimen under uniaxial tensile loading (AS4/3501-6).

The second test method is the 10° off-axis test.^{12,25} The 10° angle is chosen to minimize the effects of longitudinal and transverse stress components σ_1 and σ_2 on the shear response. The specimen is a 6-ply unidirectional coupon with the fibers oriented at 10° with the loading axis, 1.27 cm (0.5 in.) wide and approximately 23 cm (9 in.) long. It is tabbed with tapered tabs and instrumented with a two-gage rosette on each side of the test section. The two gages A and B of the rosette are oriented at 45° and -45° with the fiber direction as shown in Figure 8.22. The algebraic difference of the strain readings of gages A and B gives the in-plane shear strain directly

$$\gamma_6 = \epsilon_A - \epsilon_B \tag{8.28}$$

This difference is read directly by the gage instrumentation when the two gages are connected to adjacent arms of the Wheatstone bridge.

The specimen is subjected to a uniaxial tensile stress σ_x up to failure. The intralaminar shear stress referred to the fiber coordinate system is given by

$$\tau_6 = -\sigma_x \sin\theta \cos\theta = 0.171 \sigma_x \tag{8.29}$$

where $\theta = -10^\circ$. The in-plane shear modulus is obtained by plotting τ_6 versus γ_6 and taking the initial slope of the curve. The ultimate values of τ_6 and γ_6 define the shear strength and ultimate shear strain. A typical shear stress versus shear strain curve obtained from a 10° off-axis carbon/epoxy specimen is shown in Figure 8.23. This method tends to underestimate the ultimate properties due to interaction of the transverse tensile stress across the fibers.

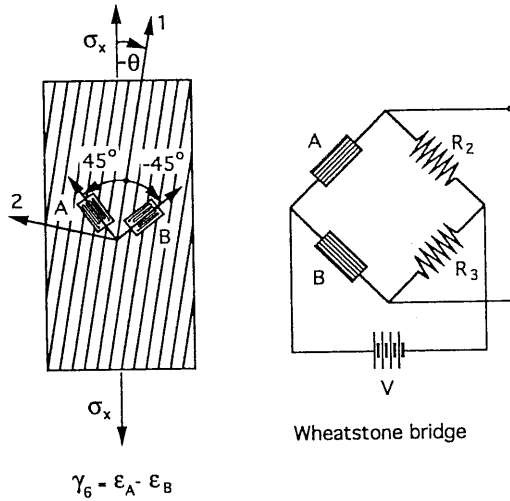


Fig. 8.22 Arrangement of strain gages on an off-axis composite specimen for measurement of in-plane shear strain.

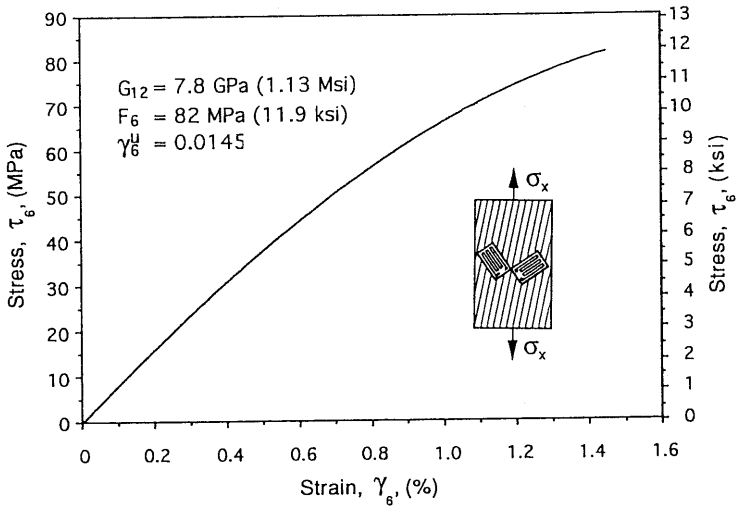


Fig. 8.23 Shear stress versus shear strain in $[10]_6$ carbon/epoxy specimen under uniaxial tensile loading (AS4/3501-6).

The third method of determining shear properties is the rail shear test, the two-rail or the three-rail test as described in ASTM standard D4255-83.⁵ In the two-rail test a rectangular composite coupon is gripped along its long edges by two pairs of rails that are loaded in a direction nearly parallel to the edges. In the three-rail test a rectangular composite coupon is clamped between three parallel pairs of rails (Fig. 8.24). The load is applied to one end of the middle

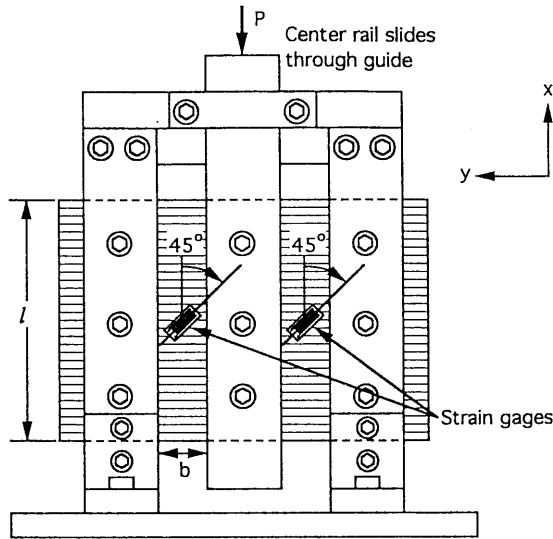


Fig. 8.24 Three-rail shear test fixture.

rails and reacted at the opposite ends of the two outer pairs of rails. The average shear stress applied to the specimen is

$$\tau_6 = \frac{P}{2lh} \tag{8.30}$$

where

P = Load

l = Specimen length along rails

h = Specimen thickness

The shear strain is obtained from a single gage placed at the center of the exposed specimen at 45° with the rail axes,

$$\gamma_6 = 2(\epsilon_x)_{\theta=45^\circ} \tag{8.31}$$

Sometimes a three-gage rectangular rosette, with additional gage elements in the x - and y -directions, is used to ensure that the state of stress at the center of the specimen is pure shear. This condition is best approximated when the aspect ratio between length and width of exposed specimen section is large, usually 8:1. The state of stress near the ends is not pure shear, and the large normal stress concentrations at the ends may result in premature failures.

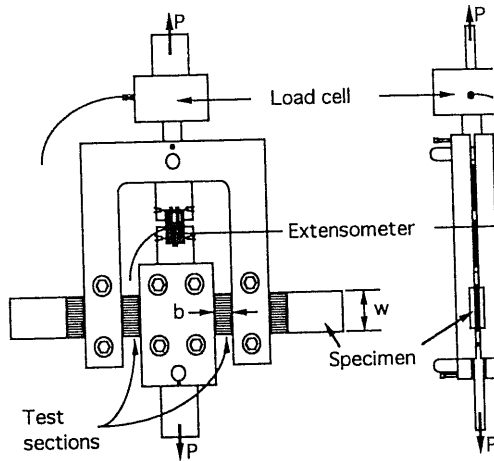


Fig. 8.25 Modified three-rail shear test fixture.^{26,27}

Modifications of the three-rail shear test have been proposed.^{26,27} The modified fixture allows the use of standard tensile coupons (Fig. 8.25). The aspect ratio of the two test sections is 2:1. The shear deformation is determined by means of an extensometer, which measures the relative motion of the central rails with respect to the outer ones. The Timoshenko beam theory is used to account for bending effects in the determination of the shear modulus:²⁷

$$G_{12} = \frac{6Pb E_1 w^2}{10\delta E_1 hw^3 - 5Pb^3} \quad (8.32)$$

where

δ = Deflection measured by extensometer

w = Specimen height (or coupon width)

h = Specimen thickness

b = Test section width

This fixture can be applied to 90° and $[0/90]_{ns}$ crossply coupons as well. In the latter case it has been used to monitor shear modulus degradation due to matrix cracking, and the results showed excellent agreement with theoretical predictions.^{26,27}

The fourth method is the torsion method utilizing a solid rod or a hollow tubular specimen subjected to torque. For a tubular unidirectional specimen with the fibers in the axial direction, the maximum shear stress and shear strain are

$$(\tau_6)_{\max} = \frac{2T r_o}{\pi (r_o^4 - r_i^4)} \quad (8.33)$$

$$(\gamma_6)_{\max} = \psi r_o = (\epsilon_x)_{\theta=45^\circ} - (\epsilon_x)_{\theta=-45^\circ} = 2 (\epsilon_x)_{\theta=45^\circ} \quad (8.34)$$

where

r_i, r_o = Inner and outer radii

ψ = Angle of twist per unit length

$(\epsilon_x)_{\theta=45^\circ}, (\epsilon_x)_{\theta=-45^\circ}$ = Surface strains at 45° and -45° with tube axis

For a thin-wall tube Eq. (8.33) can be approximated as follows:

$$(\tau_6)_{\max} \cong \frac{T}{2 \pi \bar{r}^2 h} \quad (8.35)$$

where $\bar{r} = \frac{1}{2} (r_o + r_i)$, the mean radius. For a solid rod, $r_i = 0$ in Eq. (8.33). The shear strain can be obtained by measuring the angle of twist or the strains at 45° and/or -45° with strain gages. Although the tube torsion test seems very desirable from the mechanics point of view, tubular specimens are difficult to make and load. The solid rod torsion test is less desirable because of the shear stress gradient across the section.

A new torsion method was developed recently.^{28,29} It utilizes thin rectangular coupons of the type used in tensile loading (Fig. 8.26). A closed form solution was obtained for such a specimen under torsion relating the applied torque, T , with the angle of twist, ψ , in terms of the shear moduli of the lamina. For a unidirectional laminate twisted about the longitudinal (fiber) axis, the torque-twist relationship is

$$T = \frac{1}{3} a \psi G_{12} h^3 \left(1 - \frac{\tanh \beta}{\beta} \right) \quad (8.36)$$

where

a = Specimen width

ψ = Angle of twist per unit length

h = Specimen thickness

$$\beta = \frac{a}{2h} \sqrt{10 G_{13}/G_{12}} \quad (8.37)$$

G_{12}, G_{13} = In-plane and out-of-plane shear moduli

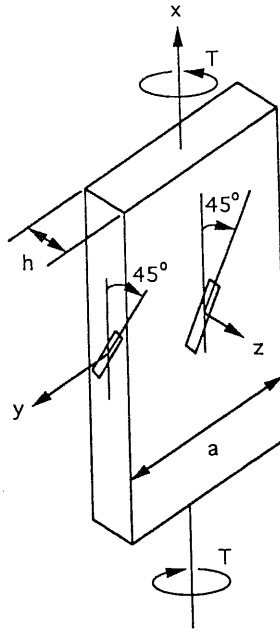


Fig. 8.26 Rectangular coupon under torsion for determination of shear moduli.²⁹

For a unidirectional laminate twisted about the transverse axis

$$\beta = \frac{a}{2h} \sqrt{10 G_{23}/G_{12}} \quad (8.38)$$

where G_{23} = Out-of-plane shear modulus in the transverse 2–3 plane.

The three shear moduli of a unidirectional composite, G_{12} , G_{13} and G_{23} , can be determined by conducting selected tests on unidirectional prismatic coupons and measuring the torque and angle of twist. A minimum of three tests would be needed, e.g., two tests with 0° specimens of different cross-sectional dimensions (h , a) and one test with a 90° specimen. However, direct measurement of the overall angle of twist does not yield accurate results because of end effects from the specimen tabs and grips. In the method described by Tsai and Daniel,²⁹ all three shear moduli can be obtained from two tests of a unidirectional material twisted about the fiber and transverse to the fiber direction. In each test the strains are measured on the face and on the edge of the coupon at 45° with the torque axis. Typical curves of applied torque versus surface and edge strains at 45° for a $[0_{32}]$ carbon/epoxy specimen are shown in Figure 8.27. Results of the complete shear modulus characterization for a carbon/epoxy material (AS4/3501-6) are

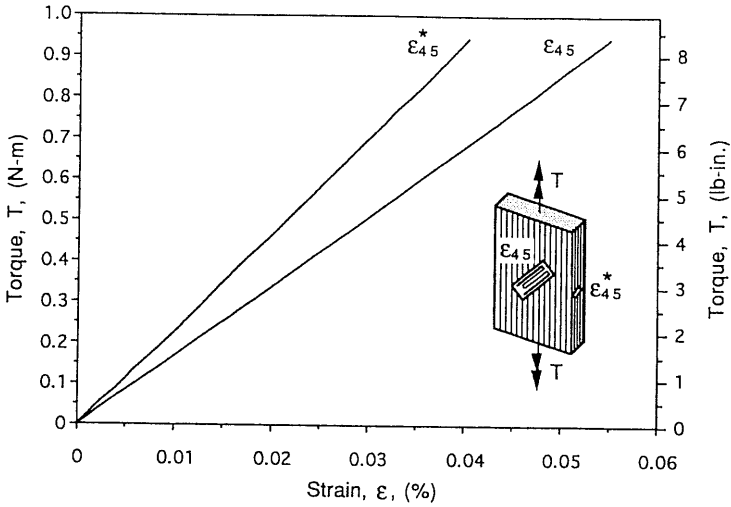


Fig. 8.27 Torque versus surface and edge strains at 45° with torque axis for [0₃₂] carbon/epoxy specimen (AS4/3501-6).²⁹

$$G_{12} = 6.90 \text{ GPa (1.00 Msi)}$$

$$G_{13} = 6.97 \text{ GPa (1.01 Msi)}$$

$$G_{23} = 3.73 \text{ GPa (0.54 Msi)}$$

Another type of shear test is based on the fact that a shear force transmitted through a section between two edge notches produces a nearly uniform shear stress along the section. Two test methods and fixtures are based on this principle, the Arcan and Iosipescu tests. The Arcan fixture is illustrated in Figure 8.28.³⁰ The specimen is a short coupon with two 90° notches. The coupon is mounted on the fixture through a bolted specimen holder. The load can be applied at various orientations with respect to the section through the notches. This allows the application of any biaxial state of stress from pure shear to transverse tension or any combination thereof. Pure shear loading is obtained for $\alpha = 0^\circ$. In the Iosipescu test the specimen is a beam with two 90° notches loaded in the fixture shown in Figure 8.29.³¹ In both cases the average shear stress applied through the notched section of the specimen is

$$\tau_6 = \frac{P}{lh} \tag{8.39}$$

where

l = Specimen height at notch location

h = Specimen thickness

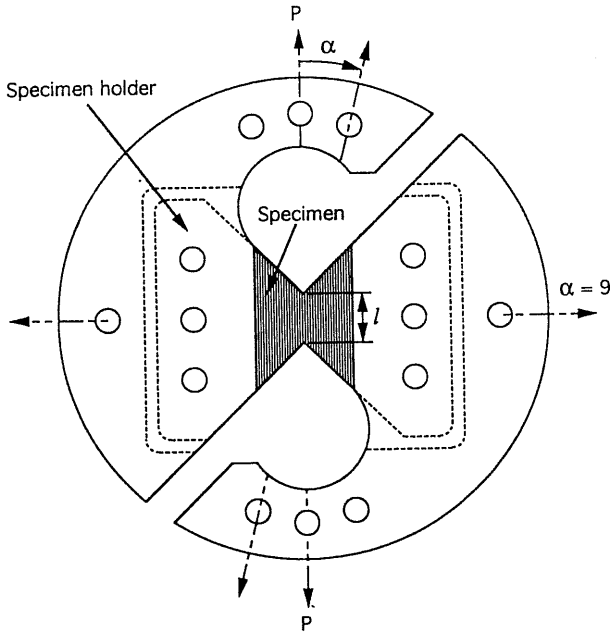


Fig. 8.28 Arcan loading fixture and specimen holder for pure shear and mixed mode loading.³⁰

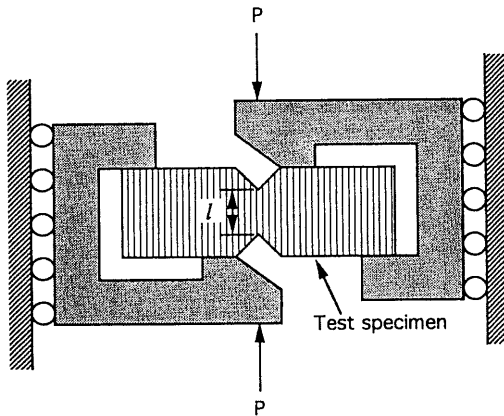


Fig. 8.29 Schematic of loading fixture for Iosipescu shear test.³¹

The shear strain, γ_6 , can be measured with a strain gage located at the center of the notched section at 45° with the loading direction as in the case of the three-rail shear specimen (Eq. 8.31). The in-plane shear modulus, G_{12} , is obtained as the slope of the τ_6 versus γ_6 curve. The ultimate value of τ_6 yields the in-plane shear strength F_6 of the lamina.

The Arcan test can also be used to measure the out-of-plane (interlaminar) shear modulus, G_{31} , by bonding the faces of a thick unidirectional lamina to the specimen holder in Figure 8.28. The relative motion of the two parts of the specimen holder must then be measured as a function of applied load.

8.7 Determination of Interlaminar Strength

8.7.1 Interlaminar Shear Strength

Interlaminar shear strength is a measure of the in situ shear strength of the matrix layer between plies. There is no method available for exact determination of this property. Approximate values of the interlaminar shear strength, or apparent interlaminar shear strength, can be obtained by various tests.

The most commonly used test is the short beam under three-point bending (Fig. 8.30). The beam is machined from a relatively thick (at least 16 plies thick) unidirectional laminate with the fibers in the axial direction and is loaded normally to the plies (in the 3-direction). (ASTM D2344-84.)⁵ Some doubts have been raised about the validity of results obtained from thin laminates (less than 16 plies thick) because of local compressive failure near the loaded points. Better results are obtained with thicker (approximately 50-ply thick) laminates.^{32,33} Because of its simplicity, the short beam shear test is used as a quality control (qualification) test of the lamination process and related matrix-dominated properties of the composite.

If the beam is sufficiently short compared with its depth, shear failure will take place at the midplane in the form of delamination. This is true only sufficiently far away from the load and reaction points, where a parabolic shear stress distribution through the thickness can be assumed. A finite element analysis has shown that the shear stress distribution is skewed near the load and reaction points and that interlaminar shear stresses larger than those predicted

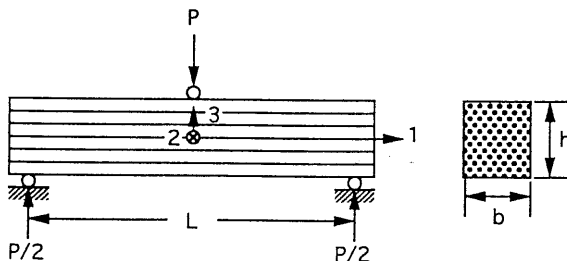


Fig. 8.30 Short beam shear test for measurement of interlaminar shear strength.

by classical beam theory exist.³⁴ The apparent interlaminar shear strength obtained from classical beam theory is given by

$$F_{31} \cong \frac{3P}{4bh} \quad (8.40)$$

where

P = Load at failure initiation

b = Width of beam

h = Depth of beam (laminate thickness)

If the beam is too long compared with its depth, flexural failure (tensile or compressive) may take place at the outer plies of the beam. To ensure interlaminar shear failure prior to flexural failure, the span to depth ratio must satisfy the relationship

$$\frac{2L}{h} < \frac{F_1}{F_{31}} \quad (8.41)$$

where

L = Beam span

F_1 = Flexural strength of beam in fiber direction (smaller of F_{1t} or F_{1c})

For a typical carbon/epoxy 15- to 20-ply laminate, a span length $L = 1$ cm (0.4 in.), width $b = 0.64$ cm (0.25 in.), and thickness $h = 1.9$ to 2.5 mm (0.075 to 0.100 in.) are used.

Another test proposed for the same purpose is the double-notch shear test as described in ASTM specification D3846-79 (1985).⁵ The specimen is a unidirectional coupon 79.5 mm (3.13 in.) long, 12.7 mm (0.50 in.) wide, and 2.54 to 6.60 mm (0.100 to 0.260 in.) thick (Fig. 8.31). Two parallel notches or grooves are machined, one on each face of the specimen, 6.4 mm (0.25 in.) apart and of depth equal to half the specimen thickness. When this specimen is loaded in uniaxial tension or compression, shear failure results along the midplane of the specimen between the notches. In the case of compressive loading, a supporting fixture is recommended to prevent buckling as shown in ASTM D3846-79 (1985).⁵ The interlaminar shear strength is then given by

$$F_{31} \cong \frac{P}{wl} \quad (8.42)$$

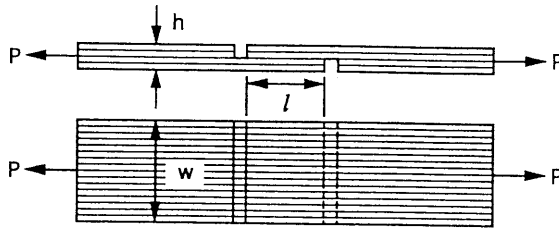


Fig. 8.31 Double-notch specimen for determination of interlaminar shear strength.

where P is the failure load, l is the distance between notches, and w the width of the specimen.

A stress analysis of the notched specimen showed that the interlaminar shear stress along the midplane between the notches is nonuniform, but becomes more uniform as the distance between the notches decreases.³⁵ For shear failure to take place between the notches, the following condition must be satisfied (for tensile or compressive loading):

$$\frac{F_{31}}{F_{1t}} < \frac{h}{2l} \quad (8.43)$$

or

$$\frac{F_{31}}{F_{1c}} < \frac{h}{2l}$$

where

F_{1t}, F_{1c} = Longitudinal tensile and compressive strength of the lamina

h = Specimen thickness

The interlaminar shear strength can also be measured by means of the Arcan test discussed before. The faces of a unidirectional coupon are bonded to the specimen holder of Figure 8.28 and the failure load recorded. The interlaminar shear strength is obtained by an expression similar to Eq. (8.42), where now l is the length and w is the width of the coupon.

8.7.2 Interlaminar Tensile Strength

Determination of interlaminar tensile strength has the following objectives:

1. Assessment of laminate integrity in the out-of-plane direction (3- or z -direction) for quality control of the lamination process.

2. Generation of design allowables for thick composite laminates subjected to three-dimensional states of stress.
3. Evaluation of laminate resistance to delamination caused by interlaminar tensile stresses near free edges under in-plane loading.

There are two approaches for determining the interlaminar tensile strength (F_{3t}), direct and indirect ones.

The direct approach is similar to that used for determination of in-plane transverse tensile strength (F_{2t}).³ Solid or hollow cylindrical specimens with slightly reduced cross section in the gage section can be machined from relatively thick laminates as shown in Figure 8.32a,b. The specimens are bonded at the ends to metallic tabs. For thinner laminates ring specimens are cut and bonded to metallic discs (Fig. 8.32c). These types of tests of course are valid when the tensile strength of the adhesive bond is higher than the interlaminar tensile strength of the composite. Furthermore, there is a problem with stress concentration due to possible Poisson's ratio mismatch between the composite and metallic tabs. The only results that are valid are those corresponding to failure in the reduced section away from the metallic tabs.

An indirect determination of F_{3t} was suggested in conjunction with the edge delamination tension test (EDT), to be discussed in the following section.^{36,37} This test, however, is complex and involves the combined effects of both interlaminar shear and interlaminar tensile stress at the edges. A better indirect test, the so-called split ring test, was originally suggested for characterization of filament wound composite elements.³⁸ This test was recently modified and improved.³⁹ It consists of a curved laminated beam specimen loaded in tension,

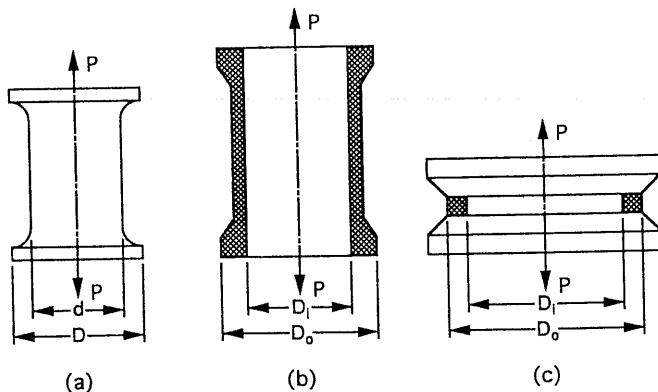


Fig. 8.32 Specimens for direct determination of interlaminar tensile strength.³ (a) Solid cylindrical specimen for thick laminates. (b) Hollow cylindrical specimen for thick laminates. (c) Ring specimen for thin laminates.

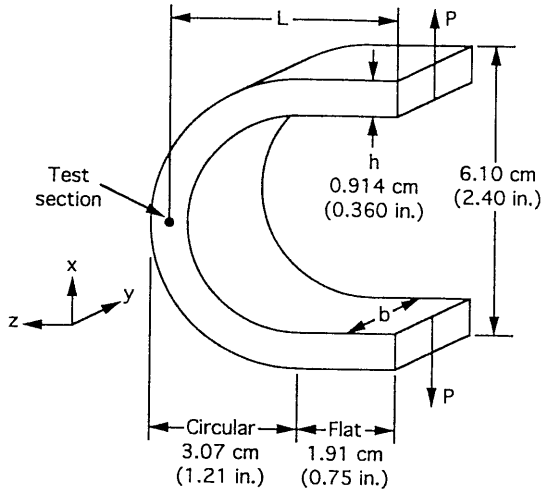


Fig. 8.33 Semicircular curved beam specimen for determination of interlaminar tensile strength.³⁹

as shown in Figure 8.33. Under this loading a pure interlaminar radial tensile stress, σ_z , is induced in the apex of the specimen test section. For semicircular geometry this stress can be closely estimated by the following relation:

$$\sigma_z = \frac{3 PL}{2 bh R} \quad (8.44)$$

where

P = Applied tensile load

L = Distance between load and test section

b = Beam width

h = Beam thickness

R = Mean radius of circular section

Test results obtained with this specimen are characterized by high scatter and low mean value of F_{3r} . Better results were obtained by using a “scarfed circular specimen” with significantly reduced test section and also by using specimens with elliptical geometry.³⁹ Regardless of the experimental approach used, the quality of the results can be assessed by how close the values of F_{3r} are to those of F_{2r} .

8.8 Determination of Interlaminar Fracture Toughness

As discussed previously (see Sect. 7.14), interlaminar crack propagation can occur under opening, forward shearing, tearing, or a combination thereof; therefore delamination fracture toughness can be characterized by stress intensity factors or strain energy release rates corresponding to modes I, II, and III. Several test methods have been developed for modes I, II, and III and combination thereof. Reviews of some of these methods have been published.^{40,41}

8.8.1 Mode I Testing

The most commonly used specimens for mode I characterization are the double cantilever beam (DCB) specimen⁴⁰ and the width-tapered double cantilever beam (WTDCB) specimen.⁴² These specimens have been used by a number of investigators for determination of mode I delamination fracture toughness.^{40,42-54} A height-tapered double cantilever beam (HTDCB) specimen has also been proposed for the study of rate effects on interlaminar fracture toughness.⁵⁵

Methods of analysis for the DCB specimen were discussed in Section 7.14. In the beam analysis or compliance method the specimen is assumed to consist of two identical cantilever beams with built-in ends and length equal to the length of the crack. For quasistatic loading the critical energy release rate is given by

$$G_{Ic} = \frac{12 P^2}{E_1 b^2 h} \left[\left(\frac{a}{h} \right)^2 + \frac{E_1}{10 G_{31}} \right] \quad (7.52 \text{ bis})$$

where

P = Maximum applied load at crack extension

b = Specimen width

h = Cantilever beam thickness

E_1 = Longitudinal modulus (in fiber direction)

G_{31} = Transverse shear modulus

a = Crack length

Another commonly used method of analysis is the area method. The energy released per unit area of crack extension is simply calculated as

$$G_{Ic} = \frac{1}{2b\Delta a} (P_1 \delta_2 - P_2 \delta_1) \tag{7.53 bis}$$

where the load P_1 corresponding to opening deflection δ_1 drops to load P_2 corresponding to deflection δ_2 after an increment Δa in crack length (see Fig. 7.30).

The uniform DCB specimen is usually 22.9 cm (9 in.) long, 2.54 cm (1 in.) wide, and 3 to 3.6 mm (0.120 to 0.140 in.) thick, with an initial artificial crack of 3.81 cm (1.5 in.) length at one end. This crack is produced by inserting a 0.025 mm (0.001 in.) thick folded polytetrafluoroethylene (PTFE, Teflon) film at the midplane of the laminate near one end. Metallic piano hinges are bonded to the cracked end of the specimen as shown in Figure 8.34 to allow for unrestrained rotation at that end during load introduction.

The specimen is loaded in a testing machine at a low crosshead rate of the order of 0.5 to 1.3 mm/min (0.02 to 0.05 in/min) in order to produce stable crack growth. The opening deflection is determined by measuring the crosshead displacement or by means of a linear variable differential transformer (LVDT) extensometer. A continuous load-deflection curve is obtained as shown in Figure 8.35. Incremental crack lengths are marked on this curve during the test. Crack extension is monitored in several different ways. At low crosshead rates crack extension can be monitored visually. At higher rates the crack can be monitored either by means of strain gages mounted on the top face of the specimen or by means of a conductive paint circuit applied to the edge of the DCB specimen.^{48,50,55}

The use of the uniform DCB specimen requires monitoring of the crack length a , which becomes more difficult at high loading rates. This problem is

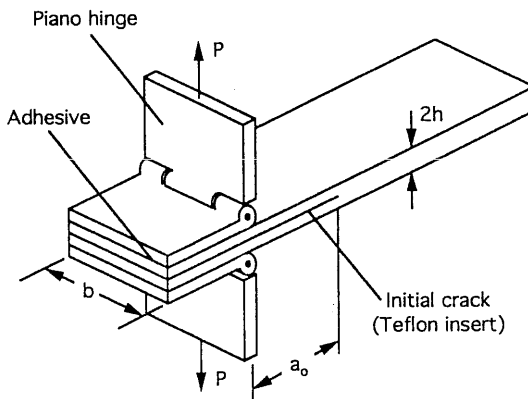


Fig. 8.34 Double cantilever beam specimen with initial crack and attached hinges for loading.

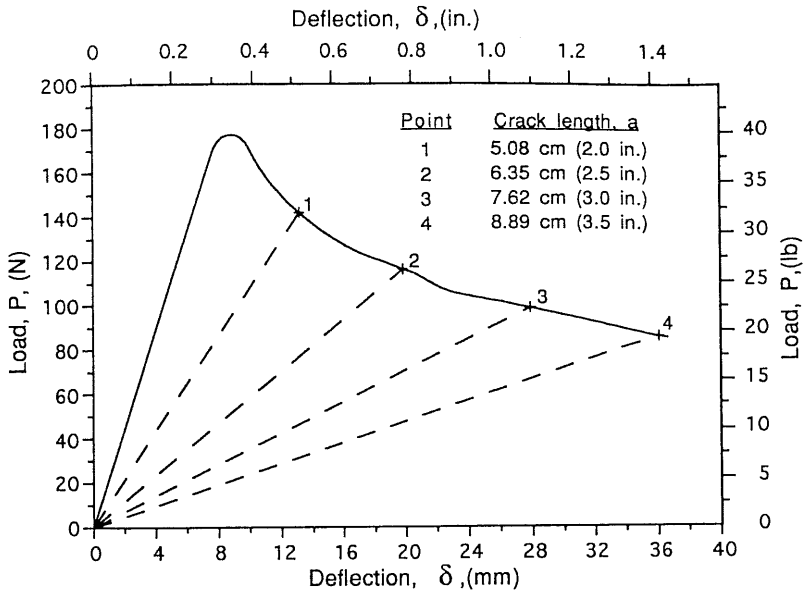


Fig. 8.35 Load versus crack opening deflection for uniform DCB specimen with an initial crack of $a_0 = 3.81$ cm (1.5 in.) loaded at a crosshead rate of 0.0085 mm/s (0.02 in./min) (AS4/3501-6 carbon/epoxy).⁵⁰

alleviated with the WTDCB, which has the property of constant rate of change of compliance with crack length, i.e., $dC/da = \text{constant}$. For this reason this specimen does not require exact monitoring of the crack length and yields a constant crack velocity for a constant opening deflection rate.⁵³ The critical strain energy release rate based on the compliance method is

$$G_{Ic} = \frac{12 P^2 k^2}{E_1 h^3} \left[1 + \frac{1}{10} \frac{E_1}{G_{31}} \left(\frac{h}{a} \right)^2 \right] \quad (8.45)$$

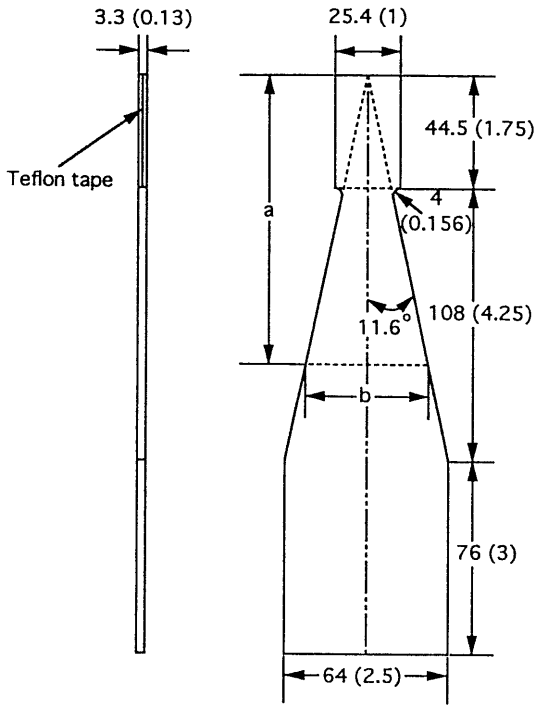
where

$$k = \frac{a}{b}$$

b = Beam width at crack length a

An alternative expression based on the area method is

$$G_{Ic} = \frac{P_1 \delta_2 - P_2 \delta_1}{a_2^2 - a_1^2} k \quad (8.46)$$



All dimensions are in mm (in.)

Fig. 8.36 Typical dimensions in mm (in.) of a width-tapered double cantilever beam (WTDCB) specimen.⁵³

where a_1 and a_2 are crack lengths corresponding to loads P_1 and P_2 and deflections δ_1 and δ_2 , respectively.

Typical dimensions for a WTDCB specimen are given in Figure 8.36. A rectangular section is provided near the end to facilitate the attachment of hinges for load introduction. A continuous load-deflection curve obtained with a carbon/epoxy WTDCB specimen is shown in Figure 8.37.

Typical results of critical strain energy release rates for various types of carbon fiber composites are shown in Table 8.1.⁴¹ These results demonstrate the effectiveness of the DCB test in manifesting the significantly higher (approximately one order of magnitude higher) G_{Ic} values of composites with tough thermoplastic matrices like PEEK compared to those with standard epoxy matrices.

8.8.2 Mode II Testing

Delamination fracture toughness for pure mode II can be obtained by testing in three-point bending the same type of DCB specimen used for mode I (Fig. 8.38).

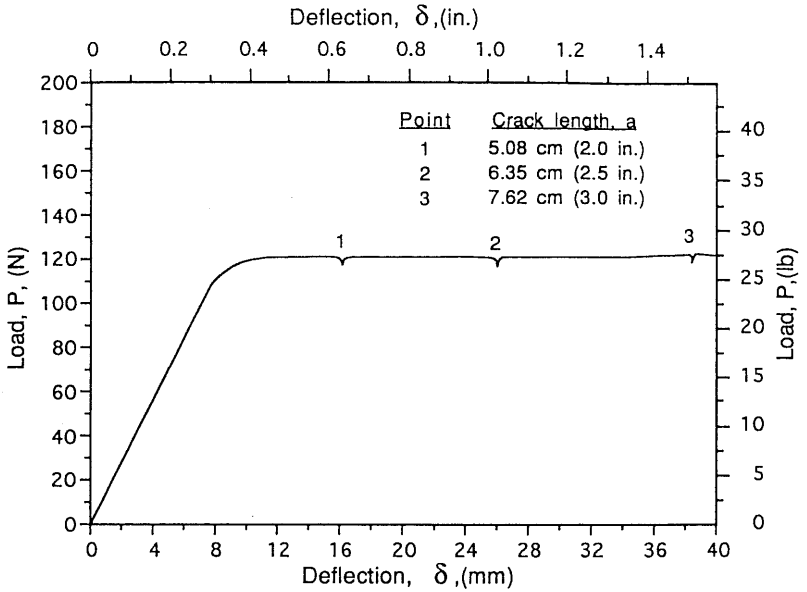


Fig. 8.37 Load versus crack opening deflection for WTDCB specimen loaded at a crosshead rate of 0.85 mm/s (2 in./min) (T300/F-185 carbon/epoxy).⁵⁰

Table 8.1 Mode I Critical Strain Energy Release Rates for Various Carbon Fiber Composite Materials

Material	Type of test	Strain energy release rate, G_{Ic} $J m^{-2}$ (lb/in.)	Reference
T300/5208	DCB	103 (0.59)	Ramkumar and Whitcomb ⁴⁹
	DCB	88 (0.50)	Wilkins et al. ⁴⁶
AS4/3501-6	DCB	198 (1.13)	Aliyu and Daniel ⁴⁸
	DCB	190 (1.08)	Gillespie et al. ⁵¹
	HTDCB	189 (1.08)	Daniel et al. ⁵³
AS4/3502	DCB	160 (0.91)	Whitney et al. ⁴⁰
T300/F-185	WTDCB	1,880 (10.73)	Daniel et al. ⁵⁰
AS4/PEEK	DCB	1,750 (9.99)	Gillespie et al. ⁵¹
	DCB	1,460 (8.33)	Prel et al. ⁵⁴

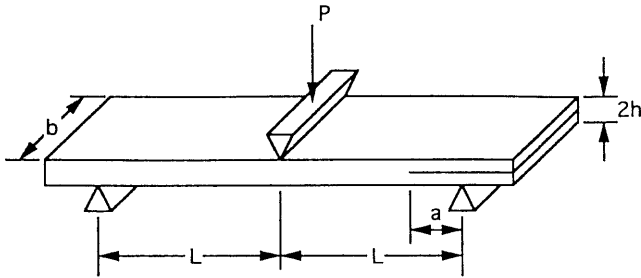


Fig. 8.38 End-notched flexure (ENF) specimen for determination of mode II interlaminar fracture toughness.

This test is referred to as the end-notched flexure (ENF) test.⁵⁶ The width of the specimen is usually 2.54 cm (1 in.), the crack length also 2.54 cm (1 in.), and the total span 10.16 cm (4 in.). The specimen is first loaded as a DCB specimen in mode I up to the point of crack initiation. Then it is loaded in flexure as shown in Figure 8.38 until further crack growth occurs at the maximum load. A load-deflection curve is recorded. Independently, a compliance calibration is performed by testing similar specimens with various crack lengths. The strain energy release rate based on linear beam theory with linear elastic behavior, including effects of shear deformation, is given by

$$G_{IIc} = \frac{9 P^2 a^2}{16E_1 b^2 h^3} \left[1 + 0.2 \frac{E_1}{G_{31}} \left(\frac{h}{a} \right)^2 \right] \tag{8.47}$$

Neglecting shear deformation, the above is expressed in terms of the measured compliance C as

$$G_{IIc} = \frac{9 P^2 a^2 C}{2b (2L^3 + 3a^3)} \tag{8.48}$$

Since the ENF test is relatively new, only a limited amount of data has been published.^{54,57-61}

In general, mode II interlaminar fracture toughness may be obtained from mixed mode tests. One such test is the end-loaded split laminate (ELS) test (Fig. 8.39).⁵⁸ In this case, the expression for G_{IIc} , neglecting shear deformation, is similar to the one for the ENF test.

$$G_{IIc} = \frac{9 P^2 a^2}{4 E_1 b^2 h^3} \tag{8.49}$$

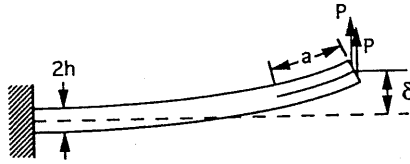


Fig. 8.39 End loaded split laminate (ELS) specimen for determination of mode II interlaminar fracture toughness.

The Arcan test configuration can be used for pure mode II as well as any combination of modes I and II by attaching an end-notched coupon in the specimen holder (Fig. 8.40).⁶² Additional mixed mode tests used for computation of G_{IIc} include the end-notched cantilever beam (ENCB) and the cantilever beam with enclosed notch (CBEN).⁵⁴

Typical results for mode II critical strain energy release rates are summarized in Table 8.2 for various types of carbon/epoxy composites.⁴¹ These results show how the ENF test manifests the higher (approximately three times higher) G_{IIc} values of composites with tough thermoplastic matrices like PEEK compared to composites with standard epoxy matrices.

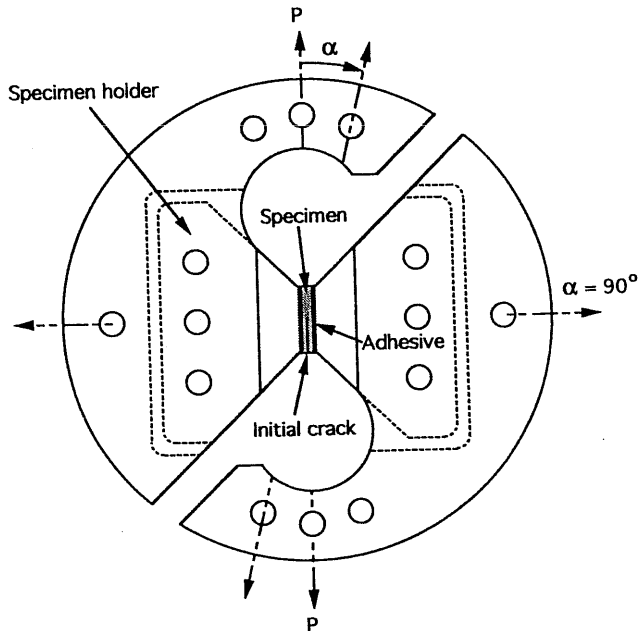


Fig. 8.40 Specimen holder and loading fixture for pure and mixed mode interlaminar fracture testing in Arcan fixture.⁶²

Table 8.2 Mode II Critical Strain Energy Release Rates for Various Carbon Fiber Composite Materials

Material	Type of test	Strain energy release rate, G_{IIc} $J m^{-2}$ (lb/in.)	Reference
T300/5208	CLS	433 (2.47)	Ramkumar and Whitcomb ⁴⁹
	CLS	154 (0.88)	Wilkins et al. ⁴⁶
T300/914	ENF	518 (2.96)	Prel et al. ⁵⁴
	CBEN	496 (2.83)	Prel et al. ⁵⁴
AS1/3501-6	ENF	458 (2.61)	Russell and Street ⁵⁶
AS4/PEEK	ENF	1,765 (10.07)	Russell and Street ⁵⁶
	ENF	1,109 (6.33)	Prel et al. ⁵⁴
	CBEN	1,860 (10.62)	Prel et al. ⁵⁴
	ENCB	1,780 (10.16)	Prel et al. ⁵⁴
AS4/3502	ELS	543 (3.10)	Corletto and Bradley ⁵⁸
	ENF	587 (3.35)	Corletto and Bradley ⁵⁸

8.8.3 Mixed Mode Testing

Mixed mode (I and II) fracture toughness has been measured by a variety of test methods such as the cracked-lap shear (CLS), mixed mode bending (MMB), edge delamination tension (EDT), and the Arcan specimen. The CLS specimen shown in Figure 8.41 has been used for composite materials as well as adhesive bond evaluation.^{42,46} Uniaxial loading is applied to one arm (strap) of a split unidirectional laminate. The load transfer to the other arm (lap) produces both shear (mode II) and peel (mode I) stresses along the interface between the lap and strap arms. The relative magnitudes of G_I and G_{II} can be modified by adjusting the relative thicknesses of the strap and lap parts. The exact determi-

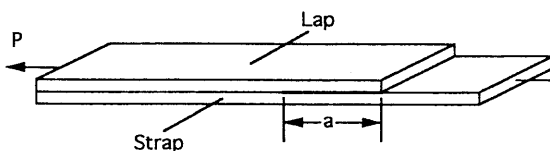


Fig. 8.41 Cracked-lap shear specimen.

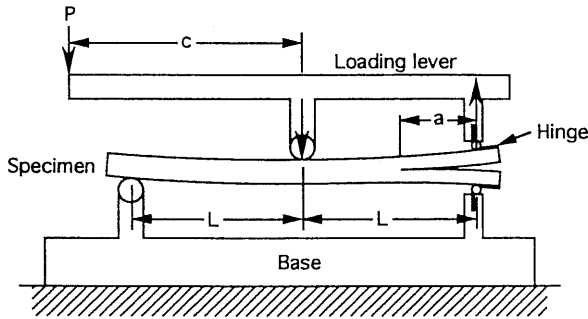


Fig. 8.42 Mixed-mode bending specimen and test apparatus.⁶⁴

nation of the two fracture toughness components is usually done by means of finite-element analysis.⁶³

The mixed mode bending specimen is shown in Figure 8.42.⁶⁴ The individual components of fracture toughness are determined as follows:

$$G_{Ic} = \frac{3 P^2 a^2}{4 b^2 h^3 L^2 E_1} (3c - L)^2 \quad (8.50)$$

$$G_{IIc} = \frac{9 P^2 a^2}{16 b^2 h^3 L^2 E_1} (c + L)^2 \quad (8.51)$$

Their ratio

$$G_{Ic}/G_{IIc} = \frac{4}{3} \frac{(3c - L)^2}{(c + L)^2}, \quad c \geq \frac{L}{3} \quad (8.52)$$

is only a function of the load position c and half span length L .

The EDT test utilizes $[(\pm\theta)_2/90/90]_s$ and $[\pm\theta/0/90]_s$ laminates designed to delaminate at the edges under tensile loading.^{65,66} The orientation θ is usually 30° in the first laminate and 35° in the second. In these laminates, a noticeable change in the load-deflection curve occurs at the onset of edge delamination. The total critical strain energy release rate associated with edge delamination growth in an unnotched composite laminate is given by⁶⁵

$$G_c = \frac{\epsilon_c^2 h}{2} \left(\bar{E}_x - \bar{E}_x^* \right) \quad (8.53)$$

where

ϵ_c = Tensile strain at delamination onset

h = Specimen thickness

\bar{E}_x = Laminate modulus before delamination

\bar{E}_x^* = Laminate modulus after total delamination along one or more interfaces

The value of G_c is independent of delamination size, but it depends on the laminate lay-up, which determines \bar{E}_x , and on the location of the delaminated surfaces, which determines \bar{E}_x^* . The two moduli are determined by both laminate plate theory and the rule of mixtures. The total strain energy release rate above consists of components G_I , G_{II} , and G_{III} . As in the case of the CLS specimen, numerical analyses are required to determine the individual components.

The Arcan test configuration can be used in principle to apply any desired combination of mode I and mode II interlaminar loading (Fig. 8.40).⁶²

8.8.4 Mode III Testing

Compared with mode I and mode II testing, relatively little work has been reported on mode III testing. A split DCB specimen made by bonding the composite laminate between two aluminum bars has been described (Fig. 8.43).⁶⁷ These bars are loaded in the direction parallel to the crack plane and normal to the beam axis. As in the case of the mode I DCB test, the load drops suddenly as the crack extends, causing some uncertainty in the crack length corresponding

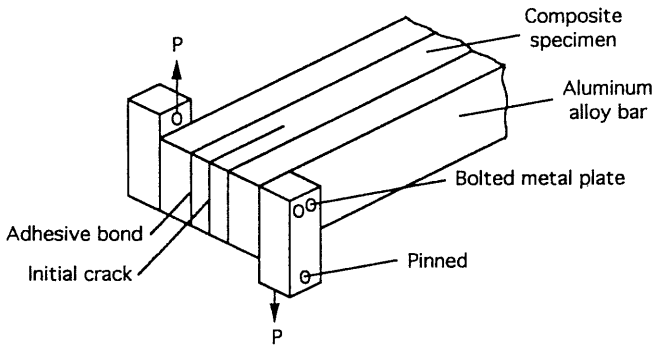


Fig. 8.43 Split cantilever beam specimen for determination of mode III interlaminar fracture toughness.⁶⁷

to the critical load. Finite element analysis of this specimen shows that at the delamination front there is a G_{II} component in addition to the G_{III} component. Furthermore, the G_{II} component increases near the free edges. One conservative way to determine G_{IIIc} from such a test is to assume that $G_{IIc} = G_{IIIc}$.

A new test method was proposed recently for determination of G_{IIIc} .⁶⁸ The specimen is a doubly-split DCB, as shown in Figure 8.44. The symmetry of the specimen ensures self-balancing and prevents twisting. The uncertainty in identifying and measuring the correct crack length at the critical load and the so-called stick-slip phenomenon are eliminated by adding a support to the doubly-split DCB specimen, as shown in Figure 8.44. The strain energy release rate for this specimen is given as

$$G_{IIIc} = \frac{3 P^2 e^2}{E b h^4} \quad (8.54)$$

where

e = Distance between the end load and the support

E = Modulus of laminate along beam axis

b = Width of outer split beams

h = Laminate thickness

The fracture toughness in this case is independent of crack length ($a + e$), and the critical tearing load P remains constant as the crack propagates.

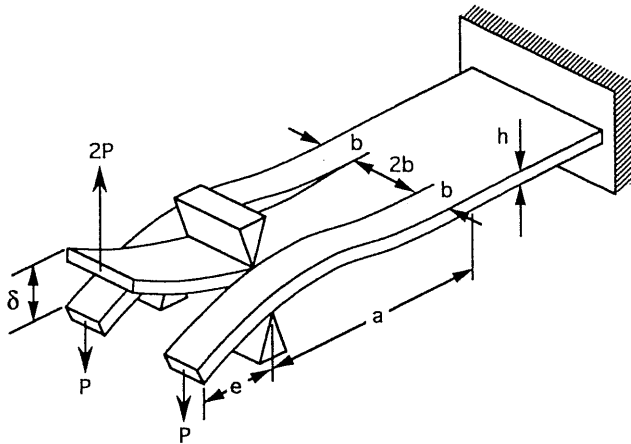


Fig. 8.44 Doubly-split double cantilever beam specimen for determination of mode III fracture toughness.⁶⁸

8.9 Biaxial Testing

8.9.1 Introduction

Failure theories, such as the Tsai–Wu theory, can predict FPF of multidirectional laminates under any state of in-plane stress. Ultimate failure, however, is difficult to predict analytically on the basis of lamina properties because of nonlinear behavior and interaction of failure modes. To check or verify analytical predictions and to generate useful failure envelopes for design purposes, it is necessary to conduct extensive testing of composite laminates under biaxial states of stress. The application of a general in-plane biaxial state of stress, including normal tension and compression and shear components, poses a difficult problem in composite testing. Some of the basic requirements for a biaxial test specimen are:

1. A significant volume of the material must be under a homogeneous state of stress.
2. Primary failure must occur in the test section.
3. The state of stress in the test section must be known or easily determined without the need for secondary measurements or analysis.
4. It must be possible to vary the three in-plane stress components ($\bar{\sigma}_x$, $\bar{\sigma}_y$, $\bar{\tau}_s$) independently.

A variety of specimen types and techniques have been proposed and used for biaxial testing of laminates. They include the off-axis coupon or ring, the crossbeam sandwich specimen, bulge plate, rectangular plate under biaxial tension, and the thin-wall tubular specimen.

8.9.2 Off-Axis Uniaxial Test

Uniaxial loading of a unidirectional lamina along a direction other than one of the principal axes produces a biaxial state of stress (Fig. 8.45). The state of stress referred to the principal material axes under uniaxial stress σ_x is obtained from the transformation relations in Eq. (3.57):

$$\begin{aligned}\sigma_1 &= m^2 \sigma_x \\ \sigma_2 &= n^2 \sigma_x \\ \tau_6 &= -mn \sigma_x\end{aligned}\tag{8.55}$$

where $m = \cos\theta$ and $n = \sin\theta$.

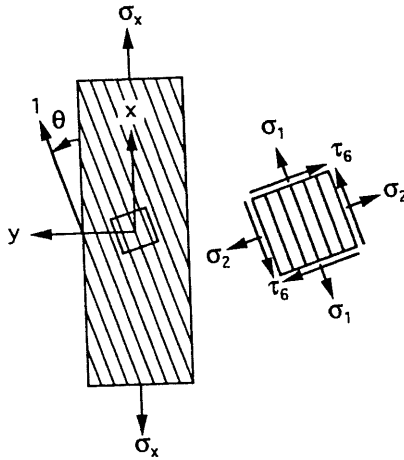


Fig. 8.45 Off-axis specimen for biaxial testing of unidirectional lamina.

The off-axis specimen has been used successfully in coupon and ring form.⁶⁹⁻⁷² In the latter case thin-wall rings with the principal material axes at an angle with the circumferential direction are subjected to internal pressure loading. Some of the limitations of the off-axis specimen are:

1. The biaxial normal stresses are always of the same sign.
2. There is no possibility for independent variation of the three stress components (non-proportional loading).
3. Erroneous stiffness and strength results may be obtained when using tensile coupon specimens of dimensions and with clamping conditions customarily used in testing along principal axes.

If the applied stress σ_x were uniform throughout, i.e., if the specimen were free to deform, the specimen strains would be

$$\epsilon_x = \frac{1}{E_x} \sigma_x$$

$$\epsilon_y = -\frac{\nu_{xy}}{E_x} \sigma_x \quad (3.74 \text{ bis})$$

$$\gamma_s = \frac{\eta_{xs}}{E_x} \sigma_x$$

which means that a rectangular coupon would deform into a parallelogram-shaped one as shown in Figure 8.46a, due to shear coupling. If the specimen

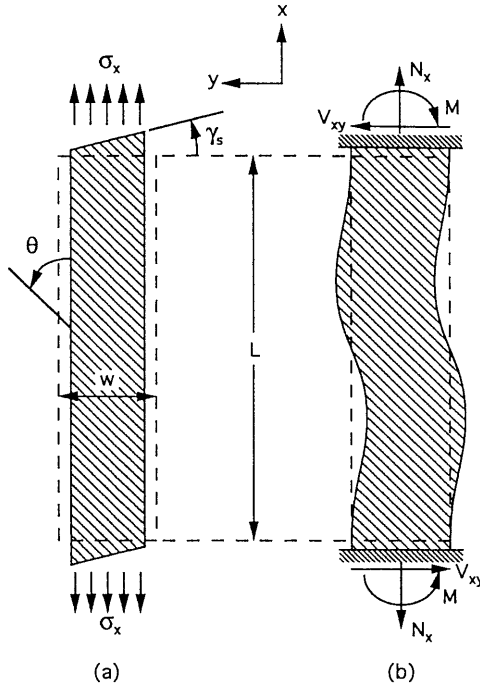


Fig. 8.46 Effect of end constraint on off-axis tensile specimen: (a) free ends and (b) clamped ends.⁷³

is clamped at the ends during loading, the shear deformation is constrained and the specimen deforms, as shown in Figure 8.46b.⁷³ This constraint induces a shear and bending moment at the ends as shown that disturb the stress field uniformity in the specimen. It was shown analytically that a uniform state of stress and strain will exist at the center of the specimen if the aspect ratio L/w (length/width) is sufficiently large.⁷⁴ Furthermore, an expression was obtained for the error involved and a correction factor for determination of the true axial modulus as follows:⁷⁴

$$E_x = E_x^* (1 - \zeta) \tag{8.56}$$

and

$$\zeta = \frac{6 S_{xs}^2}{S_{xx} \left[6 S_{ss} + S_{xx} \left(\frac{2L}{w} \right)^2 \right]} = \frac{\eta_{xs}^2}{\frac{E_x}{G_{xy}} + \frac{2}{3} \left(\frac{L}{w} \right)^2} \tag{8.57}$$

where

E_x = True axial modulus

$E_x^* = \frac{\sigma_x}{\epsilon_x}$ = Apparent (uncorrected) axial modulus

ζ = Correction factor

S_{xx}, S_{xs}, S_{ss} = Compliance parameters of off-axis lamina (functions of θ)

E_x, G_{xy}, η_{xs} = Engineering parameters of off-axis lamina (see Chapter 3)

L = Specimen length

w = Specimen width

The shear coupling effect in a uniaxially loaded off-axis specimen as characterized by the correction factor ζ in Eq. (8.57) depends on the following variables:

1. Clamping conditions.
2. Degree of anisotropy of the composite which affects the ratio E_x/G_{xy} .
3. Shear coupling parameter η_{xs} which depends primarily on the off-axis angle θ and becomes predominant in the range $10^\circ < \theta < 45^\circ$.
4. The specimen aspect ratio or length to width ratio L/w .

Of these variables, the first and last are the only ones that can be varied in testing a given material at a given off-axis angle. When the aspect ratio L/w is large enough, the shear coupling effect becomes independent of clamping conditions.⁷⁵ For an E-glass/epoxy specimen with a ratio $L/w = 24$, small differences were observed in strength and stiffness for clamped and hinged end conditions ($\zeta < 0.05$). Reliable biaxial data were obtained for E-glass/epoxy with brittle and ductile matrices using the off-axis specimen. Partial failure envelopes were obtained by varying the off-axis angle θ in the range $10^\circ \leq \theta \leq 90^\circ$ (Fig. 8.47).⁷²

Off-axis testing is not limited to the unidirectional lamina. Multidirectional symmetric laminates can be tested under uniaxial loading at an angle with one of the principal laminate axes (\bar{x}, \bar{y}). The off-axis laminate can also be tested in compression by using it as a skin in a honeycomb-core sandwich beam under pure bending. Within the limitations stated before the specimen is reliable and simple to use.

8.9.3 Crossbeam Sandwich Specimen

The crossbeam sandwich specimen consists of two intersecting beams subjected to pure bending. In one of the many types discussed, the laminate is used as

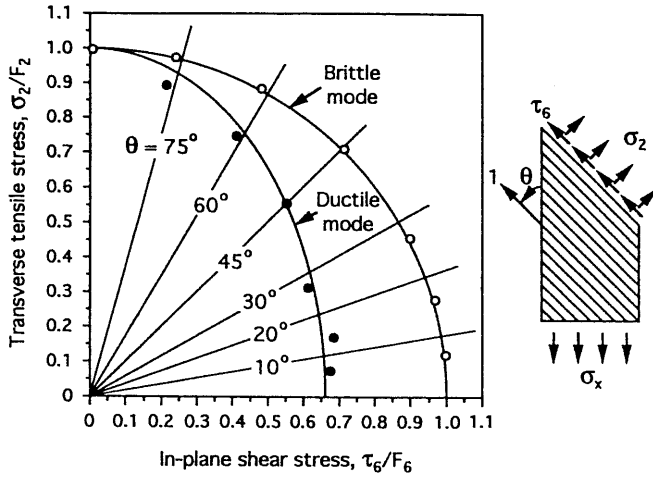


Fig. 8.47 Brittle and ductile failure envelopes for interfiber matrix failure in off-axis specimens under uniaxial tensile loading (length to width ratio: $L/w = 24$; “brittle” composite is E-glass/Epon 828-Z; “ductile” composite is E-glass/Epon 815-Versamid 140).⁷²

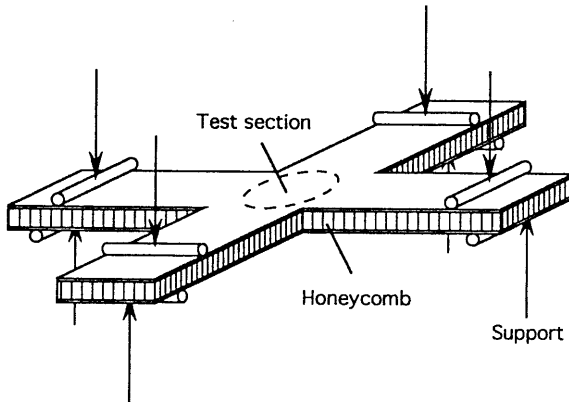


Fig. 8.48 Crossbeam sandwich specimen for biaxial testing of composite laminates.

one skin of a honeycomb-core sandwich (Fig. 8.48). This type of specimen allows, in principle, the application of tension–tension, tension–compression, and compression–compression loading in the central test section. One of the major limitations of this specimen is the disturbing influence of the corners on stress distributions in the test section and on fracture initiation at the points of stress concentration. The state of stress in the test section cannot be determined from the specimen geometry and applied loads without prior knowledge of the material properties.

8.9.4 Flat Plate Specimen

The flat plate specimen is usually a square plate subjected to tension-tension loading on its sides through fiberglass tabs. A variety of biaxial states of stress (in the tension-tension-shear space) can be achieved by rotating the principal material axes with respect to the loading directions. Nonproportional loading is possible to some degree. To ensure stress homogeneity within a reasonable test section and failure within this region, it is necessary to design the tabs and transition region very carefully.

A typical geometry of a plate specimen designed for equal biaxial tensile loading is shown in Figure 8.49.^{76,77} The composite specimen is a 40.6×40.6 cm (16×16 in.) square plate with the corners cut off. It is tabbed with glass/epoxy tabs that have a 20.3 cm (8 in.) diameter cutout. Loading is introduced by means of four whiffle-tree grip linkages designed to apply four equal loads to each side of the specimen. A photograph of such a biaxial specimen with the loading grip linkages is shown in Figure 8.50.

There are two problems with this type of specimen. The state of stress in the test section is not easily determined from the applied loads because of the unknown load sharing between the tab and the specimen. This problem can be resolved by prior calibration of the system and by ensuring (or assuming) that the tab stiffness remains constant throughout the test. The other problem is premature failure at the corners due to stress concentrations. This problem can be alleviated by proper design of the tab geometry. The specimen is most suitable when the influence of biaxial stress on notches is investigated.^{76,77}

The uniformity or homogeneity of the state of stress in the test section has been verified experimentally by means of photoelastic coatings.^{76,77} In the case of unequal biaxial loading, an elliptical reduced thickness region (or tab cutout in this case) has been proposed to ensure uniform biaxial stresses throughout the test section.⁷⁸ The ellipse is selected to satisfy the relation

$$\frac{b}{a} = \sqrt{\frac{\bar{\sigma}_y}{\bar{\sigma}_x}} \quad (8.58)$$

where $\bar{\sigma}_x$, $\bar{\sigma}_y$ are the average stresses along the two loading directions, and a and b are the major and minor semi-axes of the ellipse along the corresponding directions.

8.9.5 Thin-Wall Tubular Specimen

Of the various biaxial test specimens mentioned, the tubular specimen appears to be the most versatile and offers the greatest potential. It offers the possibility

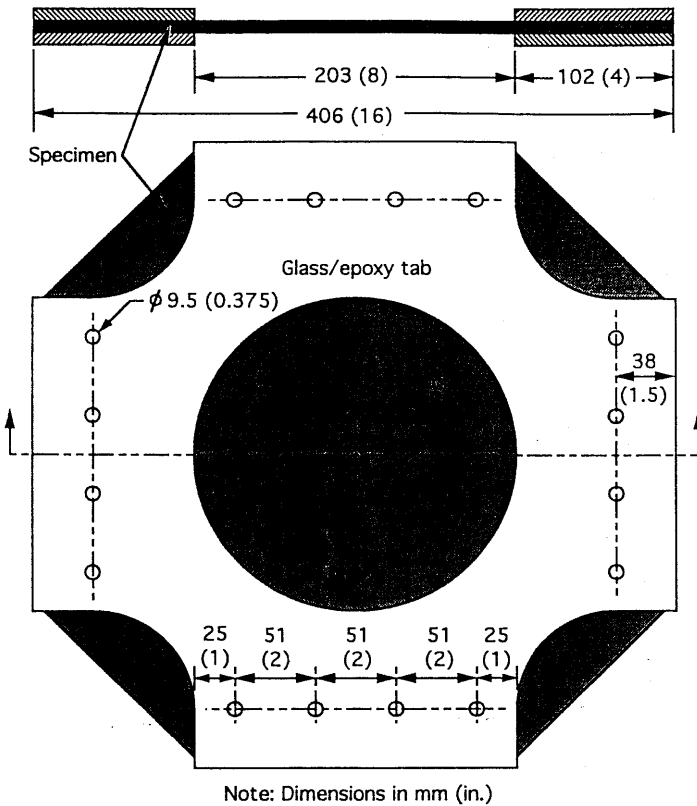


Fig. 8.49 Geometry of plate specimen for biaxial testing.⁷⁶

of applying any desired biaxial state of stress with or without proportional loading. A state of generalized plane stress can be achieved by the independent application of axial loads, internal or external pressure, and torque. Tubular specimens have been used successfully with metals because stress concentrations in the load introduction region are relieved by plastic yielding. This is not the case with brittle-like materials such as composites. For this reason no entirely satisfactory solution has been found to date. To achieve the full potential of the thin-wall tubular specimen, the following requirements must be met:

1. The tube must be loaded without constraints that would produce local extraneous or non-homogeneous stresses.
2. Surface pressures on the laminate in the test section, used for producing circumferential or axial stresses, should be minimized to avoid adding a high radial stress component resulting in a triaxial state of stress.
3. Functional or material failures of the load-introduction tabs must be avoided.

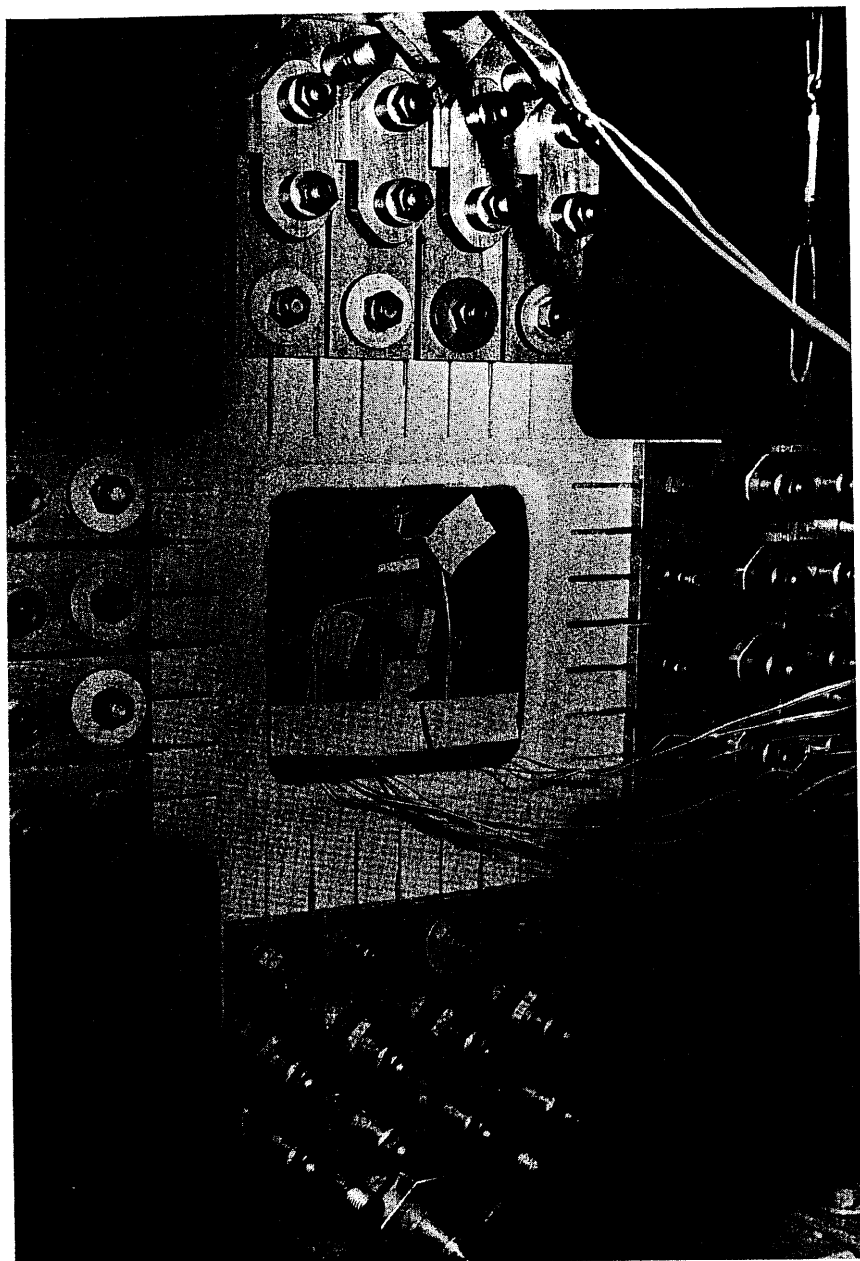


Fig. 8.50 Whiffle-tree linkage grips for load introduction in biaxial plate specimen.⁷⁶

4. Undesirable buckling prior to material failure must be avoided.
5. The cost of specimen fabrication, equipment, and testing process must not be prohibitive.

A general biaxial state of stress is produced by means of internal and external pressures p_i and p_o , longitudinal load P_x (which can also be applied by means of p_i and p_o), and torque T_x about the longitudinal axis. The axial, circumferential, and shear stresses are obtained as

$$\begin{aligned}\bar{\sigma}_x &= \frac{P_x}{2 \pi \bar{r} h} \\ \bar{\sigma}_\theta &= (p_i - p_o) \frac{\bar{r}}{h} - \frac{1}{2} (p_i + p_o) \\ \tau_s &= \frac{T_x}{2 \pi \bar{r}^2 h}\end{aligned}\tag{8.59}$$

where \bar{r} is the mean radius and h the tube thickness.

Testing of composite tubular specimens has been discussed by several investigators who analyzed the various problems arising in this type of specimen.⁷⁹⁻⁸² One of the most frequent and most critical problems encountered is that of introducing and maintaining a uniform biaxial state of stress in the specimen test section and inducing failure in the test region. Some testing of tubular specimens has been done without any provision for relieving end constraints.^{82,83} To overcome or minimize end constraints and gripping problems the concepts of tab and grip pressurization have been used.^{69,84} These concepts, however, have not been implemented with full success because of the inherent difficulty of the problem.

A typical tubular specimen geometry is illustrated in Figure 8.51. The specimen is designed to have end tabs for gripping and load introduction. These tabs are made of epoxy or glass/epoxy premachined and bonded to the specimen ends. The stiffness of these tabs in the axial and circumferential directions relative to those of the composite tube can be varied by varying the glass/epoxy lay-up and the tab thickness. This specimen geometry has been analyzed extensively using finite element methods.⁸⁵ The objective of these analyses was to minimize stress discontinuities in the transition between the test section and tabbed section of the specimen by varying the tab materials and geometry and the tab-compensating pressure.

The preparation of tubular specimens must be done very carefully to ensure that the specimen is of a quality similar to that of flat laminates fabricated and cured in an autoclave. Composite tubes can be fabricated in any desired ply orientation and stacking sequence. Fabrication techniques have been developed

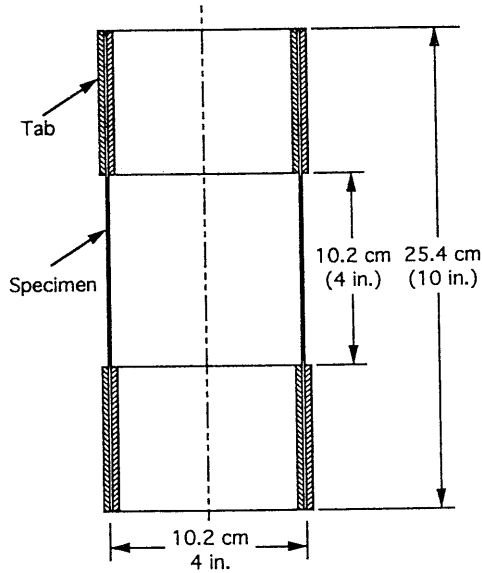


Fig. 8.51 Thin-wall tubular specimen for biaxial testing of composites.⁸⁵

and are described in the technical literature.⁸⁶⁻⁸⁸ One procedure consists of wrapping the prepreg composite tape around a cylindrical perforated mandrel and then, by means of internal pressure, expanding the prepreg tube against the wall of a cylindrical cavity mold. The glass/epoxy tabs required for the specimen are fabricated as tubes in a similar manner. They are subsequently machined to size and bonded on the composite tube.

The complete system for biaxial testing of composite tubular specimens requires the introduction and control of internal and external pressures on the specimen, internal and external compensating pressures on the tabs, grip activation pressure, axial load, and torque. The axial loads and torques are introduced through segmented collet grips at the tabs by means of linear and torque actuators. All pressures applied directly to the specimen or to the actuators are applied and controlled independently of each other with an electrohydraulic system.

The problem of biaxial testing of tubular specimens is inherently difficult and is not amenable to a complete solution. The analysis to date shows that it is possible to obtain valid tests in many cases for a variety of laminates over large portions of the failure envelope.

8.10 Characterization of Composites with Stress Concentrations

8.10.1 Introduction

The behavior of composite laminates with stress concentrations is of great interest in design because of the resulting strength reduction and life reduction due to damage growth around these stress concentrations. Stress distributions and stress concentrations around notches can be determined by linear elastic analysis, finite element methods, and experimental methods. The problem of failure of notched composite laminates has been dealt with by several approaches. One approach is based on concepts of linear elastic fracture mechanics carried over from homogeneous isotropic materials.^{89,90} A second approach is based on actual stress distributions in the vicinity of the notch and makes use of simplified stress fracture criteria.⁹¹ According to the average stress criterion proposed, failure occurs when the average stress over an assumed characteristic dimension from the boundary of the notch equals the tensile strength of the unnotched material. Comparison with results from uniaxial tensile tests showed satisfactory agreement between predicted and measured strengths for a narrow range of values of the characteristic dimension. In a similar approach, lamina failure criteria are used, and a characteristic dimension (volume) is postulated.⁹² Failure is said to occur if the average state of stress (or strain) on the boundary of this characteristic volume falls on the failure envelope of the lamina.

Experimental methods using strain gages, photoelastic coatings, and moiré have proven very useful in studying the deformation and failure of composite laminates with circular holes and through-the-thickness cracks of various sizes.⁹³ The effects of laminate lay-up, stacking sequence, notch size, and far-field stress biaxiality on failure have been investigated. The approach used was to load composite plate specimens with holes or cracks under uniaxial and biaxial tension, measure deformations by means of experimental strain analysis techniques, and determine strain distributions, failure modes, and strength reduction ratios. Experimental results are compared with predictions based on linear elastic fracture mechanics, an average stress criterion, and a progressive degradation model. A review of theoretical and experimental results on notched composite laminates is given by Awerbuch and Madhukar.⁹⁴

8.10.2 Laminates with Holes

Stress distributions around a circular hole in an infinite plate can be obtained by anisotropic elasticity.⁹⁵ For an orthotropic laminate with a hole under uniaxial

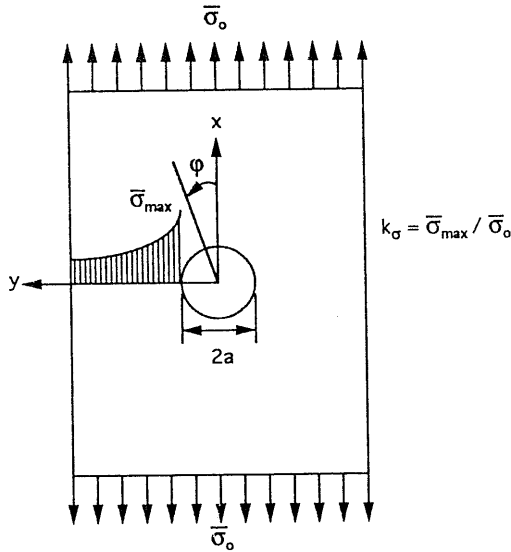


Fig. 8.52 Composite laminate with circular hole under uniaxial tensile loading.

loading along a principal axis x the maximum stress is the circumferential stress on the hole boundary at $\phi = 90^\circ$ (Fig. 8.52). The stress concentration at this location is obtained as

$$k_\sigma = \frac{\bar{\sigma}_{max}}{\bar{\sigma}_o} = 1 + \sqrt{2 \left[\sqrt{\frac{\bar{E}_x}{\bar{E}_y} - \bar{\nu}_{xy}} \right] + \frac{\bar{E}_x}{\bar{G}_{xy}}} \quad (8.60)$$

where

$\bar{\sigma}_o$ = Applied far-field average stress

$\bar{\sigma}_{max}$ = Maximum circumferential stress on hole boundary (at $\phi = 90^\circ$)

\bar{E}_x, \bar{E}_y = Average Young's moduli in the x - and y -directions

\bar{G}_{xy} = Average shear modulus

$\bar{\nu}_{xy}$ = Average Poisson's ratio

The x - and y -axes are principal axes of the laminate.

The circumferential stress on the hole boundary at $\phi = 0^\circ$ is given by

$$(\bar{\sigma}_\phi)_{\phi=0^\circ} = -\bar{\sigma}_x \sqrt{\frac{\bar{E}_y}{\bar{E}_x}} \quad (8.61)$$

Although the exact stress distribution along the transverse axis through the hole is known, the following approximate expression can be more useful:⁹⁶

$$\frac{\bar{\sigma}_x(0, y)}{\bar{\sigma}_o} \cong 1 + \frac{1}{2} \rho^{-2} + \frac{3}{2} \rho^{-4} - \frac{k_\sigma - 3}{2} \left(5\rho^{-6} - 7\rho^{-8} \right) \quad (8.62)$$

where

$\bar{\sigma}_x(0, y)$ = Axial stress along the y -axis

$\bar{\sigma}_o$ = Applied far-field axial stress

$$\rho = \frac{y}{a}$$

a = Hole radius

k_σ = Anisotropic stress concentration factor (obtained by Eq. 8.60 for large plate)

The influence of laminate lay-up on stress distribution and stress concentration is clearly illustrated by the fringe patterns of a photoelastic coating around the hole of boron/epoxy plates. These were 66 cm (26 in.) long and 25.4 cm (10 in.) wide laminates of various lay-ups with a 2.54 cm (1 in.) diameter central hole. They were loaded in longitudinal tension to failure. Figure 8.53a shows that, for the $[0/\pm 45/0/90]$, laminate, the stress distribution is similar to that of an isotropic plate and the stress concentration factor is close to 3. Figure 8.53b shows that, for a $[0/90]_{2s}$ crossply laminate, the stress gradient at the hole boundary is sharp and the stress concentration factor is high (approximately 5). The influence of the hole along the transverse axis extends over a distance of approximately half the radius. On the other hand, the fringe pattern for the $[\pm 45]_{2s}$ angle-ply laminate in Figure 8.53c shows that the gradient is very mild, the stress concentration factor is moderate (approximately 2), and the influence of the hole extends throughout the plate.

The influence of material and stacking sequence on failure was studied for a variety of lay-ups.⁹⁷ Some results are listed in Table 8.3. The ultimate strength is a function of both stress concentration and percentage of 0° plies. Laminates with a high percentage of 0° plies, but with sufficient number of 45° plies to mollify the stress concentration factor, are the strongest. The $[0/90]_{2s}$ lay-up with 50% 0° plies is not strong because of the high stress concentration factor. The $[\pm 45]_{2s}$ lay-up is the weakest because of the absence of 0° plies, although the stress concentration factor is the lowest. Stacking sequence was also found to have a noticeable influence on strength and failure patterns. Stacking sequences

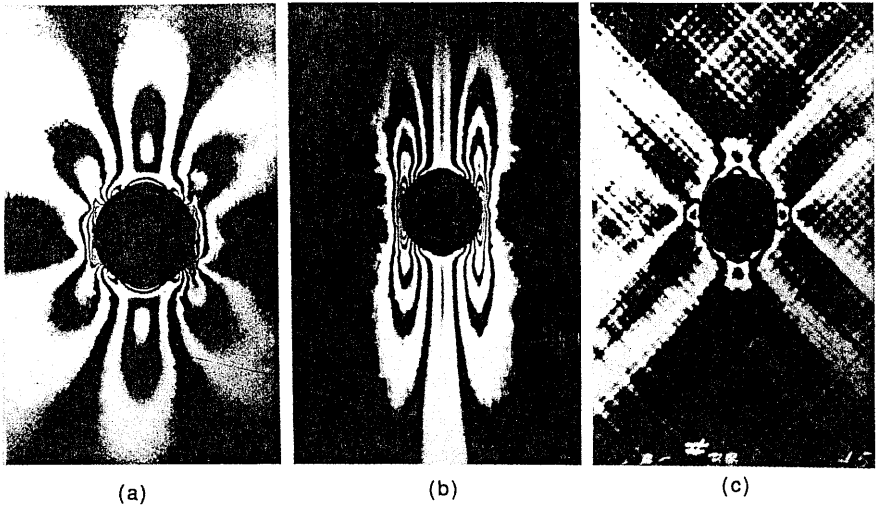


Fig. 8.53 Isochromatic fringe patterns in photoelastic coating around hole in boron/epoxy plates of different lay-ups under uniaxial tensile loading.⁹⁷ (a) $[0/\pm 45/0/90]_s$, $\bar{\sigma}_o = 293$ MPa (42.4 ksi). (b) $[0/90]_{2s}$, $\bar{\sigma}_o = 170$ MPa (24.6 ksi). (c) $[\pm 45]_{2s}$, $\bar{\sigma}_o = 77$ MPa (11.1 ksi).

resulting in tensile interlaminar normal stresses near the boundary of the hole reduce the strength of the laminate. In some cases stacking sequence variations can cause drastic differences in strength related to changes in failure modes from catastrophic to noncatastrophic (see Fig. 7.26).

The influence of hole diameter for uniaxially loaded plates can be described by using the average stress criterion.⁹¹ According to this criterion, failure occurs when the axial stress, averaged over a characteristic distance a_o from the hole boundary, equals the strength \bar{F}_o of the unnotched laminate (Fig. 8.54). The strength reduction ratio, ratio of notched to unnotched strength, is expressed as

$$k_F = \frac{\bar{F}_N}{\bar{F}_o} = \frac{2}{(1 + \xi)[2 + \xi^2 + (k_\sigma - 3)\xi^6]} \quad (8.63)$$

where

$$\xi = \frac{a}{a + a_o}$$

Experimental results obtained for uniaxially loaded $[0_2/\pm 45]_s$ carbon/epoxy laminates with holes of various diameters are in good agreement with predictions based on the average stress criterion for a characteristic length $a_o = 5$ mm,

Table 8.3 Effect of Laminate Lay-Up and Stacking Sequence on Stress Concentration and Strength of Boron/Epoxy Plates with Circular Holes under Uniaxial Tensile Loading

Lay-up	Axial modulus \bar{E}_x , GPa (Msi)	Measured stress		Predicted stress		Notched strength \bar{F}_N , MPa (ksi)	Unnotched strength \bar{F}_0 , MPa (ksi)	Strength ratio $k_F = \bar{F}_N/\bar{F}_0$
		concentration factor k_c	concentration factor k_c	concentration factor k_c	concentration factor k_c			
[0/90/0/90] _s	115.2 (16.70)	4.82	5.80	194 (28.1)	617 (89.5)	0.314		
[0 ₂ /±45/0] _s	133.9 (19.40)	3.58	3.68	498 (72.2)	807 (117.0)	0.617		
[±45/0 ₂ /0] _s	127.3 (18.45)	4.02	3.68	426 (61.7)	807 (117.0)	0.529		
[0/±45/0/90] _s	115.2 (16.70)	3.34	3.45	291 (42.2)	669 (97.0)	0.435		
[0 ₂ /±45/90] _s	116.3 (16.85)	3.15	3.45	291 (42.2)	669 (97.0)	0.435		
[0/±45/90] _s	79.5 (11.52)	3.08	3.00	180 (26.1)	457 (66.2)	0.394		
[45/90/0/-45] _s	81.4 (11.80)	3.10	3.00	213 (30.9)	459 (66.5)	0.465		
[±45/0/±45] _s	59.3 (8.59)	2.46	2.45	206 (29.9)	378 (54.8)	0.546		
[±45/±45] _s	19.9 (2.88)	2.06	1.84	125 (18.1)	137 (19.9)	0.909		
[45 ₂ /-45] ₂	20.2 (2.93)	2.55	1.84	115 (16.6)	137 (19.9)	0.833		

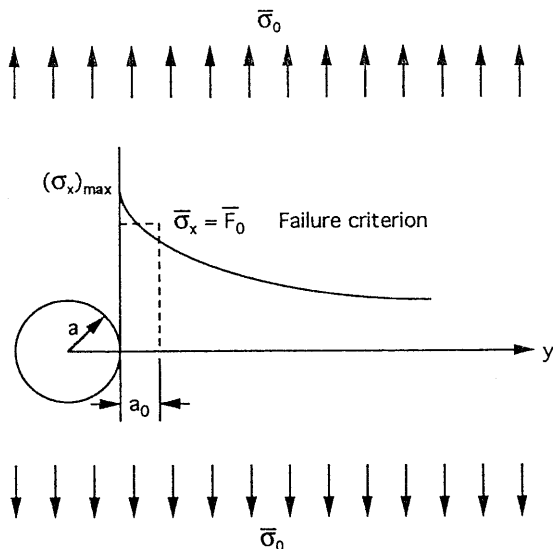


Fig. 8.54 Stress distribution and average stress criterion for uniaxially loaded composite plate with hole.

as shown in Figure 8.55. The laminates were 12.7 cm (5 in.) wide, 56 cm (22 in.) long with central holes of diameters ranging from 0.64 cm (0.25 in.) to 2.54 cm (1 in.). One interesting result observed in this and other similar cases is the existence of a threshold hole diameter, approximately 1.5 mm in this case, below which the laminate becomes notch insensitive.

The behavior of biaxially loaded composite plates with holes has been studied experimentally.^{76,98} A typical failure pattern of a $[0/\pm 45/90]_s$ carbon/epoxy plate with a hole under equal biaxial tensile loading is shown in Figure 8.56. The strength reduction ratio, ratio of notched biaxial strength to unnotched uniaxial strength, is plotted versus hole radius in Figure 8.57. These ratios are higher than corresponding values for uniaxial loading by approximately 30%. The variation of strength reduction ratio with hole diameter was satisfactorily described by using an average biaxial stress criterion. Radial and circumferential stresses around the hole were averaged over an annulus of 3 mm width and compared with the biaxial strength envelope for the unnotched quasi-isotropic laminate. Results were also in good agreement with predictions based on the Tsai–Wu failure criterion for the individual lamina and a progressive degradation model.⁹⁹ The strength reduction ratios for uniaxial and equal biaxial tensile loading represent lower and upper bounds for any biaxial tensile loading of this laminate. The strength reduction for any other tensile biaxiality ratio would fall between these two bounds and could be estimated approximately by interpolation.

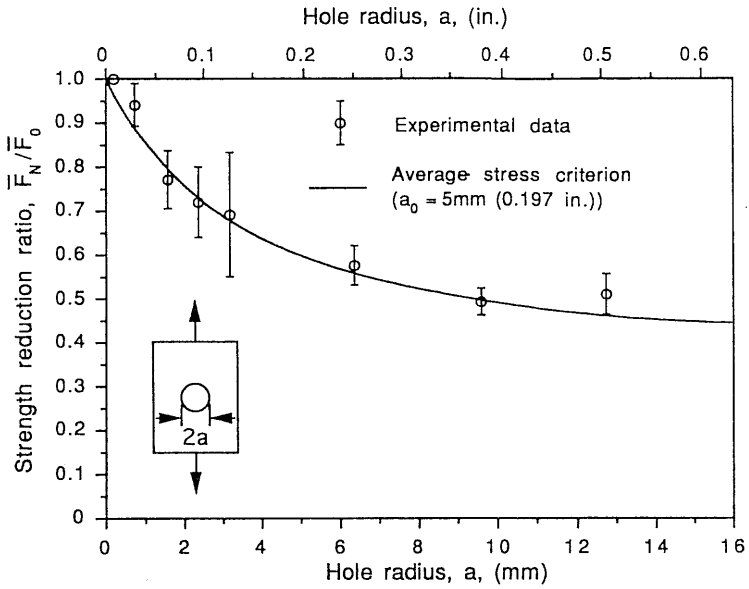


Fig. 8.55 Strength reduction as a function of hole radius for $[0_2/\pm 45]_s$ carbon/epoxy plates with circular holes under uniaxial tensile loading.⁹³

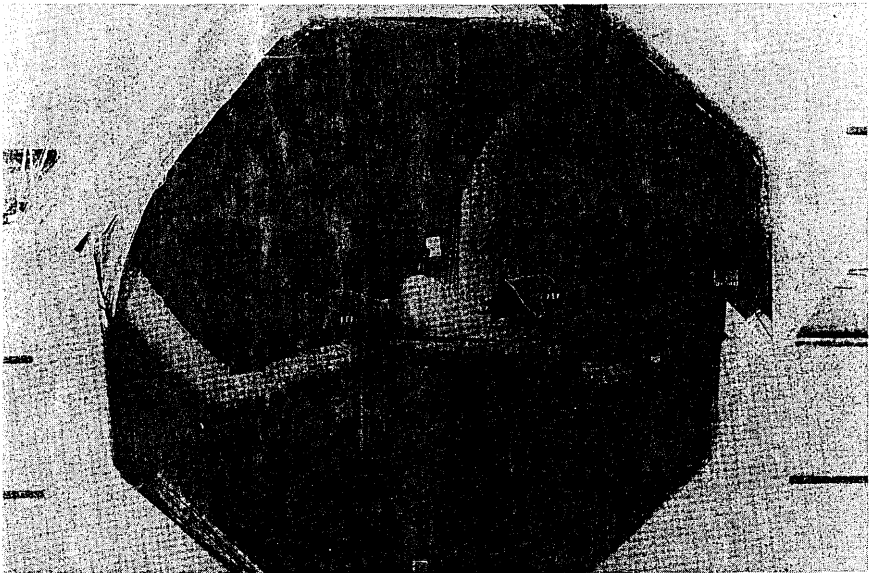


Fig. 8.56 Failure pattern in $[0/\pm 45/90]_s$ carbon/epoxy specimen with 1.91 cm (0.75 in.) hole under equal biaxial tensile loading.⁷⁶

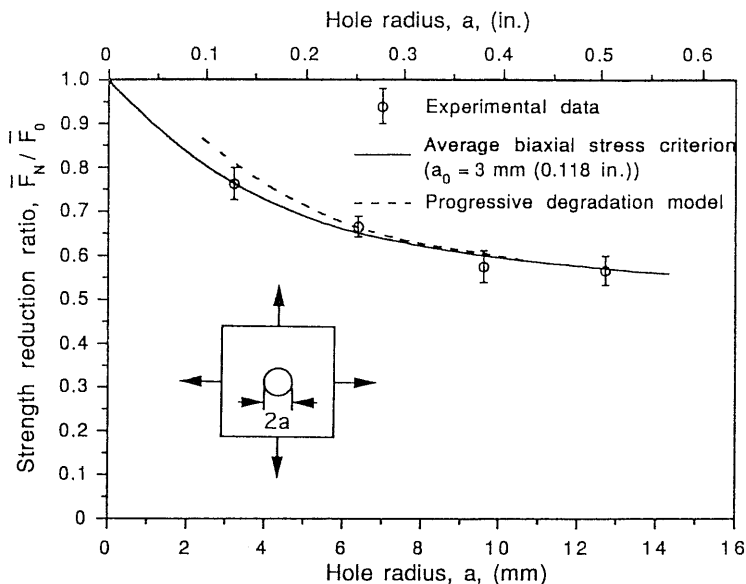


Fig. 8.57 Strength reduction as a function of hole radius for $[0/\pm 45/90]_s$ carbon/epoxy plates with circular holes under equal biaxial tensile loading.⁷⁶

8.10.3 Laminates with Cracks

Through-the-thickness cracks introduce much more severe stress concentrations in composite laminates. Stress distributions near a crack tip in an orthotropic material have been obtained in terms of mode I and mode II stress intensity factors and the laminate compliances.¹⁰⁰ An expression for the axial stress ahead of the crack, obtained as a limiting case of the solution for an elliptical hole, is (Fig. 8.58)¹⁰¹

$$\bar{\sigma}_x = \frac{\bar{\sigma}_o y}{\sqrt{y^2 - a^2}} \quad (8.64)$$

where

$\bar{\sigma}_x$ = Axial stress along transverse axis

$\bar{\sigma}_o$ = Applied far-field stress

a = Half crack length

The failure of composite laminates with through-the-thickness cracks also can be described by the semi-empirical average stress criterion.⁹¹ According to

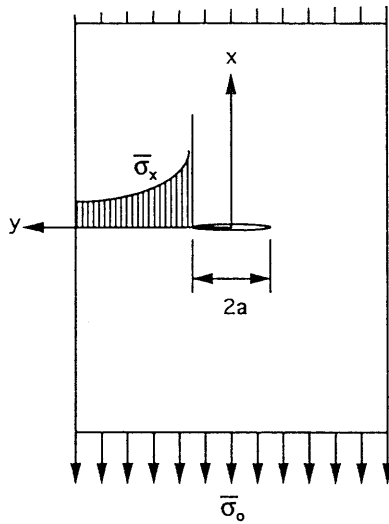


Fig. 8.58 Composite laminate with through-the-thickness transverse crack under uniaxial tensile loading.

this criterion, failure occurs when the axial stress averaged over a characteristic distance a_o from the crack tip equals the unnotched strength of the material. Using the stress distribution of Eq. (8.64), the average stress criterion predicts the following strength reduction ratio

$$k_F = \frac{\bar{F}_N}{\bar{F}_o} = \sqrt{\frac{a_o}{a_o + 2a}} \tag{8.65}$$

where \bar{F}_N and \bar{F}_o are the notched and unnotched laminate strengths, respectively and a_o the characteristic length dimension.

The deformation and failure of carbon/epoxy plates with cracks of different lengths have been investigated by experimental techniques.^{102,103} In general, failure at the tip of the crack takes the form of a damage zone consisting of ply subcracking along fiber directions, local delaminations, and fiber breakage in adjacent plies along the initial subcracks. The strain distribution around the crack tip and the phenomenon of damage zone formation and growth for a uniaxially loaded plate are vividly illustrated by the isochromatic fringe patterns in the photoelastic coating (Fig. 8.59). A noticeable characteristic is the apparent extension of the damage zone at a 45° angle with the crack direction. The size of this zone increases with applied stress up to some critical value at which point the specimen fails catastrophically. Far-field strains and the crack opening displacement were obtained from moiré fringe patterns around the crack.

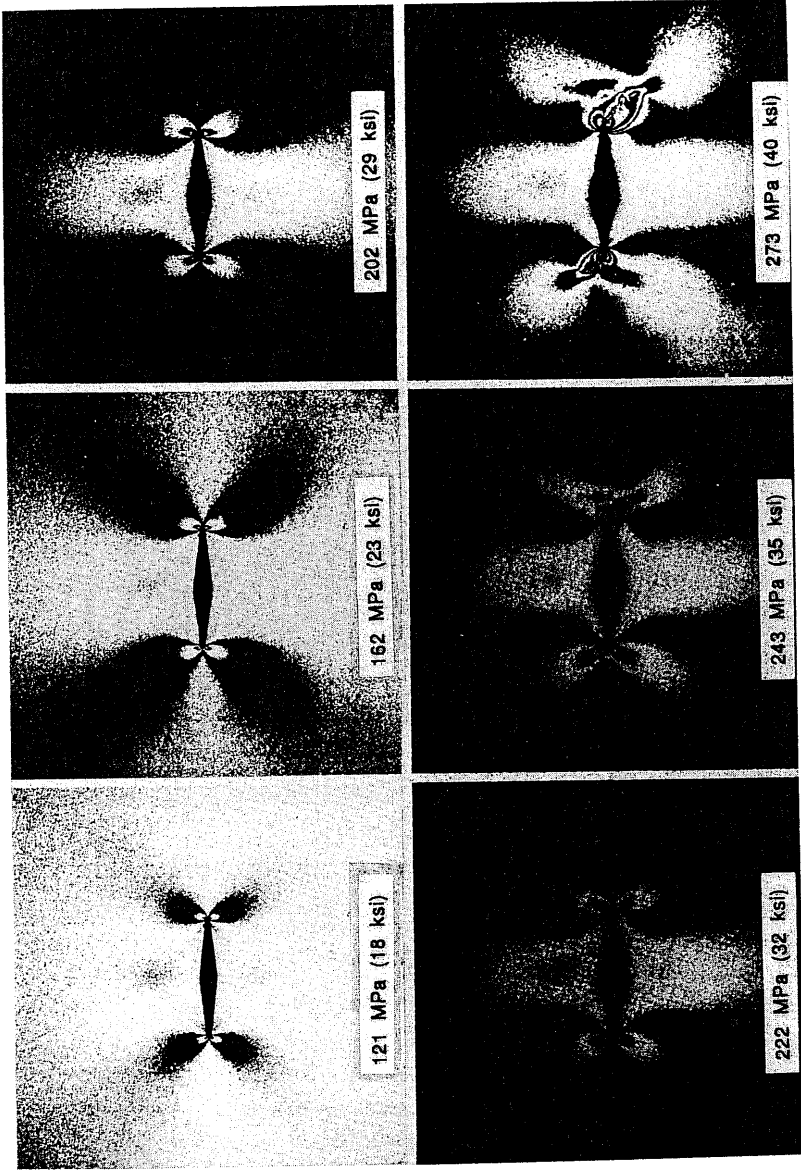


Fig. 8.59 Isochromatic fringe patterns in photoelastic coating around 1.27 cm (0.50 in.) crack of $[0/\pm 45/90]$, carbon/epoxy specimen at various levels of applied stress.¹⁰²

Experimental results for the strength reduction ratio agree well with predictions based on the average stress criterion using a characteristic dimension $a_o = 5$ mm (Fig. 8.60). Comparison of these results with those from similar specimens with circular holes shows that strength reduction in this case is nearly independent of notch geometry, i.e., specimens with holes and cracks of the same size have nearly the same strength. Experimental results for specimens with holes along with predictions based on an average stress criterion for holes are also shown in Figure 8.60.

The result above can also be analyzed by linear-elastic fracture mechanics. If the half crack length a is adjusted to include the length a_o of the damage zone near the crack tip, the critical stress intensity factor is given by

$$K_{Ic} = \bar{F}_N \sqrt{\pi(a + a_o)} \tag{8.66}$$

The length of the damage zone can be taken equal to the characteristic dimension a_o in the average stress criterion (5 mm). It can also be approximated by the diameter of the damage zone near failure as detected by the photoelastic coating. It is shown in Figure 8.61 that the critical stress intensity factor, as modified to account for the critical damage zone at the crack tip, is nearly constant with crack length.

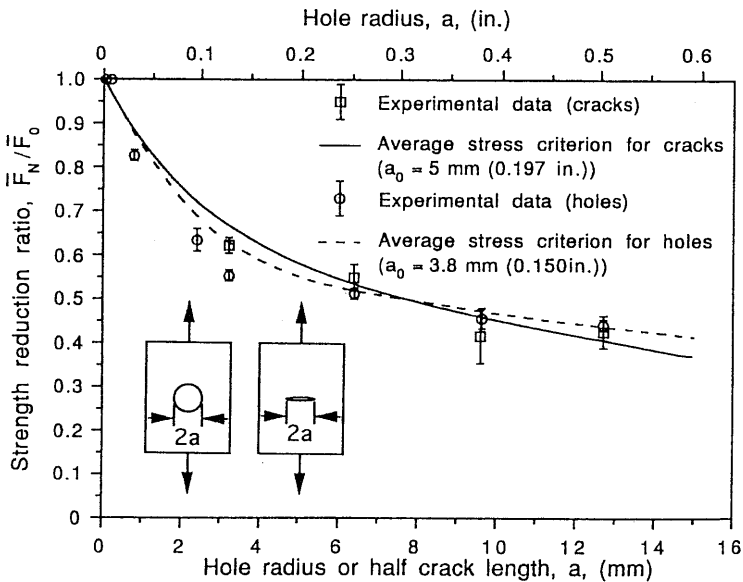


Fig. 8.60 Strength reduction as a function of hole radius or crack length for $[0/\pm 45/90]_s$ carbon/epoxy plates with circular holes and transverse cracks under uniaxial tensile loading.¹⁰²

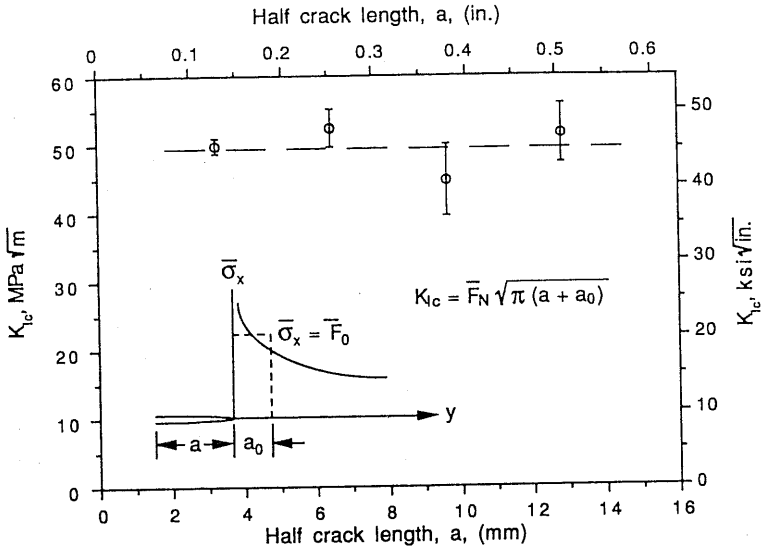


Fig. 8.61 Critical stress intensity factor as a function of crack length for $[0/\pm 45/90]_s$ carbon/epoxy plates with transverse cracks under uniaxial tensile loading.¹⁰²

Similar studies have been conducted with quasi-isotropic plates under biaxial loading having cracks of various lengths.^{77,104} Under these loading conditions it is not possible to use simplified failure criteria as discussed before. However, experimental results can be compared satisfactorily with predictions based on a maximum stress criterion for the individual lamina and a progressive degradation model.

The strength of notched laminates in general is a measure of notch sensitivity and toughness. This has prompted the recommendation of simple test methods for qualitative evaluation of laminate toughness by NASA and SACMA (Suppliers of Advanced Composite Materials Association). In the NASA specification quasi-isotropic laminates with holes are tested in tension and compression.¹⁰⁵ The SACMA recommendation is aimed at determining the tensile and compressive strength of the unidirectional material by testing laminates with holes.¹⁰⁶

8.11 Summary and Discussion

Methods of physical and mechanical characterization of constituent and composite materials were reviewed. The physical and mechanical characterization of the fiber and matrix constituents is necessary for the application of

micromechanics in understanding and predicting the macroscopic behavior of composite materials. In the macromechanical approach, the unidirectional lamina is considered the basic building block, and its full characterization is essential for any subsequent theoretical, numerical, or experimental analysis of composite structures. Many of the methods discussed have been standardized and the relevant ASTM specifications were mentioned in the text. A summary of test methods for characterization of the unidirectional lamina is given in Table 8.4.

In the case of compressive testing variations of the Celanese and IITRI test fixtures are widely used, with modifications being introduced by many investigators. A recent round robin test program by ASTM did not result in definitive conclusions. Considerable discussion and research is currently directed toward compression testing of thick composite sections.

There is still some debate as to the best methods for determining in-plane shear properties. The $[\pm 45]_{2s}$ coupon is standardized by ASTM, but the 10° off-axis specimen may be more realistic. An ASTM round robin program on in-plane shear testing, including the rail shear test, did not prove conclusive. Many types of tests may yield reasonable values for the in-plane shear modulus, but the ultimate properties determined are not always reliable. The interlaminar shear test is primarily a quality control test.



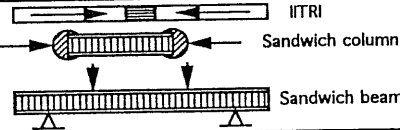
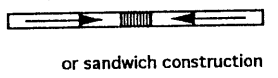
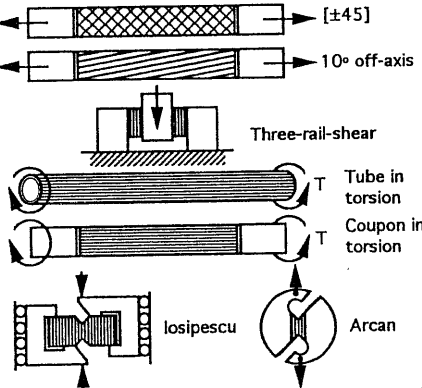
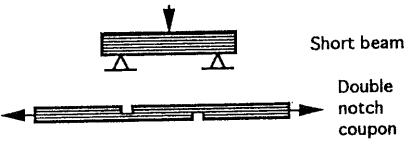
The problem of biaxial testing is still not under control. However, in many specific cases valid data can be obtained. There is great need for valid biaxial data. Biaxial fatigue data in general are not available.

Interlaminar fracture toughness is an important property, mainly for selection and ranking of different matrices for high damage tolerance, and it is well characterized in mode I by the double cantilever beam specimen. A variety of test methods and specimens are being investigated for modes II and III and mixed modes. Many of these tests, however, require finite element analysis to separate the various component modes of fracture toughness.

Stress and failure analysis around stress concentrations was discussed at some length. However, most of the work to date deals with well-defined flaws, such as holes and through-the-thickness cracks. There is need to extend this work to study more realistic defects, such as partial delaminations, scratches, and impact damaged areas. Fatigue behavior of laminates with notches, especially under biaxial loading, remains to be studied systematically.

Several areas of mechanical characterization were not addressed in this review. For example, fatigue testing is very important in studying damage mechanisms, damage accumulation, and the attendant degradation of stiffness and residual strength. Some specifications for fatigue testing are given in ASTM specifications D3479-76 and D4762-88. Fatigue studies must be extended to include spectrum fatigue loading and environmental effects. Future efforts will be directed toward methods of accelerated testing for determining the reliability and life of structures.

Table 8.4 Test Methods for Mechanical Characterization of Unidirectional Lamina

Tested Property (ASTM Standard)	Specimen Configuration	Elastic Properties	Strength Parameters
Longitudinal Tension (D3039-76)		E_1, ν_{12}	F_{1t}, ϵ_{1t}^u
Transverse Tension (D3039-76)		E_2, ν_{21}	F_{2t}, ϵ_{2t}^u
Longitudinal Compression (D3410-87) (C364-61) (C393-62)		E_1	F_{1c}, ϵ_{1c}^u
Transverse Compression (D3410-87) (C364-61) (C393-62)		E_2	F_{2c}, ϵ_{2c}^u
In-Plane Shear (D3518-76) (D4255-83)		G_{12}	F_6, γ_6^d
Interlaminar Shear (for quality assessment) (D2344-84) (D3846-79)			F_{31}

Environmental effects on mechanical properties are important and must be evaluated by special testing. The extent of property degradation as a function of temperature and moisture concentration must be measured for the various materials. Special testing procedures are needed to evaluate time effects, both long-term (creep) and short-term (dynamic) effects. Creep testing is useful in determining the viscoelastic characteristics of the composite, i.e., time-dependent stiffnesses and compliances. It can be conducted at various temperatures to obtain

master curves covering many decades of time. When creep tests are carried to ultimate failure, results can be used to predict the life of composite structures. A variety of methods have been developed for high rate testing to evaluate short-term effects. Closely related to this is impact testing and evaluation of impact damage tolerance.

Another important area of experimental characterization not covered in this chapter is nondestructive evaluation (NDE). A variety of NDE techniques are used for evaluating the integrity of composite materials and structures. They include radiographic (X-ray and neutron), optical (moiré, birefringent coatings, holographic interferometry, and speckle shearing interferometry), thermographic, acoustic (acoustic wave, acoustic emission), embedded sensors, ultrasonic, and electromagnetic techniques. The most widely used methods, especially for polymer matrix composites, are ultrasonic and X-radiographic techniques. They are used to detect and characterize flaws introduced during fabrication and in service, such as delaminations, porosity, matrix cracking, fiber-matrix debonding, fiber misalignment, inclusions and fiber fractures. The discussion of NDE methods and their application to composites is beyond the scope of this book.

References

1. J. M. Whitney, I. M. Daniel, and R. Byron Pipes, *Experimental Mechanics of Fiber Reinforced Composite Materials*, Monograph No. 4, Society for Experimental Mechanics, Bethel, CT, Prentice-Hall, Englewood Cliffs, NJ, Rev. Ed., 1985.
2. I. M. Daniel, "Methods of Testing Composite Materials," in *Fracture Mechanics and Methods of Testing*, G. C. Sih and A. M. Skudra, Vol. Eds., in *Handbook of Fibrous Composites*, A. Kelly and Y. N. Rabotnov, Eds., North Holland Publishing Co., Amsterdam, 1985, pp. 277-373.
3. Y. M. Tarnopol'skii and T. Kincis, *Static Test Methods for Composites*, G. Lubin, translation Ed., Van Nostrand Reinhold Co., New York, 1985 [originally published in Russian, 1981].
4. I. M. Daniel, "Composite Materials," in *Handbook on Experimental Mechanics*, A. S. Kobayashi, Ed., VCH Publishers, New York, 1993, pp. 829-904.
5. *ASTM Standards and Literature References for Composite Materials*, 2nd Ed., American Society for Testing and Materials, Philadelphia, PA, 1990.
6. H. D. Wagner, S. L. Phoenix, and P. Schwartz, "A Study of Statistical Variability in the Strength of Single Aramid Filaments," *J. Composite Materials*, Vol. 18, 1984, pp. 312-338.
7. J. A. DiCarlo, "Creep of Chemically Vapor Deposited SiC Fibers," *J. Materials Sci.*, Vol. 21, 1986, pp. 217-224.
8. C.-L. Tsai and I. M. Daniel, "Method for Thermomechanical Characterization of Single Fibers," *Composites Sci. Technol.*, Vol. 50, 1994, pp. 7-12.
9. N. J. Hillmer, "Thermal Expansion of Chemically Vapor Deposited Silicon Carbide Fibers," in *Symposium on High Temperature Composites*, Proceedings of the

- American Society for Composites, Technomic Publishing Co., Lancaster, PA, June 13-15, 1989, pp. 206-213.
10. "Standard Test Method for Tensile Properties of Thin Plastic Sheetings," in ASTM Designation D882-83, 1984, *Annual Book of ASTM Standards*, Section 8, Plastics, Vol. 08.01, American Society for Testing and Materials, Philadelphia, pp. 469-480.
 11. W. Freeman and M. D. Campbell, "Thermal Expansion Characteristics of Graphite Reinforced Composite Materials," *Composite Materials: Testing and Design* (Second Conference), ASTM STP 497, American Society for Testing and Materials, Philadelphia, 1972, pp. 121-142.
 12. I. M. Daniel and T. Liber, *Lamination Residual Stresses in Fiber Composites*, NASA CR-134826, NASA-Lewis Research Center, Cleveland, OH, 1975.
 13. I. M. Daniel, T. Liber, and C. C. Chamis, "Measurement of Residual Strains in Boron/Epoxy and Glass/Epoxy Laminates," in *Composite Reliability*, ASTM STP 580, American Society for Testing and Materials, Philadelphia, 1975, pp. 340-351.
 14. A. S. D. Wang, R. B. Pipes, and A. Ahmadi, "Thermoelastic Expansion of Graphite-Epoxy Unidirectional and Angle-Ply Composites," in *Composite Reliability*, ASTM STP 580, American Society for Testing and Materials, Philadelphia, 1975, pp. 574-585.
 15. E. Wolff, *Measurement Techniques for Low Expansion Materials*, Vol. 9, National SAMPE Technical Conference Series, Society for the Advancement of Material and Process Eng., Covina, CA, Oct. 1977.
 16. R. R. Johnson, M. H. Kural, and G. B. Mackey, *Thermal Expansion Properties of Composite Materials*, NASA CR-165632, NASA-Lewis Research Center, Cleveland, OH, 1981.
 17. D. E. Bowles, D. Post, C. T. Herakovich, and D. R. Tenney, "Moiré Interferometry for Thermal Expansion of Composites," *Exp. Mechanics*, Vol. 21, 1981, pp. 441-448.
 18. S. S. Tompkins, D. E. Bowles, and W. R. Kennedy, "A Laser-Interferometric Dilatometer for Thermal-Expansion Measurements of Composites," *Exp. Mechanics*, Vol. 26, 1986, pp. 1-6.
 19. S. S. Tompkins, "Techniques for Measurement of the Thermal Expansion of Advanced Composite Materials," in *Metal Matrix Composites: Testing, Analysis, and Failure Modes*, ASTM STP 1032, W. S. Johnson, Ed., American Society for Testing and Materials, Philadelphia, 1989, pp. 54-67.
 20. S. Gazit and O. Ishai, "Hygroelastic Behavior of Glass-Reinforced Plastics Exposed to Different Relative Humidity Levels," in *Proceedings of Conference on Environmental Degradation of Engineering Materials*, Virginia Polytechnic Inst., Blacksburg, VA, Oct. 1977, pp. 383-392.
 21. H. T. Hahn and R. Y. Kim, "Swelling of Composite Laminates," in *Environmental Effects on Composite Materials*, ASTM STP 658, J. R. Vinson, Ed., American Society for Testing and Materials, Philadelphia, 1978, pp. 98-120.
 22. G. Yaniv, G. Peimanidis, and I. M. Daniel, "Method for Hygrothermal Characterization of Graphite/Epoxy Composite," *J. Composites Technol. Res.*, Vol. 9, 1987, pp. 21-25.
 23. K. E. Hofer and P. N. Rao, "A New Static Compression Fixture for Advanced Composite Materials," *J. Test Eval.*, Vol. 5, 1977, pp. 278-283.
 24. B. W. Rosen, "A Simple Procedure for Experimental Determination of the Longitudinal Shear Modulus of Unidirectional Composites," *J. Composite Materials*, Vol. 6, 1972, pp. 552-554.

25. C. C. Chamis and J. H. Sinclair, "Ten-Degree Off-Axis Test for Shear Properties in Fiber Composites," *Exp. Mech.*, Vol. 17, 1977, pp. 339-346.
26. G. Yaniv, I. M. Daniel, and J.-W. Lee, "Method for Monitoring In-Plane Shear Modulus in Fatigue Testing of Composites," *Test Methods and Design Allowables for Fibrous Composites*, Second Vol., ASTM STP 1003, C. C. Chamis, Ed., American Society for Testing and Materials, Philadelphia, 1989, pp. 276-284.
27. C.-L. Tsai and I. M. Daniel, "The Behavior of Cracked Crossply Composite Laminates Under Simple Shear Loading," *Composites Engineering*, Vol. 1, 1991, pp. 3-11.
28. C.-L. Tsai, I. M. Daniel, and G. Yaniv, "Torsional Response of Rectangular Composite Laminates," *J. of Appl. Mech.*, Vol. 112, 1990, pp. 383-387.
29. C.-L. Tsai and I. M. Daniel, "Determination of In-Plane and Out-of-Plane Shear Moduli of Composite Materials," *Exp. Mech.*, Vol. 30, 1990, pp. 295-299.
30. M. Arcan, Z. Hashin, and A. Voloshin, "A Method to Produce Uniform Plane Stress States with Applications to Fiber Reinforced Materials," *Exp. Mech.*, Vol. 18, 1978, pp. 141-146.
31. D. E. Walrath and D. F. Adams, "The Iosipescu Shear Test as Applied to Composite Materials," *Exp. Mech.*, Vol. 23, 1983, pp. 105-110.
32. J. M. Whitney and C. E. Browning, "On Interlaminar Beam Experiments for Composite Materials," in *Proceedings of the V International Congress on Experimental Mechanics*, Society for Experimental Mechanics, Bethel, CT, 1984, pp. 97-101.
33. C. E. Browning, F. L. Abrams, and J. M. Whitney, "A Four-Point Shear Test for Graphite/Epoxy Composites," in *Composite Materials: Quality Assurance and Processing*, ASTM STP 797, C. E. Browning, Ed., American Society for Testing and Materials, Philadelphia, 1983, pp. 54-74.
34. C. A. Berg, J. Tirosch, and M. Israeli, "Analysis of Short Beam Bending of Fiber Reinforced Composites," *Composite Materials: Testing and Design* (Second Conference), ASTM STP 497, American Society for Testing and Materials, Philadelphia, 1972, pp. 206-218.
35. G. Menges and R. Kleinholz, "Comparison of Different Methods for the Determination of Interlaminar Shear Strength" [in German], *Kunststoffe*, Vol. 59, 1969, pp. 959-966.
36. N. J. Pagano and R. B. Pipes, "Some Observations on Interlaminar Strength of Composite Laminates," *Int. J. Mech. Sci.*, Vol. 15, 1972, pp. 679-688.
37. A. Harris and O. Orringer, "Investigation of Angle-Ply Delamination for Interlaminar Strength Test," *J. Composite Materials*, Vol. 12, 1978, pp. 285-289.
38. V. P. Nikolaev, "A Method of Testing the Transverse Tensile Strength of Wound Articles," *Mekhanika Polymerov* [Polymer Mechanics; in Russian], Vol. 9, 1973, pp. 675-677.
39. C. C. Hiel, M. Sumich, and D. P. Chappell, "A Curved Beam Test for Determination of the Interlaminar Tensile Strength of a Laminated Composite," *J. Composite Materials*, Vol. 25, 1991, pp. 854-868.
40. J. M. Whitney, C. E. Browning, and W. Hoogsteden, "A Double Cantilever Beam Test for Characterizing Mode I Delamination of Composite Materials," *J. Reinforced Plastics Composites*, Vol. 1, 1982, pp. 297-313.
41. N. Sela and O. Ishai, "Interlaminar Fracture Toughness and Toughening of Laminated Composite Materials: A Review," *Composites*, Vol. 20, 1989, pp. 423-435.
42. T. R. Brussat, S. T. Chin, and S. Mostovoy, *Fracture Mechanics for Structural Adhesive Bonds*, Phase II, AFML-TR-77-163, Wright-Patterson Air Force Base, Dayton, OH, 1978.
43. W. D. Bascom, R. J. Bitner, R. J. Moulton, and A. R. Siebert, "The Interlaminar

- Fracture of Organic-Matrix Woven Reinforced Composites," *Composites*, Vol. 11, 1980, pp. 9–18.
44. F. X. de Charentenay and M. Benzeggagh, "Fracture Mechanics of Mode I Delamination in Composite Materials," *Advances in Composite Materials*, in Proc. ICCM 3, Vol. 1, A. R. Bunsell, C. Bathias, A. Martrenchar, D. Menkes, G. Verchery, Eds., Pergamon Press, New York, 1980, pp. 186–197.
 45. D. F. Devitt, R. A. Schapery, and W. L. Bradley, "A Method for Determining Mode I Delamination Fracture Toughness of Elastic and Viscoelastic Composite Materials," *J. Composite Materials*, Vol. 14, 1980, pp. 270–285.
 46. D. J. Wilkins, J. R. Eisenmann, R. A. Camin, W. S. Margolis, and R. A. Benson, "Characterizing Delamination Growth in Graphite-Epoxy," in *Damage in Composite Materials: Basic Mechanisms, Accumulation, Tolerance, Characterization*, K. L. Reifsnider, Ed., ASTM STP 775, American Society for Testing and Materials, Philadelphia, 1982, pp. 168–183.
 47. D. L. Hunston and W. D. Bascom, "Effects of Layup; Temperature and Loading Rate in DCB Tests of Interlaminar Crack Growth," *Composite Technol. Rev.*, Vol. 5, 1983, pp. 118–119.
 48. A. A. Aliyu and I. M. Daniel, "Effects of Strain Rate on Delamination Fracture Toughness of Graphite/Epoxy," in *Delamination and Debonding of Materials*, ASTM STP 876, W. S. Johnson, Ed., American Society for Testing and Materials, Philadelphia, 1985, pp. 336–348.
 49. R. L. Ramkumar and J. D. Whitcomb, "Characterization of Mode I and Mixed Mode Delamination Growth in T300/5208 Graphite/Epoxy," in *Delamination and Debonding of Materials*, ASTM STP 876, W. S. Johnson, Ed., American Society for Testing and Materials, Philadelphia, 1985, pp. 315–335.
 50. I. M. Daniel, I. Shareef, and A. A. Aliyu, "Rate Effects on Delamination Fracture-Toughness of a Toughened Graphite/Epoxy," in *Toughened Composites*, ASTM STP 937, N. J. Johnston, Ed., American Society for Testing and Materials, Philadelphia, 1987, pp. 260–274.
 51. J. W. Gillespie, L. A. Carlsson, and A. J. Smiley, "Rate Dependent Mode I Interlaminar Crack Growth Mechanisms in Graphite/Epoxy and Graphite/PEEK," *Composites Sci. Technol.*, Vol. 28, 1987, pp. 1–15.
 52. W. S. Johnson and P. D. Mangalgiri, "Investigation of Fiber Bridging in Double Cantilever Beam Specimens," *J. Composites Technol. Res.*, Vol. 9, 1987, pp. 10–13.
 53. I. M. Daniel, G. Yaniv, and J. W. Auser, "Rate Effects on Delamination Fracture Toughness of Graphite/Epoxy Composites," in *Composite Structures—4* (Proceedings of Fourth International Conference on Composite Structures, Paisley, Scotland, 1987), I. H. Marshall, Ed., Elsevier Applied Science, New York, 1987, pp. 2.258–2.272.
 54. Y. J. Prel, P. Davies, M. L. Benzeggagh, and F. X. de Charentenay, "Mode I and Mode II Delamination of Thermosetting and Thermoplastic Composites," in *Composite Materials: Fatigue and Fracture*, Second Volume, ASTM STP 1012, Paul A. Lagace, Ed., American Society for Testing and Materials, Philadelphia, 1989, pp. 251–269.
 55. G. Yaniv and I. M. Daniel, "Height-Tapered Double Cantilever Beam Specimen for Study of Rate Effects on Fracture Toughness of Composites," in *Composite Materials: Testing and Design*, ASTM STP 972, J. D. Whitcomb, Ed., American Society for Testing and Materials, Philadelphia, 1988, pp. 241–258.
 56. A. J. Russell and K. N. Street, "Moisture and Temperature Effects on the Mixed-

- Mode Delamination Fracture of Unidirectional Graphite/Epoxy," in *Delamination and Debonding of Materials*, ASTM STP 876, W. S. Johnson, Ed., American Society for Testing and Materials, Philadelphia, 1985, pp. 349-370.
57. L. A. Carlsson, J. W. Gillespie, and R. B. Pipes, "Analysis and Design of End-Notched Flexure (ENF) Specimen for Mode II Testing," *J. Composite Materials*, Vol. 30, 1986, pp. 594-604.
 58. C. R. Corletto and W. L. Bradley, "Mode II Delamination Fracture Toughness of Unidirectional Graphite/Epoxy Composites," in *Composite Materials: Fatigue and Fracture*, Second Volume, ASTM STP 1012, Paul A. Lagace, Ed., American Society for Testing and Materials, Philadelphia, 1989, pp. 201-221.
 59. T. K. O'Brien, G. B. Murri, and S. A. Salpekar, "Interlaminar Shear Fracture Toughness and Fatigue Thresholds for Composite Materials," in *Composite Materials: Fatigue and Fracture*, Second Volume, ASTM STP 1012, Paul A. Lagace, Ed., American Society for Testing and Materials, Philadelphia, 1989, pp. 222-250.
 60. O. Ishai, H. Rosenthal, N. Sela, and E. Drucker, "Effect of Selective Adhesive Interleaving on Interlaminar Fracture Toughness of Graphite/Epoxy Composite Laminate," *Composites*, Vol. 19, 1988, pp. 49-54.
 61. N. Sela, O. Ishai, and L. Banks-Sills, "The Effect of Adhesive Thickness on Interlaminar Fracture Toughness of Interleaved CFRP Specimens," *Composites*, Vol. 20, 1989, pp. 257-264.
 62. L. Arcan, M. Arcan, and I. M. Daniel, "SEM Fractography of Pure and Mixed-Mode Interlaminar Fractures in Graphite/Epoxy Composites," in *Fractography of Modern Engineering Materials*, J. Masters and J. Au, Eds., ASTM STP 948, American Society for Testing and Materials, Philadelphia, 1987, pp. 41-67.
 63. W. S. Johnson, "Stress Analysis of the Cracked-Lap-Shear Specimen: An ASTM Round Robin," *J. Test. Eval.*, Vol. 15, 1987, pp. 303-324.
 64. J. H. Crews, Jr., and J. R. Reeder, *A Mixed-Mode Bending Apparatus for Delamination Testing*, NASA Tech-Memorandum 100662, NASA-Langley Research Center, Hampton, VA, 1988.
 65. T. K. O'Brien, "Characterization of Delamination Onset and Growth in a Composite Laminate," in *Damage in Composite Materials*, ASTM STP 775, K. L. Reifsnider, Ed., American Society for Testing and Materials, Philadelphia, 1982, pp. 140-167.
 66. T. K. O'Brien, "Mixed-Mode Strain-Energy-Release Rate Effects on Edge Delamination of Composites," in *Effects of Defects in Composite Materials*, ASTM STP 836, American Society for Testing and Materials, Philadelphia, 1984, pp. 125-142.
 67. S. L. Donaldson, "Mode III Interlaminar Fracture Characterization of Composite Materials," *Composites Sci. Technol.*, Vol. 32, 1988, pp. 225-249.
 68. G. Yaniv and I. M. Daniel, "New Test Method and Monitoring Technique to Evaluate Mode III and Mixed Mode Fracture Toughness in Composite Laminates," in *Composites: Design, Manufacture and Application*, Proceedings of Eighth International Conference on Composite Materials (ICCM/VIII), S. W. Tsai and G. S. Springer, Eds., Honolulu, 1991, pp. 36-A-1 to 15.
 69. B. W. Cole and R. B. Pipes, *Utilization of the Tubular and Off-Axis Specimens for Composite Biaxial Characterization*, AFFDL-TR-72-130, Wright Aeronautical Labs, Dayton, OH, 1972.
 70. R. E. Rowlands, "Analytical-Experimental Correlation of Polyaxial States of Stress in Thornel-Epoxy Laminates," *Exp. Mechanics*, Vol. 18, 1978, pp. 253-260.

71. V. D. Azzi and S. W. Tsai, "Anisotropic Strength of Composites," *Exp. Mech.*, Vol. 5, 1965, pp. 283-288.
72. O. Ishai, "Failure of Unidirectional Composites in Tension," *J. Eng. Mech. Div.*, Proc. of the ASCE, Vol. 97, No. EM2, 1971, pp. 205-221.
73. J. C. Halpin, *Primer on Composite Materials: Analysis*, Rev. Ed., Technomic Publishing Co., Inc., Lancaster, PA, 1984.
74. N. J. Pagano and J. C. Halpin, "Influence of End Constraint in the Testing of Anisotropic Bodies," *J. Composite Materials*, Vol. 2, 1968, pp. 18-31.
75. O. Ishai and R. E. Lavengood, "Characterizing Strength of Unidirectional Composites," *Composite Materials: Testing and Design*, ASTM STP 460, American Society for Testing and Materials, Philadelphia, 1970, pp. 271-281.
76. I. M. Daniel, "Behavior of Graphite/Epoxy Plates With Holes Under Biaxial Loading," *Exp. Mech.*, Vol. 20, 1980, pp. 1-8.
77. I. M. Daniel, "Biaxial Testing of Graphite/Epoxy Laminates with Cracks," in *Test Methods and Design Allowables for Fibrous Composites*, C. C. Chamis, Ed., ASTM STP 734, American Society for Testing and Materials, Philadelphia, 1981, pp. 109-128.
78. C. W. Bert, B. L. Mayberry, and J. D. Ray, "Behavior of Fiber-Reinforced Plastic Laminates Under Biaxial Loading," in *Composite Materials: Testing and Design*, ASTM STP 460, American Society for Testing and Materials, Philadelphia, 1969, pp. 362-380.
79. N. J. Pagano and J. M. Whitney, "Geometric Design of Composite Cylindrical Characterization Specimens," *J. Composite Materials*, Vol. 4, 1970, pp. 360-378.
80. J. M. Whitney, G. C. Grimes, and P. H. Francis, "Effect of End Attachment on the Strength of Fiber-Reinforced Composite Cylinders," *Exp. Mechanics*, Vol. 13, 1973, pp. 185-192.
81. T. L. Sullivan and C. C. Chamis, "Some Important Aspects in Testing High Modulus Fiber Composite Tubes in Axial Tension," in *Analysis of the Test Methods for High Modulus Fibers and Composites*, ASTM STP 521, American Society for Testing and Materials, Philadelphia, 1973, pp. 277-292.
82. T. R. Guess and F. P. Gerstle, Jr., "Deformation and Fracture of Resin Matrix Composites in Combined Stress States," *J. Composite Materials*, Vol. 7, 1977, pp. 448-464.
83. U. Hütter, H. Schelling, and H. Krauss, "An Experimental Study to Determine Failure Envelope of Composite Materials with Tubular Specimens under Combined Loads and Comparison with Several Classical Criteria," Proc. of Specialists Meeting on *Failure Modes of Composite Materials with Organic Matrices and Their Consequences on Design*, North Atlantic Treaty Organization, AGARD-CP-163, 1975, pp. 3-1 to 3-11.
84. U. S. Lindholm, A. Nagy, L. M. Yeakley, and W. L. Ko, *Design of a Test Machine for Biaxial Testing of Composite Laminate Cylinders*, AFFDL-TR-75-83, Wright Aeronautical Labs, Dayton, OH, 1975.
85. I. M. Daniel, T. Liber, R. Vanderby, and G. M. Koller, "Analysis of Tubular Specimen for Biaxial Testing of Composite Laminates," in *Advances in Composite Materials* (Proc. Third International Conference Composite Materials, ICCM 3), Vol. 1, A. R. Bunsell, C. Bathias, A. Martrenchar, D. Menkes, G. Verchery, Eds., Pergamon Press, New York, 1980, pp. 840-855.
86. B. W. Cole and R. B. Pipes, *Filamentary Composite Laminates Subjected to Biaxial Stress Fields*, AFFDL-TR-73-115, Wright Aeronautical Labs, Dayton, OH, 1974.

87. D. N. Weed and P. H. Francis, "Process Development for the Fabrication of High Quality Composite Tubes," *Fibre Sci. Tech.*, Vol. 10, 1977, pp. 89–100.
88. T. Liber, I. M. Daniel, R. H. Labeledz and T. Niirio, *Fabrication and Testing of Composite Ring Specimens*, (Proc. 34th Annual Tech. Conf., Reinf. Plastics/Composites Institute), The Society of the Plastics Industry, New York, Sect. 22-B, 1979.
89. M. E. Waddoups, J. R. Eisenmann, and B. E. Kaminski, "Microscopic Fracture Mechanisms of Advanced Composite Materials," *J. Composite Materials*, Vol. 5, 1971, pp. 446–454.
90. T. A. Cruse, "Tensile Strength of Notched Laminates," *J. Composite Materials*, Vol. 7, 1973, pp. 218–229.
91. J. M. Whitney and R. J. Nuismer, "Stress Fracture Criteria for Laminated Composites Containing Stress Concentrations," *J. Composite Materials*, Vol. 8, 1974, pp. 253–265.
92. E. M. Wu, *Failure Criteria to Fracture Mode Analysis of Composite Laminates*, Proc. of Specialists Meeting on *Failure Modes of Composite Materials and their Consequences on Design*, North Atlantic Treaty Organization, AGARD CP-163, 1975, pp. 2-1 to 2-11.
93. I. M. Daniel, *Failure Mechanisms and Fracture of Composite Laminates with Stress Concentrations* (Proceedings of the Seventh International Conference on Experimental Stress Analysis), Technion, Israel Institute of Technology, Haifa, Israel, 1982, pp. 1–20.
94. J. Awerbuch and M. S. Madhukar, "Notched Strength of Composite Laminates; Predictions and Experiments—A Review," *J. Reinforced Plastics Composites*, Vol. 4, 1985, pp. 3–159.
95. S. G. Lekhnitskii, *Theory of Anisotropic Elastic Body*, P. Fern, translator, J. J. Brandstatter, Ed., Holden-Day, San Francisco, 1963.
96. H. J. Konish and J. M. Whitney, "Approximate Stresses in an Orthotropic Plate Containing a Circular Hole," *J. Composite Materials*, Vol. 9, 1975, pp. 157–166.
97. I. M. Daniel, R. E. Rowlands, and J. B. Whiteside, "Effects of Material and Stacking Sequence on Behavior of Composite Plates with Holes," *Exp. Mech.*, Vol. 14, 1974, pp. 1–9.
98. I. M. Daniel, "Biaxial Testing of $[0_2/\pm 45]_s$ Graphite/Epoxy Plates with Holes," *Exp. Mech.*, Vol. 22, 1982, pp. 188–195.
99. K. H. Lo and E. M. Wu, "Failure Strength of Notched Composite Laminates," in *Advanced Composite Serviceability Program*, J. Altman, B. Burroughs, R. Hunziker, and D. Konishi, Eds., AFWAL-TR-80-4092, Wright Aeronautical Labs, Dayton, OH, 1980.
100. G. C. Sih, P. C. Paris, and G. R. Irwin, "On Cracks in Rectilinearly Anisotropic Bodies," *Int. J. Fracture Mech.*, Vol. 1, 1965, pp. 189–203.
101. S. G. Lekhnitskii, *Anisotropic Plates* (translated from second Russian edition by S. W. Tsai and T. Cheron), Gordon and Breach, Science Publishers, Inc., New York, 1968.
102. I. M. Daniel, "Strain and Failure Analysis in Graphite/Epoxy Laminates with Cracks," *Exp. Mech.*, Vol. 18, 1978, pp. 246–252.
103. Y. T. Yeow, D. H. Morris, and H. F. Brinson, "The Fracture Behavior of Graphite/Epoxy Laminates," *Exp. Mech.*, Vol. 19, 1979, pp. 1–8.
104. I. M. Daniel, "Mixed Mode Failure of Composite Laminates with Cracks," *Exp. Mech.*, Vol. 25, 1985, pp. 413–420.
105. *Standard Tests for Toughened Resin Composites*, Rev. Ed., NASA Reference Pub-

lication 1092, July 1983.

106. *Open-Hole Compression Properties of Oriented Fiber-Resin Composites*, Recommended Method SRM 3-88, SACMA, Suppliers of Advanced Composite Materials Association, 1988.

Answers to Selected Problems

Chapter 3

3.11 (c)

3.13 $\nu = 0.189$ and $\nu \cong 0.205$

3.15 $(G_{xy})_{\theta=45^\circ} = 9.40 \text{ GPa}$

$(G_{xy})_{\theta=45^\circ} \cong 10.45 \text{ GPa}$

3.18 $(\nu_{xy})_{\theta=30^\circ} = 0.298$

3.22 $\eta_{sx} = -0.241$ at $\theta = 29.4^\circ$

$\eta_{sx} = 0.189$ at $\theta = 62.8^\circ$

3.26 $\epsilon'_2 = \epsilon_2 + k_E \epsilon_1$

3.28 (a) $\eta_{sx} = \frac{G_{xy}}{\tau_s} \left(\epsilon_x - \frac{\sigma_x}{E_x} \right)$

(b) $\gamma_s = 0.167 \times 10^{-3}$

3.31 (a) $k = -\eta_{sx}$

(b) $\nu_{xy} = -\eta_{xy} \eta_{sy}$

(c) $\eta_{xs} \eta_{sx} = 1$

$$3.33 \quad E_1 = 61.82 \text{ GPa}$$

$$E_2 = 11.15 \text{ GPa}$$

$$G_{12} = 5.32 \text{ GPa}$$

$$3.34 \quad \text{Mechanics of materials: } E_2 = 7.56 \text{ GPa}$$

$$\text{Halpin-Tsai: } E_2 = 8.13 \text{ GPa}$$

$$3.36 \quad \text{Mechanics of materials: } G_{12} = 2.68 \text{ GPa}$$

$$\text{Halpin-Tsai: } G_{12} = 3.84 \text{ GPa}$$

Chapter 4

$$4.1 \quad E_1 = 46.1 \text{ GPa}$$

$$F_{1t} = 1,388 \text{ MPa (increases linearly with } E_f)$$

$$4.3 \quad E_1 = 127 \text{ GPa}$$

$$F_{1t} = 180.7 \text{ MPa}$$

$$4.5 \quad \sigma_o^u = 80 \text{ MPa; in-plane shear failure mode}$$

$$4.7 \quad F_{xt} = 142 \text{ MPa, } \theta = 38.2^\circ$$

$$4.9 \quad \sigma_o^u = 211.1 \text{ MPa}$$

$$4.12 \quad \theta_1 = 31.4^\circ, \quad \theta_2 = 58.6^\circ$$

$$4.14 \quad F_s = 122 \text{ MPa}$$

$$4.16 \quad F_o = 78.5 \text{ MPa (Tsai-Hill); } F_o = 79.7 \text{ MPa (Max. stress)}$$

$$4.18 \quad \sigma_o^u = 98.3 \text{ MPa}$$

Chapter 5

$$5.1 \quad \text{(a) Antisymmetric angle-ply laminate, } A_{xs} = A_{ys} = D_{xs} = D_{ys} = 0$$

$$B_{xx} = B_{xy} = B_{yy} = B_{ss} = 0$$

$$\text{(b) Balanced laminate}$$

$$A_{xs} = A_{ys} = 0$$

(c) Symmetric crossply laminate

$$B_{ij} = 0, A_{xs} = A_{ys} = D_{xs} = D_{ys} = 0$$

(d) Balanced laminate

$$A_{xs} = A_{ys} = 0$$

$$5.4 \quad B_{xs} = \frac{h^2}{4n} Q_{xs}(\alpha) \quad (\text{see Eq. 3.67 for transformation of } Q_{xs})$$

$$5.7 \quad B_{xs} = B_{ys} = B_{sx} = B_{sy} = \frac{(E_1 - E_2)t^2}{4(1 - \nu_{12}\nu_{21})}$$

$$B_{xx} = B_{yy} = B_{xy} = B_{ss} = 0$$

$$5.8 \quad A_{xx} = 60.49 \text{ MN/m}$$

$$A_{xy} = 17.28 \text{ MN/m}$$

$$A_{yy} = 26.68 \text{ MN/m}$$

$$A_{ss} = 20.68 \text{ MN/m}$$

$$A_{xs} = A_{ys} = A_{sx} = A_{sy} = 0$$

$$5.10 \quad A_{xx} = A_{yy} = 9.55 E_o t \cong 7.50 E_o t$$

$$A_{xy} = 7.15 E_o t \cong 7.50 E_o t$$

$$A_{ss} = 7.75 E_o t \cong 7.50 E_o t$$

$$A_{xs} = A_{ys} = A_{sx} = A_{sy} = 0$$

$$B_{xs} = B_{ys} = B_{sx} = B_{sy} = 3.52 E_o t^2 \cong 3.75 E_o t^2$$

$$B_{xx} = B_{xy} = B_{yy} = B_{ss} = 0$$

$$D_{xx} = D_{yy} = 3.18 E_o t^3 \cong 2.50 E_o t^3$$

$$D_{xy} = 2.38 E_o t^3 \cong 2.50 E_o t^3$$

$$D_{ss} = 2.58 E_o t^3 \cong 2.50 E_o t^3$$

$$D_{xs} = D_{ys} = D_{sx} = D_{sy} = 0$$

$$5.15 \quad \bar{E}_x = 25.3 \text{ GPa}, \bar{G}_{xy} = 37.6 \text{ GPa}, \bar{\nu}_{xy} = 0.688$$

$$5.17 \quad \bar{\nu}_{xy} = 0.648$$

$$5.19 \quad \bar{\nu}_{xy} = 0.281$$

$$5.21 \quad N_o = 1,035 \text{ N/m}$$

$$5.23 \quad r = 7.67$$

$$5.25 \quad \bar{E}_x = 58.41 \text{ GPa}, \bar{G}_{xy} = 23 \text{ GPa}, \bar{\nu}_{xy} = 0.27$$

Chapter 6

$$6.1 \quad \alpha_1 = 8.19 \times 10^{-6}/^\circ\text{C}$$

$$\alpha_2 = 55.8 \times 10^{-6}/^\circ\text{C}$$

$$6.3 \quad \alpha_1 = 4.05 \times 10^{-6}/^\circ\text{C}$$

$$\alpha_2 = 4.35 \times 10^{-6}/^\circ\text{C}$$

$$6.5 \quad N_x^T = N_y^T = 25.12t \text{ MPa}$$

$$N_s^T = 0$$

$$6.8 \quad \bar{\alpha}_x = -3.47 \times 10^{-6}/^\circ\text{C}$$

$$6.10 \quad r \cong 4$$

$$6.12 \quad \bar{\alpha}_x = -0.81 \times 10^{-6}/^\circ\text{C}$$

$$\bar{\alpha}_y = 5.34 \times 10^{-6}/^\circ\text{C}$$

$$6.14 \quad \Delta c = 0.856\%$$

$$6.16 \quad \sigma_{1e} = -155 \text{ MPa}, \sigma_{2e} = 30 \text{ MPa}$$

$$6.18 \quad \sigma_{1e} = -107.0 \text{ MPa}$$

$$\sigma_{2e} = 20.3 \text{ MPa}$$

$$\tau_{6e} = 0$$

$$6.20 \quad \sigma_x = -\frac{2E_x}{\eta_{xs}}(\alpha_1 - \alpha_2)mn \Delta T$$

$$6.22 \quad \sigma_x = -1,354 \text{ MPa}$$

$$6.24 \quad N_x = 497 \text{ kN/m}$$

Chapter 7

7.2 Maximum stress criterion:

$$\bar{F}_{xt} = 425 \text{ MPa}$$

$$\bar{F}_{xc} = 770 \text{ MPa}$$

Tsai-Wu criterion:

$$\bar{F}_{xt} = 423 \text{ MPa}$$

$$\bar{F}_{xc} = 1,049 \text{ MPa}$$

$$7.4 \quad (a) \quad \bar{F}_{xt} = 129 \text{ MPa}, \bar{F}_{xt} \cong 93 \text{ MPa}$$

$$(b) \quad \bar{F}_{xt} = 95 \text{ MPa}, \bar{F}_{xt} \cong 98 \text{ MPa}$$

$$(c) \quad \bar{F}_{xt} = 139 \text{ MPa}, \bar{F}_{xt} \cong 142 \text{ MPa}$$

$$7.6 \quad (a) \quad \bar{F}_s = 126 \text{ MPa}, \bar{F}_s \cong 114 \text{ MPa}$$

$$(b) \quad \bar{F}_s = 155 \text{ MPa}, \bar{F}_s \cong 152 \text{ MPa}$$

$$(c) \quad \bar{F}_s = 446 \text{ MPa}, \bar{F}_s \cong 431 \text{ MPa}$$

$$7.8 \quad \bar{F}_o = 71 \text{ MPa (by both Tsai-Wu and maximum stress criteria)}$$

$$7.10 \quad \bar{F}_{xc} = 483 \text{ MPa}$$

$$7.13 \quad \bar{F}_x = 374 \text{ MPa, in-plane shear mode}$$

7.14 Maximum stress criterion:

$$\bar{F}_{xt} = 134 \text{ MPa, transverse tensile failure}$$

$$\bar{F}_{xc} = 751 \text{ MPa, longitudinal compressive failure}$$

Tsai-Wu criterion

$$\bar{F}_{xt} = 128 \text{ MPa}$$

$$\bar{F}_{xc} = 511 \text{ MPa}$$

$$7.16 \quad \bar{F}_s = 168 \text{ MPa (Tsai-Wu)}$$

$$\bar{F}_s = 264 \text{ MPa (Maximum stress)}$$

Transverse tensile failure

- 7.18 (a) $\sigma_{1e} = -\sigma_{2e} = -20.9 \text{ MPa}$, $\tau_{6e} = -12.1 \text{ MPa}$
 (b) $\sigma_1 = 1.09 \bar{\sigma}_x$, $\sigma_2 = -0.092 \bar{\sigma}_x$, $\tau_6 = -0.236 \bar{\sigma}_x$
 (c) $\bar{F}_{xt} = 250 \text{ MPa}$ (maximum stress criterion)
 $\bar{F}_{xt} = 263 \text{ MPa}$ (Tsai-Wu criterion)
 In-plane shear failure
- 7.20 $\bar{F}_{ULF} = \bar{F}_{xt}^u = 1,140 \text{ MPa}$
 $\varphi_L = 0.373$
- 7.22 $\bar{F}_{FPF} = 301 \text{ MPa}$
 $\bar{F}_{ULF} = 760 \text{ MPa}$
 $\varphi_L = 0.396$
- 7.24 (d)
- 7.26 (a) $\sigma_1 = 51.9 \text{ MPa}$, $\sigma_2 = 23.1 \text{ MPa}$, $\tau_6 = 22.7 \text{ MPa}$
 (b) $\sigma_{1e} = -\sigma_{2e} = -20.9 \text{ MPa}$, $\tau_{6e} = -12.1 \text{ MPa}$
 (c) $\sigma_1 = 31 \text{ MPa}$, $\sigma_2 = 44 \text{ MPa}$, $\tau_6 = 10.6 \text{ MPa}$
- 7.28 $h_a = 4.88 \text{ mm}$ by maximum stress criterion
 $h_a = 4.10 \text{ mm}$ by Tsai-Wu criterion
 Transverse tensile failure

Index

- Acid digestion method, 307
Adams, D. F., 71, 74–76, 96, 98, 100, 329
Advanced Composites Design Guide, 192, 194
Aeolotropic material. *See* General anisotropic material
Aliyu, A. A., 277, 338, 340
Allowable laminate thickness, 250, 252
Alumina fibers, 28–29
American Society for Testing and Materials (ASTM) standards, 300–301, 305–8, 313, 316–22, 324–25, 331–33
Angle-ply laminates
 coefficients of thermal expansion, 212–13
 interlaminar stresses, 265–67
 properties of, 173–75, 178–81
 strengths of, 246–49
 stress concentration, 359–61
Anisotropy
 definition of, 14–15
 degrees of, 26
Antisymmetric laminates, 158–62
 angle-ply, 161–62
 crossply, 159–61
Aramid/epoxy. *See* Kevlar/epoxy
Aramid fibers, 27–30; *see also* Kevlar fibers
Arcan, M., 329
Arcan test. *See* Shear testing
Area method (for strain energy release rate), 277–78
Arnon, U., 191, 194
Artificial limb, 5
Automobile spring, 6
Average stress criterion, 357, 360, 362, 364, 367
Azzi, V. D., 114, 348
B-2 stealth bomber, 7
Balanced laminates, 157–62
Balanced symmetric laminates. *See* Orthotropic laminates
Beaumont, P. W. R., 256
Bending coupling stiffnesses. *See* Laminate, stiffnesses of
Bending laminate stiffnesses. *See* Laminate, stiffnesses of
Berry, J. M., 88, 90
Bert, C. W., 352
Betti's reciprocal law, 53
Biaxial testing, 347–56, 362–63
 crossbeam sandwich test, 350
 flat plate test, 352
 off-axis test, 347
 thin-wall tube test, 352
Bicycle frame, 5
Boeing 757 aircraft, 6
Boron/aluminum, 35
Boron/epoxy
 coefficients of thermal expansion, 197
 properties, 35
Boron fibers, 27–30
Boron/polyimide
 coefficients of thermal expansion, 197
 properties, 35

- Bounding method, 72
Bradley, W. L., 341, 343
Brinson, H. F., 365
Broutman, L. J., 280, 284
Browning, C. E., 277, 331, 336
Buckling of fibers. *See* Microbuckling of fibers
Burnout method. *See* Ignition method
- Calcium aluminosilicate, 31
Carbon/carbon composites, 20–21
Carbon/epoxy
 coefficients of thermal expansion, 197, 212–14
 critical strain energy release rates, 340, 343
 engineering constants, 34, 35, 65–66
 hygric strains, 312
 hygrothermal effects on, 190–94
 strength reduction in plates with holes, 363
 thermal strains, 197
Carbon fibers, 27–30
Carbon matrix, 31
Carbon/PEEK, 34
Carbon/polyimide
 coefficients of thermal expansion, 197
 properties, 35
Carpet plots
 for coefficient of thermal expansion, 213–14
 for laminate engineering properties, 181–83
 for strength of laminates, 248–49
Celanese test. *See* Compressive testing
Ceramic fibers, 27–30
Ceramic matrices, 31
Ceramic matrix composites, 20–21
Chamis, C. C., 216, 221, 310, 323
Characteristic damage state (CDS), 255, 259
Characterization of composite materials. *See* Testing of composite materials
Characterization of constituent materials, 300–305
Cina, B., 91, 96
Classical lamination theory (CLT), 142–153
- Coefficients of hygric expansion. *See* Coefficients of moisture expansion
Coefficients of moisture expansion
 of balanced/symmetric laminates, 207–12
 measurement of, 310–12
 of multidirectional laminate, 206–9
 prediction of, 195–98
 of unidirectional lamina, 194–98
Coefficients of thermal expansion
 of balanced/symmetric laminates, 207–9
 of fibers, 303–5
 measurement of, 309–11
 of multidirectional laminate, 206–14
 prediction of, 195–98
 of unidirectional lamina, 194–98
Compliance method (for strain energy release rate), 277
Compliances
 of general anisotropic material, 38, 40
 of lamina, 47
 of specially orthotropic material, 42
 of transversely isotropic material, 45
 transformation of, 60, 162–64
Composite materials
 advantages and limitations of, 5–10
 applications of, 4–7
 classification of, 19–21
 current status, 10–11
 definition of, 3
 future prospects, 10–11
 history of, 4
 interphase of, 3
 matrix of, 3
 performance map, 32
 properties of, 31–36
 reinforcement of, 3
 significance of technology, 10
 typical stress-strain curves, 33, 36
 types of, 19–21
Compressive testing
 Celanese test, 316
 IITRI test, 316–18
 measurement of properties, 316–20
 sandwich specimens, 318–20
Computational procedure
 for calculation of residual stresses, 225–27

- for calculation of warpage, 225–27
- for determination of laminate strengths, 244–46
- for hygrothermoelastic analysis, 225–27, 252–54
- for lamina elastic constants, 64–65
- for lamina safety factor, 120–22
- for lamina strength, 120–24
- for laminate engineering properties, 177–78
- for laminate safety factors, 244–46
- for multiple ply failure analysis, 263–65
- for stress and failure analysis of laminates, 244–46
- Concepts and characteristics, 12–36
- Constitutive relations; *see also* Stress-strain relations
 - for laminate, 149–52
- Continuous fiber composites, 19–20
- Conventional materials
 - advantages and limitations, 5–10
 - performance ranking, 13
 - structural performance, 12–13
- Corletto, C. R., 341, 343
- Coupling stiffnesses. *See* Laminate, stiffnesses of
- Cracked-lap shear specimen, 343–44
- Crews, J. H., 344
- Critical strain energy release rates, 336–346
- Critical stress intensity factor, 367–68
- Crossbeam sandwich specimen, 350–51
- Crossply laminates
 - interlaminar stresses, 266, 268–69
 - progressive failure, 254–59
 - stress concentration, 359–61
- Daniel, I. M., 72, 90, 96, 98, 190, 191, 196–97, 216–24, 256–59, 266, 269–71, 277, 283, 300, 302–05, 310, 311, 323, 326, 327, 338, 339, 340, 346, 352–54, 356, 357, 359, 362–68
- Degrees of anisotropy, 26–27
- Delamination, 265, 331, 334
- Delamination fracture toughness. *See* Interlaminar fracture toughness
- Delamination modes, 275
- Density, measurement of, 306
- Design
 - for damage tolerance, 278–79, 281
 - for dynamic stability, 278–80
 - for environmental stability, 278–79, 281
 - methodology, 278–81
 - objectives, 278–81
 - optimization, 251, 283–89
 - process (example), 278, 281–89
 - for stiffness, 278–80
 - for strength, 278–80
- Design considerations, 166–68
- Deviatoric strain energy theory. *See* Tsai-Hill theory
- DiCarlo, J. A., 300
- Discontinuous fiber composites, 19–20
- Donaldson, S. L., 345
- Doner, D. R., 71, 74–76, 96, 98, 100
- Dong, S. B., 142
- Double cantilever beam (DCB)
 - specimen, analysis of, 276–78; *see also* Interlaminar fracture toughness
- Doubly-split DCB specimen, 346
- Dvorak, G. J., 256
- E-glass/epoxy
 - failure envelopes, 121, 351
 - off-axis strength, 112, 120
 - properties, 34
- E-glass fibers, 27–30
- Edge effects, 265–72; *see also* Interlaminar stresses
 - angleply laminates, 265–67
 - crossply laminates, 266–69
 - effects of stacking sequence, 268–72
- Elastic constants; *see also* Stiffnesses; Compliances
 - comparison between unidirectional and angle-ply laminates, 178–81
 - micromechanical predictions of, 70–76
 - number of, 48
 - transformation of, 57–65, 162–64
- Eldror, I., 91, 96
- End constraints on off-axis specimen, effect of, 348–50
- End-loaded split (ELS) laminate test, 341–42

- End-notched flexure (ENF) test, 339–341
- Engineering constants, relations for, 48–54
- Engineering properties of laminates. *See* Laminate, engineering properties of
- Environmental effects. *See* Hygrothermal effects
- Epoxy, 30–32
- Experimental methods. *See* Testing of composite materials
- Extensional stiffnesses. *See* Laminate, stiffnesses of
- Fabrication
of composite tubes, 355–56
methods, 9
- Failure analysis of laminates, 234–98
- Failure of laminates, types of, 235
- Failure mechanisms, 85–106
in-plane shear, 105
longitudinal compressive, 90–96
longitudinal tensile, 85–93
transverse compressive, 99, 105
transverse tensile, 99–104
- Failure patterns
in-plane shear, 106
in laminates with holes, 363
longitudinal compressive, 95, 96
longitudinal tensile, 92, 94
transverse tensile, 101–4
- Failure theories, 106–20
applicability of, 126–29
comparison of, 127
maximum strain, 111–14
maximum stress, 108–11
Tsai-Hill, 114–16
Tsai-Wu, 116–23
- Fiber breaks, 88–90
- Fiber characterization, 300–305
- Fiber/matrix debonding, 89, 90
- Fiber/matrix interphase. *See* Interphase
- Fiber strength utilization, 261, 280, 286
- Fiber volume ratio
definition of, 4, 26
measurement of, 306–9
- Fiber weight ratio, 26
- Fibers
advantages and disadvantages, 28
performance map, 30
properties, 27–30
specific modulus, 30
specific strength, 30
stress-strain curves, 29
testing of, 300–305
types of, 27–29
- First-ply-failure (FPF)
definition of, 235
safety factors for, 235–38
stress analysis for, 235–38
strength components for, 238–42
Tsai-Wu criterion, 236–37
- Flat plate specimen (for biaxial testing), 352–54
- Flexural laminate stiffnesses. *See* Laminate, stiffnesses of
- Force-deformation relations, 149–52
- Force resultants. *See* Multidirectional laminates
- Fracture mechanics
in analysis of laminates with cracks, 367–68
in analysis of interlaminar fracture, 275–78
- Fracture toughness. *See* Interlaminar fracture toughness; Laminates with cracks
- Gatti, A., 88, 90
- General anisotropic material
definition of, 15
stress-strain relations, 37–41
- Generalized Hooke's law, 37–41
- Gillespie, J. W., 340
- Glass fibers, 27–30
- Gol'denblat, I. I., 116
- Gotro, J. T., 216–24
- Graphite/epoxy, 35
- Graphite fibers, 27–30
- Hahn, H. T., 216
- Halpin, J. C., 72, 261, 349
- Halpin-Tsai relations, 72–76
- Harper, B. D., 216
- Hashin, Z., 72, 74–76, 196, 256, 329
- Hellan, K., 275–76

- Heterogeneity, definition of, 14; *see also* Inhomogeneity, definition of
- Hiel, C. C., 334
- Highsmith, A. L., 256
- Hill, R., 71, 114
- Hillmer, N. J., 303
- Hofer, K. E., 316
- Holes, laminates with. *See* Laminates with holes
- Homogeneity, definition of, 13
- Hong, C. S., 256
- Hoogsteden, W., 277, 336
- Hooke's law. *See* Generalized Hooke's law
- Hybrid composites, 22, 23
- Hybrid failure envelope, 128
- Hyer, M. W., 221
- Hygric strains, measurement of, 312
- Hygroelastic isotropy. *See* Hydrothermoelastic isotropy
- Hygroelastic stability. *See* Hydrothermoelastic stability
- Hygrothermal effects, 189–228, 250–54
 on laminate safety factor, 250–54
 on laminate strength, 250–54
 on mechanical behavior, 190–94
 physical and chemical, 189–90
- Hygrothermal force resultants, 201
- Hygrothermal forces, physical
 significance of, 204–5
- Hygrothermal lamina strains, 198–200
- Hygrothermal moment resultants, 202
- Hygrothermal stress-strain relations, 206
- Hydrothermoelastic effects, 190
- Hydrothermoelastic isotropy, 209–10
- Hydrothermoelastic stability, 209–10
- Hydrothermoelastic stress analysis, 213–15
 computational procedure for, 225–27
- Hydrothermoelastic stress and failure analysis, 250–54
- Hydrothermoelastic stress-strain relations, 200–203
- Ignition method, 307
- Image analysis method, 307–9
- IITRI test method. *See* Compressive testing
- Ineffective fiber length, 88
- Inhomogeneity, definition of, 14
- Initial laminate failure. *See* First-ply-failure
- In-plane shear modulus
 measurement of, 321–31
 prediction of, 74–76
- In-plane shear strength
 measurement of, 321–31
 prediction of, 100
- Interactive tensor polynomial theory.
See Tsai-Wu theory
- Interlaminar failure, 235
- Interlaminar fracture toughness
 fracture mechanics, 275–78
 measurement of, 336–46; *see also* Mixed mode testing; Mode I testing; Mode II testing; Mode III testing
- Interlaminar shear strength,
 measurement of, 331–33
- Interlaminar strength, 106, 272
- Interlaminar stresses, 265–75; *see also* Edge effects
- Interlaminar tensile strength,
 measurement of, 333–35
- Interphase
 definition of, 3
 role of, 4
- Intralaminar shear modulus. *See* In-plane shear modulus
- Intralaminar shear strength. *See* In-plane shear strength
- Iosipescu shear test. *See* Shear testing
- Irwin, G. R., 364
- Ishai, O., 102, 103, 191, 194, 277, 280, 283, 284, 336, 351
- Isotropy, definition of, 14
- Jones, R. M., 53, 142
- Karalekas, D., 216
- Kevlar/epoxy
 coefficients of thermal expansion, 197
 properties, 34
 thermal strains, 197
- Kevlar fibers, 27–30
- Kincis, T., 300, 334
- Kink band. *See* Kink zone
- Kink zone, 91, 95

- Kinking (of fibers), 90, 91, 95
 Konish, H. J., 359
 Kopnov, V. A., 116
 Krishnamachari, S., 280, 284
- Lamina; *see also* Unidirectional lamina
 definition of, 21
 definition of basic properties, 25–26
- Laminate; *see also* Multidirectional laminates
 definition of, 21
 compliances of, 152–53
 efficiency ratio of, 261–62, 280, 286
 engineering properties of, 168–84
 stiffness-strength ratio of, 280
 stiffnesses of, 149–52, 166
- Laminates with cracks, 364–68
 strength reduction of, 365–68
- Laminates with holes, 269, 271, 357–64
 biaxial testing of, 362–63
 failure pattern of, 363
 strength reduction of, 360–64, 367
- Lamination residual stresses, 216
- Laws, N., 256
- Lay-up, laminate, 22, 23
- Lee, J.-W., 90, 256–58, 326
- Lekhnitskii, S. G., 357, 364
- Liber, T., 216, 310, 323, 356
- Lim, S. G., 256
- Lithium aluminosilicate (LAS), 31
- Longitudinal compressive failure. *See* Longitudinal compressive strength
- Longitudinal compressive strength
 measurement of, 316–20
 prediction of, 90–96
- Longitudinal modulus
 of fiber, 300–303
 measurement of, 312–16
 prediction of, 72
- Longitudinal tensile failure. *See* Longitudinal tensile strength
- Longitudinal tensile strength
 of fiber, 300–303
 measurement of, 312–16
 prediction of, 85–93
- Macromechanics, definition of, 23–25
- Masters, J. E., 255
- Material response, 15–19
- Material symmetry
 plane of, 15
 principal axes, 15
- Material types, 13
- Matrix material
 definition of, 3
 role of, 4
 stress-strain curves of, 31–32
 types of, 30–31
- Matrix characterization, 304–5
- Matrix cracking, 93
- Matrix volume ratio
 definition of, 26
 measurement of, 308–9
- Matrix weight ratio, 26
- Maximum strain theory, 111–14
 failure envelope, 114
- Maximum stress theory, 108–12
 failure envelope, 110, 112
 off-axis strength, 110–12
- Mazor, A., 191
- Mechanics of materials approach,
 70–75, 85–87
- Metal matrix composites, 20–21
- Metals, properties of, 36
- Microbuckling of fibers, 90, 91, 94,
 95
- Micromechanics
 definition of, 23–25
 of lamina elastic constants, 70–76
 of lamina failure, 85–106
 of lamina hygrothermal properties,
 194–98
- Mixed mode testing, 343–45
 cracked-lap shear (CLS) test,
 343–44
 edge delamination tension (EDT)
 test, 343–45
 mixed mode bending (MMB) test,
 343–44
- Mode I testing, 336–40
 double cantilever beam (DCB)
 specimen, 336–38
 width-tapered DCB (WTDCB)
 specimen, 336–40
- Mode II testing, 339–43
 Arcan fixture, 342
 cantilever beam with enclosed
 notch (ENCB), 342–43

- end-loaded split laminate (ELS)
 - test, 341–42
- end-notched cantilever beam
 - (ENCB) test, 342
- end-notched flexure (ENF) test, 341
- Mode III testing, 345–46
 - doubly split DCB specimen, 346
 - split double cantilever beam (DCB) specimen, 345–46
- Modulus reduction ratio, 256–59
- Moiré technique, 224, 266
- Moisture concentration
 - effect on mechanical behavior, 190–94
 - measurement of, 311–12
- Moisture effects. *See* Hygrothermal effects
- Moment deformation relations, 149–52
- Moment resultants. *See*
 - Multidirectional laminates
- Morris, D. H., 365
- Mullin, J., 88, 90
- Multidirectional laminates
 - carpet plots for engineering properties, 181–83
 - carpet plots for strength, 248–49
 - classical lamination theory, 142
 - coefficients of thermal and moisture expansion, 206–14
 - compliances, 152–53
 - computational procedures for stress and failure analysis, 244–46, 252–54
 - computational procedure for hygrothermoelastic analysis, 225–27, 252–54
 - design considerations, 166–68
 - elastic behavior, 142–84
 - force and moment resultants, 146–49
 - load-deformation relations, 149–52
 - safety factors, 235–37
 - stiffnesses, 149–152
 - strain-displacement relations, 143–45
 - strength components, 238–44
 - stress and failure analysis, 234–98
 - types of failure, 235
- Notches, laminates with. *See*
 - Laminates with cracks;
 - Laminates with holes
- Nuismer, R. J., 357
- O'Brien, T. K., 344
- Off-axis uniaxial test, 347–51
- Ogin, S. L., 256
- Orthotropic laminates, 162–64
- Orthotropy, definition of, 14–15
- Out-of-plane shear moduli,
 - measurement of, 327–29
- Pagano, N. J., 167, 266, 267, 269, 270, 272, 349
- Paris, P. C., 364
- Particulate composites, 19–20
- Paul, B., 72
- Peimanidis, G., 190, 191, 311
- Phoenix, S. L., 300
- Photoelastic methods, 25, 271, 360, 366
- Physical characterization, 306–12
- Pipes, R. B., 167, 266, 267, 269, 270, 300
- Pister, K. S., 142
- Plane stress, 45
- Ply. *See* Lamina
- Ply discount method, 261, 264
- Poisson's ratio; *see also* Engineering constants, relations for
 - of lamina, 25, 49–55, 61–67
 - of laminates, 168–71, 174–83
 - measurement of, 312–15
 - prediction of, 73
 - reciprocity relations, 52, 53, 62
 - of various types of materials, 15–18
- Poly-ether-ether ketone (PEEK), 30
- Polyester, 30
- Polyimide, 30
- Polymer matrix composites, 20–21
- Polymeric matrices, 30–32
- Polysulfone, 30
- Porosity. *See* Void volume ratio
- Prel, Y. J., 340, 343
- Prepreg, 10
- Principal coordinate axes for lamina, 21
- Principal modulus ratio, 280
- Principal strength ratio, 280

- Progressive degradation model, 357, 362, 364, 368
- Progressive laminate failure, 254-65
- Properties of composite materials, 31-36
- Quasi-isotropic laminates, 164-66
- Rail shear test, 324-26
- Ramkumar, R. L., 340, 343
- Ranking of laminates, 288-89
- Rao, P. N., 316
- Reeder, J. R., 344
- Reifsnider, K. L., 255, 256
- Reinforcement
 definition of, 3
 role of, 4
- Reissner, E., 142
- Residual stresses, 99, 215-21
- Riley, M. B., 71
- Rosen, B. W., 88, 89, 91, 321
- Rowlands, R. E., 269-71, 359
- Rule of mixtures, 72, 73, 85-87
- Russell, A. J., 341, 343
- S-glass/epoxy
 coefficients of thermal expansion, 197
 properties, 34
 thermal strains, 197
- S-glass fibers, 27-30
- Safety factors
 for lamina, 121
 for laminate, 235-37, 250-54
- Sandwich test specimens, 318-20, 350-51
- Schapery, R. A., 194-95
- Schwartz, P., 300
- Sela, N., 277, 336
- Self-consistent field method, 71-72
- Shareef, I., 338
- Shear coupling coefficients
 definition of, 18
 of lamina, 62
 of laminates, 170-71, 178-79, 181
- Shear coupling effect, 18, 348-50
- Shear coupling stiffnesses. *See*
 Laminate, stiffnesses of
- Shear lag analysis, 256-57
- Shear modulus; *see also* In-plane shear modulus
 of laminates, 169-71, 174, 177-80, 183
 measurement of, 321-31
- Shear strength. *See* In-plane shear strength; Interlaminar shear strength, measurement of
- Shear testing
 [± 45], angle-ply specimen, 321-22
 Arcan test, 329-31
 double-notch shear test, 332-33
 Iosipescu test, 329-30
 measurement of in-plane shear properties, 321-31
 10° off-axis specimen, 323-24
 rail shear tests, 324-26
 short beam shear test, 331-32
 torsion tests, 326-29
- Shikhmanter, L., 91, 96
- Short fiber composites, 19-20; *see also* Discontinuous fiber composites
- Sih, G. C., 364
- Silicon carbide/aluminum
 properties, 35
 temperature effects, 190, 192
- Silicon carbide/ceramic, 35
- Silicon carbide fibers, 27-30
- Sinclair, J. H., 323
- Smith, P. A., 256
- Specially orthotropic material, 41-42
- Specific modulus. *See* Specific stiffness
- Specific stiffness, 7, 30, 32, 280
- Specific strength, 7, 30, 32
- Split cantilever beam specimen, 345-46
- Springer, G. S., 189
- Stacking sequence
 definition of, 22
 effects of, 265, 268-71, 359-61
- Stavsky, Y., 142
- Stiffness degradation. *See* Stiffness reduction factors; Stiffness reduction of laminate
- Stiffness reduction factors, 264
- Stiffness reduction of laminate, 254-59
- Stiffnesses
 bending, 151-52
 coupling, 151-52
 extensional, 151-52

- of general anisotropic material, 37, 39–41
 - inversion of, 152–53
 - of isotropic material, 47
 - of lamina, 46–47
 - of laminates, 151–52
 - of specially orthotropic material, 41
 - transformation of, 59–60, 162–64
 - of transversely isotropic material, 45
- Strain concentration factor, 96, 98
- Strain-displacement relations, 143–45
- Strain energy release rate; *see also* Interlaminar fracture toughness fracture mechanics, 275–78 measurement of, 336–46
- Strain gage method, 310–12, 315, 321–25
- Strain-stress relations. *See* Stress-strain relations
- Strain transformation, 55–57
- Strains
 - hygric, 312
 - hygrothermal, 198–99
 - at a point in laminate, 145
 - tensor, 37
 - thermal, 197, 310–11
 - transformation of, 55–57
 - ultimate, 112, 301, 313
- Street, K. N., 341, 343
- Strength
 - basic parameters of lamina, 107
 - biaxial, 125–26, 347–56
 - comparison between unidirectional and angle-ply laminates, 246–49
 - of fibers, 28, 300–301
 - in-plane shear, 100, 106, 321–24
 - interlaminar, 106, 272, 331–35
 - of lamina, 85–130
 - of laminates, 234–272
 - longitudinal, 85–97, 312–20
 - notched, 360–61
 - transverse, 93–105, 312–20
 - of typical composites, 34–35
- Strength reduction ratio, of notched laminates, 360–68
- Stress analysis of laminates, 234–98
- Stress concentrations, composites with, 357–68
- Stress concentration factor
 - macromechanical (laminate), 358–61
 - micromechanical, 95, 96, 98–100
- Stress intensity factor, 364–68
- Stress-strain relations
 - for thin lamina, 54–55
 - of general anisotropic material, 37–41
 - hygrothermoelastic, 200–203
 - hygrothermal, 206
 - of isotropic material, 47–48
 - of orthotropic material under plane stress, 45–47
 - of specially orthotropic material, 41–42
 - of transversely isotropic material, 42–45
- Stress transformation, 55–57
- Stresses
 - hygrothermal, 213–15
 - interlaminar, 265–75
 - residual, 215–21
 - tensor, 37
 - transformation of, 55–57
- Symmetric balanced laminates. *See* Orthotropic laminates
- Symmetric laminates, 153–57, 235–44
 - angle-ply, 157
 - with isotropic layers, 155
 - with specially orthotropic layers (crossply), 156–57
 - stress and failure analysis of, 235–44
- Talreja, R., 256
- Tarnopol'skii, Y. M., 300, 334
- Temperature, effect of, 190–94
- Tensile testing
 - of fibers, 300–303
 - measurement of lamina properties, 312–16
 - ring specimen, 315
 - specimen geometry, 313
- Test methods for unidirectional lamina, summary of, 370
- Testing of composite materials, 299–378; *see also* Biaxial testing; Compressive testing; Interlaminar fracture toughness;

- Testing of composite materials (*cont.*)
see also Interlaminar tensile strength, measurement of;
 Shear testing; Tensile testing
- Thermal forces, 201
- Thermal moments, 202
- Thermal strains, 197, 303–305, 310–11
- Thermal stresses. *See* Residual stresses
- Thermoelastic isotropy. *See*
 Hygrothermoelastic isotropy
- Thermoelastic stability. *See*
 Hygrothermoelastic stability
- Thermoplastic, 30
- Thermoset, 30
- Thin-wall tubular specimen, 352–56
- Torsion coupling stiffnesses. *See*
 Laminate, stiffnesses of
- Torsion tube test, 326–27
- Transformation
 computational procedure for, 64–65
 of elastic parameters, 57–60
 of engineering constants, 64
 of lamina stiffnesses and compliances, 59–60
 of laminate stiffnesses and compliances, 162–64
 of stress and strain, 55–57
 of stress-strain relations, 61
- Transverse compressive failure. *See*
 Transverse compressive strength
- Transverse compressive strength
 measurement of, 316–20
 prediction of, 99, 105
- Transverse modulus
 measurement of, 312–15
 prediction of, 73–74
- Transverse tensile failure. *See*
 Transverse tensile strength
- Transverse tensile strength
 measurement of, 312–15
 prediction of, 93–104
- Transversely isotropic material,
 42–45
- Tsai, C.-L., 257, 259, 300, 302–305,
 326, 327
- Tsai-Hill criterion. *See* Tsai-Hill
 theory
- Tsai-Hill theory, 114–16
 off-axis strength, 116, 120
- Tsai, S. W., 72, 74–76, 114, 117, 283
- Tsai-Wu criterion; *see also* Tsai-Wu
 theory
 for first-ply-failure, 236–37
 with hygrothermal stresses, 250
- Tsai-Wu theory, 116–22
 biaxial strength, 125–26
 failure envelope, 121
 lamina strength components, 121–24
 off-axis strength, 120
 safety factor, 121–23
- Ultimate laminate failure, 235, 259–65
- Ultimate strains, measurement of,
 301–302, 312–15
- Unidirectional composites, properties
 of, 33–36
- Unidirectional lamina
 characterization of, 312–31
 coefficients of thermal and moisture
 expansion, 194–98
 determination of strength
 components, 121–24
 elastic behavior, 37–84
 failure mechanisms, 85–106
 hydrothermal strains, 198–200
 macromechanical failure theories,
 106–20
 macromechanical strength
 parameters, 107
 measurement of compressive
 properties, 316–20
 measurement of shear properties,
 321–31
 measurement of tensile properties,
 312–16
 micromechanics of failure, 85–106
 off-axis strength, 110–12
- Void volume ratio
 definition of, 26
 measurement of, 307–9
- Voloshin, A., 329
- von Mises yield criterion, 114
- Wagner, H. T., 300
- Walrath, D. E., 329
- Wang, T.-M., 216, 221–24
- Warp (of laminate), 221–24
- Weitsman, Y., 216
- Whitcomb, J. D., 340, 343

- Whiteside, J. B., 269–71, 359
Whitney, J. M., 71, 277, 300, 331, 336,
357, 359
Wilkins, D. J., 340, 343
Wolff, E., 310
Wooh, S.-C., 283
Woven-glass/epoxy, 34, 66–7
Wu, E. M., 117, 357
- X-radiography, 256
- Yaniv, G., 190, 191, 311, 326, 327, 339,
346
- Yeow, Y. T., 365
Young's modulus; *see also*
Engineering constants, relations
for
of fiber, 300–303
of lamina, 61–66
of laminates, 168–83
measurement of, 312–15
of off-axis lamina, 348–50
prediction of, 72
- Zewi, I. G., 216–24

